DYNAMICS OF PAVEMENT STRUCTURES

G. MARTINČEK

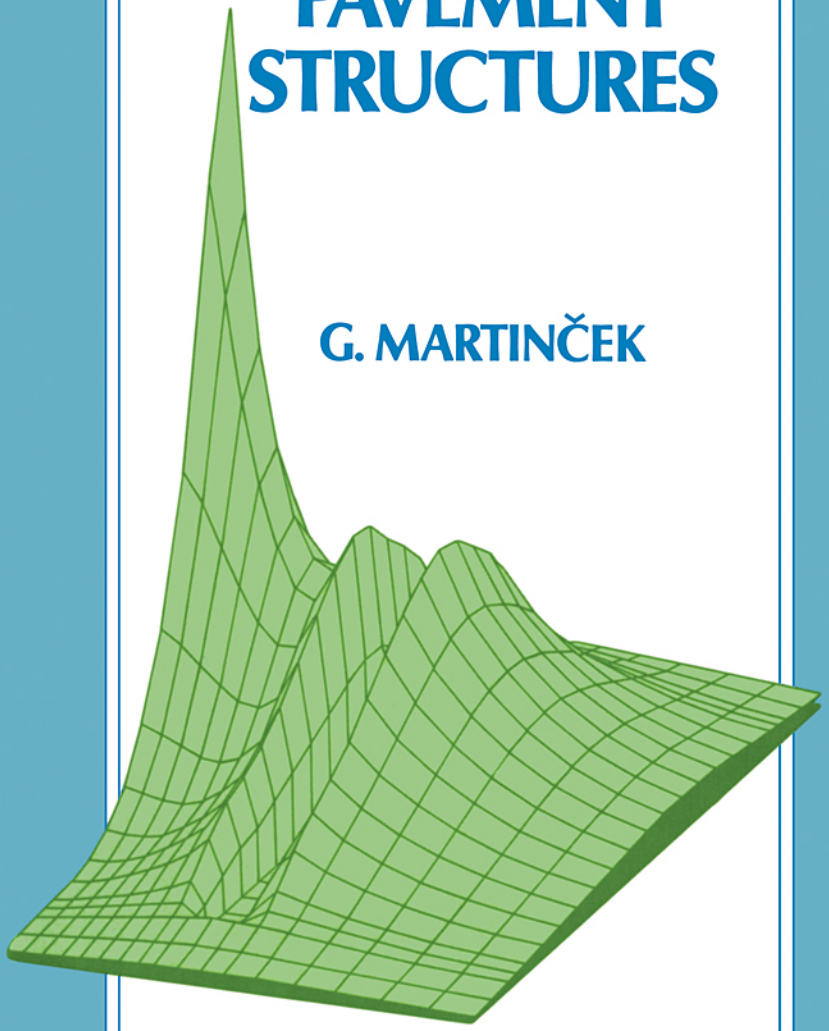

Taylor & Francis
Taylor & Francis Group

DYNAMICS OF PAVEMENT STRUCTURES

DYNAMICS OF PAVEMENT STRUCTURES

G.Martinček

Formerly Head of the Department of Dynamics
Institute of Construction and Architecture
Slovak Academy of Sciences
Bratislava, Slovak Republic

Taylor & Francis
Taylor & Francis Group
LONDON AND NEW YORK

By Taylor & Francis
2 Park Square, Milton Park, Abingdon, Oxon, OX14 4RN

This edition published in the Taylor & Francis e-Library, 2010.

To purchase your own copy of this or any of
Taylor & Francis or Routledge's collection of thousands of eBooks
please go to www.eBookstore.tandf.co.uk.

Co-published in with Ister Science Press Limited
Ister Science Press, Ltd., Staromestská 6, 811 03 Bratislava, Slovak Republic

ISBN 0-203-86077-2 Master e-book ISBN

ISBN (Taylor & Francis) 0 419 18100 8
ISBN (Ister Science Press) 80 88683 08 4

A catalogue record for this book is available from the British Library

Publisher's Note

The publisher has gone to great lengths to ensure the quality of this reprint but points out that some imperfections in the original may be apparent

CONTENTS

PREFACE

The basic criterion for the assessment of designs for pavement structures in highway and runway engineering, in terms of their service life and their operational characteristics, is their social effectiveness. Road surfaces must have the required bearing capacity and durability, and must provide for safe and comfortable driving over long periods. Specialists in transport engineering pay considerable attention to the improvement of material quality, reduction in the thickness of pavements, improvement in design methods and to other problems involved in the construction, operation and reconstruction of roads.

The loading of pavement structures is principally dynamic loading under mobile forces, the contact of which with the surface unevennesses of the pavement causes a dynamic state of stress. The current state of pavement design, in which these structures are designed only with regard to static loading, is basically a consequence of the insufficient development of dynamic theory, of the insufficient preparation of design engineers in dynamics, and of the absence of practical solutions. The aim of this book is at least partly to fill these voids, to inspire interest in the problem, and to strengthen the cooperation between specialists from industry and theoretical and research workers.

The starting point for developing the dynamics of pavement structures is detailed knowledge of the dynamic properties of materials and structures through the application and development of dynamic testing methods. This book summarizes data gathered over several years by the author and his team at the Institute of Civil Engineering and Architecture at the Slovak Academy of Sciences, in the developing field of dynamic investigation of road surfaces and road construction materials, based on the principle low-energy vibration methods.

Systematic experimental testing of real highway pavements carried out over several years and of various rigid and flexible pavement structures on the test track, served as the empirical basis for identifying acceptable theoretical models of pavement structures that agree closely with both the dynamic behaviour of structural materials and the total dynamic reaction of road pavements and airfield runways. A layered pavement structure can be modelled in terms of an equivalent plate on a subgrade. The stress states determined by using the principle of this model were compared with the stresses determined by using the layered medium for a large number of various pavement structures, and they have shown substantial agreement. The fundamental advantage of the model of an equivalent plate on a subgrade is that it makes it possible to deal with the decisive and typical tasks of pavement dynamics, which cannot be solved in a simple way by using the model of the layered medium.

The aim throughout this book is to demonstrate practical application, and the differences between the dynamic and static approaches. It contains a considerable number of numerical examples in the sphere of pavement evaluation and design.

The importance of pavement dynamics is not just theoretical. As pavement dynamics develops, it should be able to give answers to the practical requirements of design engineers, and hence its importance will continually be increasing.

It is a pleasure to acknowledge the important contributions that Milan Pokorný and Jiří Špitálsky made during the preparation and development of the experimental arrangements and during the measurements of highway pavements.

Gustáv Martinček

LIST OF SYMBOLS

a – radius of circular area

a, $\tilde{a}$ – acceleration

a_{ik} – coefficients of equation system

a_k – coefficients of Fourier series

a_T – shift factor

$A_1, A_2, A_3, \ldots$ – anti-resonance extrema

A_{kj} – coefficients of equation system

ARF – amplitude reduction factor

b – dimensionless parameter

b_{ik} – coefficients of equation system

B, B_0, B_1, B_2 – barrier thicknesses

B_{kj} – coefficients of equation system

$\boldsymbol{B}^*_\omega$ – complex bulk modulus

c, c_s – phase velocities of stress-wave propagation

c_1 – velocity of dilatational waves

$c_2, c_{2I}, c_{2II}, c_{2s}$ – velocities of shear waves

c_0, c_{01} – velocities of longitudinal waves in one-dimensional medium

c_s – velocity of longitudinal waves in two-dimensional medium

c_R, c_{Rz}, c_{Rs} – velocities of surface Rayleigh waves

c_p – dimensionless speed of load

c_{kj} – coefficients of equation system

C – dimensionless phase velocity, measure of surface irregularities

C_{ba} – barrier stiffness

$C_p(\tau)$ – covariance

C_P – dimensionless speed

d_{ik} – coefficients of equation system

$D, \bar{\boldsymbol{D}}, D^*$ – plate stifnesses, stiffness of layered system

D_1, D_2, D_k – partial stiffnesses

D_{kj} – coefficients of equation system

e – distance of central axis
E, E_ω, E_z, E_s – moduli of elasticity
E_{kj} – coefficients of equation system
$\boldsymbol{E}^*_\omega$, E^* – complex moduli of elasticity
E_1 – real part of complex modulus of elasticity
E_2 – imaginary part of complex modulus of elasticity
f, f_1, f_t, f_{T0}, f_T, f_a, f_b – frequencies
^{F}f – Fourier transform of function
F – dimensionless wave number, area
$\tilde{F}$ – harmonic variable force
F_{kj} – coefficients of equation system
F_u, $\hat{F}_u$ – corner forces
$F(z)$ – auxiliary function
$F(\imath\omega)$ – frequency characteristic
g – gravitational acceleration
G, G_I, G_{II}, G_ω – shear moduli of elasticity
$\boldsymbol{G}^*_\omega$ – complex shear modulus of elasticity
G_1, G_2, G_k – shear moduli of layer material
$G(r; t)$, $G_0(r; t)$, G_{ba} – Green functions, fundamental solutions
G_{kj} – coefficients of equation system
h, h_i – plate or layer thickness
h_{eq} – thickness of equivalent plate or layer
$H_0^{(2)}$, $H_1^{(2)}$ – Hankel's functions
H_n, $\hat{H}_n$ – equivalent shear forces
H_{kj} – coefficient of equation system
i – imaginary unit, integer
I – mass moment of inertia, parameter of global dynamic vehicle transfer
j – integer
J – moment of inertia
J_p – polar moment of inertia
J_t – modulus of stiffness in torsion
J_0, J_1 – Bessel's functions of the first kind
k – integer, real number
k_d – coefficient of mass increase
K_1 – coefficient of uniform compression
K_2 – coefficient of shear transmission
K_3 – coefficient of equivalent inertia
K_1^*, K_2^* – complex stiffness characteristics

$\boldsymbol{K_4^*}$ – complex coefficient of nonlinear compression

K_{ww}, $K_{wp,}$ K_{wM}, K_{wQ}, ... K_{QQ} – influence functions

l – distance, length of cantilever element

l_0 – length of unevenness

L – distance, chosen length

m – mass

M – object mass, moment of torsion

M, M_x, M_y, M_{nn}, $\widehat{\boldsymbol{M}}_{\mathbf{nn}}$ – bending moments

M_j – partial bending moment

M_r, $\widehat{\boldsymbol{M}}_{\boldsymbol{r}}$ – radial bending moments

M_φ, M_{t}, $\widehat{\boldsymbol{M}}_{\mathbf{t}}$ – tangential bending moments

${}^{\mathrm{F}}M$, ${}^{\mathrm{F}}M_2$ – Fourier transforms of bending moment

M_{xy}, M_{nt}, $\widehat{\boldsymbol{M}}_{\mathbf{nt}}$ – twisting moments

n – integer

N – number of nodal points

p, p_0 – intensity of normal load

${}^{\mathrm{H}}p$ – Hankel's load transform

${}^{\mathrm{F}}p$ – Fourier load transform

P – normal force

P_0 – force amplitude

P_1 – weight of unsprung load

P_2 – weight of spring-loaded part

P_{k}, P_{kk} – right-hand sides of equation system

q – vertical reaction of half-space or subgrade

${}^{\mathrm{H}}q$ – Hankel's transform of subgrade reaction

Q, Q_n, $\widehat{\boldsymbol{Q}}_{\boldsymbol{n}}$ – shear forces, transverse forces

Q_j – partial shear force

Q_{r}, Q_{rs} – transverse forces

${}^{\mathrm{F}}Q$, ${}^{\mathrm{F}}Q_0$ – Fourier transforms of transverse force

r – radial coordinate, radius of inertia

$\vec{\boldsymbol{r}}$ – radius vector

R, R' – radius, variable distances

R_1, R_2, R_3, ... – resonance extrema

${}^{\mathrm{F}}R$ – Fourier transform of dynamic load component

S – arbitrary component of state vector, region

S_0 – region

S_∞ – unbounded region

${}^{\mathrm{F}}S$ – Fourier transform of arbitraty state vector component

$S_p(\omega)$ – power spectral density
$S_s(\omega)$ – spectral density of state vector component
t – time coordinate
t_1 – dimensionless time
T – temperature, dimensionless time
T_0 – reference temperature
u_ϑ – tangential displacement
${}^{H}u$ – Hankel's transform of displacement
v – subgrade deflection, variable
V_s – coefficient of variation
w, w_0, w_1, w_2 – deflections, displacements
w_0 – depth of unevenness
w_L – linear deflection
${}^{H}w$ – Hankel's transform of displacement
${}^{F}w, {}^{F}w_0$ – Fourier transform of displacement
x – coordinate
y – coordinate
Y_0, Y_1 – Bessel's functions of the second kind
z – coordinate
z_0 – distance
Z^* – dimensionless mechanical impedance function
α, α_0 – wave number
α_1, α_2 – arguments
β – dimensionless frequency
γ – angular displacement, dimensionless characteristic of subgrade
γ_R, γ_J – real and imaginary part of angular displacement
γ_1, γ_2 – complex arguments
$\Gamma, \bar{\Gamma}$ – boundaries
$\delta, \delta_E, \delta_G, \delta_B$ – damping factors
$\delta(\xi), \delta(\eta_1)$ – Dirac generalized functions
Δ – curvature
$\Delta\varphi$ – phase difference
ε – strain, ratio of moduli
ε_0 – strain amplitude
$\varepsilon_{11}, \varepsilon_{12}, \varepsilon_{13}$ – ratios of velocities
ζ – dimensionless wave number
$\vec{\zeta}$ – radius vector of boundary point
η – argument, dimensionless coordinate, dimensionless wave number, ratio of wave lengths
η_1, η_2 – complex arguments

$\vec{\eta}$ – radius vector of boundary point

ϑ – logarithmic decrement, angle

$\vartheta, \vartheta_w, \vartheta_q, \vartheta_M$ – dynamic coefficients

κ – function of Poisson's ratio, ratio of wave velocities

κ_0 – function of Poisson's ratio

$\Lambda, \Lambda_1, \Lambda_2, \Lambda_i$ – wavelengths

μ, μ_s – Poisson's ratio

μ_0 – Poisson's ratio function

v – speed of moving load

ξ – dimensionless coordinate

ξ_1, ξ_2 – arguments

$\vec{\xi}$ – radius vector of loading point

$\varrho, \varrho_1, \varrho_{II}, \varrho_z, \varrho_s$ – material densities

ϱ, ϱ' – variable distances

$\sigma, \sigma_x, \sigma_r, \sigma_z, \sigma_s$ – normal stresses

σ_0 – stress amplitude

${}^H\sigma$ – Hankel's transform of stress

σ_s^2 – variance

$\tau, \tau_{xy}, \tau_{z\vartheta}, \tau_{r\vartheta}$ – tangential stresses

${}^H\tau$ – Hankel's transform of stress

φ – phase angle, angle, angular displacement

${}^F\varphi, {}^F\varphi_0$ – Fourier transforms of angular displacement

φ_{kj} – angles between the radius vectors

$\varphi_1(\mu), \varphi_2(\mu)$ – functions of Poisson's ratio

ϕ, ϕ_1, ϕ_2 – functions of Poisson's ratio

ψ – ratio of densities

ω – angular frequency

Ω, Ω_0 – dimensionless frequencies

Ω_0 – parameter of pulse duration

INTRODUCTION

This book is an attempt to summarize and solve the problems connected with a very important but often neclected subject: the dynamics of pavement structures.

Chapter 1 deals with dynamic methods of diagnosis. The principle of the methods, the experimental technique, the measurement procedures and the basic theoretical assumptions make up the general framework of knowledge necessary for the practical application of the methods. Chapter 1 presents the mechanical impedance methods devised for use in testing viscous and elastic materials, and based on the principle of the forced vibration of the test bodies or the subgrade. From the point of view of practical applications, the main part of this chapter contains detailed and simplified procedures for measuring the phase velocities of the propagation of stress waves in flexible and rigid road surfaces, the interpretation of the measurement results, and methods for the determination of rigidity and elasticity characteristics of pavement sections. The methods described are complemented by numerous results obtained from measurement of real pavement structures under construction or already completed.

The model of an equivalent plate on subgrade, as the result of dynamic diagnosis, provides a dynamic theory that makes it possible to determine the dynamic deflection and the principal internal forces of real layered pavement structure. The relationships for the calculation of stresses in a layered pavement structure are presented in Chapter 2.

The various variants of the dynamic theory of an equivalent plate on subgrade are analysed in Chapter 3. From studies of the vibration of a layer in contact with half-space and stress-wave propagation in a layer on half-space without shear contact, attention is concentrated on the vibration of a plate on halfspace and on the technical theory of a plate on subgrade using a simplified dynamic model of the soil base. The solutions, in integral and closed form are complemented by numerous numerical results.

Chapter 4 presents studies performed in order to determine the state vector components under dynamic loading of a half-plate on subgrade, of a plate strip on subgrade, of a plate on subgrade with joints and of a plate on inhomogeneous subgrade. All these problems have been solved by the reduction of a partial differential equation to an ordinary one using Fourier's integral transformation and by the application of the method of initial parameters. Numerous results of parametric numerical study have made it possible to compare the extreme values of flexural moments and subgrade reactions under particular schemes of dynamic loading for rigid and flexible pavements.

The typical problem of pavement dynamics is the dynamic interaction of the equivalent plate with the subgrade under a moving load. These problems are solved in Chapter 5 for a load moving along the boundary of a half-plate on subgrade. The solutions of the influence of periodical and isolated unevennesses under a moving load and load system with two degrees of freedom and the effect of a moving random load with extensive numerical data

give well-arranged material for evaluating of the dynamic behaviour of rigid and flexible pavement structures.

Chapter 6 deals with the dynamic response of the equivalent plate with free boundaries on an unbounded soil base. Starting from derived fundamental solutions for the subgrade and a plate on subgrade, the boundary integral equations according to the theorem of reciprocity and their solution using boundary elements are presented with the numerical application on a square and rectangular plate on subgrade. The analysis of the dynamic response of a bounded plate resting on unbounded subgrade using the method of boundary elements confirms that the dynamic increment under a harmonic and pulse load is significant and that the derived procedures make it possible to obtain the corresponding dynamic coefficients.

The method of boundary integral equations offers us the possibility of studying very interesting problems concerning the influence of arbitrarily shaped holes in a plate on subgrade during the propagation of vibration. The results of the theoretical and numerical analysis are given in Chapter 7 and they confirm that the influence of the hole causes the concentration of vibration about the hole. The concentration is significant, especially at resonance frequencies, when the hole becomes an amplifier of vibration.

The dynamic response of an unbounded plate on a non-linear soilbase under stationary and pulsed loads is the subject of Chapter 8. Many numerical applications make it possible to evaluate the influence of non-linearity on the dynamic behaviour of an equivalent plate on subgrade.

The effects of vibration-isolating barriers in the soil base in the case of vibration propagation evoked by traffic is analysed in Chapter 9. The application of the method of boundary elements for various kinds of barrier from different materials, trench barriers or sheet piling barriers offers advanced procedures for evaluating the vibration-isolating effect in the screening zone behind the barrier.

This book is probably the first attempt to summarize and solve systematically the main problems of pavement dynamics. It should be of interest not only to readers who are acquainted with the problems of pavement dynamics, but to students and skilled practising engineers as well.

1
DYNAMIC DIAGNOSIS OF PAVEMENT STRUCTURES

Dynamic diagnostic methods are based on the principle of the direct and indirect measurement of stress-wave velocities and their damping in the material medium.

Usually the vibration sources used have a small excitation energy. The testing is therefore non-destructive as the resulting dynamic stresses are slight and cannot affect the state of the original medium.

However, it is quite possible to use dynamic methods with a large excitation energy, which can be used to evaluate the bearing capacity of pavement structures and replace the static loading tests [1.1–1.3].

Dynamic testing can be classified according to the nature of the vibration process used into stationary vibration methods and pulse (impact) methods.

Stationary vibration methods use sources, that generate harmonic vibration at a specific frequency and inject it into the object under test. The applied frequency can be swept from the lowest frequencies to high ultrasonic frequencies.

The dynamic response of the object under test varies according to whether it is a bounded body, with dimensions comparable with the wavelength of the vibration process, or whether its dimensions are so large that it can be considered as an unbounded medium.

For a test sample that is a bounded body, a state of stationary forced vibration will arise characterized by amplitude and the phase of vibration motion at an arbitrary point of the sample. As the excitation frequency is changed, so the amplitude and phase angle of the resulting vibration will change and the phenomena of resonance and anti-resonance will result in extreme or significant values. Measurement of these extreme or significant amplitudes, together with the phase angles and corresponding frequencies, will provide parameters that can be used to assess the viscoelastic material characteristics of the test specimen.

If the harmonic exciting force is acting on an unbounded medium, such as a soil base or a structure with large dimensions like a pavement structure, the process of stress-wave propagation will occur. The amplitude of the stress-waves diminishes with distance because of dispersion and damping. Measurement the stress-waves velocities and the corresponding amplitudes of vibration provides parameters for assessing of the viscoelasticity and other characteristics of the tested structure.

The dynamic response of a medium or structure under pulse-impact force is the resultant effect of the spectrum of stress waves propagated in the medium. In practice the velocity of

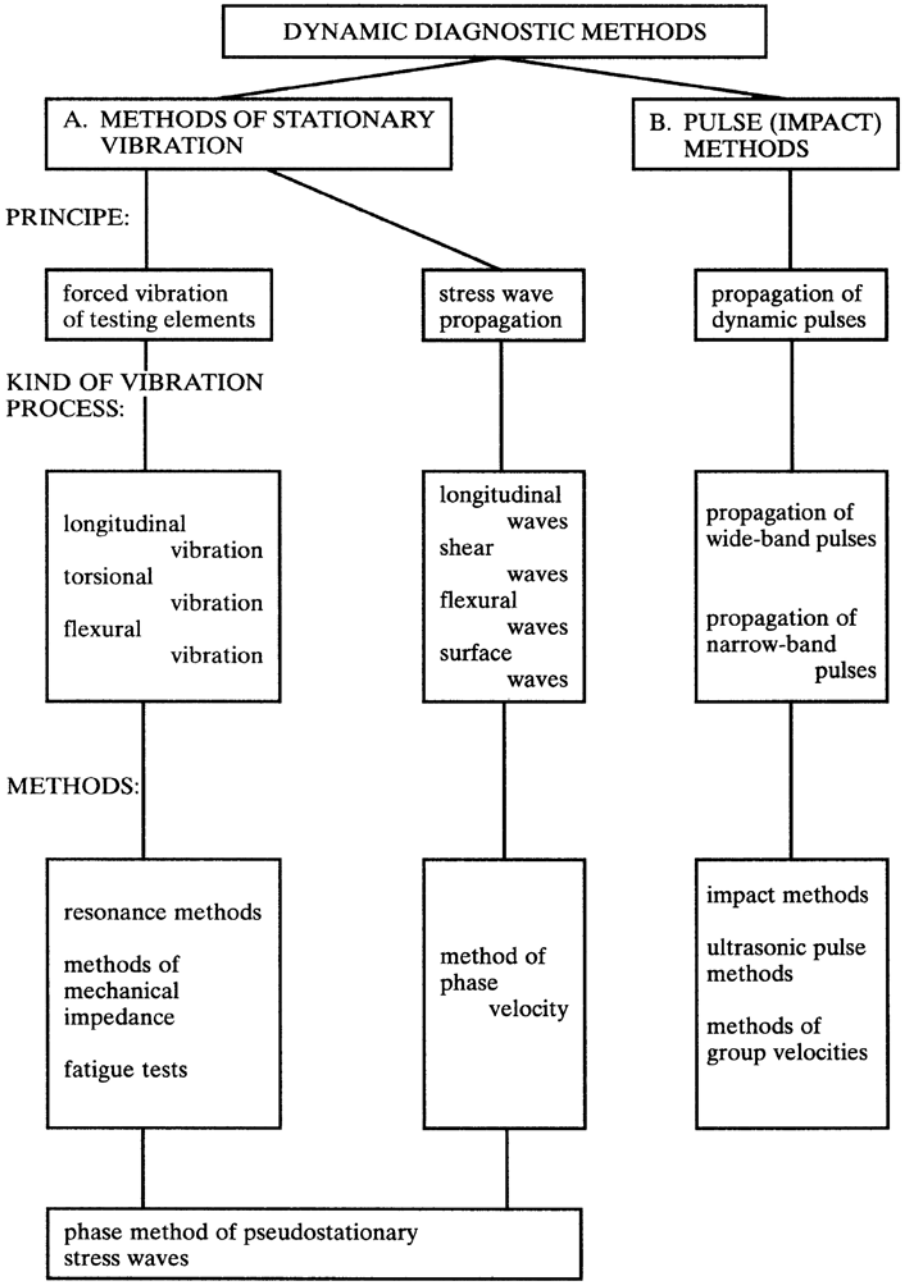

Fig. 1.1. Dynamic diagnostic methods.

pulse propagation and the amplitude of vibration are used as parameters of the quality and properties of the tested structures or medium.

The various dynamic diagnostic methods are set out in Fig.1.1.

1.1 Stress-wave velocity measurement method

The method used to measure the velocity of the propagated stress waves is derived from the method of dynamic non-destructive testing, which is particularly advantageous for assessing the properties and characteristics of plane structures and elements.

The distinguished English specialist R.Jones in the sphere of non-destructive testing started to use stress-wave velocity measurement to assess the elasticity characteristics, and thickness of pavement structures over time and under the influence of traffic [1.4–1.6]. References [1.7–1.9] refer to the intensive investigation and search for possible applications of the stress-wave velocity method. The results of our investigations, in which the theoretical and methodical investigations are summarized, are given in references [1.10–1.15].

1.1.1 Principle of method and experimental technique

The method is based upon the principle of phase-velocity measurement, in which the phase difference is measured between the vibration of the source, which transmits sinusoidal stress waves of a set frequency into the test object, and the vibration of the pick-up. The pick-up is placed at various distances from the source, and a phase difference of 360° corresponds to change of a pick-up distance of about one wavelength.

The phase velocity of stress-wave propagation, c, is related to the frequency f by the relationship

$$c=f\Lambda. \tag{1.1}$$

The apparatus for measuring phase velocities is shown schematically in Fig. 1.2. The generator consists of (1) an electrodynamic or magnetostrictive vibrator, (2) a power amplifier, and (3) a sinewave generator whose frequency can be set at anything from 20 Hz to 25 kHz. The evaluation part consists of (4) an accelerometer, (5) a narrow-band filter and (6) a phasemeter that can measure from 0° to 360° ± 1°. The apparatus has a suitable power supply.

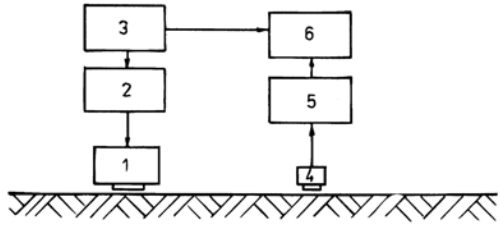

Fig. 1.2. Schematic diagram of apparatus for measuring phase velocities.

It can be seen from equation (1.1) that the decisive parameter is the wavelength Λ. Its determination can be realized in several ways.

First, if the wavelength Λ is small in comparison with the dimensions of the object, so that it is possible to take readings at a number of point, Λ is determined as follows.

1. The vibrator is acting at one point of the object.
2. The pick-up is moved along a selected line, and the phasemeter is used to determine the phase difference between the vibrator and the pick-up that corresponds to k times an angle of 360°.
3. The distance l that corresponds to the phase difference $k.2\pi$ is determined.
4. The wavelength Λ is given by the relationship $\Lambda=l/k$.

Second, if the wavelength is large and, because of the dimensions of the object or the power of the apparatus, measurements can only be made at a distance equalling one or a few wavelengths, then Λ is determined as follows.

1. The measuring line is set on the object and divided into an abscissa with equal intervals, such as 20, 10 or 5 cm.
2. The vibrator is placed at the starting point of the measuring line.
3. The pick-up location is changed to each of the discrete points of divided line in turn.
4. The phase difference is measured for every pick-up location.
5. The values of the phase angle are in a linear relationship with the pick-up distances and the slope of this linear relationship determines the average value of wavelength Λ.

Figure 1.3 shows a typical relationship between the measured phase angle φ and distance l. The results were obtained on the cement concrete plate of a pavement structure. The frequency of the vibration was f=28000 Hz and the intervals of the points on the measuring line were 2.0 cm.

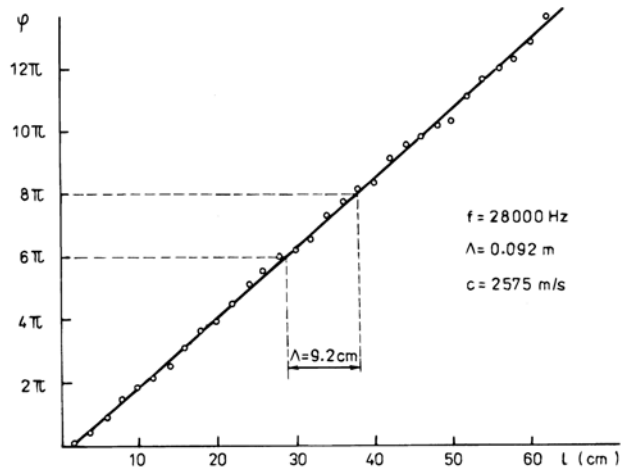

Fig. 1.3. Measured phase angle φ versus distance l.

Various disturbances can arise during the measurement process. The measurement precision is influenced by the nature of the pick-up's acoustic contact with the object at discrete points of the measuring line. This influence manifests itself as deviations in the linear relationship of φ versus l, as shown in Fig. 1.3.

Other reasons for disturbance exist in the bounded dimensions of the test object. The interference of direct and reflected waves, or the interference of waves of various kinds manifest themselves as a wave-like disturbance of the linear relationship of φ and l. This can be seen in Fig. 1.4 for a duralumin plate and longitudinal waves of frequency f=18000 Hz.

The interference of direct and reflected waves in a bounded test object can give rise to standing waves at resonant frequencies. In such a rare case the measurement of wavelength is difficult.

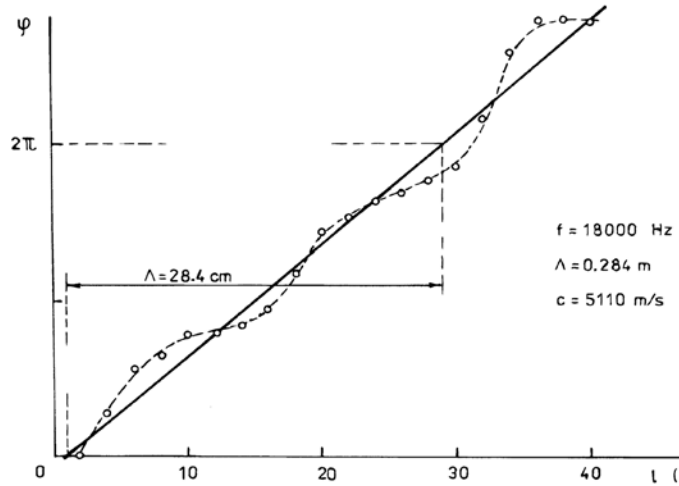

Fig. 1.4. Influence of reflected waves on relationship of phase angle to distance.

The third way in which the wavelength can be determined is by measuring the phase difference between the vibrations of two pick-up's the positions of which are constant [1.16]. This method makes it possible to automate measurement. The apparatus is shown schematically in Fig. 1.5. Two accelerometers (1, 2) with the same phase-frequency characteristic

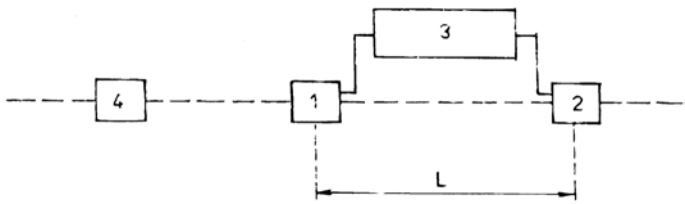

Fig. 1.5. Schematic diagram of apparatus for measuring phase difference.

are placed in contact with the tested object at a constant distance L. The outputs of the accelerometers are connected to the inputs of the phasemeter (3). The vibrator (4) transmits harmonic stress waves with frequency f into the tested medium. By the successive changing of frequency in the range f_1–f_n the phase difference $\Delta\varphi$ of accelerometer vibrations is

measured. The distance L has to fulfil the condition $L<\Lambda_1$, if Λ_1 is the wavelength corresponding to the frequency f_1. By changing the frequency f, the phase difference $\Delta\varphi$ changes too. The phase difference $\Delta\varphi=2\pi$ corresponds to the frequency when the wavelength Λ is just equal to the distance L. The variation of $\Delta\varphi$ versus frequency f (Fig. 1.6) makes it possible to determine the wavelength Λ on the basis of the measured value $\Delta\varphi=k2\pi$ in the frequency range (f_1, f_n). The wavelength is determined by the expression

$$\Lambda = \frac{2\pi L}{\Delta\varphi} = \frac{L}{k} \tag{1.2}$$

where k is an arbitrary real number.

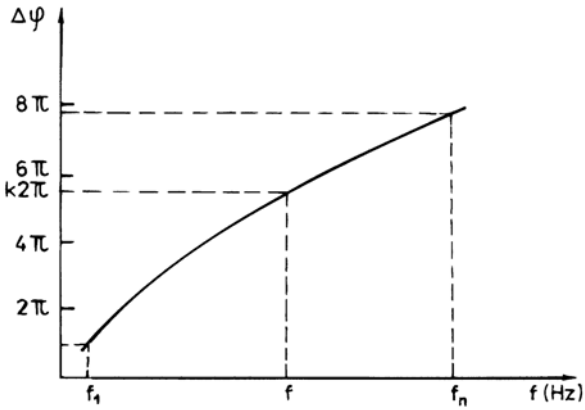

Fig. 1.6. Variation of phase difference $\Delta\varphi$ with frequency.

1.1.2 Theoretical assumptions

The theory underlying the problem of stress-wave propagation in a plane and layered medium is based on the assumption of a wider application of the phase velocity method.

Many questions of stress-wave propagation are known, especially in the geophysical literature, but the problems of layered pavement structures on a subgrade are theoretically so complex that they do not allow for exact numerical results to be obtained. This section can only outline the basics of the subject. For more detail, the reader is referred to special monographs, such as [1.17] and [1.18]. A study of the many problems of stress-wave propagation that are necessary for dynamic non-destructive diagnosis can be found in [1.13].

Dilatational and shear waves in unbounded media

It is well known that dilatational and shear waves propagate in a homogenous isotropic and elastic unbounded medium. They propagate without dispersion: that is, their velocity does not depend on the frequency or the wavelength.

The velocity of dilatational waves, c_1, is determined by the relationship

$$c_1 = \left(\frac{E(1-\mu)}{\varrho(1+\mu)(1-2\mu)}\right)^{1/2} \tag{1.3}$$

in which E is the modulus of elasticity, ϱ is the density of the material and μ is Poisson's ratio.

The velocity of shear waves, c_2, is given by

$$c_2 = \left(\frac{G}{\varrho}\right)^{1/2} \tag{1.4}$$

if G is the shear modulus of elasticity.

The motion of mass particles in shear-wave propagation is perpendicular to the direction of wave propagation.

Surface stress waves on the half-space

The stress waves that propagate on the half-space surface and diminish with depth are termed, surface Rayleigh waves. In the isotropic, homogenous and elastic half-space they propagate without wave dispersion, and their velocity c_R is given by the frequency equation

$$\kappa^6 - 8\kappa^4 - (24 - 16\mu_0^2)\kappa^2 + (16\mu_0^2 - 16) = 0 \tag{1.5}$$

if

$$\kappa = \frac{c_R}{c_2} \tag{1.6}$$

and

$$\mu_0^2 = \frac{1-2\mu}{2(1-\mu)} \tag{1.7}$$

The velocity of surface-wave propagation, c_R, is always smaller than the velocity of shear waves, c_2. The values of the velocity ratios c_R/c_2 and c_R/c_0 in relationship to Poisson's ratio μ are given in Tab. 1.1. The velocity c_0 of longitudinal waves in a one-dimensional medium is given by the very well-known relationship $c_0 = \sqrt{E/\varrho}$.

Table 1.1. Values of the velocity ratios.

μ	0	0.10	0.20	0.30	0.40	0.50
c_R/c_2	0.874	0.892	0.910	0.927	0.941	0.953
c_R/c_0	0.618	0.601	0.587	0.575	0.562	0.549

By using the method of phase velocities on pavement structures, the measured velocities at very high frequencies correspond to the velocity c_R of the surface layer medium, if the wavelength Λ is small compared with the surface layer thickness.

Symmetrical and asymmetrical stress waves in a plate with free surfaces

In an isotropic elastic plate (layer) with free surfaces, wave propagation is partly symmetrical, in view of the neutral plane of the plate (longitudinal waves), and partly asymmetrical (flexural waves).

The longitudinal stress waves are defined by the frequency equation

$$\frac{\tanh(sh/2)}{\tanh(qh/2)} = \frac{4\pi^2 h^2/\Lambda^2 (qh/2)(sh/2)}{\left[\pi^2 h^2/\Lambda^2 + (sh/2)^2\right]^2} \tag{1.8}$$

where

$$\frac{qh}{2} = \pi \frac{h}{\Lambda}\left(1 - \frac{c^2}{c_1^2}\right)^{1/2} \tag{1.9}$$

$$\frac{sh}{2} = \frac{\pi h}{\Lambda}\left(1 - \frac{c^2}{c_2^2}\right)^{1/2}. \tag{1.10}$$

The frequency equation (1.8) is fulfilled by a series of dispersion curves of phase velocity c. The velocity c of stress-wave propagation depends upon the ratio of plate thickness h to wavelength Λ. The variation of the first three branches of phase velocity versus the ratio h/Λ is shown in Fig. 1.7.

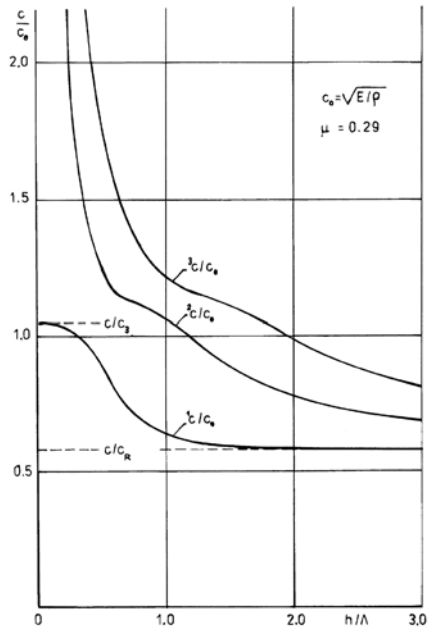

Fig. 1.7. Dispersion curves of phase velocity for symmetrical stress waves in a plate.

The first, fundamental branch of phase velocity begins from the value of velocity in the two-dimensional medium, c_3, by a large wavelength Λ according to the relationship

$$c_3 = \left(\frac{E}{\varrho(1-\mu^2)}\right)^{1/2}. \tag{1.11}$$

Succesively with the shortening of the wavelength the phase velocity c becomes smaller, and at very short values Λ is approaching the value of the surface-wave velocity, c_R.

The dispersion of flexural waves is determined by the frequency equation in the form

$$\frac{\tanh(qh/2)}{\tanh(sh/2)} = \frac{4\pi^2h^2/\Lambda^2(qh/2)(sh/2)}{\left[\pi^2h^2/\Lambda^2 + (sh/2)^2\right]^2}. \tag{1.12}$$

The curves for the first three branches of phase velocity c are drawn in Fig. 1.8. The fundamental curve of the phase velocity starts at zero for $h/\Lambda \to 0$. The phase velocity increases with increasing h/Λ, and are approaching the value c_R at very short values of Λ or as $h/\Lambda \to \infty$.

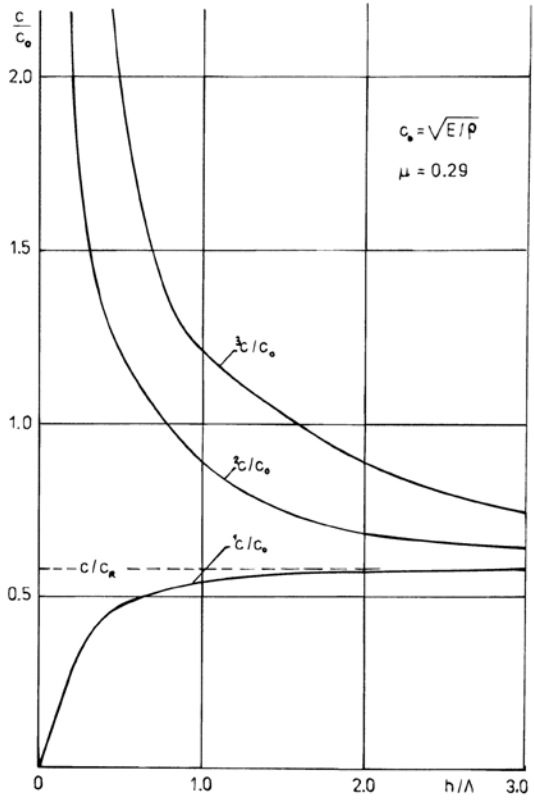

Fig. 1.8. Dispersion curves of phase velocity for asymmetrical stress waves in a plate.

The fundamental dispersion curve of the phase velocity for flexural waves in a plate is decisive for application to pavement structures.

Based on the results of detailed measurements of phase velocity in concrete and asphalt pavements it has been proved that the phase velocity corresponds to the characteristic course of this fundamental dispersion curve. Naturally, the pavement structure is in contact with the subgrade and so the problem arises of how this contact influences the variation of the dispersion curve. Because of the difficult numerical solution of this problem, the influence of the subgrade was investigated experimentally on two-dimensional models and in a state of plane stress. The results of experiments on Duralumin models of various widths l in contact with an acrylic plane medium are plotted in Fig. 1.9. The variations of the dispersion curves of phase velocity for the first two branches of symmetrical waves (A_1, A_2) and the first two branches of

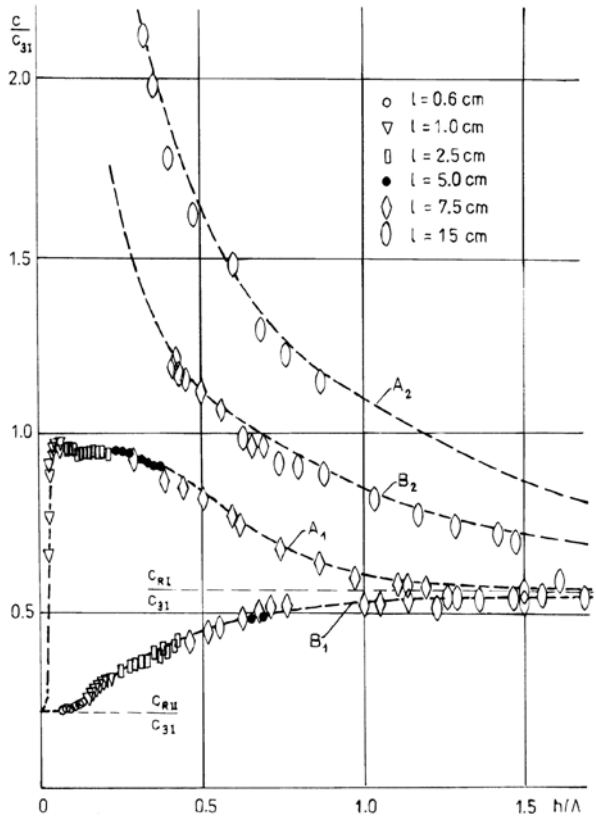

Fig. 1.9. Results of experiments on Duralumin models of various width l in contact with an acrylic plane medium.

asymmetrical waves (B_1, B_2) are identical to the theoretical courses for stress wave propagation in two-dimensional models with free boundaries for the values $l/\Lambda>0.10–0.15$ In the range of ratios $l/\Lambda<0.10–0.15$ the courses of the experimental dispersion curves are different; the

fundamental dispersion curves (A_1, B_1) are approaching the value of Rayleigh waves c_{RII} of the acrylic medium.

These results clearly prove that the fundamental dispersion curves for a plate with free surfaces may also be used for a plate on a subgrade for $h/\Lambda>0.15$. At lower frequencies (that is at larger wavelength) the influence of the subgrade manifests itself in a marked change of the curves and the phase velocities approach the velocity of surface waves in the subgrade medium.

Because of the basic importance of the fundamental dispersion curve for flexural waves in a plate for the dynamic diagnosis of pavement structures, it is helpful to present the possibility of its calculation in an elementary way. We have established according to the theory of flexural vibration of the plate, considering the influence of shear and rotational inertia [1.14], relationships that give results identical to the values gained by the numerical solution of the transcendent equation (1.12).

The phase velocity c of the fundamental dispersion curve for flexural stress waves in the plate is given by the relationship

$$(c/c_0)^2 = p - \sqrt{p^2 - q} \tag{1.13}$$

where

$$p = \varphi_1(\mu) + \frac{\Lambda^2}{h^2}\varphi_2(\mu) \tag{1.14}$$

if

$$\varphi_1(\mu) = \frac{1}{2(1-\mu^2)} + \frac{\kappa_0}{4(1+\mu)} \tag{1.15}$$

$$\varphi_2(\mu) = \frac{3\kappa_0}{4\pi^2(1+\mu)} \tag{1.16}$$

$$\kappa_0 = \left(\frac{0.87 + 1.12\mu}{1+\mu}\right)^2 \tag{1.17}$$

and

$$q = \frac{\kappa_0}{2(1-\mu^2)(1+\mu)}$$

$$c_0 = \left(\frac{E}{\varrho}\right)^{1/2}. \tag{1.18}$$

Table 1.2 lists the values of the ratio c/c_0 as related to the ratios h/Λ and Poisson's ratio. The ratio $c/c_0=0$ for $h/\Lambda=0$ and for $h/\Lambda\to\infty$ c/c_0 is given by

$$\frac{c}{c_0} = \left(\frac{\kappa_0}{2(1+\mu)}\right)^{1/2}. \tag{1.19}$$

Table 1.2. Values of the fundamental dispersion curve of flexural waves in the plate versus h/Λ. and Poisson's ratio μ.

	h/Λ	0.1	0.2	0.3	0.4	0.6	0.8	1.0	1.5	2.0	3.0
$\frac{c}{c_0}$	μ=0	0.197	0.314	0.390	0.455	0.511	0.548	0.565	0.590	0.598	0.603
	μ=0.1	0.192	0.313	0.389	0.448	0.509	0.541	0.560	0.580	0.592	0.596
	μ=0.2	0.188	0.308	0.387	0.443	0.501	0.535	0.550	0.572	0.579	0.585
	μ=0.3	0.185	0.307	0.381	0.438	0.499	0.528	0.545	0.560	0.566	0.571
	μ=0.4	0.182	0.306	0.368	0.433	0.496	0.524	0.540	0.557	0.562	0.567
	μ=0.5	0.179	0.298	0.355	0.428	0.494	0.518	0.528	0.537	0.542	0.545

Shear stress waves in a layer on subgrade

Shear stress waves in a layer on subgrade with thickness h and with the polarization of the particles in motion in a horizontal plane are characterized by the frequency equation

$$G_{\mathrm{I}} d_{\mathrm{I}} \sin d_{\mathrm{I}} h - G_{\mathrm{II}} d_{\mathrm{II}} \cos d_{\mathrm{I}} h = 0 \tag{1.20}$$

where

$$d_{\mathrm{I}} = f_0 \left(\frac{c^2}{c_{2\mathrm{I}}^2} - 1\right)^{1/2} \tag{1.21}$$

$$d_{\mathrm{II}} = f_0 \left(1 - \frac{c^2}{c_{2\mathrm{II}}^2}\right)^{1/2}. \tag{1.22}$$

G_{I} is the shear modulus of elasticity for the layer medium, G_{II} is the shear modulus of the subgrade material, f_0 is the wave number, and $c_{2\mathrm{I}}$, $c_{2\mathrm{II}}$ are the velocities of shear waves in an unbounded medium of the layer or subgrade, given by

$$c_{2\mathrm{I}} = \left(\frac{G_{\mathrm{I}}}{\varrho_{\mathrm{I}}}\right)^{1/2}, \qquad c_{2\mathrm{II}} = \left(\frac{G_{\mathrm{II}}}{\varrho_{\mathrm{II}}}\right)^{1/2}. \tag{1.23}$$

A real solution of the frequency equation (1.20) exists if $c_{2\mathrm{I}} < c_{2\mathrm{II}}$, and in such a case Love's waves propagate at the surface of the system. The variations of the first three dispersion curves are plotted in Fig. 1.10 for $c_{2\mathrm{II}}/c_{2\mathrm{I}}$=2.437. It can be seen that the phase velocities of stress-wave propagation are approaching to the velocity of shear waves in the layer, as h/Λ increases.

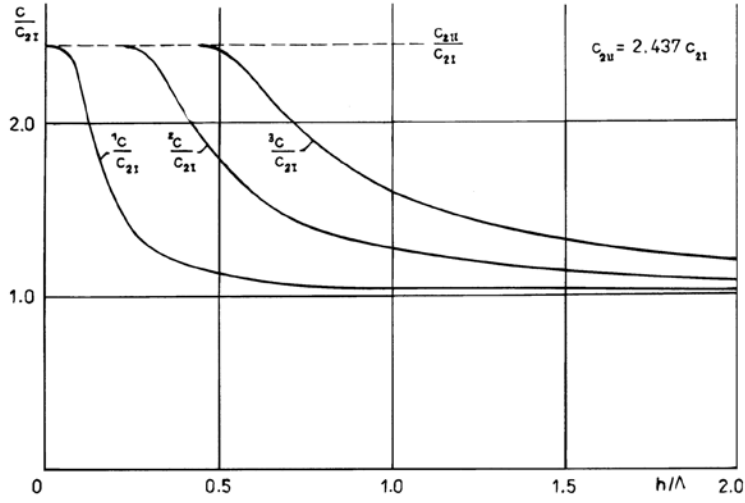

Fig. 1.10. Dispersion curves of Love's stress-wavevelocities in a layer on subgrade.

The other case is more important for pavement structures, when the plate or layer medium is stiffer than the subgrade medium. Then only a complex solution can be established, as

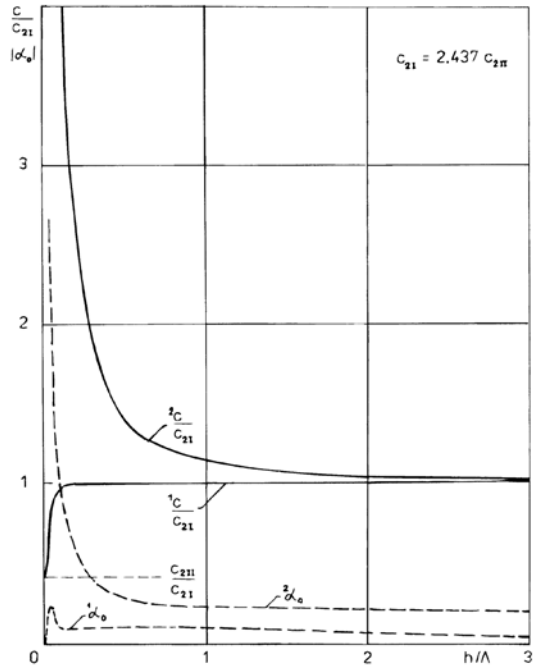

Fig. 1.11. Dispersion curves of shear stress waves in a layer on subgrade.

the energy dispersion in the subgrade has to be included. The numerical solution of the frequency equation (1.20) indicates that the results are very similar to the results for the plate or layer with free surfaces. The contact with the subgrade manifests itself as energy dispersion in the subgrade, but the influence on the velocities is visible only at the lowest frequencies for the ratios $h/\Lambda<0.1$, when the phase velocities are approaching the velocity of shear waves in the subgrade [1.19, 1.20].

The first two dispersion curves for phase velocity c and dispersion coefficient α_0 are plotted in Fig. 1.11.

The problems of stress-wave propagation described above are only typical basic tasks, which can help in the understanding of wave dispersion and propagation in connection with the application of the method of phase velocities to pavement structures.

Of course, pavement structures are complicated multilayered systems on subgrade. The analysis of stress-wave propagation in such systems and numerical solutions are difficult. The other aspect of the behaviour of real pavement structures is the viscoelasticity of the material, especially in bitumen layers, cohesive soil layers and in the subgrade. These characteristics and the non-homogeneity of the materials, influence the results obtained by the assumption that the pavement layers and subgrade are elastic, isotropic and homogeneous media.

1.2 Mechanical impedance methods

The generally known resonance method belongs to the category of dynamic non-destructive methods. It presents a system of procedures for the determination of the modulus of elasticity of materials on the basis of measured natural frequencies of specimens or elements in various geometrical forms. Usually the fundamental natural frequencies are measured, which serve in the calculation of the elasticity characteristics using the corresponding theoretical relationships of vibration theory. It is possible to assess the logarithmic decrement of vibration as a damping characteristic after the width of the resonance curve.

These procedures can be applied without difficulty on concrete, ceramic and similar materials, but they fail when used for testing materials with distinct viscoelastic behaviour such as the bituminous materials of road construction or cohesive soil material. The considerable damping of such materials causes the resonance zone to weaken, and it may be suppressed to a such extent that the measurement cannot be realized.

The testing of viscoelastic materials on the principle of the forced vibration of specimens is possible by another way, using mechanical impedance methods.

1.2.1 Complex modulus of elasticity

The typical property of the viscoelastic behaviour of materials is the dependence of their elastic and damping characteristics on temperature and loading time with respect to the frequency of the dynamic loading process.

The analysis of the dynamic response of structures made from viscoelastic materials, the theory of design and quality control require the assessment of their viscoelastic properties over a large range of temperatures and frequencies.

There are various formulations of viscoelastic behaviour in linear viscoelasticity, but the conception of complex modulus is the most useful [1.21–1.23]. Provided that the sinusoidal variable stress acts upon the element from the linear viscoelastic material, then the deformation of the element alters in time with the same frequency but a phase in arrears.

If the stress σ is expressed by the relationship

$$\sigma = \sigma_0 e^{i\omega t} \tag{1.24}$$

where σ_0 is the stress amplitude and ω is the angular frequency, then the strain ε is given in the form

$$\varepsilon = \varepsilon_0 e^{i(\omega t - \varphi)} \tag{1.25}$$

where φ is the phase angle.

The complex modulus of elasticity E^* established according to the relationships (1.24) and (1.25) is expressed by the equation

$$E^* = E_1 + iE_2 = \frac{\sigma}{\varepsilon} = \frac{\sigma_0}{\varepsilon_0} e^{i\varphi} \tag{1.26}$$

The real part of the complex modulus, E_1, is given by

$$E_1 = \frac{\sigma_0}{\varepsilon_0} \cos\varphi \tag{1.27}$$

and the imaginary part, E_2, is given by

$$E_2 = \frac{\sigma_0}{\varepsilon_0} \sin\varphi. \tag{1.28}$$

The absolute value of the complex modulus of elasticity is the ratio of stress and strain amplitudes expressed by the relationship

$$|E^*| = \frac{\sigma_0}{\varepsilon_0} = (E_1^2 + E_2^2)^{1/2}. \tag{1.29}$$

If the ratio of the imaginary and real parts of the complex modulus is indicated by the damping factor δ_E according to the relationship

$$\delta_E = \tan\varphi = \frac{E_2}{E_1} \tag{1.30}$$

the complex modulus of elasticity is given in the form

$$E^*_{\omega,T} = E_{\omega,T}(1 + \mathrm{i}\delta_{\mathrm{E}}) \tag{1.31}$$

and its absolute value is

$$|E^*_{\omega,T}| = E_{\omega,T}(1 + \delta^2_{\mathrm{E}})^{1/2}. \tag{1.32}$$

The subscripts ω and T refer to the value of complex modulus at a given frequency ω and temperature T. The coherence of the damping factor δ_{E} and the logarithmic decrement ϑ is determined by the approximate expression

$$\vartheta \approx \pi\delta_{\mathrm{E}}. \tag{1.33}$$

The viscoelastic behaviour of a material for a given temperature is fully defined by the assessment of the values δ_{E} and $|E^*|$ for all frequencies.

The complex shear modulus or complex bulk modulus can be expressed in a similar way.

1.2.2 Function of mechanical impedance

The mechanical impedance at the driving point of the harmonic vibrating system is defined as the ratio of the exciting force to the velocity of motion at this point. It is the so-called mechanical impedance of the driving point and is a complex function.

If the motion velocity is related to another point, the complex ratio of the driving force and the motion velocity determines the so-called mechanical transfer impedance.

The inverse value of the mechanical impedance determines the mechanical mobility.

From the point of view of contemporary measurement techniques it is more advantageous to assess a normalized mechanical impedance Z^*, which is defined [1.22] as the ratio of the harmonic variable force $\tilde{F}$ to the product of acceleration $\tilde{a}$ at the driving point of the vibrating object and the object mass M

$$Z^* = \frac{\tilde{F}}{\tilde{a}M} \tag{1.34}$$

Z^* is a dimensionless complex function, the behaviour of which depends on the shape and dimensions of the vibrating object, and on the kind of vibration, and the elasticity and viscosity of the object material.

Mechanical impedance by flexural vibration

By using the flexural forced vibration of a tested object the most advantageous scheme in practice is the flexural vibration of a cantilever element at the free end of which a harmonic force $\tilde{F}$ is acting, or a test specimen with free ends and the exciting force $\tilde{F}$ in the middle of the specimen length. (Fig. 1.12).

The cantilever testing element is satisfactory for bituminous pavement materials with appreciable damping. Normalized prismatic elements with dimensions 5×5×30 cm or cylindrical elements may be used.

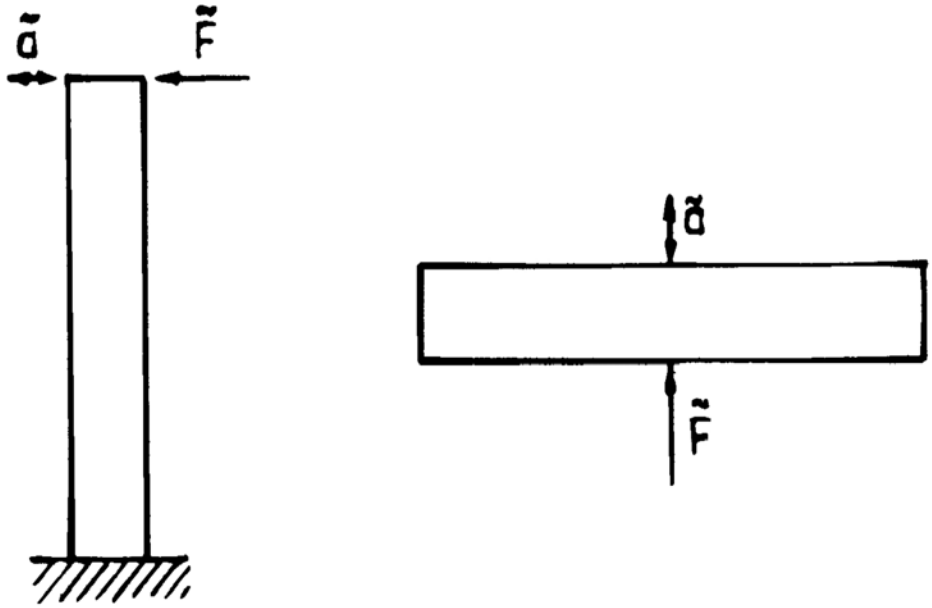

Fig. 1.12. Schematic diagram of mechanical impedance methods using flexural vibration of elements.

Many studies [1.24–1.29] have been performed in which the characteristics of the complex modulus of elasticity are determined after various schemes of element vibration, in which the amplitudes of force and deformation or deflection and the phase angle of the vibration process of these quantities are measured. All these procedures, theoretically often reduced in the system with one degree of freedom, have a common feature in that they can be applied only for very low frequencies below the fundamental natural frequency of the test element. Our effort is to prepare methods and procedures for the assessment of viscoelastic characteristics that would give the possibility of evaluating viscoelastic parameters in a wide frequency range by using just the resonance and antiresonance frequencies of the tested element [1.30–1.35].

The normalized mechanical impedance for a cantilever element in flexural vibration without the influence of shear and rotational inertia is given by the relationship [1.14]

$$Z^* = \frac{1 + \cosh n^* l \cos n^* l}{n^* l(\cos n^* l \cosh n^* l - \sin n^* l \sinh n^* l)} \tag{1.35}$$

where

$$n^*l = \left(\frac{\omega^2 l^4 \varrho}{E_\omega^* r^2}\right)^{1/4} = \frac{nl}{(1+\mathrm{i}\delta_E)^{1/4}} \tag{1.36}$$

if l is the length of the cantilever element, r is the radius of inertia of the cross section to the axis perpendicular to the vibration plane and

$$nl = \left(\frac{\omega^2 l^4 \varrho}{E_\omega r^2}\right)^{1/4}. \tag{1.37}$$

For use in practice it is preferable to establish the normalized mechanical impedance according Timoshenko's more accurate differential frequency of motion [1.36].

The variations of the calculated absolute value of normalized mechanical impedance in dB depending on the frequency parameter nl for the values of damping factor δ=0.05 and δ=0.5 are plotted in Fig. 1.13 The normalized mechanical impedance presents minima and maxima. The minima of the function 20 log $|Z^*|$, i.e. R_1, R_2, R_3,…represent resonances and correspond to the natural frequencies of an element that is clamped at the bottom and free at the top. The maxima A_1, A_2, A_3,… represent anti-resonances and correspond to the natural frequencies of an element that is clamped and simply supported at the top. It can be seen that the differences of resonance and anti-resonance extrema are a function of the damping factor δ.

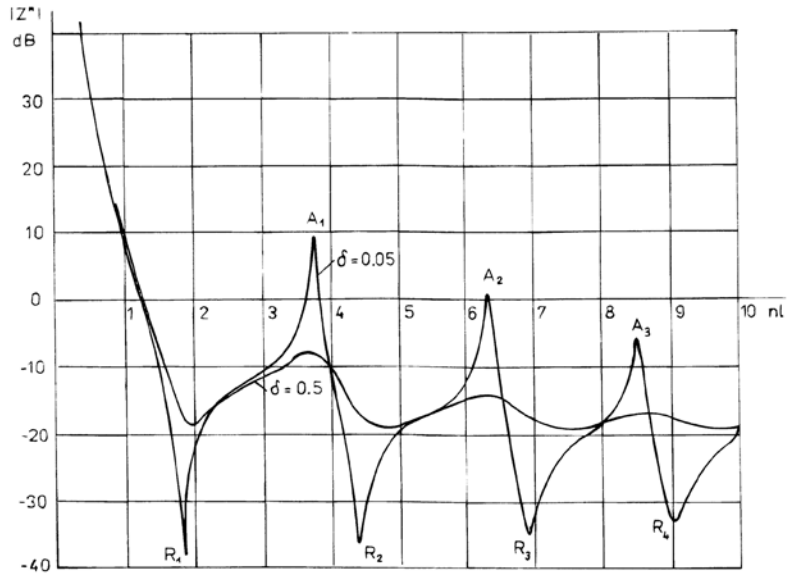

Fig. 1.13. Theoretical curves of mechanical impedance function $|Z^*|$ versus frequency parameter nl.

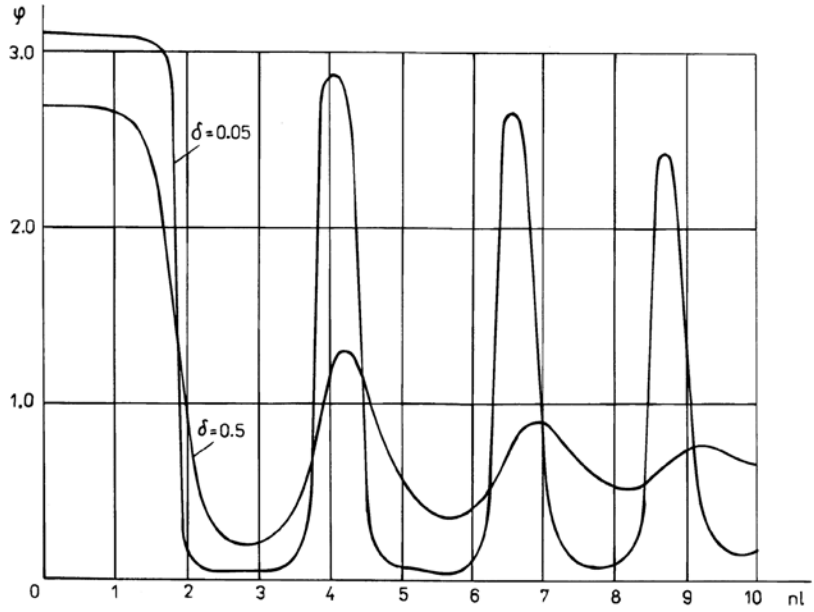

Fig. 1.14. Curves of phase angle φ versus frequency parameter *nl.*

The variations of phase angle φ depending on the frequency parameter *nl* in Fig. 1.14 present intense changes at the zone of resonance and anti-resonance frequencies. The phase angles and their differences depend on the damping factor δ.

The function of normalized mechanical impedance Z^* in the case of a flexural vibrating testing element (prismatic, cylindrical) with free ends, excited in the middle of its length, is given by the relationship [1.14]

$$Z^* = \frac{1}{n^* l} \frac{\sinh n^* l \cos n^* l + \cosh n^* l \sin n^* l}{(1 + \cosh n^* l \cos n^* l)} \tag{1.38}$$

where l is half the element length. Equation (1.38) is valid for the elementary theory without the influence of shear and rotational inertia.

By the same procedure as for a cantilever element the variations of the functions $|Z^*|(nl)$ and $\varphi(nl)$ can be prepared.

Mechanical impedance by the longitudinal and torsional vibration of elements with a constant cross-section

The longitudinal and torsional vibration of a prismatic or cylindrical element with a constant cross-section is described by a similar differential equation of motion [1.14]. Provided that the harmonic variable force or torsional moment is acting at one end of the element and the second end is free, the normalized mechanical impedance Z^* may be established in the form

$$Z^* = \frac{1}{n^* l} \tan n^* l \tag{1.39}$$

if for forced longitudinal vibration

$$n^* l = \left[\frac{\omega^2 \varrho l^2}{E_\omega (1 + \mathrm{i}\delta_\mathrm{E})} \right]^{1/2} \tag{1.40}$$

and for torsional vibration

$$n^* l = \left[\frac{\omega^2 \varrho l^2 J_\mathrm{p}}{G_\omega (1 + \mathrm{i}\delta_\mathrm{G}) J_\mathrm{t}} \right]^{1/2} \tag{1.41}$$

In equations (1.40) and (1.41) l is the length of the test element, J_p is a polar moment of inertia in the element cross-section, J_t is a modulus of stiffness in torsion (for a prismatic element with square cross-section $J_\mathrm{p}/J_\mathrm{t}$=1.183, for a circular cylindrical element $J_\mathrm{p}/J_\mathrm{t}$=1.0), and $G_\omega(1+\mathrm{i}\delta_\mathrm{G})$ is a complex modulus of clasticity in shear.

The normalized mechanical impedance (1.39) is a complex function. Its absolute value and phase angle may be expressed depending on the frequency parameter *nl,* which has the form

$$nl = \left(\frac{\omega^2 \varrho l^2}{E_\omega} \right)^{1/2} \tag{1.42}$$

for longitudinal vibration and

$$nl = \left(\frac{\omega^2 \varrho l^2}{G_\omega} \frac{J_\mathrm{p}}{J_\mathrm{t}} \right)^{1/2} \tag{1.43}$$

for torsional vibration.

The function $|Z^*|$ depending on the parameter *nl* forms the anti-resonance and resonance extrema. The resonance minima correspond to the natural frequencies of an element with free ends and the anti-resonance maxima correspond to the natural frequencies of an element that is free at one end and clamped at the other end. The differences of the extrema of the function $|Z^*|$ in dB depend on the damping parameter of the element material.

1.2.3 Measurement method

The anti-resonance and resonance frequencies and the differences ΔZ^* of the extrema can be obtained from the measured variations of the mechanical impedance function $|Z^*|$. In practice the realization of the measurement of $|Z^*|$ is obtained by observation or recording of the variation of an exciting force or torsional moment depending on the frequency for constant amplitude of acceleration at the driving point.

Table 1.3. Frequency parameter nl and differences $\Delta|Z^*|$ of mechanical impedance function extrema depending on damping parameter δ for cantilever element.

δ	nl							$\Delta\|Z^*\|$ (dB)					
	R_1	A_1	R_2	A_2	R_3	A_3	R_4	R_1-A_1	A_1-R_2	R_2-A_2	A_2-R_3	R_3-A_3	A_3-R_4
0.05	1.86	3.74	4.40	6.30	6.90	8.49	9.01	47.12	45.88	37.12	35.75	29.56	27.98
0.10	1.86	3.73	4.41	6.30	6.94	8.47	9.07	35.23	34.08	25.35	24.32	18.52	17.22
0.12	1.86	3.73	4.42	6.29	6.95	8.47	9.10	32.15	31.05	22.60	21.47	15.86	14.68
0.14	1.86	3.73	4.43	6.29	6.97	8.46	9.13	29.57	28.35	20.20	19.16	13.74	12.67
0.16	1.87	3.73	4.45	6.29	7.00	8.46	9.17	27.37	26.38	18.18	17.23	11.99	11.03
0.18	1.87	3.73	4.46	6.29	7.02	8.46	9.20	25.45	24.53	16.45	15.59	10.54	9.67
0.20	1.87	3.73	4.47	6.28	7.05	8.46	9.23	23.76	22.91	14.96	14.19	9.31	8.52
0.25	1.88	3.73	4.51	6.28	7.12	8.47	9.32	20.26	19.61	11.98	11.42	6.96	6.35
0.30	1.89	3.72	4.56	6.29	7.20	8.50	9.40	17.53	17.09	9.77	9.39	5.30	4.82
0.35	1.91	3.72	4.61	6.30	7.28	8.53	9.48	15.32	15.10	8.07	7.83	4.09	3.72
0.40	1.92	3.72	4.66	6.32	7.36	8.57	9.56	13.51	13.49	6.72	6.62	3.19	2.91
0.45	1.94	3.73	4.72	6.34	7.44	8.62	9.65	11.98	12.17	5.64	5.65	2.51	2.30
0.50	1.96	3.73	4.78	6.36	7.52	8.67	9.73	10.68	11.08	4.78	4.88	1.99	1.83
0.60	2.00	3.74	4.91	6.43	7.68	8.80	9.91	8.61	9.38	3.45	3.71	1.27	1.21
0.70	2.04	3.76	5.03	6.51	7.86	8.94	–	7.05	8.14	2.54	2.91	0.82	–
0.80	2.09	3.77	5.16	6.59	8.04	9.10	–	5.82	7.20	1.88	2.35	0.54	–
0.90	2.14	3.79	5.26	6.68	8.23	9.26	–	4.86	6.50	1.40	1.95	0.36	–
1.00	2.19	3.82	5.43	6.76	8.43	9.42	–	4.09	5.94	1.04	1.65	0.24	–

On the basis of the determined resonance and anti-resonance frequencies the real parts of moduli E_ω or G_ω can be calculated.

For longitudinal vibration of the test sample the relationship is valid in the form

$$E_\omega = \frac{16 l^2 f_l^2 \varrho}{k^2} \tag{1.44}$$

where f_l is the frequency of the extreme and k=1, 2, 3…for f_l corresponding sucsessively to the extrema A_1, R_1, A_2, R_2,…

For torsional vibration the real part of the complex modulus G_ω is expressed by the relationship

$$G_\omega = \frac{16 l^2 f_t^2}{k^2} \frac{J_p}{J_t} \tag{1.45}$$

in which f_t is the frequency of the extreme and k=1, 2, 3…for f_t corresponding to the extrema A_1, R_1, A_2, R_2,…

For schemes of flexural vibration of the element the equation is valid in the form

$$E_\omega = \frac{\omega^2 l^4 \varrho}{(nl)^4 r^2} \tag{1.46}$$

where ω is the angular frequency of the resonance or anti-resonance extrema, l is the length of the tested cantilever specimen, or half the element length for a specimen with free ends.

Table 1.3 lists the values of the frequency parameter nl in equation (1.46) for the corresponding extreme frequencies depending on damping parameter δ for a cantilever prismatic element with dimension ratios 1:1:6 or for a cylindrical element with the ratio of diameter d and l equal to 0.193. Table 1.4 lists the values of nl for elements with free ends excited in the middle of their length.

The differences of extreme values of normalized mechanical impedance $\Delta|Z^*|$ in dB, obtained by measurement, give the possibility of evaluating the damping parameter δ_E or δ_G. The theoretical values of $\Delta|Z^*|$ for longitudinal and torsional vibration are plotted in Figs. 1.15 and 1.16, for flexural vibration of the cantilever specimen in Table 1.3 and for flexural vibration of an element with free ends in Table 1.5.

Table 1.4. Frequency parameter nl of mechanical impedance function extrema for element with free ends.

δ	Frequency parameter nl									
	A_1	R_1	A_2	R_2	A_3	R_3	A_4	R_4	A_5	R_5
0.025	1.8749	2.3656	4.6933	5.5000	7.8525	8.6432	10.991	11.788	14.130	14.925
0.050	1.8744	2.3674	4.6911	5.5043	7.8459	8.6541	10.978	11.806	14.109	14.950
0.075	1.8734	2.3704	4.6875	5.5128	7.8355	8.6717	10.959	11.836	14.081	15.000

0.100	1.8722	2.3745	4.6826	5.5240	7.8225	8.6949	10.937	11.873	14.048	15.050
0.125	1.8706	2.3797	4.6765	5.5385	7.8038	8.7248	10.912	11.914	14.016	15.100
0.150	1.8687	2.3860	4.6696	5.5553	7.7909	8.7547	10.887	11.960	13.986	15.150
0.175	1.8666	2.3933	4.6619	5.5748	7.7740	8.7898	10.864	12.009	13.960	15.150
0.200	1.8642	2.4017	4.6539	5.5961	7.7562	8.8312	10.843	12.058	13.938	15.300
0.225	1.8616	2.4108	4.6448	5.6199	7.7414	8.8668	10.824	12.108	13.921	15.350
0.250	1.8589	2.4209	4.6358	5.6449	7.7262	8.9074	10.808	12.158	13.909	15.400

δ	Frequency parameter *nl*									
	A_6	R_6	A_7	R_7	A_8	R_8	A_9	R_9	A_{10}	R_{10}
0.025	17.250	18.100	20.405	21.225	23.542	24.369	26.678	27.519	29.814	30.667
0.050	17.250	18.100	20.367	21.275	23.493	24.432	26.620	27.591	29.745	30.751
0.075	17.200	18.150	20.300	21.350	23.450	24.500	26.550	27.700	29.700	30.850
0.100	17.150	18.250	20.271	21.412	23.385	24.591	26.502	27.766	29.621	30.934
0.125	17.100	18.300	20.230	21.483	23.345	24.666	26.463	27.837	29.585	31.017
0.150	17.100	18.300	20.199	21.552	23.315	24.741	26.434	27.920	29.559	31.098
0.175	17.050	18.400	20.176	21.620	23.295	24.809	26.420	27.998	29.545	31.184
0.200	17.050	18.500	20.159	21.691	23.283	24.891	26.408	28.084	29.534	31.284
0.225	17.050	18.500	20.149	21.776	23.273	24.969	26.398	28.184	29.516	31.403
0.250	17.000	18.600	20.142	21.841	23.266	25.066	26.384	28.303	29.491	31.562

δ	Frequency parameter *nl*									
	A_{11}	R_{11}	A_{12}	R_{12}	A_{13}	R_{13}	A_{14}	R_{14}	A_{15}	R_{15}
0.025	32.949	33.800	36.100	36.950	39.200	40.100	42.350	43.250	45.500	46.400
0.050	32.871	33.900	36.000	37.050	39.100	40.250	42.250	43.400	45.400	46.550
0.075	32.800	34.000	35.900	37.200	39.050	40.350	42.150	43.500	45.300	46.650
0.100	32.737	34.100	35.850	37.250	39.000	40.450	42.100	43.600	45.250	46.750
0.125	32.709	34.200	35.850	37.350	38.950	40.550	42.100	43.700	45.250	46.850
0.150	32.691	34.300	35.800	37.450	38.950	40.600	42.100	43.800	45.200	46.950
0.175	32.677	34.350	35.800	37.550	38.950	40.750	42.050	43.950	45.150	47.150
0.200	32.659	34.500	35.750	37.700	38.900	40.900	41.950	44.150	45.050	47.450
0.225	32.631	34.600	35.700	37.900	38.800	41.150	–	–	–	–
0.250	32.569	34.850	–	–	–	–	–	–	–	–

Table 1.5. Differences of extreme values of normalized mechanical impedance Δ|Z*| versus damping parameter δ for flexural vibration of an element with free ends.

δ	Extremes differences Δ|Z*| *(dB)*							
	A_1-R_1	R_1-A_2	A_2-R_2	R_2-A_3	A_3-R_3	R_3-A_4	A_4-R_4	R_4-A_5
0.025	63.242	52.995	55.729	46.4747	46.3917	40.5907	40.6237	36.2939
0.050	51.250	41.022	43.776	34.5814	34.5574	28.8351	28.9471	24.7145
0.075	44.290	34.0927	36.8777	27.7743	27.8423	22.2342	22.4612	18.3590
0.100	39.408	29.2510	32.0770	23.0896	23.2746	17.7992	18.1602	14.1960
0.125	35.676	25.5685	28.4455	19.5898	19.9078	14.5700	15.0710	11.3550
0.150	32.682	22.6304	25.5644	16.8484	17.3084	12.1040	12.7430	9.0320
0.175	30.204	20.1841	23.2091	14.6347	15.2397	10.1610	10.9300	7.3270
0.200	28.108	18.1810	21.2440	12.8090	13.5570	8.5940	9.4840	5.9790
0.225	26.3074	16.4463	19.5763	11.2753	12.1633	7.3060	8.3060	4.8930
0.250	24.7414	14.9466	18.1466	9.9728	10.9938	6.2340	7.3420	4.0070
δ	Extremes differences Δ|Z*| *(dB)*							
	A_5-R_5	R_5-A_6	A_6-R_6	R_6-A_7	A_7-R_7	R_7-A_8	A_8-R_8	R_8-A_9
0.025	35.9604	32.6360	32.6750	29.9286	29.9836	27.551	27.667	25.491
0.050	24.8236	21.494	21.641	18.908	19.071	16.788	17.000	15.014
0.075	18.602	15.431	15.711	13.112	13.439	11.282	11.608	9.765
0.100	14.602	11.542	11.968	9.506	9.954	7.908	8.351	6.617
0.125	11.774	8.836	9.393	7.044	7.600	5.654	6.203	4.559
0.150	9.696	6.864	7.503	5.245	5.930	4.071	4.710	3.146
0.175	8.064	5.327	6.133	3.960	4.708	2.928	3.648	2.155
0.200	6.859	4.208	5.068	2.971	3.796	2.086	2.877	1.448
0.225	5.870	3.269	4.228	2.203	3.109	1.461	2.315	0.942
0.250	5.073	2.571	3.585	1.625	2.588	0.997	1.906	0.581
δ	Extremes differences Δ|Z*| *(dB)*							
	A_9-R_9	R_9-A_{10}	$A_{10}-R_{10}$	$R_{10}-A_{11}$	$A_{11}-R_{11}$	$R_{11}-A_{12}$	$A_{12}-R_{12}$	$R_{12}-A_{13}$
0.025	25.591	23.787	23.878	22.239	22.327	20.808	20.891	19.532
0.050	15.165	13.453	13.722	12.187	12.399	11.045	11.258	10.021
0.075	10.093	8.485	8.825	7.424	7.756	6.501	6.830	5.710
0.100	7.060	5.561	5.999	4.686	5.117	3.954	4.376	3.339
0.125	5.097	3.683	4.210	2.978	3.491	2.405	2.905	1.938
0.150	3.767	2.429	3.032	1.869	2.452	1.430	1.995	1.088
0.175	2.849	1.576	2.243	1.139	1.780	0.812	1.428	0.576
0.200	2.205	0.988	1.711	0.657	1.346	0.420	1.077	0.254
0.225	1.753	0.584	1.353	0.341	1.069	0.178	0.869	0.076
0.250	1.439	0.311	1.119	0.141	0.903	–	–	–

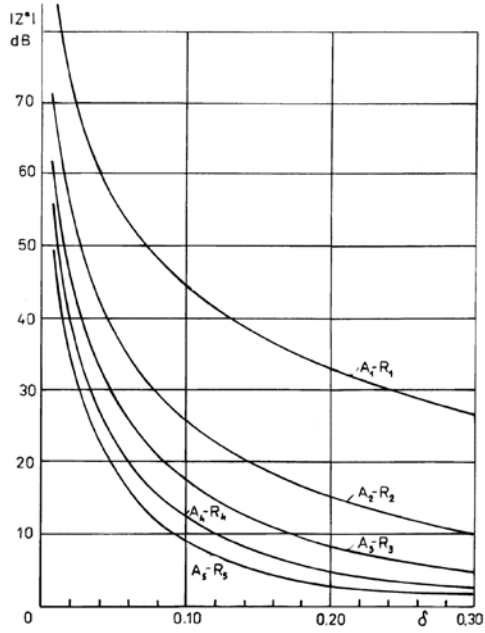

Fig. 1.15. Differences of mechanical impedance function extrema for longitudinal vibration of specimen.

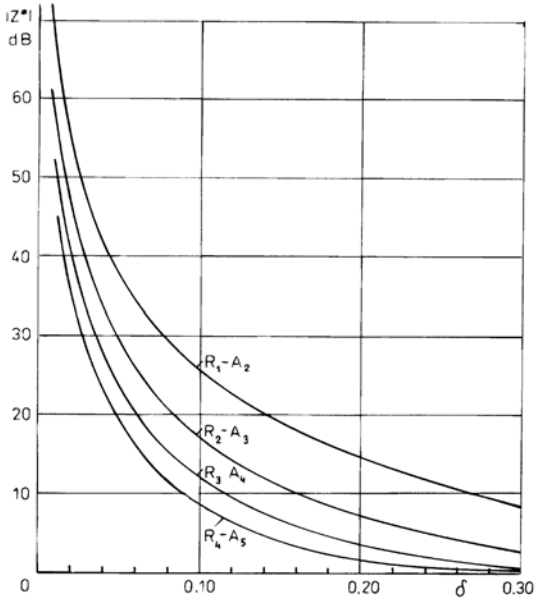

Fig. 1.16. Differences of mechanical impedance function extrema for torsional vibration of specimen.

1.2.4 Experimental apparatus

The experimental arrangement for using the mechanical impedance method is more complicated than that currently used for measuring of resonance frequencies. It is necessary to measure not only frequencies also the force or torsional moment and acceleration. It is usual to automate the measuring process: that is, to record continuously the values of the force amplitude or torsional moment amplitude by constant amplitude of acceleration in a wide frequency range.

The block diagram of the experimental arrangement realized by M.Pokorny, which has been used for application to cantilever samples and flexural vibration is shown in Fig. 1.17.

The sine-wave signal from an automatic generator leads to the power amplifier and electrodynamic vibrator. The vibration is transferred through the impedance head into the test specimen. The impedance head gives the possibility of measuring the amplitude of the force by using a preamplifier and voltmeter and recording the variation in the force amplitude with frequency.

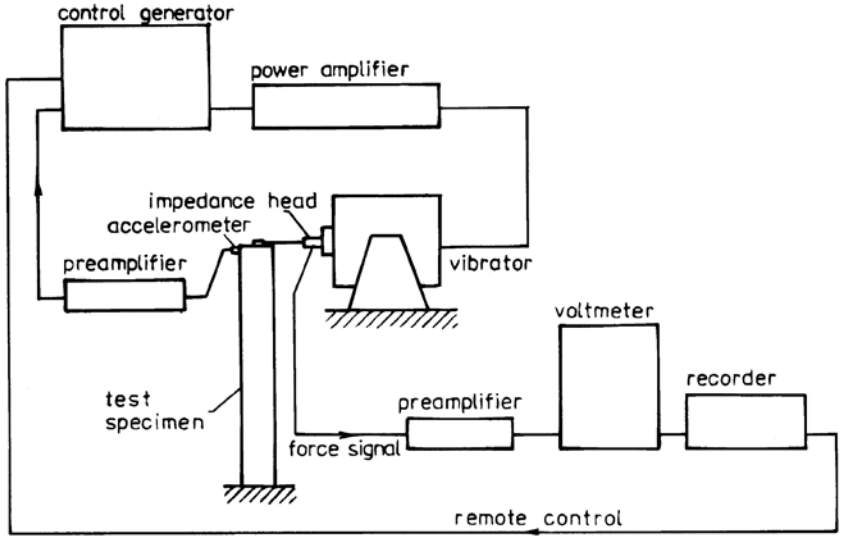

Fig. 1.17. Block diagram of experimental arrangement for mechanical impedance method.

The signal from the accelerometer leads through the preamplifier to the control generator and serves to regulate the specimen vibration in such a way that the amplitude of acceleration at the exciting point of the specimen is constant during the measuring process.

The block diagram of the arrangement and testing for the application of the mechanical impedance method to longitudinally and torsionally vibrated test samples is shown in Fig. 1.18. The test procedure and the composition of the instruments and transducers is similar to that in Fig. 1.17.

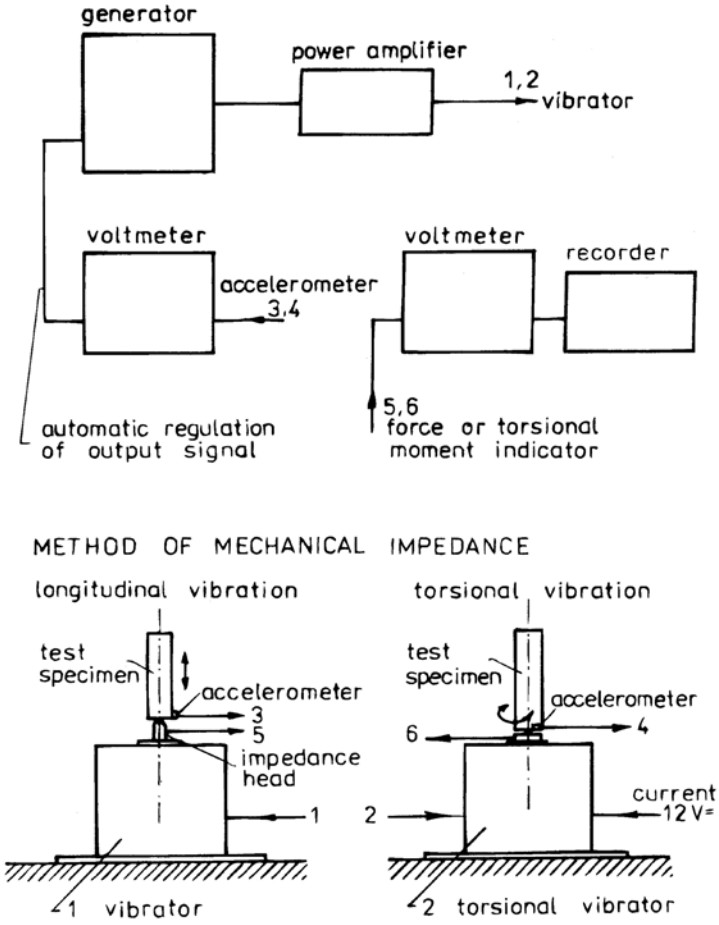

Fig. 1.18. Block diagram of arrangement and testing for application of mechanical impedance method to longitudinally and torsionally vibrated test samples.

The basic elements of the arrangement for torsional vibration are a torsional vibrator and a torsional moment meter, which have to be developed specially for this purpose. A detailed description of these elements is to be found in [1.37].

1.2.5 Application to non-destructive testing of the subgrade

The mechanical impedance method can be applied to dynamic testing of the material characteristics in the subgrade by using vibrators with a small generating energy of stationary vibration [1.38].

The scheme of testing that applies in practice is based on the vertical vibration of a thick circular plate with mass *m* situated on the surface of the subgrade through a circular contact

area with radius *a*. The vibration of the plate is excited by the harmonic variable vertical force of an electrodynamic vibrator, which is put trough a force-meter on the mass *m*.

The theoretical variation of the function *Z** of normalized mechanical impedance has been established in [1.14] by using the concepts of the complex bulk modulus $B^*_\omega = B_\omega(1 + i\delta_B)$ and the complex modulus in shear $G^*_\omega = G_\omega(1 + i\delta_G)$. The dependence of the function *Z** on the dimensionless frequency $\Omega = \omega a/c_2$ is given by the variation of the absolute value $|Z^*|$ and phase angle φ. The curves of $|Z^*|$ and φ versus Ω are plotted in Fig. 1.19 for damping parameters

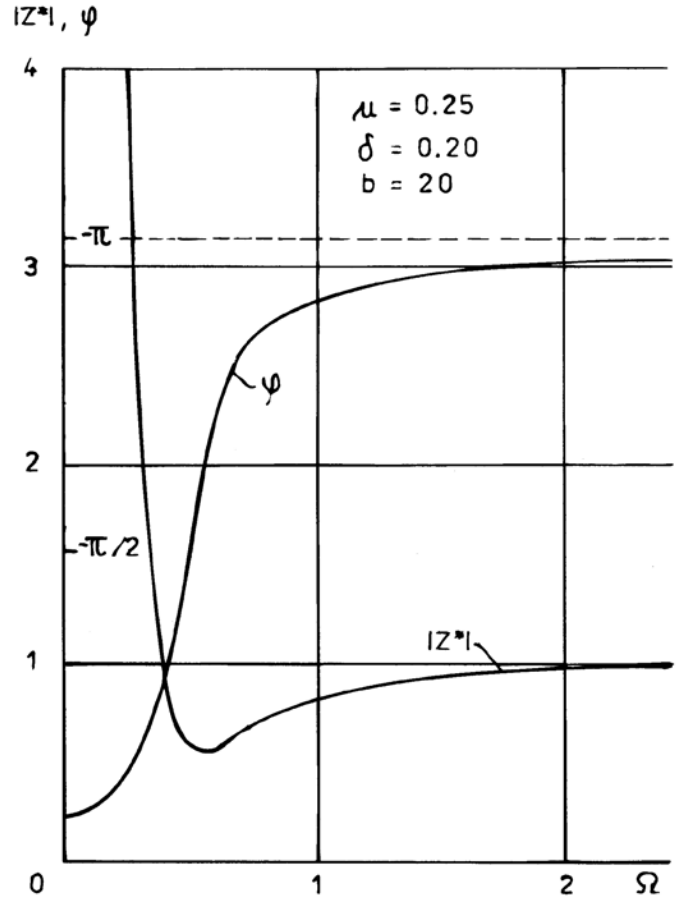

Fig. 1.19. Theoretical curves of mechanical impedance function $|Z^*|$ and phase angle φ versus frequency Ω for a vibrating mass on subgrade.

$\delta_B = \delta_G = \delta = 0.20$, Poisson's ratio $\mu = 0.25$ and for dimensionless parameter $b = m/\varrho a^3 = 20$. The phase angle φ approaches the value $\varphi = -\delta$ at low frequencies. The absolute value $|Z^*|$ has its minimum in the resonance zone of the vibrating mass on the subgrade.

The theoretical variation of $|Z^*|$ for various values of δ, $\mu = 0.35$ and parameter $b = 11$ suitable for the interpretation of experimental results are plotted in Fig. 1.20.

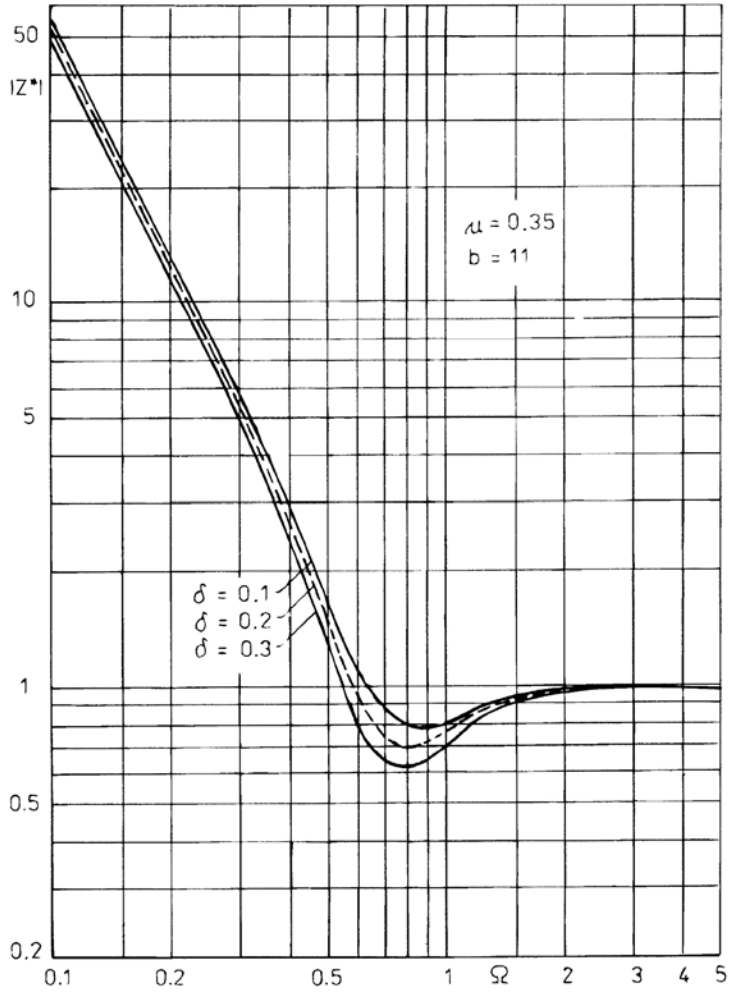

Fig. 1.20. Theoretical variations of $|Z^*|$ with frequency Ω for various values of damping factor δ.

The experimental testing arrangement can be realized according to the scheme shown in Fig. 1.21. The mass consists of a thick circular steel plate with radius a=126 mm and thickness h=100 mm. The contact circular area F=500 cm^2 and the mass m=39.5 kg. The parameter b of the system is approximately $b \approx 11$. In the middle of the mass at the centre of gravity, is situated the piezoelectric accelerometer. The force pick-up is piezoelectric too, produced specially for the purpose, with diameter 68 mm; it is fixed on the vibrating area of the electrodynamic vibrator. The vibrator is connected to the generator through the power amplifier and the signals from the force pick-up and from the accelerometer lead to the voltmeters.

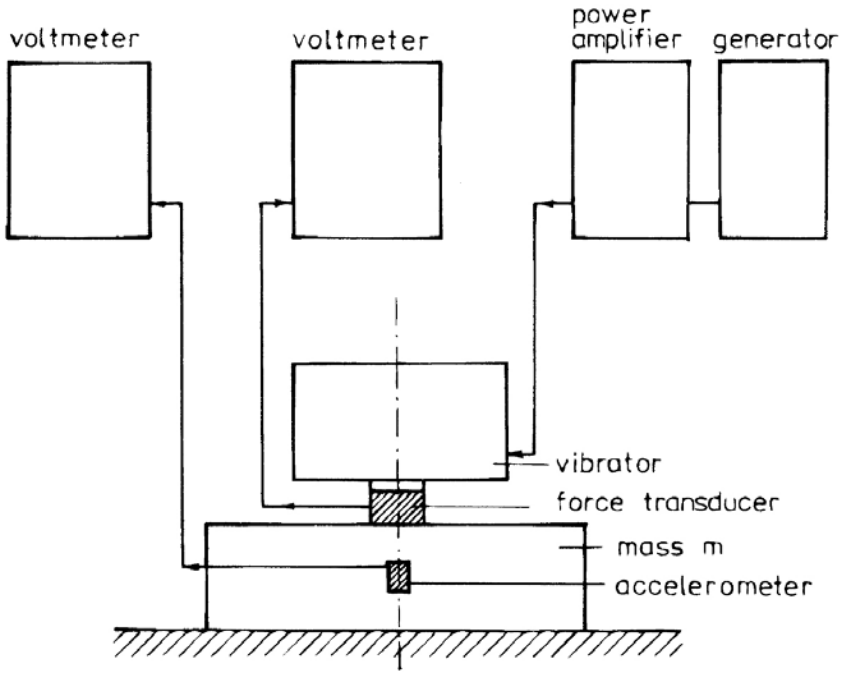

Fig. 1.21. Schematic diagram of testing arrangement for determination of subgrade charateristics by mechanical impedance method.

The testing takes place in such a way that for individual frequencies the amplitude of the force will be assessed by the constant amplitude of acceleration. The variation of the force with frequency is then proportional to the variation of the mechanical impedance function $|Z^*|$. The measurements can also be realized by a more complicated arrangement with an automatic record of the mechanical impedance function $|Z^*|$ in dB, as described for the application to testing elements.

The procedure for the evaluation of viscoelastic characteristics consists of the determination of damping parameter δ, complex modulus of elasticity in shear G_ω^* and Poisson's ratio μ.

The damping parameter δ of the subgrade material may be determined by using the special measurement of phase angle φ for the mechanical impedance function at very low frequencies, when $\varphi \approx -\delta$.

The value of Poisson's ratio μ is found from the extreme ordinate of measured function of mechanical impedance by using the theoretical variations in Fig. 1.22.

The real parts of the complex modulus G_ω are found from the measured variation of $|Z^*|$ by comparison with the theoretical curve.

If we are satisfied with the estimate of Poisson's ratio μ for subgrade material at an average value of μ=0.35, then the damping parameter δ can be assessed on the basis of the measured extreme value $|Z^*|_{\min}$ after the diagram in Fig. 1.22.

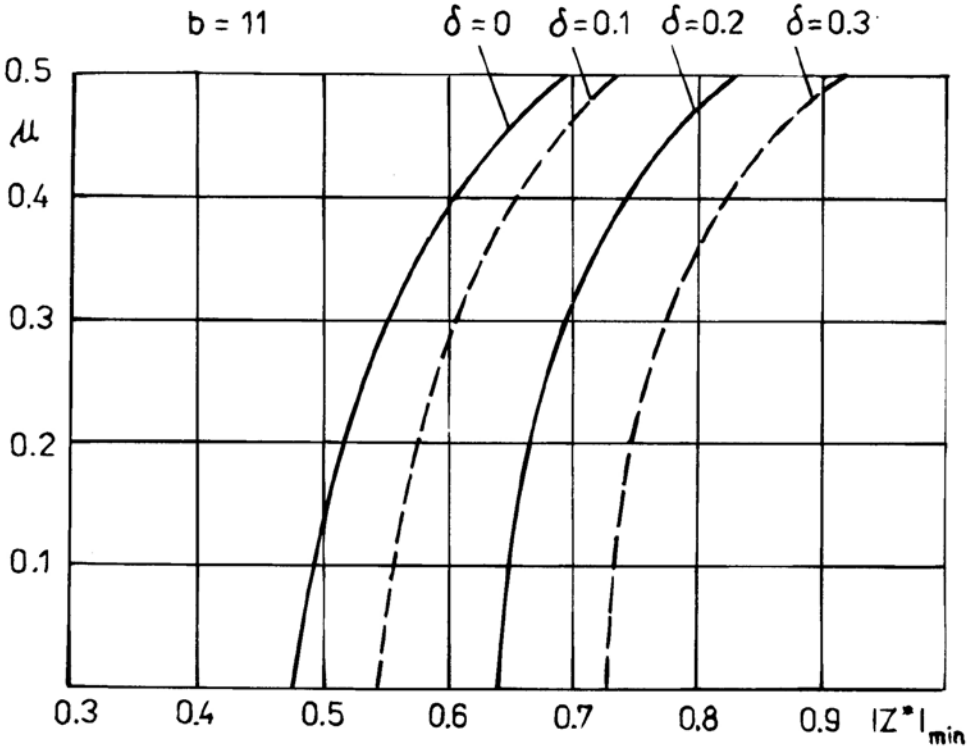

Fig. 1.22. Theoretical diagram for determination of Poisson's ratio μ according to extreme ordinate of mechanical impedance function $|Z^*|_{min}$.

1.2.6 Dynamic viscoelastic properties of bituminous materials

The bituminous materials of road construction have distinct features of viscoelastic behaviour. Measurements were performed with the mechanical impedance method using the scheme of cantilever elements measuring 5×5×30 cm from various bituminous materials. The results of measurements at temperature T=10, 20 and 40 °C, in the form of isochrones and damping parameter variations, are shown in Fig. 1.23 for mastic asphalt, in Fig. 1.24 for an open-cover asphalt layer, in Fig. 1.25 for a dense-cover asphalt layer, and in Fig. 1.26 for asphalt concrete.

The values of the damping parameter δ are average values because it does not present a regular and distinct change with frequency. The dependence of δ on temperature T is very strong.

The change of the complex modulus values is very distinct not only in their dependence on temperature T but also on the vibration frequency.

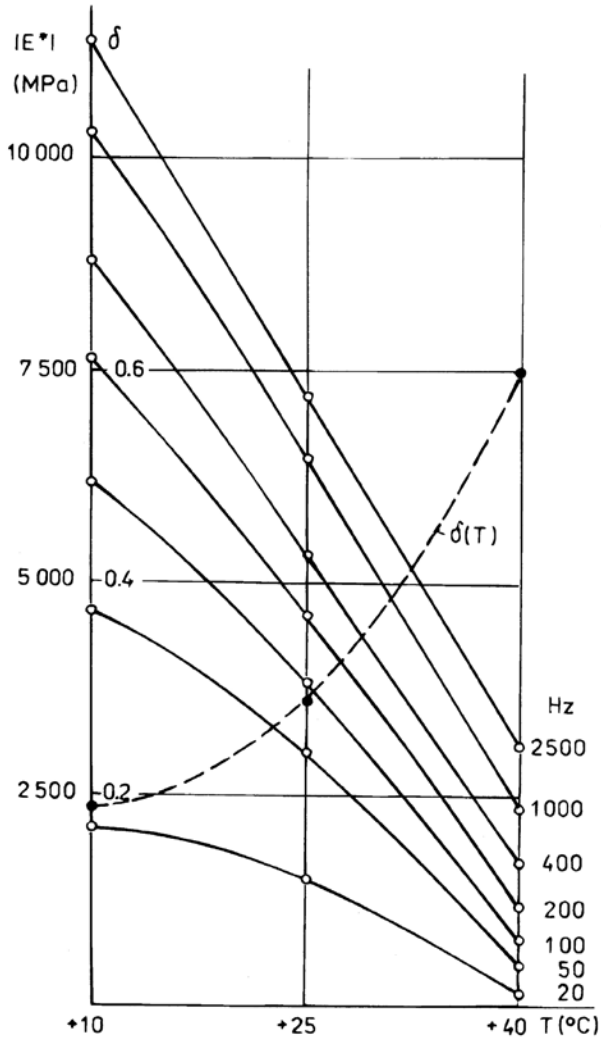

Fig. 1.23. Isochrones and damping parameter variations for mastic asphalt.

The measurements were made by using mechanical impedance method on a series of 15 specimens of asphalt concrete in the temperature range −25 to +45 °C. The mean values of the measurement results at a frequency of 20 Hz and at resonance and anti-resonance natural frequencies are plotted in Fig. 1.27 as isotherms and in Fig. 1.28 as isochrones, together with the dependence of damping factor δ on temperature. The complex modulus of elasticity $|E^*|$ alters from the value $|E^*|$=400 MPa at frequency 20 Hz and temperature T=45 °C to the value $|E^*|$=21000 MPa at frequency 3000 Hz and temperature T=−25 °C. The damping factor δ has the value $\delta\approx$0.16 at temperature T=−25 to −5 °C and at temperature T=+45 °C attains to the value δ=0.84.

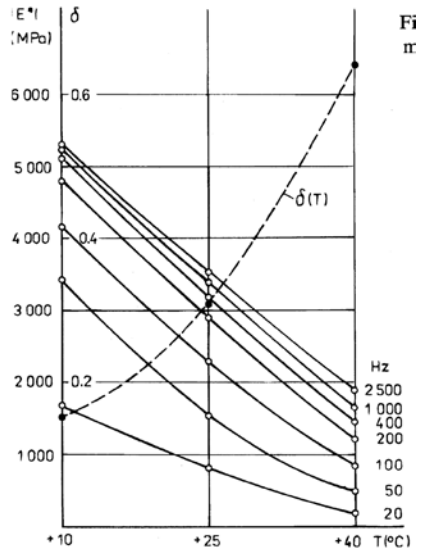

Fig. 1.24. Isochrones and damping parameter variations for open-cover asphalt.

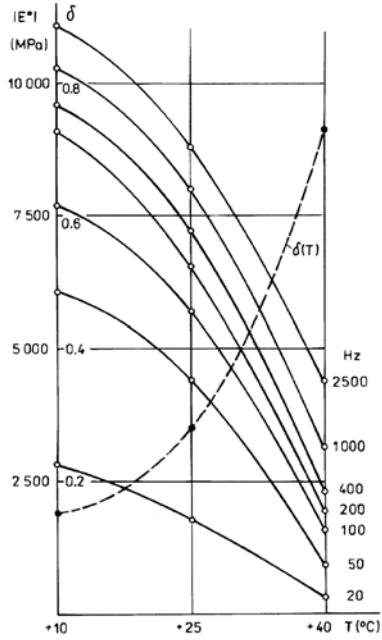

Fig. 1.25. Isochrones and damping parameter variations for dense-cover asphalt.

Similar measurements were performed on a series of 15 specimens of bitumen-coated sand and gravel material at temperatures from −25 °C to +45 °C. The results of these

measurments are evaluated in the graphs in Figs 1.29, 1.30. The damping factor $\delta(T)$ changes in the range 0.155~0.54 and the absolute value of complex modulus of elasticity $|E^*|$ in the range $|E^*|$=500−23000 MPa.

These results for measurements obtained on pavement bituminous materials demonstrate that the method of normalized mechanical impedance is an effective means of direct investigation of the dynamic viscoelastic properties in a wide frequency range. It makes possible to compare the directly measured properties with the viscoelastic properties determined from static creep testing by using the principle of superposition of time and temperature, [1.39–1.40]. The realization of this principle is combined with the fulfiling of the criterion of a linear thermo-rheological material, which is defined as a material whose temperature changes change only the position of the viscoelasticity function on a time or frequency scale but not the general shape of the function.

The principle of superposition of time and temperature may be used in the case of the dynamic isotherms in Figs. 1.27 and 1.29 to demonstrate that the viscoelastic response

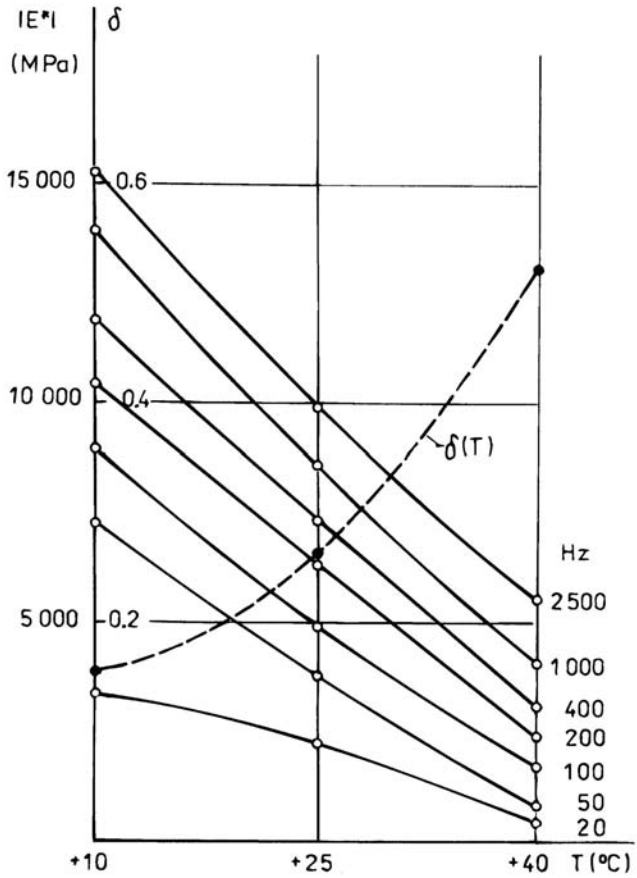

Fig. 1.26. Isochrones and damping parameter variations for asphalt concrete.

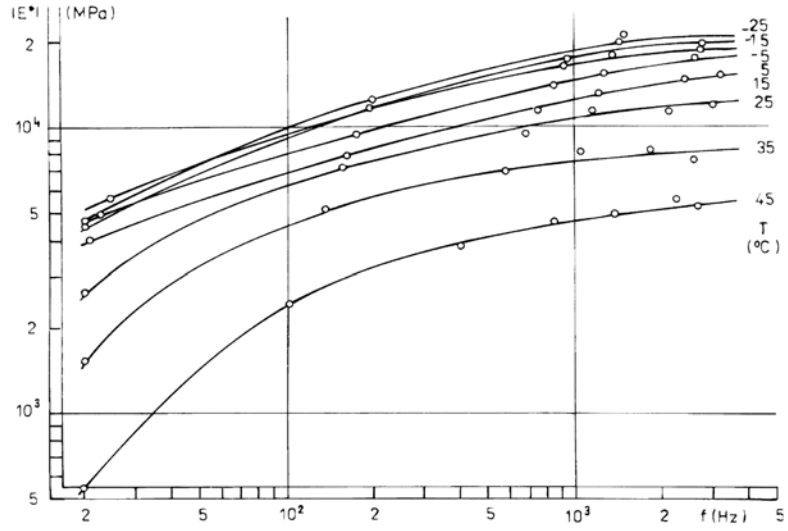

Fig. 1.27. Isotherms for asphalt concrete

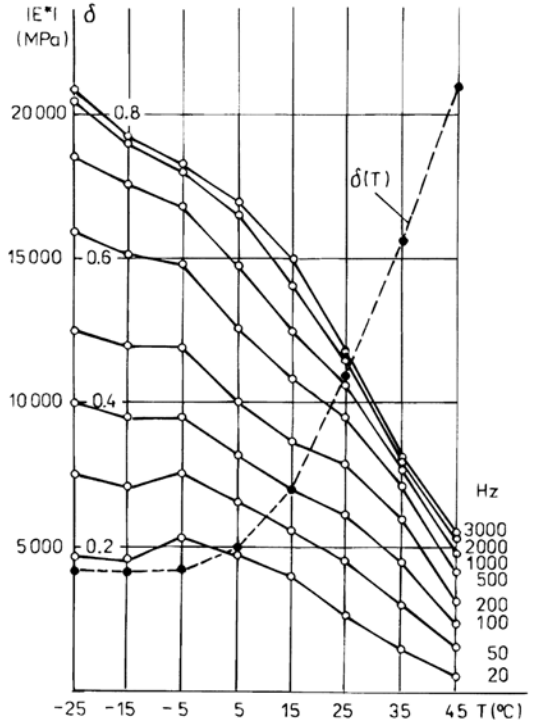

Fig. 1.28. Isochrones for asphalt concrete.

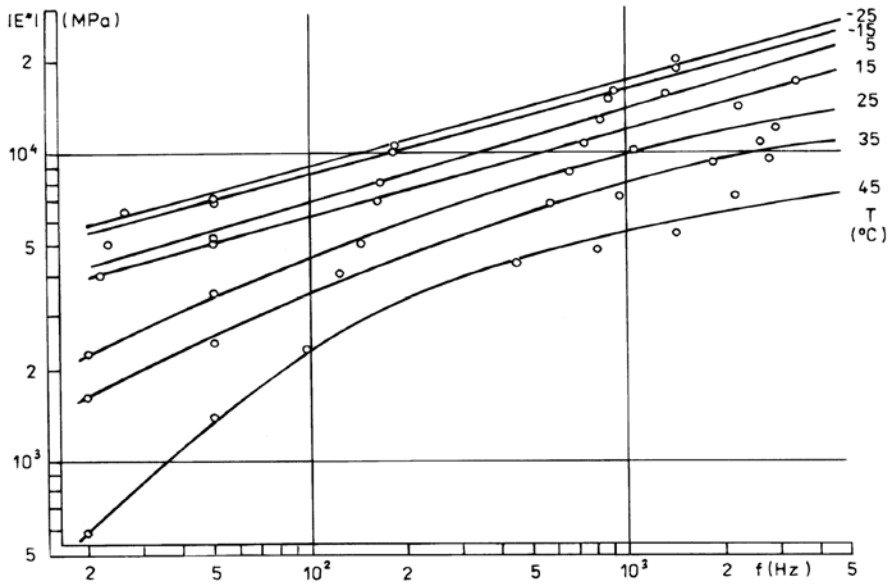

Fig. 1.29. Isotherms for precoated sand and gravel.

of the bituminous materials tested is only approximately thermorheologically linear. From the practical point of view it is advantageous to assume that this criterion is valid for the complex modulus of elasticity. The damping factor δ is more or less constant for every temperature and is independent of frequency. The principle of superposition of time and temperature cannot be used for the damping factor.

The isotherms, i.e. the functions of the relationships of the complex modulus of elasticity versus frequency obtained by measuring at various temperatures, give these relations in a certain limited frequency range. Supposing that material is approximately thermorheologically linear we can compile a fundamental isotherm for the reference temperature T_0, the variation of which will run in a substantially wider frequency range, by shifting single isotherms along the boundary scale.

The shift factor a_T may be established according to the relationship

$$a_T = \frac{f_{T_o}}{f_T} \tag{1.46}$$

where f_{T_0} is the frequency corresponding to a certain fixed value of the complex modulus of elasticity $|E^*|$ at reference temperature T_0 and f_T is the frequency corresponding to the same value of $|E^*|$ at temperature T.

In practice, in the determination of the shift factor a_T from the isotherm variations obtained by measurement, it is necessary first to access the partial shift factors Δa_T, which correspond to two neighbouring temperatures. The shift factor a_T is given by the product of partial shift factors Δa_T successively from the reference temperature T_0. In this way

the fundamental isotherme at the reference temperature T_0=+25 °C has been compiled for asphalt concrete and for bitumencoated sand and gravel material.

The shift factor a_T and reduced frequencies together with corresponding moduli |*E**| were evaluated for three values *f*=20 Hz, *f*=500 Hz, *f*=3000 Hz and *f*=4000 Hz

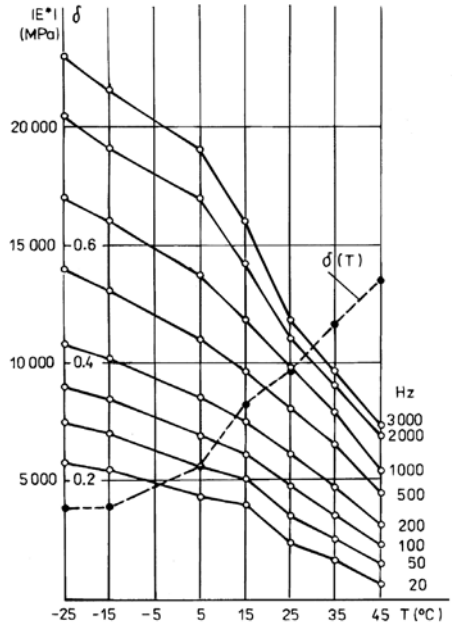

Fig. 1.30. Isochrones for precoated sand and gravel.

Table 1.6. Compilation of fundamental isotherm for asphalt concrete.

T(°C)	Δa_T	a_T	*f*(Hz)	|*E*| (MPa)
−25	1.25	7.7	3850	16000
−15	2.00	6.15	3080	14800
+5	1.85	3.07	1530	12700
+15	1.66	1.66	830	10800
T_0=+25°C	1	1	500	9600
+35	0.30	0.30	150	7150
+45	0.16	0.048	24	4050
−25	1.125	2.94	59	4700
−15	0.87	2.61	52	4500
+5	1.50	3.0	60	4700
+15	2.0	2.0	40	4000
+25	1	1	20	2650
+35	0.475	0.475	9.5	1500
+45	0.40	0.19	3.8	540

−25	2.5	96.0	288000	21000
−15	3.75	38.4	115000	19000
+5	2.73	10.2	30600	17000
+15	3.75	3.75	11250	15000
+25	1	1	3000	11900
+35	0.073	0.073	219	8050
+45	0.050	0.0036	11	5500

respectively. The results are compiled in Table 1.6 for asphalt concrete and in Table 1.7 for bitumen-coated sand and gravel. The variations of the fundamental isotherms are plotted in Figs. 1.31 and 1.32.

The fundamental isotherms at a reference temperature determined by the described above procedure characterize the viscoelastic properties of a material over a wide frequency range. Together with the shift factor a_T they serve for the determination of viscoelastic behaviour at an arbitrary temperature T.

Table 1.7. Compilation of fundamental isotherm for bitumen-coated sand and gravel.

T(°C)	Δa_T	a_T	f(Hz)	$\|E\|$ (MPa)
−25	1.25	7.05	3520	14000
−15	1.82	5.64	2820	13200
+5	1.61	3.09	1550	11050
+15	1.92	1.92	960	9600
T_0=+25°C	1	1	500	8100
+35	0.50	0.50	250	6500
+45	0.32	0.16	80	4400
−25	1.25	13.20	266	5800
−15	2.25	10.65	213	5450
−5	1.35	4.72	94.5	4300
+15	3.5	3.5	70	3950
+25	1	1	20	2200
+35	0.50	0.50	10	1550
+45	0.363	0.181	3.62	589
−25	1.29	13.20	52800	25000
−15	1.48	10.25	41000	23400
+5	1.90	6.92	27700	21000
+15	3.64	3.64	14550	17000
+25	1	1	4000	12000
+35	0.42	0.42	1680	9700
+45	0.40	0.16	640	7600

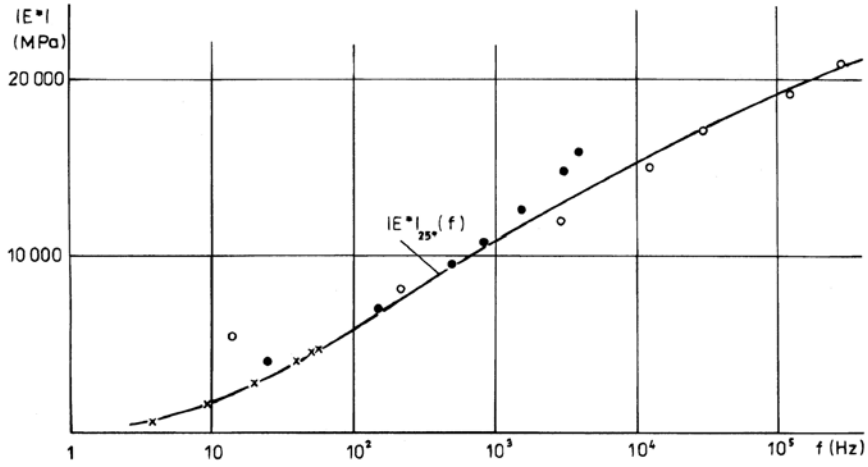

Fig. 1.31. Form of fundamental isotherm for asphalt concrete.

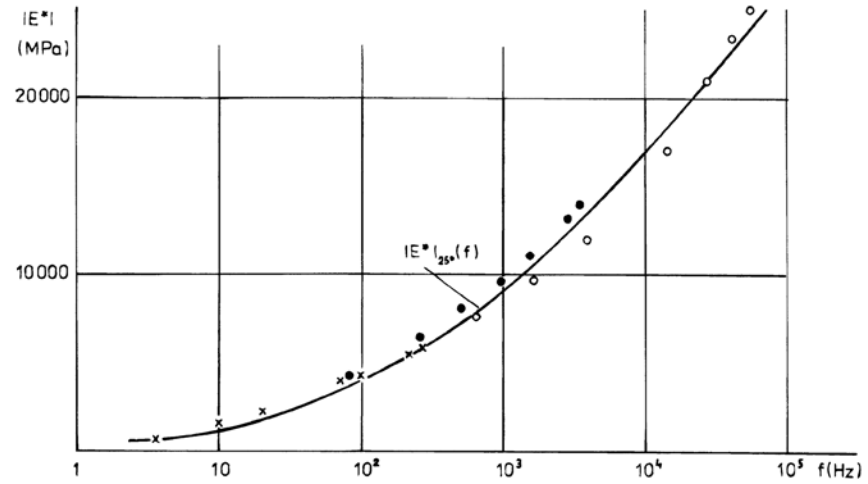

Fig. 1.32. Form of fundamental isotherm for precoated sand and gravel.

1.2.7 Dynamic viscoelastic properties of soil materials

The dynamic viscoelastic properties of cohesive or stabilized soil materials can be investigated by applying the mechanical impedance method and the schemes of torsional and longitudinal vibration of cylindrical elements.

Measurements were performed on a series of test specimens from the loess and bentonite soil materials. The specimens were cylindrical with a diameter of 4 cm and a length of 8.7 cm. The density of the compacted soil materials was $\varrho = 2060\ \mathrm{kg/m^3}$ for loess and

$\varrho = 1610\ \mathrm{kg/m^3}$ for bentonite. The test samples were compacted at moisture w=17% for loess or w=52% for bentonite and then placed in a desiccator.

By applying the mechanical impedance method and the torsional and longitudinal vibration of the tested elements, the process of change of the viscoelastic properties was studied. The change of the soil structure as a consequence of the thixotropy and the moisture change gives rise to a change of viscoelastic characteristics. The results of the measurement are compiled in the graphs in Figs. 1.33–1.37 for loess and in Figs. 1.38–1.42 for bentonite.

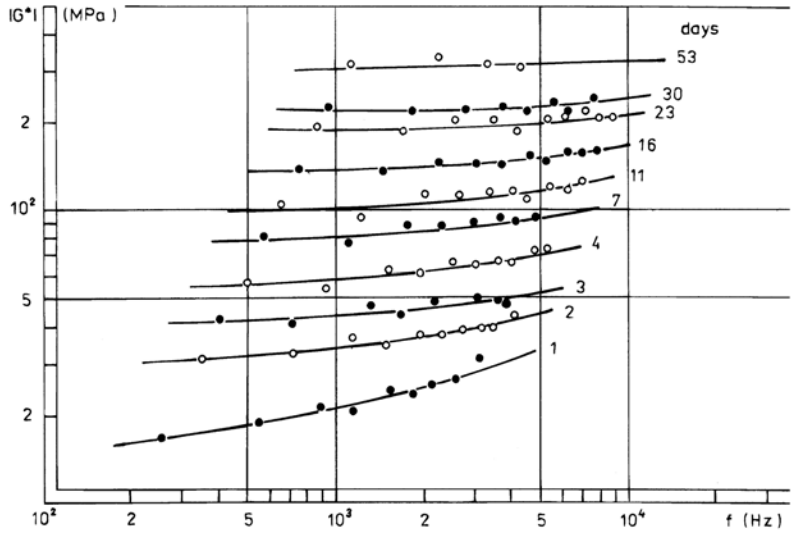

Fig. 1.33. Relationship of complex modulus |*G**| to frequency, for loess.

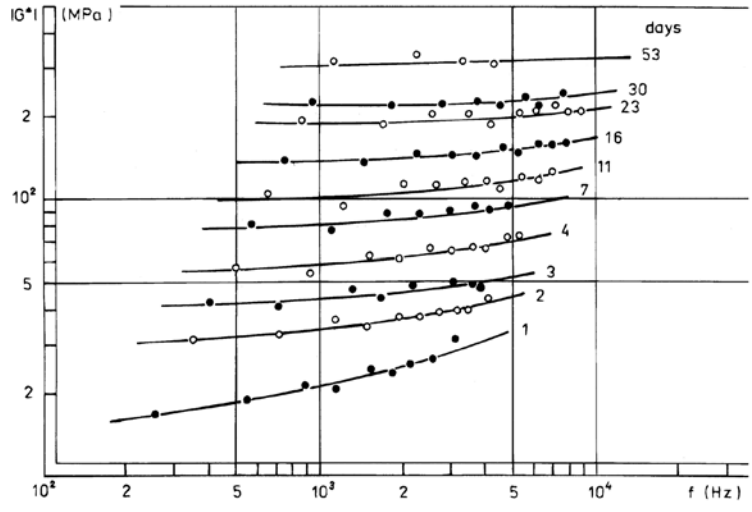

Fig. 1.34. Relationship of complex modulus |*E**| to frequency, for loess.

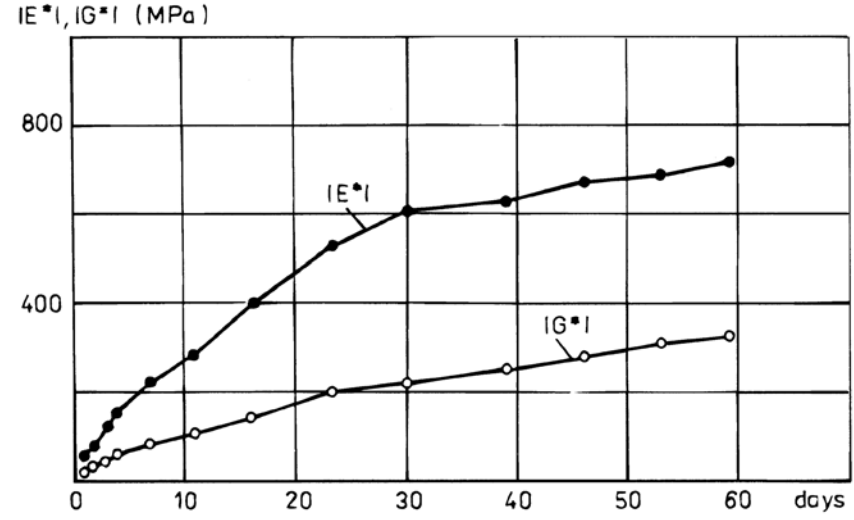

Fig. 1.35. Evolution of $|G^*|$ and $|E^*|$ over time after compacting, for loess.

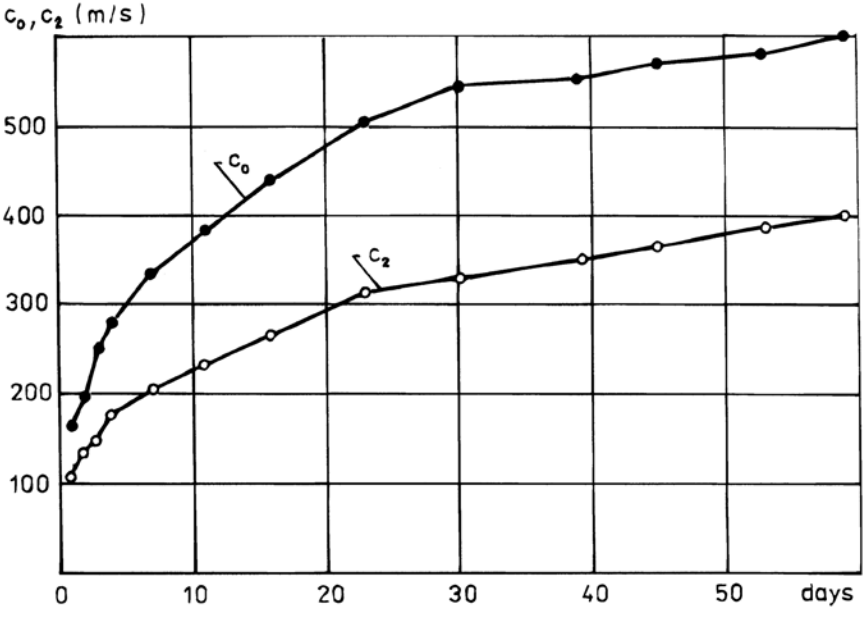

Fig. 1.36. Evolution of stress-wave velocities c_2 and c_0 over time after compacting, for loess.

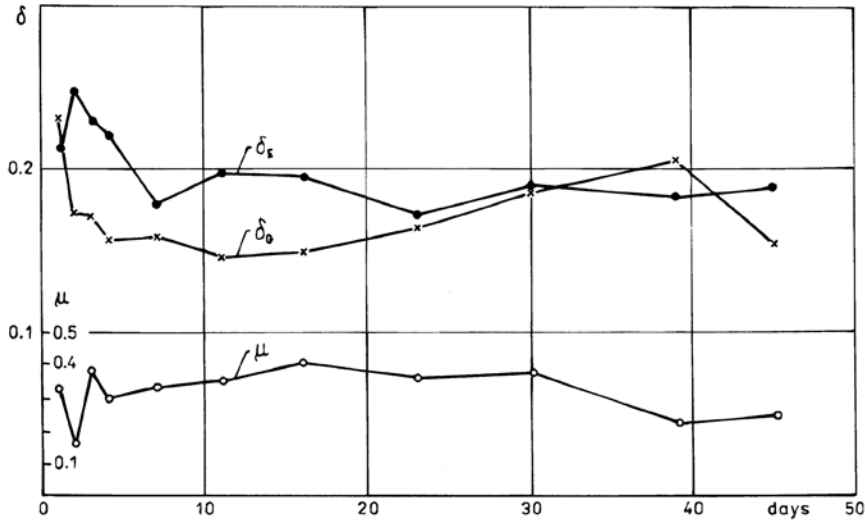

Fig. 1.37. Evolution of damping parameter δ and Poisson's ratio μ over time, for loess.

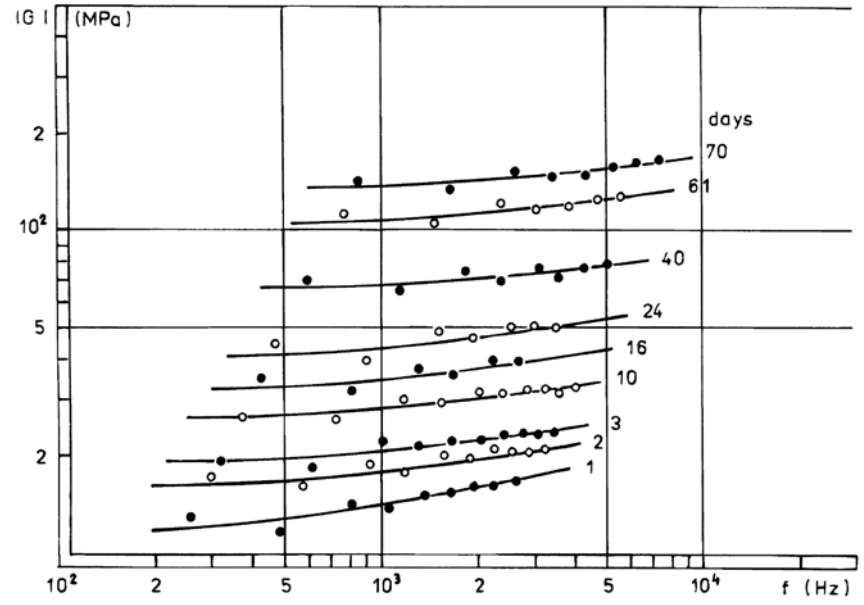

Fig. 1.38. Relationship of complex modulus $|G^*|$ to frequency, for bentonite.

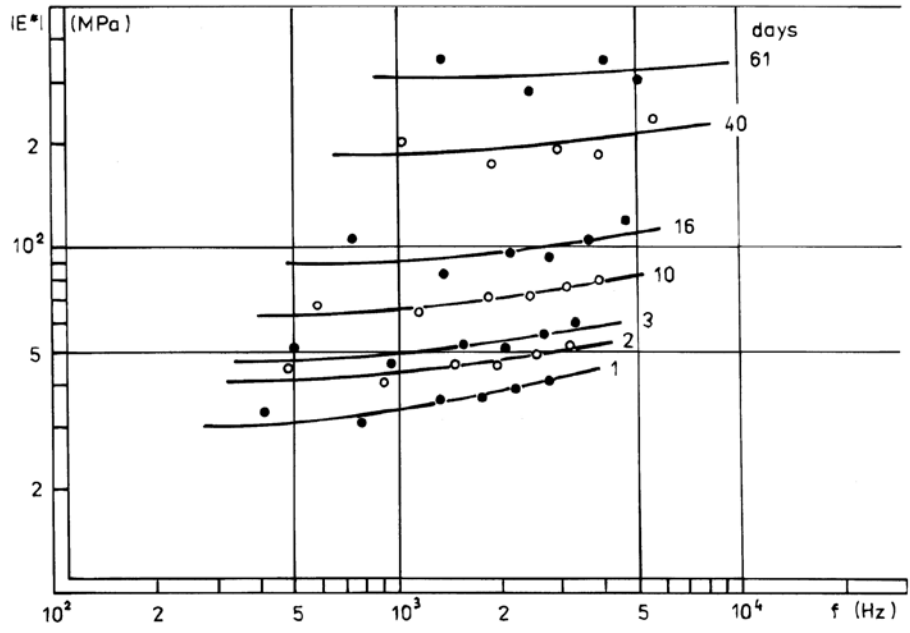

Fig. 1.39. Relationship of complex modulus |*E**| to frequency, for bentonite.

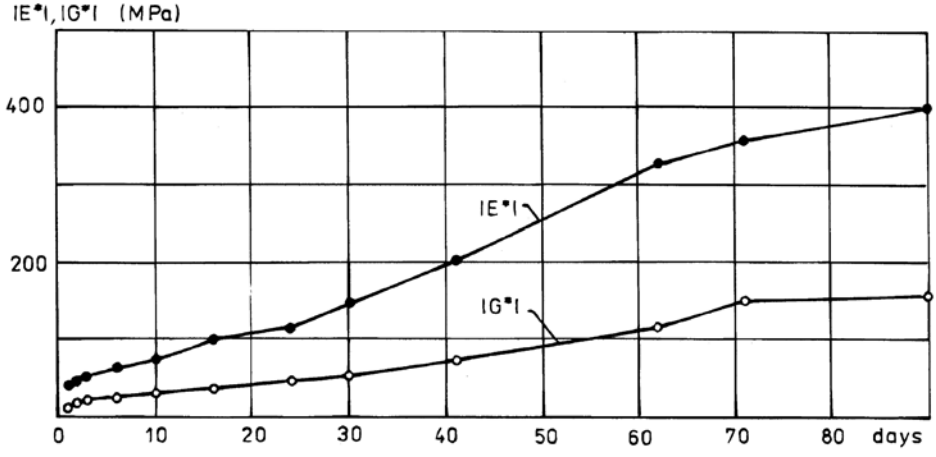

Fig. 1.40. Evolution of |*G**| and |*E**| over time after compacting, for bentonite.

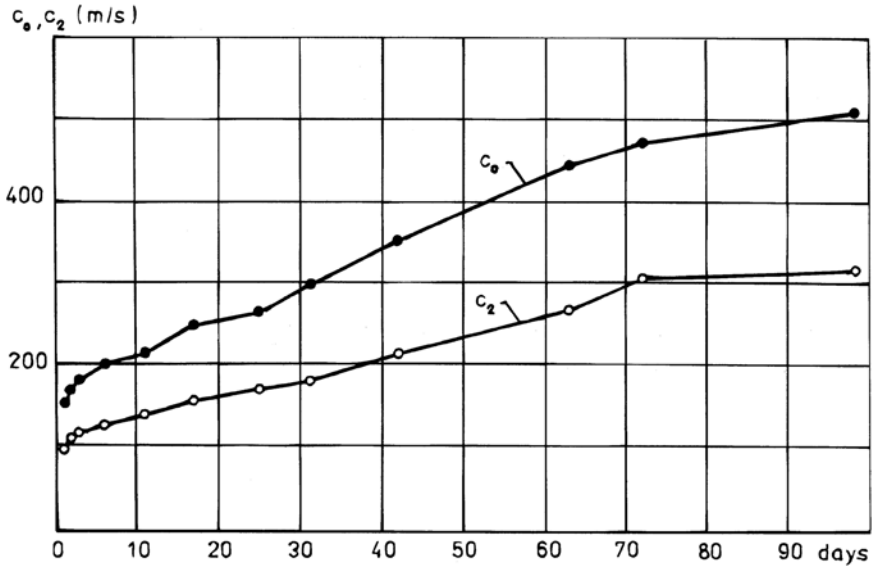

Fig. 1.41. Evolution of stress-wave velocities c_2 and c_0 over time after compacting, for bentonite.

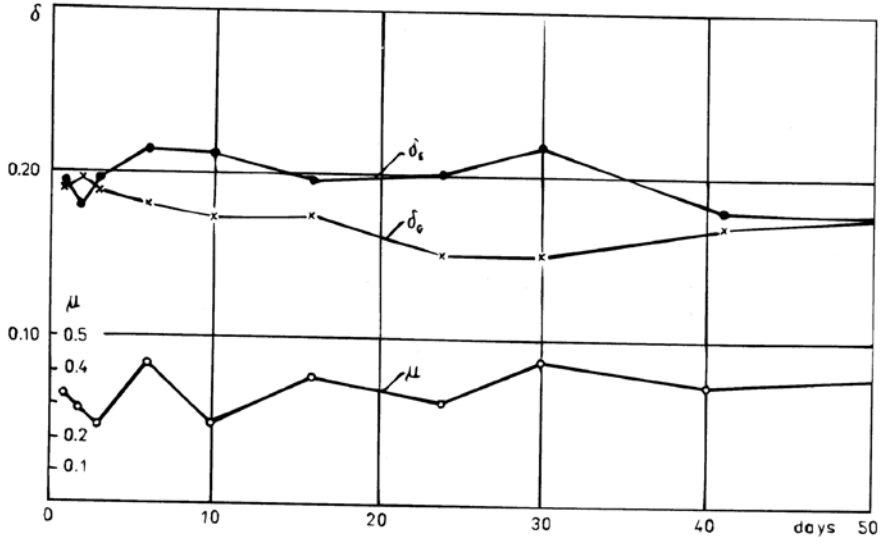

Fig. 1.42. Evolution of damping parameter δ and Poisson's ratio μ over time, for bentonite.

The real parts of the complex moduli E_ω, G_ω were calculated according to equations (1.44), (1.45) and the absolute values of the complex moduli were expressed by the relationships

$$|E^*_\omega| = E_\omega(1+\delta^2_E)^{1/2}$$
$$|G^*_\omega| = G_\omega(1+\delta^2_G)^{1/2} \tag{1.47}$$

The velocities of shear stress waves, c_2, and longitudinal stress waves, c_0, were calculated according to the relationships

$$c_2 = \frac{4lf_t}{k}\eta \tag{1.48}$$

$$c_0 = \frac{4lf_l}{k}\eta \tag{1.49}$$

where

$$\eta = \sqrt{\frac{2D^2}{1+D}} \tag{1.50}$$

if

$$D = \sqrt{1+\delta^2} \tag{1.51}$$

Poisson's ratio μ follows from the values of $|E^*|$ and $|G^*|$.

The dependence of the complex moduli $|G^*|$ and $|E^*|$ on the frequency measured at the various times of evolution affirm the distinct change of the material structure and at the same time the typical relationship $|G^*|$ and $|E^*|$ from the frequency. The values of the moduli increase with increased frequency, especially at the beginning of time evolution. In the later evolution the dynamic behaviour of soil materials approaches elastic behaviour.

1.3 Dynamic diagnosis of the subgrade

The subgrade is formed from soil materials of various kinds. Such a medium can (only very approximately) be defined as an elastic half-space. In applying dynamic methods for determining subgrade material characteristics one has to consider that the soil material has viscoelastic properties, which manifest themselves partly in the dependence of elastic characteristics on the frequency and partly in the existence of strong damping as a consequence of the internal friction and space dispersion of energy. The other special property of the subgrade is its inhomogeneity, which can similarly influence the results obtained by methods of dynamic diagnosis and their interpretation.

1.3.1 Application of the phase velocity method

The procedures for measuring stress-wave velocity, as described in section 1.1, may be used in testing pavement subgrade and road and highway soil bodies. The measured values

of phase velocity, and their dependence on frequency or wavelength, serve as an assessment of the elastic characteristics of the subgrade material, for an evaluation of its viscoelastic properties and its inhomogeneity.

Reference [1.41] describes the results of measurements on soil subgrade material. The aim of this testing was to evaluate the depth and quality of subgrade material compacted by a rubber-tyred compactor and vibratory roller.

The results of measurements on the sand and clay soils of highway subgrades versus the number of passes of the vibratory roller are given in Table 1.8. The measurements were accomplished at frequencies of 20–5000 Hz, the values of Rayleigh-wave velocity c_{Rz} corresponding to the high frequencies. The moduli of elasticity E_z were established according to the relationship $E_z=(c_{Rz}/0.57)^2$ ϱ_z. After ten passes of the vibratory roller the results indicate that the upper layer of the compacted subgrade body has disintegrated.

Table 1.8. Results of measurements on subgrade [1.42].

Number of passes	Number of specimen	Density (kg/m^3)	Moisture (%)	Surface-wave velocity, c_R (m/s)	Modulus of elasticity, E (MPa)
4	1	1751	9.1	170	156
	2	1757	6.3		
10	3	1576	9.5	150	110
	4	1618	8.3		
16	5	1792	8.3	155	130
	6	1713	8.7		

The results of measurements on the loess material of the subgrade versus the number of passes of the rubber-tyred compactor are given in Table 1.9.

Table 1.9. Influence of number of passes on the characteristics of loess subgrade [1.42].

Number of passes	Density (kg/m^3)	Moisture (%)	c_R (m/s)	E (MPa)
4	2080	13.9	148	140
8	2130	11.4	150	147
12	2135	13.6	163	175

The results of measurements of the clayed subgrade versus the number of passes of the rubber-tyred compactor and various thicknesses of the compacted layer are given in Table 1.10. Increasing the number of passes of the compactor for a thickness of the compacted layer 50 cm produced the disintegration of the compacted surface zone of the layer.

Table 1.10. Results of measurements on clay subgrade [1.42].

Layer thickness (cm)	Number of passes	Density (kg/m^3)	Moisture (%)	Surface-wave velocity c_R (m/s)	E (MPa)
20	2	2033	20.4	138	120
	6	2027	19.4	150	141
	10	2075	20.9	158	160
50	2	2070	20.1	150	143
	6	2031	19.7	132	109
	10	2048	19.9	112	79

The measurements were carried out by using the phase velocity method on the highway subgrade [1.42]. This subgrade was formed from an embankment of 5–6 m height from clay-loess soil material, with a surface layer of sand-clay soil material with a thickness of 40–50 cm. The tests were performed in two sections, the first one of which was insufficiently compacted. The results are plotted in Fig. 1.43 for the first section and in Fig. 1.44 for the second section. While the velocities c_{Rz} on the second section do not depend on the frequencies, the results in the first section indicate the influence of inhomogeneity or viscoelastic behaviour (curve 2) and insufficient compaction (curve 1).

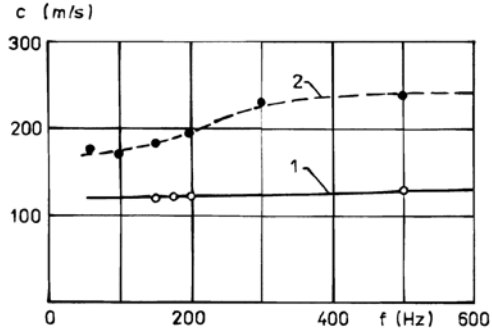

Fig. 1.43. Phase velocities of surface waves on highway subgrade.

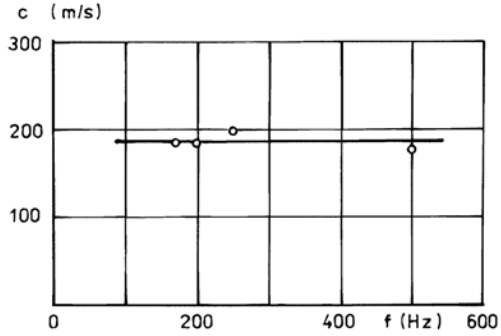

Fig. 1.44. Phase velocities of surface waves on highway subgrade.

1.3.2 Application of the mechanical impedance method

The highway subgrade described in the previous section has served as the realization of testing by the mechanical impedance method using the procedure described in section 1.2.5. We have used the scheme of the vertical vibration of the mass on the subgrade. The measurements were carried out on two localities for the first section and on three localities for the second section. The localities correspond to the places where the phase velocities of stress wave propagation were determined.

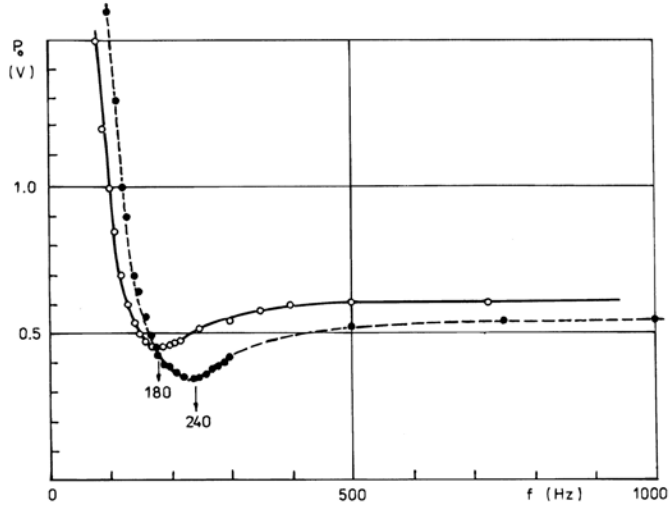

Fig. 1.45. Curves of measured functions of mechanical impedance of highway subgrade: section 1.

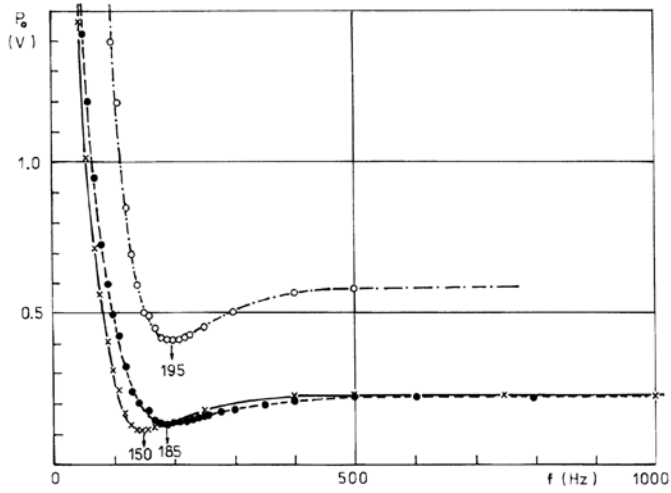

Fig. 1.46. Curves of measured functions of mechanical impedance of highway subgrade: section 2.

The curves of measured force amplitude P_0 (in volts) at constant amplitude of acceleration A of vertical mass vibration versus frequency f (in Hz) are drawn in Fig. 1.45 for the first section and in Fig. 1.46 for second section. These curves are proportional to the variation of the mechanical impedance function and quite unambiguously correspond to the theoretical curve of $|Z^*|$.

The interpretation and evaluation of the measured results is to be formed in Tables 1.11–1.15. The evaluation was carried out assuming a value of Poisson's ratio μ=0.35, and the damping parameter δ was determined from the extreme ordinate $|Z^*_{\min}|$. It is necessary to add some notes to the evaluation procedure. The measured values of the frequencies f (in Hz) and force amplitudes P_0 (in volts) are in the first two columns of the tables. With

Table 1.11. Evaluation of the measured results on highway subgrade. Section 1, first measurement. Amplitude of acceleration, A=0.003V; μ=0.35; δ=0.3.

Frequency (Hz)	P_0 (V)	$\|Z^*\|$	Ω_{theor}	c_2 (m/s)	$c_{2,corr}$ (m/s)	G (MPa)
60	2.20	4.070	0.355	133.5	150.5	40.8
70	1.80	3.330	0.390	142.0	154.7	43.1
80	1.50	2.770	0.425	148.5	158.0	44.9
90	1.20	2.220	0.475	149.5	158.5	45.2
100	1.00	1.845	0.500	158.0	162.7	47.6
110	0.85	1.570	0.540	161.0	164.2	48.5
120	0.70	1.290	0.590	161.5	164.5	48.7
130	0.60	1.110	0.640	161.0	164.2	48.5
140	0.54	0.995	0.675	164.0	165.7	49.4
150	0.50	0.924	0.715	166.0	166.7	50.0
160	0.48	0.888				
180	0.46	0.850	0.850	167.5	167.5	50.5
200	0.47	0.870				
220	0.48	0.888				
250	0.52	0.960				
300	0.54	0.995				
350	0.58	1.070				
400	0.60	1.105				
500	0.61	1.125		174.5	174.5	54.8
750	0.59	1.085				

Table 1.12. Evaluation of the measured results on highway subgrade. Section 2, second measurement. A=0.003V; μ=0.35; δ=0.1.

Frequency (Hz)	P_0 (V)	$\|Z^*\|$	Ω_{theor}	c_2 (m/s)	c_{2corr} (m/s)	G (MPa)
60	4.00	7.370	0.262	181.0	209.0	78.6
70	2.90	5.350	0.301	183.5	210.0	79.4
80	2.40	4.420	0.328	193.0	215.0	83.2
90	2.00	3.680	0.355	200.0	218.5	85.9
100	1.60	2.950	0.392	201.0	219.0	86.3
110	1.30	2.398	0.420	207.0	222.0	88.7
120	1.00	1.845	0.465	205.0	221.0	87.9
130	0.90	1.660	0.480	214.0	225.5	91.5
140	0.70	1.290	0.530	209.0	223.0	89.5
150	0.65	1.198	0.550	215.5	226.0	91.9
160	0.56	1.032	0.580	218.0	227.5	93.2
170	0.50	0.922	0.610	220.0	228.5	93.9
180	0.42	0.775	0.660	216.0	226.5	92.3
190	0.41	0.755	0.680	221.0	220.0	94.4
200	0.39	0.719	0.700	226.0	231.5	96.5
210	0.37	0.682	0.725	229.0	233.0	97.7
220	0.35	0.645				
230	0.35	0.645				
240	0.34	0.626	0.800	237.0	237.0	101.1
250	0.35	0.645				
260	0.36	0.663				
270	0.38	0.700				
280	0.39	0.719				
290	0.40	0.737				
300	0.42	0.774				
500	0.52	0.959				
750	0.54	0.995		238.0	238.0	102.0
1000	0.55	1.014				

regard to the parameters and calibrations of the experimental arrangement used, the values of mechanical impedance $|Z^*|$ in the third column of the tables are calculated according to the relationship

$$|Z^*| = 0.00553\frac{P_0}{A}. \tag{1.52}$$

The steep part of the curve of $|Z^*|$ at low frequencies, extending to the value at the resonance frequency and the values at high frequencies were used in the evaluation of the measurements.

The values Ω_{theor} (column 4 of the tables) were determined according to the theoretical variation of the mechanical impedance function for individual measured values of $|Z^*|$.

Table 1.13. Evaluation of the measured results on highway subgrade. Section 2, first measurement. A=0.001V; μ=0.35; δ=0.05.

Frequency (Hz)	P_0 (Volt)	$\|Z^*\|$	Ω_{theor}	c_2 (m/s)	c_{2corr} (m/s)	G (MPa)
50	1.450	8.030	0.240	165.0	165.0	49.0
60	1.000	5.530	0.285	166.0	165.5	49.3
70	0.700	3.870	0.330	167.5	166.2	49.7
80	0.560	3.100	0.365	173.0	169.0	51.4
90	0.400	2.210	0.420	169.0	167.0	50.2
100	0.300	1.660	0.460	171.5	168.2	50.9
110	0.230	1.270	0.520	167.5	166.2	49.7
120	0.160	0.885	0.580	163.5	164.2	48.5
130	0.125	0.692	0.620	166.0	165.5	49.3
140	0.110	0.609	0.680	163.0	164.0	46.1
150	0.105	0.581	0.720	165.0	165.0	49.0
160	0.110	0.610				
170	0.120	0.665				
180	0.130	0.720				
200	0.145	0.805				
250	0.180	0.995				
300	0.200	1.105				
400	0.220	1.219				
500	0.220	1.219				
750	0.220	1.219		182.0	182.0	59.6

The velocity of shear stress waves $c_2 = \sqrt{G_z/\varrho_z}$ can be determined by using the relationship in the form

$$c_2 = \frac{\omega a}{\Omega} = \frac{2\pi f \cdot 0.126}{\Omega} = 0.791\frac{f}{\Omega}. \tag{1.53}$$

The values of the velocity c_2 (column 5 of the tables) determined in this way have to be corrected, because they were assessed on the basis of the theoretical variation of $|Z^*|$ for a steady value G, which is independent of frequency. From the practical point of view it is sufficient to determine the corrected values c_{2cor} as the arithmetic mean of the given value of c_2 and the value of c_2 for the resonance frequency. The real parts of the complex modulus G_z are in the last column of the tables provided that ϱ_z=1800 kg/m^3.

The values of c_2 at high frequencies, when $|Z^*|_{theor}$ is practically equal to 1.0, can be determined by the relationship

$$c_2 = \sqrt{\frac{|Z^*|_{exp}}{|Z^*|_{theor}}}\, c_2(f_{res}) \approx \sqrt{|Z^*|_{exp}}\, c_2(f_{res}) \tag{1.54}$$

where $c_2(f_{res})$ is the value of the velocity for the resonance frequency fres.

Table 1.14. Evaluation of the measured results on highway subgrade. Section 2, Second measurement. A=0.001V; μ=0.35; δ=0.25.

Frequency (Hz)	P_0 (V)	$\|Z^*\|$	Ω_{theor}	c_2 (m/s)	c_{2corr} (m/s)	G (MPa)
26	6.500	35.900	0.120	171.5	177.2	56.5
30	4.800	27.500	0.138	172.0	177.5	56.7
40	2.700	14.950	0.185	171.0	177.0	56.4
50	1.700	9.400	0.229	172.5	177.7	56.8
60	1.200	6.650	0.270	175.5	179.2	57.8
70	0.950	5.260	0.300	184.0	183.5	60.6
80	0.730	4.050	0.337	187.0	185.0	61.6
90	0.600	3.320	0.370	192.0	187.5	63.3
100	0.500	2.770	0.400	197.5	190.2	65.1
110	0.440	2.430	0.420	207.0	195.0	68.4
120	0.320	1.770	0.480	197.5	190.2	65.1
130	0.240	1.330	0.540	190.5	186.7	62.7
140	0.200	1.105	0.580	191.0	187.0	62.9
150	0.180	0.997	0.620	191.5	187.2	63.1
160	0.180	0.997	0.620	204.0	193.5	67.4
170	0.140	0.775	0.720	187.0	185.0	61.6
185	0.135	0.748	0.800	183.0	183.0	60.3
200	0.140	0.775				
210	0.140	0.775				
230	0.145	0.804				
250	0.160	0.886				
300	0.180	0.997				
350	0.195	1.080				
400	0.200	1.105				
500	0.220	1.218		202.5	202.5	73.8
600	0.220	1.218				

The values of elasticity modulus E_z determined according to the results of measurement by the mechanical impedance method and the phase velocity method are to be formed in Table 1.16.

The modulus of elasticity E_z was calculated according to the test results of the phase velocity method by using the relationship in the form

$$E_z = \left(\frac{c_{Rz}}{0.57}\right)^2 \varrho_z \tag{1.55}$$

in which c_{Rz} corresponds to the measured phase velocities. The comparison with modulus values in Table 1.15 is quite satisfactory and at the same time confirms the supposition that the values of the moduli have to refer to the vibration frequency.

Table 1.15. Evaluation of the measured results on highway subgrade. Section 2, third measurement. A=0.003V; μ=0.35; δ=0.28.

Frequency (Hz)	P_0 (V)	$\|Z^*\|$	Ω_{theor}	c_2 (m/s)	c_{2corr} (m/s)	G (MPa)
75	2.70	4.980	0.320	185.0	185.2	61.7
80	2.30	4.250	0.340	186.0	185.7	62.1
90	1.80	3.320	0.375	189.0	187.2	63.1
100	1.40	2.580	0.410	192.5	189.0	64.3
110	1.20	2.210	0.440	199.0	192.2	66.5
120	0.85	1.570	0.510	186.0	185.7	62.1
130	0.70	1.290	0.551	186.0	185.7	62.1
140	0.60	1.110	0.600	184.5	185.0	61.6
150	0.50	0.922	0.660	180.0	182.7	60.1
160	0.50	0.922	0.660	191.5	188.5	63.9
170	0.45	0.830	0.720	186.5	186.0	62.3
195	0.42	0.775	0.830	185.5	185.5	61.9
250	0.46	0.850				
300	0.50	0.922				
400	0.57	1.050				
500	0.58	1.070		192.0	192.0	66.4

Table 1.16. Comparison of the measured characteristics of subgrade material.

Section number	Measurement number	E(MPa) method Mechanical impedance	E(MPa) method Phase velocity	Note
1	1	110–136.5	82.5–93.7	Insufficient compaction
	2	212–276	170–318	Sufficient compaction
	1	132–161		
2	2	152–199	187.0	
	3	167–179		

The methods of dynamic diagnosis of the subgrade are also useful in cases of a subgrade with sub-base layers. We can present the results of measurements on the highway subgrade

with a 25 cm thick sandgravel layer and with a 15 cm thick cement-stabilized layer. By using the method of mechanical impedance the resonance frequency f_{res}=450 Hz has been determined. Provided that μ=0.35 and δ=0.20 the characteristic values will be determined as c_2=445 m/s, G=396 MPa and E=1070 MPa, if ϱ=2000 kg/m^3. By using the phase velocity method the values of c=435 m/s was measured at the frequency 450 Hz.

In the same structure but with the 4 cm thick bituminous interlayer the resonance frequency f_{res}=550 Hz is the result of mechanical impedance measuring. Then the characteristic data are: c_2=543 m/s, G=590 MPa, E=1595 MPa supposing the same values of μ, δ and ϱ. The velocity of surface waves determined by using the phase velocity method at the frequency f=550 Hz is c_2=510 m/s. The corresponding modulus of elasticity E given by equation (1.55) will be E=1600 MPa. Once again, the values obtained by the mechanical impedance method and by the phase velocity method compare favourably. However, we have used for the evaluation the theory of a viscoelastic homogeneous half-space, although in these cases the structure is a layered subgrade. We can suppose that by using the theory of a viscoelastic homogeneous half-space with the conception of complex moduli of elasticity depending on an arbitrary function of frequency, the behaviour of a layered half-space may be expressed adequately as well. While for a viscoelastic subgrade material the change of moduli of elasticity depending on frequency causes the viscoelasticity, for the layered subgrade this change of modulus is the result of the inghomogeneity of the subgrade. The resulting effect, for the layered subgrade, is qualitatively same, because the sub-base layers of pavement structures cause an increase of the moduli with increasing frequency.

1.4 Diagnosis of dynamic elasticity and rigidity of layered pavement structures

The method of phase velocity of stress-wave propagation can be used both in the process of construction and in the course of road and airfield servicing as a serviceable and effective means of diagnostic testing. Though these methods cannot replace bearing capacity tests, they offer rich information on structural material properties, pavement stiffness, as well as on the overall quality of the pavement structures.

The results of the dynamic diagnosis also help in the formation and identification of acceptable theoretical models that agree closely with both the dynamic behaviour of structural materials and the total dynamic response of pavements.

When applying the phase velocity method on layered pavement structures the phase velocities of stress waves of various kinds can be measured, depending on the arrangement of the transducers (vibrator and pick-up). The basic possibilities for the transducer arrangement are shown in Figs. 1.47–1.52. The arrangement of Fig. 1.47 is suitable for the determination of flexural waves, the arrangement of Fig. 1.48 for longitudinal waves, that in Fig.1.49 shear waves and that in Fig. 1.50 boundary Rayleigh waves. The arrangements in Fig. 1.51 and 1.52 partly replace those in Figs. 1.47 and 1.48.

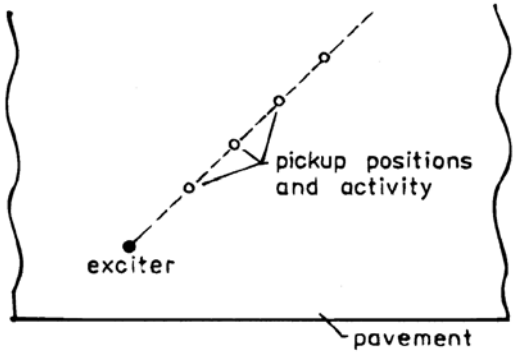

Fig. 1.47. Transducer arrangement for determination of flexural-wave velocities.

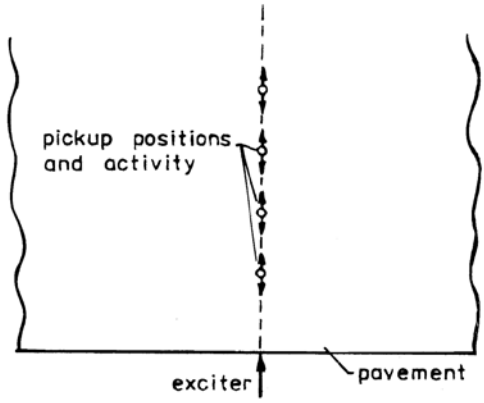

Fig. 1.48. Transducer arrangement for determination of longitudinal-wave velocities.

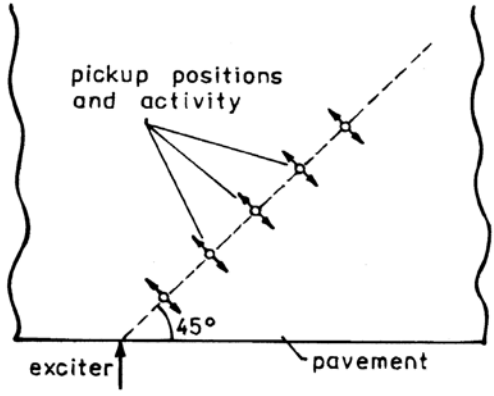

Fig. 1.49. Transducer arrangement for determination of shear-wave velocities.

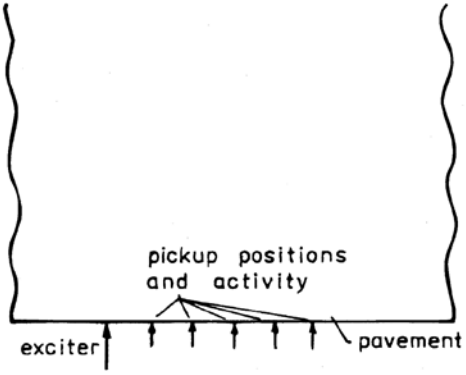

Fig. 1.50. Transducer arrangement for determination of boundary—surface—wave velocities.

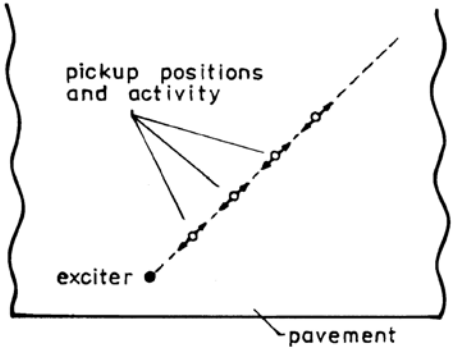

Fig. 1.51. Alternative transducer arrangement for measurement of longitudinal-wave velocities.

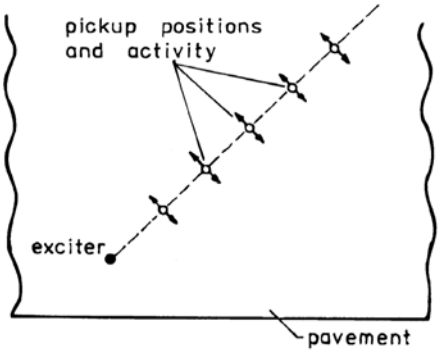

Fig. 1.52. Alternative transducer arrangement for measurement of shear-wave velocities.

The influence of the reciprocal contact of the pavement layers and the influence of the contact with the subgrade obviously transform the properties and the regularities of individual kinds of stress wave, but for the sake of this survey it is advantageous to retain the categorization of the wave types as for a layer with free surfaces.

1.4.1 Determination of the characteristics of rigidity and elasticity using detailed measurement

If the measurement of the phase velocities of stress-wave propagation is conducted on pavement structures after the schemes of Figs. 1.47–1.52 and over a wide frequency range (35–35000 Hz), the results of the testing will have the form of dispersion curves. Their variation with frequency or wavelength makes it possible to assess the characteristics of elasticity and stiffness of the pavement structures.

Typical results of measurements on rigid pavement structures [1.43], [1.44] are in Figs. 1.53 and 1.54. The structure of the pavement layers was as follows: 22 cm thick cement concrete surfacing, 5 cm thick coated sand and gravel, 12 cm thick layer of bitumen stabilization, and 8 cm thick layer of lime stabilization. The total thickness of the pavement structure is 47 cm.

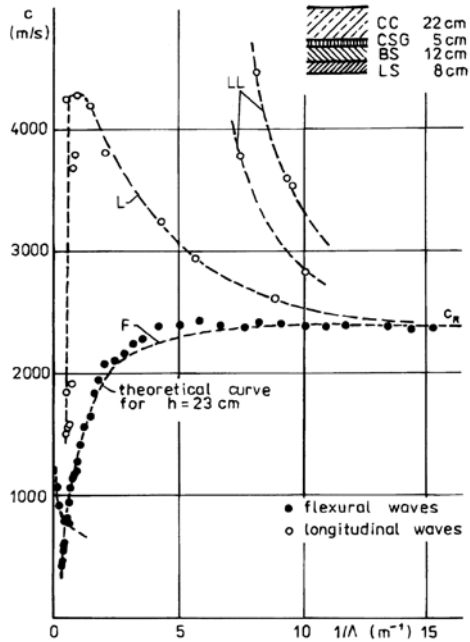

Fig. 1.53. Typical results of phase velocity measurement in rigid pavement.

According to the results in Fig. 1.53 the velocity of surface waves at high frequencies is c_R=2420 m/s. The corresponding velocity of longitudinal waves $c_0 = \sqrt{E/\varrho}$ can be

obtained according to the ratios in Table 1.1. Provided that μ=0.20, the value of velocity c0 will be $c_0=c_R/0.587$=4120 m/s. It is simple to determine the modulus of elasticity E for pavement cement concrete surfacing using the formula $E = c_0^2\varrho$ if we know or suppose the density ρ.

By the variation of the dispersion curve for flexural waves F and comparison of the experimental values with the theoretical ones, the equivalent thickness of the pavement structure may be determined. At very low frequencies a part of the dispersion relation S is formed that corresponds to stress waves propagated in the stabilization layers. The basic dispersion curve of longitudinal waves L has the same characteristic course as the free layer,

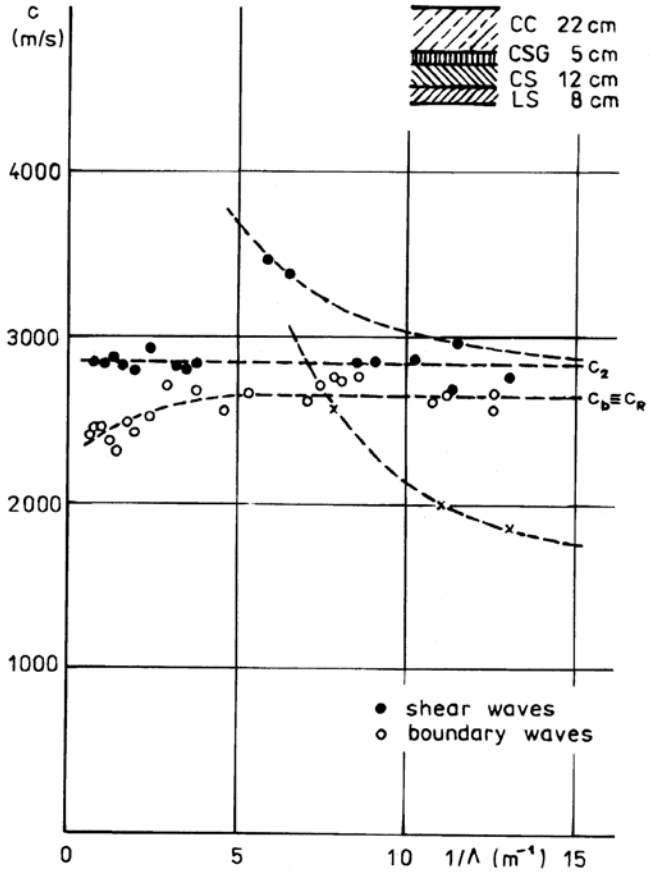

Fig. 1.54. Results of measurement of shear and boundary-surface-wave velocities on rigid pavement.

but at low frequencies the velocities radically decrease under the influence of the contact with the subgrade and approach the velocity of the surface waves in the subgrade. Part of the measured velocities forms the higher modes of dispersion curves LL.

The phase velocities in Fig. 1.53 were measured using the schemes of Figs. 1.47 and 1.48. The measured velocity values according to the schemes of Figs. 1.49 and 1.50 are plotted in Fig. 1.54. It is shown that the mean value of the shear-wave velocity c_2 according to the basic mode is c_2=2850 m/s, and the velocity of the boundary Rayleigh waves at high frequencies is c_{bound}=2400–2600 m/s.

The experimental values indicated by cross marks belong to the stress waves that propagate in the interlayer of coated sand and gravel or the bitumen stabilization layer. At high frequencies the dispersion curve approaches the velocity of shear waves $c_2 = \sqrt{G/\varrho}$ for these materials.

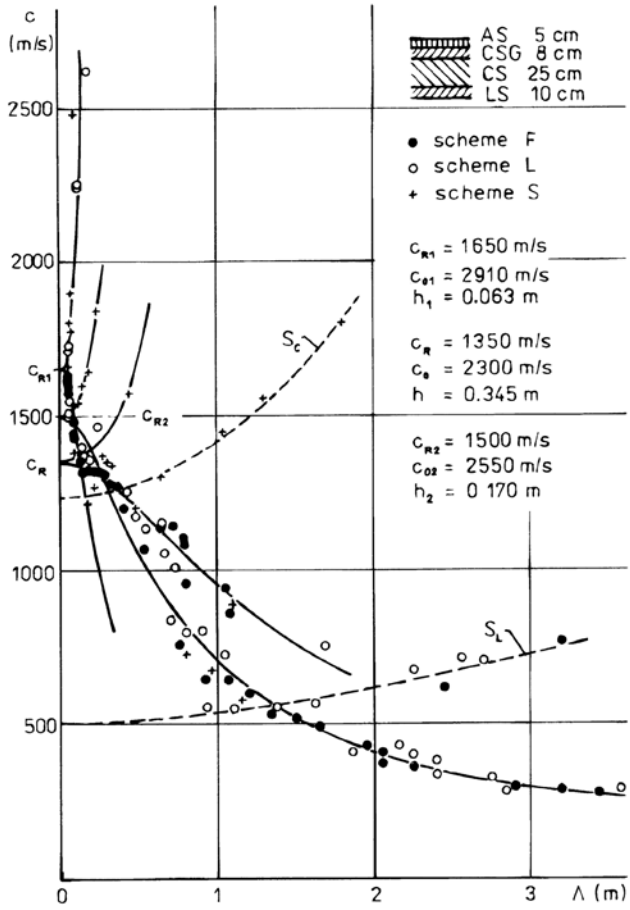

Fig. 1.55. Typical results of phase velocity measurement on flexible pavement.

On the sections of flexible pavement structures the phase velocities of stress waves propagation may be measured according to the scheme in Fig. 1.47 for flexural waves. It is convenient to complete these results by measuring according to the schemes in Figs. 1.51 and 1.52. All these schemes can be indicated as schemes F, L, S.

Typical results of detailed measurement in the frequency range 35–35000 Hz on the section of flexible pavement are shown in Fig. 1.55. The structure of the pavement layers was as follows: 5 cm thick asphalt surfacing, 8 cm thick bitumen-coated sand and gravel, 10 cm thick layer of cement stabilization (better quality), 15 cm thick layer of cement stabilization, and 10 cm thick layer of lime stabilization. The thickness of the pavement structure was 48 cm.

The results in Fig. 1.55 show that in the frequency range 35000–8000 Hz the greatest part of the frequency was propagated in the surface layer of asphalt surfacing, when the velocity of surface waves $c_{R_1} = 1650$ m/s and corresponding to a pavement surface temperature T=23–28 °C. The velocity of longitudinal wave $c_{01} = \sqrt{E/\varrho}$ supposing μ=0.30 will be c_{01}=2910 m/s. The mean thickness of the equivalent free layer, evaluated according to the experimental results, is h_1=0.063 m.

In the frequency range 8000–800 Hz the pavement structure acts as a whole and the flexural waves and their velocities represent the whole stiffness of the pavement. The corresponding velocity of surface waves c_R for the equivalent free layer, which represents the whole dynamic stiffness, is determined by the value c_R=1350 m/s. Then c_0=2300 m/s if μ=0.20 or c_0=2380 m/s if μ=0.30 and the thickness of the equivalent free layer is h_2=0.345 m.

In the frequency range 800–50 Hz the decisive part of the vibration energy of flexural waves probably propagates in the layers of asphalt surfacing and bitumen-coated sand and gravel, having the velocity c_{R2}=1500 m/s, c_{02}=2640 m/s and the thickness of equivalent free layer h_2=0.170 m.

Theoretical variations in the dispersion curves of flexural and longitudinal waves are drawn for all three response cases in Fig. 1.55 as solid lines.

The broken dispersion lines in Fig. 1.55 following the experimental results, belong to stress waves propagating in the layers lime stabilization layer (curve S_l) and in the cement stabilization layers (curve S_c). They have the typical form of dispersion curves for shear waves, which approach at high frequencies the velocity of shear waves c_2: hence for the lime stabilization layer c_2=500 m/s and for the cement stabilization layer c_2=1240 m/s.

In view of the complicated interpretation of the experimental results on flexible pavements, detailed measurements was accomplished on seven different flexible pavements of the circular test track [1.45].

The measurement procedure was chosen according to the schemes in Figs. 1.47, 1.51 and 1.52, which can be indicated as schemes F, L and S. At some frequencies, in particular at lower frequencies, measurement according to schemes L and S is not possible. The results for measured phase velocities are the same for all three schemes at a considerable number of frequencies. But in many cases the values of phase velocity measured according to schemes L and S are different compared with the velocity c obtained according to scheme F and contribute decisively to the generallization of the dispersion knowledge for stress-wave propagation of various kinds.

It is necessary to call attention to a phenomenon that was recorded by the measurement and evaluation of phase differences. In some cases the points of the phase diagram do not present only one linear dependence of the phase angle φ with the distance l; at a certain distance, the measured values create another linear dependence (Fig. 1.56). This signifies that two different wavelengths Λ_1, Λ_2 and two corresponding phase velocities can be evaluated from the measurements.

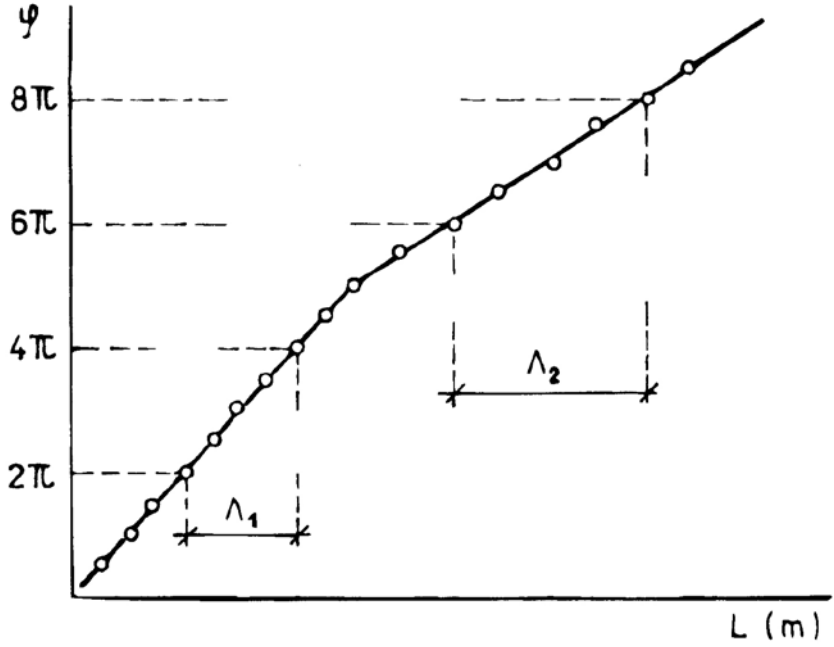

Fig. 1.56. Phase diagram showing two kinds of stress wave.

The subgrade of the pavement sections was created from clayed earth. The structure of the pavement sections was as follows:

Section 1:	closed asphalt carpet	CAC	4 cm
	bitumen-coated sand		
	and gravel	BSG	20 cm
	sand and gravel	SG	20 cm
			44 cm
Section 2:	closed asphalt carpet	CAC	4 cm
	coated sand and gravel	CSG	20 cm
	cement stabilization	CS	20 cm
			44 cm
Section 3:	closed asphalt carpet	CAC	4 cm
	coated sand and gravel	CSG	20cm
	open asphalt carpet	OAC	20cm
	mastic asphalt membrane	MA	2 cm
			44 cm

Section 4:	closed asphalt carpet	CAC	4 cm
	coated sand and gravel	CSG	10 cm
	coated tuff	CT	20 cm
	lime stabilization	LS	15 cm
			49cm
Section 5:	asphalt concrete	AC	8 cm
	coated sand and gravel	CSG	10 cm
	coated crushed material	CCM	5 cm
	cement stabilization	CS	20 cm
	lime stabilization	LS	15 cm
			58 cm
Section 6:	asphalt concrete	AC	8 cm
	coated sand and gravel	CSG	10 cm
	cement stabilization	CS	17 cm
	sand and gravel	SG	15 cm
			50cm
Section 7:	mastic asphalt	MA	4 cm
	asphalt concrete	AC	5 cm
	cement concrete	CC	15 cm
			24 cm

Using the phase velocity method the measurements were made in the frequency range 50–35000 Hz. The results are plotted in Figs 1.57– 1.63 in the form of variations of phase velocity c with the wavelength Λ. The marks F, L indicate the dispersion curves of flexural and longitudinal waves when the pavement structure acts as a whole, the marks F_1, L_1 indicate the dispersion curves of flexural and longitudinal waves when only the surfacing pavement layer is active; and the S_k dispersion curves relate to the shear-wave propagation in the interlayers. The k subscript marks the k th layer, numbered from the top down. The temperature T of the pavement surface is also indicated. The assessed variation of dispersion curves are in all cases in agreement with the structure of the tested pavement sections.

Interpretation and exploitation possibilities of the detailed measurement results

In general it can be stated that, on rigid pavements, it is possible to find out the velocities of flexural, longitudinal, shear and boundary waves. The dynamic moduli of elasticity for the material of the concrete plate of rigid pavements will be calculated according to the values of the measured velocities of surface waves c_R, the velocities of shear waves c_2 or the velocities of boundary waves c_{bound}. The velocity of surface waves c_R is the value that the basic dispersion curves of phase velocity for flexural and longitudinal waves achieve, at high frequencies or (which is the same thing) at small wavelengths. The velocity $c_0 = \sqrt{E/\varrho}$ will be determined according to the theoretical ratios in Table 1.1. Then the dynamic modulus of elasticity E is given by the relationship

$$E = c_0^2 \varrho \tag{1.56}$$

if ρ is the density of the surfacing concrete material.

The shear modulus of elasticity G will be determined according to the measured value of shear-wave velocity c_2 by the relationship

$$G = c_2^2 \varrho. \tag{1.57}$$

The equivalent thickness of the pavement, h, and the dynamic flexural rigidity of the pavement structure is determined by using the experimental results of the dispersion curve for flexural waves and their comparison with the theoretical values according to equation (1.13) or Table 1.2. The equivalent thickness is greater than the thickness of the cement concrete surfacing if the contact of the surfacing is with the underlying structure. In the case of failed contact the equivalent thickness is practically equal to the thickness of the concrete surfacing.

The characteristic feature of the measurement results on flexible pavements is that the measured velocities of stress-wave propagation form dispersion curves of flexural and longitudinal waves of a double kind. The curves F_1 and L_1 are related to the surface part of the pavement structure whereas the dispersion curves F and L correspond to the pavement structure as a whole.

The velocities of surface waves in the surface part of the pavement, c_{R1}, and the velocity of surface waves, c_R, which corresponds to the activity of the whole pavement structure, will be determined according to the variation of dispersion curves at high frequencies. These values c_{R1} and c_R, as shown in Figs. 1.57–1.63, are influenced by the temperature

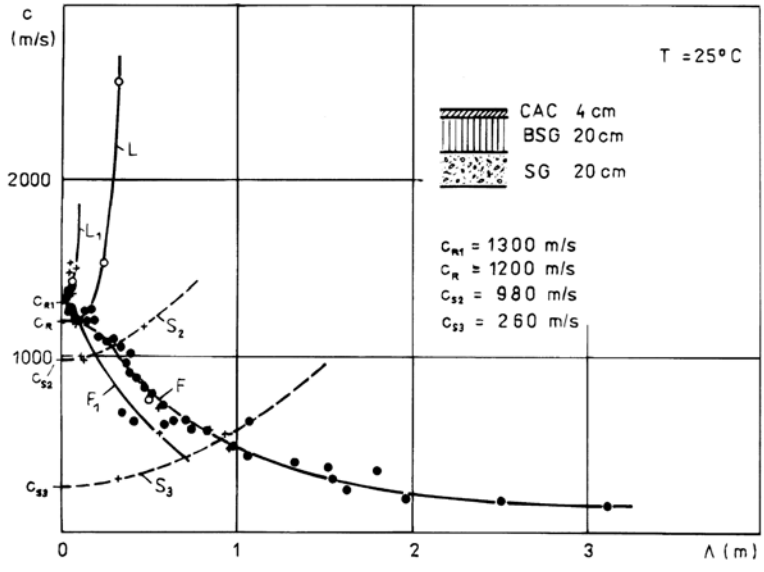

Fig. 1.57. Measured phase velocities on pavement section 1.

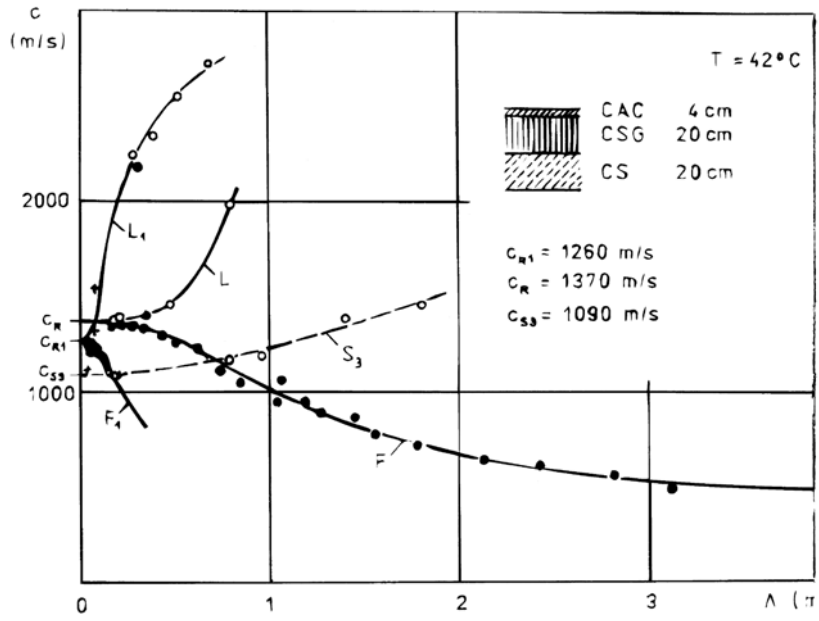

Fig. 1.58. Measured phase velocities on pavement section 2.

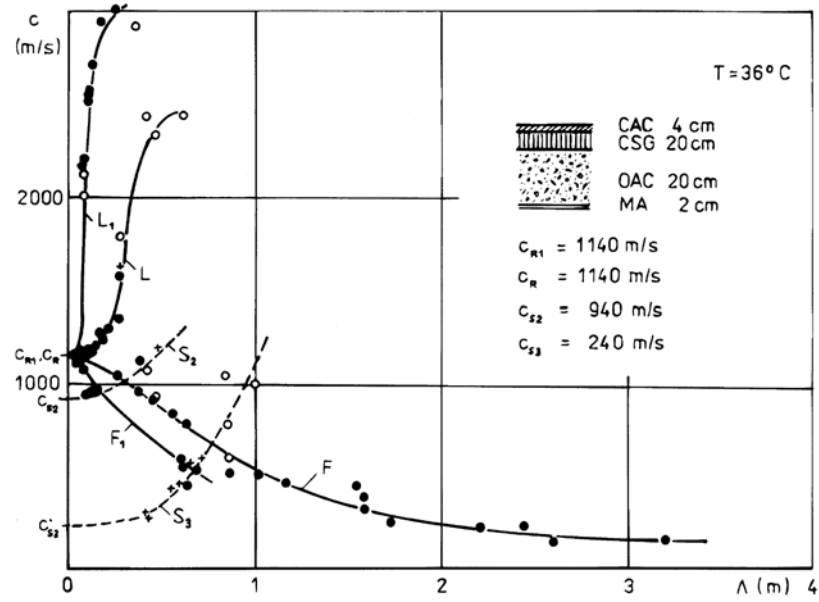

Fig. 1.59. Measured phase velocities on pavement section 3.

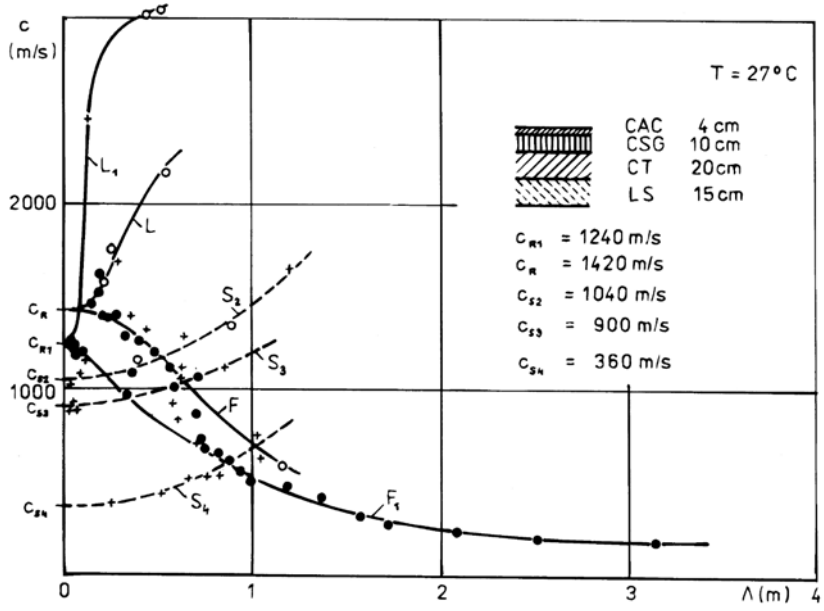

Fig. 1.60. Measured phase velocities on pavement section 4.

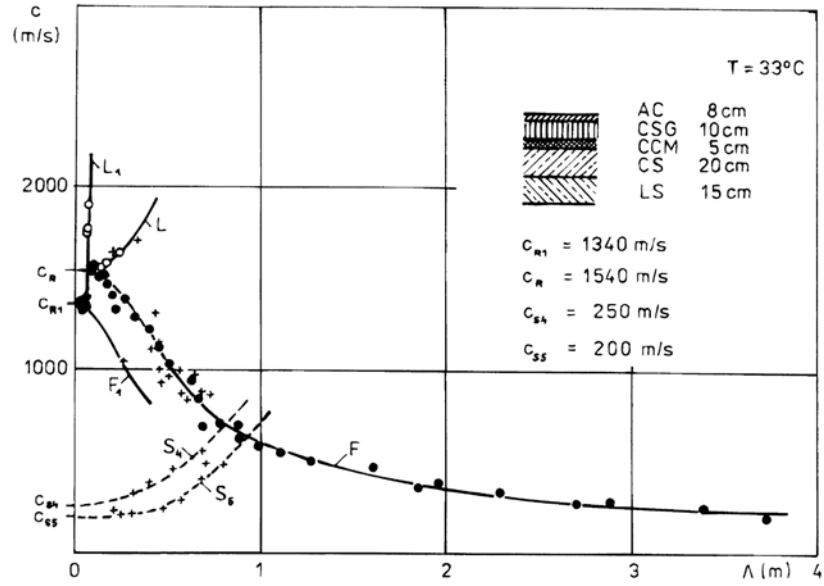

Fig. 1.61. Measured phase velocities on pavement section 5.

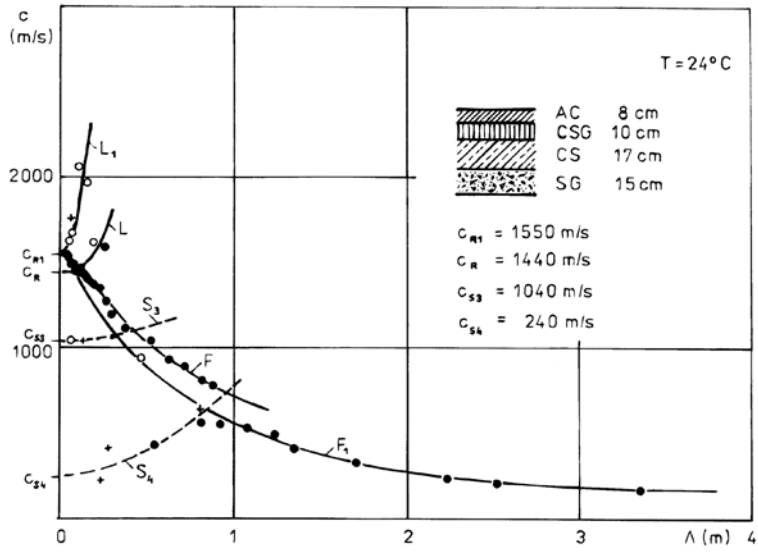

Fig. 1.62. Measured phase velocities on pavement section 6.

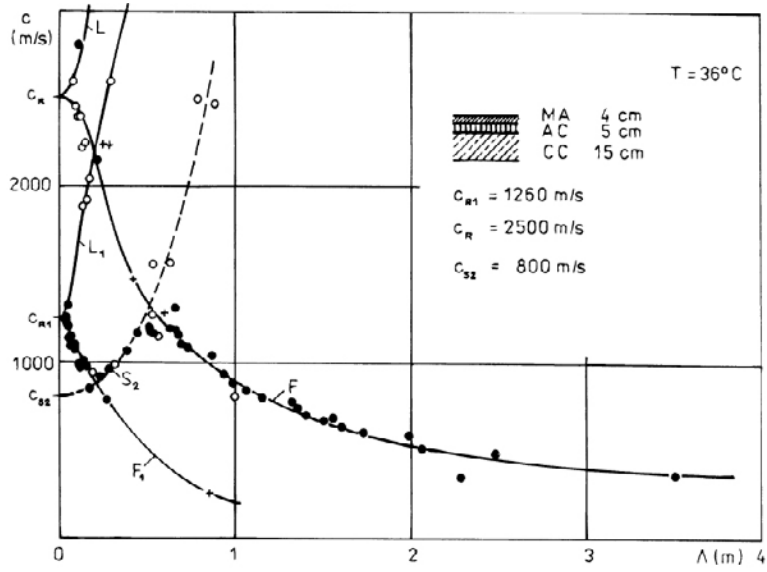

Fig. 1.63. Measured phase velocities on pavement section 7.

of the material. Except for sections 1 and 6, when the temperature of the surface material does not differ from the temperature of the rest of the structure, the velocities c_{R1} of all the pavement sections have lower values in comparison with c_R as a consequence of the higher temperature of the surfacing material.

The measured values of c_{R1} and c_R make it possible to determine the velocities c_0 and the variation of phase velocity c for flexural waves with the wavelengths Λ as a base for the determination of the mean equivalent thickness h_1 or h.

The procedure for the evaluation of the equivalent thickness is given in references [1.10] and [1.13]. In view of the laborious evaluation of this parameter, the generalized procedure will be given here.

Guillemin [1.8] presented the interpretation of the measured results of flexural-wave velocities, expressing the dispersion curve by the exponential relationship

$$\frac{c}{c_R} = A e^{B(\Lambda/h)} \tag{1.58}$$

where A, B are functions of the minimal velocities ratio c/c_R. The mean equivalent thickness h and the velocity of surface waves, c_R, are determined by using the set of measured values Λ of c and specially compiled nomograms. It is necessary to remark that the results of this measurement do not cover the high-frequency range and not permit the determination of the value of c_R with acceptable precision.

The results of our measurements, which were effected in the frequency range to 35000 Hz, make it possible to assess the values of c_{R_1} and c_R quite precisely, especially if the dispersion curves F_1, L_1 or F, L are formed. In these conditions it is more advantageous to start from the known values of surface-wave velocities c_{R_1} and c_R, and to determine the equivalent thicknesses h_1 and h by using the Lamb dispersion curve.

The basic dispersion curve for flexural stress waves in the free layer is expressed by the simple relationships in equations (1.13)—(1.18). From the equation (1.13) the relationship of the wavelength Λ to the layer thickness h and phase velocity c is expressed in the form

$$\Lambda = h\left[(\phi\left(1 + \phi_1 + \frac{c^2}{c_0^2} + \phi_2\frac{c_0^2}{c^2}\right)\right]^{1/2} \tag{1.59}$$

where ϕ, ϕ_1 and ϕ_2 are functions of Poisson's ratio μ, given by the relationships

$$\phi = -\pi^2\left[\frac{2}{3\kappa_0(1-\mu)} + \frac{1}{3}\right] \tag{1.60}$$

$$\phi_1 = -\frac{2(1-\mu^2)}{2+\kappa_0(1-\mu)} \tag{1.61}$$

$$\phi_2 = \frac{-\kappa_0}{2(1+\mu)+\kappa_0(1-\mu^2)} \tag{1.62}$$

and κ_0 is determined by equation (1.17).

For $\Lambda/h \to 0$ the phase velocity c approaches the velocity of surface waves, c_R, and is given according to equation (1.13) by the relationship

$$\frac{c_R}{c_0} = \sqrt{\frac{\kappa_0}{2(1+\mu).}} \tag{1.63}$$

All these equations are necessary for the evaluation and interpretation of the measured results according to the basic dispersion curve of flexural stress waves.

The input data are:

c_R—determined by measurement

μ—approximated or determined on specimens the set of measured wavelengths and phase velocities *c:*

Λ_1, c_1

Λ_2, c_2

.

.

.

Λ_n, c_n

The output data describing the characteristics of pavement structure are:

1. the velocity c_0 calculated according to the relationship

$$c_0 = c_R \sqrt{\frac{2(1+\mu)}{\kappa_0}}$$

if

$$\kappa_0 = \left(\frac{0.87 + 1.12\mu}{1+\mu}\right)^2$$

2. the individual thicknesses of equivalent layer h_i, calculated according to the equation

$$h_i = \Lambda_i \left[\frac{1}{\phi\left(1 + \phi_1 \frac{c_i^2}{c_0^2} + \phi_2 \frac{c_0^2}{c_i^2}\right)}\right]^{1/2}$$

if, ϕ, ϕ_1, ϕ_2 are given in the form (1.60), (1.61), (1.62)

3. the mean value of equivalent thickness h given by the relationship

$$h = \frac{\sum_{i=1}^{n} h_i}{n}$$

4. the dynamic stiffness of the unit pavement strip EJ reduced by density ϱ calculated according to the relationship

$$\frac{EJ}{\varrho} = \frac{c_0^2 h^3}{12} \tag{1.64}$$

5. the values of wavelengths Λ_k for theoretical variations of dispersion curve corresponding to the thickness h calculated according to the relationship

$$\Lambda_k = h\left[\phi\left(1 + \phi_1 \frac{c_k^2}{c_0^2} + \phi_2 \frac{c_0^2}{c_k^2}\right)\right]^{1/2}$$

where $c_k = kc_R$, if k=0.9, 0.8, 0.7,…,0.1.

The outlined procedure was used for the evaluation of measured results on seven pavement sections on the circular test track. The characteristics of the equivalent surface layer and the layer that is equivalent to the whole pavement structure are presented in Table 1.17.

Table 1.17. Evaluation of measurement on pavement sections of the circular test track.

Section number	Surface layer				Whole structure			
	c_R (m/s)	c_0 (m/s)	h (m)	EJ/ϱ	c_R *(m/s)*	c_0 *(m/s)*	h *(m)*	EJ/ϱ
1	1300	2209	0.096	363	1200	2039	0.159	1400
2	1260	2141	0.122	687	1370	2328	0.405	29950
3	1140	1937	0.110	421	1140	1937	0.176	1714
4	1240	2107	0.136	935	1420	2413	0.246	7210
5	1340	2280	0.114	638	1540	2617	0.157	2192
6	1550	2634	0.106	696	1440	2447	0.179	2870
7	1260	2141	0.057	70	2500	4248	0.123	2785
EJ in Nm^2; density ϱ in kg/m^3								

The experimental results obtained by detailed measurement on the pavement structures form dispersion curves of type S, which correspond to shear stress waves propagating through the interlayers of the pavement. The common feature of dispersion curves S is that the phase velocity c decreases with decreasing of wavelength Λ and comes asymptotically near the velocity of shear waves $c_s = \sqrt{G/\varrho}$ in the interlayer. This velocity c_s may be used as the bass for the determination of the elasticity characteristic of the interlayer material.

It is convenient to use the empirical formula for the relationship between velocity c and the wavelength Λ in the form

$$c = A + B\Lambda^2 \tag{1.65}$$

The parameters *A, B* will be obtained by the method of least squares from experimental values

$$A = \frac{\sum c - B\sum \Lambda^2}{n} \tag{1.66}$$

$$B = \frac{\sum c\Lambda^2 - \sum c \sum \Lambda^2/n}{\sum \Lambda^4 - \left(\sum \Lambda^2\right)^2/n} \tag{1.67}$$

where n is the number of experimental values.

The value of phase velocity c_s is the phase velocity c for $\Lambda \to 0$; then according to equation (1.65) it follows that

$$c_s = A. \tag{1.68}$$

1.4.2 Simplified procedures for assessment of the elasticity and rigidity characteristics of pavement structures

The most general and most significant characteristic is the dynamic flexural stiffness of the pavement structure, which can be determined according to the measured variation of the dispersion curve for flexural stress waves and its comparison with the theoretical one. The dynamic flexural stiffness EJ of pavement structures is given by equation (1.64). It can be seen that this characteristic of the equivalent layer corresponding to the pavement structure is given by two unknown parameters: the thickness of the equivalent layer, h, and the velocity $c_0 = \sqrt{E/\varrho}$. Therefore only two values of phase velocity c and wavelength Λ determined at two frequencies, are needed for their calculation [1.12, 1.45].

If the phase velocity c and wavelength Λ measured at the first frequency f_a are denoted by c_a, Λ_a and at the second frequency f_b by c_b, Λ_b, then according to equation (1.59) two equations may be written. From these equations a biquadratic equation is performed for the calculation of the value c_0, which is established from the equation

$$c_0^2 = \frac{-(\eta - 1) \pm \left[(\eta - 1)^2 - 4\phi_1\phi_2(\eta c_a^2 - c_b^2)\left(\eta/c_a^2 - 1/c_b^2\right)\right]^{1/2}}{2\phi_2\left(\eta/c_a^2 - 1/c_b^2\right)}. \tag{1.69}$$

The positive sign before the square root in equation (1.69) is valid if $c_a < c_b$, whereas the negative sign is valid if $c_a > c_b$.

The ratio η is given in the form

$$\eta = \frac{\Lambda_b^2}{\Lambda_a^2} \tag{1.70}$$

By using the calculated value c_0 the second characteristic-equivalent thickness h is determined according to equation (1.59).

The choice of frequencies

The best approximation of the dispersion curve of flexural stress waves that describes the characteristics and dynamic stiffness of the pavement structure can be stated if the measurement is carried out at two frequencies that are sufficiently far apart.

The most suitable frequencies for rigid pavements are f_a=20000 Hz and f_b=250Hz.

When measuring flexible pavements or pavements under construction the best frequency f_b is 250 Hz. The choice of the frequency f_a depends on the condition that the measured wavelength Λ_a is shorter than 1/10 of the wavelength Λ_b. Sometimes the frequency f_a=10000 Hz is satisfactory.

Comparison of simplified procedures with detailed measurement

The results of detailed measurement on five different sections of rigid pavement structures are in reference [1.44]. A comparison of the characteristics of the equivalent layer and the dynamic stiffness according to the detailed measurement and measurement at only two frequencies is given in Table 1.18.

Table 1.18. Comparison of rigid pavement characteristics according to detailed and simplified measurement.

Section number	Detailed measurement			Simplified procedure		
	h (m)	c_0 (m/s)	EJ/ϱ	h *(m)*	c_0 *(m/s)*	EJ/ϱ
1	0.176	4460	8990	0.169	4610	8580
2	0.230	4096	17100	0.220	4310	16400
3	0.176	4250	8170	0.171	4340	7860
4	0.217	4210	15050	0.191	4350	11050
5	0.229	4040	16300	0.210	4190	13600
EJ in Nm^2; density ϱ in kg/m^3						

A comparison of the characteristics of the equivalent layer according to the detailed and simplified procedures on seven sections of flexible pavements of the circular test track is given in Table 1.19.

Table 1.19. Comparison of flexible pavement characteristics according to detailed and simplified measurement.

Section number	Detailed measurement			Simplified procedure		
	h (m)	c_0 (m/s)	EJ/ϱ	h *(m)*	c_0 *(m/s)*	EJ/ϱ
1	0.159	2039	1400	0.159	2100	1480
2	0.405	2328	29950	0.386	2380	27200
3	0.176	1937	1714	0.181	1998	1975
4	0.246	2413	7210	0.153	1650	2080
5	0.157	2617	2192	0.154	2820	2420
6	0.179	2447	2870	0.189	2500	3520
7	0.123	4248	2785	0.171	3990	6630
EJ in Nm^2; density ϱ in kg/m^3						

It can be seen that the characteristics of the equivalent pavement structures determined by using the simplified procedure at two frequencies correspond very well to the values obtained by detailed measurement on rigid and flexible pavements. More substantial differences are only found in sections 4 and 7 of the flexible pavements. But section 7 has a special structure and on pavement section 4 the dispersion curve representing the whole flexural rigidity was determined only in a narrow frequency range.

1.4.3 Evaluation of the rigidity of layered pavements using deflection determined by means of stress-wave velocities

The dispersion curve of quasi-flexural stress waves gives the variation of the phase velocity of flexural waves with the wavelength or frequency. The position and the shape of the dispersion curve plotted as phase velocity c versus wavelength Λ depend on the rigidity of the pavement structure and on the rigidity of the subgrade. At short wavelengths, i.e. at high frequencies, the dispersion curve goes from the value of phase velocity c_R in the surface layer of the pavement. As the wavelenght increases, the phase velocity decreases, and at $\Lambda \rightarrow \infty$, i.e. at very small frequencies, the phase velocity approaches the value c_{Rs}, which corresponds to the velocity of surface Rayleigh waves in the subgrade. The characteristic form of the dispersion curve in a pavement lying on a subgrade is indicated in Fig. 1.64.

The theoretical solution and in particular the numerical results for the case of propagation of quasi-flexural waves in a layer lying on a subgrade has not yet been obtained because of the excessive complexity of the frequency transcendental equation. The characteristic form of the dispersion curve in Fig. 1.64 was confirmed not only by means of pavement measurements but also by detailed experimental study on plane models.

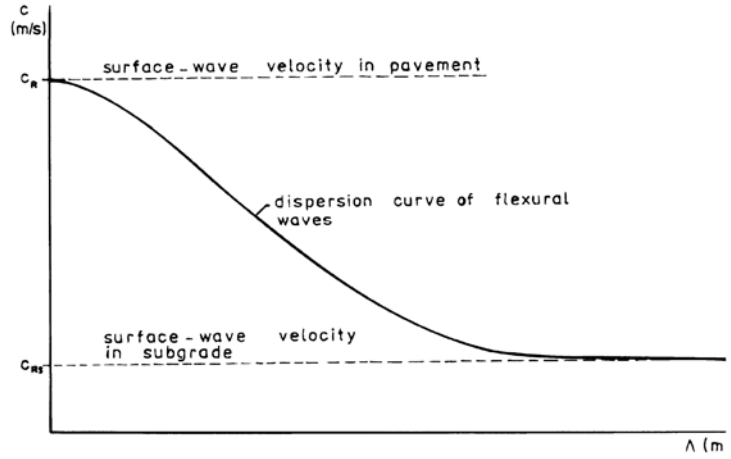

Fig. 1.64. Form of dispersion curve for quasi-flexural stress waves in layered pavement structure lying on subgrade.

In some cases, especially in flexible pavements, the continual variation of the dispersion curve may be interrupted as a consequence of imperfect contact of the pavement layers.

These irregularities are, however, a reflection of the real activity of the pavement structure and its dynamic stiffness.

The variation of the dispersion curve for quasi-flexural stress waves is, in a certain wavelength range, identical with the form of the dispersion curve for flexural waves in the equivalent layer with free boundaries. At large wavelengths it deviates from this and approaches asymptotically the wave velocity in the subgrade, c_{Rs} (Fig. 1.65).

So it is possible to suppose that for $\Lambda<\Lambda_1$ the pavement structure acts as the equivalent plate with thickness h and stiffness $EJ = c_0^2 h^3 \varrho/12$, while the velocity of longitudinal waves, c_0, and the thickness of the equivalent plate, h, follow from the variation of the dispersion curve. The corresponding algorithm for the determination of c_0 and h was given in sections 1.4.1 and 1.4.2. At wavelengths $\Lambda>\Lambda_1$ the influence of the pavement structure is practically negligible and the system acts as a half-space with the characteristics of the subgrade.

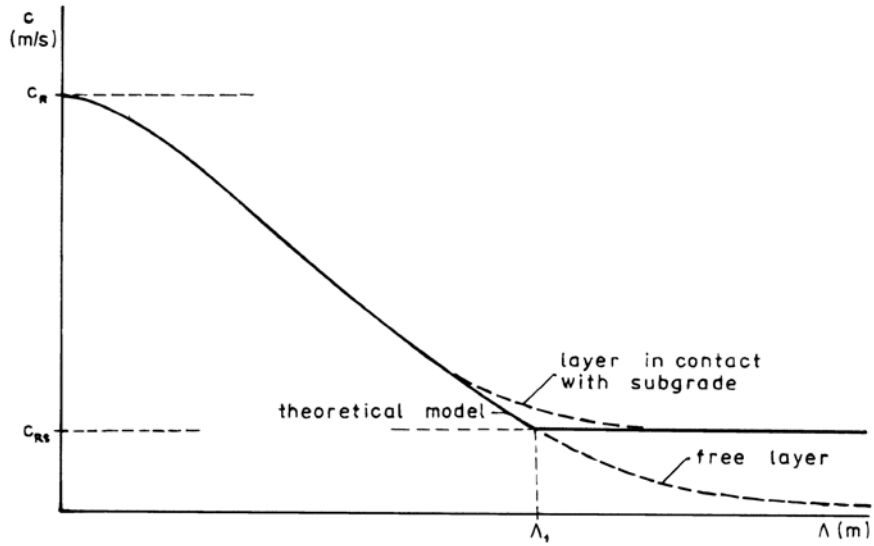

Fig. 1.65. Theoretical dispersion curve for layered pavement on subgrade for use in pavement deflection computation.

From these facts about the response of pavement structures, which are confirmed by the results of the phase velocity method, we shall attempt further to derive the theory and method of rigidity evaluation for layered pavement structures using the deflection determined according to the results of measurement by the phase velocity method of stress-wave propagation.

What are the advantages of the method of pavement rigidity evaluation by deflection? Above all, the evaluation of pavement rigidity by deflection has been, until now the usual procedure for classifying the rigidity and quality of pavements. It includes the subgrade reaction, whereas the dynamic stiffness of the pavement is the principal characteristic that evaluates the pavement structure proper.

Deflection assessment from the results of non-destructive testing using the phase velocity method removes the need for the laborious determination of deflection characteristics with costly loading tests. It also eliminates the inaccuracy in the determination of deflection data influenced by the load time because it uses parameters obtained in a defined dynamic regime.

The formation of the procedure for pavement rigidity evaluation using deflection requires the derivation of theoretical relationships of deflection for the half-space and the plate that is equivalent to a layered pavement structure, under a normal load in a circular area with radius *a*. It is necessary to state the coherence of these theoretical relationships with the characteristics of flexural stress-wave propagation in the pavement lying on the subgrade. The synthesis will determine the resulting relationship for deflection on the basis of parameters ascertained by the phase-velocity method on real structures.

The procedure, which is developed in detail in [1.14], gives the relationships for pavement deflection w and curvature Δ under normal vertical load p_0, uniformly distributed on a circular contact area with radius a, in the form

$$w = \frac{p_0(1-\mu_s)a}{c_{2s}^2 \varrho_s} \int_0^{\eta_1} \frac{J_1(\eta)}{\eta} \mathrm{d}\eta + \frac{p_0 a^2}{\varrho h} \int_{\eta_1}^{\infty} \frac{J_1(\eta)}{\eta^2 c^2} \mathrm{d}\eta \tag{1.71}$$

$$\Delta = \frac{p_0(1-\mu_s)}{c_{2s}^2 \varrho_s a} \int_0^{\eta_1} \eta J_1(\eta) \mathrm{d}\eta + \frac{p_0}{\varrho h} \int_{\eta_1}^{\infty} \frac{J_1(\eta)}{c^2} \mathrm{d}\eta \tag{1.72}$$

where $J_1(\eta)$ is a Bessel function of the first kind, first order with real argument η.

The limit value η_1, corresponding to the wavelength Λ_1, is determined from the condition of deflection equality for the equivalent layer and half-space according to the relationship

$$\eta_1 = \sqrt[3]{\frac{12 c_{2s}^2 \varrho_s (1+\mu_s)}{h^3 c_0^2 \varrho}}. \tag{1.73}$$

In the equations (1.71) and (1.72) c_{2s} is the velocity of shear waves in the subgrade, μ_s and ϱ_s are Poisson's ratio and density respectively for the subgrade material, and ϱ, h and c_0 are characteristics of the equivalent layer. The phase velocities c are given in the form

$$c^2 = c_0^2 \left(p - \sqrt{p^2 - q} \right) \tag{1.74}$$

if

$$p = \frac{1}{2(1-\mu^2)} + \frac{\kappa_0}{4(1+\mu)} \left(1 + \frac{12a^2}{h^2 \eta^2} \right) \tag{1.75}$$

$$q = \frac{\kappa_0}{2(1-\mu^2)(1+\mu)} \tag{1.76}$$

κ is given by the equation (1.17) and μ is Poisson's ratio for the equivalent plate material.

In the case of normal loading with intensity p_0 through a rigid circular slab, the stress distribution on the contact area does not correspond to a uniform load distribution. The pavement deflection in the loaded area, w_0, is given in the form

$$w_0 = \frac{p_0 a(1-\mu_s)}{2c_{2s}^2 \varrho_s} \int_0^{\eta_1} \frac{\sin\eta}{\eta} d\eta + \frac{p_0 a^2}{2\varrho h} \int_{\eta_1}^{\infty} \frac{\sin\eta}{\eta^2 c^2} d\eta. \tag{1.77}$$

It follows from the structure of the relationships for deflections w, w_0 or curvature Δ that these values can be calculated according to the characteristics assessed by using the algorithms of paragraphs 1.4.1 or 1.4.2. The calculation of w, w_0 or Δ may be realized by applying computers.

Let us now apply this procedure for pavement calculation to the pavement sections of the circular test track. For this purpose we can use the results of the simplified measurements which are given in Table 1.18. The values of deflection w and curvature Δ calculated according to equations (1.71) and (1.72) and deflection w_0 calculated according to equation (1.77) are listed in Table 1.20. The following input data were substituted: c_{2s}=160 m/s, μ_s=0.40, ϱ_s=1800 kg/m^3, μ=0.30, ϱ=2200 kg/m^3, a=0.178 m. .

Table 1.20. Deflections and curvatures of pavement sections computed according to the measured phase velocities.

Section number	Deflection w (m)	Curvature Δ (m^{-1})	Deflection w_0 (m)
1	$0.1168\times10^{-2}p_0$	$0.1556\times10^{-1}p_0$	$0.8855\times10^{-3}{}_{P0}$
2	$0.5701\times10^{-3}p_0$	$0.2223\times10^{-2}p_0$	$0.3905\times10^{-3}p_0$
3	$0.1082\times10^{-2}p_0$	$0.1270\times10^{-1}p_0$	$0.8191\times10^{-3}p_0$
4	$0.1056\times10^{-2}p_0$	$0.1173\times10^{-1}p_0$	$0.8052\times10^{-3}p_0$
5	$0.1005\times10^{-2}p_0$	$0.1021\times10^{-1}p_0$	$0.7715\times10^{-3}p_0$
6	$0.9391\times10^{-3}p_0$	$0.8534\times10^{-3}p_0$	$0.6954\times10^{-3}p_0$
7	$0.7583\times10^{-3}p_0$	$0.4493\times10^{-2}p_0$	$0.5881\times10^{-3}p_0$
Normal load intensity p_0 in MPa			

Table 1.21. Comparison of pavement deflections determined using different methods.

Section number	Deflections w (mm)					
	Static testing		Damped impact testing	Benkelman's deflectograph	Phase velocity method	
	T (°C)	w			w	T (°C)
1	27	0.72 (0.13–0.14)	(0.135–00.389) 0.207 (0.059–0.144)	(0.662–1.115) 0.9145 (0.170–0.530)	0.585	25
2	18	0.135 (0.26–0.30)	0.107 (0.081–0.178)	0.318 (0.260–1.215)	0.285	42

3	18	0.28	0.122 (0.071–0.146)	0.622 (0.365–1.41)	0.541	36
4	21	0.44 (0.21–0.41)	0.109 (0.056–0.083)	0.694 (0.381–1.182)	0.528	27
5	18.5	0.31	0.073 (0.052–0.26)	0.745 (0.466–1.58)	0.502	33
6	30	0.35 (0.14–0.31)	0.147 (0.054–0.616)	0.937 (0.052–0.446)	0.469	24
7	38	0.225	0.235	0.269	0.397	36

The pavement section rigidity, expressed by using w or Δ, gives the sequence: 2, 7, 6, 5, 4, 3, 1. Pavement section 2 presents the highest dynamic stiffness, section 1 the lowest.

The results of deflection measurements on these pavement sections by static tests using the load bridge, Benkelman deflectograph and by damped impact tests with a pulse time of 0.03 s are in the study [1.46]. Table 1.21 gives a survey of measured deflection values in mm under a normal load intensity of 0.5 MPa: the range of measured values (in parenthesis) and the mean values. The deflections determined according to the measured phase velocities are given in the last column of the table.

The measured deflection values using the damped impact test or Benkelman deflectograph display a considerable dispersion. A comparison is possible only with the values of the static test or with the mean values of all measurements. Table 1.22 gives a survey of the comparative values. The deflection values obtained by the phase velocity method are compared with the mean values in the first three columns of the table. The temperature of the pavement section material was not considered. The classification of pavement sections is given by the sequence 2, 7, 6, 5, 4, 3, 1 for the phase velocity method and by 2, 7, 3, 5, 4, 6, 1 for the mean values of direct deflection measurements.

Table 1.22. Comparison of pavement deflections determined by the phase velocity method and by static testing.

Section number	w (mm) Mean values of all measurements	w (mm) w_0 (mm) Phase velocity method		w (mm) Static testing	w (mm) Phase velocity method (temperature correction)
1	0.614	0.585	0.443	0.72	0.595
2	0.186	0.285	0.180	0.135	0.165
3	0.341	0.541	0.409	0.28	0.451
4	0.414	0.528	0.403	0.44	0.498
5	0.376	0.502	0.385	0.31	0.442
6	0.478	0.469	0.348	0.35	0.499

The comparison of the deflections obtained according to the phase velocity method with the deflections of the static load test is given in the second half of Table 1.22. At the same time the deflections according to the phase velocitiy method were reduced at a comparable temperature by using the reduction 0.005 mm at 1 °C. The stiffness of the pavement section determines the sequence 2, 7, 5, 3, 4, 6, 1 for the phase velocity method and 2, 7, 3, 5, 6, 4, 1 for static load testing.

With the exception of section 1 the deflection values w, determined according to the phase velocity method, are a little greater than the values from the static tests. This follows from the fact, that these values are determined as the maximal deflection at r=0 by the supposition of a uniformly distributed normal load on the circular area, while the static deflections correspond to the mean values under the rigid load slab.

The values of deflections w_0 present good global agreement with the deflections obtained by direct measurement.

It can be gathered from these results that the comparisons demonstrate the reality and objectivity of pavement evaluation by the deflection based on the measured phase velocities of stress-wave propagation.

1.4.4 Diagnosis of dynamic elasticity and rigidity of highway pavement sections

Diagnostic measurements on highway pavement structures were performed over a few years in collaboration with construction enterprises. The aim of these measurements was to verify these advanced new procedures for the complex evaluation of dynamic elasticity and rigidity in layered pavement structures and to obtain qualitative parameters for highway construction.

Description of pavement structures, measurement results and evaluation

The structure of the pavement layers on highway sections was as follows: a 24 cm thick cement concrete plate, a 4 cm thick bituminous interlayer, a 15 cm thick cement stabilization layer, and a 35 cm thick layer of sand and gravel. The total thickness was 78 cm. The subgrade was formed of loess-clay material or clay-sand material with boulders.

Diagnostic measurements were made on pavement sections in which the cement concrete surfacing was manufactured half or one year ago. Table 1.23 gives some of the measurement results. The values of wavelengths and velocities Λ_a, Λ_b, c_a, c_b are the mean values from the measuring results on the inner and outer lanes. The atmospheric temperature was 6–10 °C**.**

A summary of the characteristics used to evaluate the dynamic elasticity and rigidity of the measured highway sections is given in Table 1.24.

The homogeneity of concrete production may be evaluated by the determination of the standard deviation and coefficient of variation for the set of measured values of c_0, as given in Table 1.25. As the strength of cement concrete is empirically found to be approximately proportional

Table 1.23. Results of measurement on highway pavements.

Section number	Section in km	Frequency f (Hz)	Wavelength Λ (m)	Phase velocity c (m/s)
		20000	0.1175	2350
1	8.8	250	2.917	729
		20000	0.125	2500
2	9.0	250	2.782	696
		20000	0.121	2420
3	9.3	250	2.895	724
		20000	0.119	2380
4	9.5	250	3.217	804
		20000	0.1187	2375
5	9.7	250	3.202	801
		20000	0.1162	2325
6	9.9	250	2.920	730
		20000	0.1175	2350
7	14.0	250	2.665	666
		20000	0.120	2400
8	137.0	250	2.795	699
		20000	0.1203	2405
9	137.0	250	2.937	734

Table 1.24. Summary of evaluated characteristics for pavement elasticity and rigidity.

Section number	Section in km	$c_0 = \sqrt{\frac{E}{\varrho}}$ (m/s)	h (m)	EJ (Nm^2)	Deflection w (m)	Curvature Δ (m^{-1})
1	8.8	4038	0.304	38049ϱ	$0.4160\times10^{-3}p_0$	$0.1149\times10^{-2}p_0$
2	9.0	4324	0.255	25738ϱ	$0.4518\times10^{-3}p_0$	$0.1459\times10^{-2}p_0$
3	9.3	4166	0.289	34795ϱ	$0.4234\times10^{-3}p_0$	$0.1204\times10^{-2}p_0$
4	9.5	4075	0.371	70610ϱ	$0.3659\times10^{-3}p_0$	$0.0762\times10^{-2}p^0$
5	9.7	4067	0.368	68929ϱ	$0.3677\times10^{-3}p_0$	$0.0775\times10^{-2}p_0$
6	9.9	3993	0.308	38969ϱ	$0.4142\times10^{-3}p_0$	$0.1137\times10^{-2}p_0$
7	14.0	4060	0.249	21245ϱ	$0.4737\times10^{-3}p_0$	$0.1708\times10^{-2}p_0$
8	137.0	4138	0.270	28077ϱ	$0.4410\times10^{-3}p_0$	$0.1398\times10^{-2}p_0$
9	137.0	4135	0.300	38448ϱ	$0.4145\times10^{-3}p_0$	$0.1129\times10^{-2}p_0$
Density ϱ in kg/m^3, normal load intensity p_0 in MPa						

to the fourth power of the velocity c_0, the coefficient of variation for concrete strength will be given by the fourth multiple of the variation coefficient for the velocity, i.e. by $v\approx0.092$.

A variation coefficient for concrete strength of under 10% indicates a good standard of concrete production and placement.

Table 1.25. Evaluation of the homogeneity of cement concrete surfacing in highway pavements.

Section number	Section in km	n	c_0	Mean value of c_0	ε	ε^2
		(km/s)	(km/s)			
1	8.8	1	4.038		-0.073	0.005329
2	9.0	2	4.324		0.213	0.045369
3	9.3	3	4.166		0.055	0.003025
4	9.5	4	4.075		-0.036	0.001296
5	9.7	5	4.067	4.111	-0.044	0.001936
6	9.9	6	3.993		-0.118	0.013924
7	14.0	7	4.060		-0.051	0.002601
8	137.0	8	4.138		0.027	0.000729
9	137.0	9	4.135		0.024	0.000576
Σ			36.996		0.641	0.074785

Variance $\sigma^2 = \sum_{i=1}^{n} \varepsilon_i^2/n - 1 = 0.074785/8 = 0.009348$
Standard deviation σ=0.09668
Coefficient of variation v=σ/c_{0mean}=0.09668/4.111=0.023

The standard deviation σ can be assessed directly from the measured values of stress-wave velocity at the frequency f=20000 Hz, which corresponds to the velocities of surface Rayleigh waves in the concrete plate.

The values of the equivalent thickness h and dynamic flexural stiffness EJ, which are characteristics of the rigidity for the layered pavement structure as a whole, have considerably greater dispersion.

This suggests that the layers of cement stabilization and bituminous interlayers on particular sections have very different qualities or thicknesses, so that the cement concrete plate does not always have the same thickness.

It can be seen that the quality of the concrete surfacing, on its own, does not guarantee high stiffness of the pavement structure. The highest velocity c_0, i.e. the highest quality of concrete, was obtained on the pavement section 2, but the stiffness of the total structure is one of the weakest.

The evaluation of pavement rigidity by deflection is very near to the method of quality and rigidity evaluation that has been used until now. It is the most objective evaluation because it includes the activity of the subgrade as well.

Provided that the intensity of normal load p_0=0.5 MPa, the greatest deflections will be in the sections 7 (0.237 mm) and 2 (0.226 mm). The pavement sections with the greatest stiffness 4 and 5 present deflection values of 0.183 mm.

The measurement was made again on the same pavement sections 1–6 after eight months. Repeated measurement gives a valuable opportunity to compare results or to evaluate changes in the structure.

Table 1.26. Comparison of repeated measurement results on highway pavements.

Section number	Section in km	Frequency f(Hz)	Wave length Λ (m)		Phase velocity c (m/s)	
			Measurement 1.	Measurement 2.	Measurement 1.	Measure-ment 2
		20000	0.1175	0.1191	2350	2382
1	8.8	250	2.917	2.865	729	716
		20000	0.1250	0.1274	2500	2548
2	9.0	250	2.782	2.593	696	648
		20000	0.1210	0.1220	2420	2440
3	9.3	250	2.895	2.777	724	694
		20000	0.1190	0.1200	2380	2400
4	9.5	250	3.217	3.200	804	800
		20000	0.1187	0.1212	2375	2424
5	9.7	250	3.202	3.235	801	809
		20000	0.1162	0.1200	2325	2400
6	9.9	250	2.920	3.000	730	750

The results of measured wavelengths A and phase velocities c at the frequencies f=20000 Hz and f=250 Hz are compared in Table 1.26. A simple comparison of the characteristic values

Table 1.27. Comparison of repeated evaluation results for highway pavements.

Sec. num.	Sec-tion in km	$c_0 = \sqrt{E/\varrho}$ (m/s)		h (m)		EJ (Nm^2)		Deflection w (m)	
		1. meas.	2. meas.	1. meas	2. meas.	1. meas.	2. meas.	1. meas.	2. meas.
1	8.8	4038	4099	0.304	0.287	38049 ϱ	33244 ϱ	$0.4160\times10^{-3}p_0$	$0.4280\times10^{-3}p_0$
2	9.0	4324	4442	0.255	0.213	25738 ϱ	15930 ϱ	$0.4518\times10^{-3}p_0$	$0.5042\times10^{-3}p_0$
3	9.3	4166	4213	0.289	0.261	34795 ϱ	26266 ϱ	$0.4234\times10^{-3}p_0$	$0.4504\times10^{-3}p_0$
4	9.5	4075	4112	0.371	0.363	70 610 ϱ	67406 ϱ	$0.3659\times10^{-3}p_0$	$0.3691\times10^{-3}p_0$
5	9.7	4067	4153	0.368	0.367	68929 ϱ	71262 ϱ	$0.3677\times10^{-3}p_0$	$0.3649\times10^{-3}p_0$
6	9.9	3992	4122	0.308	0.315	38969 ϱ	44293 ϱ	$0.4142\times10^{-3}p_0$	$0.4022\times10^{-3}p_0$
Density ϱ in kg/m^3 normal load intensity p_0 in MPa									

for 1 and 2 measurements documents the high degree of reproducibility. A summary of the characteristics of dynamic elasticity and rigidity of the highway sections is given in Table 1.27.

Table 1.28. Measurement results on highway pavement structures.

Number of meas.	Section in km	Frequency (Hz)	Λ_a (m)	c_a (m/s)	Frequency (Hz)	Λ_b (m)	c_b (m/s)
1	44.950	20000	0.1141	2282	250	3.038	759.5
2	45.200	20000	0.1117	2234	250	3.054	763.8
3	45.400	20000	0.1136	2272	250	3.055	763.8
4	45.650	20000	0.1147	2294	250	3.000	750.0
5	45.750	20000	0.1153	2306	250	2.973	743.2
6	45.900	20000	0.1179	2358	250	3.057	764.2
7	46.100	20000	0.1169	2338	250	3.186	796.5
8	48.260	20000	0.1172	2344	250	3.163	790.7
9	46.700	20000	0.1159	2318	250	2.951	737.7
10	47.000	20000	0.1141	2282	250	2.857	714.2
11	47.100	20000	0.1134	2268	250	3.094	773.5
12	47.300	20000	0.1167	2334	250	3.026	756.5

It can be seen that the velocities c_0 increased after eight months, i.e. the dynamic modulus of elasticity increased by approximately 2–6%. The equivalent thickness h of the sections 1–5 decreased and that of the section 6 increased. There are similar changes in the parameters of rigidity. The maximum rigidity is again present in the pavement sections 4 and 5, while the minimum rigidity is again in the pavement section 2.

The changes of section rigidity may be caused by changes in the contact of the pavement layers or by building site traffic.

Comparison of the quality parameters of concrete surfacing from direct measurements on highway pavements with the values of laboratory testing on core samples

The diagnostic measurements of phase velocities c_a, c_b and wavelengths Λ_a, Λ_b at the frequencies f=20000 Hz and 250 Hz were carried out on 12 highway pavement sections in km 44.950–47.300 (Table 1.28). The results of the evaluation are given in Table 1.29.

At the same time three core samples were taken from the concrete surfacing at every measurement site. The dynamic modulus of elasticity E was measured in the laboratory by using the core samples, with the resonance method and longitudinal vibration of the cylindrical core samples. Data about the dimensions of the tested cylindrical core samples, about the density ϱ and the comparison of the values of the elasticity modulus are given in Table 1.30.

It can be seen that direct measurements on pavement structures make it possible to obtain from the measured values of velocity c_0 qualitative parameters that are equivalent to the values determined on test samples bored from the concrete surfacing of the pavement structure.

Table 1.29. Evaluation of elasticity and rigidity for highway pavement sections.

Number of meas.	$c_0\sqrt{E/\varrho}$ (m/s)	h_{ekv} (m)	EJ/ϱ EJ (Nm^2)	Deflection $w/p_0\times10^3$ w (m)	Deflection $w_0/p_0\times10^3$ w_0 (m)
1	3910	0.344	51862	0.3905	0.2785
2	3824	0.357	55545	0.3856	0.2729
3	3891	0.350	54153	0.3872	0.2766
4	3933	0.333	47393	0.3977	0.2853
5	3956	0.324	44323	0.4025	0.2920
6	4044	0.335	51389	0.3904	0.2801
7	4002	0.371	68198	0.3689	0.2601
8	4014	0.364	64780	0.3726	0.2650
9	3978	0.317	41917	0.4079	0.2964
10	3919	0.301	34777	0.4250	0.3096
11	3883	0.361	59005	0.3918	0.2704
12	4003	0.332	48839	0.4018	0.2849

Table 1.30. Comparison of dynamic moduli of elasticity in cement concrete sufacing obtained by using resonance and phase velocity methods.

Number of meas.	Core diameter (m)	Length of core sample (m)	Density ϱ (kg/m^3)	Modulus of elasticity E Resonance method (MPa)	Phase velocity method (MPa)
1	0.150	0.250	2339	35 580	35 760
2	0.150	0.242	2328	35 500	34 040
3	0.150	0.260	2272	35 280	34 400
4	0.150	0.245	2310	36 790	35 730
5	0.1485	0.255	2312	33 580	36 180
6	0.1485	0.240	2382	38 610	38 950
7	0.1485	0.249	2356	37 950	37 732
8	0.1485	0.238	2351	36 570	37 870
9	0.150	0.267	2289	34 110	36 220
10	0.1497	0.238	2348	35 270	36 060
11	0.1497	0.268	2282	33 830	34 410
12	0.1497	0.247	2335	35 590	37 410

1.4.5 Testing pavements under construction

The methods of dynamic diagnosis and evaluation can also be applied to pavements under construction. In this section we present the results of measurements on six sections of pavement under construction. The structure of the pavement was as follows: an 8 cm thick first layer of cement stabilization with aggloporite (40% aggloporite, 12% cement), a 19 cm thick second layer of cement stabilization with aggloporite (40% aggloporite, 10% cement), and a 24 cm thick sub-base layer. At the time of measurement the first layer of cement stabilization was 15 days old and the second layer was 8 weeks old. The material density of these layers was ϱ=1900 kg/m^2.

Tests using the simplified phase velocity method were performed at frequencies 250 and 10000 Hz or 15000 Hz. The results of the measurement and evaluation are given in

Table 1.31. The qualitative parameters of evaluation were determined on the basis of measured phase velocities at frequencies 250 and 10000 Hz or at frequencies 250 and 15000 Hz. It can be seen that the differences are very small.

The results of this evaluation hint at considerable rigidity difference in the measured sections, which is supported by differences in the equivalent thickness *h,* in the tiffness *EJ* and in the values of deflection *w.*

Many other detailed measurements were made on pavements under various kinds of construction [1.43]. The structure of these sections was as follows:

measurements 1 and 3:	The subgrade was formed by a 4 m thick embankment from clayed sand and gravel, compacted slightly.
measurements 2 and 9:	A 5 m embankment from clayed sand and gravel, 20 cm thick layer of crushed stone with grain size 32–64 mm, a bituminous spraying and 3 cm thick scattering of crushed gravel with grain size 8–16 mm, and a 10 cm thick layer of coated sand and gravel. The temperature of the surfacing material, T=43 °C (measurement 2) or T=15 °C (measurement 9).
measurements 7 and 8:	The subgrade (the original material), 25 cm thick layer of sand and gravel, and a 24 cm thick layer of cement stabilization.
measurements 4, 5 and 6:	A 4 m embankment (clayed sand and gravel or original material), 25 cm thick layer of sand and gravel, 24 cm thick layer of cement stabilization, and a 4 cm thick layer of coated sand and gravel. The temperature of the surfacing material, T=27–30 °C.
measurement A:	A similar structure as in sections 4, 5 and 6. T=30 °C.
measurement B:	the completed section A with a 24 cm thick layer of cement concrete surfacing.

The results of measurements 1 and 3 on the subgrade determined the velocity of surfaces waves c_R=140–180 m/s, while at high frequencies (short wavelengths) this velocity achieved the value c_R=250 m/s. This corresponds to compacted subgrade surfacing. Dynamic moduli of elasticity for the subgrade material, obtained according to the relationship $E_s = (c_R/0.57)^2 \varrho$, are E_s=95–180 MPa, provided that ϱ_s=1800 kg/m^3 and in the compacted surface layer E_s=345 MPa.

Measurements on the other sections of pavement under construction generated typical variations of dispersion curves for quasi-flexural stress waves and allow the use of the usual evaluation procedures.

Table 1.32 summarizes the characteristics obtained for dynamic elasticity and rigidity of pavement sections.

Measurements 2 and 9 on the same section, which had atypical base and sub-base layers, document very weak rigidity. The deflections and the curvatures reached the highest values. The influence of different temperatures on the surface bituminous layer manifests itself as a change in the pavement characteristics, as can be seen in Table 1.32.

Measurements 7 and 8 on the same section with the finished layer of cement stabilization give substantially higher rigidity characteristics, although the low value of h suggests that the thickness of the cement stabilization layer does not reach the prescribed value of 24.0 cm.

Sections 4, 5 and 6 belong to the pavements with finished base layers; that is in addition to the cement stabilization layer they have a bituminous membrane. It can be seen from the results in Table 1.32 that the rigidity of the pavement sections increased and the dynamic stiffness, deflection and curvature are very similar for all three sections.

Table 1.31. Measurement results using phase velocity method on pavements under construction.

Number of meas.	Section in km	Frequency (Hz)	Λ_a (m)	c_a (m/sec)	Frequency (Hz)	Λ_a (m)	c_a (m/s)	Frequency (Hz)	Λ_b (m)	c_b (m/s)
1	108.880	15000	0.0928	1392	10000	0.1392	1392	250	2.437	609.25
2	108.940	15000	0.0871	1306	10000	0.1336	1336	250	2.054	513.50
3	109.000	15000	0.0839	1258	10000	0.1218	1218	250	1.636	409.00
4	109.070	15000	0.0834	1251	10000	0.1228	1228	250	2.129	532.25
5	109.180	15000	0.0876	1314	10000	0.1268	1268	250	1.781	445.25
6	109.240	15000	0.0975	1462	10000	0.1451	1451	250	1.515	378.75

Number of meas.	$c_0 = \sqrt{E/\varrho}$ (m/s)	h_{ekv} (m)	EJ/ϱ (EJ/Nm^2)	$c_0 = \sqrt{E/\varrho}$ (m/s)	h_{ekv} (m)	EJ/ϱ $EJ/(Nm^2)$	w_0/p_0 p_0(m)
1	2388	0.385	27093	2376	0.387	27373	0.3576×10^{-3}
2	2310	0.273	9038	2236	0.284	9549	0.4782×10^{-3}
3	2137	0.182	2298	2173	0.179	2242	0.7174×10^{-3}
4	2108	0.332	13524	2136	0.326	13194	0.4390×10^{-3}
5	2212	0.210	3788	2263	0.205	3659	0.6267×10^{-3}
6	2710	0.119	1028	2539	0.125	1006	0.8611×10^{-3}
	according to the measurement for f=10000 Hz and 250 Hz			according to the measurement for f=15000 Hz and 250 Hz			
Note: ϱ in kg/m^3; p_0 in MPa.							

Table 1.32. Evaluation of dynamic elasticity and rigidity of pavements under construcion.

Number of meas.	$c_0 = \sqrt{\frac{E}{\varrho}}$ (m/s)	h (m)	EJ/ϱ EJ in (Nm^2)	Deflection w/p_0 w in (m)	Curvature Δ/p_0 Δ in (m^{-1})
2	1436	0.096	151	$1.5703.10^{-3}$	$5.9785.10^{-2}$
9	2494	0.076	223	$1.3957.10^{-3}$	$4.3715.10^{-2}$
7–8	2621	0.143	1674	$0.8684.10^{-3}$	$1.1623.10^{-2}$
4	2040	0.253	5591	$0.6598.10^{-3}$	$0.5749.10^{-2}$
5	2450	0.204	4215	$0.6924.10^{-3}$	$0.6378.10^{-2}$
6	1503	0.321	6238	$0.6756.10^{-3}$	$0.6372.10^{-2}$
A	2633	0.264	10667	$0.5449.10^{-3}$	$0.3358.10^{-2}$
B	3958	0.425	100400	$0.3428.10^{-3}$	$0.0621.10^{-2}$
density ϱ in (kg/m^3) normal load intensity p_0 in (MPa)					

Lastly, the evaluation of section A with all base layers and the subsequent evaluation B on the same section but with cement concrete surfacing demonstrate conclusively that there is a radical change in the rigidity characteristics due to the activity of the cement concrete pavement surfacing.

Figure 1.66 gives a summary of the rigidities obtained by dynamic diagnostic measurements on highway pavement structures expressed in terms of the determined deflections w_0 versus the normal load p_0.

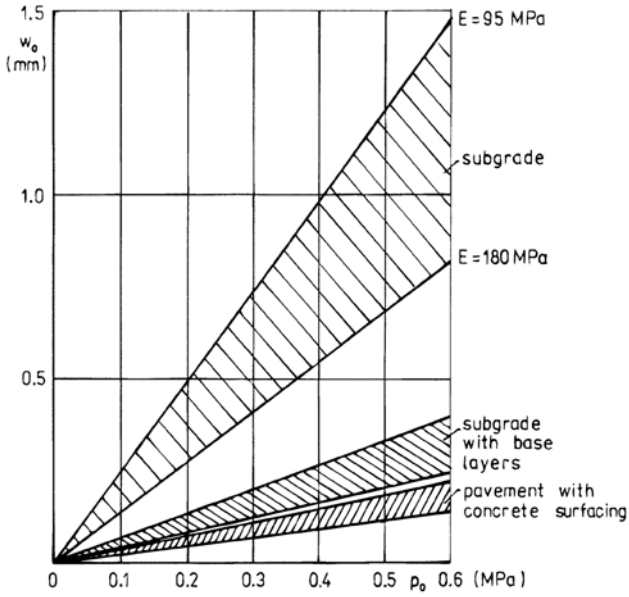

Fig. 1.66. Survey of rigidities obtained by diagnostic measurement on highway pavements according to deflection.

The results of measurements using phase velocity method and their evaluation, performed on the various sections of pavements under construction, document the efficiency of the testing method and the proposed evaluation procedures. They are a reliable means for evaluating the properties and quality of pavement structures during their construction.

1.4.6 Influence of base and sub-base layers on the overall rigidity of pavement structures

The test results on six sections of highway pavement under construction with base layers of cement stabilization and aggloporite, given in Table 1.31, can be used to evaluate the influence of the base layers on overall pavement rigidity. After the cement concrete surfacing was finished, tests were made on the same sections of pavement structure. The results of the measurements and the determined evaluation parameters are given in Table 1.33.

Table 1.33. Evaluation of pavements after completion of cement concrete surfacing.

Number of meas.	Section in km	Frequency (Hz)	Λ_a (m)	c_a (m/s)	Frequency (Hz)	Λ_b (m)	c_b (m/s)
1	109.880	20000	0.1159	2318	250	3.383	845
2	109.940	20000	0.1130	2260	250	3.209	802
3	110.000	20000	0.1182	2364	250	3.207	801
4	110.070	20000	0.1155	2310	250	3.408	852
5	110.180	20000	0.1196	2392	250	3.279	819
6	110.240	20000	0.1185	2370	250	2.970	742

Number of meas.	$c_0 = \sqrt{\frac{E}{\varrho}}$ (m/s)	h_{ekv} (m)	$EJ\ \varrho$ EJ in (Nm^2)	w_0/p_0 w_0 in (m)
1	3961	0.428	102333	$0.2344.10^{-3}$
2	3864	0.393	75345	$0.2538.10^{-3}$
3	4048	0.371	69755	$0.2603.10^{-3}$
4	3946	0.437	108426	$0.2309.10^{-3}$
5	4094	0.384	79255	$0.2510.10^{-3}$
6	4070	0.313	42181	$0.2952.10^{-3}$
Note: ϱ in (kg/m^3), p_0 in (MPa)				

A comparison of the rigidity characteristics of the finished pavement structures with those of the base-layer structures (Table 1.31) shows the decisive influence of the rigidity of the subgrade and sub-base and base layers on the overall stiffness of the finished pavement structure. Sections 1 and 4, which presented the greatest base-layer rigidity, are also the sections with the greatest overall rigidity of finished pavement structure. Section 6, with the smallest rigidity of the base-layer structure, is the section with the smallest stiffness of

the finished pavement section. It can be said that, for equal quality of concrete surfacing, the dynamic stiffnesses of finished pavements reflect the rigidity of the subgrade and base layers.

The overall dynamic stiffness of pavement structures is also important from the point of view of a comparison with the rigidity of adequate physico-mathematical models, which could appropriately describe the properties and action of layered pavements.

Let us consider the perfect contact of all pavement layers and compare it with a model in which the shear contact at the pavement interlayer is interrupted. We shall use the determined characteristics of elasticity and rigidity of the base layers in Table 1.31 and the elasticity characteristics of the concrete surfacing from Table 1.33. It is possible to calculate the equivalent thickness h and dynamic stiffness in flexion EJ for the sections studied and for two assumptions of contact for pavement action. These results may be compared with the experimental values given in Table 1.33. The comparisons are summarized in Table 1.34.

Table 1.34. Comparison of theoretical and experimental rigidity parameters for finished pavement structures.

Section number	h_{ekv} (m)			$EJ/\varrho.10^{-3}$ EJ in (Nm^2)		
	perfect contact	without shear contact at interlayer	experiment	perfect contact	without shear contact	experiment
1	0.540	0.335	0.428	217.5	49.9	102.3
2	0.452	0.291	0.393	115.5	30.7	75.3
3	0.367	0.262	0.372	67.8	24.6	69.7
4	0.477	0.305	0.437	141.2	36.9	108.4
5	0.390	0.268	0.384	82.5	26.8	79.2
6	0.346	0.254	0.313	57.6	22.5	42.2

It can be seen that the equivalent thickness and dynamic stiffness in flexion determined according to measurements using the phase velocity method fall between the values calculated assuming perfect contact of the layers and those assuming interrupted shear contact at the interlayer. The interaction of the pavement layers will change over time owing to volume changes and traffic. This trend will be manifested as a decrease of the real values of the rigidity parameters.

The complex method of dynamic diagnosis of pavement structure presented here permits advanced possibilities to investigate and observe non-destructively the changes in the rigidity and quality of pavement structures over time factor or due to the effect of traffic [1.41, 1.47].

Knowledge of the dynamic behaviour of the subgrade and pavement materials, and of the dynamic parameters of pavement rigidity, which may be acquired through the application of dynamic testing methods, together constitute the starting point for the development of acceptable theoretical models of a layered pavement system.

2
MODEL OF THE EQUIVALENT PLATE ON SUBGRADE

The results of dynamic diagnosis also serve for the formation and identification of acceptable theoretical models of pavement structures which closely agree with both the dynamic behaviour of structural materials and the total dynamic reaction of road pavements or airfield runways.

The model of the equivalent plate on subgrade is a model by means of which the behaviour of layered pavement structures may be expressed. The layered pavement structure itself is too complex a model to be used as a basis for the solution of dynamic tasks.

The dynamic theory of the equivalent plate lying on subgrade makes it possible to determine the dynamic deflection and all decisive internal forces of a real layered pavement structure.

2.1 Calculation of cross-section quantities of equivalent plate and calculation of stress in layered pavement structures

A comparison of the state of stress in layered plates obtained by a more exact solution applying the finite elements method with the results of a simplified technical solution has been realized in [2.1]. The simplified solution was established on the assumption that the normal line to the central plane of the layered plate will keep the normal to the plate under a load too. The comparison demonstrated that this technical theory is, from a practical point of view, suitable for the determination of stresses in the layered plate.

Let us assume a layered pavement structure with n layers as shown in the Fig. 2.1. By assuming the retention of the normal line to the central plane the deformation ε_x changes linearly in relation to the coordinate z. The stresses σ_x are linear in every layer and their

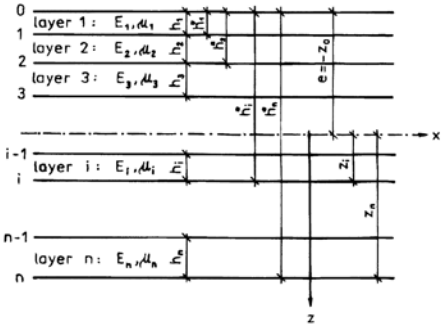

Fig. 2.1. Schematic diagram of layered pavement structure.

plots form lines, which cross a central axis. This central axis is situated at a distance $e=-z_0$ from the surface of the layered pavement.

The distance e is determined by the equilibrium condition of the normal forces $\int\sigma_x dz=0$ in the cross-section of the unit width of the layered pavement. The equation is [2.1]

$$e = \frac{\sum_{i=1}^{n} E_i h_i \, (h_{i-1}^* + h_i/2)/(1-\mu_i^2)}{\sum_{i=1}^{n} E_i h_i/(1-\mu_i^2)} \tag{2.1}$$

where

$$h_i^* = \sum_{j=1}^{i} h_j. \tag{2.2}$$

The normal stresses $\sigma_{x,i}$ in the i th layer under a bending moment M are established according to the relationship

$$\sigma_{x,i} = Mz \frac{E_i/(1-\mu_i^2)}{D} \tag{2.3}$$

if the stiffness of the layered system D is given in the form

$$D = \frac{1}{3}\sum_{i=1}^{n} \frac{E_i}{1-\mu_i^2}(z_i^3 - z_{i-1}^3). \tag{2.4}$$

The tangential stresses τ_{xz} of pavement structure with perfect contact of the layers are determined by the relationship

$$\tau_{xz}^j = \frac{QS_z^l}{\bar{D}} \tag{2.5}$$

where Q is the shear force, the stiffness $\bar{D}$ is given in the form

$$\bar{D} = \frac{1}{3}\sum_{i=1}^{n} E_i\left(z_i^3 - z_{i-1}^3\right) \tag{2.6}$$

and S_z^l is expressed by the relationship

$$S_z^l = \frac{1}{2}\sum_{i=1}^{l-1} E_i(z_{i-1}^2 - z_i^2) + \frac{1}{2}E_l(z_{l-1}^2 - z^2). \tag{2.7}$$

Equation (2.7) is valid for an arbitrary point of the l th layer of the structure.

2.1.1 Calculation of stress in layered structures with defective layer contact

The influence of volume changes and traffic in a layered pavement structure manifests itself as defective shear contact at the interface of some of the layers. For instance, in cement concrete highway pavements it is supposed that shear contact failure appears in the region of the bituminous interlayer.

In such a case the total stiffness D is the sum of the partial stiffnesses D_1, D_2,…D_k of the layered pavement parts, the contact interfaces of which do not transmit the tangential stresses. The following equation is valid:

$$D=D_1+D_2+...D_k. \tag{2.8}$$

Equations (2.1) and (2.4) can be used for calculating the individual central axis positions or partial stiffnesses.

The total bending moment M straining the pavement structure is divided into the partial values M_j according to the relationship

$$M_j = \frac{D_j}{D} M. \tag{2.9}$$

The partial shear force Q_j is established from the equation

$$Q_j = \frac{\kappa_j G_j h_{\mathrm{eq},j}}{\kappa G h_{\mathrm{eq}}} Q \tag{2.10}$$

while the following relationship is valid:

$$\kappa G h_{\mathrm{eq}} = \kappa_1 G_1 h_{\mathrm{eq},1} + \kappa_2 G_2 h_{\mathrm{eq},2} + \ldots + \kappa_k G_k h_{\mathrm{eq},k}. \tag{2.11}$$

The coefficients κ, κ_1,…κ_k express the influence of non-uniformity in shear stress distribution along the thickness.

In practice the following simplified relationships can be used:

$$Q_j = \frac{G_j h_{\mathrm{eq},j}}{G h_{\mathrm{eq}}} Q \tag{2.12}$$

and

$$G h_{\mathrm{eq}} = G_1 h_{\mathrm{eq},1} + G_2 h_{\mathrm{eq},2} + \ldots G_k h_{\mathrm{eq},k} \tag{2.13}$$

in which h_{eq} is the equivalent thickness of the total structure and $h_{\mathrm{eq},j}$ are the equivalent thicknesses of the j th part of the layered system.

By the determination of the partial quantities M_j and Q_j it is possible to use the similar relationships (2.3), (2.5) to calculate the normal and tangential stresses in the parts of the layered system with partial stiffnesses D_j, $\bar{D}_j$.

2.1.2 Coherence of layered pavement stiffness with the characteristics of the equivalent plate

The physical model of the equivalent plate in the case of a layered pavement is defined by the equivalent thickness h_{eq} and the elasticity characteristics corresponding to the material of the surface layer. Equality of the stiffness D_{ekv} for the equivalent plate and the stiffness D for the real layered system has to be fulfilled. It is expressed by the equation

$$\frac{E_1 h_{eq}^3}{12(1-\mu_1^2)} = D. \tag{2.14}$$

Table 2.1. Composition and charasteristics of pavement materials.

Layer number	Material	Thickness	alternative a)		alternative b)	
		(m)	E(MPa)	μ	E(MPa)	μ
1	cement concrete	0.24	38000	0.20	38000	0.20
2	bituminous interlayer	0.04	5000	0.35	2500	0.35
3	cement stabilization	0.15	10000	0.25	8000	0.25
4	sand and gravel	0.35	500	0.35	300	0.35

The thickness of the equivalent plate, h_{eq}, according to equation (2.14) is given in the form

$$h_{eq} = \sqrt[3]{\left[\frac{4(1-\mu_1^2)}{E_1}\sum_{i=1}^{n}\frac{E_i}{1-\mu_i^2}(z_i^3 - z_{i-1}^3)\right]} \tag{2.15}$$

for perfect contact of all layers and in the form

$$h_{eq} = \sqrt[3]{\left[\frac{12(1-\mu_1^2)}{E_1}(D_1 + D_2 + \ldots + D_k)\right]} \tag{2.16}$$

for defective shear contact at the interfaces of the partial structures of the layered system.

Equation (2.15) can be used to calculate the partial equivalent thicknesses, h_{eq}.

2.1.3 Variations of normal and tangential stress for highway cement concrete pavements with perfect layer contact

Provided that the composition and characteristics of pavement materials in two alternatives correspond to the values in Table 2.1, the results of the solution are as follows

Alternative (a)

e=0.1638 m, h_{eq}=0.371 m, D=168.36×10^6 N m^2

Normal stresses:

σ_{01}/M=−38.51, σ_{11}/M=17.92, σ_{12}/M=2.57, σ_{22}/M=3.93,

σ_{23}/M=7.36, σ_{33}/M=16.87, σ_{34}/M=0.90, σ_{44}/M=2.08

Tangential stresses:

τ_{01}/Q=0.0, τ_1/Q=3.03, τ_{11}/Q=τ_{12}/Q=2.37,

τ_{22}/Q=τ_{23}/Q=2.26, τ_3/Q=2.491, τ_{33}/Q=τ_{34}/Q=0.554,

τ_4/Q=0.613, τ_{44}/Q=0.0

Alternative (b)

e=0.154 m, h_{eq}=0.347 m, D=137.59×10^6 N m^2

Normal stresses:

σ_{01}/M=−44.31, σ_{12}/M=24.73, σ_{12}/M=1.78, σ_{22}/M=2.60

σ_{23}/M=7.81, σ_{33}/M=17.11, σ_{34}/M=0.68, σ_{44}/M=1.55

Tangential stresses:

τ_{01}/Q=0.0, τ_1/Q=3.70, τ_{11}/Q=τ_{12}/Q=2.90,

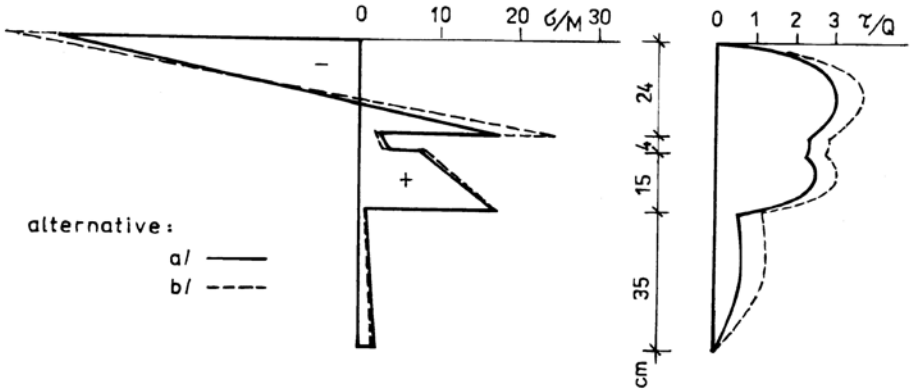

Fig. 2.2. Variation of stresses in layered pavement.

τ_{22}/Q=τ_{23}/Q=2.83, τ_{44}/Q=3.06, τ_{33}/Q=τ_{34}/Q=1.16,
τ_4/Q=1.208, τ_{44}/Q=0.0

The stress variations are depicted graphically in Fig.2.2.

2.1.4 Variations of normal and tangential stress for highway cement concrete pavements with defective shear contact in the bituminous interlayer

The structure and material characteristics of the pavement layers are assumed to be the same as in the previous section, but the shear contact at interface 1, i.e. at the interface of the cement surfacing layer and the bituminous interlayer is interrupted.

The results of the solution are as follows.

Alternative (a)

e_1=0.12 m, D_1=45.6×10^6 N m^2

e_2=0.128 m, D_2=19.19×10^6 N m^2

h_{eq}=0.2698 m, D=64.79×10^6 N m^2

Normal stresses:

σ_{01}/M=−73.30, σ_{11}/M=73.30, σ_{12}/M=−11.34, σ_{22}/M=−7.82,

σ_{23}/M=−14.64, σ_{33}/M=10.06, σ_{34}/M=0.537, σ_{44}/M=3.615

Shear stresses:

τ_{01}/Q=0.0, τ_1/Q=5.34, τ_{11}/Q=τ12/Q=0.0,

τ_{22}/Q=τ_{23}/Q=0.124,

τ_3/Q=0.347, τ_{33}/Q=τ_{34}/Q=0.236, τ_4/Q=0.198, τ_{44}/Q=0.0

Alternative (b)

e_1=0.12 m, D_1=45.6×10^6 Nm^2

e_2=0.1276 m, D_2=11.9×10^6 Nm^2

h_{eq}=0.2593 m, D=57.5×10^6 Nm^2

Normal stresses:

σ_{01}/M=−82.60, σ_{11}/M=82.60, σ_{12}/M=−6.32, σ_{22}/M=−4.34,

σ_{23}/M=−13.00, σ_{33}/M=9.25, σ_{34}/M=0.371, σ_{44}/M=2.45

Shear stresses:

τ_{01}/Q=0.0, τ_1/Q=5.55, τ_{11}/Q=τ_{12}/Q=0.0,

τ_{22}/Q=τ_{23}/Q=0.0673,

τ_3/Q=0.2593, τ_{33}/Q=τ_{34}/Q=0.1619, τ_4/Q=0.1368,

τ_{44}/Q=0.0

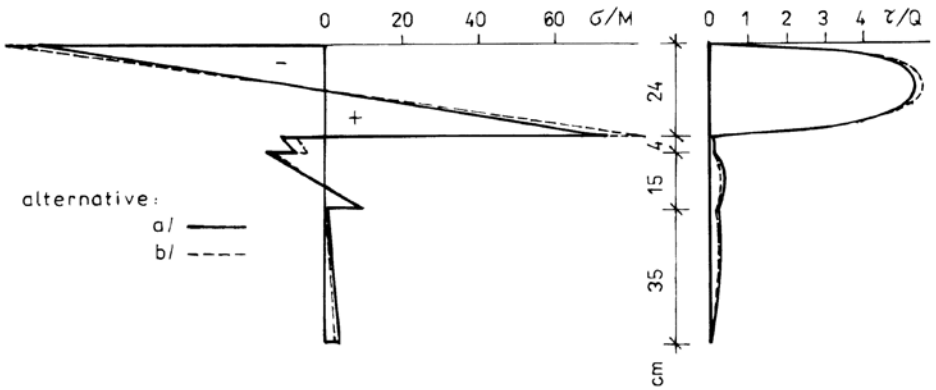

Fig. 2.3. Variation of stresses in layered pavement with defective shear contact in bituminous interface.

The variations of the stresses are drawn in Fig. 2.3. It can be seen from a comparison of the results for the two cases of layered pavement activity that the defective shear contact in the bituminous interface leads to a considerable decrease in pavement stiffness and to an increase in the normal and shear stresses in the layer of concrete surfacing. The normal tension stresses and the shear stresses in the sub-base layers are considerably reduced.

3
VARIANTS OF THE DYNAMIC THEORY OF THE EQUIVALENT PLATE ON SUBGRADE

On the basis of the experimental studies described in Chapter 1 the following working hypotheses can be formulated.

1. The dynamic properties and behaviour of the layered pavement structure are sufficiently similar to the dynamic properties and behaviour of the equivalent layer that is in contact with the subgrade.
2. The elasticity characteristics for the material of the equivalent layer and its thickness and the total flexural stiffness of the system have to express the dynamic behaviour of the real structure according to the same dispersion curve of quasi-flexural stress waves.
3. The equivalent layer lying on the subgrade allows the modelling of various states of the total dynamic flexural stiffness of the real structure, which are dependent on the subgrade stiffness, subbase and surface layers of the pavement and on the contact quality at the layer interfaces.

In conformity with these hypotheses the layer in contact with the half-space is one of the possible models. Such a system has to be analysed on the basis of the equations of elasticity theory with corresponding boundary conditions on the surface and contact conditions for the stresses and displacements at the interface of the layer and the halfspace. This system fulfills the required criteria, and guarantees a precise mathematical formulation of the accepted physical model, although difficulties can be expected in the numerical solution of the dynamic task.

The other possibility is the layer (or plate) on subgrade without shear contact. This system fulfills the required criteria as well. It can be proved that the interrupted shear contact has a slight influence on the typical dispersion curve for stress-waves velocities. For the equivalent plate on a half-space the formulation, by using the differential equation of motion with the influence of shear and rotational inertia and at the same time the halfspace reaction, secures a sufficiently precise mathematical formulation of the model and extensive possibilities for the numerical solution of the dynamic problems.

At last it is possible to use the technical theories of the layer (plate) on the subgrade in which the simplified physical model of the subgrade is accepted. The system is mathematically formulated by the differential equation of motion for the plate with the influence of subgrade reaction. Although these systems assume the simplified subgrade action, they have the widest application in the solution of miscellaneous dynamic problems. They also make it possible to formulate special cases of subgrade, such as a subsoil layer with a given thickness lying on an unyielding subgrade.

Applying either variant to the formulation of the dynamic theory of the equivalent layer lying on subgrade, it is inevitable that we have to consider the viscoelastic behaviour of the materials. The materials of pavement structures on a bituminous base and the materials of the subbase layers and subgrade present marked viscoelastic properties. In determinig the dynamic behaviour of pavement structures these viscoelastic materials are manifested partly by strong damping of vibration and partly by changes of the elastic characteristics with frequency and (for bituminous material) with temperature as well.

From the point of view of applications the dynamic viscoelasticity, the most acceptable form of definition for the viscoelastic behaviour of materials is the concept of complex moduli. This concept is in harmony with the current trend towards the development and utilization of numerical methods and computer techniques, and at the same time is based on experimental determinations of the dynamic viscoelastic characteristics over a wide frequency range.

The concept of complex moduli of elasticity formulates the dynamic viscoelastic behaviour of materials as a stationary harmonic process. The complex shear modulus $G^*_{\omega,T}$ and complex bulk modulus $B^*_{\omega,T}$ are expressed by the relationships

$$G^*_{\omega,T} = G_{\omega,T}(1 + \mathrm{i}\delta_G \mathrm{sgn}\omega) \tag{3.1}$$

$$B^*_{\omega,T} = B_{\omega,T}(1 + \mathrm{i}\delta_B \mathrm{sgn}\omega) \tag{3.2}$$

in which $G^*_{\omega,T}$, $B^*_{\omega,T}$ are the real parts of the complex moduli, δ_G is the damping parameter of the shear effect, and δ_B is the damping parameter of the volume effect. The subscripts ω, T indicate that the values of the complex moduli relate to a given angular frequency ω and temperature T.

Assuming equal rheological regularities for the changes of volume and form, then $\delta_B=\delta_G=\delta$ and Poisson's ratio μ is independent of frequency. The fact that the definition of the viscoelastic behaviour of complex moduli is realized for a stationary harmonic process must not be a barrier for the solution of a periodic vibration problems under pulse impact loading. It is possible to use the Fourier integral transformation and the results of stationary vibration as a starting point. Of course the initial conditions cannot be fulfilled during this procedure.

3.1 Layer in contact with the half-space

A layer in contact with the half-space is one of the variants of the dynamic theory of the equivalent plate (layer) on subgrade. The torsional and vertical vibration of the layer on the half-space are two actual problems of this system.

The problem of the vertical vibration of an isotropic elastic half-space under a harmonically variable normal load on a circular area and the vertical vibration of a mass with a circular contact area on the half-space has been solved by Reissner [3.1] and Šechter [3.2]. A summary of the results of [3.2] is to be found in [3.3]. The same task was also analysed by Bycroft [3.4].

The torsional vibration of the elastic half-space under a torsional harmonically variable load acting on a circular contact area was first analysed approximately by Reissner

[3.5] and subsequently has been analysed precisely by Reissner and Sagochi [3.6] and Bycroft [3.4].

Commencing from this knowledge and taking the viscoelastic behaviour as the basis of the conception of complex moduli we shall study actual problems of layer vibration in contact with the half-space.

3.1.1 Torsional vibration of layer on viscoelastic half-space

The differential equation of motion by torsional vibration in cylindrical coordinates has the form

$$\frac{\partial^2 u_\vartheta}{\partial r^2}+\frac{1}{r}\frac{\partial u_\vartheta}{\partial r}-\frac{u_\vartheta}{r^2}+\frac{\partial u_\vartheta}{\partial z^2}=\frac{\varrho}{G^*}\frac{\partial^2 u_\vartheta}{\partial t^2} \tag{3.3}$$

where u_ϑ is the tangential displacement, ϱ is the density and G^* is the complex shear modulus.

The shear stresses are determined by the equations

$$\tau_{z\vartheta}=G^*\frac{\partial u_\vartheta}{\partial z}$$

$$\tau_{r\vartheta}=G^*\left(\frac{\partial u_\vartheta}{\partial r}-\frac{u_\vartheta}{r}\right). \tag{3.4}$$

We assume stationary harmonic vibration:

$$u_\vartheta=u_\vartheta(r,z)\mathrm{e}^{\mathrm{j}\omega t} \tag{3.5}$$

and use the Hankel integral transformation

$${}^{\mathrm{H}}u_\vartheta(\alpha,z)=\int_0^\infty ru_\vartheta(r,z)J_1(\alpha r)\mathrm{d}r \tag{3.6}$$

The solution of differential equation (3.3) is then given by the relationship

$${}^{\mathrm{H}}u_\vartheta=U_1(\xi^*)\mathrm{e}^{-\xi^* z}+U_2(\xi^*)\mathrm{e}^{\xi^* z} \tag{3.7}$$

where

$$\xi^*=\sqrt{\alpha^2-\frac{\omega^2}{c_2^{*2}}} \tag{3.8}$$

if

$$c_2^* = \sqrt{\frac{G^*}{\varrho}} \tag{3.9}$$

Let the harmonic variable torsional moment $M(t)=Me^{i\omega t}$ act on layer I with thickness h, which is in contact with the half-space. The boundary conditions on the surface at $z=0$ are given in the form

$$\begin{aligned} \tau_{z\vartheta}^{\mathrm{I}} &= \frac{2Mr}{\pi a^4}, \quad 0 < r < a \\ \tau_{z\vartheta}^{\mathrm{I}} &= 0, \quad r > a \end{aligned} \tag{3.10}$$

for the case of linear distribution of the shear stresses on a circular contact area with radius a, and in the form

$$\begin{aligned} \tau_{z\vartheta}^{\mathrm{I}} &= \frac{3Mr}{4\pi a^3 (a^2 - r^2)^{1/2}}, \quad 0 < r < a \\ \tau_{z\vartheta}^{\mathrm{I}} &= 0, \quad r > a \end{aligned} \tag{3.11}$$

for the case of stress distribution under a rigid plate, which is supposed to be the same as in the static case.

The conditions at the interface between the layer and halfspace, i.e. at $z=h$, have the form

$$\begin{aligned} u_{\vartheta}^{\mathrm{I}} &= u_{\vartheta} \\ \tau_{z\vartheta}^{\mathrm{I}} &= \tau_{z\vartheta} \end{aligned} \tag{3.12}$$

The application of the Hankel integral transformation to equations (3.10) and (3.11) gives the transforms of stresses

$${}^{\mathrm{H}}\tau_{z\vartheta}^{\mathrm{I}} = \frac{2}{\pi}\frac{M}{a^2}\frac{J_2(\alpha a)}{\alpha}$$

or

$${}^{\mathrm{H}}\tau_{z\vartheta}^{\mathrm{I}} = \frac{3M}{4\pi a^2 \alpha}\left[\frac{\sin(\alpha a)}{\alpha a} - \cos(\alpha a)\right] \tag{3.14}$$

Provided that in the solution of equation (3.7) for the half-space only the term with negative exponent is selected in accordance with its physical meaning, the displacements ${}^{\mathrm{H}}u^{\mathrm{I}}_{\vartheta}$, ${}^{\mathrm{H}}u_{\vartheta}$ and stresses ${}^{\mathrm{H}}\tau^{\mathrm{I}}_{z\vartheta}$, ${}^{\mathrm{H}}\tau_{z\vartheta}$ can be expressed. By using the boundary conditions and conditions at the interface a system of equations is established, which gives the expressions for the functions U in the form

$$U_1^{\mathrm{I}} = \frac{{}^{\mathrm{H}}\tau^{\mathrm{I}}_{z\vartheta}}{G_{\mathrm{I}}^*} \frac{-B^*}{\xi_{\mathrm{I}}^*(A^* + B^*)} \tag{3.15}$$

$$U_2^{\mathrm{I}} = \frac{{}^{\mathrm{H}}\tau^{\mathrm{I}}_{z\vartheta}}{G_{\mathrm{I}}^*} \frac{A^*}{\xi_{\mathrm{I}}^*(A^* + B^*)} \tag{3.16}$$

$$U_1 = \frac{{}^{\mathrm{H}}\tau^{\mathrm{I}}_{z\vartheta}}{G_{\mathrm{I}}^*} \frac{A^* \mathrm{e}^{-\xi_{\mathrm{I}}^* h} - B^* \mathrm{e}^{\xi_{\mathrm{I}}^* h}}{\xi_{\mathrm{I}}^*(A^* + B^*)\mathrm{e}^{-\xi_{\mathrm{I}}^* h}} \tag{3.17}$$

where

$$A^* = \left(\frac{G^*}{G_{\mathrm{I}}^*}\,\xi^* - \xi_{\mathrm{I}}^*\right)\mathrm{e}^{-\xi_{\mathrm{I}}^* h} \tag{3.18}$$

$$B^* = \left(\frac{G^*}{G_{\mathrm{I}}^*}\,\xi^* + \xi_{\mathrm{I}}^*\right)\mathrm{e}^{\xi_{\mathrm{I}}^* h} \tag{3.19}$$

and

$$\xi_{\mathrm{I}}^* = \sqrt{\alpha^2 - \frac{\omega^2}{c_{2\mathrm{I}}^{*2}}} \quad , \quad \xi^* = \sqrt{\alpha^2 - \frac{\omega^2}{c_2^{*2}}}. \tag{3.20}$$

The complex velocities of shear waves in the layer and halfspace are in the form $c^*_{2,\mathrm{I}} = \sqrt{G_{\mathrm{I}}^*/\varrho_{\mathrm{I}}}$, $c_2^* = \sqrt{G^*/\varrho}$, if $G_{\mathrm{I}}^* = G_{\mathrm{I}}(1 + \mathrm{i}\delta_{\mathrm{I}})$, $G^*=G(1+\mathrm{i}\delta)$.

After rearranging, if the ratios are denoted according to the relationships

$$\varepsilon = \frac{G}{G_{\mathrm{I}}} \tag{3.21}$$

$$\psi = \frac{\varrho}{\varrho_{\mathrm{I}}} \tag{3.21}$$

$$\alpha a = \eta, \quad \Omega = \frac{\omega a}{c_2}, \quad c_2 = \sqrt{\frac{G}{\varrho}} \tag{3.22}$$

the original displacements in the layer and in the half-space for the case of linear distribution of shear stresses from torsional moment M are given by the relationships

$$u_\vartheta^{\mathrm{I}} = \frac{2M}{\pi a^2 G}\int_0^\infty H_{\mathrm{I}}^* J_2(\eta) J_1\left(\eta\frac{r}{a}\right)\mathrm{d}\eta \tag{3.23}$$

$$u_\vartheta = \frac{2M}{\pi a^2 G}\int_0^\infty H^* J_2(\eta) J_1\left(\eta\frac{r}{a}\right)\mathrm{d}\eta. \tag{3.24}$$

In the case of shear stress distribution, which corresponds to equation (3.11), the relationships are given in the form

$$u_\vartheta^{\mathrm{I}} = \frac{3M}{4\pi a^2 G}\int_0^\infty H_{\mathrm{I}}^*\left(\frac{\sin\eta}{\eta} - \cos\eta\right) J_1\left(\eta\frac{r}{a}\right)\mathrm{d}\eta \tag{3.25}$$

$$u_\vartheta = \frac{3M}{4\pi a^2 G}\int_0^\infty H^*\left(\frac{\sin\eta}{\eta} - \cos\eta\right) J_1\left(\eta\frac{r}{a}\right)\mathrm{d}\eta. \tag{3.26}$$

The terms marked by H_{I}^* and H^* have the form

$$H_{\mathrm{I}}^* = \frac{\varepsilon(\bar{A}^* \mathrm{e}^{\xi_{\mathrm{I}}^* z/a} - \bar{B}^* \mathrm{e}^{-\xi_{\mathrm{I}}^* z/a})}{(1+\mathrm{i}\delta_{\mathrm{I}})(\bar{A}^* + \bar{B}^*)\xi_{\mathrm{I}}^*} \tag{3.27}$$

$$H^* = \frac{\varepsilon(\bar{A}^* \mathrm{e}^{\xi_{\mathrm{I}}^* h/a} - \bar{B}^* \mathrm{e}^{-\xi^* z/a})\mathrm{e}^{-\xi_{\mathrm{I}}^* z/a}}{(1+\mathrm{i}\delta_{\mathrm{I}})(\bar{A}^* + \bar{B}^*)\xi_{\mathrm{I}}^* \mathrm{e}^{-\xi^* h/a}} \tag{3.28}$$

if

$$\bar{A}^* = \left[\varepsilon\xi^* \frac{(1+\mathrm{i}\delta)}{(1+\mathrm{i}\delta_{\mathrm{I}})} - \xi_{\mathrm{I}}^*\right]\mathrm{e}^{-\xi_{\mathrm{I}}^* h/a} \tag{3.29}$$

$$\bar{B}^* = \left[\varepsilon\xi^* \frac{(1+\mathrm{i}\delta)}{(1+\mathrm{i}\delta_{\mathrm{I}})} + \xi_{\mathrm{I}}^*\right]\mathrm{e}^{-\xi_{\mathrm{I}}^* h/a} \tag{3.30}$$

$$\xi^* = \sqrt{\eta^2 - \frac{\Omega^2}{1+\mathrm{i}\delta}} \tag{3.31}$$

$$\xi_1^* = \sqrt{\eta^2 - \frac{\Omega^2 \varepsilon}{\psi(1 + i\delta_1)}}. \tag{3.32}$$

The original displacements (3.23)–(3.26) are given by improper integrals, the sub-integral functions of which are complex functions of a real variable, have no discontinuities in the domain of integration and the improper integrals converge. They can be calculated by numerical integration using computers.

3.1.2 Torsional vibration of mass on layered half-space

A rigid disk with mass m and circular contact area of radius a lies on the layered half-space. The harmonically variable moment of torsion $M=M_0e^{i\omega t}$ acting on the disk causes torsional vibration. The equation of motion is valid in the form

$$I\frac{d^2\gamma}{dt^2} + M(t) = M_o e^{i\omega t} \tag{3.33}$$

where I is the mass moment of inertia, $M(t)$ is the reaction of the subbase, and γ is the angular displacement of the disk. For a circular disk with thickness h_d and radius a, I is given in the form $I = \pi a^4 h_d \varrho/2 = ma^2/2$.

The angular displacement γ corresponds to the mean angular displacement of the layered half-space under the disk. It can be determined by using the Rayleigh theorem of reciprocity [3.4] from the condition that expressed the equality of deformation work of affected torsional moment on the mean angular displacement with the work of the supposed distribution of tangential stresses on the contact circular area.

For instance, by stress distribution according to equation (3.11) the equation is valid in the form

$$M\gamma = \int_0^a \frac{2\pi r\, 3Mr\, dr}{4\pi a^3 (a^2 - r^2)^{1/2}}$$
$$\times \int_0^\infty \frac{3M}{4\pi a^2 G} \frac{\varepsilon(\bar{A}^* - \bar{B}^*)\,(\sin\eta/\eta - \cos\eta) J_1\left(\eta \frac{r}{a}\right) d\eta}{(1 + i\delta_1)(\bar{A}^* + \bar{B}^*)\,\xi_1^*}. \tag{3.34}$$

After integration with respect to the variable r the angular displacement γ is given by the relationship

$$\gamma = \frac{9}{8}\frac{M}{\pi a^3 G} \int_0^\infty \frac{\varepsilon(\bar{A}^* - \bar{B}^*)\,(\sin\eta - \eta\cos\eta)^2 d\eta}{(1 + i\delta_I)(\bar{A}^* + \bar{B}^*)\eta^3 \xi_1^*}. \tag{3.35}$$

The mean dynamic angular displacement of the disk in a general form is given by the relationship

$$\gamma = \frac{-M}{Ga^3}(\gamma_R + i\gamma_J)e^{i\omega t} \tag{3.36}$$

where the real and imaginary part of mean angular displacement γ_R, γ_J will be obtained by numerical calculation of the improper integrals (3.35).

By substitution of (3.36) into (3.33) the sub-base reaction $M(t)=Me^{i\omega t}$ can be expressed, if

$$M = \frac{M_0}{1 + B\Omega^2\gamma_R + iB\Omega\gamma_J} \tag{3.37}$$

and

$$B = \frac{m}{2\varrho a^3}. \tag{3.38}$$

The amplitude-frequency characteristic is given by the equation

$$\frac{|\gamma|Ga^3}{M_0} = \frac{\sqrt{\gamma_R^2 + \gamma_J^2}}{\sqrt{(1 + B\Omega^2\gamma_R)^2 + (B\Omega^2\gamma_J)^2}} \tag{3.39}$$

and the phase-frequency characteristic by the relationship

$$\varphi = \arctan\frac{\gamma_J}{\gamma_R + B\Omega^2(\gamma_R^2 + \gamma_J^2)}. \tag{3.40}$$

The function of normalized mechanical impedance Z^*, which for stationary forced harmonic vibration is defined [1.22] as the ratio of the torsional exciting moment to the multiple of the angular displacement acceleration and mass moment of inertia for the disk, is given in absolute value by the relationship

$$|Z^*| = \frac{\sqrt{(1 + B\Omega^2\gamma_R)^2 + (B\Omega^2\gamma_J)^2}}{B\Omega^2\sqrt{\gamma_R^2 + \gamma_J^2}}. \tag{3.41}$$

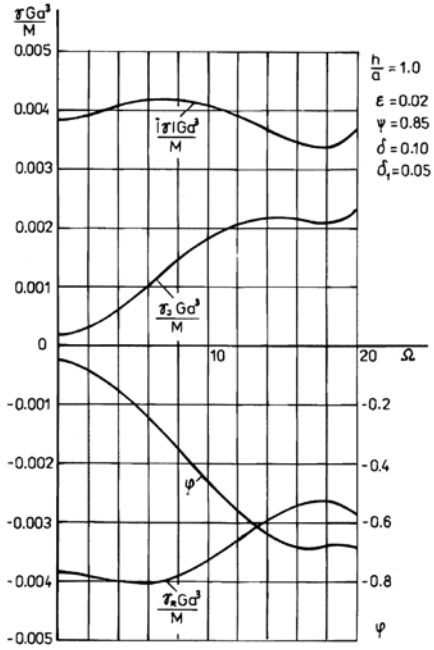

Fig. 3.1. Variation of mean dynamic angular displacement of layered half-space.

The variations of the mean dynamic angular displacements of the layered half-space, of the amplitudes of torsional vibration for the mass on the subbase and of the mechanical impedance functions are plotted in Figs. 3.1–3.3. They were calculated according to equations (3.35), (3.39) and (3.41) for the following parameter values: ε=0.02, γ=0.85, δ=0.1, δ_1=0.05, h/a=1.0.

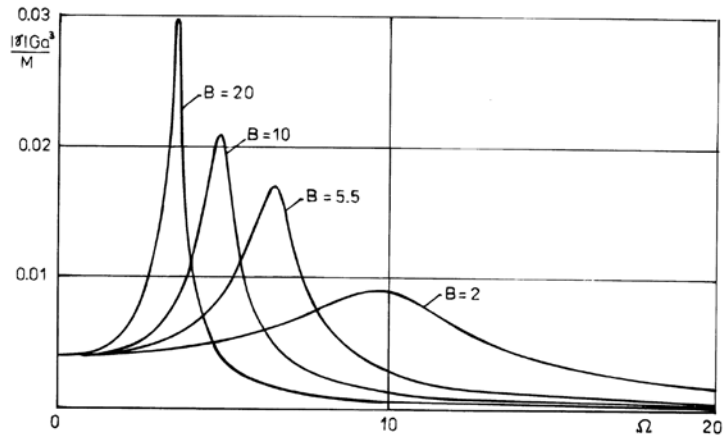

Fig. 3.2. Amplitude-frequency characteristics for torsional vibration of mass on layered half-space.

The dependence of the mean dynamic angular displacements of the layered half-space, $|\gamma|$, on the ratio of the layer thickness h to the radius a for fixed values of the frequency Ω is shown in Fig. 3.4. It can be seen that the amplitudes of dynamic angular displacements for $h/a>1$ are stable whereas for $h/a<1$ the amplitudes increase rapidly with decreasing h/a.

The amplitude of dynamic angular displacement is linearly dependent on the value ε, which follows from equation (3.35). For instance, the dependence of $|\gamma|$ on ε for $h/a=1.5$ is shown in Fig. 3.5.

3.1.3 Vertical vibration of layer on viscoelastic half-space

Starting from the scheme of relationships between the general stress tensor and general strain tensor we can express the relationships between the tensor of the mean normal

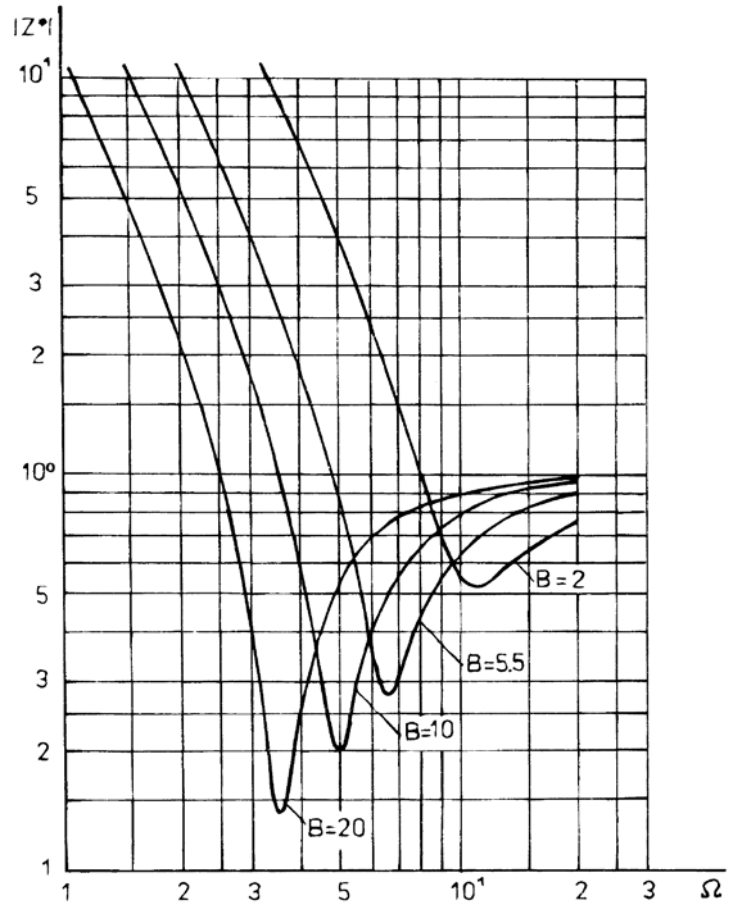

Fig. 3.3. Mechanical impedance functions for torsional vibration of mass on layered half-space.

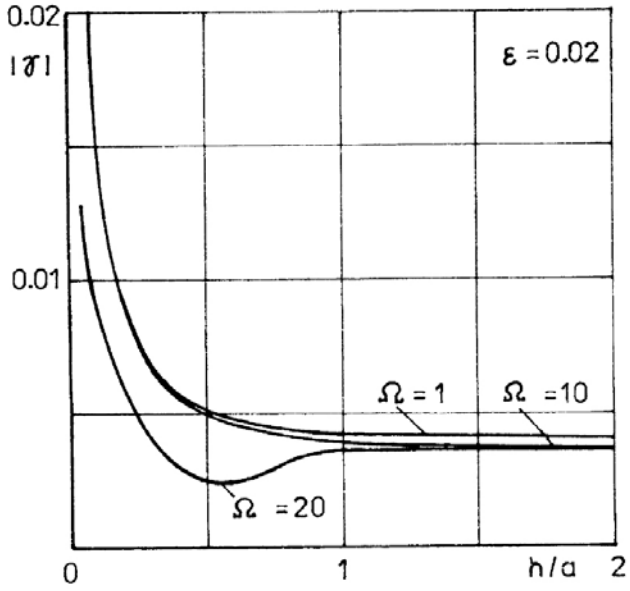

Fig. 3.4. Dependence of mean dynamic angular displacement |γ| on ratio *h/a* for fixed values of Ω.

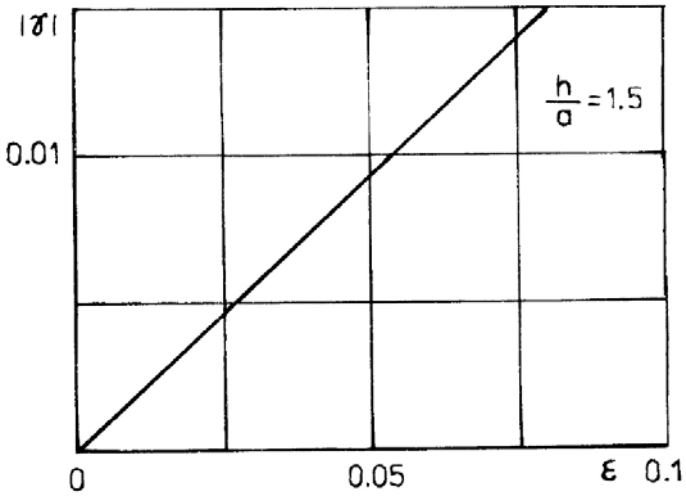

Fig. 3.5. Variation of amplitude of dynamic angular displacement |γ| with ratio *ε*.

stresses and the tensor of the mean normal deformations by using the complex bulk modulus *B**, and the relationships between the stress deviator and strain deviator by using the

complex modulus G^*. In the case of axial symmetry and cylindrical coordinates (r, φ, z), the equations of motion have the form

$$\begin{aligned}
\varrho\frac{\partial^2 u}{\partial t^2} &= \left(B^* + \tfrac{4}{3}G^*\right)\left(\frac{\partial^2 u}{\partial r^2} + \frac{1}{r}\frac{\partial u}{\partial r} - \frac{u}{r^2} + \frac{\partial^2 w}{\partial r \partial z}\right) \\
&\quad + G\left(\frac{\partial^2 u}{\partial z^2} - \frac{\partial^2 w}{\partial r \partial z}\right) \\
\varrho\frac{\partial^2 w}{\partial t^2} &= \left(B^* + \tfrac{4}{3}G^*\right)\left(\frac{\partial^2 u}{\partial r \partial z} + \frac{1}{r}\frac{\partial u}{\partial z} + \frac{\partial^2 w}{\partial z^2}\right) \\
&\quad + G^*\left(\frac{\partial^2 w}{\partial r^2} + \frac{1}{r}\frac{\partial w}{\partial r} - \frac{1}{r}\frac{\partial u}{\partial z} - \frac{\partial^2 u}{\partial r \partial z}\right)
\end{aligned} \tag{3.42}$$

where u is horizontal displacement, w is vertical displacement and ϱ is density.

The stresses are given by the relationships

$$\begin{aligned}
\sigma_r &= \left(B^* + \tfrac{4}{3}G^*\right)\frac{\partial u}{\partial r} + \left(B^* - \tfrac{2}{3}G^*\right)\left(\frac{u}{r} + \frac{\partial w}{\partial z}\right) \\
\sigma_z &= \left(B^* + \tfrac{4}{3}G^*\right)\frac{\partial w}{\partial z} + \left(B^* - \tfrac{2}{3}G^*\right)\left(\frac{u}{r} + \frac{\partial u}{\partial r}\right) \\
\sigma_\varphi &= \left(B^* + \tfrac{4}{3}G^*\right)\frac{u}{r} + \left(B^* - \tfrac{2}{3}G^*\right)\left(\frac{\partial u}{\partial r} + \frac{\partial w}{\partial z}\right) \\
\tau_{rz} &= \tau_{zr} = G^*\left(\frac{\partial u}{\partial z} + \frac{\partial w}{\partial r}\right)
\end{aligned} \tag{3.43}$$

Let us make use of Hankel's integral transformation on the functions of variable r in the equations of motion (3.42), i.e. for the function $u(r, z, t)$ in the form

$${}^{\mathrm{H}}u(\alpha, z, t) = \int_0^\infty ru(r, z, t)J_1(\alpha r)\mathrm{d}r \tag{3.44}$$

and for the function $w(z, t)$ according to the relationship

$$^{\mathrm{H}}w(\alpha, z, t) = \int_0^\infty rw(r, z, t)J_0(\alpha r)\mathrm{d}r. \tag{3.45}$$

Supposing that the steady harmonically variable vibration corresponds to the relationships

$$\begin{aligned} ^{\mathrm{H}}u(\alpha, z, t) &= {}^{\mathrm{H}}u(\alpha, z)\mathrm{e}^{\mathrm{i}\omega t} \\ ^{\mathrm{H}}w(\alpha, z, t) &= {}^{\mathrm{H}}w(\alpha, z)\mathrm{e}^{\mathrm{i}\omega t} \end{aligned} \tag{3.46}$$

the system of ordinary differential equations is established in the form

$$\begin{aligned} (B^* + \tfrac{1}{3}G^*)\alpha\frac{\mathrm{d}^{\mathrm{H}}w}{\mathrm{d}z} &= \left[\varrho\omega^2 - (B^* + \tfrac{4}{3}G^*)\alpha^2 + G^*\frac{\mathrm{d}^2}{\mathrm{d}z^2}\right]{}^{\mathrm{H}}u \\ -(B^* + \tfrac{1}{3}G^*)\alpha\frac{\mathrm{d}^{H}u}{\mathrm{d}z} &= \left[\varrho\omega^2 + (B^* + \tfrac{4}{3}G^*)\frac{\mathrm{d}^2}{\mathrm{d}z^2} - G^*\alpha^2\right]{}^{\mathrm{H}}w. \end{aligned} \tag{3.47}$$

If an auxiliary function *F(z)* is used according to the relationships

$$^{\mathrm{H}}u = \alpha(B^* + \tfrac{1}{3}G^*)\frac{\mathrm{d}}{\mathrm{d}z}F \tag{3.48}$$

$$^{\mathrm{H}}w = \left[\varrho\omega^2 - (B^* + \tfrac{4}{3}G^*)\alpha^2 + G^*\frac{\mathrm{d}^2}{\mathrm{d}z^2}\right]F \tag{3.49}$$

the first of equations (3.47) will be fulfilled identically, and by substituting into the second of equations (3.47), the differential equation is established after rearranging into the form

$$\begin{aligned} &\frac{\mathrm{d}^4F}{\mathrm{d}z^4} + \frac{\mathrm{d}^2F}{\mathrm{d}z^2}\left[-2\alpha^2 + \omega^2\left(\frac{1}{c_1^{*2}} + \frac{1}{c_2^{*2}}\right)\right. \\ &\left. + F\left[\alpha^4 - \omega^2\alpha^2\left(\frac{1}{c_1^{*2}} + \frac{1}{c_2^{*2}}\right) + \frac{\omega^4}{c_1^{*2}c_2^{*2}}\right] = 0\right. \end{aligned} \tag{3.50}$$

where the complex velocity of dilatational waves is given by

$$c_1^* = \sqrt{\frac{B^* + \frac{4}{3}G^*}{\varrho}} \tag{3.51}$$

and the complex velocity of shear waves by

$$c_2^* = \sqrt{\frac{G^*}{\varrho}}. \tag{3.52}$$

The roots of the characteristic equation for (3.50) are

$$q^2 = \alpha^2 - \frac{\omega^2}{c_1^{*2}} \tag{3.53}$$

$$s^2 = \alpha^2 - \frac{\omega^2}{c_2^{*2}}. \tag{3.54}$$

Hence the auxiliary function *F(z)* is given by the equation

$$F(z) = A_1^* \, e^{q^* z} + A_2^* \, e^{-q^* z} + A_3^* \, e^{s^* z} + A_4^* \, e^{-s^* z} \tag{3.55}$$

if

$$q^* = \sqrt{\alpha^2 - \frac{\omega^2}{c_1^{*2}}} \quad , \quad s^* = \sqrt{\alpha^2 - \frac{\omega^2}{c_2^{*2}}} \tag{3.56}$$

and A_1^*, A_2^*, A_3^*, A_4^* are arbitrary complex functions of variable α.

The displacement transforms ${}^{H}u$, ${}^{H}w$ are determined according to equations (3.48) and (3.49). For the layer medium I the equations have the form

$${}^{H}u^{I} = \alpha \left(A_1^* q_1^* e^{q_1^* z} - A_2^* q_1^* e^{-q_1^* z} + A_3^* s_1^* e^{s_1^* z} - A_4 s_1^* e^{-s_1^* z} \right) \tag{3.57}$$

$${}^{H}w^{I} = -q_1^{*2}(A_1^* e^{q_1 * z} + A_2^* e^{-q_1^* z}) - \alpha^2 (A_3 e^{s_1^* z} + A_4 e^{-s_1^* z}) \tag{3.58}$$

while the expression $(B_1^* + \frac{1}{3} G_1^*)$ was inserted into the unknown functions A_1^*, A_2^*, A_3^*, A_4^*. For the half-space medium in accordance with the physical meaning of the problem we use only exponentially decreasing members and the displacement transforms have the form

$${}^{H}u = -\alpha (q^* A_5^* e^{-q^* z} + s^* A_6^* e^{-s^* z}) \tag{3.59}$$

$${}^{H}w = -\alpha (A_5^* q^{*2} e^{-q^* z} + \alpha^2 A_6^* e^{-s^* z}) \tag{3.60}$$

where A_5^*, A_6^* are arbitrary complex functions of a and the expression $(B^* + \frac{1}{3} G^*)$ has been inserted into the A_5^*, A_6^*.

The equations for stress transforms can be established according to the relationships (3.43). If the equation for σ_z is multiplied by the expression $rJ_0(\alpha r)$ and integrated in the

limits (0, ∞) and similarly the equation for τ_{rz} is multiplied by $rJ_1(\alpha r)$ and integrated in the limits (0, ∞), the stress transforms in the layer medium are given by the relationships

$$
\begin{aligned}
{}^{\mathrm{H}}\sigma_z^{\mathrm{I}} = {} & \left[\left(B_1^* + \tfrac{4}{3}G_1^*\right)q_1^{*2} - \left(B_1^* - \tfrac{2}{3}G_1^*\right)\alpha^2\right]\left(-A_1^* q_1^* e^{q_1^* z}\right. \\
& \left. + A_2^* q_1^* \mathrm{e}^{-q_1^* z}\right) + 2G_1^* s_1^* \alpha^2 \left(-A_3^* \mathrm{e}^{s_1^* z} + A_4^* \mathrm{e}^{-s_1^* z}\right)
\end{aligned} \tag{3.61}
$$

$$
\begin{aligned}
{}^{\mathrm{H}}\tau_{rz}^{\mathrm{I}} = {} & G_1^* \alpha \left[2q_1^{*2}\left(A_1^* \mathrm{e}^{-q_1^* z} + A_2^* \mathrm{e}^{-q_1^* z}\right)\right. \\
& \left. + (s_1^{*2} + \alpha^2)\left(A_3^* \mathrm{e}^{s_1^* z} + A_4^* \mathrm{e}^{-s_1^* z}\right)\right].
\end{aligned} \tag{3.62}
$$

The stress transforms in the half-space medium are given by the expressions

$$
\begin{aligned}
{}^{\mathrm{H}}\sigma_z = {} & \left[\left(B^* + \tfrac{4}{3}G^*\right)q^{*2} - \left(B^* - \tfrac{2}{3}G^*\right)\alpha^2\right] q^* A_5^* \mathrm{e}^{-q^* z} \\
& + 2G^* s^* \alpha^2 A_6^* \mathrm{e}^{-s^* z}
\end{aligned} \tag{3.63}
$$

$$
{}^{\mathrm{H}}\tau_{rz} = G^* \alpha \left[2q^{*\,2} A_5^* \, \mathrm{e}^{-q^* z} + (s^{*2} + \alpha^2) A_6^* \mathrm{e}^{-s^* z}\right]. \tag{3.64}
$$

Boundary conditions and contact conditions at the interface

We are interested in the vertical displacement of the layer on the half-space under a dynamic, harmonically variable normal load on the layer surface. It is assumed that the normal load is uniformly distributed on a circular area with radius *a,* according to the variation that corresponds to the static contact problem of a rigid disk on the half-space. The boundary conditions at the layer surface for z=0 are

$$
\begin{aligned}
&\text{(a)} && \sigma_z^{\mathrm{I}} = p_0 \, \mathrm{e}^{\mathrm{i}\omega t} \, , && 0 < r < a \\
& && \sigma_z^{\mathrm{I}} = 0 \, , && r > a \\
& && \tau_{rz}^{\mathrm{I}} = 0 \\
&\text{(b)} && \sigma_z^{\mathrm{I}} = \frac{P \mathrm{e}^{\mathrm{i}\omega t}}{2\pi a (a^2 - r^2)^{1/2}} , && 0 < r < a \\
& && \sigma_z^{\mathrm{I}} = 0, && r > a \\
& && \tau_{rz}^{\mathrm{I}} = 0
\end{aligned} \tag{3.65}
$$

where p_0 is the load intensity and P is the normal force.

By using Hankel's integral transformation the transforms are expressed in the form

(a)
$$ {}^{\mathrm{H}}\sigma_z^{\mathrm{I}} = \frac{p_0 a J_1(\alpha a)}{\alpha} \tag{3.66} $$

(b)
$$ {}^{\mathrm{H}}\sigma_z^{\mathrm{I}} = \frac{P}{2\pi a}\,\frac{\sin(\alpha a)}{\alpha}. \tag{3.67} $$

The contact conditions at the interface of the layer and the half-space are

$$ \begin{aligned} ({}^{\mathrm{H}}u^{\mathrm{I}})_{z=h} &= ({}^{\mathrm{H}}u)_{z=h} \\ ({}^{\mathrm{H}}w^{\mathrm{I}})_{z=h} &= ({}^{\mathrm{H}}w)_{z=h} \\ ({}^{\mathrm{H}}\sigma_z^{\mathrm{I}})_{z=h} &= ({}^{\mathrm{H}}\sigma_z)_{z=h} \\ ({}^{\mathrm{H}}\tau_{rz}^{\mathrm{I}})_{z=h} &= ({}^{\mathrm{H}}\tau_r z)_{z=h}. \end{aligned} \tag{3.68} $$

By substituting into the boundary and contact conditions and rearranging, the system of equations in Table 3.1 is obtained for the calculation of unknown complex functions $A_1^*, A_2^*, \ldots A_6^*$. This system can only be solved numerically for fixed values of angular frequency ω and α.

The originals of the displacements and stresses were obtained by the inverse of Hankel's transformation according to the relationships

$$ u(r,z,t) = \mathrm{e}^{\mathrm{i}\omega t} \int_0^\infty \alpha\, {}^{\mathrm{H}}u\,(\alpha,z)\, J_1(\alpha r)\mathrm{d}\alpha $$

$$ w(r,z,t) = \mathrm{e}^{\mathrm{i}\omega t} \int_0^\infty \alpha\, {}^{\mathrm{H}}w\,(\alpha,z)\, J_0(\alpha r)\mathrm{d}\alpha $$

Table 3.1. System of equations.

A_1^*	A_2^*	A_3^*	A_4^*	A_5^*	A_6^*	Right-hand side
$-q_l^* a_1^*$	$q_l^* a_1^*$	$-2s_l^*\alpha^2$	$2s_l^*\alpha^2$			$(\sigma_z^I)_{z=0}/G_l^*$
$2q_l^{*2}$	$2q_l^{*2}$	$(s_l^{*2}+\alpha^2)$	$(s_l^{*2}+\alpha^2)$			0
$q_l^* e^{q_l^* h}$	$-q_l^* e^{-q_l^* h}$	$s_l^* e^{s_l^* h}$	$-s_l^* e^{-s_l^* h}$	$a_3^* q^* e^{-q^* h}$	$a_3^* s^* e^{-s^* h}$	0
$-q_l^{*2} e^{q_l^* h}$	$-q_l^{*2} e^{-q_l^* h}$	$-\alpha^2 e^{s_l^* h}$	$-\alpha^2 e^{-s_l^* h}$	$a_3^* q^{*2} e^{-q^* h}$	$a_3^* \alpha^2 e^{-s^* h}$	0
$-a_1^* q_l^* e^{q_l^* h}$	$a_1^* q_l^* e^{-q_l^* h}$	$-2s_l^*\alpha^2 e^{s_l^* h}$	$2s_l^*\alpha^2 e^{-s_l^* h}$	$-a_2^* q^* e^{-q^* h}$	$-2a_4^* s^* \alpha^2 e^{-s^* h}$	0
$2q_l^{*2} e^{q_l^* h}$	$2q_l^{*2} e^{-q_l^* h}$	$(s_l^{*2}+\alpha^2) e^{s_l^* h}$	$(s_l^{*2}+\alpha^2) e^{-s_l^* h}$	$-2a_4^* q^{*2} e^{-q^* h}$	$-a_4^* (s^{*2}+\alpha^2) e^{-s^* h}$	0

where $a_1^* = \frac{B_l^* + \frac{1}{3}G_l^*}{G_l^*} q_l^{*2} - \frac{B_l^* - \frac{2}{3}G_l^*}{G_l^*} \alpha^2$

$a_2^* = \frac{B^* + \frac{1}{3}G^*}{G_l^*} q^{*2} - \frac{B^* - \frac{2}{3}G^*}{G_l^*} \alpha^2$

$a_3^* = \frac{B^* + \frac{1}{3}G^*}{B_l^* + \frac{1}{3}G_l^*}$

$a_4^* = \frac{G^*}{G_l^*}$

$$\sigma_z(r,z,t) = \mathrm{e}^{\mathrm{i}\omega t} \int_0^\infty \alpha \, {}^{\mathrm{H}}\sigma_z \, (\alpha, z) \, J_0(\alpha r) \mathrm{d}\alpha$$

$$\tau_{rz}(r,z,t) = \mathrm{e}^{\mathrm{i}\omega t} \int_0^\infty \alpha \, {}^{\mathrm{H}}\tau_{rz} \, (\alpha, z) \, J_1(\alpha r) \mathrm{d}\alpha \tag{3.69}$$

The sub-integral functions are complex functions of the real variable α; they have no discontinuities in the integration limits in view of the viscoelastic behaviour of the layer medium and half-space medium. It is possible to suppose that the improper integrals converge and can be evaluated by numerical integration. The numerical study is very laborious, however, and is not suitable for practical use.

3.2 Stress waves in layer on half-space without shear contact

The interpretation of the measurement results obtained on the pavement structures is based on the suppositon of the continual dispersion curve of quasi-flexural stress waves in the equivalent layer on a subgrade. This dispersion curve for the long wavelengths approaches the velocity of surface waves at the subgrade in consequence of the pavement contact with the subgrade. It is interesting to know whether this variance of the dispersion curve is also regular in the case of interrupted shear contact between the layer and the half-space. Such a study is also significant for the technical theories of the equivalent plate on a subgrade.

The relationships derived in the previous chapter make it possible to study the influence of imperfect contact at the interface of the layer and the halfspace on the variance of the dispersion curves of stress-wave propagation.

3.2.1 Boundary and contact conditions at the interface

Supposing the same boundary conditions as given by the relationships (3.64), (3.65) or (3.66), (3.67), the contact conditions at the interface of the layer and halfspace are

$$({}^{\mathrm{H}}u^{\mathrm{I}})_{z=h} = ({}^{\mathrm{H}}u)_{z=h}$$

$$({}^{\mathrm{H}}w^{\mathrm{I}})_{z=h} = ({}^{\mathrm{H}}w)_{z=h} \tag{3.70}$$

$$({}^{\mathrm{H}}\sigma_z^{\mathrm{I}})_{z=h} = ({}^{\mathrm{H}}\sigma_z)_{z=h}$$

$$\left({}^{\mathrm{H}}\tau_{rz}^{\mathrm{I}}\right)_{z=h} = 0$$

$$\left({}^{\mathrm{H}}\tau_{rz}\right)_{z=h} = 0.$$

By using the conditions (3.70) the complex functions A_5^*, A_6^* are eliminated in the form

$$A_5^* = \frac{\mathrm{e}^{q^* h}}{b_1^*}\left(A_1^*\, q_l^{*2}\, \mathrm{e}^{q_l^* h} + A_2^*\, q_l^{*2}\, \mathrm{e}^{-q_l^* h} + A_3^* \alpha^2 \mathrm{e}^{s_l^* h} + A_4^* \alpha^2 \mathrm{e}^{-s_l^* h}\right)$$

$$A_6^* = \frac{-2q^{*2}}{s^{*2} + \alpha^2}\, \mathrm{e}^{-q^* h + s^* h} + A_5^* \tag{3.71}$$

and the system of equations in Table 3.2 is given for the unknown complex functions $A_1^*, A_2^*, A_3^*, A_4^*$.

3.2.2 Frequency equation

The frequency equation of the problem can be established as a determinant of matrix coefficients for the homogenous system of equations in Table 3.2. By adding and subtracting the first and second column of matrix coefficients like the third and fourth column, together with other rearrangements, the elements of matrix coefficients in dimensionless form are given by the relationships

$$a_{11} = 0$$

$$a_{12} = -(S_1^2 + F^2)$$

$$a_{13} = 0$$

$$a_{14} = -2S_1F^2$$

$$a_{21} = 2Q_1$$

$$a_{22} = 0$$

$$a_{23} = S_1^2 + F^2$$

$$a_{24} = 0$$

Table 3.2. System of equations.

A_1^*	A_2^*	A_3^*	A_4^*	Right-hand side
$-q_1^* a_1^*$	$q_1^* a_1^*$	$-2s_1^*\alpha^2$	$2s_1^*\alpha^2$	$\frac{P}{G_1 a}\frac{\sin(\alpha a)}{2\pi\alpha(1+i\delta_1)}$
$2q_1^{*2}$	$2q_1^{*2}$	a_1^*	a_1^*	0
$2q_1^{*2}e^{q_1^* h}$	$2q_1^{*2}e^{-q_1^* h}$	$a_1^* e^{s_1^* h}$	$a_1^* e^{-s_1^* h}$	0
$\left(\frac{q_1^{*2}}{b_1^*}-\frac{a_1^* q_1^*}{b_2^*}\right)\frac{e^{q_1^* h}}{e^{-q_1^* h}}$	$\left(\frac{q_1^{*2}}{b_1^*}+\frac{a_1^* q_1^*}{b_2^*}\right)$	$\left(\frac{\alpha^2}{b_1^*}-\frac{2s_1^*\alpha^2}{b_2^*}\right)\frac{e^{s_1^* h}}{e^{-q_1^* h}}$	$\left(\frac{\alpha^2}{b_1^*}+\frac{2s_1^*\alpha^2}{b_2^*}\right)\frac{e^{-s_1^* h}}{e^{-q_1^* h}}$	0

where $a_1^* = s_1^* + \alpha^2$

$$b_1^* = \frac{q^{*2}(s^{*2}-\alpha^2)}{s^{*2}+\alpha^2}$$

$$b_2^* = -\frac{G_1^*}{G_1^*} q^* \frac{\left[\left(s^{*2}+\alpha^2\right)^2 - 4q^* s^* \alpha^2\right]}{s^{*2}+\alpha^2}$$

right side in case a): $\frac{p_0 a J_1(\alpha a)}{G_1 \alpha(1+i\delta_1)}$

$$a_{31} = 2Q_1(e^{Q_1} + e^{-Q_1})$$

$$a_{32} = 2Q_1(e^{Q_1} - e^{-Q_1})$$

$$a_{33} = (S_1^2 + F^2)(e^{S_1} + e^{-S_1})$$

$$a_{34} = (S_1^2 + F^2)(e^{S_1} - e^{-S_1})$$

$$a_{41} = \frac{\left[-\frac{G^*}{G_1^*}Q_1R - Q(S^2 - F^2)(S_1^2 + F^2)\right]e^{Q_1}}{2(S^2 + F^2)}$$

$$+\frac{\left[-\frac{G^*}{G_1^*}Q_1R + Q(S^2 - F^2)(S_1^2 + F^2)\right]e^{-Q_1}}{2(S^2 + F^2)}$$

$$a_{42} = \frac{\left[-\frac{G^*}{G_1^*}Q_1R - Q(S^2 - F^2)(S_1^2 + F^2)\right]e^{Q_1}}{2(S^2 + F^2)}$$

$$-\frac{\left[-\frac{G^*}{G_1^*}Q_1R + Q(S^2 - F^2)(S_1^2 + F^2)\right]e^{-Q_1}}{2(S^2 + F^2)}$$

$$a_{43} = \frac{F^2\left[-\frac{G^*}{G_1^*}R - 2QS_1(S^2 - F^2)\right]e^{S_1}}{2(S^2 + F^2)}$$

$$+\frac{F^2\left[-\frac{G^*}{G_1^*}R + 2QS_1(S^2 - F^2)\right]e^{-S_1}}{2(S^2 + F^2)}$$

$$a_{44} = \frac{F^2\left[-\frac{G^*}{G_1^*}R - 2QS_1(S^2 - F^2)\right]e^{S_1}}{2(S^2 + F^2)} \tag{3.72}$$

$$-\frac{F^2\left[-\frac{G^*}{G_1^*}R + 2QS_1(S^2 - F^2)\right]e^{-S_1}}{2(S^2 + F^2)}$$

where

$$\begin{gathered} F=\alpha h \\ Q=q^{*}h \\ Q_1 = q_1^{*}h \\ S=s^{*}h \\ S_1 = s_1^{*}h \end{gathered} \tag{3.73}$$

and

$$\begin{gathered} R=(S^2+F^2)-4QSF^2 \\ G^{*}=G(1+\mathrm{i}\delta) \\ G_1^{*} = G_1(1+\mathrm{i}\delta_1). \end{gathered} \tag{3.74}$$

The determinants of the matrix coefficients equal to zero have the form

$$\begin{gathered} a_{12}\,[a_{21}\,a_{33}\,a_{44}+a_{41}\,a_{23}\,a_{34}-a_{21}\,a_{34}\,a_{43}-a_{31}\,a_{23}\,a_{44}] \\ +a_{14}\,a_{21}\,a_{32}\,a_{43}+a_{31}\,a_{42}\,a_{23}-a_{41}\,a_{32}\,a_{23}-a_{21}\,a_{42}\,a_{33}]=0. \end{gathered} \tag{3.75}$$

3.2.3 Curves of dispersion for stress-wave phase velocities

The frequency equation (3.75) for the layer on a half-space without shear contact makes it possible to obtain the dispersion variances of stress-wave propagation in the system. The number of dispersion curves that determine the dependence of the propagation characteristics on the frequency or wavelength is infinite, as is the number of natural frequencies of vibration of bodies with continually distributed mass.

The process of determination of the dispersion curve variances from equation (3.75) can be carried out using two alternatives, as follows.

(a) The complex values of wave number F in dimensionless form are found for fixed values of frequency, by which the frequency equation (3.75) is fulfilled.

The concretization of such a procedure is in the formation of a dimensionless frequency β in the form

$$\beta = \frac{\omega h}{c_2^{\mathrm{I}}} \tag{3.76}$$

and the relationships

$$Q_1 = \sqrt{F^2 - \varepsilon_{11}^2\,\frac{\beta^2}{1+\mathrm{i}\delta_1}} \tag{3.77}$$

$$Q = \sqrt{F^2 - \varepsilon_{12}^2 \frac{\beta^2}{1 + \mathrm{i}\delta}} \tag{3.78}$$

$$S_1 = \sqrt{F^2 - \frac{\beta^2}{1 + \mathrm{i}\delta_1}} \tag{3.19}$$

$$S = \sqrt{F^2 - \varepsilon_{22}^2 \frac{\beta^2}{1 + \mathrm{i}\delta}} \tag{3.80}$$

where

$$\varepsilon_{11} = \frac{c_2^{\mathrm{I}}}{c_1^{\mathrm{I}}} \tag{3.81}$$

$$\varepsilon_{12} = \frac{c_2^{\mathrm{I}}}{c_1} \tag{3.82}$$

$$\varepsilon_{22} = \frac{c_2^{\mathrm{I}}}{c_2}. \tag{3.83}$$

Every quantity representing the state of stress or deformation of the system is by stress-wave propagation from the source, proportionate to the expression $\mathrm{e}^{\mathrm{i}(\omega t - \alpha r)}$. The wave number α. has to be complex, considering the viscoelastic behaviour of the material and the dissipation of energy into the halfspace. The physically real solutions correspond to the complex roots of the wave number, the imaginary part of which is negative.

The phase velocity c is determined in dimensionless form by the equation

$$\frac{c}{c_2^{\mathrm{I}}} = \frac{\beta}{F_{\mathrm{R}}} \tag{3.84}$$

where $F_{\mathrm{R}}=2\pi h/\Lambda$ is the real part of the dimensionless wave number.

The imaginary part F_{J} of the dimensionless wave number represents the damping and dissipation laws of stress-wave propagation in the system medium.

b) The second procedure commences from the complex phase velocity $c^*=c_{\mathrm{R}}+\mathrm{i}c_{\mathrm{J}}$. The dimensionless complex phase velocity C corresponds to the relationship

$$C = \frac{c^*}{c_2^{\mathrm{I}}} \tag{3.85}$$

and the expressions for Q_1, Q, S_1, S are put into the form

$$Q_1 = \beta \sqrt{\frac{1}{C^2} - \frac{\varepsilon_{11}^2}{1 + \mathrm{i}\delta_1}} \tag{3.86}$$

$$Q = \beta \frac{1}{C^2} - \frac{\varepsilon_{12}^2}{1 + \mathrm{i}\delta} \tag{3.87}$$

$$S_1 = \beta \sqrt{\frac{1}{C^2} - \frac{1}{1 + \mathrm{i}\delta_1}} \tag{3.88}$$

$$S = \beta \sqrt{\frac{1}{C^2} - \frac{\varepsilon_{22}^2}{1 + \mathrm{i}\delta}}. \tag{3.89}$$

The complex values of dimensionless phase velocity C are found for fixed values of frequency β, by which the frequency equation (3.75) is fulfilled.

If

$$\beta = CF \tag{3.90}$$

then the real and imaginary parts of the wave number are given by

$$F_{\mathrm{R}} = \frac{\beta\, C_{\mathrm{R}}}{C_{\mathrm{R}}^2 + C_{\mathrm{J}}^2} \tag{3.91}$$

$$F_{\mathrm{J}} = \frac{-\beta\, C_{\mathrm{R}}}{C_{\mathrm{R}}^2 + C_{\mathrm{J}}^2}. \tag{3.92}$$

Then the phase velocity c in dimensionless form is as follows

$$\frac{c}{c_2^{\mathrm{I}}} = \frac{C_{\mathrm{R}}^2 + C_{\mathrm{J}}^2}{C_{\mathrm{R}}}. \tag{3.93}$$

At the same time the relationships for the calculation of C_{R} and C_{J} by means of the real and imaginary part of the wave number are valid

$$C_{\mathrm{R}} = \frac{\beta\, F_{\mathrm{R}}}{F_{\mathrm{R}}^2 + F_{\mathrm{J}}^2} \tag{3.94}$$

$$C_{\mathrm{J}} = \frac{-\beta\, F_{\mathrm{J}}}{F_{\mathrm{R}}^2 + F_{\mathrm{J}}^2}. \tag{3.95}$$

It follows from this that physically real values of the complex dimensionless velocity C, which fulfil the frequency equation (3.75) have to be a number with a positive imaginary part.

In practice the realization of the procedure for the determination of the complex roots of frequency equation (3.75) is very laborious. Application of numerical methods of linear or quadratic interpolation, or the methods of iteration that are known and used for finding the real roots of transcendental equations, give favourable results only in a limited frequency range.

The determination of the roots for frequency equation (3.75) and the basic forms of the dispersion curves was possible only by using the method of finding the zero contour lines for the real and imaginary part of the function. Their point of intersection gives the approximate value of the complex root.

3.2.4 Numerical results

A numerical study was carried out for characteristics corresponding to the highway cement concrete structure with parameters:

ε_{11}=0.5765, ε_{12}=6.5500, ε_{22}=13.6500, $\varrho_1/\varrho = 1.333$, δ_1=0.10, δ=0.20, μ_1=0.25, μ=0.35

The variations of the dispersion curves for the real and imaginary part of the wave number F_R, F_J versus frequency β in the case of longitudinal and flexural waves are drawn in Fig. 3.6. It can be seen that F_R^0 at low values of frequency β approaches the line that represents surface waves in the halfspace. The values F_R^P move at low frequencies on the line corresponding to the dilatational waves of the layer medium. At high frequencies the dispersion variances F_R^0 and F_R^P approach the line that represents surface waves in the layer medium.

The relationships of phase velocities and F_J versus frequency β are drawn in Fig. 3.7 and the relationship of dimensionless phase velocities c/c_2^I and the cofficient of damping and dissipation F_J versus the ratio h/Λ are drawn in Fig. 3.8.

It can be stated that the forms of the basic dispersion curves of phase velocities for longitudinal and flexural waves correspond at higher frequencies or lower wavelengths to the forms of the dispersion curves that are valid for the free layer. The contact of the layer and the half-space without shear contact is apparent in the region $h/\Lambda<0.15$, where the phase velocities of flexural waves decrease and approach the velocity of surface waves in the half-space medium if the ratio h/Λ. approaches zero.

The phase velocities of longitudinal waves in the region $h/\Lambda<0.15$ achieve values that exceed the velocity of dilatational waves in the layer, c_1^I, but for $h/\Lambda\rightarrow 0$ they decrease intensively. It cannot in practice be confirmed, whether the values approach the value c_R for $h/\Lambda\rightarrow 0$.

The influence of the contact conditions at the interface of the pavement structure and half-space as derived from theoretical and numerical solutions can be supported by the results of measurements on pavement structures. These are acting as the equivalent layer on a subgrade. The contact conditions with the subgrade are complex. They correspond to imperfect contact, the quality of which changes with time from perfect contact to a non-shear or to the local loss of contact with the subgrade.

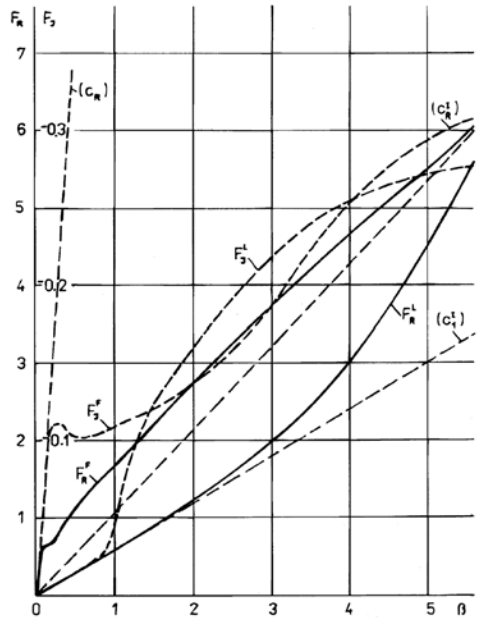

Fig. 3.6. Variation of real and imaginary part of wave mumber F_R, F_J versus frequency β for longitudinal and flexural waves in layer on half-space.

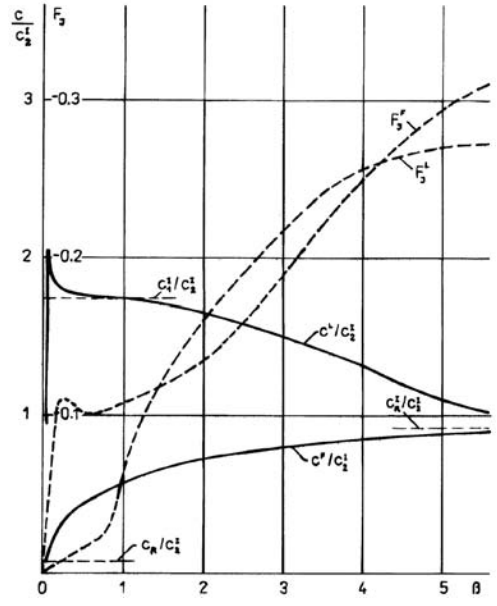

Fig. 3.7. Relationship of phase velocities c/c_2^I and coefficient of dissipation F_J to frequency β.

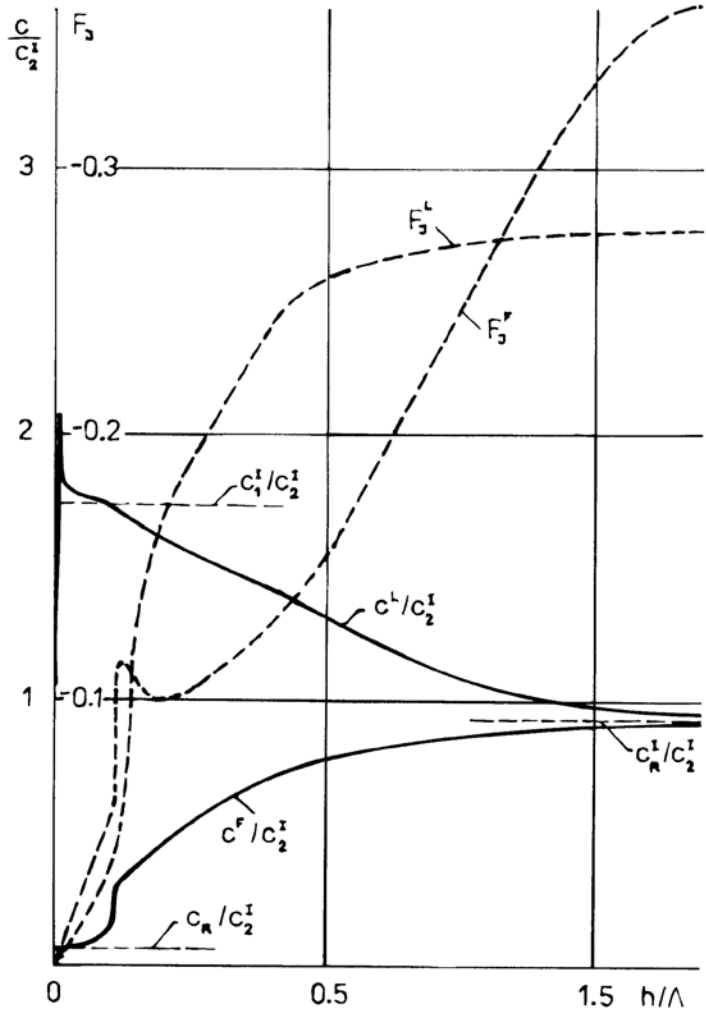

Fig. 3.8. Relationship of phase velocities c/c_2^I and dissipation coefficient F_J versus ratio h/Λ.

The direct measurement of phase velocities in the range of very low frequencies is difficult considering the great wavelength Λ. It is possible to evaluate the phase velocities according to the results of measurement by the mechanical impedance method [1.38, 3.7].

The relationships of the velocities of flexural stress waves c versus the ratio h/Λ on eight sections of flexible pavement determined by measurement are shown in Fig. 3.9. The average thickness of the equivalent pavement layer was approximately h=0.40 m and the surface-wave velocity of the subgrade, c_R=80–120 m/s. Measurement by the mechanical impedance method was made in the frequency range 25–1500 Hz and evaluation of the phase velocities was carried out according to the results below the resonance frequencies.

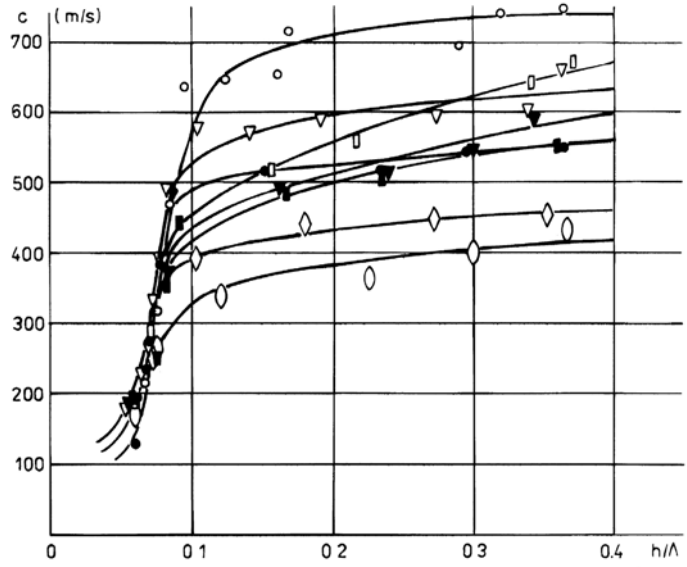

Fig. 3.9. Relationship of velocities of flexural stress waves, c, versus ratio h/Λ on sections of flexible pavement.

The form of the dispersion curve for longitudinal stress waves may be compared with the experimental one obtained from measurements on a plane model [3.8], formed by a duralumin strip in contact with acrylon medium. The results of direct measurement of phase velocities are plotted in Fig. 3.10 and manifest a similar form of dispersion as for the theoretical solution.

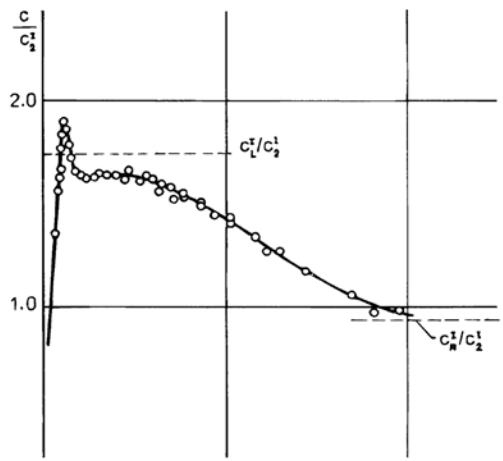

Fig. 3.10. Experimental dispersion curve for longitudinal stress waves obtained on plane model.

3.3 Plate on half-space without shear contact

The model of the equivalent layer replaced by a plate lying on the half-space without shear contact is a system that can adequately reflect the dynamic response of pavement structures and make it possible to realize the numerical calculations.

The differential equation of motion for the plate, including the influence of shear and rotational inertia [3.9, 3.10], has for unloaded elastic and isotropic plate the form

$$\nabla^2\nabla^2 w - \left(\frac{1}{c_3^2}+\frac{1}{c_R^2}\right)\frac{\partial^2\nabla^2 w}{\partial t^2}+\frac{1}{c_3^2 c_R^2}\frac{\partial^4 w}{\partial t^4}+\frac{\varrho h}{D}\frac{\partial^2 w}{\partial t^2}=0 \tag{3.96}$$

where w is the vertical deflection of the plate, and the velocity of longitudinal waves c_3 and the velocity of surface waves c_R are determined by the relationships

$$c_3=\sqrt{\frac{E}{\varrho\,(1-\mu^2)}}$$

$$c_R=\sqrt{\frac{\kappa G}{\varrho}} \tag{3.97}$$

h is the thickness of the plate, ϱ is the material density and the plate constant D is given in the form

$$D=\frac{Eh^3}{12(1-\mu^2)}. \tag{3.98}$$

The coefficient κ expresses the influence of unequable distribution of shear stresses along the plate thickness. The relationship for κ in the form

$$\kappa=\left(\frac{0.87+1.12\mu}{(1+\mu)}\right)^2 \tag{3.99}$$

was derived in [3.11] by comparing the phase velocity of propagation for flexural stress waves with the velocity of surface Rayleigh waves at a very short wavelength.

The differential operator ∇^2 in polar coordinates (r, φ) has the form

$$\nabla^2=\frac{\partial^2}{\partial r^2}+\frac{1}{r}\frac{\partial}{\partial r}+\frac{1}{r^2}\frac{\partial^2}{\partial\varphi^2}. \tag{3.100}$$

The differential equation (3.96) produces a basic dispersion curve for flexural stress waves that is practically identical to the exact solution of the theory of elasticity for a layer with free surfaces.

The higher forms of dispersion curve are reduced to only one dispersion curve, which approaches the velocity c_3 for short wavelengths.

The variation of dispersion curves for a plate with free surfaces is drawn in Fig. 3.11 for Poisson's ratio μ=0.30.

Provided that the loaded plate is lying on the half-space without shear contact, the differential equation of motion has the form

$$\nabla^2\nabla^2 w - \left(\frac{1}{c_3^2}+\frac{1}{c_R^2}\right)\frac{\partial^2\nabla^2 w}{\partial t^2} + \frac{1}{c_3^2 c_R^2}\frac{\partial^4 w}{\partial t^4} + \frac{\varrho h}{D}\frac{\partial^2 w}{\partial t^2} = \frac{p}{D} - \frac{q}{D} \tag{3.101}$$

if p is the intensity of vertical load of the plate surface and q is the vertical reaction of the half-space.

Now the basic dispersion curve for flexural stress waves corresponds to the model of the equivalent layer on a subgrade; that is, the phase velocities approach that of surface Rayleigh waves in the half-space for longwave lengths Λ.

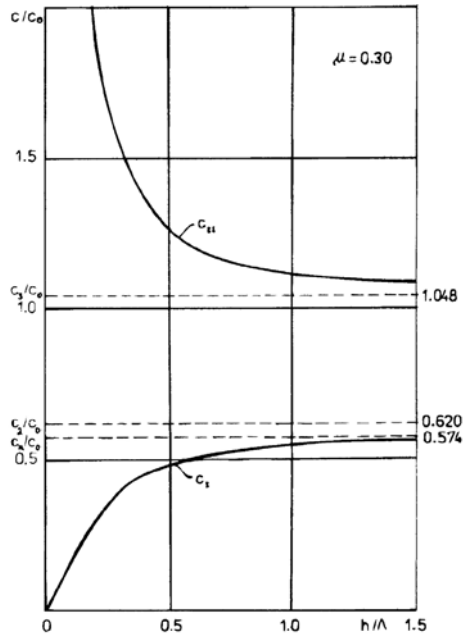

Fig. 3.11. Dispersion curves for plate with free surfaces.

3.3.1 Conditions at the interface of plate and half-space

We assume an axisymmetrical problem, with harmonic steady vibration and viscoelastic behaviour of the plate and half-space on the basis of the complex moduli concept with equal rheological parameters for the volume and form changes.

By using Hankel's integral transformation on the equation of motion (3.101) according to the relationships

$$
\begin{aligned}
{}^{\mathrm{H}}w\,(\alpha,t) &= \int_0^\infty r\, w(r,t)\, J_0(\alpha r)\, \mathrm{d}r \\
{}^{\mathrm{H}}q\,(\alpha,t) &= \int_0^\infty r\, q(r,t)\, J_0(\alpha r)\, \mathrm{d}r \\
{}^{\mathrm{H}}p\,(\alpha,t) &= \int_0^\infty r\, p(r,t)\, J_0(\alpha r)\, \mathrm{d}r
\end{aligned}
\tag{3.102}
$$

and the assumption of harmonic vibration

$$
\begin{aligned}
{}^{\mathrm{H}}w(\alpha,\, t) &= {}^{\mathrm{H}}w(\alpha)\mathrm{e}^{\mathrm{i}\omega t} \\
{}^{\mathrm{H}}q(\alpha,\, t) &= {}^{\mathrm{H}}q(\alpha)\, \mathrm{e}^{\mathrm{i}\omega t} \\
{}^{\mathrm{H}}p(\alpha,\, t) &= {}^{\mathrm{H}}p(\alpha)\, \mathrm{e}^{\mathrm{i}\omega t}
\end{aligned}
\tag{3.103}
$$

the equation is obtained from (3.101) in the form

$$
{}^{\mathrm{H}}w\left\{\alpha^4 - \left(\frac{1}{c_3^{*2}} + \frac{1}{c_{\mathrm{R}}^{*2}}\right)\alpha^2\omega^2 + \frac{1}{c_3^{*2}c_{\mathrm{R}}^{*2}}\,\omega^4 - \frac{\varrho h\omega^2}{D^*}\right\} = \frac{{}^{\mathrm{H}}p}{D^*} - \frac{{}^{\mathrm{H}}q}{D^*} \tag{3.104}
$$

The conditions at the interface of the plate and halfspace are given in the form

$$
\begin{aligned}
(\sigma_z)_{z=0} &= q(r,t),\ 0<r<\infty \\
(\tau_{rz})_{z=0} &= 0,\ 0<\mathrm{r}<\infty
\end{aligned}
\tag{3.105}
$$

The origin of the cylindrical coordinate system for the half-space is positioned at the interface of the plate and half-space.

The transform of the normal stresses on the half-space surface $({}^{\mathrm{H}}\sigma_z)_{z=0} = {}^{\mathrm{H}}q$, and for the transform of tangential stresses the equation is valid in the form

$$
{}^{\mathrm{H}}\tau_{rz} = \int_0^\infty r\, \tau_{rz}\, J_1(\alpha r)\mathrm{d}r \tag{3.106}
$$

By using equations (3.63), (3.64) for the transforms of the stresses in the half-space medium the fulfilling of the interface condition follows the system of equations

$$A_5^* q_z^* \left[\left(B_z^* + \frac{4}{3} G_z^* \right) q_z^{*2} - \left(B_z^* - \frac{2}{3} G_z^* \right) \alpha^2 \right] + A_6^* 2 G_z^* s_z^* \alpha^2 = {}^{\mathrm{H}}q$$
$$A_5^* 2 q_z^{*2} + A_6^* (s_z^{*2} + \alpha^2) = 0 \tag{3.107}$$

All quantities that refer to the half-space are indicated by the subscript z and the asterisk indicates their complex values considering the concept of complex moduli.

According to the system (3.107) the following relationships are valid:

$$A_5^* = \frac{(s_z^{*2} + \alpha^2)}{D_0^*} {}^{\mathrm{H}}q \tag{3.108}$$

$$A_6^* = \frac{-2 q_z^{*2}}{D_0^*} {}^{\mathrm{H}}q \tag{3.109}$$

if

$$D_0^* = G_z^* q_z^* \left[\left(2\alpha^2 - \frac{\omega^2}{c_{2z}^{*2}} \right)^2 - 4\alpha^2 q_z^* s_z^* \right]. \tag{3.110}$$

The transform of vertical deflection for the halfspace ${}^{\mathrm{H}}w_z$ is given according to (3.60) in the form

$${}^{\mathrm{H}}w_z = \frac{q_z^{*2} \left[(s_z^{*2} + \alpha^2)\, \mathrm{e}^{-q_z^* z} - 2\alpha^2\, \mathrm{e}^{-s_z^* z} \right]}{D_0^*} {}^{\mathrm{H}}q. \tag{3.111}$$

At the interface of the plate and half-space, i.e at z=0, considering the relationship (3.111) the following equation is valid:

$${}^{\mathrm{H}}q = \frac{D_0^*}{q_z^{*2} \left[(s_z^{*2} + \alpha^2) - 2\alpha^2 \right]} \left({}^{\mathrm{H}}w_z \right)_{z=0}. \tag{3.112}$$

Substituting (3.112) into (3.104) and considering that the vertical deflection of the plate w has to be equal to the vertical deflection of the half-space according to the relationship

$${}^{\mathrm{H}}w = \left({}^{\mathrm{H}}w_z \right)_{z=0} \tag{3.113}$$

the equation is obtained after rearrangement in the form

$${}^{\mathrm{H}}w = \frac{12(1-\mu^2)h}{E(1+\mathrm{i}\delta)} \frac{1}{F(\xi, \beta)} {}^{\mathrm{H}}p \tag{3.114}$$

where

$$F(\xi,\beta)=\xi^4-\beta^2\left(\frac{1-\mu}{2}+\frac{1}{\kappa}\right)\frac{\xi^2}{(1+\mathrm{i}\delta)}+\frac{(1-\mu)}{2\kappa}\frac{\beta^4}{(1+\mathrm{i}\delta)^2}$$

$$-\frac{6(1-\mu)\,\beta^2}{(1+\mathrm{i}\delta)}-6(1-\mu)\,\frac{G_z}{G}\,F_1(\xi,\beta) \tag{3.115}$$

if

$$F_1(\xi,\beta)=$$

$$\frac{(1+\mathrm{i}\delta_z)\left[\left(2\xi^2-\varepsilon_2^2\frac{\beta^2}{(1+\mathrm{i}\delta_z)}\right)^2-4\xi^2\sqrt{\xi^2-\varepsilon_1^2\frac{\beta^2}{(1+\mathrm{i}\delta_z)}}\sqrt{\xi^2-\varepsilon_2^2\frac{\beta^2}{(1+\mathrm{i}\delta_z)}}\right]}{(1+\mathrm{i}\delta)\varepsilon_2^2\,\frac{\beta^2}{(1+\mathrm{i}\delta_z)}\,\sqrt{\xi^2-\varepsilon_1^2\,\frac{\beta^2}{(1+\mathrm{i}\delta_z)}}} \tag{3.116}$$

and

$$\xi=\alpha h \tag{3.117}$$

$$\beta=\frac{\omega h}{c_2} \tag{3.118}$$

$$\varepsilon_1=\frac{c_2}{c_{1z}}=\frac{\sqrt{\frac{G}{\varrho}}}{\sqrt{\frac{E_z}{\varrho}\,\frac{(1-\mu_z)}{(1+\mu_z)(1-2\mu_z)}}} \tag{3.119}$$

$$\varepsilon_2=\frac{c_2}{c_{2z}} \tag{3.120}$$

where δ is the damping parameter of the plate material and δ_z is the damping parameter of the half-space material.

3.3.2 Normal dynamic load on circular contact area.

The basic type of dynamic load for the equivalent system of a pavement structure is a dynamic harmonically variable normal load of the surface on a circular area with radius *a*. We are interested in the deflection and internal forces of the plate, the subgrade reaction, the state of stresses and deformations of the half-space respectively.

The problem may be solved at the same time for two variable distributions of a normal load on a circular contact area: (a) a uniformly distributed normal load with intensity p_0; and (b) a load according to the function that corresponds to the static contact distribution of the rigid disk on the half-space.

Hankel's transforms have the form

(a)

$$^{\mathrm{H}}p = \frac{p_0 a J_1(\alpha a)\mathrm{e}^{\mathrm{i}\omega t}}{\alpha} = \frac{P}{\pi a}\,\frac{J_1(\alpha a)}{\alpha}\,\mathrm{e}^{\mathrm{i}\omega t}$$

(b)

$$^{\mathrm{H}}p = \frac{P}{2\pi a}\,\frac{\sin(\alpha a)}{\alpha}\,\mathrm{e}^{\mathrm{i}\omega t} \tag{3.121}$$

where P is the amplitude of the vertical resultant of a normal load.

3.3.3 Deflection of plate

The load transforms in the form (3.121) bring about the deflection of the equivalent plate on the half-space, the transform of which is obtained by the substitution of (3.121) into (3.114). Using the inverse of Hankel's integral transformation the deflection $w(r, t)$ is given by the relationship

(a)

$$w(r,t) = \frac{P\,\mathrm{e}^{\mathrm{i}\omega t}}{Ga}\,\frac{6(1-\mu)}{\pi}\int_0^\infty \frac{J_1\left(\xi\frac{a}{h}\right) J_0\left(\xi\frac{r}{h}\right)\mathrm{d}\xi}{(1+\mathrm{i}\delta)\,F(\xi,\beta)}$$

(b)

$$w(r,t) = \frac{P\,\mathrm{e}^{\mathrm{i}\omega t}}{Ga}\,\frac{3(1-\mu)}{\pi}\int_0^\infty \frac{\sin\left(\xi\frac{a}{h}\right) J_0\left(\xi\frac{r}{h}\right)\mathrm{d}\xi}{(1+\mathrm{i}\delta)\,F(\xi,\beta)} \tag{3.122}$$

The deflection w corresponds to the deflection of the plate including the part of the deflection caused by shear. The solutions for the other internal forces of the plate depend on the function w_1, which is given by the equation of motion [3.11] in the form

$$\nabla^2(w_1 - w) + \frac{\varrho}{\kappa G^*}\,\frac{\partial^2 w}{\partial t^2} - \frac{p(r,t)}{\kappa G^* h} + \frac{q(r,t)}{\kappa G^* h} = 0 \tag{3.123}$$

or, after Hankel's integral transformation in the form

$$-\alpha^{2\mathrm{H}}w_1 = -\alpha^{2\mathrm{H}}w + \frac{\omega^2}{c_R^{*2}}\,^{\mathrm{H}}w + \frac{^{\mathrm{H}}p}{\kappa G^* h} - \frac{^{\mathrm{H}}q}{\kappa G^* h} = 0. \tag{3.124}$$

Substituting (3.114) into (3.124) and rearranging the equation gives

$$
\begin{aligned}
{}^{\mathrm{H}}w_1 = \Bigg[\left(1 - \frac{\beta^2}{\kappa\xi^2(1+\mathrm{i}\delta)}\right) \frac{12(1-\mu^2)h}{E(1+\mathrm{i}\delta)\,F(\xi,\beta)} \\
- \frac{h}{\xi^2\kappa G(1+\mathrm{i}\delta)}\Bigg]\,{}^{\mathrm{H}}p + \frac{h}{\xi^2\kappa G(1+\mathrm{i}\delta)}\,{}^{\mathrm{H}}q.
\end{aligned}
\tag{3.125}
$$

By using (3.112), (3.113), (3.121) and inverse transformation the following equation is obtained

$$
\begin{aligned}
w_1(r,t) = \frac{P\,\mathrm{e}^{\mathrm{i}\omega t}}{Ga}\int_0^\infty \Bigg[\frac{6(1-\mu)}{\pi}\left(1 - \frac{\beta^2}{\kappa\xi^2(1+\mathrm{i}\delta)} - \frac{G_z}{G}\,\frac{F_1(\xi,\beta)}{\kappa\xi^2}\right) \\
\times \frac{1}{(1+\mathrm{i}\delta)\,F(\xi,\beta)} - \frac{1}{\pi\kappa(1+\mathrm{i}\delta)\xi^2}\Bigg] J_1\left(\xi\frac{a}{h}\right) J_0\left(\xi\frac{r}{h}\right)\mathrm{d}\xi.
\end{aligned}
\tag{3.126}
$$

Equation (3.126) is valid in the case of load (a). Load case (b) is obtained by the substitution of $J_1(\xi\frac{a}{h})$ in (3.126) with the expression $(\xi\frac{a}{h})/2$. This substitution will be valid for all components of the state vector; therefore we shall only consider solutions for load case (a).

3.3.4 Bending moments of equivalent plate

The bending moment of the plate in the radial direction is given by the relationship [3.11]

$$
\begin{aligned}
M_r &= -D^*\left[\frac{\partial^2 w_1}{\partial r^2} + \mu\frac{1}{r}\,\frac{\partial w_1}{\partial r}\right] \\
&= -\frac{Gh^3(1+\mathrm{i}\delta)}{6(1-\mu)}\left[\frac{\partial^2 w_1}{\partial r^2} + \mu\frac{1}{r}\,\frac{\partial w_1}{\partial r}\right].
\end{aligned}
\tag{3.127}
$$

Commencing from equation (3.126), the equation for the bending moment of the plate is derived, after rearrangment, in the form

$$
M_r = \frac{Ph\mathrm{e}^{\mathrm{i}\omega t}}{a}\int_0^\infty M(\xi,\beta)\left[J_0\left(\xi\frac{r}{h}\right) - (1-\mu)\frac{J_1(\xi\frac{r}{h})}{\xi\frac{r}{h}}\right] J_1\left(\xi\frac{a}{h}\right)\mathrm{d}\xi \tag{3.128}
$$

where

$$M(\xi,\beta)=\frac{1}{\pi}\left[\xi^2-\frac{\beta^2}{\kappa(1+\mathrm{i}\delta)}-\frac{G_z}{G}\,\frac{F_1(\xi,\beta)}{\kappa}\right]\frac{1}{F(\xi,\beta)}-\frac{1}{6\pi\kappa(1-\mu)}. \tag{3.129}$$

The bending moment at $r=0$ is given by the expression

$$M_r(r=0)=\frac{Ph}{a}\,\frac{(1+\mu)}{2}\,\mathrm{e}^{\mathrm{i}\omega t}\int_0^\infty M(\xi,\beta)\,J_1\left(\xi\frac{a}{h}\right)\mathrm{d}\xi. \tag{3.130}$$

The bending moment of the plate in the tangential direction is derived from the equation [3.11]

$$M_\varphi=-D^*\left[\frac{1}{r}\frac{\partial w_1}{\partial r}+\mu\frac{\partial^2 w_1}{\partial r^2}\right]=-\frac{Gh^3(1+\mathrm{i}\delta)}{6(1-\mu)}\left[\frac{1}{r}\frac{\partial w_1}{\partial r}+\mu\frac{\partial^2 w_1}{\partial r^2}\right]. \tag{3.131}$$

By using equation (3.126), performing the derivations and rearranging, the equation for M_φ is established in the form

$$M_\varphi=\frac{Ph\mathrm{e}^{\mathrm{i}\omega t}}{a}\int_0^\infty M(\xi,\beta)\left[\mu J_0\left(\xi\frac{r}{h}\right)+(1-\mu)\,\frac{1}{\xi\frac{r}{h}}J_1\left(\xi\frac{r}{h}\right)\right]J_1\left(\xi\frac{a}{h}\right)\,d\xi \tag{3.132}$$

where $M(\xi, \beta)$ is defined by equation (3.129).

The bending moment M_φ at $r=0$ is given by the relationship

$$M_\varphi(r=0)=\frac{Ph}{a}\,\frac{(1+\mu)}{2}\,\mathrm{e}^{\mathrm{i}\omega t}\int_0^\infty M(\xi,\beta)J_1\left(\xi\frac{a}{h}\right)\mathrm{d}\xi \tag{3.133}$$

which is identical to equation (3.130).

3.3.5 Transverse forces on equivalent plate

The transverse force of the equivalent plate, Q_r, is defined by the equation [3.11]

$$Q_r=\kappa G^* h\left(\frac{\partial w}{\partial r}-\frac{\partial w_1}{\partial r}\right). \tag{3.134}$$

Performing the substitution and rearrangement of the equation for Q_r gives the relationship

$$Q_r=\frac{P}{a}\,\mathrm{e}^{\mathrm{i}\omega t}\int_0^\infty-\left[\frac{6(1-\mu)}{\pi}\,\frac{\left(\beta^2+\frac{G_z}{G}F_1(\xi,\beta)\,(1+\mathrm{i}\delta)\right)}{\xi(1+\mathrm{i}\delta)\,F(\xi,\beta)}+\frac{1}{\pi\xi}\right] \tag{1.135}$$

$$\times\,J_1\left(\xi\frac{a}{h}\right)J_1\left(\xi\frac{r}{h}\right)\mathrm{d}\xi.$$

3.3.6 Reaction of subgrade

The transform of the subgrade reaction ${}^{H}q$ is determined by equation (3.112). By using the equality (3.113) and the inverse of Hankel's transformation the expression for the original function $q(r, t)$ will be given in the form

$$q = -\frac{P}{ah}\,\frac{6(1-\mu)}{\pi}\,\frac{G_z}{G}\,e^{i\omega t}\int_0^\infty \frac{F_1(\xi,\beta)}{F(\xi,\beta)}\,J_1\left(\xi\frac{a}{h}\right)J_0\left(\xi\frac{r}{h}\right)\mathrm{d}\xi. \tag{3.136}$$

All these internal forces are the basic decisive components of the state vector that are necessary for the determination of stresses in a pavement structure under dynamic load. There are no difficulties in deriving the stresses in the half-space if the dynamic reaction on the half-space surface is given.

3.3.7 Numerical calculation of components of state vector for highway pavements under construction or completed

All components of the state vector for the equivalent plate on a half-space are determined in the form of improper integrals. The sub-integral functions are complex functions of the real variable ξ, have no discontinuities in the integration region and the improper integrals converge. They can be calculated by using numerical integration and computers.

The relationships for bending moments and transverse force may be modified by separating out the parts for which direct determination of the improper integral values is possible.

The expression for transverse force Q_r (3.135) is rearranged in the form

$$Q_r = \frac{P}{a}\,e^{i\omega t}\left\{\int_0^\infty \frac{-6(1-\mu)}{\pi}\,\frac{\left(\beta^2+\frac{G_z}{G}F_1(\xi,\beta)\,(1+i\delta)\right)}{\xi(1+i\delta)\,F(\xi,\beta)}\right. \tag{3.137}$$

$$\left.\times\,J_1\left(\xi\frac{a}{h}\right)J_1\left(\xi\frac{r}{h}\right)\mathrm{d}\xi-\frac{1}{\pi}\,\frac{a/h}{2r/h}\right\},\qquad \frac{r}{h}>\frac{a}{h}$$

because the following equation is valid

$$\int_0^\infty \frac{1}{\xi}\,J_1\left(\xi\frac{a}{h}\right)J_1\left(\xi\frac{r}{h}\right)\mathrm{d}\xi=\frac{a/h}{2r/h},\qquad \frac{r}{h}>\frac{a}{h} \tag{3.138}$$

The transverse force Q_r for $r/h<a/h$ is similarly given in the form

$$Q_r = \frac{P}{a} e^{i\omega t} \left\{ -\frac{6(1-\mu)}{\pi} \frac{\left(\beta^2 + \frac{G_z}{G} F_1(\xi,\beta)\,(1+i\delta)\right)}{\xi(1+i\delta)\,F(\xi,\beta)} \right.$$

$$\left. \times J_1\left(\xi\frac{a}{h}\right) J_1\left(\xi\frac{r}{h}\right) d\xi - \frac{1}{\pi}\frac{r/h}{2a/h} \right\}. \tag{3.139}$$

Modifying the expression for bending moment in the plate (3.128) the relationship is as follows

$$M_r = \frac{Ph}{a} e^{i\omega t} \left\{ \int_0^\infty \left[\frac{1}{\pi} \left(\xi^2 - \frac{\beta^2}{\kappa(1+i\delta)} - \frac{G_z}{G} \frac{F_1(\xi,\beta)}{\kappa} \frac{1}{F(\xi,\beta)} \right) \right] \right.$$

$$\times \left[J_0\left(\xi\frac{r}{h}\right) - (1-\mu)\frac{1}{\xi\frac{r}{h}} J_1\left(\xi\frac{r}{h}\right) \right] J_1\left(\xi\frac{a}{h}\right) d\xi$$

$$\left. \frac{a/h}{12\pi\kappa\, r^2/h^2} \right\}, \text{for } r/h > a/h$$

$$+$$

$$\left. \frac{-(1+\mu)}{12\pi\kappa(1-\mu)\,a/h} \right\}, \text{for } r/h < a/h \tag{3.140}$$

because of the validity of

$$\int_0^\infty J_0\left(\xi\frac{r}{h}\right) J_1\left(\xi\frac{a}{h}\right) d\xi = 0, \qquad \frac{r}{h} > \frac{a}{h} \tag{3.141}$$

$$\int_0^\infty J_0\left(\xi\frac{r}{h}\right) J_1\left(\xi\frac{a}{h}\right) d\xi = \frac{1}{a/h}, \qquad \frac{r}{h} < \frac{a}{h} \tag{3.142}$$

and at the same time of the validity of (3.138).

It can be seen from equation (3.140) that there is a discontinuity for *r/h=a/h* as a consequence of the curvature change caused by shear deformation. From the practical point of view it is better to neglect this specific influence of the more precise plate theory and to consider the relationship for bending moment M_r at *r*=0 in the form

$$M_r(r=0) = \frac{Ph}{a} e^{i\omega t} \frac{(1-\mu)}{2} \int_0^\infty \left[\frac{1}{2\pi} \left(\xi^2 - \frac{\beta^2}{\kappa(1+i\delta)} \right.\right.$$

$$\left.\left. - \frac{G_z}{G} \frac{F_1(\xi,\beta)}{\kappa} \right) \times \frac{1}{F(\xi,\beta)} \right] J_1\left(\xi\frac{a}{h}\right) d\xi. \tag{3.143}$$

The relationships for bending moment M_φ (3.132) and (3.133) can be arranged in the same way.

For the sake of numerical calculation the limit values of functions $F(\xi, \beta \to 0)$, $F_1(\xi, \beta \to 0)$ for dimensionless frequency $\beta \to 0$ have to be obtained.

According to equation (3.115) it follows that

$$F(\xi, \beta \Rightarrow 0) = \xi^4 - \frac{6(1-\mu)G_z}{G} F_1(\xi, \beta \Rightarrow 0) \tag{3.144}$$

if after equation (3.116)

$$F_1(\xi, \beta \Rightarrow 0) = \frac{1 + \mathrm{i}\delta_z}{1 + \mathrm{i}\delta}$$

$$\times \lim_{\beta \to 0} \frac{\left[\left(2\xi^2 - \varepsilon_2^2 \frac{\beta^2}{1+\mathrm{i}\delta_z}\right)^2 - 4\xi^2 \sqrt{\xi^2 - \varepsilon_1^2 \frac{\beta^2}{1+\mathrm{i}\delta_z}} \sqrt{\xi^2 - \varepsilon_2^2 \frac{\beta^2}{1+\mathrm{i}\delta_z}}\right]}{\varepsilon_2^2 \frac{\beta^2}{1+\mathrm{i}\delta_z} \sqrt{\xi^2 - \varepsilon_1^2 \frac{\beta^2}{1+\mathrm{i}\delta_z}}} \tag{3.145}$$

$$= 2 \frac{(1 + \mathrm{i}\delta_z)}{1 + \mathrm{i}\delta} \frac{\varepsilon_1^2 - \varepsilon_2^2}{\varepsilon_2^2} \xi.$$

The limit values of the sub-integral functions in the expressions for the state vector components are at $\beta \to 0$ and at the same time $\xi \to 0$. The following equations are valid

$$\lim_{\substack{\beta \to 0 \\ \xi \to 0}} w = \frac{P}{Ga} \left[-\frac{1}{4\pi} \frac{a}{h} \frac{\varepsilon_2^2}{\frac{G_z}{G} (1 + \mathrm{i}\delta_z)(\varepsilon_1^2 - \varepsilon_2^2)} \right] \tag{3.146}$$

$$\lim_{\substack{\beta \to 0 \\ \xi \to 0}} M_r = 0 \quad , \quad \lim_{\substack{\beta \to 0 \\ \xi \to 0}} M_\varphi = 0 \tag{3.147}$$

$$\lim_{\substack{\beta \to 0 \\ \xi \to 0}} Q_r = 0 \tag{3.148}$$

$$\lim_{\substack{\beta \to 0 \\ \xi \to 0}} q = 0. \tag{3.149}$$

Motorway pavement structure under construction

The numerical calculation of state vector components is performed for the equivalent plate on a subgrade with thickness h, which substitutes for the motorway pavement structure

under construction. The structure on the subgrade is composed of a 25 cm thick sand-gravel layer, then a 24 cm thick layer of cement stabilization and a 4 cm thick asphaltic layer of coated sand and gravel.

According to actual measurements on pavements under construction [1.14], we consider these characteristic parameters for calculation:

G_z/G=0.02, a/h=1.0, $\varepsilon_2=c_2/c_{2z}$=6.518, $\varepsilon_1=c_2/c_{1z}$=3.12, μ=0.30, μ_z=0.35, δ=0.10, δ_z=0.20.

The numerical calculation was performed for 20 different frequency values β at the interval (0.1–5.0) and for β=0, the state vector components being calculated at r=0, r=h, r=2h, r=3h, r=5h and r=10h.

The approximate (but in practice sufficiently precise) values of the improper integrals were obtained by numerical integration over the interval ξ=(0.0–20.0). Because of the complex sub-integral functions for every state vector component the real part, the imaginary part and absolute value and phase angle were determined.

The variations of dynamic dimensionless deflections wGa/P with the ratio r/h at the dimensionless frequencies β=0.1, 0.2, 0.5, 1.0, 2.0, 3.0 and 5.0 are plotted in Figs. 3.12–3.15.

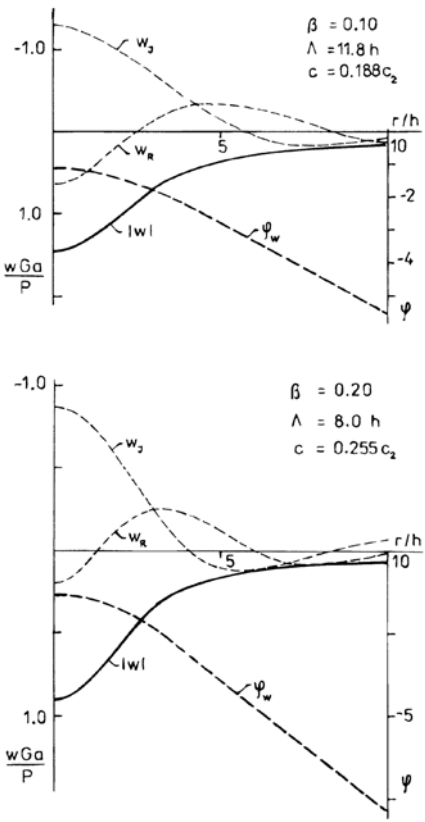

Fig. 3.12. Variations of dynamic dimensionless deflection wGa/P with ratio r/h at frequencies β=0.1 and β=0.2.

According to the stationary part of the linear course of the phase angle φ_w, the wavelength Λ and phase velocity c were determined and they are recorded in Figs. 3.12–3.15.

If the values of c/c_2 versus h/Λ are plotted (Fig. 3.16), it can be seen that they correspond to the theoretical dispersion curves for flexural stress waves in a plate under the influence of shear and rotational inertia. This is proof of the correct numerical calculation too. It is interesting that at the frequency β=3.0 a transition of the phase velocity values from the basic dispersion curve to the dispersion curve of higher forms sets in. The propagation of stress waves in the range of this transition is interrupted, as can be seen in Fig. 3.15 at frequency β=3.0.

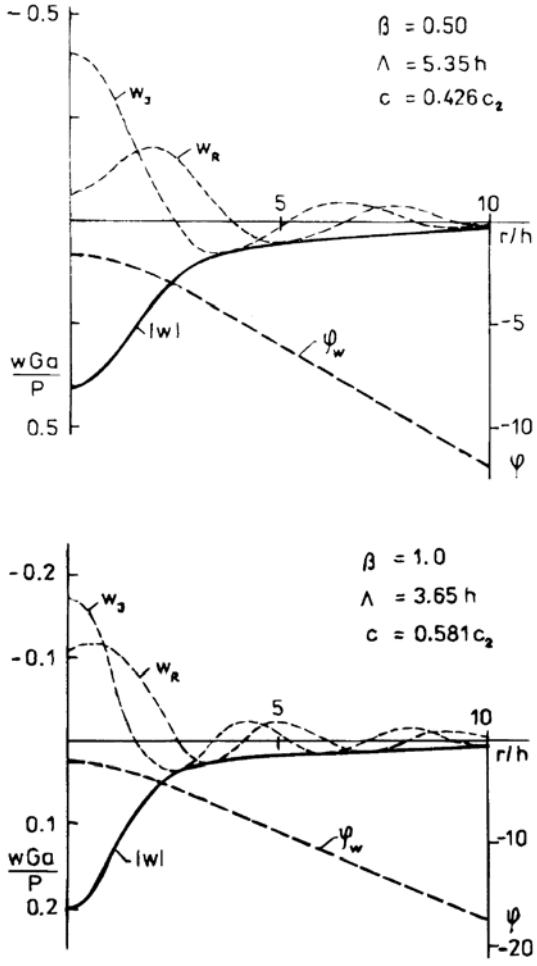

Fig. 3.13. Variation of dynamic dimensionless deflection *wGa/P* with ratio *r/h* at frequencies β=0.50 and β=1.0.

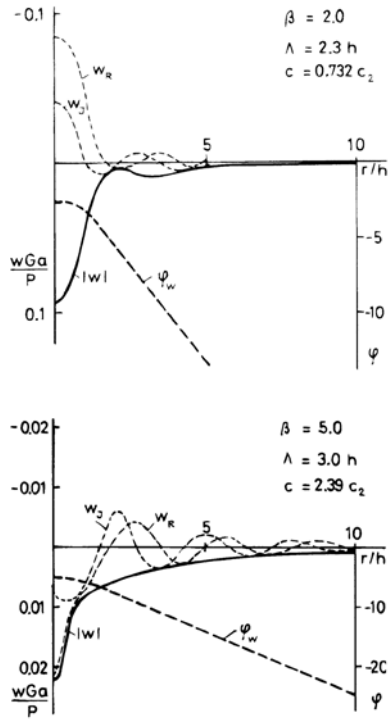

Fig. 3.14. Variation of dynamic dimensionless deflection *wGa/P* with ratio *r/h* at frequencies β=2.0 and β=5.0.

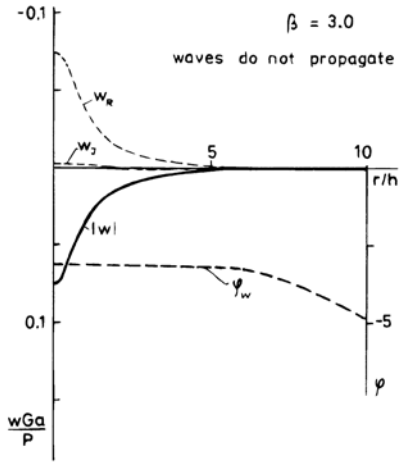

Fig. 3.15. Variation of dynamic dimensionless deflection *wGa/P* with ratio *r/h* at frequency β=3.0.

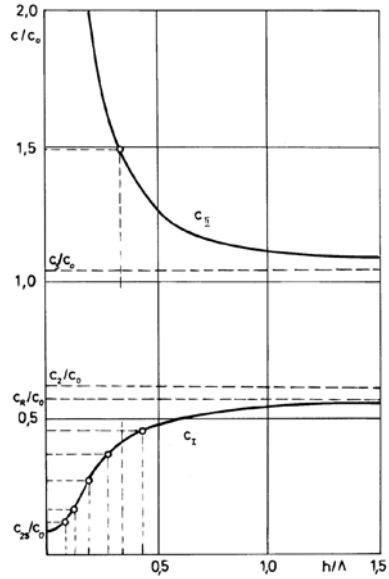

Fig. 3.16. Theoretical and experimental relationship of velocities c/c_0 to h/Λ in the plate.

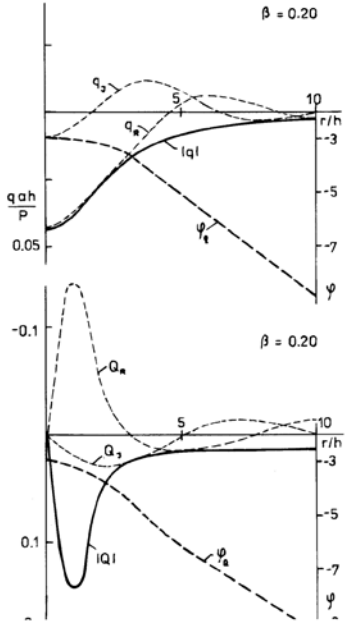

Fig. 3.17. Variation of dynamic dimensionless subgrade reaction qah/P and transverse force Qa/P in the equivalent plate on subgrade at frequency β=0.2.

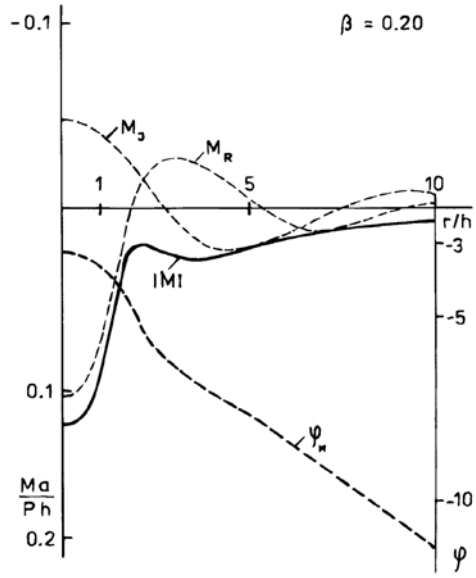

Fig. 3.18. Variation of dimensionless bending moment *Ma/Ph* with the h/Λ at frequency β=0.2.

The behaviour of the dynamic dimensionless subgrade reaction *qah/P,* bending moment *Ma/Ph* and transverse forces *Qa/P* in the equivalent plate are plotted in Figs. 3.17 and 3.18 for the frequency β=0.20.

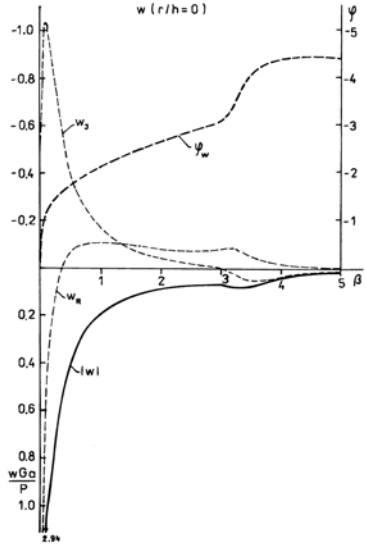

Fig. 3.19. Variation of dimensionless deflection *wGa/P* with frequency β.

Computed variations of dynamic values for the state vector components, i.e $w(r/h=0)$, $q(r/h=0)$, $M_r(r/h=1)$, $Q_r(r/h=1)$ with frequency β, are shown in Figs. 3.19–3.22.

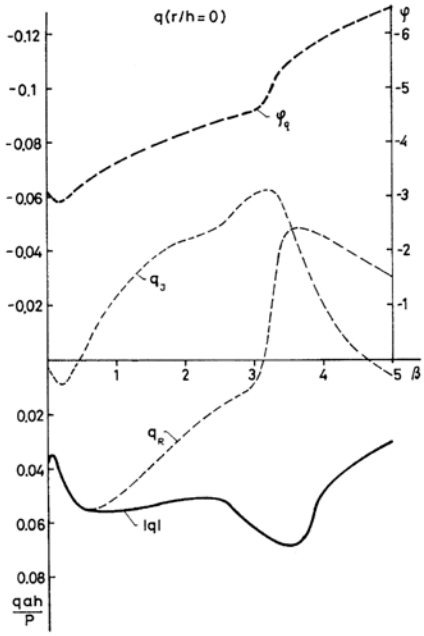

Fig. 3.20. Variation of dimensionless subgrade reaction qah/P with frequency β.

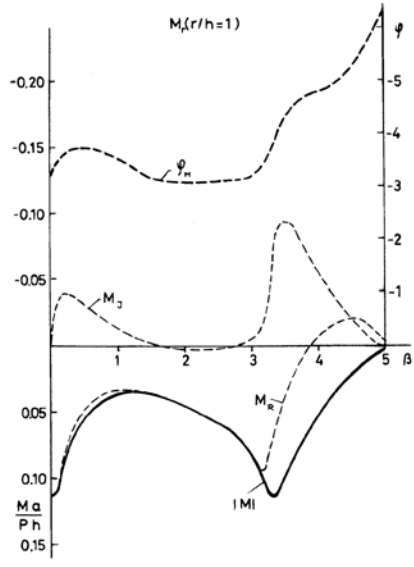

Fig. 3.21. Variation of dimensionless bending moment Ma/Ph with frequency β.

For $\beta \rightarrow 0$ the problem is approaching to the static case. The variations of the values of w and q, in Fig. 3.23 and the values of M_r and Q_r in Fig. 3.24 versus the ratio r/h for $\beta=0$ satisfy the condition of static load; that is, the phase angles are constant, and the stress waves do not propagate.

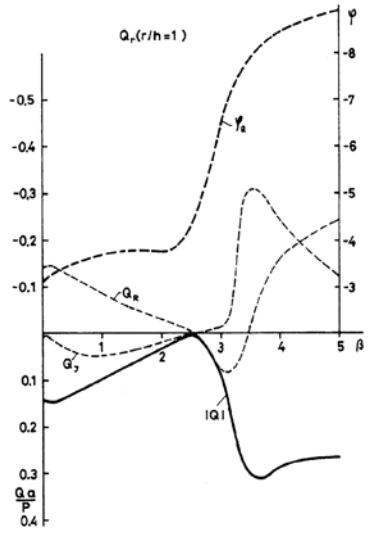

Fig. 3.22. Variation of dimensionless transverse force Qa/P with frenuency β.

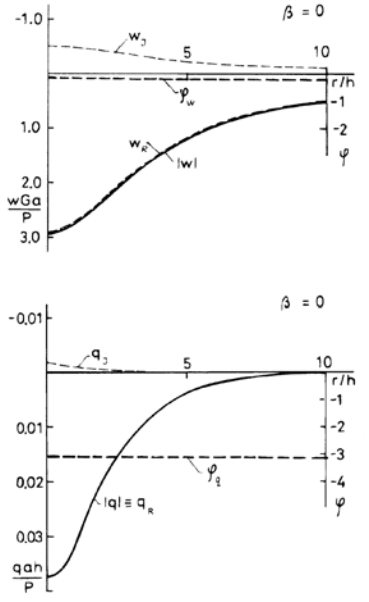

Fig. 3.23. Variation of dimensionless deflection wGa/P and subgrade reaction qah/P with ratio r/h at $\beta=0$.

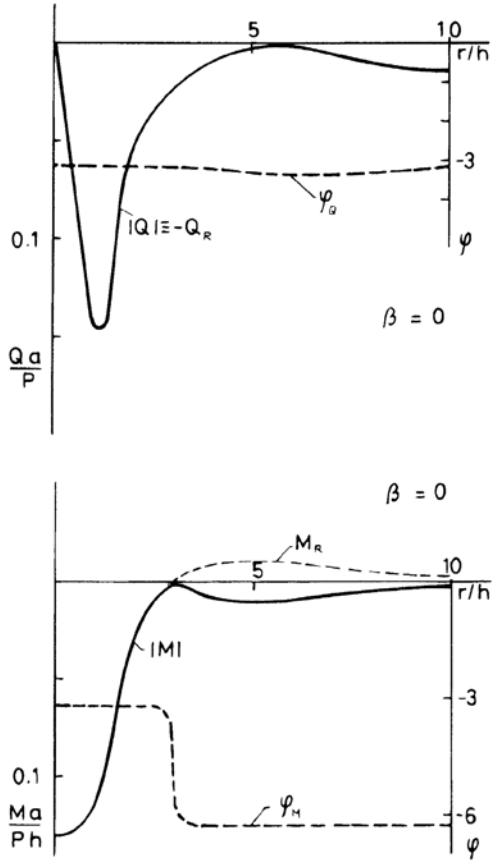

Fig. 3.24. Variation of dimensionless bending moment *Ma/Ph* and transverse force *Qa/P* with ratio *r/h* at β=0.

Motorway pavement structure

A similar numerical analysis of the state vector components was realized for a completed motorway pavement with a cement concrete surfacing 24 cm thick.

Based on diagnostic measurements carried out on completed motorway pavements, the following values of input characteristics are considered: G_z/G=0.00423, a/h=0.548, $\varepsilon_2=c_2/c_{2z}$=13.65, $\varepsilon_1=c_2/c_{1z}$=6.55, μ=0.25, μ_z=0.35, δ=0.10, δ_z=0.20.

The computed curves of the dynamic deflection characteristics w_R, w_J, $|w|$, φ_w versus the ratio *r/h* for various values of dimensionless frequency β are plotted in Figs. 3.25 and 3.26.

The variations of dynamic subgrade reaction *q,* bending moment M_r and transverse force Q_r in the equivalent plate at the frequency values β=0.5 and β=1.0 are plotted in Figs. 3.27–3.29 and at β=0, i.e for the static case, in Figs. 3.30 and 3.31.

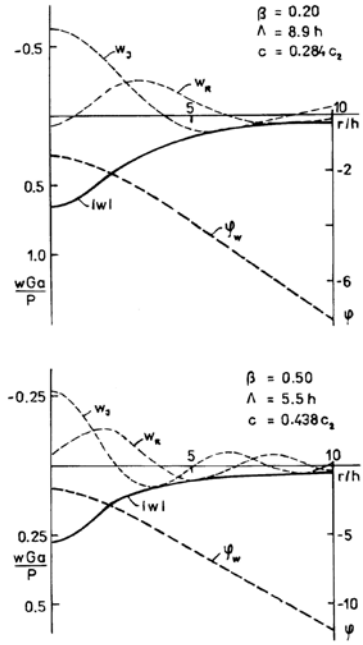

Fig. 3.25. Variation of dimensionless deflection *wGa/P* with ratio *r/h* at frequencies β=0.20 and β=0.50.

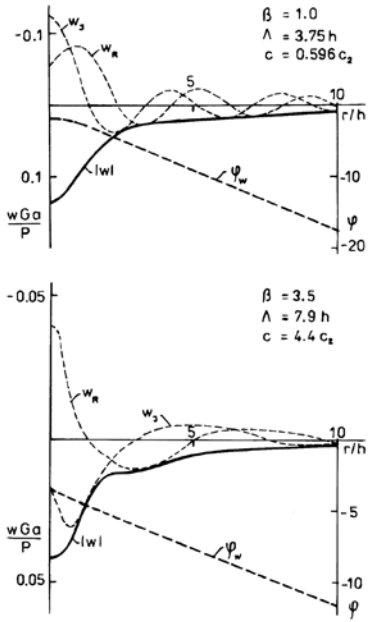

Fig. 3.26. Variation of dimensionless deflection *wGa/P* with ratio *r/h* at frequencies β=1.0 and β=3.5.

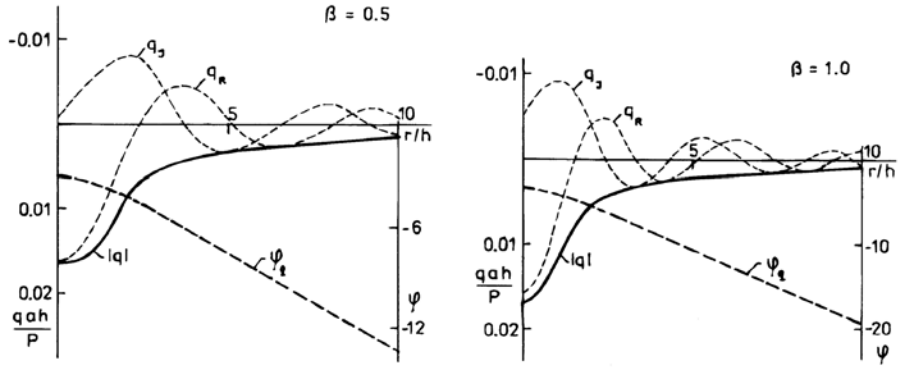

Fig. 3.27. Variation of dimensionless subgrade reaction *qah/P* with ratio *r/h* at frequencies β=0.50 and β=1.0.

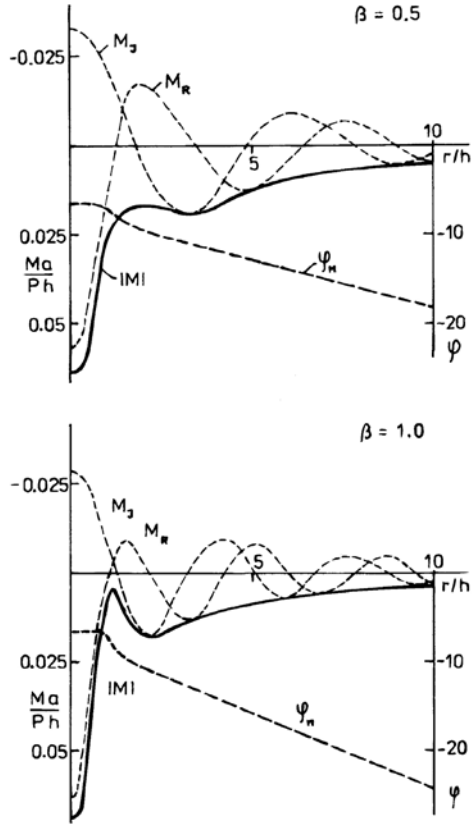

Fig. 3.28. Variation of dimensionless bending moment *Ma/Ph* with ratio *r/h* at frequencies β=0.50 and β=1.0.

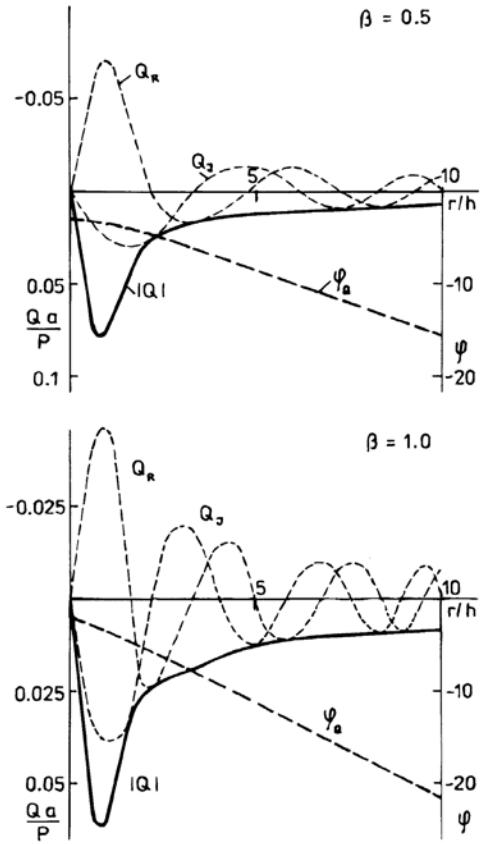

Fig. 3.29. Variation of dimensionless transverse force *Qa/P* with ratio *r/h* at frequencies β=0.50 and β=1.0.

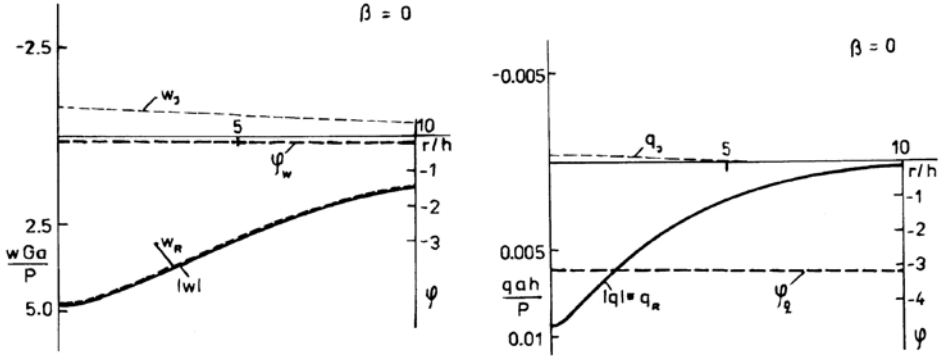

Fig. 3.30. Variation of dimensionles deflection *wGa/P* and subgrade reaction *qah/P* with ratio *r/h* at β=0.

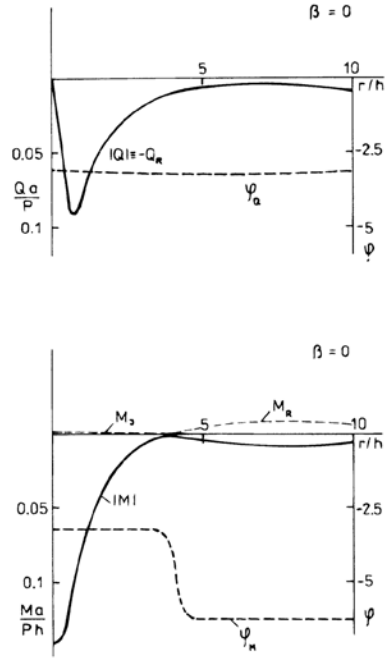

Fig. 3.31. Variation of dimensionless bending moment *Ma/Ph* and transverse force *Qa/P* with ratio *r/h* at β=0.

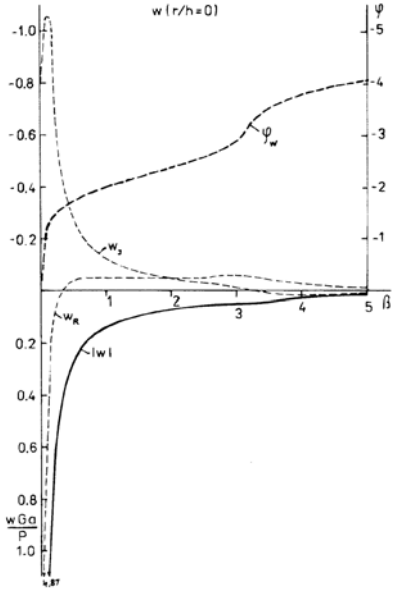

Fig. 3.32. Variation of dimensionless deflection *wGa/P* with frequency β.

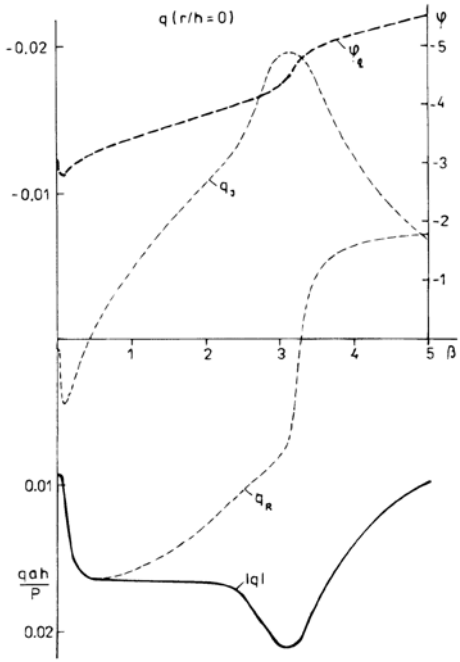

Fig. 3.33. Variation of dimensionless subgrade reaction *qah/P* with frequency *β.*

Dynamic values of the state vector components $w(r/h=0)$, $q(r/h=0)$, $M_r(r/h=1)Q_r(r/h=1)$ versus frequency β are plotted in Figs. 3.32–3.35.

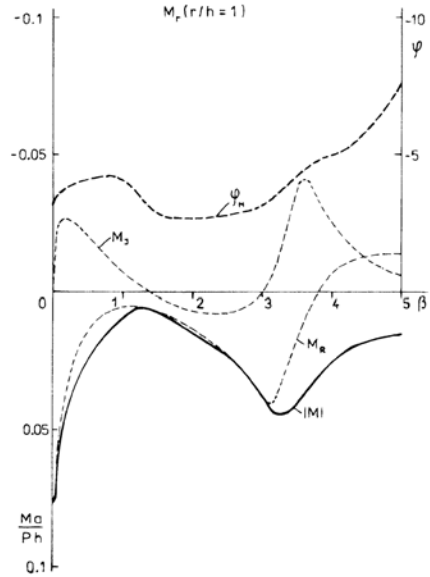

Fig. 3.34. Variation of dimensionless bending moment *Ma/Ph* with frequency

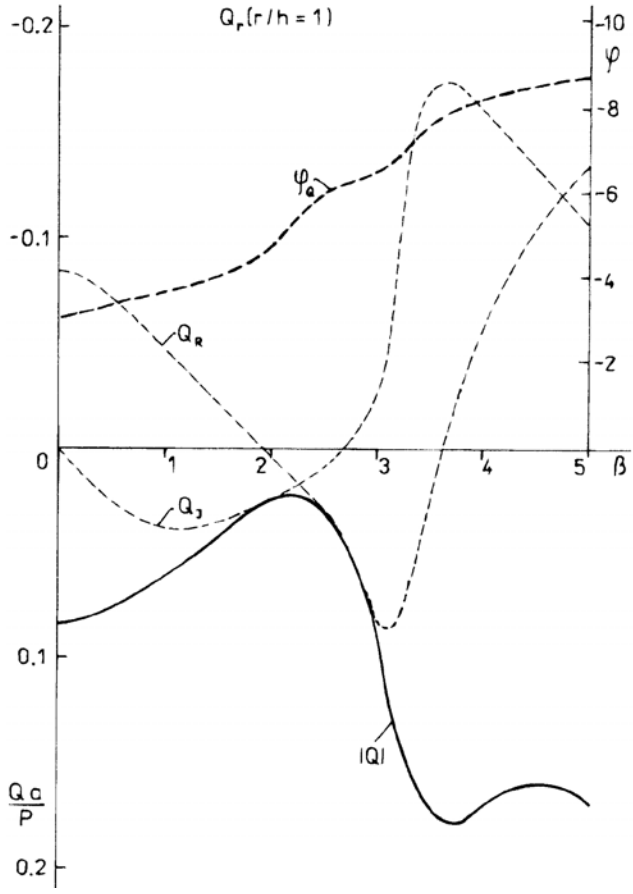

Fig. 3.35. Variation of dimensionless transverse force Qa/P with frequency β.

At the end of this numerical analysis it can be stated that the theory of the equivalent plate with the influence of shear and rotational inertia, lying on the subgrade fulfils the dynamic response of pavement structures in the frequency range=0.0–3.0 very well. This frequency range corresponds to the basic dispersion curve of phase velocities of stress wave propagation. An example of the computer program is given in Appendix 1.

3.3.8 Comparison of deflections and stresses in layered pavements according to theory of equivalent plate on subgrade and theory of layered half-space

A detailed study of the deflections, normal and shear stresses computed using the theory of the equivalent plate on subgrade presented in this chapter, compared with the theory of the layered half-space according to [3.12], has been performed in [3.13] for various structures of layered pavements assuming static loading.

Table 3.3. Composition of layered pavement structures.

Pavement structure	Layer material	Layer thickness (cm)	E(MPa) for 0°C 11°C 27°C	Poisson ratio μ for 00C 11°C 27°C	Density ϱ (kg/m^3)
right pavement	cement concrete	24	35000	0.30	2500
	asphalt concrete	4	5700	0.21	2300
			4200	0.33	
			2000	0.44	
	cement stabilization	20	1200	0.25	2000
	sand and gravel	15	300	0.35	2150
	sand and gravel	15	120	0.35	2100
		78 cm			
flexible pavement	mastix asphalt	4	7500	0.21	2500
			5500	0.33	
			3000	0.44	
	asphalt concrete	6	7500	0.21	2400
			5500	0.33	
			3000	0.44	
	asphalt concrete	5	7500	0.21	2400
			5500	0.33	
			3000	0.44	
	precoated aggregates	11	5700	0.21	2300
			4200	0.33	
			2000	0.44	
	mechanically hardened aggregates	18	800	0.25	2200
	sand and gravel	20	120	0.35	2100
		64 cm			
subgrade			30	0.35	1700
			45	0.35	1800
			60	0.35	1900

Here we present only the results for one rigid pavement structure and one flexible pavement. The composition of the layered structures, the layer thicknesses, moduli of material elasticity at 0 °C, 11 °C, 27 °C and material densities are given in Table 3.3.

The computed radial nomal stresses σ_r at r=0 and shear stresses τ at r=a in pavement structures under static load p=0.5 MPa, uniformly distributed on a circular area with radius a=0.2033 m, are plotted in Figs. 3.36 and 3.37. The deflection values in mm and vertical normal stresses σ_z as a subgrade reaction for temperatures 0 °C, 11 °C, 27 °C are also shown.

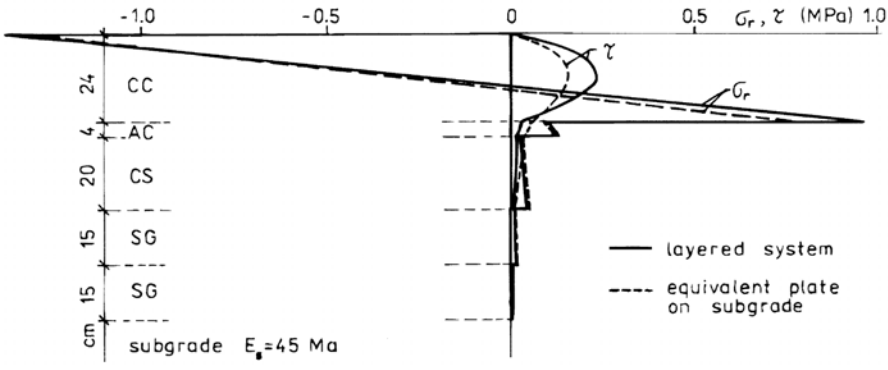

T(°C)	deflection (mm)		σz (MPa)	
	laymed	eq. plate	laymed	eq. plate
0	0.235	0.250	0.0038	0.0042
11	0.242	0.251	0.0038	0.0042
27	0.244	0.252	0.0039	0.0043

Fig. 3.36. Comparison of stresses and deflections computed according to the theory of equivalent plate on subgrade and theory of layered half-space for rigid pavement.

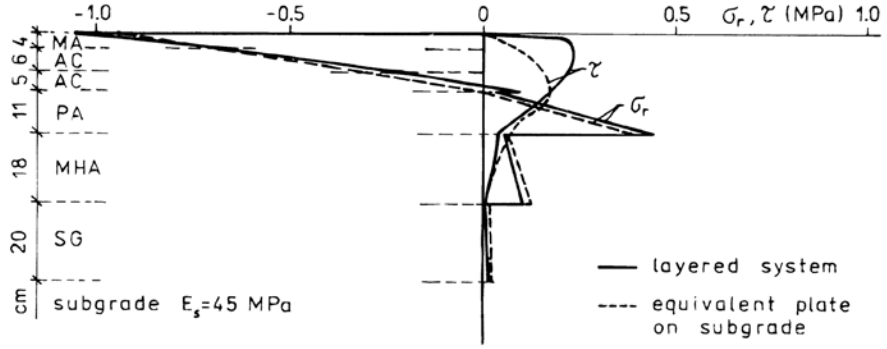

T(°C)	deflection (mm)		σz (MPa)	
	laymed	eq. plate	laymed	eq. plate
0	0.391	0.385	0.0092	0.0098
11	0.413	0.399	0.0100	0.0105
27	0.466	0.429	0.0121	0.0121

Fig. 3.37. Comparison of stresses and deflections according to theory of the equivalent plate on subgrade and theory of layered half-space for flexible pavement.

One remark has to be made concerning stress calculation below the neutral axis when applying the theory of the equivalent plate on subgrade. The radial and shear stresses have to be computed on the assumption that the loading p on a circular surface area with radius

a is extended with depth and the load *p* is reduced by the ratio $(a+e)/(a+h_i)$, where *e* is the distance of the neutral axis from the surface and h_i is the distance of the *i* th level from the surface.

Comparison of the values computed according to the theory of the equivalent plate on subgrade with the values obtained using the theory of the layered half-space indicates a very good level of agrement. However the fundamental advantage of the model of the equivalent plate on subgrade is the possibility of solving of decisive typical problems of pavement dynamics that cannot be solved in a simple way using the model of the layered medium.

3.4 Technical theory of plate on subgrade

The relative complexity of the model of the equivalent plate on half-space suggests that one should study and analyse the variants of technical theory for a dynamically equivalent plate on a simplified model of the subgrade.

3.4.1 Dynamic simplified model of soil base

The simplified models of the soil base, the characteristics of which are described by two or more parameters of elasticity, form the transition between Winkler's model and the half-space theory. Such models have been presented by Filonenko-Boroditch [3.14], Pasternak [3.15], Vlasov-Leontjev [3.16] and others [3.17].

A dynamic simplified model of the soil base may be established by a differential equation of motion in the form

$$K_2\nabla^2 w - K_1 w - \varrho_z K_3 \frac{\partial^2 w}{\partial t^2} + q(r,t) = 0 \tag{3.150}$$

where *w* is vertical deflection, *q* is vertical dynamic load, K_1 is the coefficient of uniform compression in N/m^3, K_2 is the coefficient of shear transmission in N/m, K_3 is the coefficient of equivalent inertia in m, the operator ∇^2 in the case of axial symmetry is given by the relationship

$$\nabla^2 = \frac{\partial^2}{\partial r^2} + \frac{1}{r}\frac{\partial}{\partial r} \tag{3.151}$$

and ϱ_z is the material density.

Assuming, stationary dynamic problems, the viscoelastic behaviour of the subgrade material may be determined by means of the complex characteristic $K_1^* = K_1(1+\mathrm{i}\delta_z)$, $K_2^* = K_2(1+\mathrm{i}\delta_z)$, if δ_z is the damping parameter. The values of this characteristic may be determined on the basis of dynamic experiments performed on real subgrade [3.18].

The coefficient of equivalent inertia, K_3, can fulfil conditions for various behaviours of the simplified model of the subgrade [3.19]. For instance, if we assume K_3 is a constant, we can require its determination from the condition

$$c_{\mathrm{Rz}}^2 = \frac{K_2}{\varrho_z K_3} \tag{3.152}$$

where c_{Rz} is the velocity of surface-Rayleigh waves. Supposing the deflection *w(r, t)* takes the form

$$w(r,t) = w_0 H_0^{(2)}(\alpha r)\, \mathrm{e}^{\mathrm{i}\omega t} \tag{3.153}$$

where $H_0^{(2)}(\alpha r)$ is Hankel's function, $\alpha = 2\pi/\Lambda$ is the wave number and ω is the angular frequency, then from the homogeneous equation (3.150) we can obtain

$$-K_2\alpha^2 - K_1 + \varrho_z K_3 \omega^2 = 0. \tag{3.154}$$

Using the expression $\omega = ca$, where c is the phase velocity of stress waves the following relationship can be obtained

$$c = c_{\mathrm{Rz}}\sqrt{1 + \frac{K_1}{K_2\alpha^2}} = c_{\mathrm{Rz}}\sqrt{1 + \frac{K_1^2\Lambda^2}{K_2 4\pi^2}}. \tag{3.155}$$

It can be seen that at higher frequencies, when $\Lambda \to 0$, the phase velocity c approaches the velocity of surface waves c_{Rz}. The phase velocities c increase with increasing of wavelength Λ. This variant of inertial forces leads to behaviour that matches quite well the response of real soil bases.

The other formulation of inertia forces may commence from the condition that the stress-wave velocity is equal to the velocity of surface waves at very low frequencies. In this case we do not know the expression for coefficient K_3 as it is a function of variable *r,* but it is possible to formulate the condition as an equation of deflection transforms after Hankel's integral transformation of the homogeneous equation of motion (3.150). The condition is fulfilled if the following equation for the transform of inertia coefficient ${}^{\mathrm{H}}K_3$ is valid

$${}^{\mathrm{H}}K_3 = \frac{K_1}{\varrho_z c_{\mathrm{Rz}}^2}\,\frac{1}{\alpha^2}. \tag{3.156}$$

Then the phase velocity of stress-wave propagation is determined by

$$c = c_{\mathrm{Rz}}\sqrt{1 + \frac{K_2\alpha^2}{K_1}} = c_{\mathrm{Rz}}\sqrt{1 + \frac{K_2}{K_1}\,\frac{4\pi^2}{\Lambda^2}}. \tag{3.157}$$

The third variant of inertia forces, which is the closest to the homogeneous half-space, is obtained from the condition that the phase velocity c is equal to the velocity of surface waves c_{R} in a whole frequency range. The transform of inertia forces is expressed by ${}^{\mathrm{H}}K_3$ in the form

$$^{H}K_3 = \frac{K_1 + K_2\alpha^2}{\varrho_z c_{Rz}^2 \alpha^2}. \tag{3.158}$$

The simplified dynamic model of the subgrade with three characteristics gives the basis for the conception of the technical theory of the plate lying on subgrade in dynamic problems. The advantage of such an idea is that dynamic characteristics and subgrade reaction can be formulated directly in a diferential equation of motion of the plate for the cases of complex layered subgrade too.

If the subgrade reaction q in diferential motion equation (3.101) is expressed according to the subgrade equation (3.150) for the simplified dynamic model of the soil base, the differential equation of the plate on subgrade will be obtained in the form

$$\nabla^2\nabla^2 w - \left(\frac{1}{c_3^2} + \frac{1}{c_R^2}\right)\frac{\partial^2\nabla^2 w}{\partial t^2} - \frac{K_2}{D}\nabla^2 w + \frac{K_2}{D}w + \frac{1}{c_3^2 c_R^2}\frac{\partial^4 w}{\partial t^4} + \frac{\varrho h}{D}\frac{\partial^2 w}{\partial t^2} + \frac{\varrho_z K_3}{D}\frac{\partial^2 w}{\partial t^2} = \frac{p}{D}. \tag{3.159}$$

3.4.2 Dispersion curve for stress-wave phase velocities and coefficient of equivalent inertia

The technical theory of the plate on subgrade will reflect the real dynamic behaviour of the system if the curve of dispersion of phase velocities for quasi-flexural stress waves corresponds to a free plate in the high-frequency range, and in the low-frequency region will approach the velocity of surface waves in the subgrade as a consequence of the plate contact with the subgrade.

Assuming the deflection *w(r, t)* in the form (3.153), then by substitution into the homogeneous differential equation (3.159) the following relationship is obtained

$$\alpha^4 - \left(\frac{1}{c_3^2} + \frac{1}{c_R^2}\right)\alpha^2\omega^2 + \frac{K_2}{D}\alpha^2 + \frac{K_1}{D} + \frac{1}{c_3^2 c_R^2}\omega^4 - \frac{\varrho h}{D}\omega^2 - \frac{\varrho_z K_3}{D}\omega^2 = 0. \tag{3.160}$$

By using the expression $\omega = c\alpha$ the biquadratic equation for phase velocity c is given in the form

$$c^4 - c^2\left(c_3^2 + c_R^2 + \frac{\varrho h}{D}\frac{c_3^2 c_R^2}{\alpha^2} + \frac{K_3\varrho_z}{D}\frac{c_3^2 c_R^2}{\alpha^2}\right) + c_3^2 c_R^2\left(1 + \frac{K_2}{D}\frac{1}{\alpha^2} + \frac{K_1}{D}\frac{1}{\alpha^4}\right) = 0. \tag{3.161}$$

The dispersion curve of quasi-flexural waves is expressed by the relationship

$$\left(\frac{c}{c_0}\right)^2 = P_0 - \sqrt{P_0^2 - Q_0} \tag{3.162}$$

where

$$P_0 = \frac{1}{2(1-\mu^2)} + \frac{\kappa}{4(1+\mu)} + \frac{3\kappa}{(1+\mu)\alpha^2 h^2} + \frac{3\kappa\varrho_z K_3}{\varrho(1+\mu)\alpha^2 h^3} \tag{3.163}$$

$$Q_0 = \frac{\kappa}{2(1-\mu^2)(1+\mu)}\left(1 + \frac{K_2 h^2}{D}\frac{1}{\alpha^2 h^2} + \frac{K_1 h^4}{D}\frac{1}{\alpha^4 h^4}\right) \tag{3.164}$$

and

$$c_0 = \sqrt{\frac{E}{\varrho}}.$$

Assuming the formulation of inertia forces in the simplified model of the subgrade given by equation (3.156), the expressions can be writen in the form

$$\begin{aligned} P_0 &= P_1 + \frac{P_2}{\alpha^2 h^2} + \frac{P_3}{\alpha^4 h^4} \\ Q_0 &= Q_1 + \frac{Q_2}{\alpha^2 h^2} + \frac{Q_3}{\alpha^4 h^4} \end{aligned} \tag{3.165}$$

where P_1, P_2, P_3 and Q_1, Q_2, Q_3 are functions of the material characteristics of the plate and subgrade and plate thickness h only.

In the limit $a \to 0$ the ratio $(c/c_0)^2$ is given by the relationship

$$\lim_{\alpha \to 0}\left(\frac{c}{c_0}\right)^2 = \frac{Q_0}{P_0 + \sqrt{P_0^2 - Q_0}} = \frac{Q_3}{2P_3} = \frac{c_{\mathrm{Rz}}^2}{c_0^2}. \tag{3.166}$$

We can see that the phase velocity c approaches the velocity of surface waves in subgrade c_{Rz} at low frequencies, when $\alpha \to 0$.

The same result may be obtained for the formulation of inertia forces in the simplified model of the subgrade given by equation (3.158).

At very high frequencies when the wave number $\alpha \to \infty$, equation (3.161) is reduced to the form

$$c^4 - c^2(c_3^2 + c_{\mathrm{R}}^2) + c_3^2 c_{\mathrm{R}}^2 = 0. \tag{3.167}$$

One root of this biquadratic equation corresponds to the velocity of the surface waves c_{R} in the plate medium.

The dispersion curve of phase velocities for quasi-flexural waves of the plate on subgrade derived on the basis of the differential equation (3.159) with the definition of the equivalent inertia coefficient given by equations (3.156) or (3.158) fulfils the real limit conditions.

If coefficient of equivalent inertia K_3 is assumed constant, then it cannot fulfil the limit condition for $\alpha \to 0$, but its use is adequate, because the real subgrade is inhomogeneous, and surface-wave velocities increase with increased wavelength.

3.4.3 Axial symmetric dynamic load of unbounded plate on subgrade

The basic dynamic problem is a plate under an axial symmetric load of vertical harmonic variable force $P(t)=P\mathrm{e}^{\mathrm{i}\omega t}$. For pavement structures, it is a dynamic load on a circular area with radius a.

The general form of the operator

$$\nabla^2 = \frac{\partial^2}{\partial r^2} + \frac{1}{r}\frac{\partial}{\partial r} + \frac{1}{r^2}\frac{\partial^2}{\partial \varphi^2}$$

in equation (3.159) is reduced to the form

$$\nabla^2 = \frac{\partial^2}{\partial r^2} + \frac{1}{r}\frac{\partial}{\partial r}. \tag{3.177}$$

By using Hankel's integral transformation on the equation of motion (3.159) after the relationships

$$\begin{aligned} {}^{\mathrm{H}}w(\alpha,t) &= \int_0^\infty r\, w(r,t)\, J_0(\alpha r)\mathrm{d}r \\ {}^{\mathrm{H}}p(\alpha,t) &= \int_0^\infty r\, p(r,t)\, J_0(\alpha r)\mathrm{d}r \end{aligned} \tag{3.178}$$

and supposing harmonic vibration

$$\begin{aligned} {}^{\mathrm{H}}w(\alpha,t) &= {}^{\mathrm{H}}w(\alpha)\, \mathrm{e}^{\mathrm{i}\omega t} \\ {}^{\mathrm{H}}p(\alpha,t) &= {}^{\mathrm{H}}p(\alpha)\, \mathrm{e}^{\mathrm{i}\omega t} \end{aligned} \tag{3.179}$$

and complex characteristics of elasticity, we obtain the equation

$$^{H}w\left[\alpha^4 - \left(\frac{1}{c_3^{*2}} + \frac{1}{c_R^{*2}}\right)\alpha^2\omega^2 + \frac{K_2^*}{D^*}\alpha^2 + \frac{K_1^*}{D^*} + \frac{1}{c_3^{*2}\,c_R^{*2}}\omega^4 - \frac{\varrho h}{D^*}\omega^2\right.$$

$$\left. - \frac{\varrho_z K_3}{D^*}\omega^2\right] = \frac{^{H}p}{D^*}. \tag{3.180}$$

The deflection transform after rearranging is given in the form

$$^{H}w = \frac{^{H}p\xi^2}{\frac{E^*}{12h(1-\mu^2)}F(\xi,\beta)} \tag{3.181}$$

if

$$F(\xi,\beta) = \xi^6 - \xi^4\left[\frac{\beta^2}{1+\mathrm{i}\delta}\left(\frac{1-\mu}{2} + \frac{1}{\kappa}\right) - \frac{K_2^* h}{D^*}\right]$$

$$+\xi^2\left[\frac{K_1^* h^4}{D^*} + \frac{(1-\mu)}{2\kappa}\frac{\beta^4}{(1+\mathrm{i}\delta)^2}\right. \tag{3.182}$$

$$\left. - \frac{6(1-\mu)\,\beta^2}{1+\mathrm{i}\delta}\right] - \frac{6(1-\mu)\,K_1^* h\varrho_z}{\kappa_z G_z \varrho(1+\mathrm{i}\delta)}\beta^2$$

where the dimensionless quantities ξ (wave number) and β (frequency) are expressed by the relationships

$$\xi = \alpha h \tag{3.183}$$

$$\beta = \frac{\omega h}{c_2} \tag{3.184}$$

$c_2 = \sqrt{G/\varrho}$ is the velocity of shear waves in plate medium.

3.4.4 Solution in integral form

The transform ^{H}p for the case of uniformly distributed load of intensity p on a circular area with radius a is given by the relationship

$$^{H}p = \frac{pa\,J_1(\alpha a)\,e^{i\omega t}}{\alpha} = \frac{P}{\pi a}\,\frac{J_1(\alpha a)}{\alpha}\,e^{i\omega t} \tag{3.185}$$

where P is the amplitude of total vertical force.

Using the inverse of Hankel's integral transformation the deflection $w(r, t)$ according to equation (3.181) is obtained in the form

$$w(r,t) = \frac{ph}{E}\,e^{i\omega t}\,\frac{12(1-\mu^2)a}{h}\int_0^\infty \xi^2 J_1\left(\xi\frac{a}{h}\right)\frac{J_0\left(\xi\frac{r}{h}\right)d\xi}{(1+i\delta)\,F(\xi,\beta)}. \tag{3.186}$$

The subgrade reaction according to equation (3.150) can be expressed in the form

$$q = (K_1^* - \varrho_z\omega^2 K_3)w - K_2^*\nabla^2 w \tag{3.187}$$

and then by the relationship

$$q(r,t) = p\,e^{i\omega t}\,12(1-\mu^2)\frac{a}{h}\int_0^\infty \frac{(1+i\delta_z)\,F_q(\xi,\beta)\,J_1\left(\xi\frac{a}{h}\right)\,J_0\left(\xi\frac{r}{h}\right)d\xi}{(1+i\delta)\,F(\xi,\beta)} \tag{3.188}$$

where

$$F_q(\xi,\beta) = \frac{K_2}{Eh}\xi^4 + \frac{K_1 h}{E}\xi^2 - \frac{K_1 h\varrho_z}{\kappa_z G_z 2(1+\mu)\varrho}\beta^2. \tag{3.189}$$

According to the more accurate theory of a plate subject to shear and rotatory inertia [3.10] the expression for function w_1 has to be derived. For the motion of a plate element in the vertical direction (the derivation and description is in [1.13]) the equation is valid in the form of equation (3.123) or, after Hankel's integral transformation and supposed harmonic vibration in the form of equation (3.124).

Substituting (3.185), (3.181) and the transform ^{H}q and by inverse transformation the function w_1 is given by the relationship

$$w_1(r,t) = \frac{ph}{E}\,e^{i\omega t}\,\frac{12(1-\mu^2)a}{h}\int_0^\infty \frac{F_1(\xi,\beta)\,J_1\left(\xi\frac{a}{h}\right)\,J_0\left(\xi\frac{r}{h}\right)d\xi}{1+i\delta} \tag{3.190}$$

where

$$F_1(\xi,\beta) = \left[\xi^2 - \frac{\beta^2}{\kappa(1+i\delta)} + \frac{(1+i\delta_z)\,2(1+\mu)}{(1+i\delta)\kappa}\left(\frac{K_1 h}{E} + \frac{K_2}{Eh}\xi^2\right)\right.$$
$$\left. - \frac{(1+i\delta_z)\varrho_z}{(1+i\delta)\varrho}\,\frac{K_1 h}{G_z\kappa_z\kappa}\,\frac{\beta^2}{\xi^2}\right]\,\frac{1}{F(\xi,\beta)} - \frac{1}{6\kappa(1-\mu)\xi^2} \tag{3.191}$$

The bending moment in the radial direction, M_r is defined by equation (3.127), and after substituting (3.190) and rearranging, the following expression is obtained

$$M_r = ph^2 e^{i\omega t} \frac{a}{h} \int_0^\infty F_M(\xi, \beta) \left[J_0\left(\xi \frac{r}{h}\right) - (1-\mu) \frac{J_1\left(\xi \frac{r}{h}\right)}{\xi \frac{r}{h}} \right] J_1\left(\xi \frac{a}{h}\right) d\xi \tag{3.192}$$

where

$$F_M(\xi, \beta) = \frac{M(\xi, \beta)}{F(\xi, \beta)} - \frac{1}{6\kappa(1-\mu)} \tag{3.193}$$

if

$$M(\xi, \beta) = \xi^4 - \frac{\beta^2 \xi^2}{\kappa(1+i\delta)} + \frac{(1+i\delta z)}{(1+i\delta)} \frac{2(1+\mu)}{\kappa} \left(\frac{K_1 h}{E} + \frac{K_2 \xi^2}{Eh} \right) \xi^2 - \frac{(1+i\delta_z)}{(1+i\delta)} \frac{\varrho_z}{\varrho} \frac{K_1 h}{G_z \kappa_z \kappa} \beta^2. \tag{3.194}$$

The transverse force on the plate, Q_r given by equation (3.134), after substituting (3.186) and (3.190), is obtained in the form

$$Q_r = phe^{i\omega t} 6(1-\mu) \frac{a}{h} \int_0^\infty F_Q(\xi, \beta) J_1\left(\xi \frac{a}{h}\right) J_1\left(\xi \frac{r}{h}\right) d\xi \tag{3.195}$$

$$F_Q(\xi, \beta) = \frac{Q(\xi, \beta)}{F(\xi, \beta)} - \frac{1}{6(1-\mu)\xi} \tag{3.196}$$

if

$$Q(\xi, \beta) = \frac{-\beta^2 \xi}{1+i\delta} + \frac{(1+i\delta_z)}{(1+i\delta)} 2(1+\mu) \left(\frac{K_1 h}{E} + \frac{K_2 \xi^2}{Eh} \right) \xi - \frac{(1+i\delta_z)}{(1+i\delta)} \frac{\varrho_z}{\varrho} \frac{K_1 h}{G_z \kappa_z} \frac{\beta^2}{\xi}. \tag{3.197}$$

With regard to the validity of equations (3.138), (3.141) and (3.142) the expressions for bending moment and transverse force may be modified as follows

for $r/h > a/h$

$$M_r = ph^2 e^{i\omega t} \frac{a}{h} \left\{ \int_0^\infty \frac{M(\xi,\beta)}{F(\xi,\beta)} \left[J_0\left(\xi \frac{r}{h}\right) - (1-\mu) \frac{J_1(\xi \frac{r}{h})}{\xi \frac{r}{h}} \right] J_1\left(\xi \frac{a}{h}\right) d\xi \right.$$

$$\left. + \frac{a/h}{12\kappa r^2/h^2} \right\} \tag{3.198}$$

$$Q_r = phe^{i\omega t} 6(1-\mu) \frac{a}{h} \left\{ \int_0^\infty \frac{Q(\xi,\beta)}{F(\xi,\beta)} J_1\left(\xi \frac{a}{h}\right) J_1\left(\xi \frac{r}{h}\right) d\xi \right.$$

$$\left. - \frac{1}{6(1-\mu)} \frac{a/h}{2r/h} \right\}. \tag{3.199}$$

The bending moment M_r at r=0 for a plate on subgrade is given by the relationship

$$M_r(r=0) = ph^2 e^{i\omega t} \frac{a}{h} \left\{ \int_0^\infty \frac{M(\xi,\beta)}{F(\xi,\beta)} \frac{(1+\mu)}{2} J_1\left(\xi \frac{a}{h}\right) d\xi \right\}. \tag{3.200}$$

All components of the state vector for a plate on subgrade are determined by improper integrals. The sub-integral functions are complex functions of a real variable, and have no discontinuities in the region of integration. The integrals converge and can be evaluated by using numerical integration and computers with satisfactory precision for practical use.

3.4.5 Solution in closed form

The deflection transform ${}^{H}w$ was determined in its general form by equations (3.181) and (3.182). Hankel's transform of concentrated force with amplitude P is given by the relationship

$${}^{H}p = \frac{P}{2\pi} \tag{3.201}$$

Using the inverse of Hankel's integral transformation the dynamic deflection is

$$w(r,t) = \frac{Pe^{i\omega t}\, 6(1-\mu^2)}{\pi E h (1+i\delta)} \int_0^\infty \frac{\xi^3 J_0(\xi \frac{r}{h})}{F(\xi,\beta)} d\xi \tag{3.202}$$

If the Bessel function $J_0(\xi \frac{r}{h})$ is expressed [1.18] by the relationship

$$J_0\left(\xi\frac{r}{h}\right)=\frac{-\mathrm{i}}{\pi}\int_0^{\infty}\left(\mathrm{e}^{\mathrm{i}\xi(r/h)\cosh u}-\mathrm{e}^{-\mathrm{i}\xi(r/h)\cosh u}\right)\mathrm{d}u \tag{3.203}$$

and substituted into equation (3.202), the deflection after modification is given in the form

$$w(r,t)=\frac{P\mathrm{i}6(1-\mu^2)\,\mathrm{e}^{\mathrm{i}\omega t}}{\pi^2Eh(1+\mathrm{i}\delta)}\int_0^{\infty}\mathrm{d}u\int_{-\infty}^{\infty}\frac{\xi^3\mathrm{e}^{-\mathrm{i}\xi(r/h)\cosh u}}{F(\xi,\beta)}\mathrm{d}\xi. \tag{3.204}$$

The interior integral computed by using the method of residua in the lower complex half-plane is expressed in the form

$$\int_{-\infty}^{\infty}\frac{\xi^3\mathrm{e}^{-\mathrm{i}\xi(r/h)\cosh u}}{F(\xi,\beta)}\mathrm{d}\xi=-2\pi\mathrm{i}\sum_{k=1}^{3}\left[\frac{\xi^3\,\mathrm{e}^{-\mathrm{i}\xi(r/h)\cosh u}}{6\xi^4-4\xi^2A+2B}\right]_{\xi=\xi_k} \tag{3.205}$$

if

$$\begin{aligned}A&=\frac{\beta^2}{1+\mathrm{i}\delta}\left(\frac{1-\mu}{2}+\frac{1}{\kappa}\right)-\frac{K_2^*h}{D^*}\\ B&=\frac{K_1^*h^4}{D^*}+\frac{(1-\mu)}{2\kappa}\,\frac{\beta^4}{(1+\mathrm{i}\delta)^2}-\frac{6(1-\mu)\beta^2}{(1+\mathrm{i}\delta)}\end{aligned} \tag{3.206}$$

ξ_1, ξ_2, ξ_3 are the complex roots of the bicubic equation $F(\xi, \beta)$=0, which can be determined in the lower complex half-plane. Because of the validity of the equation

$$\frac{2\mathrm{i}}{\pi}\int_0^{\infty}\mathrm{e}^{-\mathrm{i}\xi_k(r/h)\cosh u}\,\mathrm{d}u=H_0^{(2)}\left(\xi_k\frac{r}{h}\right) \tag{3.207}$$

the dynamic deflection of a plate on subgrade is determined by the relationship

$$w(r,t)=\frac{-P\,\mathrm{e}^{\mathrm{i}\omega t}3(1-\mu^2)\mathrm{i}}{Eh(1+\mathrm{i}\delta)}\sum_{k=1}^{3}\frac{\xi_k^2}{3\xi_k^4-2A\xi_k^2+B}\;H_0^{(2)}\left(\xi_k\frac{r}{h}\right) \tag{3.208}$$

where $H_0^{(2)}\left(\xi_k\frac{r}{h}\right)$ is Hankel's function with the complex argument.

The solution of equation (3.208) offers the possibility of obtaining expressions of similar structure for other components of the state vector.

3.4.6 Compensation of subgrade inertia by coefficient of mass increase of plate

The relatively complex solutions from the previous section, which are too complex for practical numerical analysis, force us to find the possibility of simplified solutions.

If we assume that the inertia forces of the subgrade are included in the inertia forces of the plate by means of the coefficient of mass increase of the plate, k_d, then the differential equation of motion for a plate on subgrade is determined in the form

$$\nabla^2\nabla^2 w - \left(\frac{1}{c_3^{*2}} + \frac{1}{c_R^{*2}}\right)\frac{\partial^2\nabla^2 w}{\partial t^2} - \frac{K_2^*}{D^*}\nabla^2 w + \frac{K_1^*}{D^*}w + \frac{1}{c_3^{*2}c_R^{*2}}\frac{\partial^4 w}{\partial t^4} + \frac{k_d\varrho h}{D}\frac{\partial^2 w}{\partial t^2} = \frac{p(r,t)}{D^*} \tag{3.209}$$

where the coefficient of mass increase, k_d, is a constant for every frequency of stationary harmonic vibration. Provided that $w(r, t)=w(r)e^{i\omega t}$, the homogeneous equation (3.209) may be writen in the form

$$(\nabla^2 + \gamma_1^2)(\nabla^2 + \gamma_2^2)w = 0 \tag{3.210}$$

if

$$\gamma^2 h^2 = \wp + \Im$$

$$\gamma_2^2 h^2 = \wp - \Im$$

and

$$\wp = \tfrac{1}{2}\left[\left(\frac{1-\mu}{2} + \frac{1}{\kappa}\right)\frac{\beta^2}{1+i\delta} - \frac{K_2}{Eh}\frac{12(1-\mu^2)(1+i\delta_z)}{(1+i\delta)}\right] \tag{3.212}$$

$$\Im = \sqrt{\left\{\wp^2\left[\frac{K_1 h}{E}\frac{12(1-\mu^2)(1+i\delta_z)}{1+i\delta} + \frac{(1-\mu)\beta^4}{2\kappa(1+i\delta)^2} - \frac{6(1-\mu)k_d\beta^2}{1+i\delta}\right]\right\}} \tag{3.213}$$

β is the dimensionless frequency according to equation (3.184); h is the plate thickness.

Equation (3.210) can be expressed as a system of Bessel equations:

$$\frac{d^2 w}{dr^2} + \frac{1}{r}\frac{dw}{dr} + \gamma_1^2 w = 0$$

$$\frac{d^2w}{dr^2}+\frac{1}{r}\frac{dw}{dr}+\gamma_2^2 w=0 \tag{3.214}$$

and the solution of the homogeneous equation (3.209) is obtained in the form

$$w(r)=A_1J_0(\gamma_1 r)+A_2Y_0(\gamma_r)+A_3J_0(\gamma_2 r+A_4Y_0(\gamma_{2r}) \tag{3.215}$$

where $J_0(\gamma_{1r}), J_0(\gamma_{2r})$ are Bessel functions of the first kind and zero order and $Y_0(\gamma_{1r})$, $Y_0(\gamma_{2r})$ are Bessel functions of the second kind and zero order. A_1, A_2, A_3, A_4 are arbitrary constants.

Because the arguments γ_1, γ_2 are complex, it is better to write the solution (3.125) in the form of linear combinations of Bessel functions

$$w(r)=A_1^*\,H_0^{(2)}\left(\eta_1\frac{r}{h}\right)+A_2^*\,H_0^{(2)}\left(\eta_2\frac{r}{h}\right) \tag{3.216}$$

where

$$\eta_1=\gamma_1 h,\ \eta_2=\gamma_2 h. \tag{3.217}$$

Hankel's functions $H_0^{(2)}$, $H_0^{(1)}$, i.e. Bessel functions of the third kind are solely from Bessel functions which approach zero by the infinite values of complex arguments. The boundary conditions for $r\to\infty$ are fulfilled in this manner as from a physical point of view it is evident that $w(r)\to 0$ for $r\to\infty$. A_1^*, A_2^* are arbitrary complex constants.

Hankel's functions $H_0^{(2)}$ converge on zero for $r\to\infty$ if complex roots η_1, η_2 have a positive real part and a negative imaginary part whereas Hankel's functions $H_0^{(1)}$ converge on zero for $r\to\infty$, if complex roots η_1, η_2 have a positive real and imaginary part too.

The complex constants A_1^*, A_2^* are determined from the conditions that the deflection at $r\to 0$ is finite and the transverse force of the system concentrated on a circle with radius r is at the limit at $r\to 0$ equal to the concentrated force P.

The imaginary parts of Hankel's functions have the members $\frac{2}{\pi}\ln\frac{|\eta_1|r}{2h}$ and $\frac{2}{\pi}\ln\frac{|\eta_2|r}{2h}$ which at $r\to 0$ approach the infinite. The condition of finite deflection at $r=0$ gives the equation

$$A_1^*\ln r+A_2^*\ln r=0. \tag{3.218}$$

It is evident that the following equation has to be valid

$$A_2^*=-A_1^*. \tag{3.219}$$

The transverse force of the system that is necessary to express the second boundary condition cannot be identical to the transverse force of the plate. Starting from the differential equation of the system in the form

$$\nabla^2\nabla^2 w+\frac{2\wp}{h^3}\nabla^2 w+\frac{\Im}{h^2}w=\frac{P}{D^*} \tag{3.220}$$

we can see that the increase of transverse force of the system, i.e. $(\frac{\mathrm{d}}{\mathrm{d}r}+\frac{1}{r})Q_{\mathrm{rs}}$ is expressed by members $D^*(\nabla^2\nabla^2 w+\frac{2\wp}{h^2}\nabla^2 w)$. Then the transverse force of the system Q_{rs} is given in the form

$$Q_{\mathrm{rs}}=D^*\left[\frac{\mathrm{d}^3 w}{\mathrm{d}r^3}+\frac{1}{r}\frac{\mathrm{d}^2 w}{\mathrm{d}r^2}-\frac{1}{r^2}\frac{\mathrm{d}w}{\mathrm{d}r}+\frac{2\wp}{h^2}\frac{\mathrm{d}w}{\mathrm{d}r}\right] \tag{3.221}$$

The second boundary condition has the form

$$\left(Q_{\mathrm{rs}}=\frac{P}{2\pi r}\right)_{r\to 0}. \tag{3.222}$$

As the following relationships are valid:

$$\left(\frac{\mathrm{d}^3}{\mathrm{d}r^3}+\frac{1}{r}\frac{\mathrm{d}^2}{\mathrm{d}r^2}-\frac{1}{r^2}\frac{\mathrm{d}}{\mathrm{d}r}\right)H_0^{(2)}\left(\eta\frac{r}{h}\right)=\frac{\eta^3}{h^3}H_1^{(2)}\left(\eta\frac{r}{h}\right) \tag{3.223}$$

$$\frac{\mathrm{d}}{\mathrm{d}r}H_0^{(2)}\left(\eta\frac{r}{h}\right)=-\frac{\eta}{h}H_1^{(2)}\left(\eta\frac{r}{h}\right) \tag{3.224}$$

and the function $\frac{\eta}{h}H_1^{(2)}(\eta\frac{r}{h})$ in the limit transition for $r\to 0$ is approaching $\mathrm{i}2/\pi r$, the boundary condition (3.222) has the form

$$A_1^*\left(\frac{\eta_1^2}{h^2}-\frac{2\wp}{h^2}\right)\frac{2}{\pi r}+A_2^*\left(\frac{\eta_2^2}{h^2}-\frac{2\wp}{h^2}\right)\frac{2}{\pi r}=\frac{P}{2\pi r}\frac{1}{D^*\mathrm{i}} \tag{3.225}$$

By using equation (3.219) the following relationship for A_1^* is obtained:

$$A_1^*=\frac{Ph^2}{4D^*\mathrm{i}}\frac{1}{\eta_1^2-\eta_2^2}=\frac{Ph^2}{8D^*\mathrm{i}\Im}=\frac{-P\,3(1-\mu^2)\mathrm{i}}{2Eh\Im(1+\mathrm{i}\delta)} \tag{3.226}$$

and the dynamic deflection of a plate on subgrade is determined by the expression

$$w(r,t)=\frac{-P\,e^{\mathrm{i}\omega t}\,3(1-\mu^2)\mathrm{i}}{2Eh\Im\,(1+\mathrm{i}\delta)}\left[H_0^{(2)}\left(\eta_1\frac{r}{h}\right)-H_0^{(2)}\left(\eta_2\frac{r}{h}\right)\right]. \tag{3.227}$$

3.4.7 Components of the state vector under a dynamic load uniformly distributed on a circular area

The fundamental solution (3.227) for a plate on subgrade under a concentrated harmonic variable force forms the basis of generalization for other axial symmetric dynamic loads.

Let us indicate the arguments: $\eta_1 r/h=\xi_1$, $\eta_2 r/h=\xi_2$ and, $\eta_1 a/h=\alpha_1$, $\eta_2 a/h=\alpha_2$ where a is the distance of the concentrated force from the origin of the coordinate system. Then according to Fig. 3.38 the distance between points A and B is determined by equation

$$z_1 = \sqrt{\alpha_1^2 + \xi_1^2 - 2\alpha_1\xi_1 \cos(\vartheta - \varphi)} \tag{3.228}$$

For a load $p_1 e^{i\omega t}$ uniformly divided along a circle with radius a, the elementary deflection at the point B with the coordinates (ξ, φ) under elementary load $p_1 a \mathrm{d}\vartheta$ on circle section $a\mathrm{d}\vartheta$ has to be expressed. In conformity with the fundamental solution (3.227) and by integration the deflection is expressed by the relationship

$$w = \frac{-p_1\, e^{i\omega t}\, 3(1-\mu^2)\mathrm{i}}{2Eh^3(1+i\delta)} \int_0^{2\pi} \left[\frac{\alpha_1 h}{\eta_1} H_0^{(2)}(z_1) - \frac{\alpha_2 h}{\eta_2} H_0^{(2)}(z_2)\right] \mathrm{d}\vartheta \tag{3.229}$$

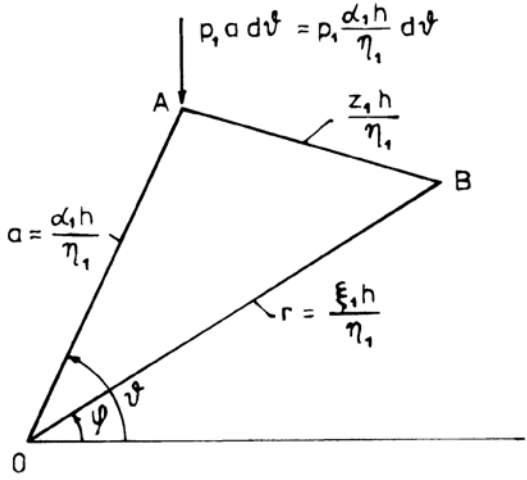

Fig. 3.38. Scheme of distances.

and after substitution of the expression (3.228) and the same for z_2 the deflection is determined by the eqaution

$$w = -\frac{p_1\, e^{i\omega t} 3(1-\mu^2)\mathrm{i}}{2Eh^3(1+i\delta)} \left[\int_0^{2\pi} \frac{\alpha_1 h}{\eta_1} H_0^{(2)}\left(\sqrt{\alpha^2 + \xi_1^2 - 2\alpha_1\xi_1 \cos(\vartheta - \varphi)}\right) \mathrm{d}\vartheta \right. \tag{3.230}$$

$$\left. - \int_0^{2\pi} \frac{\alpha_2 h}{\eta_2} H_0^{(2)}\left(\sqrt{\alpha_2^2 + \xi_2^2 - 2\alpha_2\xi_2 \cos(\vartheta - \varphi)}\right) \mathrm{d}\vartheta \right]. \tag{3.230}$$

From the theory of Bessel functions the formulae are wellknown [3.20]

$$H_0^{(2)}\left(\sqrt{\alpha_1^2+\xi_1^2-2\alpha_1\xi_1\ \cos(\vartheta-\varphi)}\right)$$
$$=2\sum_0^{\infty}{}'J_n(\xi_1)\ H_n^{(2)}(\alpha_1)\ \cos n(\vartheta-\varphi) \tag{3.231}$$

for $\xi_1 \leq \alpha_1$ and

$$H_0^{(2)}\left(\sqrt{\alpha_1^2+\xi_1^2-2\alpha_1\xi_1\ \cos(\vartheta-\varphi)}\right)$$
$$=2\sum_0^{\infty}{}'J_n(\alpha_1)\ H_n^{(2)}(\xi_1)\ \cos n(\vartheta-\varphi) \tag{3.232}$$

for $\xi_1 \geq \alpha_1$. The prime (') by the summation sign signifies that for $n=0$ the expression has to be divided by 2. Similar expressions apply for arguments α_2, ξ_2.

By integration over the limits $(0, 2\pi)$, only the first member from the sum, i.e for $n=0$, is different from zero. Then the dynamic deflection expressed for $\xi_1 \leq \alpha_1$, $\xi_2 \leq \alpha_2$, i.e for $r \leq a$ is given by the relationship

$$w = p_1\ e^{i\omega t} A^* \left[\frac{\alpha_1}{\eta_1}\ J_0(\xi_1)\ H_0^{(2)}(\alpha_1) - \frac{\alpha_2}{\eta_2} J_0(\xi_2)\ H_0^{(2)}(\alpha_2)\right] \tag{3.233}$$

and for $\xi_1 \geq \alpha_1$, $\xi_2 \geq \alpha_2$, i.e. for $r \geq a$, by

$$w = p_1\ e^{i\omega t} A^* \left[\frac{\alpha_1}{\eta_1} J_0(\alpha_1)\ H_0^{(2)}(\xi_1) - \frac{\alpha_2}{\eta_2} J_0\ (\alpha_2)\ H_0^{(2)}(\xi_2)\right] \tag{3.234}$$

where

$$A^* = -\frac{\pi\ 3(1-\mu^2)i}{E\Im\ (1+i\delta)}. \tag{3.235}$$

For a harmonic load uniformly distributed on an annulus with radii a^{II} and a^{I}, if $a^{I} < a^{II}$ the following expression is used

$$p_1 = p\ \frac{d\alpha_1 h}{\eta_1} = p\ \frac{d\alpha_2 h}{\eta_2}. \tag{3.236}$$

The dynamic deflection for $r \leq a^{I}$ is expressed in the form

$$w = p\, e^{i\omega t} A^{*} h \left[\int_{\alpha_1^{I}}^{\alpha_1^{II}} \frac{\alpha_1}{\eta_1^2}\, J_0(\xi_1)\, H_0^{(2)}(\alpha_1)\, d\alpha_1 - \int_{\alpha_2^{I}}^{\alpha_2^{II}} \frac{\alpha_2}{\eta_2^2}\, J_0(\xi_2)\, H_0^{(2)}(\alpha_2) d\alpha_2 \right] \tag{3.237}$$

As in general the following expression is valid

$$\frac{d}{dx}\left[x^n\, H_n^{(2)}(x)\right] = x^n\, H_{n-1}^{(2)}(x) \tag{3.238}$$

and for $n=1$

$$\int x\, H_0^{(2)}(x) dx = x\, H_1^{(2)}\,(x) \tag{3.239}$$

the resulting relationship for deflection at $r \leq a^{I}$ has the form

$$w = p e^{i\omega t} A^{*} h \left\{ \left[\alpha_1^{II} H_1^2(\alpha_1^{II}) - \alpha_1^{I} H_1^{(2)}(\alpha_1^{I})\right] \frac{J_0(\xi_1)}{\eta_2^2} - \left[\alpha_2^{II} H_1^{(2)}(\alpha_2^{II}) - \alpha_2^{I} H_1^{(2)}(\alpha_2^{I})\right] \frac{J_0(\xi_2)}{\eta_2^2} \right] \right\} \tag{3.240}$$

and for $r \geq a^{II}$

$$w = p e^{i\omega t} A^{*} h \left\{ \left[\alpha_1^{II} J_1(\alpha_1^{II}) - \alpha_1^{I} J_1(\alpha_1^{I})\right] \frac{H_0^{(2)}(\xi_1)}{\eta_1^2} - \left[\alpha_2^{II} J_1(\alpha_2^{II}) - \alpha_2^{I} J_1(\alpha_2^{I})\right] \frac{H_0^{(2)}(\xi_2)}{\eta_2^2} \right] \right\} \tag{3.241}$$

For a point in the annulus, i.e for $a^{I} \leq r \leq a^{II}$, equation (3.234) has to be integrated for $\alpha^{I} \leq \alpha \leq \xi$ and equation (3.233) for $\xi \leq \alpha \leq \alpha^{II}$. The relationship is obtained in the form

$$w = p e^{i\omega t} A^{*} h \left\{ \int_{\alpha_1^{I}}^{\xi_1} \frac{\alpha_1}{\eta_1^2} J_0(\alpha_1) H_0^{(2)}(\xi_1) d\alpha_1 - \int_{\alpha_2^{I}}^{\xi_2} \frac{\alpha_2}{\eta_2^2} J_0(\alpha_2) H_0^{(2)}(\xi_2) d\alpha_2 \right.$$

$$\left. + \int_{\xi_1}^{\alpha_1^{II}} \frac{\alpha_1}{\eta_1^2} J_0(\xi_1) H_0^{(2)}(\alpha_1) d\alpha_1 - \int_{\xi_2}^{\alpha_2^{II}} \frac{\alpha_2}{\eta_2^2} J_0(\xi_2) H_0^{(2)}(\alpha_2) d\alpha_2 \right\}$$

$$= p e^{i\omega t} A^{*} h \left\{ \left[\xi_1 J_1(\xi_1) - \alpha_1^{I} J_1(\alpha_1^{I})\right] \frac{H_0^{(2)}(\xi_1)}{\eta_1^2} \right.$$

$$-\left[\xi_2 J_1(\xi_2) - \alpha_2^{\mathrm{I}} J_1(\alpha_2^{\mathrm{I}})\right] H_0^{(2)}(\xi_2)/\eta_2^2$$

$$+\left[\alpha_1^{\mathrm{II}} H_1^{(2)}(\alpha_1^{\mathrm{II}}) - \xi_1 H_1^{(2)}(\xi_1)\right] J_0(\xi_1)/\eta_1^2 \tag{3.242}$$

$$-\left[\alpha_2^{\mathrm{II}} H_1^{(2)}(\alpha_2^{\mathrm{II}}) - \xi_2 H_1^{(2)}(\xi_2)\right] J_0(\xi_2)/\eta_2^2\Bigg\}.$$

According to [3.20] Vronskian V is valid for functions J_n and $H_n^{(2)}$ in the form

$$V\left(J_n(x), H_n^{(2)}(x)\right) = \frac{-2\mathrm{i}}{\pi x} \tag{3.243}$$

or

$$-J_n(x)\ \frac{\mathrm{d}\, H_n^{(2)}(x)}{\mathrm{d}x} - H_n^{(2)}(x)\ \ \frac{\mathrm{d}J_n(x)}{\mathrm{d}x} = -\frac{2\mathrm{i}}{\pi x}. \tag{3.244}$$

In the case n=0 the following relationship is obtained

$$-J_0(x)\ H_1^{(2)}(x) + H_0^{(2)}(x)\ J_1(x) = -\frac{2\mathrm{i}}{\pi x}. \tag{3.245}$$

Applying this equation in equation (3.242), the deflection w in the point of annulus is given by the expression

$$w = p\mathrm{e}^{\mathrm{i}\omega t} A^* h \left\{ -\frac{2\mathrm{i}}{\pi}\left(\frac{1}{\eta_1^2} - \frac{1}{\eta_2^2}\right) - \frac{\alpha_1^{\mathrm{I}}}{\eta_1^2} J_1(\alpha_1^{\mathrm{I}})\ H_0^{(2)}(\xi_1) + \frac{\alpha_2^{\mathrm{I}}}{\eta_2^2} J_1(\alpha_2^{\mathrm{I}})\ H_0^{(2)}(\xi_2) \right.$$

$$\left. + \frac{\alpha_1^{\mathrm{II}}}{\eta_1^2} J_0(\xi_1)\ H_1^{(2)}(\alpha_1^{\mathrm{II}}) - \frac{\alpha_2^{\mathrm{II}}}{\eta_2^2} J_0(\xi_2)\ H_1^{(2)}(\alpha_2^{\mathrm{II}}) \right\}. \tag{3.246}$$

For a load uniformly distributed on a circular area with radius a=a^{II}, i.e a^{I}=0 or the deflection at $r \leq a^{\mathrm{II}}$ according to equation (3.246) and rearranged is given by the relationship

$$w = p\mathrm{e}^{\mathrm{i}\omega t} A^* h \left\{ -\frac{2\mathrm{i}}{\pi}\left(\frac{1}{\eta_1^2} - \frac{1}{\eta_2^2}\right) + \frac{\alpha_1^{\mathrm{II}}}{\eta_1^2} J_0(\xi_1)\ H_1^{(2)}(\alpha_1^{\mathrm{II}}) - \right.$$

$$\left. - \frac{\alpha_2^{\mathrm{II}}}{\eta_2^2} J_0(\xi_2)\ H_1^{(2)}(\alpha_2^{\mathrm{II}}) \right\} \tag{3.247}$$

and at $r \geq a^{\mathrm{II}}$ according to equation (3.241) by the expression

$$w = p\mathrm{e}^{\mathrm{i}\omega t}A^*h\left\{\frac{\alpha_1^{\mathrm{II}}}{\eta_1^2}\,J_1(\alpha_1^{\mathrm{II}})\,H_0^{(2)}(\xi_1) - \frac{\alpha_2^{\mathrm{II}}}{\eta_2^2}\,J_1(\alpha_2^{\mathrm{II}})\,H_0^{(2)}(\xi_2)\right\} \tag{3.248}$$

The state vector components for the case of a dynamic load uniformly distributed on a circular area can be derived by applying equations (3.247) and (3.248) and the procedures of the previous paragraphs. The dynamic reaction of the subgrade, q, is expressed in the form

$$q = p\mathrm{e}^{\mathrm{i}\omega t}A^*h\left\{-\frac{2\mathrm{i}}{\pi}\left(\frac{1}{\eta_1^2}-\frac{1}{\eta_2^2}\right) + J_0(\xi_1)\,H_1^{(2)}(\alpha_1^{\mathrm{II}})\left[\frac{\alpha_1^{\mathrm{II}}}{\eta_1^2}K_1^* + K_2^*\frac{\alpha_1^{\mathrm{II}}}{h^2}\right]\right.$$

$$\left. - J_0(\xi_2)\,H_1^{(2)}(\alpha_2^{\mathrm{II}})\left[\frac{\alpha_2^{\mathrm{II}}}{\eta_2^2}K_1^* + K_2^*\frac{\alpha_2^{\mathrm{II}}}{h^2}\right]\right\} \tag{3.249}$$

for $r \leq a^{\mathrm{II}}$, and

$$q = p\mathrm{e}^{\mathrm{i}\omega t}A^*h\left\{J_1(\alpha_1^{\mathrm{II}})\,H_0^{(2)}(\xi_1)\left[\frac{\alpha_1^{\mathrm{II}}}{\eta_1^2}K_1^* + K_2^*\frac{\alpha_1^{\mathrm{II}}}{h^2}\right]\right.$$

$$\left. - J_1(\alpha_2^{\mathrm{II}})\,H_0^{(2)}(\xi_2)\left[\frac{\alpha_2^{\mathrm{II}}}{\eta_2^2}K_1^* + K_2^*\frac{\alpha_2^{\mathrm{II}}}{h^2}\right]\right\} \tag{3.250}$$

for $r \geq a^{\mathrm{II}}$.

The transversal force Q_r of the plate is given by the relationships

$$Q_r = p\mathrm{e}^{\mathrm{i}\omega t}\kappa G^*A^*a^{\mathrm{II}}\left\{(1-A_{11}^*)J_1(\xi_1)\,H_1^{(2)}(\alpha_1^{\mathrm{II}})\right.$$

$$\left. -(1-A_{12}^*)J_1(\xi_2)H_1^{(2)}(\alpha_2^{\mathrm{II}})\right\} \tag{3.251}$$

for $r \leq a^{\mathrm{II}}$, and

$$Q_r = p\mathrm{e}^{\mathrm{i}\omega t}\kappa G^*A^*a^{\mathrm{II}}\left\{(1-A_{11}^*)\,J_1(\alpha_1^{\mathrm{II}})\,H_1^{(2)}(\xi_1)\right.$$

$$\left. -(1-A_{12}^*)\,J_1(\alpha_2^{\mathrm{II}})\,H_1^{(2)}(\xi_2)\right\} \tag{3.252}$$

for $r \geq a^{\mathrm{II}}$. A_{11}^*, A_{12}^* are determined by the relationships

$$A_{11}^{*} = \left(1 + \frac{K_2\, 2(1+\mu)\,(1+\mathrm{i}\delta_z)}{Eh\kappa(1+\mathrm{i}\delta)}\right) - \frac{1}{\kappa\eta_1^2}\left[\frac{\beta^2}{1+\mathrm{i}\delta} - \frac{K_1 h\, 2(1+\mu)\,(1+\mathrm{i}\delta_z)}{E(1+\mathrm{i}\delta)}\right] \tag{3.253}$$

$$A_{12}^{*} = \left(1 + \frac{K_2\, 2(1+\mu)\,(1+\mathrm{i}\delta_z)}{Eh\kappa(1+\mathrm{i}\delta)}\right) - \frac{1}{\kappa\eta_2^2}\left[\frac{\beta^2}{1+\mathrm{i}\delta} - \frac{K_1 h\, 2(1+\mu)\,(1+\mathrm{i}\delta_z)}{E(1+\mathrm{i}\delta)}\right] \tag{3.254}$$

The radial bending moment of the plate is given by the relationships for $r \leq a^{\mathrm{II}}$

$$M_r = -D^{*} p \mathrm{e}^{\mathrm{i}\omega t} A^{*} \left\{ A_{11}^{*} \frac{\alpha_1^{\mathrm{II}}}{h^2}\, H_1^{(2)}(\alpha_1^{\mathrm{II}}) \left[-J_0(\xi_1) + \frac{(1-\mu)}{\xi_1} J_1(\xi_1)\right] - A_{12}^{*} \frac{\alpha_2^{\mathrm{II}}}{h^2}\, H_1^{(2)}(\alpha_2^{\mathrm{II}}) \left[-J_0(\xi_2) + \frac{(1-\mu)}{\xi_2} J_1(\xi_2)\right] \right\} \tag{3.255}$$

and for $r \geq a^{\mathrm{II}}$

$$M_r = -D^{*} p \mathrm{e}^{\mathrm{i}\omega t} A^{*} h \left\{ A_{12}^{*} \frac{\alpha_1^{\mathrm{II}}}{h^2}\, J_1(\alpha_1^{\mathrm{II}}) \left[-H_0^{(2)}(\xi_1) + \frac{(1-\mu)}{\xi_1} H_1^{(2)}(\xi_1)\right] - A_{12}^{*} \frac{\alpha_2^{\mathrm{II}}}{h^2}\, J_1(\alpha_2^{\mathrm{II}}) \left[-H_0^{(2)}(\xi_2) + \frac{(1-\mu)}{\xi_2} H_1^{(2)}(\xi_2)\right] \right\}. \tag{3.256}$$

3.4.8 Physical model of thin plate on subgrade with rigidity defined by dispersion curve for flexural stress waves

Further simplification of the technical theory of the equivalent plate on subgrade, by fulfilling the conditions of real behaviour of the system allows the application of a physical model of a thin plate with flexural rigidity, which is a function of frequency and corresponds to the form of the dispersion curve for flexural stress waves.

The differential equation of motion for a plate on subgrade is given in the form

$$\nabla^2\nabla^2 w - \frac{K_2^{*}}{D^{*}}\, \nabla^2 w + \frac{K_1^{*}}{D^{*}} w + \frac{\varrho h}{D^{*}} \frac{\partial^2 w}{\partial t^2} + \frac{\varrho_z K_3}{D^{*}} \frac{\partial^2 w}{\partial t^2} = \frac{p}{D^{*}}. \tag{3.257}$$

The relation between the plate constant $D^*=[Eh^3(1+i\delta)]/[12(1-\mu^2)]$ and the phase velocity c of flexural waves in plate with wave number $\alpha_0=2\pi/\Lambda$ has been determined in [1.43] by the expression

$$D^* = (1 + i\delta)\,\frac{c^2}{\alpha_0^2}\,\varrho h \tag{3.258}$$

where the phase velocity is a function of wave number a or frequency ω. Because $\omega=c\alpha_0$, equation (3.258) may be modified in the form

$$D^* = \left(\frac{c}{c_2}\right)^4 \frac{Gh^3}{\beta^2}(1 + i\delta) \tag{3.259}$$

where c_2 is the velocity of shear waves in the plate medium, β is the dimensionless frequency, and δ is the damping parameter of the plate material.

If the phase velocity c of flexural waves in the plate is expressed as a function of frequency β according to the relationship that corresponds to the dispersion curve of flexural waves in the plate, the dynamic rigidity of the plate given by (3.258) will replace the behaviour of the plate according to the more accurate theory described in previous paragraphs.

In [3.11] the equation for phase velocity c of flexural waves in a plate has been derived in the form

$$\left(\frac{c}{c_2}\right)^2 = P - \sqrt{P^2 - Q} \tag{3.260}$$

where

$$P = \frac{1}{1-\mu} + \frac{\kappa}{2} + 6\kappa\,\frac{\Lambda^2}{4\pi^2 h^2} \tag{3.261}$$

$$Q = \frac{2\kappa}{1-\mu} \tag{3.262}$$

if

$$\kappa = \left(\frac{0.87 + 1.12\mu}{1+\mu}\right)^2$$

Equation (3.260) expresses the form of the dispersion curve for flexural waves, which from the practical point of view is identical with the form of the exact solution according to elasticity theory. Replacing the wave number with the dimensionless frequency β, substituting into equation (3.258) and rearranging the plate stiffness, D^* is obtained in the form

$$D^* = Gh^3(1+\mathrm{i}\delta)\left[\frac{2\left(\frac{1}{1-\mu}+\frac{\kappa}{2}\right)\beta - \sqrt{4\left(\frac{1}{1-\mu}+\frac{\kappa}{2}\right)^2\beta^2 - \frac{8\kappa}{1-\mu}\,(\beta^2-12\kappa)}}{2(\beta^2-12\kappa)}\right]^2 \tag{3.263}$$

For $\beta\to 0$ the stiffness value has to be $D^*=[Eh^3(1+\mathrm{i}\delta)]/[12(1-\mu^2)]$. It is necessary to take care of the D^* evaluation in the region of $\beta^2=12\kappa$ when the ratio forms indeterminacy of the type 0/0.

By a harmonic variable dynamic load it is sufficient to compute the plate stiffness D^* according to equation (3.263) and to solve the vibration problem of a thin plate on subgrade.

Let us summarize the relationships for the state vector components of the thin equivalent plate on subgrade with the compensation of the subgrade inertia by the coefficient of the mass increase of the plate, k_d, under a harmonic variable load uniformly distributed on a circular area with radius a^{II}. By using the analogous procedures as in previous chapters the same relationships for deflection and subgrade reaction are valid, i.e. (3.247), (3.248) and (3.249), (3.250) respectively. In these expressions the quantities $\eta_1^2 = \wp + \Im$, $\eta_2^2 = \wp - \Im$ are given in the form

$$\wp = -\frac{K_2^* h^2}{2D^*} \tag{3.264}$$

$$\Im = \sqrt{\left[\wp^2 - \frac{K_1^* h^4}{D^*} + \frac{Gk_d\beta^2 h^3}{D^*}\right]} \tag{3.265}$$

The complex constant A^* is expressed by the relationship

$$A^* = -\frac{\pi h^3 \mathrm{i}}{4D^*\Im} \tag{3.266}$$

The radial bending moment of the plate M_r is determined by the equation

$$M_r = -D^*\left[\frac{\partial^2 w}{\partial r^2} + \frac{\mu}{r}\frac{\partial w}{\partial r}\right] \tag{3.267}$$

and after substitation M_r is given in the form for $r\le a^{\mathrm{II}}$

$$M_r = -D^* p\mathrm{e}^{\mathrm{i}\omega t}A^* h\left\{\frac{\alpha_1^{\mathrm{II}}}{h^2}H_1^{(2)}(\alpha_1^{\mathrm{II}})\left[-J_0(\xi_1) + \frac{(1-\mu)}{\xi_1}J_1(\xi_1)\right]\right.$$
$$\left. - \frac{\alpha_2^{\mathrm{II}}}{h^2}H_1^{(2)}(\alpha_2^{\mathrm{II}})\left[-J_0(\xi_2) + \frac{(1-\mu)}{\xi_2}J_1(\xi_2)\right]\right\} \tag{3.268}$$

and for $r\ge a^{\mathrm{II}}$

$$M_r = -D^* p e^{i\omega t} A^* h \left\{ \frac{\alpha_1^{II}}{h^2} J_1(\alpha_1^{II}) \left[-H_0^{(2)}(\xi_1) + \frac{(1-\mu)}{\xi_1} H_1^{(2)}(\xi_1) \right] \right.$$
$$\left. - \frac{\alpha_2^{II}}{h^2} J_1(\alpha_2^{II}) \left[-H_0^{(2)}(\xi_2) + \frac{(1-\mu)}{\xi_2} H_1(\xi_2) \right] \right\}. \tag{3.269}$$

The transverse force of the system, Q_{rs} is in the case of a thin plate on subgrade determined by the relationship

$$Q_{rs} = -D^* \left[\frac{\partial^3 w}{\partial r^3} + \frac{1}{r} \frac{\partial^2 w}{\partial r^2} - \frac{1}{r^2} \frac{\partial w}{\partial r} - \frac{K_2}{D^*} \frac{\partial w}{\partial r} \right]. \tag{3.270}$$

After substitution, derivation and rearranging the expressions are determined in the form for $r \leq a^{II}$

$$Q_{rs} = D^* p e^{i\omega t} A^* \left\{ \frac{\alpha_1^{II}}{\eta_1} \left(\frac{\eta_1^2}{h^2} + \frac{K_2^*}{D^*} \right) J_1(\xi_1) H_1^{(2)}(\alpha_1^{II}) \right.$$
$$\left. - \frac{\alpha_2^{II}}{\eta_2} \left(\frac{\eta_2^2}{h^2} + \frac{K_2^*}{D^*} \right) J_1(\xi_2) H_1^{(2)}(\alpha_2^{II}) \right\} \tag{3.271}$$

and for $r \geq a^{II}$

$$Q_{rs} = D^* p e^{i\omega t} A^* \left\{ \frac{\alpha_1^{II}}{\eta_1} \left(\frac{\eta_1^2}{h^2} + \frac{K_2^*}{D^*} \right) J_1(\alpha_1^{II}) H_1^{(2)}(\xi_1) \right.$$
$$\left. - \frac{\alpha_2^{II}}{\eta_2} \left(\frac{\eta_2^2}{h^2} + \frac{K_2^*}{D^*} \right) J_1(\alpha_2^{II}) H_1^{(2)}(\xi_2) \right\}. \tag{3.272}$$

The transverse force of the plate, Q_r may be expressed by equation (3.270)–(3.272) in which the member with coefficient K_1^*/D^* is omitted. This member represents the part of the transverse force transferred by the subgrade.

3.4.9 Numerical results

Numerical calculations were performed by using computers for two variants of the technical theory of the equivalent plate on subgrade under a harmonic variable load uniformly distributed on a circular area with radius a:

(a) for the solution in integral form;
(b) for the solution in closed form and compensation of the subgrade inertia by the coefficient of the mass inecrease of the plate.

The numerical results were obtained for two types of pavement structures, represented by the equivalent plate on subgrade:

I. A highway cement concrete pavement with these input characteristics:

G_z/G=0.00423,	$a^{II}/h=a/h$=0.548
$\varepsilon_1=c_2/c_{1z}$=6.55,	$\varepsilon_2=c_2/c_{2z}$=13.65
μ=0.25,	μ_z=0.35
δ=0.10,	δ_z=0.20
K_1h/E=0.000785,	K_2/Eh=0.000825

II. A flexible pavement with these input data:

G_z/G=0.020,	$a^{II}/h=a/h$=1.00
$\varepsilon_1=c_2/c_{1z}$=3.12,	$\varepsilon_2=c_2/c_{2z}$=6.52
μ=0.30,	μ_z=0.35
δ=0.10,	δ_z=0.20
K_1h/E=0.00192,	K_2/Eh=0.00673

The numerical calculations were realized for 18 different values of dimensionless frequencies in the interval (0–3.0) or (0–5.0), and the state vector components were obtained at r=0, r=h, r=2h, r=3h, r=5h, r=7h and r=10h.

A numerical solution according to variant (b) was performed for various coefficients of the mass increase of the plate: k_d=1.0, k_d=1.25, k_d=1.50, k_d=1.75, k_d=2.0, k_d=2.5.

The variations of dimensionles deflection wE/ph, subgrade reaction q/p, transversal force of the plate Q/ph and bending moment of the plate M/ph^2 with the ratio r/h for frequencies β=0.5 and β=1.0 are plotted in Figs. 3.39–3.42. They are valid for pavement I and were obtained according to variant (b).

The variations of w, q, M and Q for β=0 are drawn in Figs. 3.43 and 3.44, which show the loss of wave character of the load process in the limited static case.

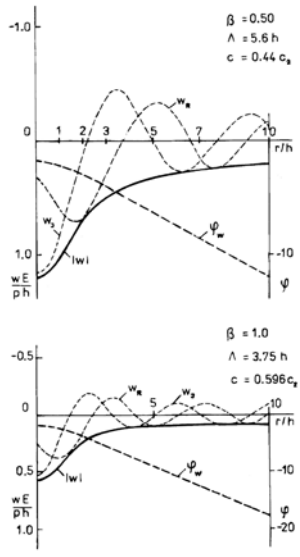

Fig. 3.39. Variation of dimensionless deflection wE/ph with ratio r/h at frequencies β=0.50 and β=1.0.

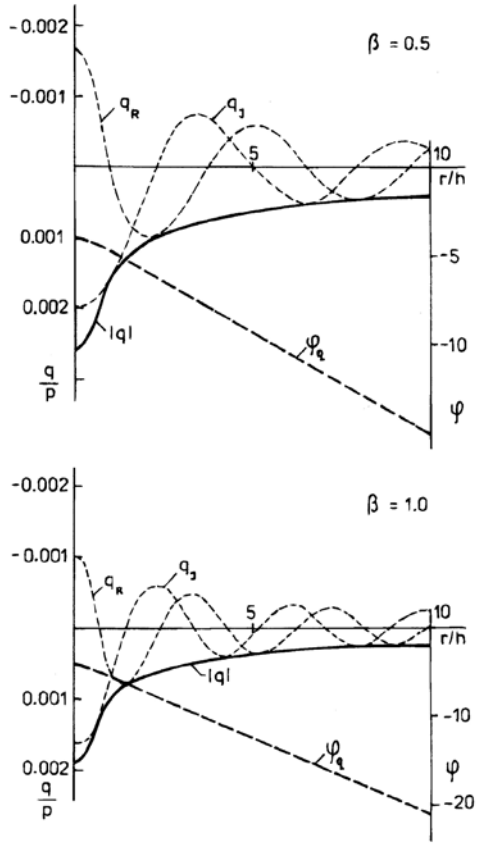

Fig. 3.40. Variation of dimensionless subgrade reaction q/p with ratio r/h at frequencies β=0.50 and β=1.0.

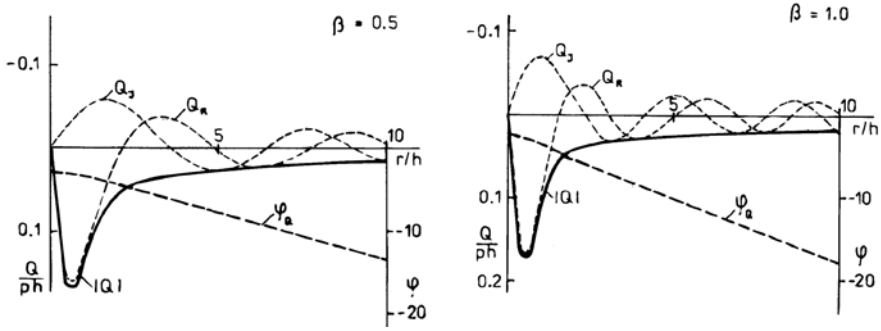

Fig. 3.41. Variation of dimensionless transverse force Q/ph with ratio r/h at frequencies β=0.50 and β=1.0.

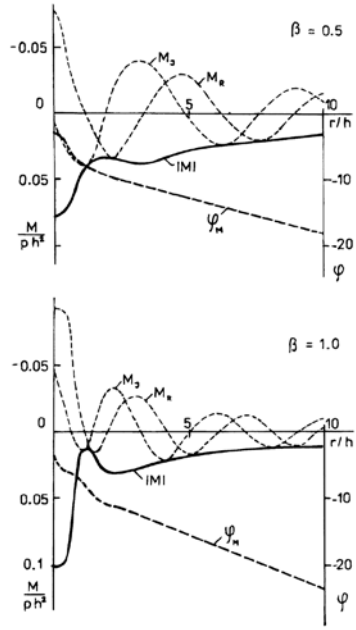

Fig. 3.42. Variation of dimensionless bending moment M/ph^2 with ratio r/h at frequencies β=0.50 and β=1.0.

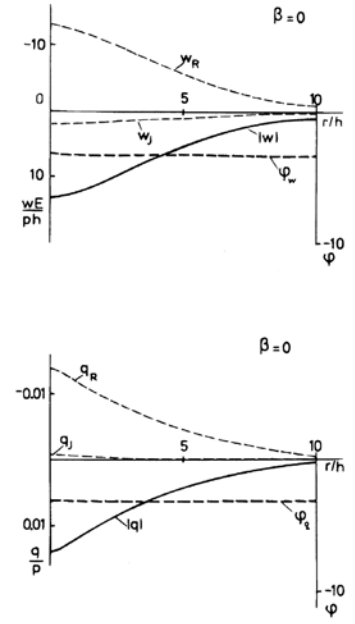

Fig. 3.43. Variation of dimensionless deflection wE/ph and subgrade reaction q/p with r/h in static case.

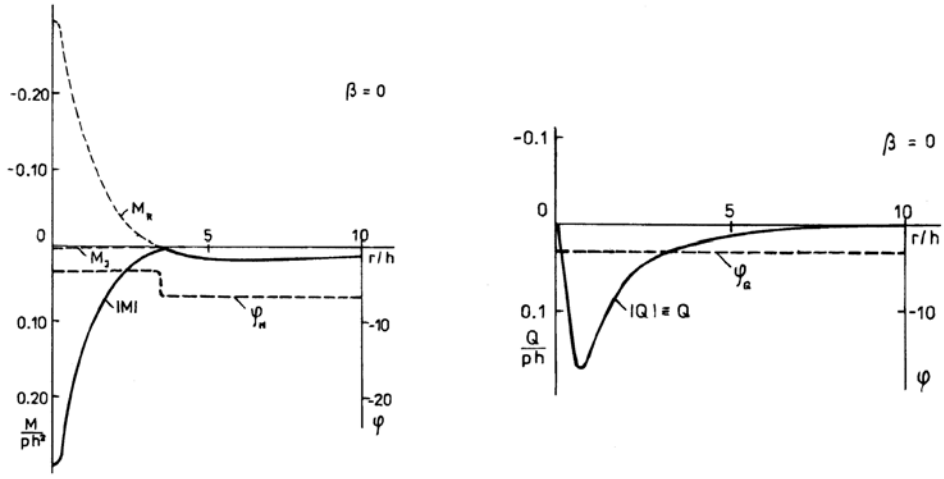

Fig. 3.44. Variation of dimensionless bending moment M/ph^2 and transverse force Q/ph with r/h in static case.

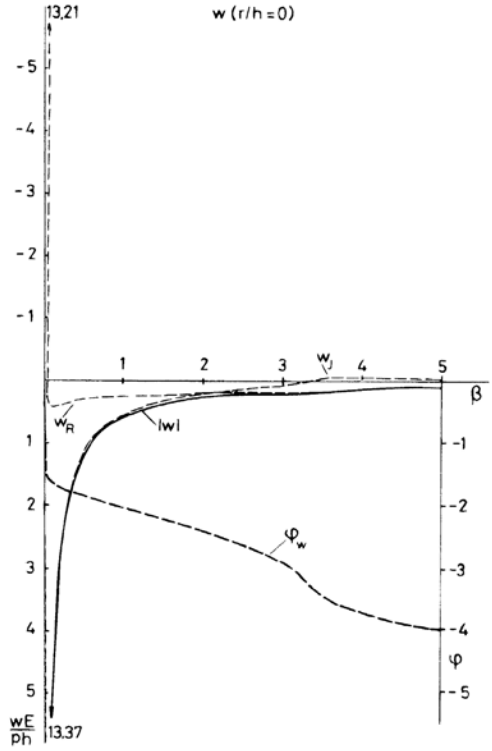

Fig. 3.45. Relationship of dimensionless deflection wE/ph to frequency β.

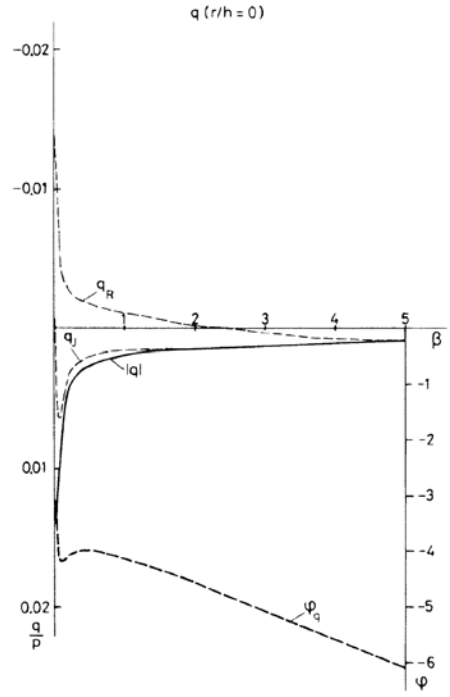

Fig. 3.46. Relationship of dimensionless subgrade reaction q/p to frequency β.

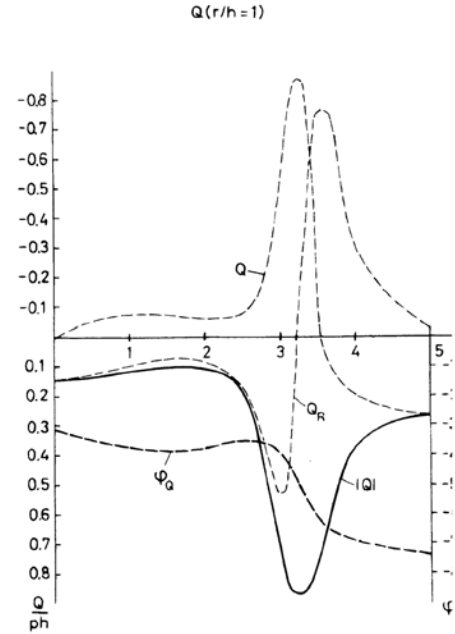

Fig. 3.47. Relationship of dimensionless transverse force Q/ph to frequency β.

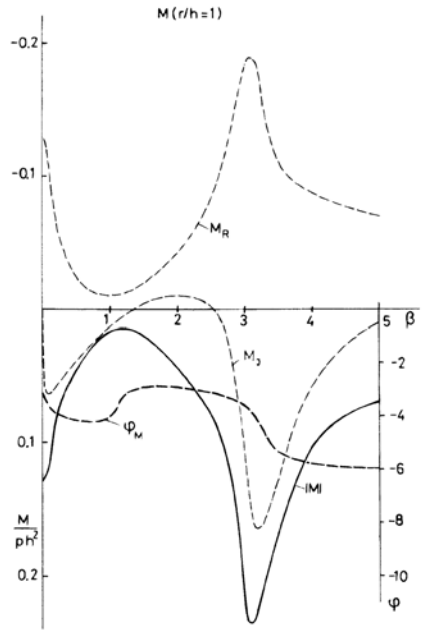

Fig. 3.48. Relationship of dimensionless bending moment M/ph^2 to frequency β.

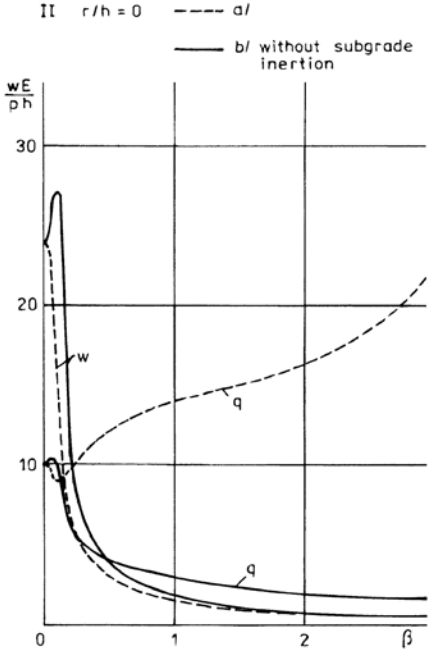

Fig. 3.49. Influence of subgrade inertia on variation of dimensionless deflection wE/ph and subgrade reaction q/p in equivalent plate on subgrade.

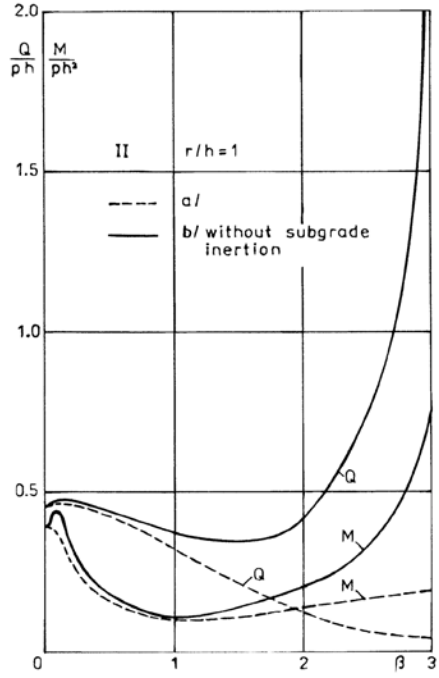

Fig. 3.50. Influence of subgrade inertia on variation of dimensionless bending moment M/ph^2 and transverse force Q/ph in equivalent plate on subgrade.

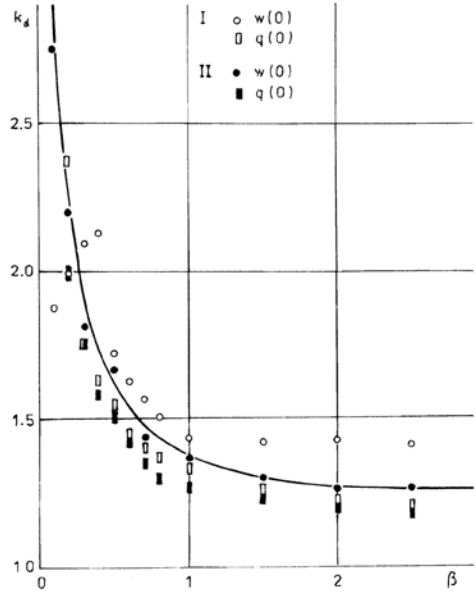

Fig. 3.51. Relationship of coefficient of mass increase of plate *kd* to frequency *β*.

The computed curves of $w(0)$, $q(0)$, $Q(r/h=1)$ and $M(r/h=1)$ versus frequency β are plotted in Figs. 3.45–3.48.

Neglecting the subgrade inertia forces considerably influences the values of the state vector components of a plate lying on a simplified model of subgrade. This can be seen from a comparison of the variations of absolute values for w and q in Fig. 3.49 and for M and Q in Fig. 3.50. These results were obtained for flexible pavement II by using the solution in integral form, i.e. variant (a).

The computed values of the state vector components for various input data of coefficient k_d, i.e coefficient of mass increase of the plate, give the opportunity to determine for an arbitrary frequency β the value of k_d in such a way that the values of state vector components are approximately identical to the values of variant (a). The values of kd versus frequency β for pavement structures I and II and by the identification of absolute values $(wE/ph)_{r/h=0}$ or $(q/p)_{r/h=0}$ are plotted in Fig. 3.51. Although the influence of pavement stiffness and the given state vector component on the form of function $k_d(\beta)$ is evident, in practice the approximate relation $k_d(\beta)$ in Fig. 3.51 is useful in the solution of a plate on subgrade according to the technical theory in variant (b).

4
DYNAMIC INTERACTION OF PLATES WITH THE SUBGRADE FOR CHARACTERISTIC LOADS

In the previous chapter the diverse variants of the theory of the equivalent plate on subgrade were analysed in connection with the basic loading case: axial symmetric harmonically variable loading of an unbounded plate on subgrade. Such a load is in the static case the design load of pavement structures.

The aim of this chapter is the study of the other characteristic loading cases in the dynamic harmonic regime. For the characteristic loading cases, we consider dynamic loading at the boundary region of the half-plate on subgrade, the state of dynamic stress about the cut transverse joint of the plate on subgrade, and the influence of the inhomogeneous subgrade on the interaction of the plate with the subgrade.

4.1 The applied variant of the theory of an equivalent plate on subgrade

The simplest variant of the technical theory of a plate on subgrade that retains the essential properties of real system behaviour is the physical model of a thin plate with flexural stiffness corresponding to the curve of dispersion of flexural stress waves in connection with the simplified model of the subgrade. If the compensation of the subgrade inertia, by the coefficient of mass increase of the plate k_d, is used, the differential equation of motion has the form

$$\nabla^2\nabla^2 w - \frac{K_2^*}{D^*}\nabla^2 w + \frac{K_1^*}{D^*}w + \frac{k_d \varrho h}{D^*}\frac{\partial^2 w}{\partial t^2} = \frac{p}{D^*} \tag{4.1}$$

in which D^* is given by equation (3.263).

The operator ∇^2 in a rectangular coordinates system is given by the expression

$$\nabla^2 = \frac{\partial^2}{\partial x^2} + \frac{\partial^2}{\partial y^2}. \tag{4.2}$$

The bending moments M_x and M_y are determined by the relationships

$$M_x = -D^*\left(\frac{\partial^2 w}{\partial x^2} + \mu\frac{\partial^2 w}{\partial y^2}\right)$$

$$M_y = -D^*\left(\frac{\partial^2 w}{\partial y^2} + \mu\frac{\partial^2 w}{\partial x^2}\right). \tag{4.3}$$

The transverse forces on the plate are determined by the expressions

$$T_x = -D^* \frac{\partial}{\partial x}\left(\frac{\partial^2 w}{\partial x^2} + \frac{\partial^2 w}{\partial y^2}\right)$$

$$T_y = -D^* \frac{\partial}{\partial y}\left(\frac{\partial^2 w}{\partial x^2} + \frac{\partial^2 w}{\partial y^2}\right) \tag{4.4}$$

and the twisting moment by

$$M_{xy} = M_{yx} = -D^*(1-\mu)\frac{\partial^2 w}{\partial x \partial y}. \tag{4.5}$$

The equivalent transverse forces of the plate including the effect of twisting moments are given in the form

$$\bar{Q}_x = \left(T_x + \frac{\partial M_{xy}}{\partial y}\right) = -D^* \frac{\partial}{\partial x}\left[\frac{\partial^2 w}{\partial x^2} + (2-\mu)\frac{\partial^2 w}{\partial y^2}\right]$$

$$\bar{Q}_y = \left(T_y + \frac{\partial Mxy}{\partial x}\right) = -D^* \frac{\partial}{\partial y}\left[\frac{\partial^2 w}{\partial y^2} + (2-\mu)\frac{\partial^2 w}{\partial x^2}\right]. \tag{4.6}$$

The transverse forces of the system (plate on subgrade) are determined by the equations

$$Q_x = -D^*\left[\frac{\partial^3 w}{\partial x^3} + (2-\mu)\frac{\partial^3 w}{\partial x \partial y^2} - \frac{K_2^*}{D^*}\frac{\partial w}{\partial x}\right]$$

$$Q_y = -D^*\left[\frac{\partial^3 w}{\partial y^3} + (2-\mu)\frac{\partial^3 w}{\partial y \partial x^2} - \frac{K_2^*}{D^*}\frac{\partial w}{\partial y}\right]. \tag{4.7}$$

The reaction of the subgrade is expressed by the relationship

$$q = K_1^* w - K_2^* \nabla^2 w. \tag{4.8}$$

4.2 Reduction of partial differential equation to an ordinary differential equation

The analysis of characteristic loading cases is possible if Fourier integral transformation, with regard to one variable, is used according to the relationships

$$^{\mathrm{F}}f(\alpha_0) = \frac{1}{2\pi}\int_{-\infty}^{\infty} f(x)\mathrm{e}^{\mathrm{i}\alpha_0 x}\mathrm{d}x \tag{4.9}$$

$$f(x) = \int_{-\infty}^{\infty} {}^{\mathrm{F}}f(\alpha)\mathrm{e}^{-\mathrm{i}\alpha_0 x}\mathrm{d}\alpha_0. \tag{4.10}$$

If we assume harmonic vibration with angular frequency ω, then by using (4.9) in equation (4.1) the ordinary differential equation is obtained in the form

$$\left[\frac{\mathrm{d}^4}{\mathrm{d}y^4} + \frac{\mathrm{d}^2}{\mathrm{d}y^2}\left(-2\alpha_0^2 - \frac{K_2^*}{D^*}\right) + \left(\alpha_0^4 + \alpha_0^2\frac{K_2^*}{D^*} + \frac{K_1^*}{D^*} - \frac{k_\mathrm{d}\varrho h\omega^2}{D^*}\right)\right]{}^{\mathrm{F}}w = \frac{{}^{\mathrm{F}}p(\alpha_0, y)}{D^*} \tag{4.11}$$

where ${}^{\mathrm{F}}w$ is the Fourier transform of the deflection and ${}^{\mathrm{F}}p$ is the transform of the external load. The integration variable α_0 presents the wave number.

Let us assume the solution of homogeneous equation (4.11) in the form ${}^{\mathrm{F}}w = \mathrm{e}^{\bar{\gamma}y}$. After substituting into (4.11), the following relationship for $\bar{\gamma}$ is obtained

$$\bar{\gamma}_{1,2}^2 = \alpha_0^2 + \frac{K_2^*}{2D^*} \pm \sqrt{\frac{K_2^{*2}}{4D^{*2}} - \frac{K_1^*}{D^*} + \frac{k_\mathrm{d}\varrho h}{D^*}\omega^2} \tag{4.12}$$

and the solution of the homogeneous equation has the form

$${}^{\mathrm{F}}w(\alpha_0, y) = A_1\mathrm{e}^{\bar{\gamma}_1 y} + A_2\mathrm{e}^{-\bar{\gamma}_1 y} + A_3\mathrm{e}^{\bar{\gamma}_2 y} + A_4\mathrm{e}^{-\bar{\gamma}_2 y}. \tag{4.13}$$

Provided the dimensionless variable

$$\eta = \frac{y}{L} \tag{4.14}$$

and dimensionless wave number

$$\alpha = \alpha_0 L \tag{4.15}$$

the Fourier transform of the deflection can be expressed in the form

$${}^{\mathrm{F}}w(\alpha, \eta) = A_1\sinh\gamma_1\eta + A_2\cosh\gamma_1\eta + A_3\sinh\gamma_2\eta + A_4\cosh\gamma_2\eta \tag{4.16}$$

if

$$\gamma_1 = \left[\alpha^2 + \frac{K_2^* L^2}{2D^*} + \left(\frac{K_2^{*2} L^4}{4D^{*2}} - \frac{K_1^* L^4}{D^*} + \frac{\varrho h \omega^2 L^4}{D^*} k_d\right)^{1/2}\right]^{1/2} \tag{4.17}$$

$$\gamma_2 = \left[\alpha^2 + \frac{K_2^* L^2}{2D^*} - \left(\frac{K_2^{*2} L^4}{4D^{*2}} - \frac{K_1^* L^4}{D^*} + \frac{\varrho h \omega^2 L^4}{D^*} k_d\right)^{1/2}\right]^{1/2} \tag{4.18}$$

and L is the chosen length.

4.2.1 Application of the method of initial parameters

In the case of arbitrary external loading or for the solution of characteristic loading cases the method of initial parameters is advantageous. The initial parameters are the transforms of the deflection ${}^{\mathrm{F}}w_0$, angular displacement ${}^{\mathrm{F}}\varphi_0$, bending moment ${}^{\mathrm{F}}M_0$ and transverse force ${}^{\mathrm{F}}Q_0$.

In accordance with equations (4.16), (4.3) and (4.7), the equations are given as follows

$${}^{\mathrm{F}}\varphi(\alpha,\eta) = \frac{1}{L}\frac{\mathrm{d}^{\mathrm{F}}w}{\mathrm{d}\eta} = \frac{1}{L}(A_1\gamma_1 \cosh\gamma_1\eta + A_2\gamma_1 \sinh\gamma_1\eta + A_3\gamma_2 \cosh\gamma_2\eta + A_4\gamma_2 \sinh\gamma_2\eta) \tag{4.19}$$

$$\begin{aligned}
{}^{\mathrm{F}}M(\alpha,\eta) &= -\frac{D^*}{L^2}\left[A_1(\gamma_1^2 - \mu\alpha^2)\sinh\gamma_1\eta + A_2(\gamma_1^2 - \mu\alpha^2)\cosh\gamma_1\eta\right. \\
&\quad \left. + A_3(\gamma_2^2 - \mu\alpha^2)\sinh\gamma_2\eta + A_4(\gamma_2^2 - \mu\alpha^2)\cosh\gamma_2\eta\right] \\
{}^{\mathrm{F}}Q(\alpha,\eta) &= -\frac{D^*}{L^2}\left\{A_1\left[\gamma_1^3 - \gamma_1\left((2-\mu)\alpha^2 + \frac{K_2^* L^2}{D^*}\right)\right]\cosh\gamma_1\eta\right. \\
&\quad + A_2\left[\gamma_1^3 - \gamma_1\left((2-\mu)\alpha^2 + \frac{K_2^* L^2}{D^*}\right)\right]\sinh\gamma_1\eta \\
&\quad + A_3\left[\gamma_2^3 - \gamma_2\left((2-\mu)\alpha^2 + \frac{K_2^* L^2}{D^*}\right)\right]\cosh\gamma_2\eta \\
&\quad \left. + A_4\left[\gamma_2^3 - \gamma_2\left((2-\mu)\alpha^2 + \frac{K_2^* L^2}{D^*}\right)\right]\sinh\gamma_2\eta\right\}.
\end{aligned} \tag{4.20, 4.21}$$

For η=0 the following expressions are obtained

$$
\begin{aligned}
{}^{\mathrm{F}}w_0 &= A_2 + A_4 \\
{}^{\mathrm{F}}\varphi_0 L &= A_1\gamma_1 + A_3\gamma_2 \\
-\frac{{}^{\mathrm{F}}M_0 L^2}{D^*} &= A_1 s_1 + A_4 s_2 \\
-\frac{{}^{\mathrm{F}}Q_0 L^3}{D^*} &= A_1 q_1 + A_3 q_2
\end{aligned}
\tag{4.22}
$$

where

$$
\begin{aligned}
s_1 &= \gamma_1^2 - \mu\alpha^2 \\
s_2 &= \gamma_2^2 - \mu\alpha^2 \\
q_1 &= \gamma_1^3 - \gamma_1\left((2-\mu)\alpha^2 + \frac{K_2^* L^2}{D^*}\right) \\
q_2 &= \gamma_2^3 - \gamma_2\left((2-\mu)\alpha^2 + \frac{K_2^* L^2}{D^*}\right).
\end{aligned}
\tag{4.23}
$$

The values of constants A_1, A_2, A_3, A_4 may be expressed from the equations system (4.22) through initial parameters by the following relationships

$$
\begin{aligned}
{}^{\mathrm{F}}w(\alpha,\eta) &= K_{ww}{}^{\mathrm{F}}w_0 + K_{w\varphi}{}^{\mathrm{F}}\varphi_0 + K_{wM}{}^{\mathrm{F}}M_0 + K_{wQ}{}^{\mathrm{F}}Q_0 \\
{}^{\mathrm{F}}\varphi(\alpha,\eta) &= K_{\varphi w}{}^{\mathrm{F}}w_0 + K_{\varphi\varphi}{}^{\mathrm{F}}\varphi_0 + K_{\varphi M}{}^{\mathrm{F}}M_0 + K_{\varphi Q}{}^{\mathrm{F}}Q_0 \\
{}^{\mathrm{F}}M(\alpha,\eta) &= K_{Mw}{}^{\mathrm{F}}w_0 + K_{M\varphi}{}^{\mathrm{F}}\varphi_0 + K_{MM}{}^{\mathrm{F}}M_0 + K_{MQ}{}^{\mathrm{F}}Q_0 \\
{}^{\mathrm{F}}Q(\alpha,\eta) &= K_{Qw}{}^{\mathrm{F}}w_0 + K_{Q\varphi}{}^{\mathrm{F}}\varphi_0 + K_{QM}{}^{\mathrm{F}}M_0 + K_{QQ}{}^{\mathrm{F}}Q_0
\end{aligned}
\tag{4.24}
$$

where K_{ww}, $K_{w\varphi}$,…K_{QQ} are the influence functions summarized in Table 4.1. The matrix of influence functions has a symmetric structure with regard to the upward diagonal.

The concept of the solution and derived expressions, as described, makes it possible to analyse characteristic cases of dynamic loading at the boundary region or about the cut transverse joints of a plate on subgrade and close to the sudden change of rigidity in the equivalent plate on subgrade as a consequence of inhomogeneous subgrade.

4.3 Dynamic load at the boundary region of a plate on subgrade

Although the design methods of pavement structures assume, as a decisive case, static loading of an unbounded pavement structure, it is known that some components of the static vector, by loading at the border of the pavement, may exceed the values of the basic loading case. We shall attempt to solve, in the next chapter, the state of stresses by dynamic loading about the border of the equivalent plate on subgrade.

4.3.1 Half-plate on subgrade

According to the scheme in Fig. 4.1 we assume a harmonic variable concentrated force $Pe^{i\omega t}$ acting at distance y_1 or dimensionless quantity $\eta_1=y_1/L$ from the boundary of the half-plate on subgrade.

For the region $\eta<\eta_1$, i.e. zone I, the relationships of the Fourier transform components derived in the form (4.24) and the corresponding matrix of influence functions in Table 4.1 are valid.

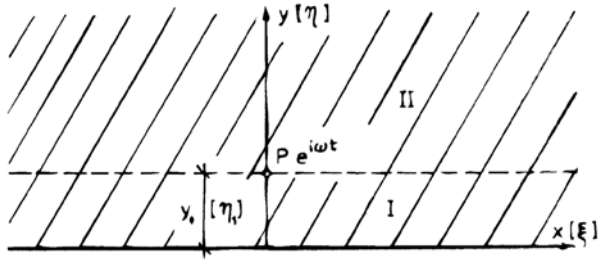

Fig. 4.1. Schematic diagram of half-plate on subgrade and system of coordinates.

Table 4.1. Matrix of influence functions.

	${}^{F}w_0$	${}^{F}\varphi_0$	${}^{F}M_0$	${}^{F}Q_0$
$F_w(\alpha,\eta)$	$K_{ww}=\frac{1}{s_1-s_2}$ $\times(-s_2\cosh\gamma_1\eta+$ $+s_1\cosh\gamma_2\eta)$	$K_{w\varphi}=\frac{L}{q_2\gamma_1-q_1\gamma_2}$ $\times(q_2\sinh\gamma_1\eta-$ $-q_1\sinh\gamma_2\eta)$	$K_{wM}=\frac{L^2}{D^*}\frac{1}{s_1-s_2}$ $\times(-\cosh\gamma_1\eta+$ $+\cosh\gamma_2\eta)$	$K_{wQ}=\frac{L^3}{D^*}\frac{1}{q_2\gamma_1-q_1\gamma_2}$ $\times(\gamma_2\sinh\gamma_1\eta-$ $-\gamma_1\sinh\gamma_2\eta)$
$F_\varphi(\alpha,\eta)$	$K_{\varphi w}=\frac{1}{L}\frac{1}{s_1-s_2}$ $\times(-\gamma_1 s_2\sinh\gamma_1\eta+$ $+\gamma_2 s_1\sinh\gamma_2\eta)$	$K_{\varphi\varphi}=\frac{1}{q_2\gamma_1-q_1\gamma_2}$ $\times(\gamma_1 q_2\cosh\gamma_1\eta+$ $+\gamma_2 q_1\cosh\gamma_2\eta)$	$K_{\varphi M}=\frac{L}{D^*}\frac{1}{s_1-s_2}$ $\times(-\gamma_1\sinh\gamma_1\eta+$ $+\gamma_2\sinh\gamma_2\eta)$	$K_{\varphi Q}=K_{wM}$
${}^{F}M(\alpha,\eta)$	$K_{Mw}=\frac{D^*}{L^2}\frac{s_1 s_2}{s_1-s_2}$ $\times(\cosh\gamma_1\eta-$ $-\cosh\gamma_2\eta)$	$K_{M\varphi}=-\frac{D^*}{L(q_2\gamma_1-q_1\gamma_2)}$ $\times(q_2 s_1\sinh\gamma_1\eta-$ $-q_1 s_2\sinh\gamma_2\eta)$	$K_{MM}=K_{\varphi\varphi}$	$K_{MQ}=K_{w\varphi}$
${}^{F}Q(\alpha,\eta)$	$K_{Qw}=\frac{D^*}{L^3(s_1-s_2)}$ $\times(q_1 s_2\sinh\gamma_1\eta-$ $-q_2 s_1\sinh\gamma_2\eta)$	$K_{Q\varphi}=K_{Mw}$	$K_{QM}=K_{\varphi w}$	$K_{QQ}=K_{ww}$

For the region $\eta>\eta_1$, i.e. zone II, the relationships of the transform components can be established in the form

$$
\begin{aligned}
{}^{\mathrm{F}}w(\alpha,\eta) &= B_1 e^{\gamma_1\eta} + B_2 e^{\gamma_2\eta} \\
{}^{\mathrm{F}}\varphi(\alpha,\eta) &= \frac{1}{L}(B_1\gamma_1 e^{\gamma_1\eta} + B_2\gamma_2 e^{\gamma_2\eta}) \\
{}^{\mathrm{F}}M(\alpha,\eta) &= -\frac{D^*}{L^2}(B_1 s_1 e^{\gamma_1\eta} + B_2 s_2 e^{\gamma_2\eta}) \\
{}^{\mathrm{F}}Q(\alpha,\eta) &= -\frac{D^*}{L^3}(B_1 q_1 e^{\gamma_1\eta} + B_2 q_2 e^{\gamma_2\eta})
\end{aligned}
\tag{4.25}
$$

assuming that the complex values γ_1, γ_2 have a negative real part. B_1, B_2 are arbitrary complex constants.

Assuming a free boundary of the half-plate on an unbounded subgrade medium, the boundary conditions are determined in the form

$$
\begin{aligned}
{}^{\mathrm{F}}M_0(\eta=0) &= 0 \\
{}^{\mathrm{F}}Q_0(\eta=0) &= {}^{\mathrm{F}}Q_z(\eta=0)
\end{aligned}
\tag{4.26}
$$

where ${}^{\mathrm{F}}Q_z$ is the Fourier transform of the reaction of free subgrade.

The reaction of the free subgrade may be determined by using the equation of the simplified model of subgrade (3.150) in the form

$$
-K_2^*\nabla^2 v + K_1^* v + \varrho_z K_3 \frac{\partial^2 v}{\partial t^2} = q(x,y)e^{i\omega t} \tag{4.27}
$$

if v is subgrade deflection.

By using Fourier integral transformation in the x direction the following equation is obtained

$$
\frac{d^2}{dy^2}{}^{\mathrm{F}}v + \left[-\frac{K_1^*}{K_2^*} - \alpha_0^2 + \varrho_z \frac{K_3^*\omega^2}{K_2^*}\right]{}^{\mathrm{F}}v = \frac{{}^{\mathrm{F}}q(\alpha_0,y)}{K_2^*}. \tag{4.28}
$$

The solution of the homogeneous equation is given for the transform of subgrade deflection ${}^{\mathrm{F}}v$ in the form

$$
{}^{\mathrm{F}}v = A\, e^{\bar{\gamma}_z y} + B^{-\bar{\gamma}_z y} \tag{4.29}
$$

where

$$\bar{\gamma}_z = \pm \sqrt{\frac{K_1^*}{K_2^*} + \alpha_0^2 - \varrho_z \frac{K_3 \omega^2}{K_2^*}}. \tag{4.30}$$

Considering only the part of solution (4.29) which is in free subgrade with the distance damped, i.e.

$${}^{\mathrm{F}}v = A\, \mathrm{e}^{\bar{\gamma}_z y} \tag{4.31}$$

and the condition that for y=0 the subgrade deflection transform has to be equal to the deflection transform of halfplate border, the following equation is given

$${}^{\mathrm{F}}v(0) = A = {}^{\mathrm{F}}w_0. \tag{4.32}$$

Then the reaction transform of the free subgrade ${}^{\mathrm{F}}Q_z$ is given by the transform of shear force at y=0 according to the relationship

$${}^{\mathrm{F}}Q_z = K_2^* \frac{\mathrm{d}^{\mathrm{F}}v}{\mathrm{d}y} = K_2^* \bar{\gamma}_z {}^{\mathrm{F}}w_0 \tag{4.33}$$

and in dimensionless form

$${}^{\mathrm{F}}Q_z = K_2^* \frac{1}{L} \gamma_z {}^{\mathrm{F}}w_0 \tag{4.34}$$

if

$$\gamma_z = \sqrt{\frac{K_1^* L^2}{K_2^*} + \alpha^2 - \frac{\varrho_z K_3 \omega^2 L^2}{K_2^*}}. \tag{4.35}$$

The contact conditions at the interface of zone I and zone II, i.e. at $\eta=\eta_1$ are given in the form

$$\begin{aligned}
{}^{\mathrm{F}}w_{\mathrm{I}}(\eta=\eta_1) &= {}^{F}w_{\mathrm{II}}(\eta=\eta_1) \\
{}^{\mathrm{F}}\varphi_{\mathrm{I}}(\eta=\eta_1) &= {}^{\mathrm{F}}\varphi_{\mathrm{II}}(\eta=\eta_1) \\
{}^{\mathrm{F}}M_{\mathrm{I}}(\eta=\eta_1) &= {}^{\mathrm{F}}M_{\mathrm{II}}(\eta=\eta_1) \\
{}^{\mathrm{F}}Q_{\mathrm{I}}(\eta=\eta_1) - {}^{\mathrm{F}}P &= {}^{\mathrm{F}}Q_{\mathrm{II}}(\eta=\eta_1)
\end{aligned} \tag{4.36}$$

where ${}^{\mathrm{F}}P$ is the Fourier transform of dynamic load.

Substituting into the boundary conditions (4.26) and contact conditions (4.36) and rearranging, the following system of equations for unknown quantities ${}^{\mathrm{F}}w$, $L\,{}^{\mathrm{F}}\varphi_0$, B_1, B_2 is obtained

${}^{F}w_0$	$L^{F}\varphi_0$	B_1	B_2	*Right-hand side*
a_{11}	a_{12}	a_{13}	a_{14}	a_{10}
a_{21}	a_{22}	a_{23}	a_{24}	a_{20}
a_{31}	a_{32}	a_{33}	a_{34}	a_{30}
a_{41}	a_{42}	a_{43}	a_{44}	a_{40}

(4.37)

where

$$a_{11} = \frac{1}{s_1 - s_2}\left(-s_2 \cosh\gamma_1\eta_1 + s_1 \cosh\gamma_2\eta_1\right)$$

$$+\frac{K_2^* L^2\gamma_z}{D^*(q_2\gamma_1 - q_1\gamma_2)}\left(\gamma_2 \sinh\gamma_1\eta_1 - \gamma_1 \sinh\gamma_2\eta_1\right)$$

$$a_{12} = \frac{1}{q_2\gamma_1 - q_1\gamma_2}\left(q_2 \sinh\gamma_1\eta_1 - q_1 \sinh\gamma_2\eta_1\right)$$

$$a_{13} = -1$$

$$a_{13} = -1$$

$$a_{10} = 0$$

$$a_{21} = \frac{1}{s_1 - s_2}\left(-\gamma_1 s_2 \sinh\gamma_1\eta_1 + \gamma_2 s_1 \sinh\gamma_2\eta_1\right) + \frac{K_2^* L^2\gamma_z}{D^*(s_1 - s_2)}$$

$$\times\left(-\cosh\gamma_1\eta_1 + \cosh\gamma_2\eta_1\right)$$

$$a_{22} = \frac{1}{q_2\gamma_1 - q_1\gamma_2}\left(\gamma_1 q_2 \cosh\gamma_1\eta_1 - \gamma_2 q_1 \cosh\gamma_2\eta_1\right)$$

$$a_{23} = -\gamma_1$$

$$a_{24} = -\gamma_2$$

$$a_{20} = 0$$

$$a_{31} = \frac{s_1 s_2}{s_1 - s_2} (\cosh \gamma_1 \eta_1 - \cosh \gamma_2 \eta_1)$$

$$+ \frac{K_2^* L^2 \gamma_z}{D^* (q_2 \gamma_1 - q_1 \gamma_2)} (q_2 \sinh \gamma_1 \eta_1 - q_1 \sinh \gamma_2 \eta_1)$$

$$a_{32} = \frac{-1}{q_2 \gamma_1 - q_1 \gamma_2} (q_2 s_1 \sinh \gamma_1 \eta_1 - q_1 s_2 \sinh \gamma_2 \eta_1)$$

$$a_{33} = s_1$$

$$a_{34} = s_2$$

$$a_{30} = 0 \tag{4.38}$$

$$a_{41} = \frac{1}{s_1 - s_2} (q_1 s_2 \sinh \gamma_1 \eta_1 - q_2 s_1 \sinh \gamma_2 \eta_1)$$

$$+ \frac{K_2^* L^2 \gamma_z}{D^* (s_1 - s_2)} (-s_2 \cosh \gamma_1 \eta_1 + s_1 \cosh \gamma_2 \eta_1)$$

$$a_{42} = \frac{s_1 s_2}{s_1 - s_2} (\cosh \gamma_1 \eta_1 - \cosh \gamma_2 \eta_1)$$

$$a_{43} = q_1$$

$$a_{44} = q_2$$

$$a_{40} = \frac{L^3}{D^*} {}^{\mathrm{F}}P.$$

In the limited case when η_1=0, the coefficients of system (4.37) have the following values

$$a_{11}=1,\quad a_{21}=0,\quad a_{31}=0,\quad a_{41}=\frac{K_2^*L^2\gamma_z}{D^*}$$

$$a_{12}=0,\quad a_{22}=1,\quad a_{32}=0,\quad a_{42}=0$$

$$a_{13}=-1,\quad a_{23}=-\gamma_1,\quad a_{33}=s_1,\quad a_{43}=q_1 \tag{4.39}$$

$$a_{14}=-1,\quad a_{24}=-\gamma_2,\quad a_{34}=s_2,\quad a_{44}=q_2$$

$$a_{10}=0,\quad a_{20}=0,\quad a_{30}=0,\quad a_{40}=\frac{L^3}{D^*}{}^{\mathrm{F}}P$$

and the solution corresponds to a half-plate on unbounded subgrade with the dynamic force acting at the boundary.

The equation system (4.37) is in general a system with a complex coefficients and the unknown initial parameters ${}^{\mathrm{F}}w_0$, ${}^{\mathrm{F}}\varphi_0$ and quantities B_1, B_2 are complex functions of dimensionless wave number α.

4.3.2 Survey of relationships for state vector components of a half-plate on subgrade

By using equations (4.24), (4.3), (4.5), (4.7), (4.8) and by inverse transformation the following expressions are obtained for the region $0<\eta<\eta_1$:

$$w(\xi,\eta)=\frac{2P}{GL}\int_0^\infty\left[{}^{\mathrm{F}}w_0K_{ww}+\frac{{}^{\mathrm{F}}\varphi_0}{L}K_{w\varphi}+{}^{\mathrm{F}}Q_0GK_{wQ}\right]\cos\alpha\xi\,\mathrm{d}\alpha$$

$$q(\xi,\eta)=\frac{2P}{L^2}\int_0^\infty\left[\left(\frac{K_1^*L}{G}+\frac{K_2^*\alpha^2}{LG}\right){}^{\mathrm{F}}w_0K_{ww}+\frac{{}^{\mathrm{F}}\varphi_0}{L}K_{w\varphi}\right. \tag{4.40}$$

$$\left.+{}^{\mathrm{F}}Q_0GK_{wQ}-\frac{K_2^*}{LG}K_{w2}\right]\cos\alpha\xi\,\mathrm{d}\alpha$$

where

$$K_{w2} = \frac{{}^{\mathrm{F}}w_0}{s_1 - s_2}(-\gamma_1^2 s_2 \cosh\gamma_1\eta + \gamma_2^2 s_1 \cosh\gamma_2\eta) + \frac{{}^{\mathrm{F}}\varphi_0}{q_2\gamma_1 - q_1\gamma_2}$$

$$\times (\gamma_1^2 q_2 \sinh\gamma_1\eta - \gamma_2^2 q_1 \sinh\gamma_2\eta) + \frac{{}^{\mathrm{F}}Q_0 GL^3}{D^*}\frac{1}{s_1 - s_2}$$

$$\times (-\gamma_1 \sinh\gamma_1\eta + \gamma_2 \sinh\gamma_2\eta)$$

$$M_y(\xi,\eta) = 2P\int_0^\infty \left[{}^{\mathrm{F}}w_0\frac{1}{GL}K_{Mw} + {}^{\mathrm{F}}\varphi_0\frac{1}{GL^2}K_{M\varphi} + {}^{\mathrm{F}}Q_0\frac{1}{L}K_{w\varphi}\right]$$

$$\times \cos\alpha\xi \mathrm{d}\alpha$$

$$Q_y(\xi,\eta) = \frac{2P}{L}\int_0^\infty \left[{}^{\mathrm{F}}w_0\frac{1}{G}K_{Qw} + {}^{\mathrm{F}}\varphi_0\frac{1}{GL}K_{Mw} + {}^{\mathrm{F}}Q_0 K_{ww}\right]\cos\alpha\xi \mathrm{d}\alpha$$

$$M_x(\xi,\eta) = -2P\int_0^\infty \frac{D^*}{GL^3}\left[-\alpha^2\left({}^{\mathrm{F}}w_0 K_{ww} + {}^{\mathrm{F}}\varphi_0\frac{1}{L}K_{w\varphi} + {}^{\mathrm{F}}Q_0 GK_{wQ}\right)\right.$$

$$\left. + \mu K_{w2}\right]\cos\xi\alpha \mathrm{d}\alpha$$

$$Q_x(\xi,\eta) = \frac{2P}{L}\int_0^\infty \frac{D^*}{GL^3}\left[-\alpha^2\left({}^{\mathrm{F}}w_0 K_{ww} + {}^{\mathrm{F}}\varphi_0\frac{1}{L}K_{w\varphi} + {}^{\mathrm{F}}Q_0 GK_{wQ}\right)\right.$$

$$\left. + K_{w2}\right]\alpha\sin\xi\alpha \mathrm{d}\alpha$$

$$M_{xy}(\xi,\eta) = 2P\int_0^\infty \frac{D^*(1-\mu)}{GL^3}\left({}^{\mathrm{F}}w_0 LK_{\varphi w} + {}^{\mathrm{F}}\varphi_0 K_{\varphi\varphi} + {}^{\mathrm{F}}Q_0 GLK_{wM}\right)$$

$$\times \alpha \sin\xi\alpha \,\mathrm{d}\alpha$$

and for the region $\eta > \eta_1$ of a half-plate on subgrade in the form

$$w(\xi,\eta)=\frac{2P}{GL}\int_0^\infty\left(B_1\,\mathrm{e}^{\gamma_1(\eta-\eta_1)}+B_2\,\mathrm{e}^{\gamma_2(\eta-\eta_1)}\right)\cos\xi\alpha\,\mathrm{d}\alpha$$

$$q(\xi,\eta)=\frac{2P}{L^2}\int_0^\infty\left(\frac{K_1^*L}{G}+\frac{K_2^*\alpha^2}{GL}\right)\left(B_1\,\mathrm{e}^{\gamma_1(\eta-\eta_1)}+B_2\,\mathrm{e}^{\gamma_2(\eta-\eta_1)}\right)\cos\xi\alpha\mathrm{d}\alpha$$

$$M_y(\xi,\eta)=2P\int_0^\infty\frac{D^*}{GL^3}\left(-B_1s_1\,\mathrm{e}^{\gamma_1(\eta-\eta_1)}-B_2s_2\,\mathrm{e}^{\gamma_2(\eta-\eta_1)}\right)\cos\xi\alpha\mathrm{d}\alpha$$

$$Q_y(\xi,\eta)=\frac{2P}{L}\int_0^\infty\frac{D^*}{GL^3}\left(-B_1q_1\,\mathrm{e}^{\gamma_1(\eta-\eta_1)}-B_2q_2\,\mathrm{e}^{\gamma_2(\eta-\eta_1)}\right)\cos\xi\alpha\mathrm{d}\alpha$$

$$M_x(\xi,\eta)=-2P\int_0^\infty\frac{D^*}{GL^3}\left[B_1(-\alpha+\mu\gamma_1^2)\,\mathrm{e}^{\gamma(\eta-\eta_1)}\right.$$

$$\left.+B_2(-\alpha^2+\mu\gamma_2^2)\,\mathrm{e}^{\gamma_2(\eta-\eta_1)}\right]\cos\xi\alpha\mathrm{d}\alpha \qquad (4.41.)$$

$$Q_x(\xi,\eta)=\frac{2P}{L}\int_0^\infty\frac{D^*}{GL^3}\left[B_1\left(-\alpha^2+(2-\mu)\gamma_1^2-\frac{K_2^*L^2}{D^*}\right)\mathrm{e}^{\gamma_1(\eta-\eta_1)}\right.$$

$$\left.+B_2\left(-\alpha^2+(2-\mu)\gamma_2^2-\frac{K_2^*L^2}{D^*}\right)\mathrm{e}^{\gamma_2(\eta-\eta_1)}\right]\alpha\,\sin\xi\alpha\mathrm{d}\alpha$$

$$M_{xy}(\xi,\eta)=2P\int_0^\infty\frac{D^*(1-\mu)}{GL^3}\left[B_1\gamma_1\,\mathrm{e}^{\gamma_1(\eta-\eta_1)}+B_2\gamma_2\,\mathrm{e}^{\gamma_2(\eta-\eta_1)}\right]$$

$$\times\,\alpha\,\sin\xi\alpha\,\mathrm{d}\alpha$$

4.3.3 Numerical results

Computers were used to calculate the components of the state vector for the equivalent half-plate on unbounded subgrade under a harmonic dynamic force $Pe^{i\omega t}$. The dynamic force with amplitude P is assumed to be concentrated in the direction y and uniformly distributed on the line segment $2a$ in the direction x. Then the force amplitude P may be expressed as $P=p2a$, where p is the load segment intensity.

The Fourier transform ${}^{F}P$ is given by the relationship

$$ {}^{F}P = \frac{P}{2a}\,\frac{1}{2\pi}\int_{-a}^{a} e^{i\alpha_0 x}\,dx = \frac{P}{2\pi}\,\frac{\sin\alpha_0 a}{\alpha_0 a}. \tag{4.42}$$

We shall present the results corresponding to the concentrated segment harmonic variable load at the boundary of the half-plate on subgrade. Input data for the system present a flexible pavement structure, which corresponds to a highway pavement under construction composed of a 25 cm thick sandgravel layer, then a 24 cm thick layer of cement stabilization and a 4 cm thick asphaltic layer. They are given by the values

$$c_2/c_{2z} = 6.52, \quad G_z/G = 0.020$$

$$\mu = 0.30, \quad \mu_z = 0.35$$

$$\delta = 0.10, \quad \delta_z = 0.20$$

$$L/h = 12.5, \quad a/L = 0.08$$

$$\frac{K_1 h}{G} = 0.00499, \quad \frac{K_2}{Gh} = 0.01750.$$

The process of numerical calculation was carried out for 21 various values of dimensionless frequencies $\beta=\omega h/c_2$ in the range (0–3.0).

The improper integrals used to define the state vector components, were computed by numerical integration in bounded interval α=(0–40). The upper value of α represents the Fourier spectrum component when the wavelength is comparable with the thickness of the equivalent half-plate and in this way also ensures sufficient precision.

As the sub-integral functions are complex functions for every component of the state vector the real and imaginary part and amplitude and phase angle φ have to be computed. According to the linear variation of phase angle φ the wavelength Λ and corresponding phase velocity c may be determined.

The variations of dimensionless deflection wGL/P, subgrade reaction qL^2/P, bending moment M_y/P and transverse force $Q_y L/P$ versus dimensionless ratio $\eta=y/L$ at the frequencies β=0.1 and β=0.5 and $\xi=x/L$=0.01 are plotted in Figs. 4.2–4.5.

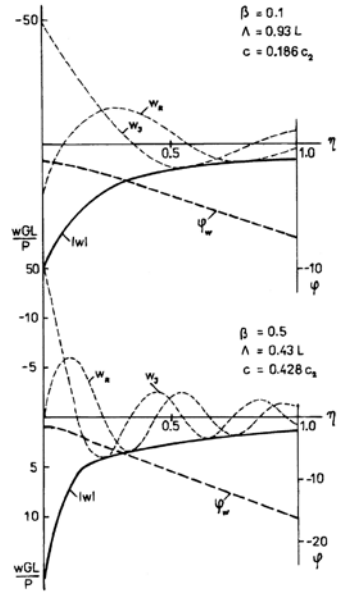

Fig. 4.2. Variation of dimensionless deflection wGL/P with ratio $\eta=y/L$ at frequencies β=0.1 and β=0.5.

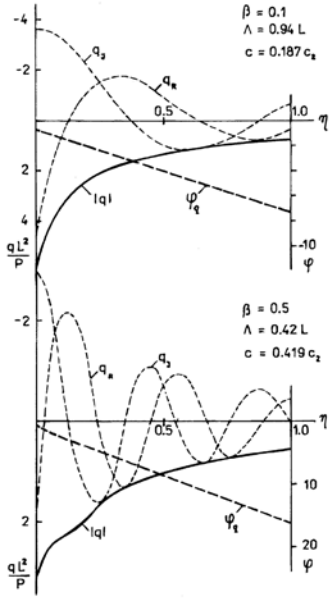

Fig. 4.3. Variation of dimensionless subgrade reaction qL^2/P with ratio $\eta=y/L$ at frequencies β=1.0 and β=0.5.

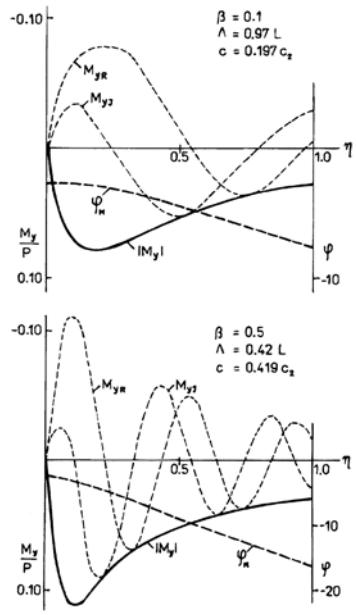

Fig. 4.4. Variation of dimensionless bending moment M_y/P with ratio $\eta=y/L$ at frequencies β=0.1 and β=0.5.

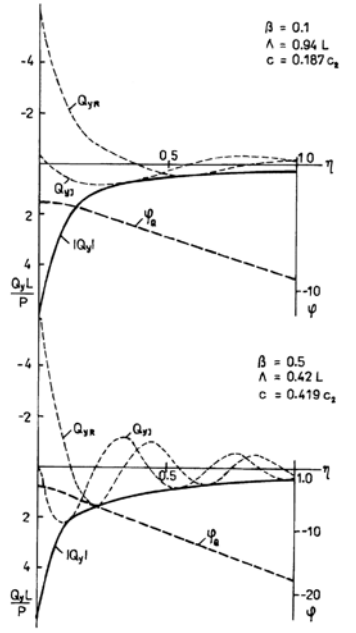

Fig. 4.5. Variation of dimensionless transverse force Q_yL/P with ratio $\eta=y/L$ at frequencies β=0.1 and β=0.5.

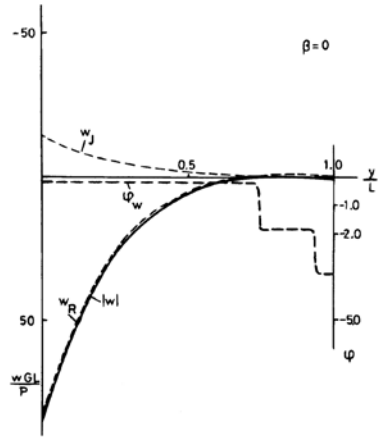

Fig. 4.6. Relationship of dimensionless deflection wGL/P to $\eta=y/L$ in static case.

The relation wGL/P versus y/L at the frequency $\beta=0$ is drawn in Fig. 4.6. The phase angle φ_w with its constant course indicates that there is no propagation of the energy. The computed curves of wGL/P, Q_yL/P, M_x/P, Q_xL/P, and M_{xy}/P versus $\xi=x/L$ at frequencies $\beta=0.1$ and $\beta=0.5$ at the halfplate boundary, i.e. at $\eta=y/L=0.01$, are plotted in Figs. 4.7–4.11.

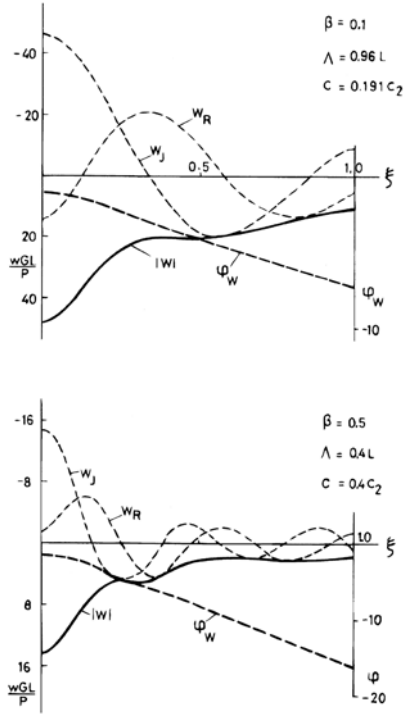

Fig. 4.7. Variation of dimensionless deflection wGL/P with ratio $\xi=x/L$ at frequencies $\beta=0.1$ and $\beta=0.5$.

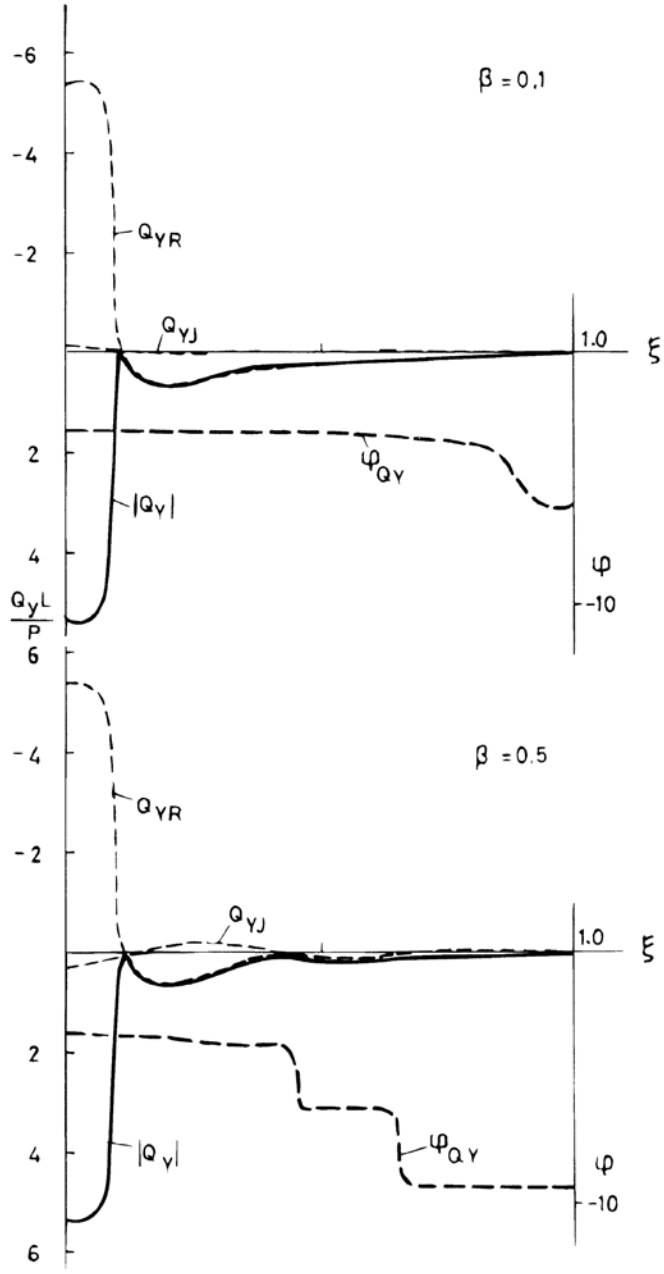

Fig. 4.8. Variation of dimensionless transverse force $Q_y L/P$ with $\xi = x/L$ at frequencies β=0.1 and β=0.5.

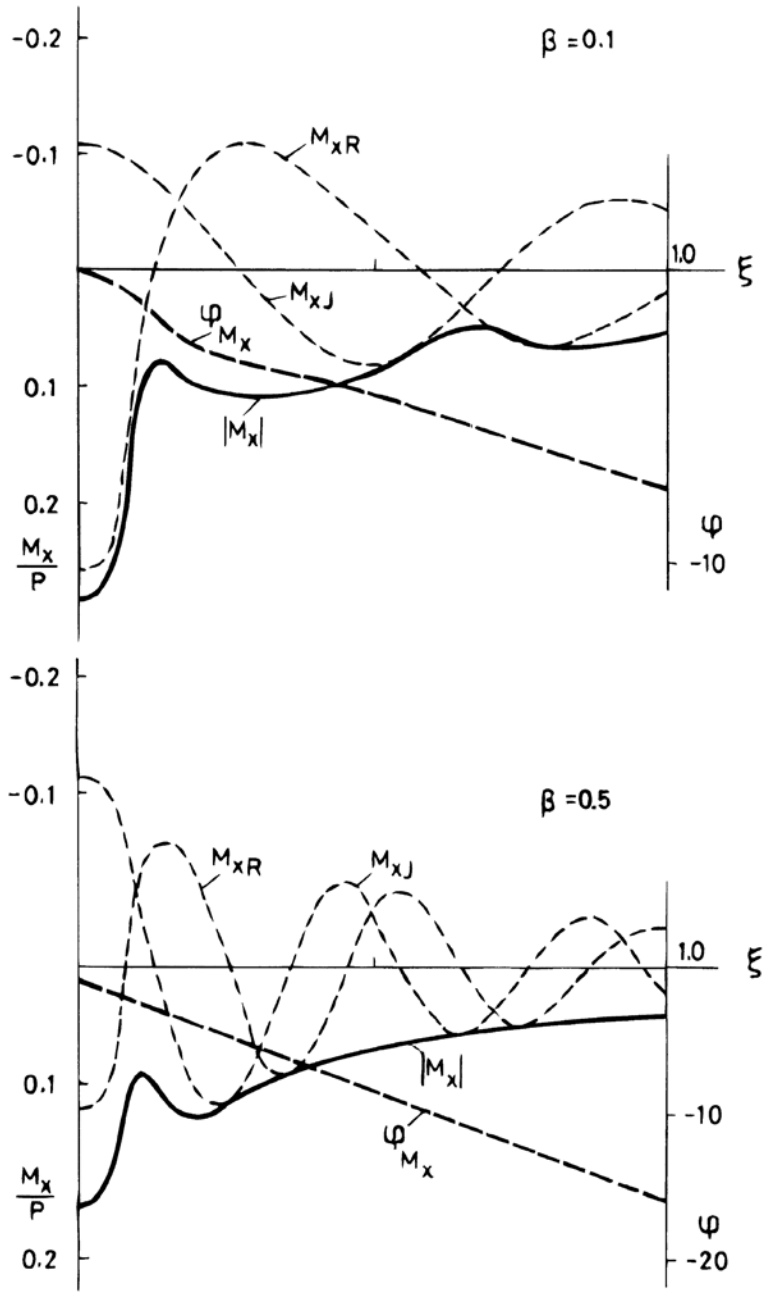

Fig. 4.9. Variation of dimensionless bending moment M_x/P with $\xi=x/L$ at frequencies β=0.1 and β=0.5.

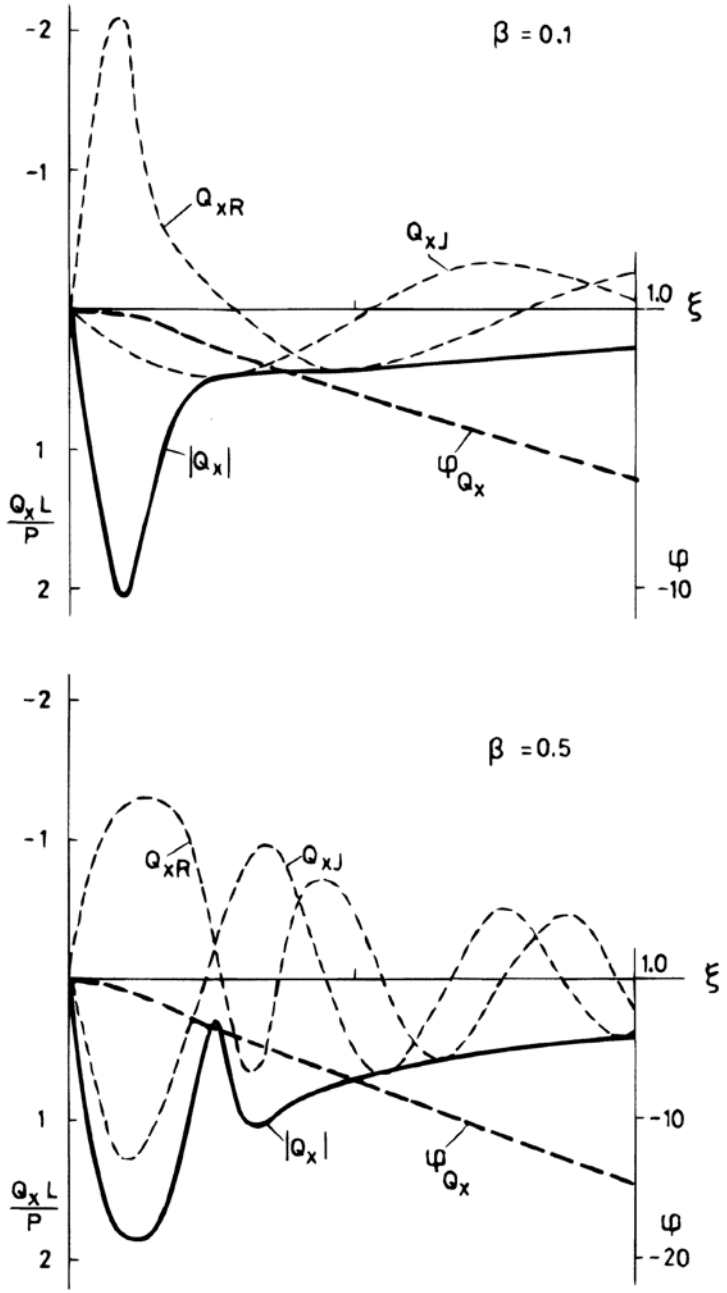

Fig. 4.10. Variation of dimensionless transverse force $Q_x L/P$ with $\xi=x/L$ at frequencies β=0.1 and β=0.5.

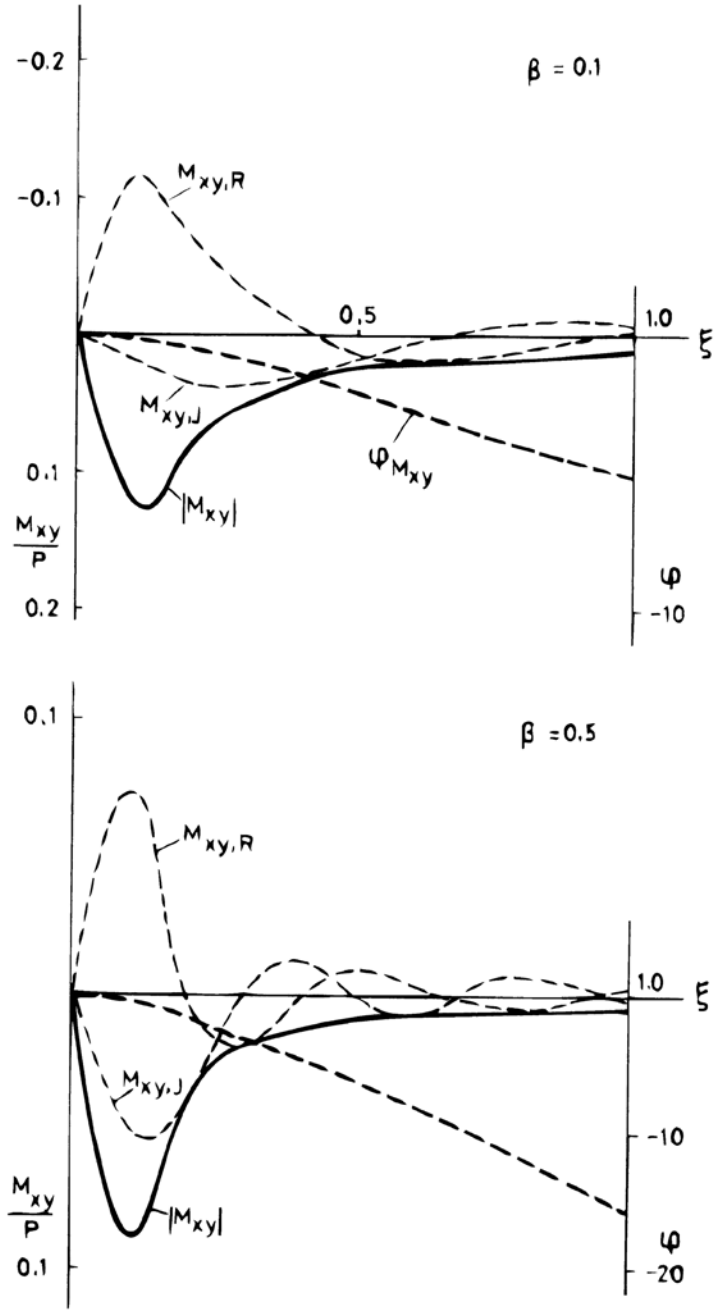

Fig. 4.11. Variation of dimensionless twisting moment M_{xy}/P with $\xi=x/L$ at frequencies β=0.1 and β=0.5.

The variations of wGL/P, qL^2/P, Q_yL/P and M_x/P with frequency β are plotted in Figs. 4.12–4.15.

In the case of a concentrated harmonic force acting at a distance $\eta=\eta_1=0.25$ from the half-plate border the computed course of deflection wGL/P versus $\eta=y/L$ for $\xi=x/L=0.01$ is plotted in Fig. 4.16 for $\beta=0.1$ and $\beta=0.5$.

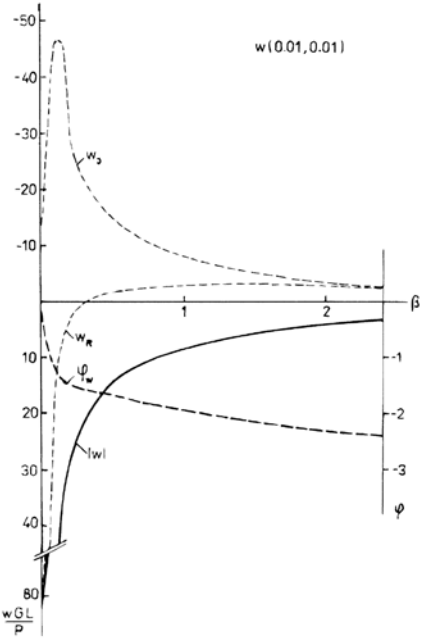

Fig. 4.12. Variation of dimensionless deflection wGL/P with frequency β.

The other calculations were carried out for the half-plate on subgrade which is equivalent to the behaviour of a rigid highway pavement structure. This pavement has the same structure as in the previous case but it is finished by means of a 24 cm thick cement concrete surfacing. The input data are

$$c_2/c_{2z} = 13.65, \quad G_z/G = 0.00423$$

$$\mu = 0.25, \quad \mu_z = 0.35$$

$$L/h = 12.5, \quad a/L = 0.0438$$

$$\delta = 0.10, \quad \delta_z = 0.20$$

$$\frac{K_1 h}{G} = 0.00196, \quad \frac{K_2}{Gh} = 0.00206.$$

The computed values of dimensionless deflections, subgrade reactions, bending moments and transverse forces in relation to the frequency β are drawn in absolute values in Figs. 4.17 and 4.18 at the locations of concentrated dynamic load at points (0.0, 0.0) and (0.0, 0.25).

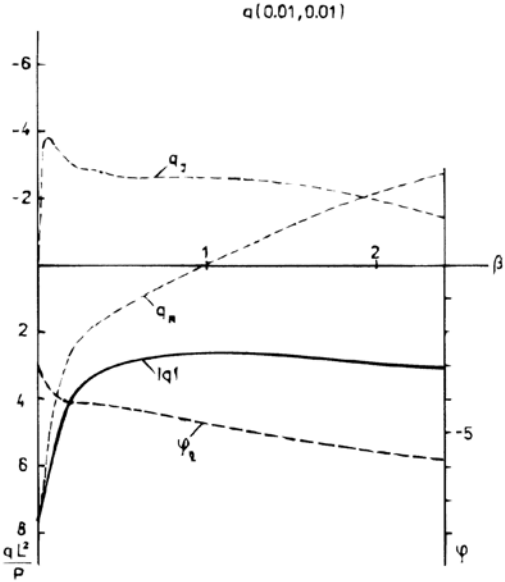

Fig. 4.13. Variation of dimensionless subgrade reaction qL^2/P with frequency β.

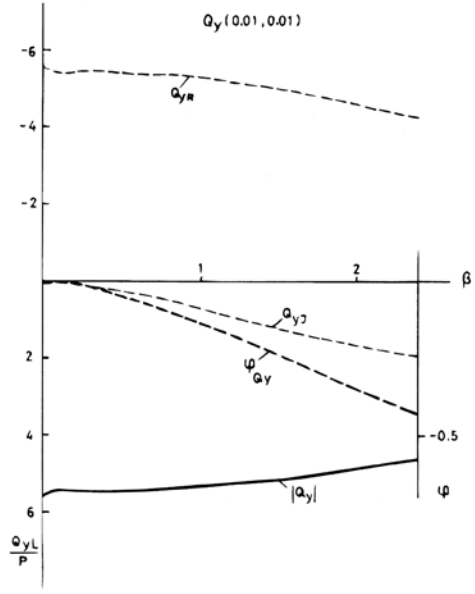

Fig. 4.14. Variation of dimensionless transverse force Q_yL/P with frequency β.

4.4 Plate strip on subgrade

Let us assume an unbounded plate strip on subgrade according to the scheme in Fig. 4.19, with a concentrated harmonic variable load $P(t)=Pe^{i\omega t}$ acting at a distance y_1 from the strip border. We consider again the dimensionless coordinates $\xi=x/L$, $\eta=y/L$, $\eta_1=y_1/L$, where L is the width of the plate strip.

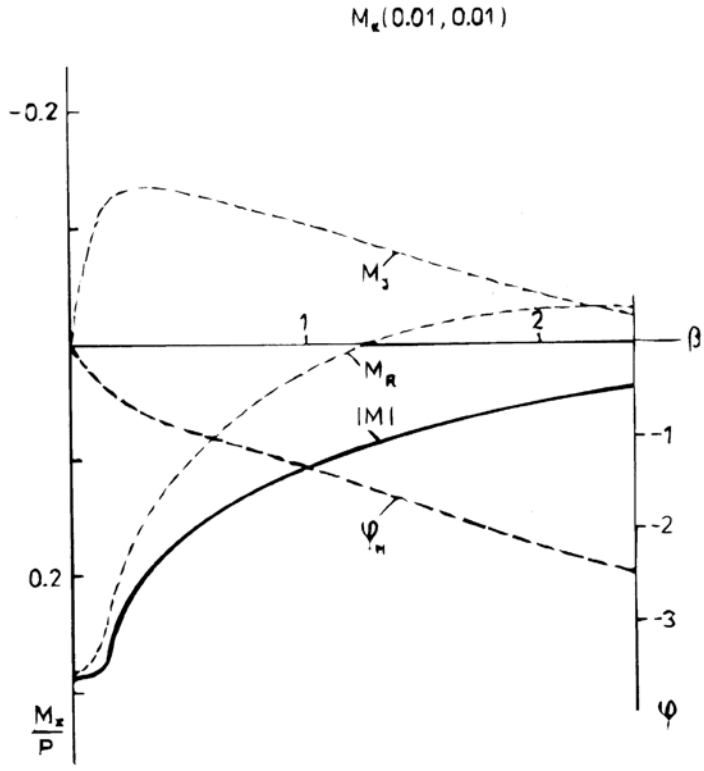

Fig. 4.15. Variation of dimensionless bending moment M_x/P with frequency β.

In the region of the unloaded plate strip the solutions (4.24) can be considered for the transforms of the state vector components. At $\eta=0$ and $\eta=1$ the boundary of the plate strip that is in contact with the unbounded subgrade, is free. The boundary conditions at $\eta=0$ are in the form

$$\begin{aligned} {}^{F}M_0(\eta=0)&=0 \\ {}^{F}Q_0(\eta=0)&={}^{F}Q_z(\eta=0) \end{aligned} \tag{4.43}$$

where ${}^{F}Q_Z$ is the transform of the free subgrade reaction given by equation (4.34).

At the section $\eta_1<\eta<1$ the following equations are valid

$$
\begin{aligned}
{}^{F}w(\eta,\alpha) &= {}^{F}w_0 K_{ww}(\eta) + {}^{F}\varphi_0 K_{w\varphi}(\eta) + {}^{F}Q_0 K_{wQ}(\eta) - {}^{F}P_1 K_{wQ}(\eta-\eta_1)\\
{}^{F}\varphi(\eta,\alpha) &= {}^{F}w_0 K_{\varphi w}(\eta) + {}^{F}\varphi_0 K_{\varphi\varphi}(\eta) + {}^{F}Q_0 K_{\varphi Q}(\eta) - {}^{F}P_1 K_{\varphi Q}(\eta-\eta_1)\\
{}^{F}M(\eta,\alpha) &= {}^{F}w_0 K_{Mw}(\eta) + {}^{F}\varphi_0 K_{M\varphi}(\eta) + {}^{F}Q_0 K_{MQ}(\eta) - {}^{F}P_1 K_{MQ}(\eta-\eta_1)\\
{}^{F}Q(\eta,\alpha) &= {}^{F}w_0 K_{Qw}(\eta) + {}^{F}\varphi_0 K_{Q\varphi}(\eta) + {}^{F}Q_0 K_{QQ}(\eta) - {}^{F}P_1 K_{QQ}(\eta-\eta_1)
\end{aligned}
\tag{4.44}
$$

At the other border of the plate strip, i.e. at η=1, the following boundary conditions have to be fulfilled

$$
\begin{aligned}
{}^{F}M(\eta=1) &= 0\\
{}^{F}Q(\eta=1) &= -{}^{F}Q_z(\eta=1) = -K_2^*\frac{1}{L}\gamma_z\,{}^{F}w(1).
\end{aligned}
\tag{4.45}
$$

After substituting and rearranging, the following system of equations is obtained

$$
\begin{aligned}
a_{11}\,{}^{F}w_0 + a_{12}\,{}^{F}\varphi_0 &= a_{10}\\
a_{21}\,{}^{F}w_0 + a_{22}\,{}^{F}\varphi_0 &= a_{20}
\end{aligned}
\tag{4.46}
$$

where

$$
\begin{aligned}
a_{11} &= \frac{s_1 s_2}{s_1 - s_2}(\cosh\gamma_1 - \cosh\ \gamma_2) + \frac{K_2^* L^2 \gamma_z}{D^*(q_2\gamma_1 - q_1\gamma_2)}\\
&\quad \times (q_2 \sinh\ \gamma_1 - q_1 \sinh\gamma_2)
\end{aligned}
\tag{4.47}
$$

$$
a_{12} = \frac{-L}{q_2\gamma_1 - q_1\gamma_2}\ (q_2 s_1 \sinh\gamma_1 - q_1 s_2 \sinh\gamma_2) \tag{4.48}
$$

$$
a_{10} = \frac{L^{3F}P}{D^*(q_2\gamma_1 - q_1\gamma_2)}\ [\,q_2 \sinh\gamma_1(1-\eta_1) - q_1\ \sinh\gamma_2(1-\eta_1)] \tag{4.49}
$$

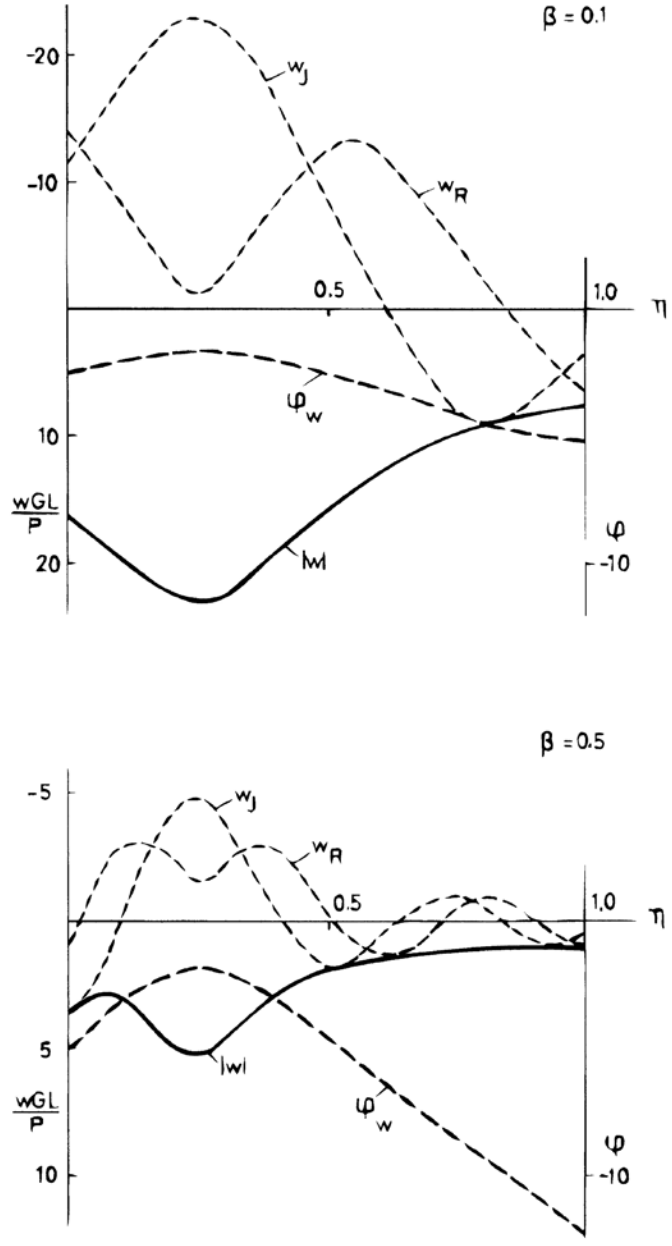

Fig. 4.16. Variation of dimensionless deflection wGL/P with $\eta=y/L$ at frequencies β=0.1 and β=0.5 in the case of harmonic force acting at distance $\eta=\eta_1$=0.25.

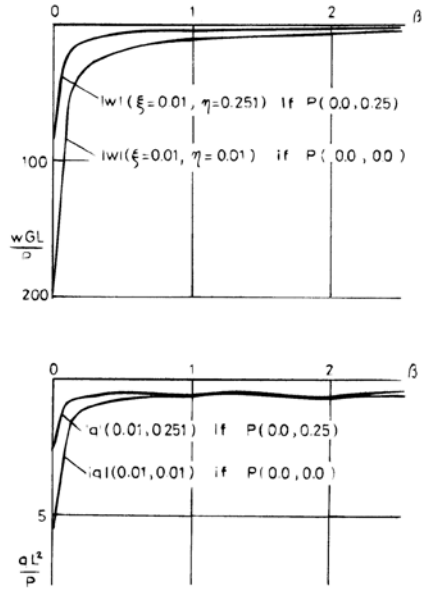

Fig. 4.17. Variation of dimensionles deflection wGL/P and subgrade reaction qL^2/P with frequency β for various force locations.

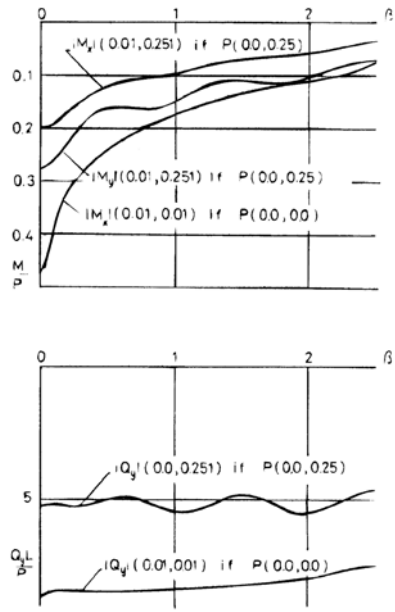

Fig. 4.18. Variation of dimensionless bending moments M/P and transverse force Q_y/P with frequency β for various force locations.

$$a_{21} = \frac{1}{s_1 - s_2}\left[q_1 s_2 \sinh\gamma_1 - q_2 s_1 \sinh\gamma_2 + \frac{2K_2^* L^2 \gamma_z}{D^*}\right.$$

$$\left. \times (-s_2 \cosh\gamma_1 + s_1 \cosh\gamma_2)\right] \tag{4.50}$$

$$+\left(\frac{K_2^* L^2 \gamma_z}{D^*}\right)^2 \frac{1}{q_2\gamma_1 - q_1\gamma_2}(\gamma_2 \sinh\gamma_1 - \gamma_1 \sinh\gamma_2)$$

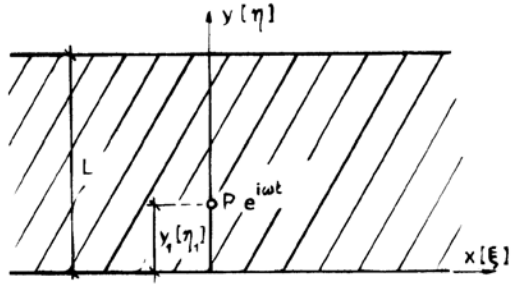

Fig. 4.19. Schematic diagram of plate strip on subgrade and system of coordinates.

$$a_{22} = \frac{s_1 s_2 L}{s_1 - s_2}(\cosh\gamma_1 - \cosh\gamma_2) + \frac{K_2^* L^2 \gamma_z}{D^*}\frac{L}{q_2\gamma_1 - q_1\gamma_2} \tag{4.51}$$

$$\times (q_2 sinh\gamma_1 - q_1 sinh\gamma_2)$$

$$a_{20} = \frac{L^3}{D^*(s_1 - s_2)}\,{}^{\mathrm{F}}P\,[-s_2\cosh\gamma_1(1-\eta_1) + s_1\cosh\gamma_2(1-\eta_1)] \tag{4.52}$$

$$-\frac{L^3}{D^*(q_2\gamma_1 - q_1\gamma_2)}\frac{K_2^* L^2\gamma_z}{D^*}\,{}^{\mathrm{F}}P\,[\gamma_2\sinh\gamma_1(1-\eta_1) - \gamma_1\sinh\gamma_2(1-\eta_1)].$$

The unknown initial parameters ${}^{\mathrm{F}}w_0$, ${}^{\mathrm{F}}\varphi_0$ can be computed from the system (4.46) and according to the relationships (4.26) and (4.34) ${}^{\mathrm{F}}Q_0$ is given.

All these initial parameters are complex functions of the dimensionless wave number α.

4.4.1 Relationships for state vector components of plate strip on subgrade

In the region of the plate strip $0 \le \eta < \eta_1$ the relationships (4.40) are valid. For the region $\eta_1 < \eta < 1$ the relationships are obtained in the form

$$w(\xi,\eta)=\frac{P}{GL}\int_0^\infty\left[{}^{\mathrm{F}}w_0\,K_{ww}(\eta)+{}^{\mathrm{F}}\varphi_0\frac{1}{L}K_{w\varphi}(\eta)+{}^{\mathrm{F}}Q_0GK_{wQ}(\eta)\right.$$

$$\left.-\frac{1}{2\pi}\,\frac{\sin\,\alpha\frac{a}{L}}{\alpha\frac{a}{L}}\,GK_{WQ}(\eta-\eta_1)\right]\,\cos\xi\alpha\,\mathrm{d}\alpha$$

$$q(\xi,\eta)=\frac{2P}{L^2}\int_0^\infty\left\{\left(\frac{K_1^*L}{G}+\frac{K_2^*\alpha^2}{LG}\right)\left[{}^{\mathrm{F}}w_0K_{ww}(\eta)+\frac{{}^{\mathrm{F}}\varphi_0}{L}K_{w\varphi}(\eta)+\right.\right.$$

$$\left.+{}^{\mathrm{F}}Q_0GK_{wQ}(\eta)-\frac{K_2^*}{GL}K_{w2}(\eta)-\frac{1}{2\pi}\,\frac{\sin\frac{\alpha a}{L}}{\frac{\alpha a}{L}}GK_{wQ}(\eta-\eta_1)\right]$$

$$-\frac{K_2^*}{GL}\left[K_{w2}(\eta)-\frac{1}{2\pi}\,\frac{\sin\frac{\alpha a}{L}}{\frac{\alpha a}{L}}\,\frac{GL^3}{D^*}\,\frac{1}{s_1-s_2}(-\gamma_1\sinh\gamma_1(\eta-\eta_1)\right.$$

$$\left.\left.+\gamma_2\sinh\gamma_2(\eta-\eta_1)\right]\right\}\cos\xi\alpha\,\mathrm{d}\alpha$$

$$M_y(\xi,\eta)=2P\int_0^\infty\left[{}^{\mathrm{F}}w_0\frac{1}{GL}K_{Mw}(\eta)+{}^{\mathrm{F}}\varphi_0\frac{1}{GL^2}K_{M\varphi}(\eta)+{}^{\mathrm{F}}Q_0\frac{1}{L}K_{w\varphi}(\eta)\right.$$

$$\left.-\frac{1}{2\pi}\,\frac{\sin\frac{\alpha a}{L}}{\frac{\alpha a}{L}}\,\frac{1}{L}K_{w\varphi}(\eta-\eta_1)\right]\,\cos\xi\alpha\,\mathrm{d}\alpha$$

$$Q_y(\xi,\eta)=\frac{2P}{L}\int_0^\infty\left[{}^{\mathrm{F}}w_0\frac{1}{G}K_{Qw}(\eta)+{}^{\mathrm{F}}\varphi_0\frac{1}{GL}K_{Mw}(\eta)+{}^{\mathrm{F}}Q_0K_{ww}(\eta)\right.$$

$$\left.-\frac{1}{2\pi}\,\frac{\sin\frac{\alpha a}{L}}{\frac{\alpha a}{L}}K_{ww}(\eta-\eta_1)\right]\,\cos\xi\alpha\,\mathrm{d}\alpha$$

$$M_x(\xi,\eta)=-2P\int_0^\infty\frac{D^*}{GL^3}\left\{-\alpha^2\left[{}^{\mathrm{F}}w_0K_{ww}(\eta)+{}^{\mathrm{F}}\varphi_0\frac{1}{L}K_{w\varphi}(\eta)\right.\right.$$

$$+{}^{\mathrm{F}}Q_0 GK_{wQ}(\eta) - \frac{1}{2\pi}\,\frac{\sin\frac{\alpha a}{L}}{\frac{\alpha a}{L}}\,GK_{wQ}(\eta-\eta_1)]$$

$$+\mu\left[K_{w2}(\eta) - \frac{1}{2\pi}\,\frac{\sinh\frac{\alpha a}{L}}{\frac{\alpha a}{L}}\,\frac{GL^3}{D^*}\,\frac{1}{s_1-s_2}(-\gamma_1\sin\gamma_1(\eta-\eta_1)\right.$$

$$\left.+\gamma_2\sinh\gamma_2(\eta-\eta_1))\right]\Big\}\cos\ \xi\alpha\mathrm{d}\alpha$$

$$Q_x(\xi,\eta)\frac{2P}{L}\int_0^\infty \frac{D^*}{GL^3}\left\{-\alpha^2\left[{}^{\mathrm{F}}w_0 K_{ww}(\eta) + {}^{\mathrm{F}}\varphi_0\frac{1}{L}K_{w\varphi}(\eta) + {}^{\mathrm{F}}Q_0 GK_{wQ}(\eta)\right.\right. \tag{4.53}$$

$$\left.-\frac{1}{2\pi}\,\frac{\sin\frac{\alpha a}{L}}{\frac{\alpha a}{L}}\,GK_{wQ}(\eta-\eta_1)\right] + K_{w2}(\eta) - \frac{1}{2\pi}\,\frac{\sin\frac{\alpha a}{L}}{\frac{\alpha a}{L}}\,\frac{GL^3}{D^*}\,\frac{1}{s_1-s_2}$$

$$\left.\times\ [-\gamma_1\sinh\gamma_1(\eta-\eta_1) + \gamma_2\ \sinh\gamma_2(\eta-\eta_1)]\right\}\alpha\sin\xi\alpha\ \mathrm{d}\alpha$$

$$M_{xy}(\xi,\eta) = 2P\int_0^\infty \frac{D^*(1-\mu)}{GL^3}\left[{}^{\mathrm{F}}w_0 LK_{\varphi w}(\eta) + {}^{\mathrm{F}}\varphi_0 K_{\varphi\varphi}(\eta)\right.$$

$$\left.+{}^{\mathrm{F}}Q_0 GLK_{wM}(\eta) - \frac{1}{2\pi}\,\frac{\sin\frac{\alpha a}{L}}{\frac{\alpha a}{L}}\,GLK_{wM}(\eta-\eta_1)\right]\ \alpha\ \sin\xi\alpha\ \mathrm{d}\alpha.$$

4.4.2 Numerical results

The procedures in sections 4.3.3 may also be used for numerical computations. With regard to the high values of the arguments of hyperbolic functions which are situated in sub-integral expressions and in equation system (4.46) too, especially at the high values of wave number α or frequency β, double precision of computing is necessary, using computers.

Naturally there are no differences in the values of the state vector components about the loaded border, calculated for a half-plate on subgrade or a plate strip on subgrade. It is possible to provide results as evidence in support of the case of border loading at the point (ξ=0, η=0). The half-plate or plate strip on subgrade are equivalent to a flexible pavement with input parameters as in section 4.3.3.

A comparison of the computed values is in Table 4.2.

Table 4.2. Comparison of values of state vector components for half-plate on subgrade and plate strip on subgrade.

Frequency	Absolute value of state vector components at the plate (ξ=0.01 η=0.01)		
β		halfplate on subgrade	plate strip on subgrade
0.0	$\frac{wGL}{P}$	81.04	81.05
0.1		48.02	45.69
0.2		28.52	27.84
0.0	$\frac{qL^2}{P}$	7.58	7.58
0.1		5.32	5.18
0.2		3.91	3.86
0.0	$\frac{Q_y L}{P}$	5.59	5.60
0.1		5.39	5.44
0.2		5.43	5.48
0.0	$\frac{M_x}{P}$	0.286	0.286
0.1		0.285	0.283
0.2		0.234	0.234

4.5 Dynamic stress state near cut transverse joints of the plate on subgrade

Rigid pavement structures are divided by longitudinal and transverse cut joints. These joints are made in cutting the cement concrete surfacing to a depth that corresponds to approximately one third of the concrete plate. After some time, as a result of volume changes and traffic, the cut joints proceed as cracks through the whole thickness of the plate.

The pavement structure cannot carry bending moments over in the direction perpendicular to the joint. The ability to transfer transverse forces remains because the cracks in the place of the joints have irregular contact areas. A similar effect may be assumed to occur in the case of cracks in flexible pavements.

In this section, we shall try to solve the case of the dynamic state of stress about the joint under a concentrated harmonic variable load. The scheme of the problem is indicated in Fig. 4.20.

The basic system is assumed to be in the form of two divided half-plates, I and II, on the subgrade with the acting unknown transverse force ${}^{F}Q_0$ of the system. Half-plate I is under an external dynamic load $Pe^{i\omega t}$. With regard to the application of Fourier integral transformation in the ξ direction, the Fourier transform of the unknown transversal force ${}^{F}Q_0$ is considered in the η direction (Fig. 4.21).

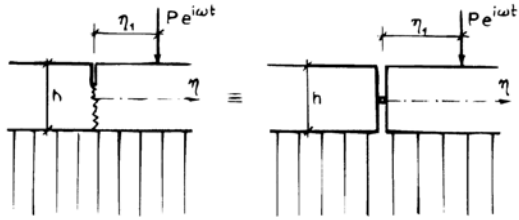

Fig. 4.20. Schematic diagram of the problem of dynamic state of stress about a pavement joint.

At the point η=0 of half-plates I and II only transverse force of the system ${}^{F}Q_0$ is acting, because the bending moment ${}^{F}M_0$=0. The condition of system continuity with regard to the supposed joint connection is required to fulfil the equation

$$ {}^{F}w_{II}(\eta = 0) = {}^{F}w_{I}(\eta = 0) \tag{4.54} $$

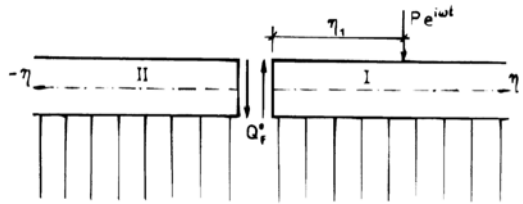

Fig. 4.21. The basic system in the form of two divided half-plates on subgrade.

4.5.1 Influence functions of a half-plate on subgrade with initial parameters of transverse force ${}^{F}Q_0$ and bending moment ${}^{F}M_0$

The solution of the differential equation of the system of a half-plate on subgrade is given for the deflection transform and other components by equations (4.25).

For η=0 the following equations are valid

$$ \begin{aligned} {}^{F}w_0 &= B_1 + B_2 \\ {}^{F}\varphi_0 L &= B_1\gamma_1 + B_2\gamma_2 \\ -\frac{{}^{F}M_0 L^2}{D^*} &= B_1 s_1 + B_2 s_2 \\ -\frac{{}^{F}Q_0 L^3}{D^*} &= B_1 q_1 + B_2 q_2 \end{aligned} \tag{4.55} $$

where ${}^{F}w$ ${}^{F}\varphi_0$, ${}^{F}M_0$, and ${}^{F}Q_0$ are initial parameters.

Assuming that at the free boundary of the half-plate on subgrade the transverse forces and bending moments are acting, then the unknown constants B_1 and B_2 being in this case unknown complex functions of wave number α, may be expressed from the last two equations (4.55) in the form

$$B_1 = \frac{1}{D^*} \frac{-q_2 {}^{F}M_0 L^2 + s_2 {}^{F}Q_0 L^3}{s_1 q_2 - s_2 q_1} \tag{4.56}$$

$$B_2 = \frac{1}{D^*} \frac{q_1 {}^{F}M_0 L^2 - s_1 {}^{F}Q_0 L^3}{s_1 q_2 - s_2 q_1}. \tag{4.57}$$

The state vector components expressed by the initial parameters and influence coefficients are given by the following relationships

$$\begin{aligned}
{}^{F}w(\alpha, \eta) &= K_{wM} {}^{F}M_0 + K_{wQ} {}^{F}Q_0 \\
{}^{F}\varphi(\alpha, \eta) &= K_{\varphi M} {}^{F}M_0 + K\varphi Q {}^{F}Q_0 \\
{}^{F}M(\alpha, \eta) &= K_{MM} {}^{F}M_0 + K_{MQ} {}^{F}Q_0 \\
{}^{F}Q(\alpha, \eta) &= K_{QM} {}^{F}M_0 + K_{QQ} {}^{F}Q_0
\end{aligned} \tag{4.58}$$

if the influence functions $K_{wM}, \ldots K_{QQ}$ are given by the matrix of Table 4.3.

Table 4.3. Matrix of influence functions.

	${}^{F}M_0$	${}^{F}Q_0$
${}^{F}w(\eta)$	$K_{wM} = \frac{L^2}{D^*} \frac{1}{s_1 q_2 - s_2 q_1} \cdot$ $(-q_2 e^{\gamma_1 \eta} + q_1 e^{\gamma_2 \eta})$	$K_{wQ} = \frac{L^3}{D^*} \frac{1}{s_1 q_2 - s_2 q_1} \cdot$ $(s_2 e^{\gamma_1 \eta} - s_1 e^{\gamma_2 \eta})$
${}^{F}\varphi(\eta)$	$K_{\varphi w} = \frac{L}{D^*} \frac{1}{s_1 q_2 - s_2 q_1} \cdot$ $(-\gamma_1 q_2 e^{\gamma_1 \eta} + \gamma_2 q_1 e^{\gamma_2 \eta})$	$K_{\varphi Q} = \frac{L^2}{D^*} \frac{1}{s_1 q_2 - s_2 q_1} \cdot$ $(\gamma_1 s_2 e^{\gamma_1 \eta} - \gamma_2 s_1 e^{\gamma_2 \eta})$
${}^{F}M(\eta)$	$K_{MM} = \frac{L^2}{s_1 q_2 - s_2 q_1} \cdot$ $(s_1 q_2 e^{\gamma_1 \eta} - s_2 q_1 e^{\gamma_2 \eta})$	$K_{MQ} = \frac{s_1 s_2 L^3}{s_1 q_2 - s_2 q_1} \cdot$ $(-e^{\gamma_1 \eta} + e^{\gamma_2 \eta})$
${}^{F}Q(\eta)$	$K_{QM} = \frac{q_1 q_2 L^3}{s_1 q_2 - s_2 q_1} \cdot$ $(e^{\gamma_1 \eta} - e^{\gamma_2 \eta})$	$K_{QQ} = \frac{L^3}{s_1 q_2 - s_2 q_1} \cdot$ $(-q_1 s_2 e^{\gamma_1 \eta} + s_1 q_2 e^{\gamma_2 \eta})$

4.5.2. Determination of unknown initial parameters for transversal force ${}^{F}Q_0$

The initial parameter ${}^{F}Q_0$ may be determined by using the condition (4.54). Half-plates I and II have the same thickness and plate stiffnesses, i.e. $D_{\mathrm{I}}^* = D_{\mathrm{II}}^*$. However, quantities s_1,

s_2, q_1 and q_2 are different be-cause γ_1 and γ_2 for half-plate II have to be considered with a positive real part with regard to negative coordinates η. So we shall distinguish the quantities s_1^{I}, s_2^{I}, q_1^{I}, q_2^{I}, for half-plate I and s_1^{II}, s_2^{II}, q_1^{II}, q_2^{II}, for half-plate II.

By using condition (4.54) for the equality of deflection of half-plate I and half-plate II at η=0, the equation for the unknown initial transverse force of the system, ${}^{\mathrm{F}}Q_0$, is obtained in the form

$$ {}^{\mathrm{F}}Q_0 = -\frac{{}^{\mathrm{F}}w_0^P \frac{D^*}{L^3}}{(s_2^{\mathrm{I}} - s_1^{\mathrm{I}})/(s_1^{\mathrm{I}} q_2^{\mathrm{I}} - s_2^{\mathrm{I}} q_1^{\mathrm{I}}) - (s_2^{\mathrm{II}} - s_1^{\mathrm{II}})/(s_1^{\mathrm{II}} q_2^{\mathrm{II}} - s_2^{\mathrm{II}} q_1^{\mathrm{II}})} \tag{4.59} $$

if ${}^{\mathrm{F}}w_0^P$ is the transform of the initial deflection for half-plate I under a dynamic harmonic load, which can be determined by the procedure as in section 4.3.1 for a half-plate on subgrade but considering the initial transverse force ${}^{\mathrm{F}}Q_0$ in the form (4.59).

4.5.3 Numerical results

The influence of the pavement joint on the values of the plate vector components was studied for the equivalent plate on subgrade under a dynamic concentrated load acting at distance η_1 from the joint. The system corresponds to the flexible pavement with input data given in section 4.3.2.

The results of the solution are plotted in Figs. 4.22–4.24 for the absolute values of wGL/P, qL^2/P, M_y/P, M_x/P and Q_yL/P versus coordinates η_1 at the point of action of the concentrated dynamic load. The variations are indicated for dimensionless frequencies $\beta=\omega h/c_2$=0, 0.1, 0.2, 0.3 of the harmonic load.

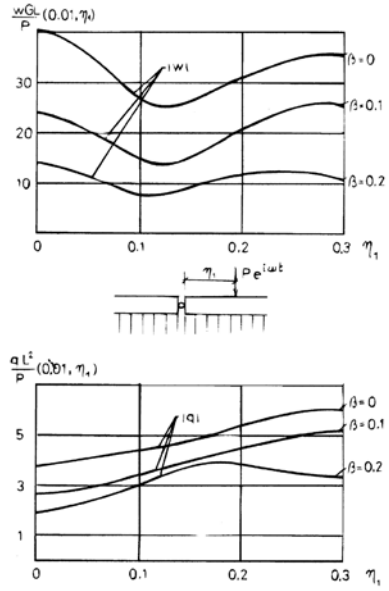

Fig. 4.22. Variation of dimensionless deflection wGL/P and subgrade reaction qL^2/P with coordinate η_1 of concentrated dynamic load.

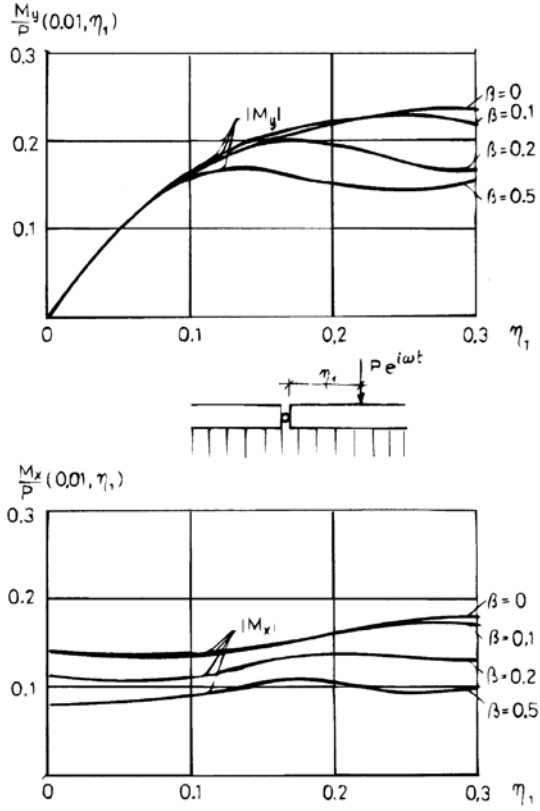

Fig. 4.23. Variation of dimensionless bending moments M_y/P and M_x/P with coordinate η_1 of concentrated dynamic load.

The variations of absolute values for the same state vector components with frequency β and positions of dynamic load η_1=0.01 and η_1=0.3 are drawn in Figs. 4.24 and 4.25.

From the variations of bending moments M_x/P, M_y/P in Fig. 4.23 and Fig. 4.25 it can be seen that the absolute values M_x/P, M_y/P by dynamic concentrated load about the joint do not reach the maximal values of M_x/P in the case of border loading of the halfplate on subgrade.

4.6 Influence of inhomogeneous subgrade on dynamic interaction of plate with subgrade

In the case of inhomogeneous subgrade or in the case of a defective drain field the result will sometimes be the moistening of the subgrade and sub-base layers. In winter the stiffness of the subgrade and sub-base layers may be extremely high in these places as a consequence of freezing temperatures. The stiffness of the pavement structure will increase too.

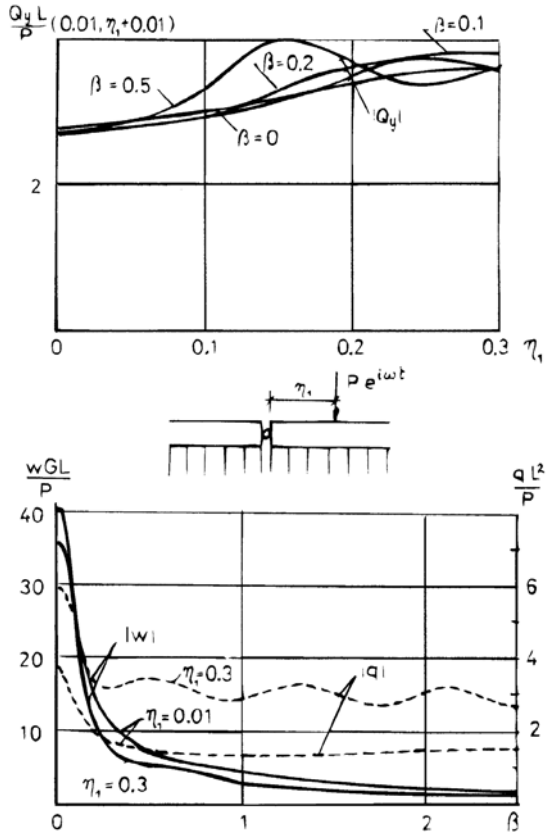

Fig. 4.24. Variation of dimensionless transverse force $Q_y L/P$ with coordinate η_1 and variation of deflection wGL/P and subgrade reaction qL^2/P with frequency β.

At the transition from normal to frozen pavement, the sudden change in pavement stiffness can be pronounced, which can unfavourably influence the state of stress under loading by vehicle transit.

4.6.1 Results of dynamic diagnosis of highway pavement at the site of failure cracks in concrete surfacing

The size of the stiffness change for pavement structures can be demonstrated using the results of dynamic diagnosis of highway pavements obtained by means of the evaluation of phase-velocity measurements. These measurements were performed in the region of cracked concrete surfacing at six different places using the procedure described in section 1.4.2. The results and evaluation of the measurements carried out in April and repeated at the same places in June are summarized in Tables 4.4 and 4.5.

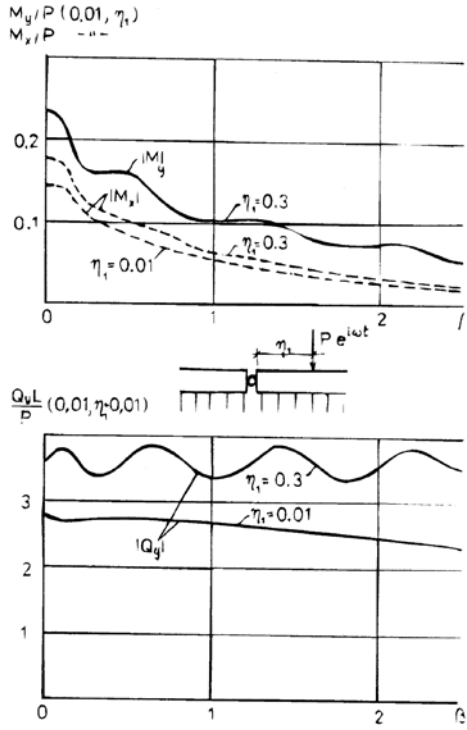

Fig. 4.25. Variation of dimensionless bending moments M/P and transverse force $Q_y L/P$ with frequency β.

As can be seen, measurement sites 1, 2, 3, 5 and 6 present approximately similar characteristics, but measurement site 4 in April gives disproportionally high stiffness, which is demonstrated by the high values of the equivalent thickness h_{eq}, dynamic flexural rigidity EJ and by the low value of deflection w_0. During the subsequent measurements in June, site 4 displayed characteristics comparable with those of the other sites.

By means of detailed investigation it was ascertained that, in the measured region of the cracked concrete surfacing, the subgrade and sub-base layers were moistened, and frozen in winter. During the measurement in April part of the section was not frozen but site 4 was still frozen, and so its rigidity was extremely high. During the measurement in June the rigidity was similar to that of the other measurement sites.

Such local volume changes and differences in pavement stiffness caused an unfavourable state of stress from traffic and the failure of the structure.

It follows from the characteristic values of the measured section number 4 that the stiffness change manifests itself in a threefold value of equivalent thickness, above a thirtyfold increase of pavement flexural stiffness and almost to a multiple of 2.5 of a deflection decrease.

It will be very interesting to analyse the influence of a sudden change in stiffness on the state of stress about the interface under a dynamic concentrated load.

Table 4.4. Results of measurements on highway pavement section in April and in June.

Measur. number	measurement in April					
	Frequency (Hz)	Λ_a (m)	c_a (m/s)	Frequency (Hz)	Λ_b (m)	c_b (m/s)
1	10000	0.1265	2530	250	2.922	730
2	10000	0.1250	2500	250	2.866	716
3	10000	0.1256	2512	250	2.957	739
4	10000	0.1266	2532	250	4.706	1176
5	10000	0.1250	2500	250	3.018	754
6	10000	0.1268	2536	250	2.885	721
	measurement in June					
1	10000	0.1179	2358	250	2.513	628
2	10000	0.1211	2422	250	2.712	678
3	10000	0.1235	2470	250	2.934	733
4	10000	0.1211	2422	250	2.743	686
5	10000	0.1197	2394	250	2.931	733
6	10000	0.1215	2430	250	2.806	701

Table 4.5. Evaluation of measurements on highway pavement section carried out in April and repeated at the same places in June.

Number of meas.	Measurement in April				Measurement in June			
	c_0 (m/s)	h_e (m)	EJ/ϱ EJ in (Nm^2)	w_0/p_0 w_0 in (m)	c_0 (m/s)	h_e (m)	EJ/ϱ EJ in (Nm^2)	w_0/p_0 w_0 in (m)
1	4364	0.279	34605	$0.356.10^{-3}$	4093	0.218	14533	$0.454.10^{-3}$
2	4315	0.272	31081	$0.367.10^{-3}$	4187	0.250	22804	$0.400.10^{-3}$
3	4328	0.289	37756	$0.348.10^{-3}$	4254	0.290	36780	$0.351.10^{-3}$
4	4310	0.813	831386	$0.165.10^{-3}$	4184	0.256	24524	$0.392.10^{-3}$
5	4302	0.304	43362	$0.335.10^{-3}$	4116	0.300	38231	$0.378.10^{-3}$
6	4379	0.271	31782	$0.364.10^{-3}$	4192	0.268	28253	$0.377.10^{-3}$

ϱ in (kg/m^3)
p_0 in (MPa)

4.6.2 Influence of sudden change of rigidity in equivalent plate on subgrade

The influence of inhomogeneous subgrade and sub-base layers may be modelled by means of a sudden change in the equivalent thickness of the plate on subgrade according to the scheme in Fig. 4.26.

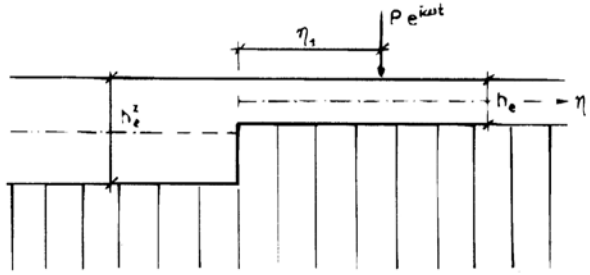

Fig. 4.26. Schematic diagram of sudden change of equivalent thickness of plate on subgrade.

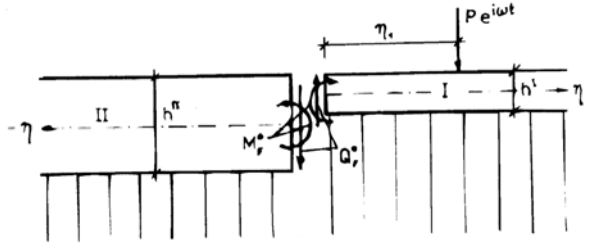

Fig. 4.27. Schematic diagram of basic system.

The basic system is assumed to be in the form of two divided half-plates on subgrade: half-plates I and II with the unknown transversal force ${}^{\mathrm{F}}Q_0$ and bending moment ${}^{\mathrm{F}}M_0$. Half-plate I is loaded by a dynamic concentrated force $P\mathrm{e}^{\mathrm{i}\omega t}$. By using the Fourier integral transformation in the ξ direction, the action of integrands ${}^{\mathrm{F}}Q_0$ and ${}^{\mathrm{F}}M_0$ in the η direction may be assumed to be in agreement with the scheme of Fig. 4.27.

The conditions of system continuity at the interface of a sudden change of rigidity is required to fulfil the following equations

$$\begin{aligned} {}^{\mathrm{F}}w_{\mathrm{I}}(\eta=0)&={}^{\mathrm{F}}w_{\mathrm{II}}(\eta=0)\\ {}^{\mathrm{F}}\varphi_{\mathrm{I}}(\eta=0)&={}^{\mathrm{F}}\varphi_{\mathrm{II}}(\eta=0). \end{aligned} \tag{4.60}$$

Using the influence functions for a half-plate on subgrade with the initial parameters ${}^{\mathrm{F}}Q_0$ and ${}^{\mathrm{F}}M_0$ according to Table 4.3, equations (4.60) yield the equation system

$$\begin{aligned} b_{11}\,{}^{\mathrm{F}}Q_0+b_{12}\,{}^{\mathrm{F}}M_0/L&=b_{10}\\ b_{21}\,{}^{\mathrm{F}}Q_0+b_{22}\,{}^{\mathrm{F}}M_0/L&=b_{20} \end{aligned} \tag{4.61}$$

where

$$b_{11}=\frac{s_2^{\mathrm{I}}-s_1^{\mathrm{I}}}{s_1^{\mathrm{I}}q_2^{\mathrm{I}}-s_2^{\mathrm{I}}q_1^{\mathrm{I}}}-d_{12}\,\frac{s_2^{\mathrm{II}}-s_1^{\mathrm{II}}}{s_1^{\mathrm{II}}q_2^{\mathrm{II}}-s_2^{\mathrm{II}}q_1^{\mathrm{II}}} \tag{4.62}$$

$$b_{12} = \frac{-q_2^{\mathrm{I}} + q_1^{\mathrm{I}}}{s_1^{\mathrm{I}} q_2^{\mathrm{I}} - s_2^{\mathrm{I}} q_1^{\mathrm{I}}} + d_{12} \frac{-q_2^{\mathrm{II}} + q_1^{\mathrm{II}}}{s_1^{\mathrm{II}} q_2^{\mathrm{II}} - s_2^{\mathrm{II}} q_1^{\mathrm{II}}} \tag{4.63}$$

$$b_{21} = \frac{\gamma_1^{\mathrm{I}} s_2^{\mathrm{I}} - \gamma_2^{\mathrm{I}} s_1^{\mathrm{I}}}{s_1^{\mathrm{I}} q_2^{\mathrm{I}} - s_2^{\mathrm{I}} q_1^{\mathrm{I}}} + d_{12} \frac{\gamma_1^{\mathrm{II}} s_2^{\mathrm{II}} - \gamma_2^{\mathrm{II}} s_1^{\mathrm{II}}}{s_1^{\mathrm{II}} q_2^{\mathrm{II}} - s_2^{\mathrm{II}} q_1^{\mathrm{II}}} \tag{4.64}$$

$$b_{22} = \frac{-\gamma_1^{\mathrm{I}} q_2^{\mathrm{I}} + \gamma_2^{\mathrm{I}} q_1^{\mathrm{I}}}{s_1^{\mathrm{I}} q_2^{\mathrm{I}} - s_2^{\mathrm{I}} q_1^{\mathrm{I}}} - d_{12} \frac{\gamma_1^{\mathrm{II}} q_2^{\mathrm{II}} + \gamma_2^{\mathrm{II}} q_1^{\mathrm{II}}}{s_1^{\mathrm{II}} q_2^{\mathrm{II}} - s_2^{\mathrm{II}} q_1^{\mathrm{II}}} \tag{4.65}$$

$$b_{10} = -{}^{\mathrm{F}}w_0^P \frac{D_{\mathrm{I}}^*}{L^3} \tag{4.66}$$

$$b_{20} = -{}^{\mathrm{F}}\varphi_0^P \frac{D_{\mathrm{I}}^*}{L^3} \tag{4.67}$$

$$d_{12} = \frac{D_{\mathrm{I}}^*}{D_{\mathrm{II}}^*}. \tag{4.68}$$

In equations (4.66) and (4.67) the quantities ${}^{\mathrm{F}}w_0^P$ and are the transforms of initial deflection and initial angular displacement of the halfplate on subgrade under a concentrated harmonic variable force $P\mathrm{e}^{\mathrm{i}\omega t}$ acting at a distance η_1 from the interface. Their values can be determined by using the procedures given in section 4.3.1.

The unknown initial parameters are expressed from equations system (4.61) by the relationships

$${}^{\mathrm{F}}Q_0 = \frac{BE_1}{BE} \tag{4.69}$$

$$\frac{{}^{\mathrm{F}}M_0}{L} = \frac{BE_2}{BE} \tag{4.70}$$

where

$$\begin{aligned} BE_1 &= b_{10}b_{22} - b_{20}b_{12} \\ BE_2 &= b_{20}b_{11} - b_{10}b_{21} \\ BE &= b_{11}b_{22} - b_{12}b_{21} \end{aligned} \tag{4.71}$$

The state vector components of the system with a sudden change of pavement stiffness will be determined applying the procedures and relationships from section 4.3.1 for the half-plate on subgrade with the initial transverse force and initial bending moment of the system, the integrands of which are determined in the form (4.69) and (4.70).

4.6.3 Numerical results

The numerical solution performed for equivalent plate I on subgrade corresponds to the rigid highway pavement structure with input data given in section 3.4.9. The sudden change in rigidity is given by the stiffness ratio $d_{12} = D_I^*/D_{II}^* = 0.05273$, which corresponds to the measured values on the pavement section. (Tables 4.4 and 4.5, measurements number 4 and 5).

Here we present the results of the numerical solution for state vector components under loading of plate I by a concentrated harmonic variable force acting at distance $\eta_1=y_1/L=0.25$ according to the scheme in Fig. 4.28.

We are interested in the dynamic state vector components of the half-plate I close to the load and sudden change of rigidity.

The variations of the state vector components with coordinate η at dimensionless frequencies $\beta=\omega h/c_2=0.1$ and $\beta=0.5$ are plotted in Figs. 4.29–4.34.

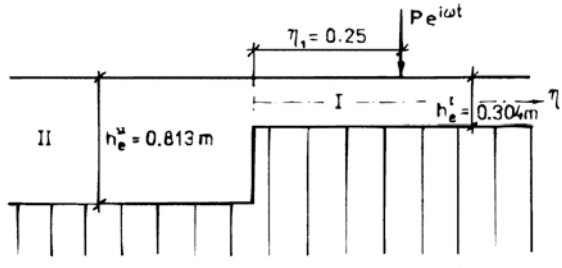

Fig. 4.28. Schematic diagram of the dynamic load and sudden change of plate thickness.

The influence of the dynamic load distance from the interface of the rigidity change was studied at various frequencies β at the point $\xi=0.01$, $\eta=0.01$. The absolute values of decisive components versus load distance η_1 are drawn in Figs. 4.35 and 4.36 for an analysed rigid pavement. Relatively high values of bending moments M_x/P and transverse forces or subgrade reactions at the interface are attained at load distances $\eta_1=0.025–0.05$, i.e. at short load distances.

The considered sudden change of rigidity determines the behaviour of half-plate I as being similar to the behaviour of an unbounded half-plate clamped at $\eta=0$. It is interesting to present the extreme values of bending moments $M_y(\xi=0, \eta=0)$ for a clamped halfplate under static load by concentrated force P at distance $\xi=0$, $\eta=\eta_1$. According to [4.1] the bending moment $M_y(0, 0)$ is independent of the load distance η_1 and has the value

$$\frac{M_y(0,0)}{P} = -\frac{1}{\pi} = -0.318. \tag{4.72}$$

In our case, which corresponds to a half-plate on subgrade with elastic clamped boundary, the bending moments $M_y(0.01, 0.01)/P$ achieve values about 0.200, approximately constant at distances $\eta_1>0.10$. With regard to the elastic clamped boundary the bending moments decrease at shorter load distances.

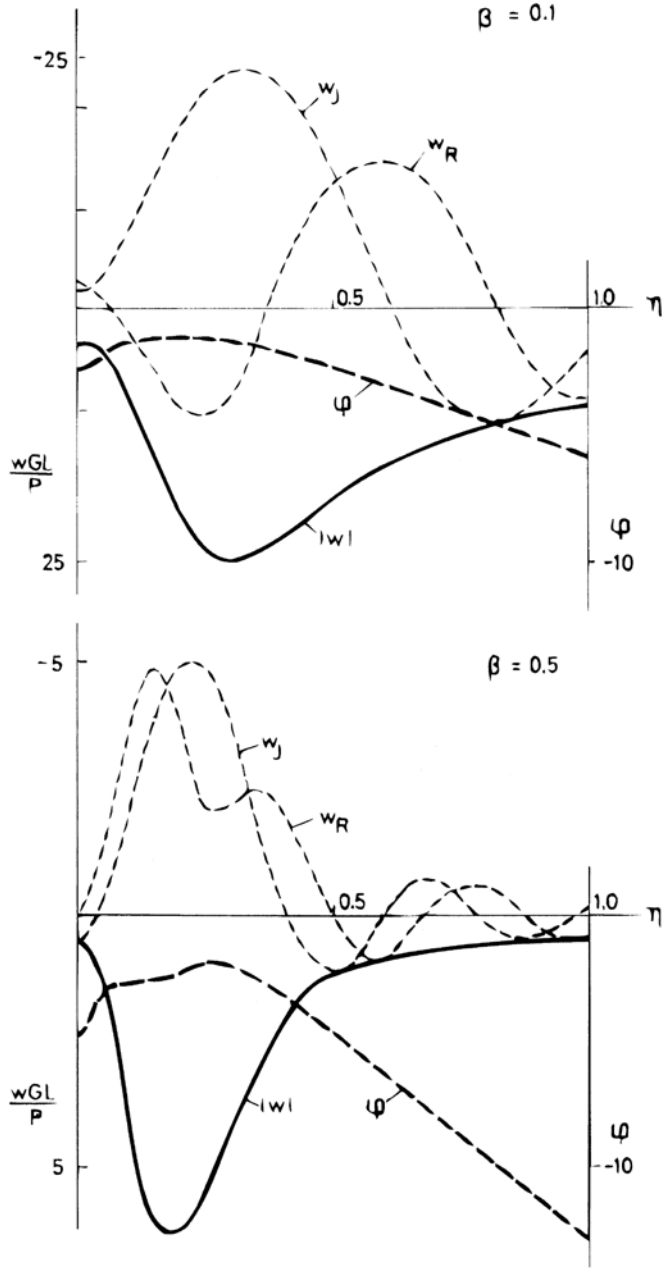

Fig. 4.29. Variation of dimensionless deflection wGL/P with ratio η at frequencies β=0.1 and β=0.5.

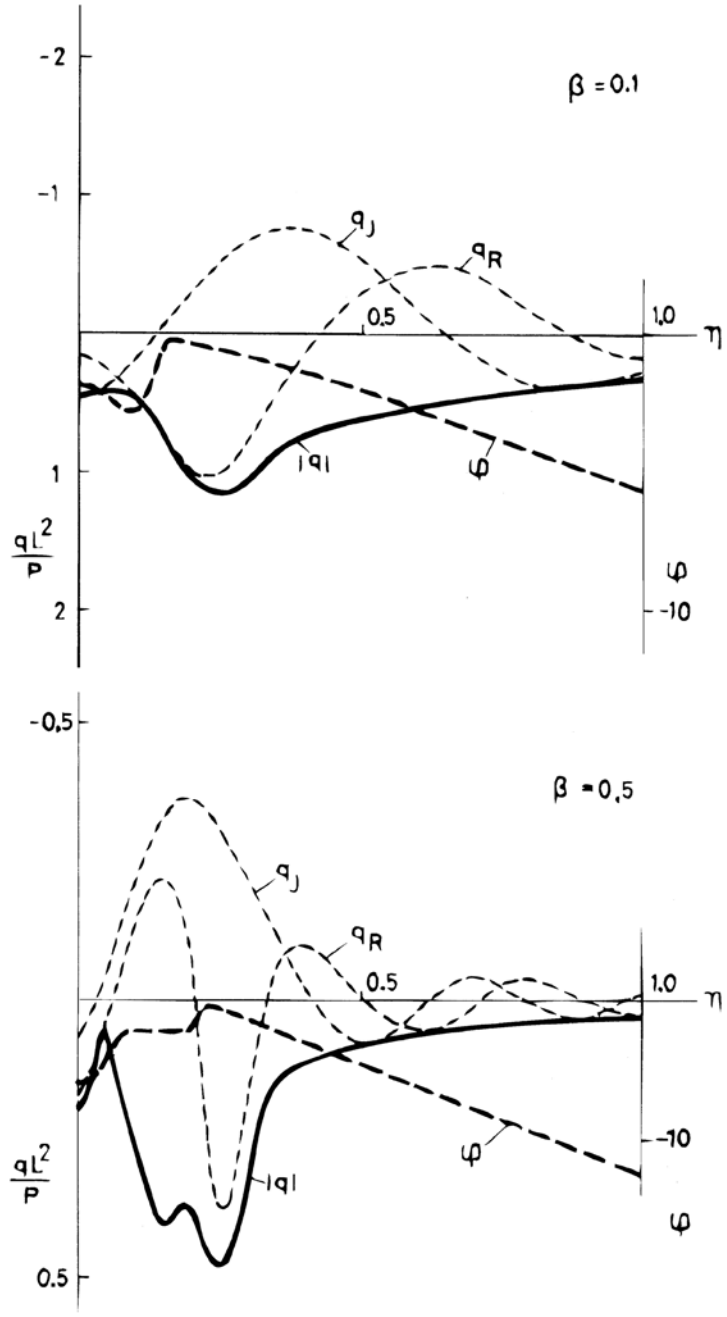

Fig. 4.30. Variation of dimensionless subgrade reaction qL^2/P with η at frequencies β=0.1 and β=0.5.

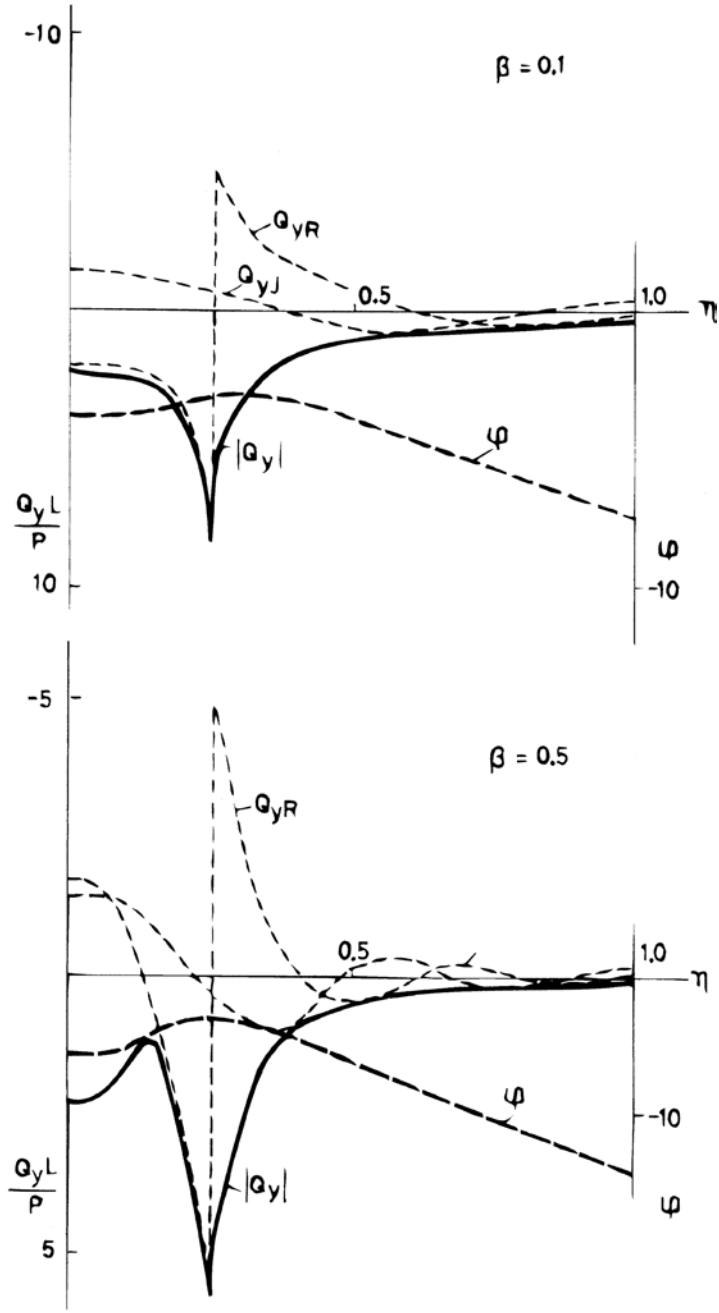

Fig. 4.31. Variation of dimensionless transverse force $Q_y L/P$ with η at frequencies β=0.1 and β=0.5.

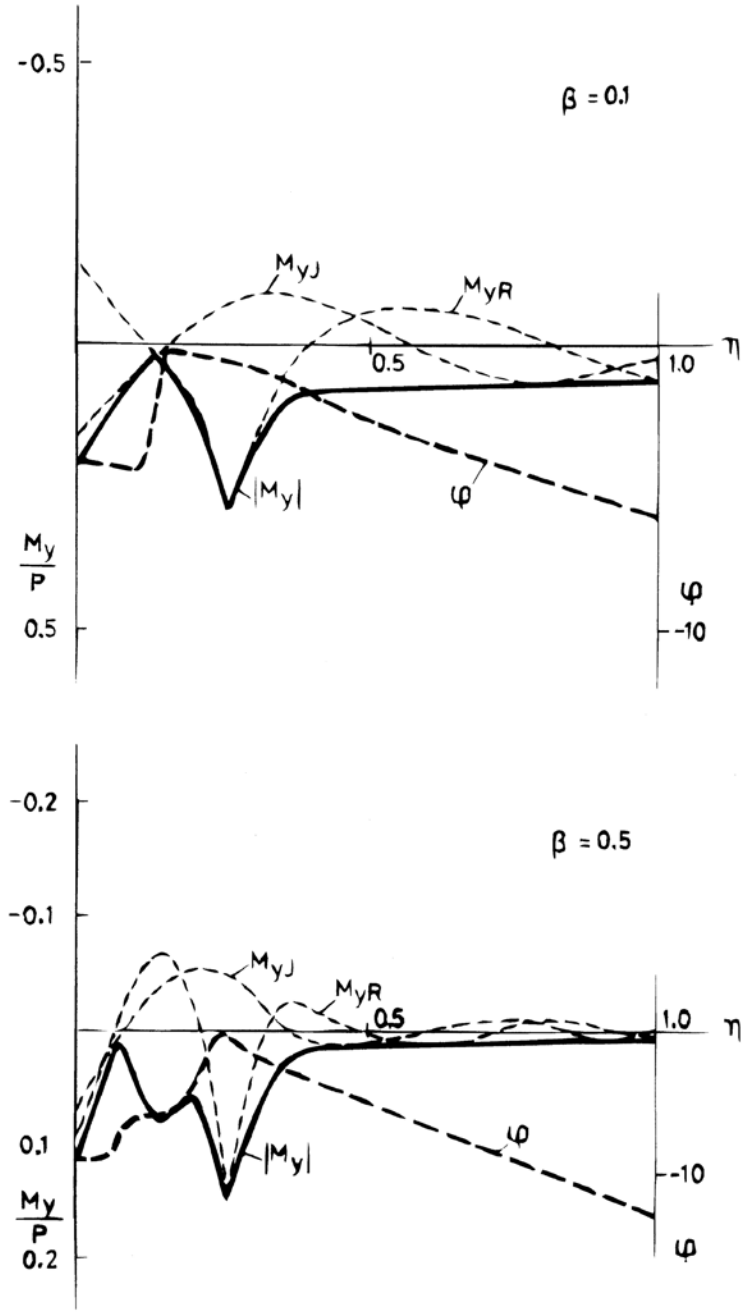

Fig. 4.32. Variation of dimensionless bending moment M_y/P with ratio η at frequencies β=0.01 and β=0.5.

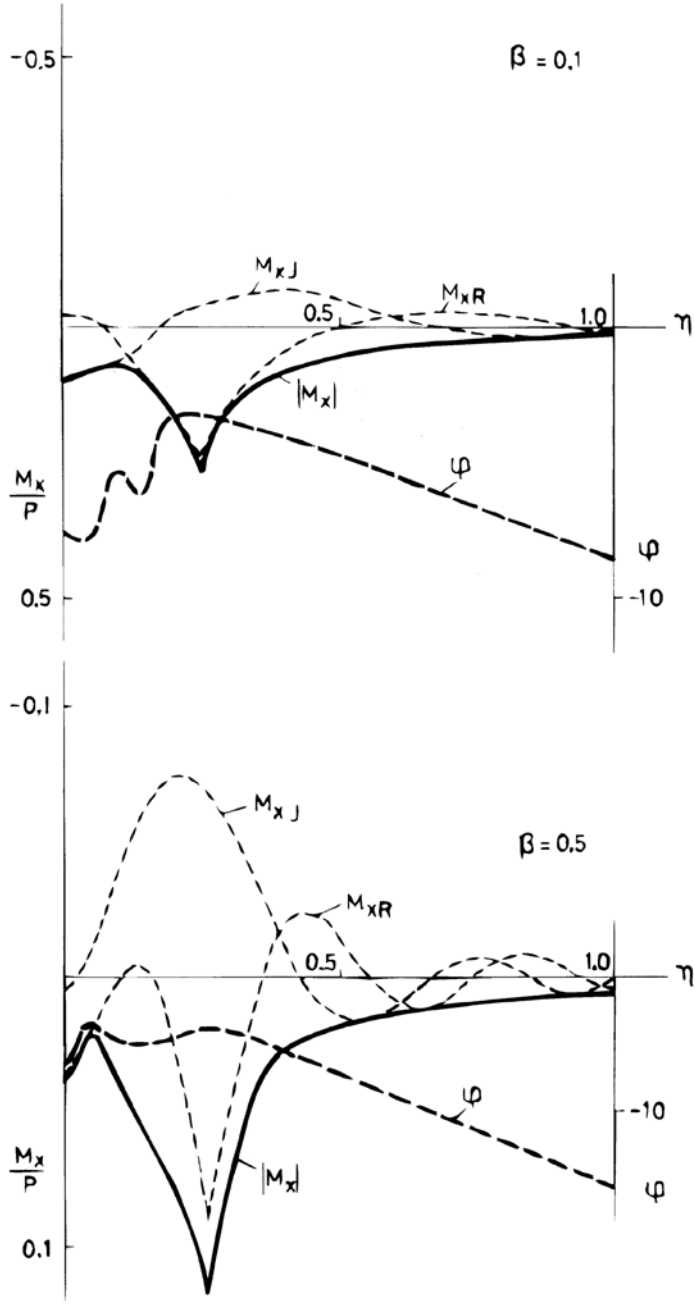

Fig. 4.33. Variation of dimensionless bending moment M_x/P with ratio η at frequencies β=0.1 and β=0.5.

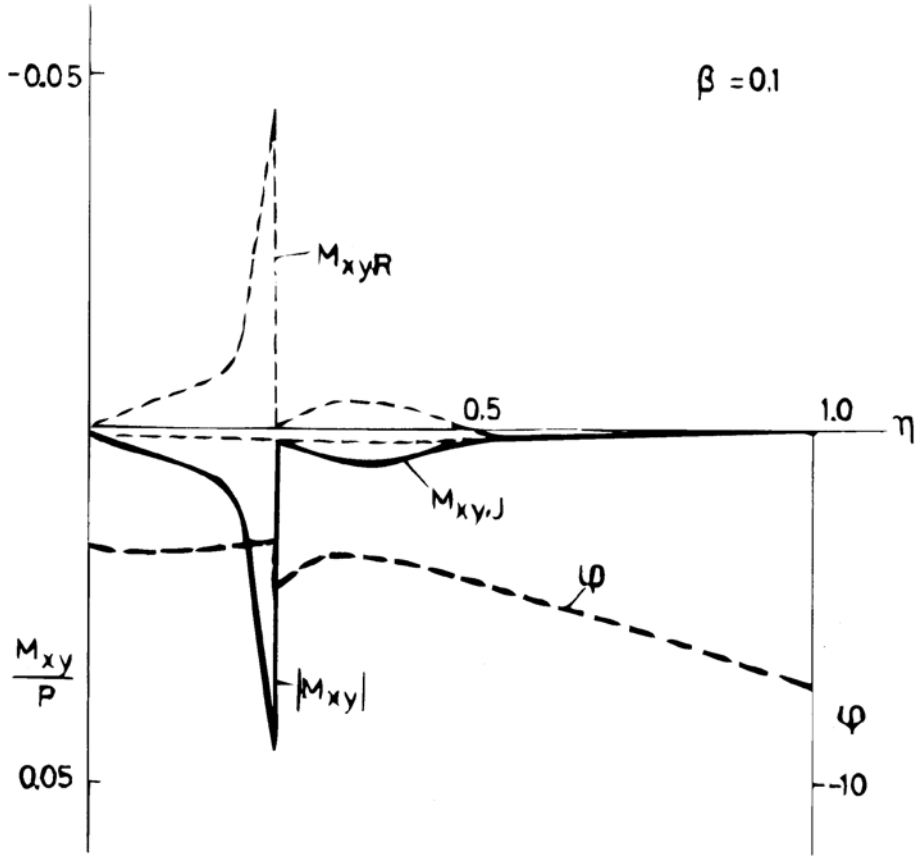

Fig. 4.34. Variation of dimensionless twisting moment M_{xy}/P with ratio η at frequency β=0.1.

4.6.4 Sudden change of rigidity situated parallel to the free boundary of half-plate on subgrade

The other variant of an homogeneous subgrade and sub-base layers offers a sudden change of rigidity that is parallel to the free boundary of the half-plate on subgrade. The scheme of this case is given in Fig. 4.37. The dynamic harmonic variable load acts at the boundary of half-plate I and the distance of the boundary from a sudden change in rigidity is indicated by coordinate $\eta_1=y_1/L$.

For the solution of this problem it is possible to use the procedure for a half-plate on subgrade described in section 4.3.1. In the region of the half-plate $\eta<\eta_1$, i.e. in zone I the relationships for state vector components in the form (4.24) and the matrix of influence functions in Table 4.1 are applied. In zone II the relationships for transforms of state vector components in the form (4.25) have to be used.

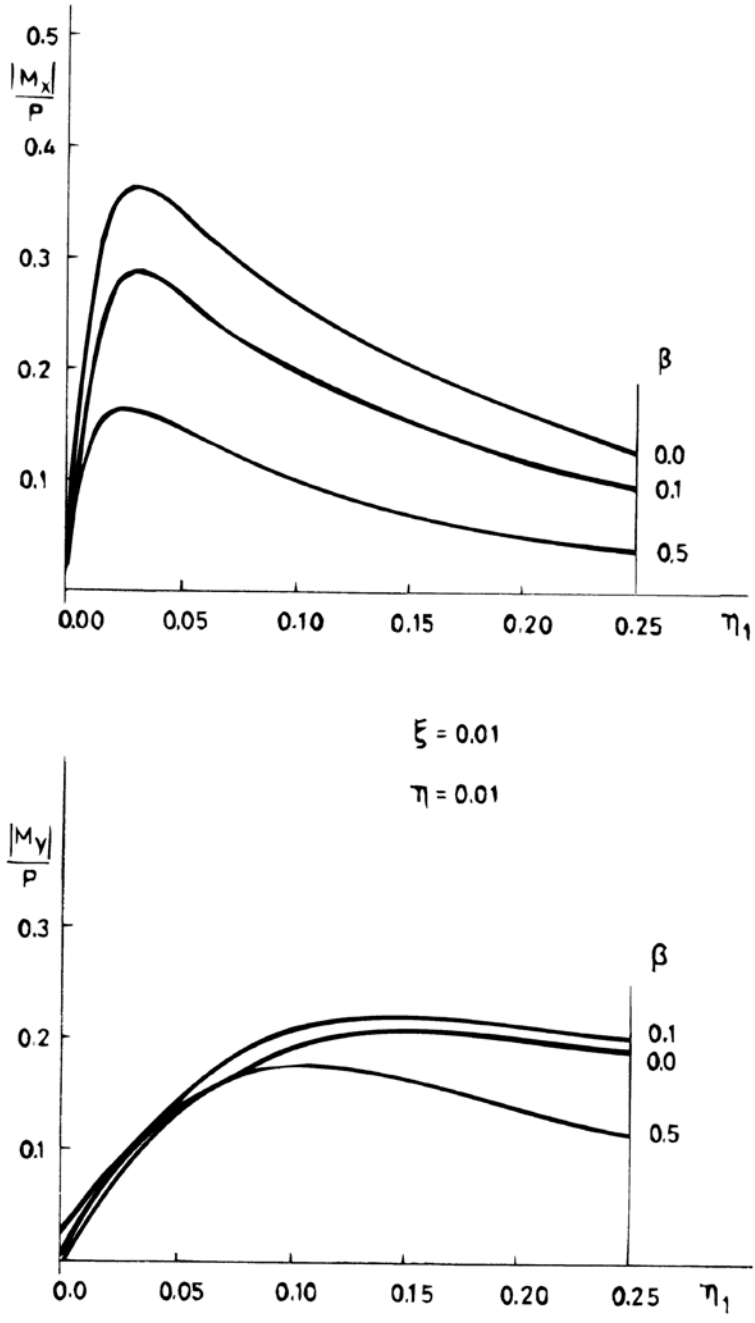

Fig. 4.35. Relationship of dimensionless bending moment $|M_x|/P$ and $|M_y|/P$ to dynamic load distance η_1.

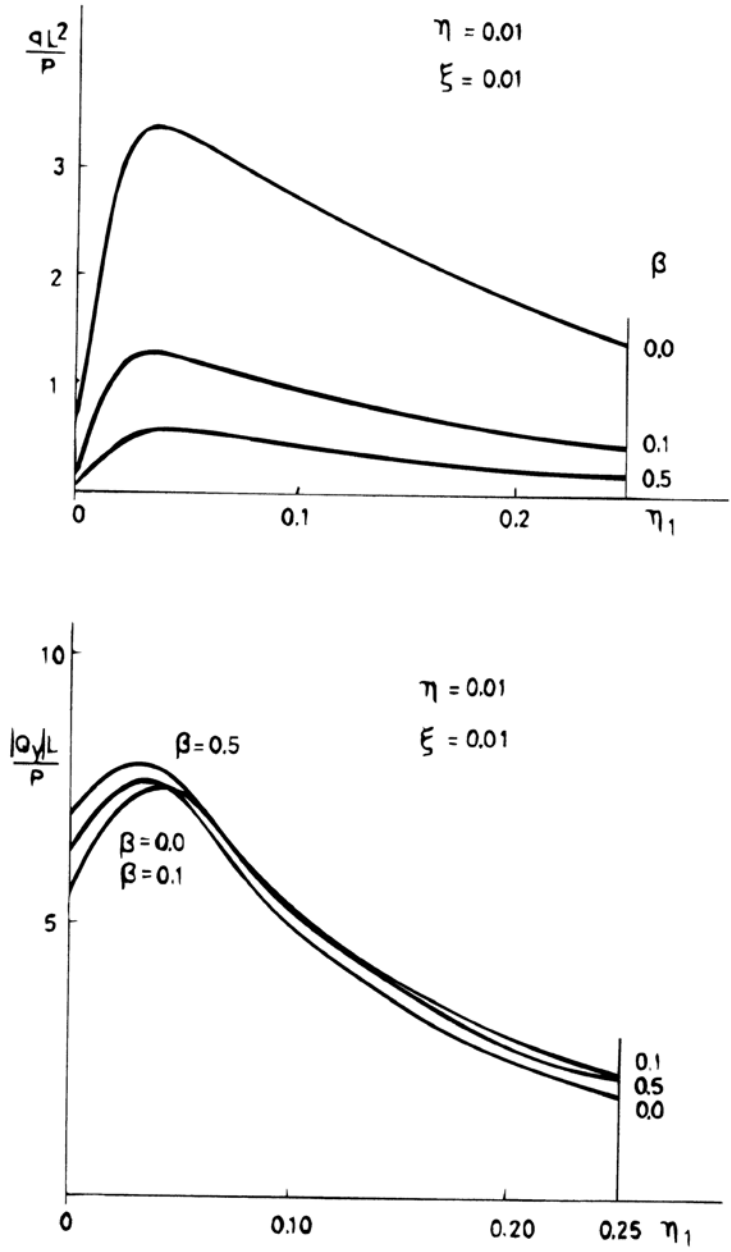

Fig. 4.36. Relationship of dimensionless subgrade reaction $|q|L^2/P$ and transverse force $|Q_y|L/P$ to dynamic load distance η_1.

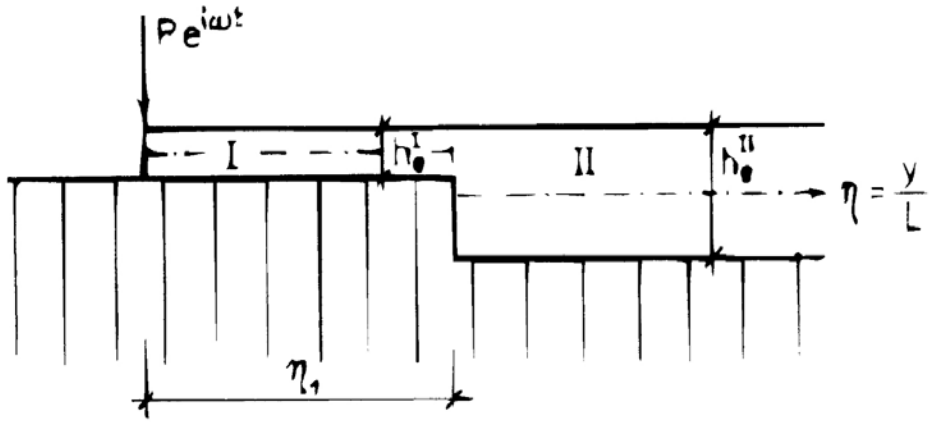

Fig. 4.37. Schematic diagram of dynamic load and sudden change of rigidity parallel with free boundary of half-plate on subgrade.

The boundary conditions at η=0 are determined by the assumption of a free boundary with acting concentrated external load $P\mathrm{e}^{\mathrm{i}\omega t}$. They are given by the equations

$$\begin{aligned} {}^{\mathrm{F}}M_0(\eta=0)&=0 \\ {}^{\mathrm{F}}Q_0(\eta=0)&={}^{\mathrm{F}}Q_z(\eta\ 0)-{}^{\mathrm{F}}P_1 \end{aligned} \tag{4.73}$$

where ${}^{\mathrm{F}}M_0$, ${}^{\mathrm{F}}Q_0$ are transforms of the initial bending moment and initial transversal force, ${}^{\mathrm{F}}Q_z$ is a transform of the subgrade transversal force and ${}^{\mathrm{F}}P_1$ is a transform of external force.

The contact conditions at the interface of zone I and zone II at $\eta=\eta_1$ are determined by the equations

$$\begin{aligned} {}^{F}w_{\mathrm{I}}(\eta=\eta_1)&={}^{\mathrm{F}}w_{\mathrm{II}}(\eta=\eta_1) \\ {}^{\mathrm{F}}\varphi_{\mathrm{I}}(\eta=\eta_1)&={}^{\mathrm{F}}\varphi_{\mathrm{II}}(\eta=\eta_1) \\ {}^{\mathrm{F}}M_{\mathrm{I}}(\eta=\eta_1)&={}^{\mathrm{F}}M_{\mathrm{II}}(\eta=\eta_1) \\ {}^{\mathrm{F}}Q_{\mathrm{I}}(\eta=\eta_1)&={}^{\mathrm{F}}Q_{\mathrm{II}}(\eta=\eta_1) \end{aligned} \tag{4.74}$$

Substituting into (4.73) and (4.74) the system of equations (4.37) is obtained, in which the coefficients a_{11}, a_{12}, a_{21}, a_{22}, a_{31}, a_{32}, a_{41}, a_{42} are given by the same relationships (4.38) but for the others the equations are given in the form

$$a_{13} = -1$$

$$a_{14} = -1$$

$$a_{10} = \frac{L^3}{D_\mathrm{I}^*} \frac{{}^{\mathrm{F}}P_1}{q_2\gamma_1 - q_1\gamma_2} (\gamma_2 \sinh \gamma_1\eta_1 - \gamma_1 \sinh \gamma_2\eta_1)$$

$$a_{23} = -\gamma_1^{\mathrm{II}}$$

$$a_{24} = -\gamma_2^{\mathrm{II}}$$

$$a_{20} = \frac{L^3}{D_\mathrm{I}^*} \frac{{}^{\mathrm{F}}P_1}{s_1 - s_2} (-\cosh \gamma_1\eta_1 + \cosh \gamma_2\eta_1)$$

(4.75)

$$\alpha_{33} = s_1^{\mathrm{II}}/d_{12}$$

$$a_{34} = s_2^{\mathrm{II}}/d_{12}$$

$$a_{30} = \frac{L^3}{D_\mathrm{I}^*} \frac{{}^{\mathrm{F}}P_1}{q_2\gamma_1 - q_1\gamma_2} (q_2 \sinh \gamma_1\eta_1 - q_1 \sinh \gamma_2\eta_1)$$

$$a_{43} = q_1^{\mathrm{II}}/d_{12}$$

$$a_{44} = q_2^{\mathrm{II}}/d_{12}$$

$$a_{40} = \frac{L^3}{D_\mathrm{I}^*} \frac{{}^{\mathrm{F}}P_1}{s_1 - s_2} (-s_2 \cosh \gamma_1\eta_1 + s_1 \cosh \gamma_2\eta_1)$$

where s_1^{II}, s_2^{II}, q_1^{II}, q_2^{II} are parameters according to (4.23) but referred to zone II of the half-plate with greater thickness.

After computation of the unknown initial parameters ${}^{\mathrm{F}}w_0$, ${}^{\mathrm{F}}\varphi_0$ the originals of the state vector components are determined according to equations (4.40) for region I and according to equations (4.41) for region II.

The numerical solutions were performed partly for the characteristics of a plate on subgrade in zone I corresponding to a rigid highway pavement structure and partly for the characteristics equivalent to flexible pavements. The sudden change of rigidity was always given by the ratio $d_{12} = D_\mathrm{I}^*/D_\mathrm{II}^* = 0.05273$.

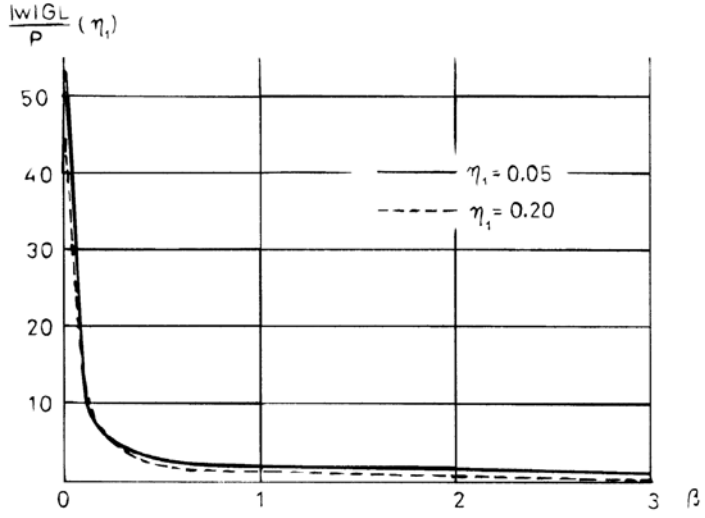

Fig. 4.38. Variation of dimensionless deflection $|w|GL/P$ with frequency β.

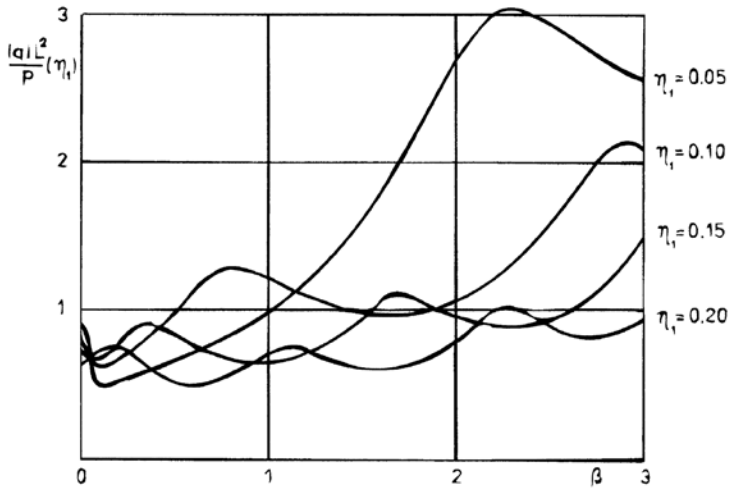

Fig. 4.39. Variation of dimensionless subgrade reaction $|q|L^2/P$ with frequency β for various interface distances η_1.

The computed amplitude-frequency characteristics of dimensionless deflections wGL/P, subgrade reaction qL^2/P, transverse forces of the system $Q_y L/P$ and bending moments M_y/P in the point $\eta=\eta_1$, i.e. at the interface of the rigidity change for plate I, are plotted in Figs. 4.38– 4.41 of rigid pavements and in Figs. 4.42 and 4.43 for M_y/P and qL^2/P for case of flexible pavements.

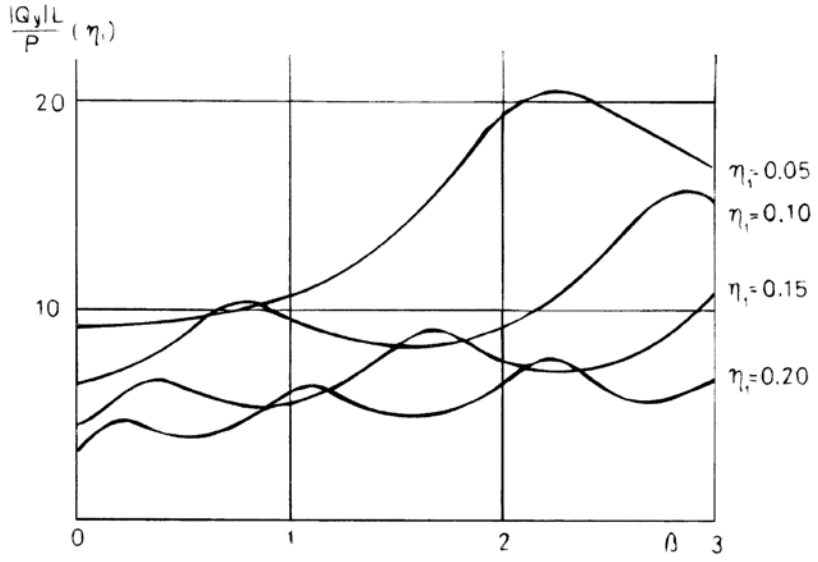

Fig. 4.40. Variation of dimensionless transverse force $|Q_y|L/P$ with frequency β for various interface distances η_1.

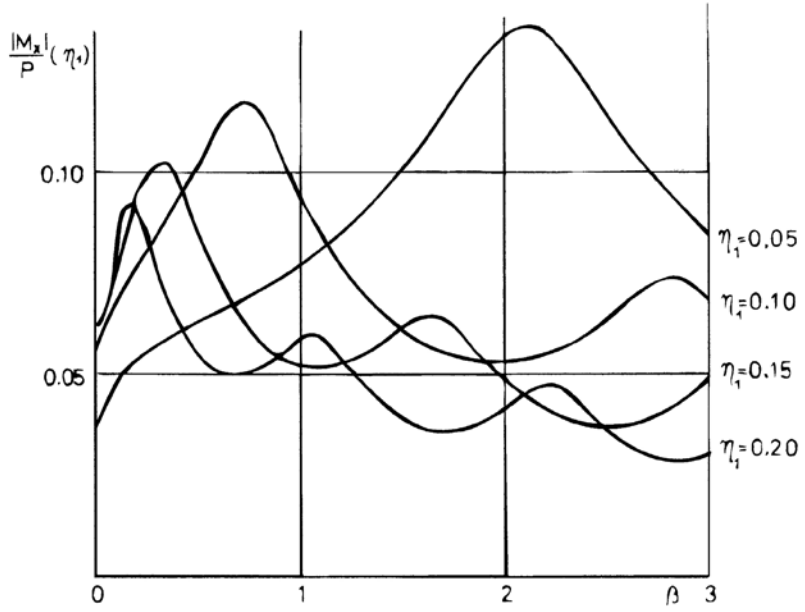

Fig. 4.41. Variation of dimensionless bending moment $|M_x|/P$ with frequency β for various interface distances η_1.

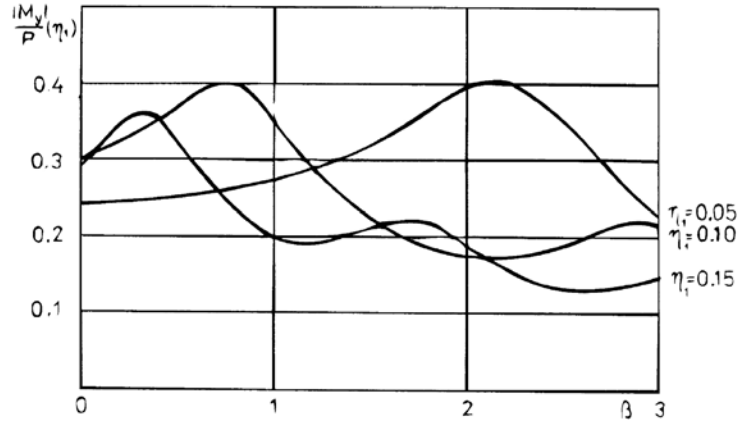

Fig. 4.42. Variation of dimensionless bending moment $|M_y|/P$ with frequency β for various interface distances η_1 and flexible pavement.

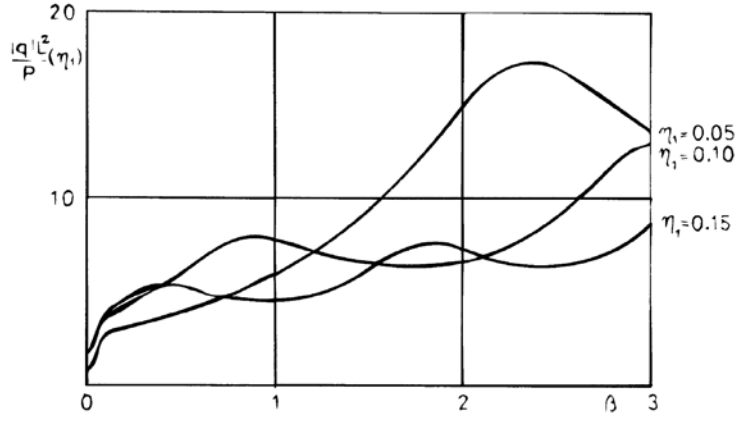

Fig. 4.43. Variation of dimensionless subgrade reaction $|q|L^2/P$ with frequency β for various interface distances η_1 and flexible pavement.

The variations of subgrade reaction, bending moments and transverse force of the system produce resonance zones and, as a consequence, a considerable increase in the values that are connected with the natural frequencies of the cantilever part of zone I.

With regard to the cantilever behaviour of plate I (Fig. 4.37) it will be interesting to compare the values of bending moments $M_y/P(\eta=\eta_1)$ for $\beta=0$ with the values of the static case of the cantilever plate strip which is clamped at one side and loaded by a concentrated force P on the free side of the strip (Fig. 4.44).

According to [4.1] the bending moment at the point $\xi=0$, $\eta=\eta_1$ under a concentrated loading force has a constant value independent from the width of plate strip, η_1. It is given by the expression

$$M_y(\eta)=\eta_1)=-0.465P. \tag{4.76}$$

In our case, which differs from this model because the plate is lying on subgrade and at the interface has an elastic clamped boundary, the values $M_y(\beta=0)=(0.320–0.385)\ P$ for rigid pavement and $M_y(\beta=0)=(0.240–0.300)\ P$ for flexible pavement were obtained. With regard to subgrade reaction the values of bending moments are smaller in comparison to the free cantilever plate. Of course, the values of bending moments M_y under a dynamic load acquire higher values as in the static case given by expression (4.76) as a consequence of resonance phenomena.

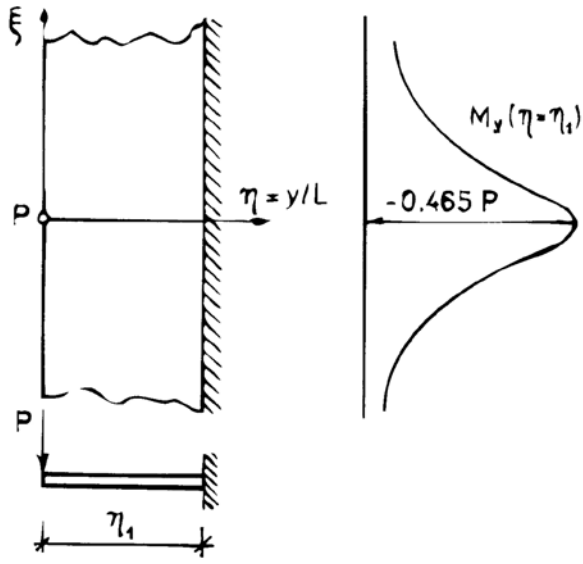

Fig. 4.44. Bending moment M_y in the static case of a cantilever plate strip.

4.7 Comparison of extreme values of flexural moments and subgrade reactions

From the point of view of design and the evaluation of stresses in the equivalent plate on subgrade or in a layered pavement structure the extreme values of bending moments M_x, M_y are decisive. For the bearing power of the subgrade the normal stresses of subgrade reaction are significant.

The extreme values of bending moments for characteristic loading cases are summarized in Table 4.6. It follows from the summary that for the equivalent plate on subgrade the bending moments of the half-plate on subgrade under the loading of the free boundary are decisive. The loading close to the joints gives smaller values but the influence of the inhomogeneous subgrade and sub-base layers modelled by a sudden change in rigidity causes a considerable increase in bending moment values, by the second loading scheme in particular.

The subgrade reactions for characteristic loading schemes are summarized in Table 4.7.

Table 4.6. Survey of bending moment values for various schemes of loading on rigid and flexible pavements.

Scheme of loading	rigid pavement	flexible pavement
	$\|M\|/P$	$\|M\|/P$
unbounded plate on subgrade	0.402	0.226
loading of the halfplate boundary	0.470	0.286
loading near the joint 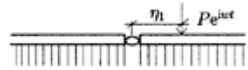	–	0.236
loading near the sudden 	0.365	0.240
loading near the sudden 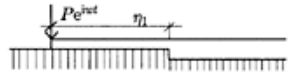	0.536	0.405

Table 4.7. Survey of subgrade reaction values for various schemes of loading on rigid and flexible pavements.

Scheme of loading	rigid pavement	flexible pavement
	$\|q\|h^2/P$	$\|q\|h^2/P$
unbounded plate on subgrade	0.0165	0.0392
loading of the halfplate boundary	0.0345	0.0486
loading near the joint	–	0.0381
loading near the sudden change of rigidity	0.0211	0.0382
loading near the sudden change of regidity	0.0345	0.1099

The maximum values of subgrade reactions are recorded by dynamic loading at the border of the half-plate on subgrade respectively in the case of the loading close to the sudden change of system rigidity.

4.8 Pulse (impact) loads of equivalent plate on subgrade

The solution of individual characteristic cases of dynamic loading for the equivalent plate on subgrade was realized by considering a harmonic variable load. They form the basic problems and starting point for the determination of the dynamic response under pulse loading.

Pulse-impact loading is a dynamic load that is actually produced by traffic and which is used for the determination of the stiffness and bearing capacity of pavement structures in highway and runway engineering as a simulator of the vehicle loads.

The shape of the force pulse that adequately corresponds to the impact loading may be expressed by the relationship [1.22]

$$P(t) = P_{\max} \frac{e^2}{4} (\omega_0 t)^2 \, e^{-\omega_0 t} \tag{4.77}$$

where ω_0 is a parameter with angular frequency extent, the choice of which changes the duration of the pulse. The time during which the pulse lasts can be determined from the condition $\omega_o t \approx 6$, i.e. $T_0 = t = 6/\omega_0$. For the purpose of the solution of the dynamic pulse loading effect the application of Fourier integral transformation is available. The conception of complex moduli applied by stationary vibration under external harmonic loading does not fulfil the principle of causality, but from a practical point of view this fact can be neglected. It manifests itself only by the inaccurate initial values of the dynamic response.

The dynamic response of the equivalent plate on subgrade under harmonic loading was determined in previous chapters by means of complex state vector components or in the form of amplitude-frequency and phase—frequency characteristics. In general it can be indicated by $S^*(\beta) = S_R(\beta) + iS_J(\beta)$, if β is a dimensionless frequency.

The transform of the loading force pulse (4.74) is given by the expression

$${}^{F}P = \int_{-\infty}^{\infty} P(t) \, e^{-i\omega t} \, dt = \frac{P_{\max} \, e^2 \omega_0^2}{2(\omega_0 + i\omega)^3} = \frac{P_{\max} \, e^2 \Omega_0^2 \, a}{2c_2 \left(\Omega_0^2 + i\beta \frac{a}{h}\right)^3} \tag{4.78}$$

where

$$\Omega_0 = \frac{\omega_0 \, a}{c_2} \tag{4.79}$$

and $c_2 = \sqrt{G/\varrho}$ is the stress-wave velocity in the medium of the equivalent plate; a is halfway from the line segment in the direction ξ on which the load is concentrated.

The Fourier transform of an arbitrary state vector component ${}^{F}S$ is given by the relationship

$${}^{F}S = S^*(\omega) \, {}^{F}P(\omega) = S^*(\beta) \, {}^{F}P(\beta). \tag{4.80}$$

Using the Fourier inverse transformation the original state vector component $S(t)$ is given by the equation

$$S(t) = \frac{1}{2\pi} \int_{-\infty}^{\infty} S^*(\omega) \, {}^{F}P(\omega) \, e^{i\omega t} d\omega = \frac{1}{2\pi} \int_{-\infty}^{\infty} S^*(\beta) \, {}^{F}P(\beta) \, e^{i\beta \frac{c_2}{h} t} d\beta \tag{4.81}$$

or in the form

$$S(T) = \frac{1}{\pi} \operatorname{Re} \left[\int_0^{\infty} S^*(\beta) P_{\max} \frac{e^2 \Omega_0^2 \, e^{i\beta T} a}{2\left(\Omega_0 + i\beta \frac{a}{h}\right)^3 h} d\beta \right] \tag{4.82}$$

where T is dimensionless time

$$T = \frac{c_2}{h} t. \tag{4.83}$$

Equation (4.82) can be computed using numerical integration and computers. A numerical procedure was performed in which the values $S^*(\beta)$ were computed at 21 discrete values β in the integration range β(0.0–3.0). The real and imaginary part of complex function $S^*(\beta)$, i.e. $S_R(\beta)$ and $S_J(\beta)$ in interval <0.0, 3.0>, were expressed by cubic splines with connection to the discrete values β, by means of which the functions $S_R(\beta)$, $S_J(\beta)$ were computed for arbitrary value β connected to the numerical integration of improper integrals.

4.8.1 Dynamic response of plate on subgrade as an analogue of flexible pavement structure

The numerical results can be presented for the case of the equivalent half-plate on subgrade under pulse loading at the boundary. The input data correspond to the flexible pavement. The dimensionless deflection $wGL/P_{max}(\xi=0, \eta=0)$, subgrade reaction $qL^2/P_{max}(\xi=0, \eta=0)$ and bending moment $M_x/P_{max}(\xi=0, \eta=0)$ versus dimensionless time T are plotted in Figs. 4.45–4.47 for various times of pulse duration given by values Ω_0=0.075, 0.15, 0.30, 0.50 and 0.75. At the same time the values of the competent quantities under the static load P_{max} are marked. It can be seen that the dynamic response values do not exceed these static ones.

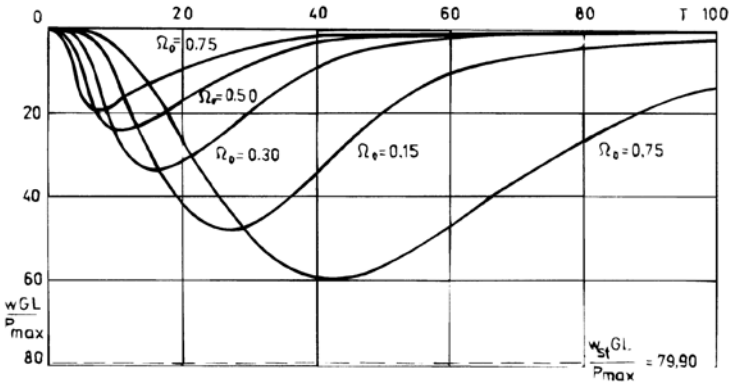

Fig. 4.45. Variation of dimensionless deflection wGL/P_{max} with time T for the equivalent half-plate on subgrade under pulsed loading.

The other situation is in the case of the boundary pulse loading of the half-plate on subgrade with a sudden change of rigidity. As can be seen in Fig. 4.48 the dynamic response computed for a sudden change of rigidity at distance η_1=0.1 and for bending moment M_y/P_{max} demonstrates that maximum values of dynamic bending moment under pulse loading exceed the

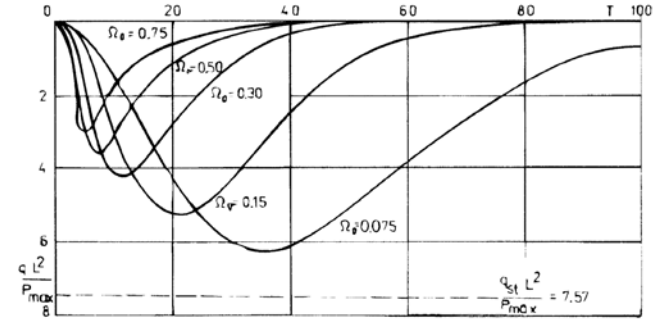

Fig. 4.46. Variation of dimensionless subgrade reaction qL_2/P_{max} with time T of the equivalent half-plate on subgrade under pulsed loading.

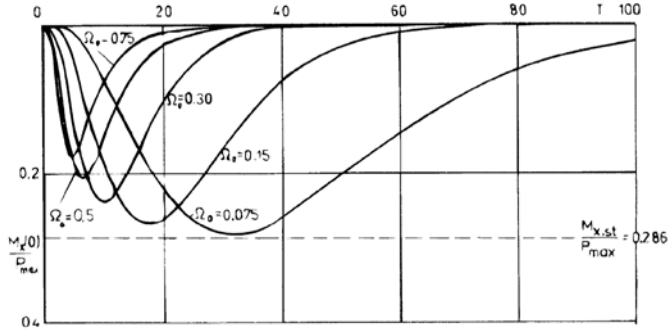

Fig. 4.47. Variation of dimensionless bending moment $M_x(0)/P_{max}$ with time T for equivalent half-plate on subgrade under pulsed loading.

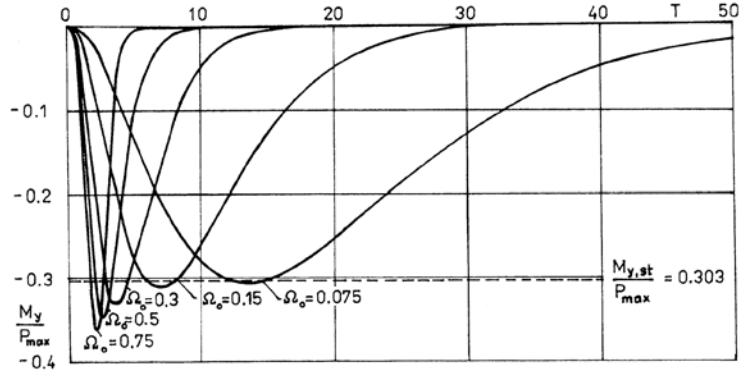

Fig. 4.48. Variation of dimensionless bending moment M_y/P_{max} with time T for equivalent half-plate on subgrade under pulsed loading.

static values under force load P_{max}. This is a reflection of the expressive increase of bending moment values in the amplitude-frequency characteristics (Fig. 4.42) as a consequence of resonance phenomena.

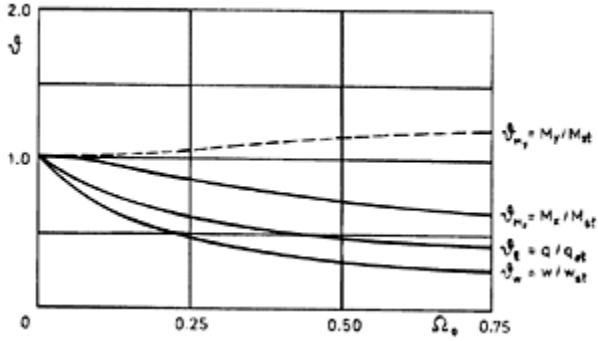

Fig. 4.49. Variation of dynamic coefficients ϑ with parameter Ω_0.

The dynamic coefficients ϑ defined by the ratio of the maximum value of the dynamic response to the static value under P_{max}, are plotted in Fig. 4.49 versus parameter Ω_0. BY increasing Ω_0, i.e. if the time of pulse duration decreases, the dynamic coefficients ϑ_w, ϑ_0 and ϑ_{M_x} decrease but the dynamic coefficient ϑ_{M_y} values are higher.

5
DYNAMIC INTERACTION OF PLATE WITH SUBGRADE UNDER A MOVING LOAD

The dynamic loads of the pavement structures in highway and runway engineering are evoked by moving vehicles and it is necessary to evaluate their effects in comparison with the effect of proposal static loads. The interaction of the plate and the subgrade under a moving load suggests the actual dynamic effect of irregularities on road surfaces too.

It is known that the decisive values of stresses and deformations for layered pavement structures can be achieved by loading at the border of the pavement. From this point of view the relevant task is to assess the dynamic response of the system under a moving concentrated load along the trajectory parallel to the border of the pavement.

5.1 Physical model of plate on subgrade as dynamic equivalent of the pavement

Numerous comparative studies on various modifications of the system of the equivalent plate resting on subgrade in previous chapters give reason to conclude that the simplest modification is the physical model of a thin equivalent plate in connection with the simplified model of subgrade. Such a model covers the essential properties of the dynamic behaviour of the system: real dispersion of flexural stress waves, the inertia of the co-acting subgrade, the dispersion of the energy into the subgrade and the damping properties of the material.

The differential motion equation has the form (3.257) or (4.1). The complex plate constant D^* is replaced by the relationship (3.258), and if the phase velocity c of the flexural stress waves is expressed by the relationship corresponding to the dispersion curve of flexural stress waves according to [3.11], the plate constant D^* will compensate for the dynamic rigidity of the equivalent plate in the sense of the refined theory of the plate taking account of the influence of shear and rotational inertia. The resulting relationship for D^* has the form (3.263) when β is given in the form

$$\beta^2 = \frac{\alpha^2 h^2}{L^2}\left(\frac{1}{1-\mu}+\frac{\kappa}{2}\right)+6\kappa - \sqrt{\left[\frac{\alpha^2 h^2}{L^2}\left(\frac{1}{1-\mu}+\frac{\kappa}{2}\right)+6\kappa\right]^2 - \frac{2\kappa}{1-\mu}\frac{\alpha^4 h^4}{L^4}}. \tag{5.1}$$

The dimensionless wave number $a=\alpha_0 L=2\pi L/\Lambda$, μ is Poisson's ratio and $\kappa=(0.87+1.12\mu)/(1+\mu)^2$. L is an arbitrary length constant.

We assume further that the load function *p(x, y, t)* is expressed as the sum of harmonic components for the functions of place or time so that the concept of complex characteristics D^*, K_1^*, K_2^* may be applied.

5.2 Load moving along boundary of half-plate on subgrade

The effect of the moving concentrated load for the unbounded plate on Winkler's subgrade has been analysed in [5.1]. Here we shall analyse the dynamic response of the system under a moving concentrated load along the trajectory, parallel to the border of the pavement, i.e. of the system of the equivalent half-plate on unbounded subgrade.

The load function is given by the relationship

$$p(x, y, t)=\delta(x-vt)\delta(y_1)P \tag{5.2}$$

where v is the speed of concentrated force P in the direction x along the trajectory with the distance y_1 from the boundary. $\delta(x-vt)$, $\delta(y_1)$ are Dirac generalized functions.

A quasi-stationary state arises assuming that the half-plate is at a standstill in connection with a moving dimensionless coordinate system:

$$\xi = \frac{1}{L}(x - vt) \quad , \quad \eta = \frac{y}{L} \tag{5.3}$$

if L is the chosen length constant.

The problem is defined as a dynamic system response at the point (ξ=0, η) under a concentrated load at the point (ξ, η_1) according to the scheme of Fig. 5.1, if the differential equation is given in the form

$$\left(\frac{\partial^2}{\partial\xi^2}+\frac{\partial^2}{\partial\eta^2}\right)^2 w(\xi,\eta) - \frac{K_2^* L^2}{D^*}\left(\frac{\partial^2}{\partial\xi^2}+\frac{\partial^2}{\partial\eta^2}\right)w(\xi,\eta) + \frac{K_1^* L^4}{D^*}w(\xi,\eta)$$

$$+\frac{k_d \varrho h}{D^*}v^2 L^2 \frac{\partial^2 w(\xi,\eta)}{\partial\xi^2} = \delta(\xi)\,\delta(\eta_1)\frac{PL^4}{D}.$$

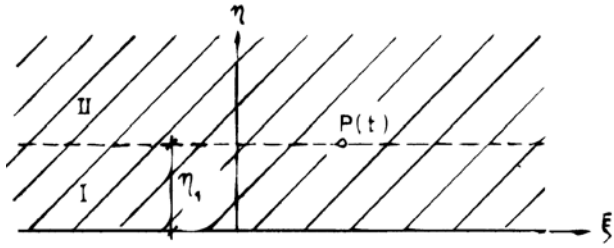

Fig. 5.1. Schematic diagram of coordinate system and load moving along boundary of half-plate on subgrade.

Applying Fourier's integral transformation for the dimension ξ in the form

$$^{F}w(\alpha,\eta)=\frac{1}{2\pi}\int_{-\infty}^{\infty}w(\xi,\eta)e^{i\alpha\xi}d\xi \tag{5.5}$$

the ordinary differential equation for Fourier's transform of deflection $^{F}w(\alpha, \eta)$ is obtained

$$\left[\frac{d^4}{d\eta^4}-\frac{d^2}{d\eta^2}\left(2\alpha^2+\frac{K_2^*L^2}{D^*}\right)+\alpha^4+\alpha^2\frac{K_2^*L^4}{D^*}+\frac{K_1^*L^4}{D^*}-\frac{k_d\varrho h}{D^*}v^2\alpha^2L^2\right]$$
$$\times\ ^{F}w(\alpha,\eta)=\delta(\eta_1)\frac{PL^4}{2\pi D^*}\frac{\sin\frac{\alpha a}{L}}{\frac{\alpha a}{L}}. \tag{5.6}$$

The concentrated load is considered in the ξ direction, divided on the line segment $2a/L$, as can be seen from the right side of equation (5.6).

The solution of homogeneous equation (5.6) lets us express the deflection transform in the form

$$^{F}w(\alpha,\eta)=A_1\sinh\gamma_1\eta+A_2\cosh\gamma_1\eta+A_3\sinh\gamma_2\eta+A_4\cosh\gamma_2\eta \tag{5.7}$$

if

$$\gamma_1^2=\alpha^2+\frac{K_2^*L^2}{2D^*}+\left(\frac{K_2^{*2}L^4}{4D^{*2}}-\frac{K_1^*L^4}{D^*}+\frac{k_d\varrho h}{D^*}v^2\alpha^2L^2\right)^{1/2} \tag{5.8}$$

$$\gamma_2^2=\alpha^2+\frac{K_2^*L^2}{2D^*}-\left(\frac{K_2^{*2}L^4}{4D^{*2}}-\frac{K_1^*L^4}{D^*}+\frac{k_d\varrho h}{D^*}v^2\alpha^2L^2\right)^{1/2}. \tag{5.9}$$

This solution can be connected with the application of the method of initial parameters in the same way as it was realized in previous chapters in the case of forced vibration under a harmonic concentrated load. It is not necessary to repeat the detailed procedures but, for the sake of completeness it is convenient to indicate that by the solution of differential equation (5.6) and using the method of initial parameters the transform of deflection for the area I is expressed in the form

$$^{F}w(\alpha,\eta)=K_{ww}\,^{F}w_0+K_{w\varphi}\,^{F}\varphi_0+K_{wM}\,^{F}M_0+K_{wQ}\,^{F}Q_0 \tag{5.10}$$

and for area II in the form

$$^{F}w(\alpha,\eta)=A_1^*e^{\gamma_1\eta}+A_2^*e^{\gamma_2\eta}. \tag{5.11}$$

The initial parameters ${}^{F}w_0$, ${}^{F}\varphi_0$, ${}^{F}M_0$, ${}^{F}Q_0$ are the transforms of deflection, angular displacement, bending moment and transverse force at η=0 and K_{ww}, $K_{w\varphi}$, K_{wM}, K_{wQ} are influence coefficients that are functions of α, v, and of stiffness parameters.

A_1^*, A_2^* in equation (5.11) are arbitrary complex constants while γ_1, γ_2, according to relationships (5.8), (5.9) have a negative real part.

The conditions of the boundary of the half-plate at η=0 have the form

$$\begin{gathered} {}^{F}M_I(0) = 0 \\ {}^{F}Q_I(0) = K_2^* \frac{\gamma_z}{L} {}^{F}w_0 \end{gathered} \tag{5.12}$$

when the right part of the second equation (5.12) presents the reaction of free subgrade and γ_z is determined by the expression

$$\gamma_z^2 = \frac{K_1^* L^2}{K_2^*} + \alpha^2 - \frac{\varrho_z K_3 v^2 \alpha^2}{K_2^*}. \tag{5.13}$$

The conditions of continuity at the interface of I and II are given in the form

$$\begin{gathered} {}^{F}w_I(\eta_1) = {}^{F}w_{II}(\eta_1) \\ {}^{F}\varphi_I(\eta_1) = {}^{F}\varphi_{II}(\eta_1) \\ {}^{F}M_I(\eta_1) = {}^{FMII(\eta} \\ {}^{F}Q_I(\eta_1) = {}^{F}Q_{II}{}^{(\eta}{}_{1}{}^{)} \end{gathered} \tag{5.14}$$

and together with the boundary conditions (5.12) enable us to determine the transforms of the initial parameters and the values of complex constants A_1^* and A_2^*. Applying these values and the relationships of plate theory the transforms of state vector components of the system can be determined.

By inverse transformation of the arbitrary component ${}^{F}S(\alpha, \eta)$ the originals are established according to the relationship

$$S(\xi, \eta) = \int_{-\infty}^{\infty} {}^{F}S(\alpha, \eta) \bar{e}^{i\alpha\xi} d\alpha = 2\mathrm{Re}\left[\int_{0}^{\infty} {}^{F}S(\alpha, \eta) e^{-i\alpha\xi} d\alpha\right]. \tag{5.15}$$

It follows from this procedure that, in contrast to forced vibration under a harmonic force, the relationships differ only in having the term $v^2\alpha^2L^2$ instead of ω^2L^4, and the numerical solution is realized for various values of load moving speed v. The dimensionless speed

$C_p=v/c_2$, if $c_2=\sqrt{G/\varrho}$ is the shear-wave velocity in the plate medium, now represents the dimensionless frequencies $\beta=\omega h/c_2$ in the case of forced vibration.

Another difference is in the conception of sub-integral complex functions during inverse transformation. Whereas sub-integral functions by forced harmonic vibration, which are complex functions of wave number square α^2, were considered with symmetrical real and imaginary parts, in the case of a moving load the sub-integral functions have to be considered with asymmetrical imaginary parts. This signifies that the complex characteristics of elasticity E^*, K_1^*, K_2^* have to be considered in the form

$$E^*=E(1+\mathrm{i}\delta\ \mathrm{sgn}\ \alpha)$$

$$K_1^* = K_1(1 + \mathrm{i}\delta_z\ \mathrm{sgn}\ \alpha) \tag{5.16}$$

$$K_2^* = K_2(1 + \mathrm{i}\delta_z\ \mathrm{sgn}\ \alpha).$$

This procedure is similar to that for an arbitrary dynamic load if Fourier's integral transformation is used on real-time functions. In such a case the complex characteristics are considered in the form (for example) $E^*=E(1+\mathrm{i}\delta\ \mathrm{sgn}\omega)$. The physical reason follows from the fact that the dynamic effect in a mechanical system manifests itself by means of propagated stress waves. If we assume that the stress of the propagated wave is in the form $\sigma(\xi)=\sigma_0 e^{i\alpha\xi}$, then the corresponding deformation as a consequence of the damping effect is shifted in phase with the angle φ and has the form $\varepsilon(\xi)=\varepsilon_0 e^{i(\alpha\xi-\varphi)}$.

5.3 Numerical results

Numerical computations using the procedure described above were realized partly on a system that is equivalent to the behaviour of highway cement concrete pavements and partly on the equivalent system for flexible pavements. The input characteristics for both pavement structures are considered to be the same as in Chapter 4.

The variations of the computed dimensionless state vector components versus ξ are plotted in Figs. 5.2–5.6 for various values of dimensionless speed $C_p=v/c_2$. They are valid for the case of a cement concrete pavement structure. The numerical results obtained for flexible pavement structures are drawn in Figs. 5.7–5.11.

The dynamic coefficient ϑ, defined as the ratio of the maximum dynamic value of state vector component to the value at zero speed of a moving load, are plotted for deflection w, subgrade reaction q and bending moment $M_x(t)$ in Figs. 5.12 and 5.13 in relation to the moving speed C_p. It is shown that the dynamic increase of the moving load effect rises with increasing C_p.

The maximum values are achieved at the speed $C_p=0.175$–0.180 for a cement concrete pavement and at $C_p=0.21$–0.22 for a flexible pavement structure. With further increase of moving speed values the dynamic coefficients drop significantly below the level of static values. The maximum values of dynamic coefficients by the considered

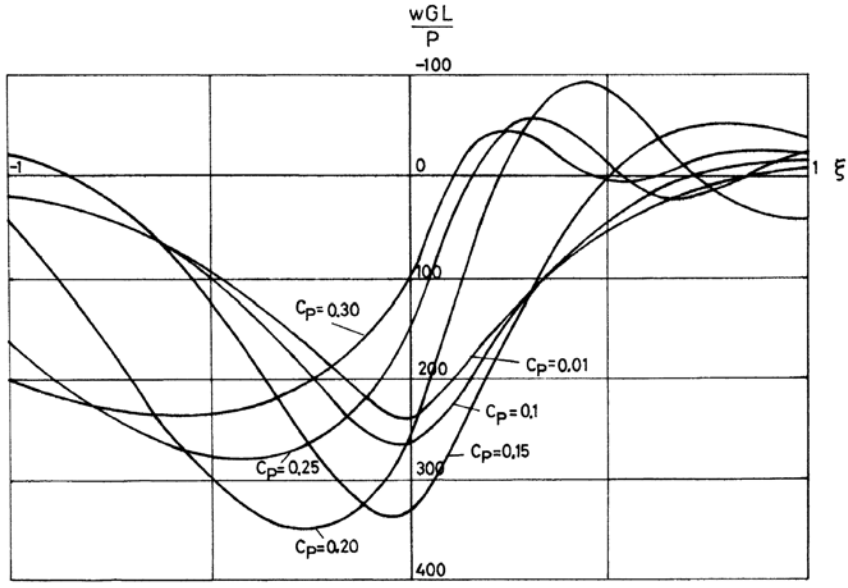

Fig. 5.2. Variation of dimensionless deflection wGL/P with ξ for various speed values C_P in rigid pavement.

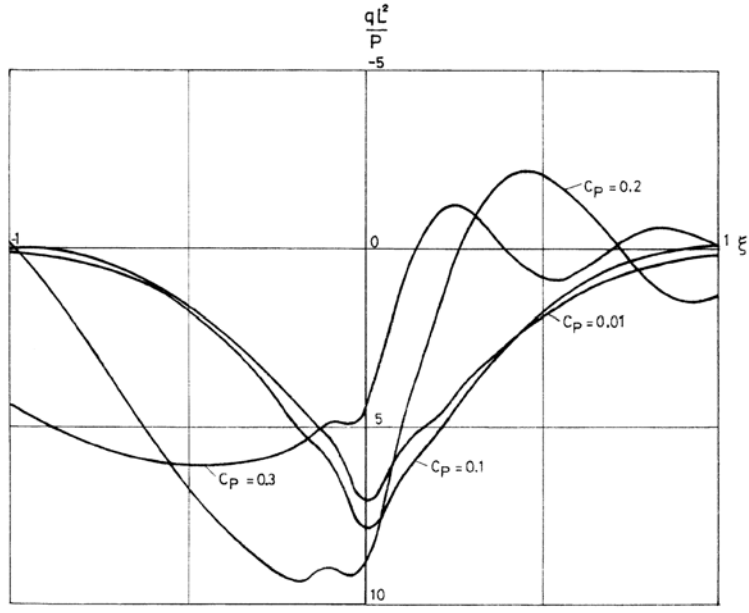

Fig. 5.3. Variation of dimensionless subgrade reaction qL^2/P with ξ for various speed values C_P in rigid pavement.

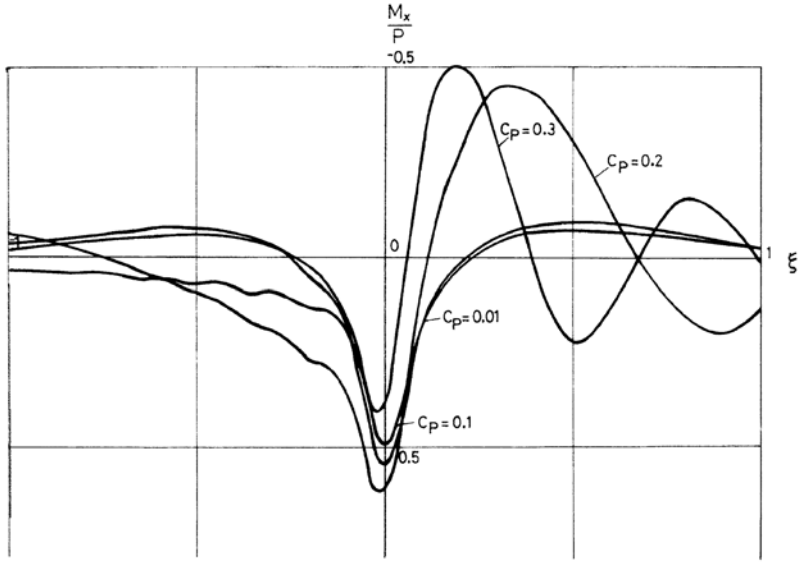

Fig. 5.4. Variation of dimensionless bending moment M_x/P with ξ for various speed values C_p in rigid pavement.

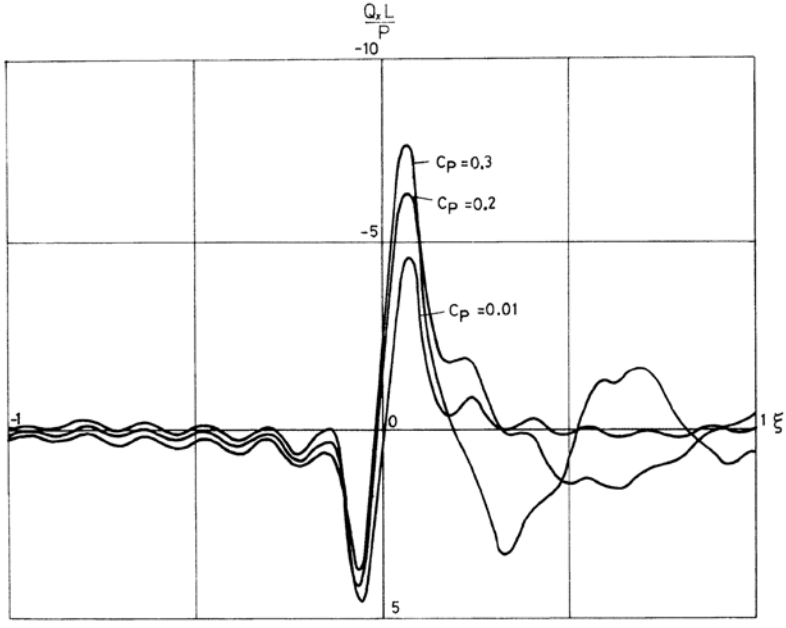

Fig. 5.5. Variation of dimensionless transverse force Q_xL/P with ξ for various speed values C_p in rigid pavement.

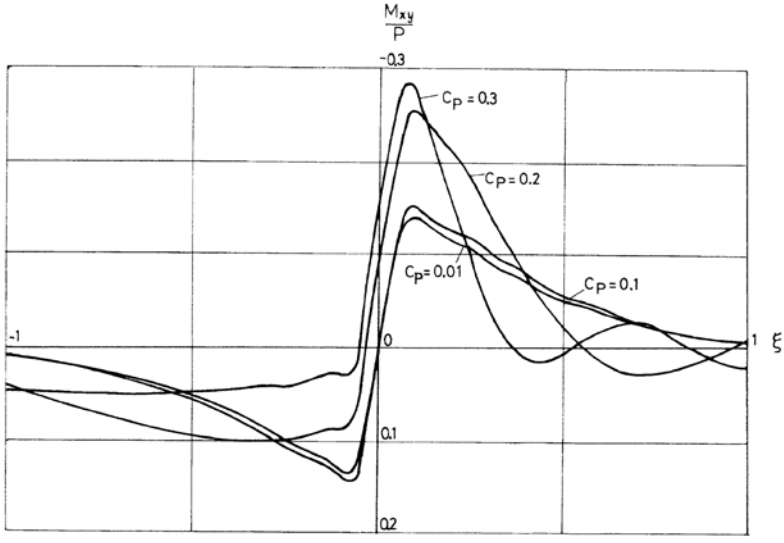

Fig. 5.6. Variation of dimensionless twisting moment M_{xy}/P with ξ for various speed values C_p in rigid pavement.

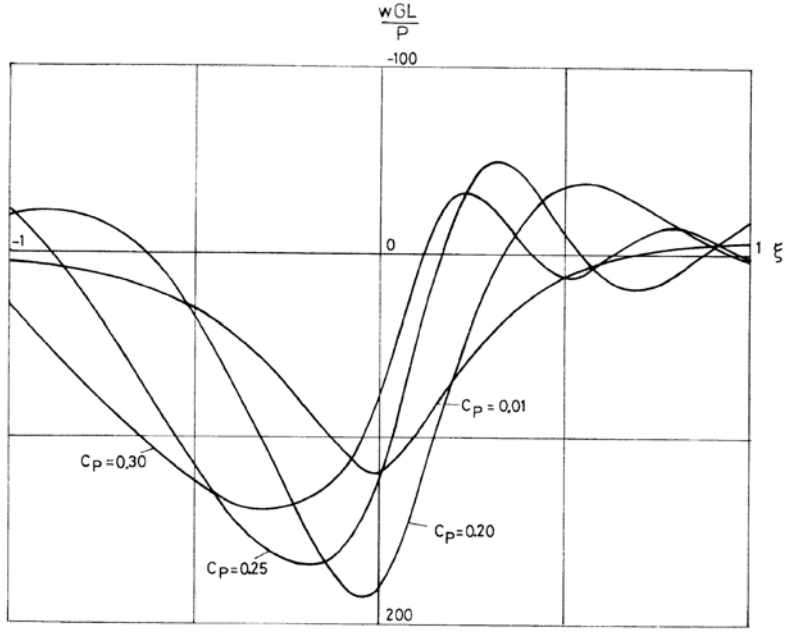

Fig. 5.7. Variation of dimensionless deflection wGL/P with ξ for various speed values C_p in flexible pavement.

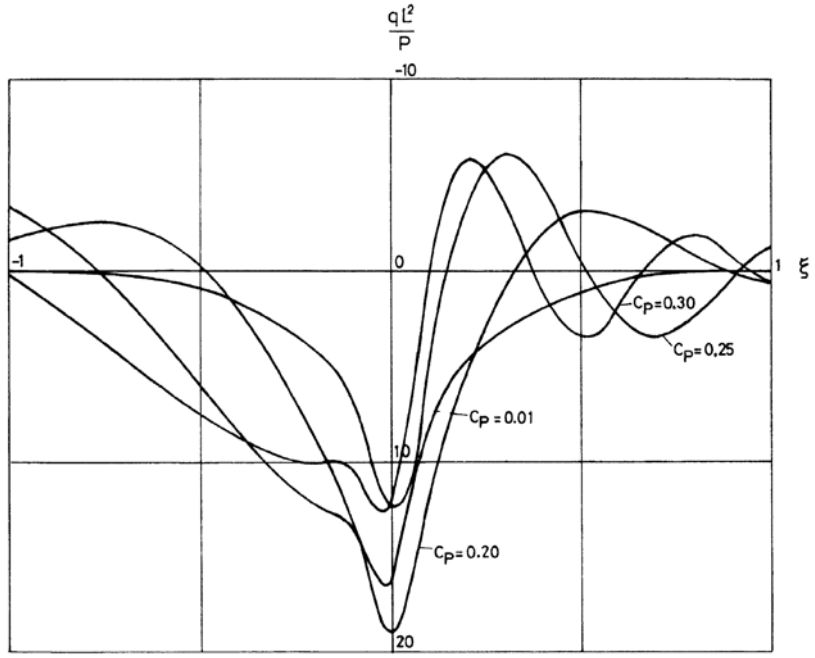

Fig. 5.8. Variations of dimensionless subgrade reaction qL^2/P with ξ for various speed values C_p in flexible pavement.

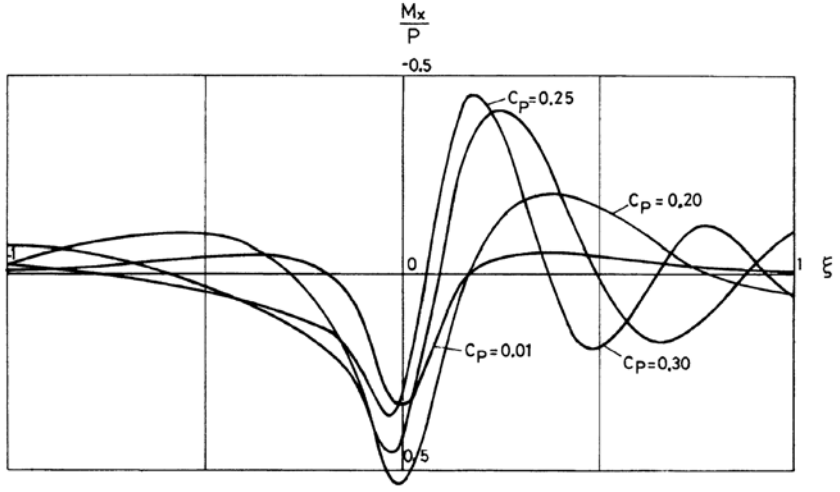

Fig. 5.9. Variation of dimensionless bending moment M_x/P with ξ for various speed values C_p in flexible pavement.

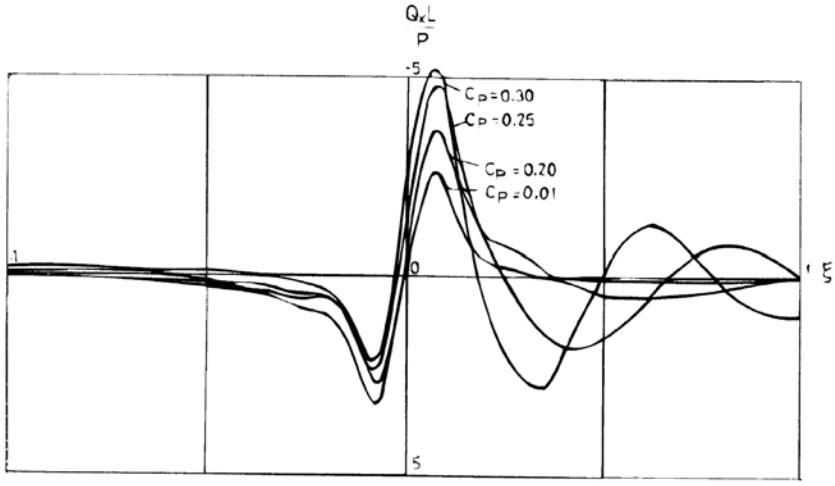

Fig. 5.10. Variation of dimensionless transverse force $Q_x L/P$ with ξ for various speed values C_p in flexible pavement.

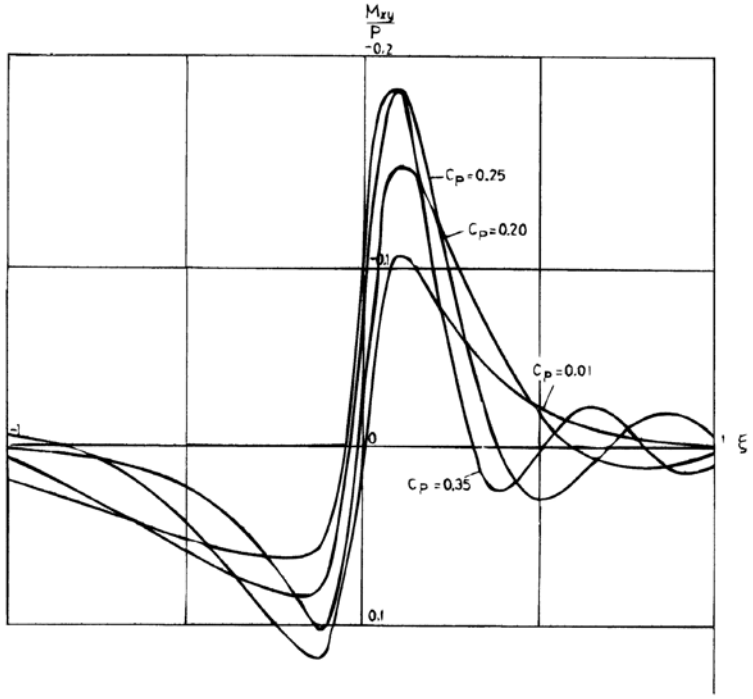

Fig. 5.11. Variation of dimensionless twisting moment M_{xy}/P with ξ for various speed values C_p in flexible pavement.

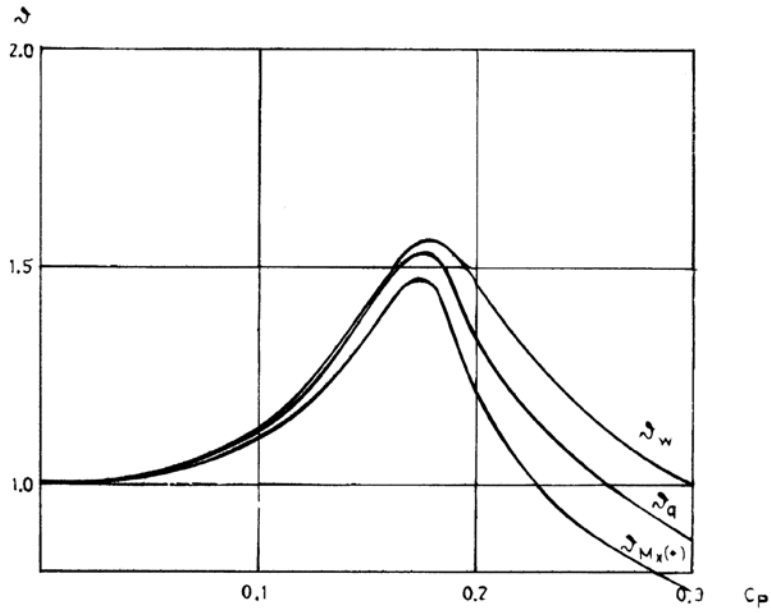

Fig. 5.12. Dynamic coefficients ϑ versus speed factor C_p in rigid pavement.

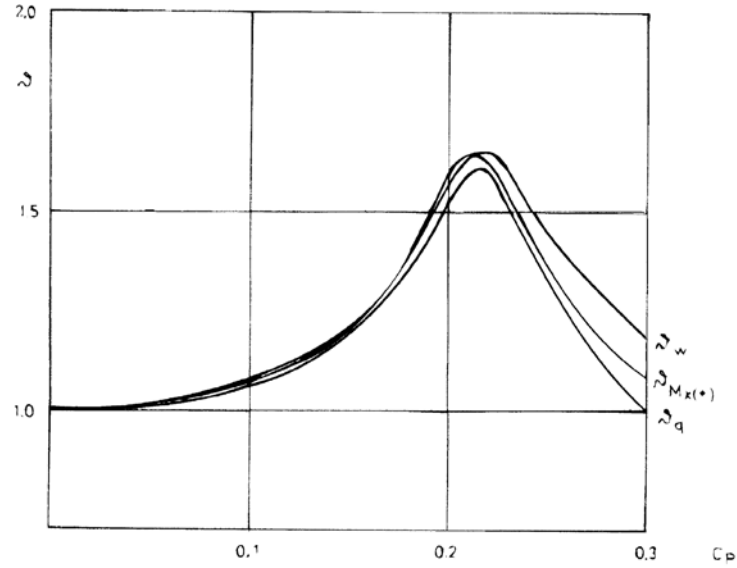

Fig. 5.13. Dynamic coefficients ϑ versus speed factor C_p in flexible pavement.

parameters of damping and dispersion are ϑ=1.47–1.56 for rigid pavements and ϑ=1.6–1.7 for flexible pavements.

The numerical results obtained accord with practical experience, which suggests that the dynamic increase of the moving load effect arises from speeds that are too high compared with current speeds of vehicles or airplanes during take off and landing. In the case of a rigid pavement, when the velocity of shear waves c_2 in the medium of the concrete plate is given by the value c_2≈2500 m/s, the critical moving speed v_{cr}=(0.175–0.18) 2500=445 m/s=1600 km/h. Similarly, for a flexible pavement, then assuming that c_2 in bituminous medium 1500 m/s, the critical speed is v_{cr}=(0.21–0.22)1500–325 m/s=1170 km/h.

5.4 Influence of unevennesses on dynamic response

From the practical point of view the most relevant task is to assess the dynamic response of the system under moving loads at the transition of surface irregularities. The dynamic increment of acting forces by transition of surf ace unevennesses is visible already by the usual speeds of the moving load.

5.4.1 Influence of periodical surfacing unevennesses under moving load

Let us assume that the surfacing unevennesses on the track are parallel to the border of the half-plate on the subgrade, with a shape given by the equation

$$w_0(z) = \tfrac{1}{2} w_0 \left(1 + \cos \frac{2\pi x}{l_0}\right) \tag{5.17}$$

and continuously repeated on the track at y=y_1. In equation (5.17) w_0 is the depth and l_0 is the length of the unevenness according to the scheme in Fig. 5.14.

For a concentrated moving load the right side of differential equation (5.4) is expressed by the relationship

$$\delta(x - vt)\ \delta(y_1)\ \frac{1}{D^*}\left(P - \frac{P}{g}\ \frac{\partial w_0(x, y, t)}{\partial t^2}\right) \tag{5.18}$$

where g is the acceleration of gravity. In this equation the effect of system deflection under a moving load is neglected.

Introducing a moving system of dimensionless coordinates (ξ, η), it follows that

$$\frac{\partial^2 w_0}{\partial t^2} = \frac{v^2}{L^2}\ \frac{\partial^2 w_0}{\partial \xi^2} \tag{5.19}$$

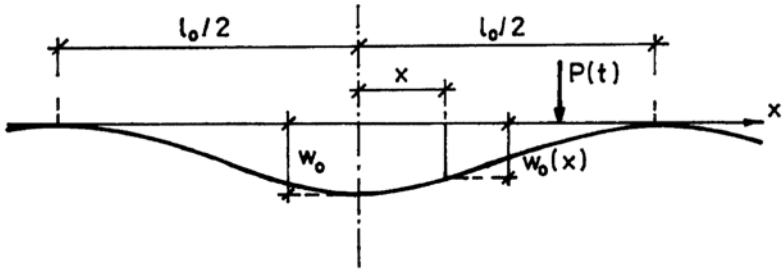

Fig. 5.14. Schematic diagram of pavement unevenness.

and the right side of differential equation (5.4) is established by the relationship

$$\frac{\delta(\xi)\,\delta(\eta_1)}{D^*}\left(P+\frac{P}{g}\frac{w_0}{2}v^2\,\frac{4\pi^2}{l_0^2}\cos 2\pi\xi\frac{L}{l_0}\right). \tag{5.20}$$

Applying Fourier's integral transformation and supposing that the moving load is divided on a line segment with length $2a$, the expression for the right side of equation (5.6) is obtained in the form

$$\frac{P}{D^*}\,\delta(\eta_1)\left[\frac{1}{2\pi}\,\frac{\sin\frac{\alpha a}{L}}{\frac{\alpha a}{L}}+\frac{\pi w_0 v^2}{\varrho l_0^2}\,\frac{1}{\frac{4\pi^2 a^2}{l_0^2}-\alpha^2\frac{a^2}{L^2}}\right.$$

$$\left.\times\left(\frac{2\pi a}{l_0}\sin\frac{2\pi a}{l_0}\cos\frac{\alpha a}{L}-\frac{\alpha a}{L}\cos\frac{2\pi a}{l_0}\sin\frac{\alpha a}{L}\right)\right]. \tag{5.21}$$

It is shown that the additional effect of acting forces evoked by unevennesses increases with the square of the moving load speed v^2, is linear with the depth w_0 of unevennesses, and is inversely proportional to the length of unevenness, l_0.

5.4.2 Influence of periodical surfacing unevennesses by a moving load system with two degrees of freedom

Again, we assume continuous unevennesses of the track surfacing according to equation (5.17), and the effect of system deflection under a moving load is neglected as it is small in comparison with the depth of the unevennesses.

The moving load is formed by a system with two degrees of freedom according to the scheme in Fig. 5.15. The total weight of load P is composed of an unsprung part and a spring-loaded part according to the expression

$$P=P_1+P_2 \tag{5.22}$$

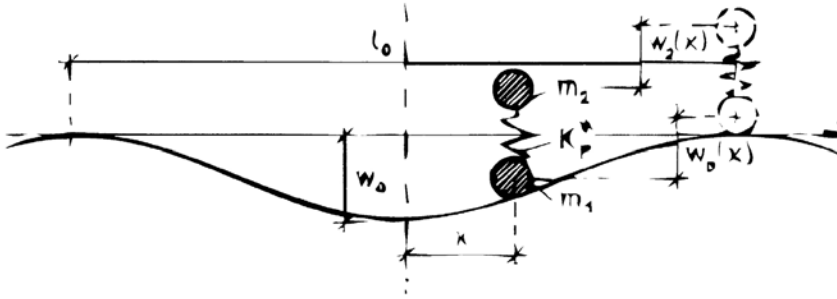

Fig. 5.15. Schematic diagram of unevenness and system of moving load.

where $P_1=m_1g$ is the weight of the unsprung part and $P_2=m_2g$ is the weight of the spring-loaded part. Both masses are connected by means of a complex spring constant K_P^* which characterizes the stiffness and damping of the connection.

The motion of the mass m_2 in a vertical direction is described by the differential equation

$$\frac{P_2}{g}\frac{\partial w_2(x,t)}{\partial t^2}+K_P^*[w_2(x,t)-w_0(x,t)]=0 \tag{5.23}$$

where $w_2(x, t)$ is the vertical displacement of spring-loaded mass m_2. Introducing the moving system of dimensionless coordinates (ξ, η) and the relationship

$$\frac{\partial^2 w_2}{\partial t^2}=\frac{v^2}{L^2}\frac{\partial w_2}{\partial \xi^2} \tag{5.24}$$

equation (5.23) is transformed into the relationship

$$\frac{\mathrm{d}^2 w_2}{\mathrm{d}\xi^2}+\frac{\Omega_0^2 L^2}{v^2}w_2=\frac{\Omega_0^2 L^2}{v^2}w_0(\xi) \tag{5.25}$$

if Ω_0 is given by the expression

$$\Omega_0=\sqrt{\frac{K_P^* g}{P_2}}. \tag{5.26}$$

The dynamic load component $R(\xi)$ evoked by the vertical motion of the spring-loaded part P_2 is determined by the expression

$$R(\xi)=K_P^*\ [w_2(\xi)-w_0(\xi)]\ \delta(\xi). \tag{5.27}$$

Using Fourier's integral transformation of equations (5.25) and (5.27) the following relationships are established:

$$^{F}R(\alpha) = K_P^*\left[^{F}\bar{w}_2(\alpha) - {}^{F}\bar{w}_0(\alpha)\right] \tag{5.28}$$

$$^{F}\bar{w}_2(\alpha) = \frac{\Omega_0^2 L^2}{v^2}\,\frac{1}{\left(\frac{\Omega_0^2 L^2}{v^2} - \alpha^2\right)}\,{}^{F}\bar{w}_0(\alpha) \tag{5.29}$$

where $^{F}\bar{w}_2(\alpha)$, $^{F}\bar{w}_0(\alpha)$ are transforms of the products $w_2(\xi)\delta(\xi)$ or $w_0(\xi)\delta(\xi)$.

Introducing equation (5.29) into equation (5.28) and rearranging the transform of the dynamic load component, $^{F}R(\alpha)$ is determined in the form

$$^{F}R(\alpha) = K_P^*\left[\frac{1}{1 - \frac{\alpha^2 v^2}{\Omega_0^2 L^2}} - 1\right]{}^{F}\bar{w}_0(\alpha). \tag{5.30}$$

The Fourier transform $^{F}\bar{w}_0(\alpha)$, assuming that the concentrated load used is divided on the line segment 20, is given by the relationship

$$^{F}\bar{w}_0(\alpha) = \frac{1}{2\pi}\,\frac{w_0}{2}\int_{-a}^{a}\left(1 + \cos\frac{2\pi\xi L}{l_0}\right)e^{i\alpha\xi}d\xi = \frac{w_0}{4\pi}\left\{\frac{2\sin\frac{\alpha a}{L}}{\alpha\frac{1}{L}} + \frac{1}{\frac{4\pi^2}{l_0^2} - \frac{\alpha^2}{L^2}}\right. \tag{5.31}$$

$$\left.\times\left[\frac{4\pi}{l_0}\,\sin\,\frac{2\pi a}{l_0}\,\cos\frac{\alpha a}{L} - \frac{2\alpha}{L}\,\cos\frac{2\pi a}{l_0}\,\sin\frac{\alpha a}{L}\right]\right\}.$$

Substituting this expression into equation (5.30) and rearranging the dynamic load component as Fourier's transform, $^{F}R(\alpha)$ has the form

$$^{F}R(\alpha) = K_P^*\,\frac{w_0}{4\pi}\left[\frac{1}{1 - \frac{\alpha^2 v^2}{\Omega_0^2 L^2}} - 1\right]\left\{\frac{\sin\frac{\alpha a}{L}}{\frac{\alpha a}{L}} + \frac{1}{\frac{4\pi^2 a^2}{l_0^2} - \frac{\alpha^2 a^2}{L^2}}\right. \tag{5.32}$$

$$\left.\times\left[\frac{2\pi a}{l_0}\,\sin\frac{2\pi a}{l_0}\,\cos\frac{\alpha a}{L} - \frac{\alpha a}{L}\,\cos\frac{2\pi a}{l_o}\,\sin\frac{\alpha a}{L}\right]\right\}.$$

At the same time the spring constant was introduced with the value $K_p^*/2a$ with regard to the assumption of a divided concentrated load on the line segment 2*a*.

The right side of equation (5.6) is determined by total expression of the Fourier's transform in the form

$$\frac{\delta(\eta_1)}{D^*}\left\{\frac{P}{2\pi}\frac{\sin\frac{\alpha a}{L}}{\frac{\alpha a}{L}}+\frac{P_1\pi w_0 v^2}{gl_0^2}\frac{1}{\frac{4\pi^2a^2}{l_0^2}-\frac{\alpha^2a^2}{L^2}}\left(\frac{2\pi a}{l_0}\sin\frac{2\pi a}{l_0}\cos\frac{\alpha a}{L}\right.\right.$$
$$\left.\left.-\frac{\alpha a}{L}\cos\frac{2\pi a}{l_0}\sin\frac{\alpha a}{L}\right)+{}^{\mathrm{F}}R(\alpha)\right\} \tag{5.33}$$

5.4.3 Influence of isolated surfacing unevenness by a moving load system with two degrees of freedom

The influence of repeated surface unevennesses studied in previous sections does not complicate the solution of moving-load problems from the point of view of an applied algorithm. It is manifested only in a more complicated form of the right side of the differential equation of motion. Of course the assumption of regular repeated unevennesses on the track surface has too high a measure of determinism, which is demonstrated by excessively high unreal values of the state vector quantities at moving speed v, when the resonance vibration of springloaded mass m_2 is setting in.

More realistic behaviour is obtained by analysis of the effect of isolated surfacing unevenness. Of course this problems is more complicated, and its solution requires a lot of computer time.

We assume the isolated unevenness of track surfacing in the form

$$w_0(\xi)=\frac{w_0}{2}\left(1+\cos 2\pi\xi\frac{L}{l_0}\right)$$
$$-\frac{l_0}{2L}<\xi<\frac{l_0}{2L}. \tag{5.34}$$

Using the expansion of the function in the Fourier series it follows that

$$w_0(\xi)=\frac{a_0}{2}+\sum_{k=1,2,\ldots}a_k\cos\frac{k2\pi\xi L}{\lambda_0} \tag{5.35}$$

if

$$a_k=\frac{4L}{\lambda_0}\int_0^{\lambda_0/2L}w_0(\xi)\cos\frac{k2\pi\xi L}{\lambda_0}\mathrm{d}\xi,\quad k=0,1,2,\ldots \tag{5.36}$$

and λ_0/L is dimensionless length period. This ratio λ_0/L has to be chosen at a sufficiently high value for the resulting effect to correspond to isolated unevenness.

According to equation (5.36), by using (5.34) we obtain

$$a_0 = w_0 \frac{l_0}{\lambda_0} \tag{5.37}$$

$$a_k = \frac{w_0 l_0}{\lambda_0} \left\{ \frac{\sin k\pi l_0/\lambda_0}{k\pi l_0/\lambda_0} + \frac{1}{2} \left[\frac{\sin \pi(1 + kl_0/\lambda_0)}{\pi(1 + kl_0/\lambda_0)} + \frac{\sin \pi(1 - kl_0/\lambda_0)}{\pi(1 - kl_0/\lambda_0)} \right] \right\}. \tag{5.38}$$

The basic zero member of the series for k=0 is determined in the form

$$w_{0,0}(\alpha\xi) = \frac{a_0}{2} = \frac{w_0}{2} \frac{l_0}{\lambda_0}. \tag{5.39}$$

The dynamic load component arising from the vertical motion of the spring-loaded mass m_2 can be derived for k=0 in the form of a Fourier transform

$${}^{F}R_0(\alpha) = K_P^* \frac{w_0}{4\pi} \frac{l_0}{\lambda_0} \left[\frac{1}{1 - \frac{\alpha^2 v^2}{\Omega_0^2 L^2}} - 1 \right] \frac{\sin \frac{\alpha a}{L}}{\frac{\alpha a}{L}} \tag{5.40}$$

The universal k-member of the series has the form

$$w_{0,k}(\xi) = a_k \cos \frac{k2\pi\xi L}{\lambda_0}. \tag{5.41}$$

The contribution of the unsprung part of the load system to the righthand side of differential equation (5.4) is expressed for k=1, 2, 3,…in the form

$$\frac{\delta(\xi)\, \delta(\eta_1)}{D^*} \frac{P_1}{g} v^2 a_k \frac{k^2 4\pi^2}{\lambda_0^2} \cos \frac{k2\pi\xi L}{\lambda_0} \tag{5.42}$$

and, by applying Fourier's integral transformation, in the form

$$\frac{\delta(\eta_1)}{D^*} \frac{P_1}{g} \frac{2\pi k^2 v^2}{\lambda_0^2} a_k \frac{1}{\frac{4\pi^2 k^2 a^2}{\lambda_0^2} - \frac{\alpha^2 a^2}{L^2}} \left(\frac{2\pi ka}{\lambda_0} \sin \frac{2\pi ka}{\lambda_0} \cos \frac{\alpha a}{L} - \frac{\alpha a}{L} \cos \frac{2\pi ka}{\lambda_0} \sin \frac{\alpha a}{L} \right). \tag{5.43}$$

The contribution of the spring-loaded part of the load system, applying a similar procedure to that in section 5.4.2, leads to the transform of dynamic load component ${}^{F}R_k(\alpha)$ in the form

$$
{}^{F}R_k(\alpha) = K_P^* \frac{a_k}{2\pi} \left[\frac{1}{1 - \frac{\alpha^2 v^2}{\Omega_0^2 L^2}} - 1 \right] \frac{1}{\frac{4\pi^2 k^2 a^2}{\lambda_0^2} - \frac{\alpha^2 a^2}{L^2}}
$$

$$
\times \left(\frac{2\pi k a}{\lambda_0} \sin \frac{2\pi k a}{\lambda_0} \cos \frac{\alpha a}{L} - \frac{\alpha a}{L} \cos \frac{2\pi k a}{\lambda_0} \sin \frac{\alpha a}{L} \right). \tag{5.44}
$$

Together, the right-hand side of differential equation (5.6) is determined by the total expression for the Fourier transform in the form

$$
\frac{\delta(\eta_1)}{D^*} \left\{ \frac{P}{2\pi} \frac{\sin \frac{\alpha a}{L}}{\frac{\alpha a}{L}} + K_P^* \frac{w_0}{4\pi} \frac{l_0}{\lambda_0} \left(\frac{1}{1 - \frac{\alpha^2 v^2}{\Omega_0^2 L^2}} - 1 \right) \frac{\sin \frac{\alpha a}{L}}{\frac{\alpha a}{L}} \right.
$$

$$
+ \sum_{k=1,2,3,\ldots} \left[\frac{P_1}{g} \frac{2\pi k^2 v^2}{\lambda_0^2} + \frac{K_P^*}{2\pi} \left(\frac{1}{1 - \frac{\alpha^2 v^2}{\Omega_0^2 L^2}} - 1 \right) \right] \frac{a_k}{\frac{4\pi^2 k^2 a^2}{\lambda_0^2} - \frac{\alpha^2 a^2}{L^2}} \tag{5.45}
$$

$$
\left. \times \left(\frac{2\pi k a}{\lambda_0} \sin \frac{2\pi k a}{\lambda_0} \cos \frac{\alpha a}{L} - \frac{\alpha a}{L} \cos \frac{2\pi k a}{\lambda_0} \sin \frac{\alpha a}{L} \right) \right.
$$

As can be seen from the composition of equation (5.45) it is necessary to solve the problem for a single member of the Fourier series and then superimpose the results.

5.4.4 Numerical results

The numerical solution was performed for the equivalent half-plate on unbounded subgrade, which corresponds to a rigid pavement structure with the same input characteristics as in previous sections. The load system moved along the border of the half-plate, i.e. on the track η_1=0, with moving speed v.

Isolated unevenness is assumed on the track. The characteristics of the unevenness are given by the ratios

$$
\frac{c_2^2 w_0}{g l_0^2} = 1\,254
$$

$$
\frac{a}{l_0} = 0.116
$$

$$
\frac{l_0}{\lambda_0} = 0.04
$$

and the characteristics of the load system by the ratios

$$\frac{P_1}{P} = 0.1$$

$$\frac{\Omega_0 a}{c_2} = 0.002(1 + 0.1i)$$

The state vector components, namely the dimensionless deflection *wGL/P,* the subgrade reaction qL^2/P and bending moment M_x/P, were computed for boundary point η=0 and various speeds of load motion.

The results of the solution obtained by considering 60 members of the Fourier series are plotted as functions of coordinate ξ in Fig. 5.16 for *wGL/P,* in Fig. 5.17 for qL^2/P and in Fig. 5.18 for bending moment M_x/P. The ascertained differences of the computed values for k=60 and k=50 did not exceed 1.5%.

It can be seen from the curves of the computed state vector components that the influence of unevenness is manifested in an increase of the values with increased dimensionless load speeds $C_p=v/c_2$. These increments of the computed state vector component values have already set in for relatively low speeds.

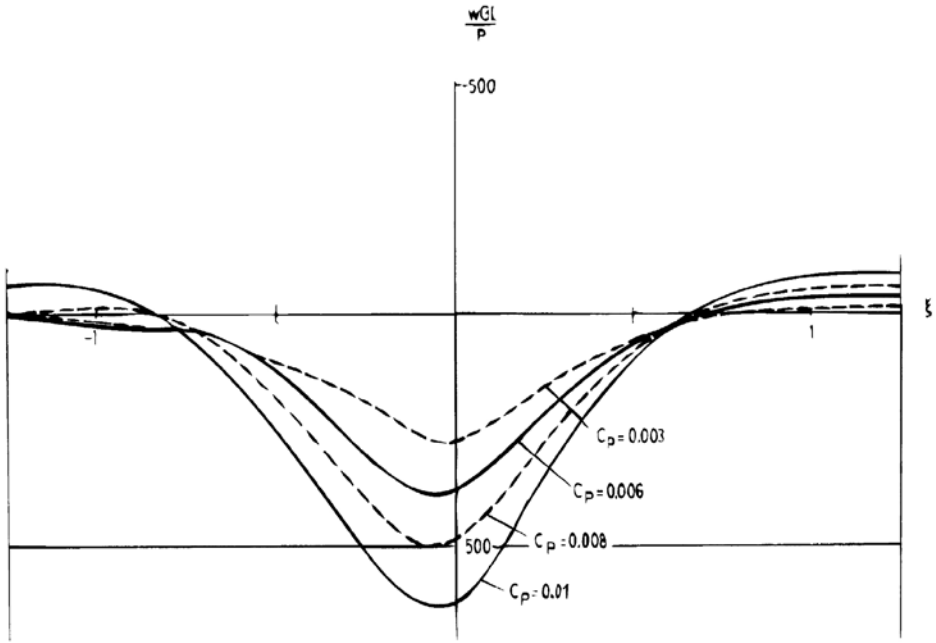

Fig. 5.16. Influence of isolated unevenness on dimensionless deflection *wGL/P* for various speed values C_p in rigid pavement.

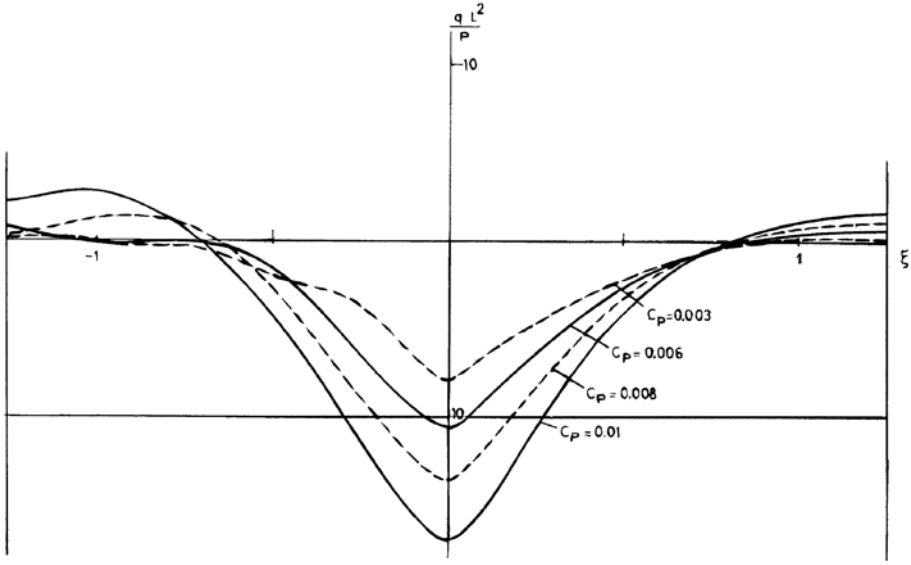

Fig. 5.17. Influence of isolated unevenness on dimensionless subgrade reaction qL^2/P for various speed values C_p in rigid pavement.

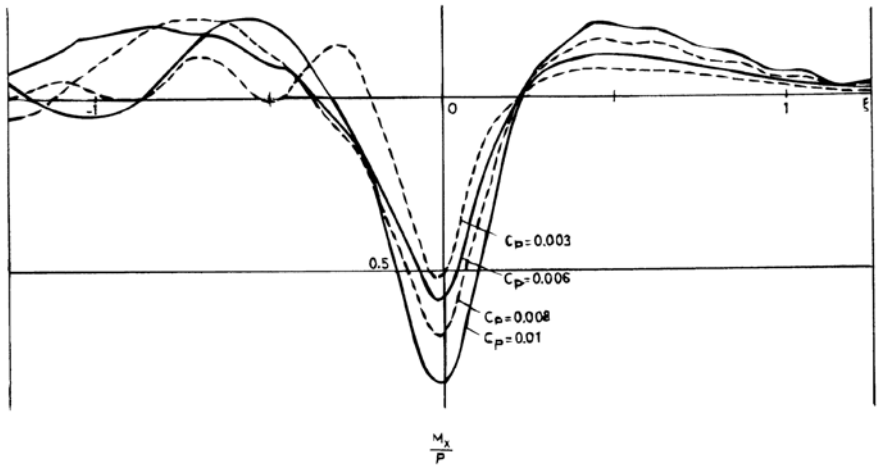

Fig. 5.18. Influence of isolated unevenness on dimensionless bending moment M_x/P for various speed values C_p in rigid pavement.

The dynamic coefficients ϑ, considered as the ratios of the dynamic values to the values that correspond to zero speed, are plotted in Fig. 5.19. There are variations of ϑ with the load speed C_p, and the dynamic effect increases with increasing C_p. Such a result is

connected of course to the assumption considered in the theoretical solution, that during the motion the load system follows the given track of unevenness. In practice the influence of motion inertia in the horizontal plane gives rise to contact interruption between the moving load system and the initial part of the track unevenness at higher load speeds. This phenomenon leads to a decrease of load forces and so to a decrease in the values of dynamic behaviour.

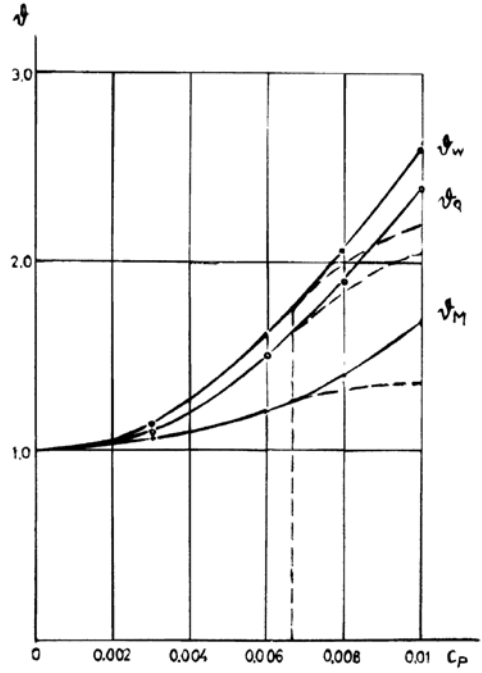

Fig. 5.19. Influence of isolated unevenness on dynamic coefficients ϑ versus speed factor C_P

The approximate determination of the speed limit value for a moving load system in the case of contact interruption with unevenness gives the relationship

$$w_0\,(l_0/4) = \frac{gT^2}{2} = \frac{gl_0^2}{2.16v^2} \tag{5.46}$$

in which it is assumed that the contact interruption is at the length $l_0/4$. In the numerical solution the characteristics of unevenness were considered by the values w_0=0.02 m and l_0=3.0 m and then the speed limit of moving load according to (5.46) is given as $v = \sqrt{9.81 \times 9/32 \times 0.01} = 16.7$ m/s ≈ 60 km/h.

This value corresponds to the dimensionless ratio $C_p=v/c_2$=16.7/2350–0.0067.

The probable curves of the decreased dynamic effects at higher moving speeds are indicated by the broken lines in Fig. 5.18.

The effect of surface unevenness for a moving load may be supported by evidence using the results of experiments on rigid cement concrete pavements [5.2]. The measured dynamic deflections versus moving speeds are reproduced in Fig. 5.20. We can see that after an initial quadratic increase of the dynamic effects the curve stars to flatten from vehicle speeds $v \approx 9$ m/s, i.e. 32.5 km/h, and attains the maximum value of dynamic coefficient $\vartheta_w \approx 2.0$.

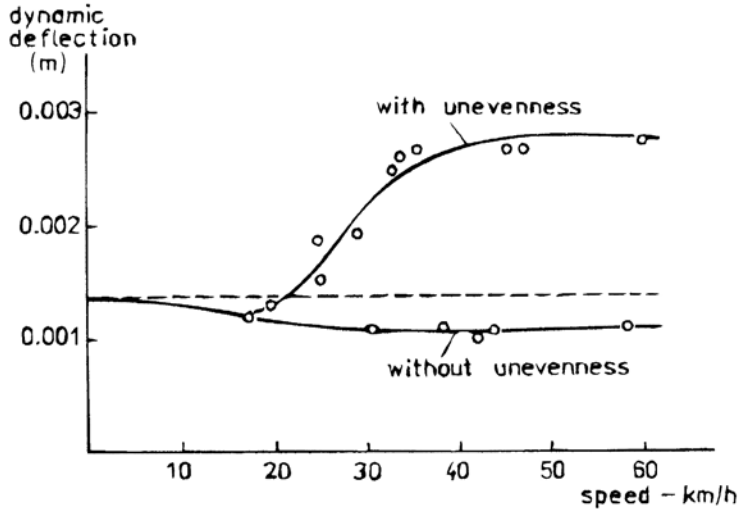

Fig. 5.20. Effect of surface unevenness under moving load according to [5.2].

5.5 Effect of moving random load

The deterministic solutions of the preceding sections enable us to determine and evaluate the effect of surface unevennesses during vehicle traverse on the dynamic values of state vector components.

They suggest that this influence is real for contemporary vehicles speeds, and provide the opportunity to evaluate quantitatively the effect of unevennesses corresponding to given parameters.

The unevennesses of track surfacing are of course random in character. As a consequence of this the moving load is also random in character, and its effect on the system is manifested as a random dynamic response. Therefore it is necessary to solve the problems of moving loads on the basis of the statistical methods of structural mechanics.

The solutions of the effect of a dynamic random moving load on a beam are indicated in [5.3], [5.4], [5.1] and elsewhere. The method of decomposition into the natural modes of vibration of the load and deflection is usually used, and often the spectral method of the stationary random process.

Let us attempt to solve our problem of the equivalent half-plate on unbounded subgrade under a random load moving along a track parallel to the free half-plate boundary.

We shall assume the external load $p(x-vt, y, t)$ as a non-stationary process with the mean (deterministic) value $E[p(x-vt, y, t)]$ and centred (random) value $\mathring{p}(x-vt, y, t)$ in the form

$$p(x-vt, y, t) = E[p(x-vt, y, t)] + \mathring{p}(x-vt, y, t). \tag{5.47}$$

For a concentrated moving load the expression is valid as follows (Fig.5.21)

$$p(x-vt, y, t)=\delta(x-vt)\,\delta(y_1)\,P(t) \tag{5.48}$$

where

$$P(t)=P+\mathring{P}(t). \tag{5.49}$$

The load $P(t)$ has the mean constant value

$$E[P(t)]=P \tag{5.50}$$

and $\mathring{P}(t)$ a random function of the time.

In the dimensionless coordinates of a moving coordinates system equation (5.48) has the form

$$p(\xi, \eta_1, t)=\delta(\xi)\delta(\eta_1). \tag{5.51}$$

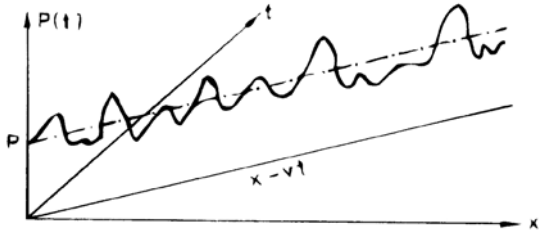

Fig. 5.21. Schematic diagram of random moving load.

The effect of loading by mean value

$$E[p(\xi, \eta_1, t)]=\delta(\xi)\,\delta(\eta_1)\,P \tag{5.52}$$

corresponds to the deterministic solution of section 5.2. The effect of the centred stochastic part of the load in the form

$$\mathring{p}(\xi, \eta_1, t) = \delta(\xi)\,\delta(\eta_1)\,\mathring{P}(t) \tag{5.53}$$

may be solved using the covariance function and corresponding power spectral densities, assuming a stationary stochastic load.

We assume the known covariance $C_p(\tau)$ and corresponding power spectral density $S_p(\omega)$ for the stationary stochastic load which are connected by the known relationships

$$C_{\mathrm{P}}(\tau) = \int_0^\infty S_{\mathrm{P}}(\omega)\ \cos\ \omega\tau \mathrm{d}\omega \tag{5.54}$$

and

$$S_{\mathrm{P}}(\omega) = \frac{2}{\pi}\int_0^\infty C_{\mathrm{P}}(\tau)\ \cos\omega\tau \mathrm{d}\tau. \tag{5.55}$$

It is necessary to determine the frequency characteristics (functions of the system response) $F(\mathrm{i}\omega)$ for state vector components at the arbitrary point of the system under a moving concentrated load acting at the point (ξ, η_1), which is a harmonic variable with the angular frequency ω.

The solution of the basic differential equation of motion (4.1) is supposed in the form

$$w(x, y, t)=w(x-vt, y)\mathrm{e}^{\mathrm{i}\omega t}. \tag{5.56}$$

Introducing the dimensionless moving coordinates system

$$\xi = \frac{1}{L}(x - vt) \quad , \quad \eta = \frac{y}{L}$$

the equation is obtained in the form

$$\begin{aligned}\frac{\partial^2 w}{\partial t^2} &= \frac{\partial^2 w}{\partial \xi^2}\ \frac{v^2}{L^2}\ \mathrm{e}^{\mathrm{i}\omega t} - 2\frac{v}{L}\ \mathrm{i}\omega\frac{\partial w}{\partial \xi}\ \mathrm{e}^{\mathrm{i}\omega t} - w(\xi,\eta)\omega^2\mathrm{e}^{\mathrm{i}\omega t} \\ &= \left(\frac{v^2}{L^2}\ \frac{\partial^2 w}{\partial \xi^2} - \frac{2v}{L}\mathrm{i}\omega\frac{\partial w}{\partial \xi} - \omega^2 w\right)\mathrm{e}^{\mathrm{i}\omega t}\end{aligned} \tag{5.57}$$

and the differential equation is established as follows

$$\begin{aligned}&\left(\frac{\partial^2}{\partial \xi^2} + \frac{\partial^2}{\partial \eta^2}\right)^2 w(\xi,\eta) - \frac{K_2^* L^2}{D^*}\left(\frac{\partial^2}{\partial \xi^2} + \frac{\partial^2}{\partial \eta^2}\right) w(\xi,\eta) + \frac{K_1^* L^4}{D^*} w(\xi,\eta) \\ &+ \frac{k_d \varrho h}{D^*}\left(v^2 L^2 \frac{\partial^2 w}{\partial \xi^2} - 2v\mathrm{i}\omega L^3 \frac{\partial w}{\partial \xi} - \omega^2 L^4 w\right) = \delta(\xi)\ \delta(\eta_1)\frac{L^4}{D^*} P.\end{aligned} \tag{5.58}$$

Using Fourier's integral transformation in the form (5.5) the ordinary differential equation for Fourier's transforms of deflection ${}^{\mathrm{F}}w(\alpha, \eta)$ is obtained in the form

$$\left[\frac{\mathrm{d}^4}{\mathrm{d}\eta^4}-\frac{\mathrm{d}^2}{\mathrm{d}\eta^2}\left(2\alpha^2+\frac{K_2^* L^2}{D^*}\right)+\alpha^4+\alpha^2\frac{K_2^* L^2}{D^*}+\frac{K_1^* L^4}{D^*}-\frac{k_d \varrho h}{D^*}\right.$$

$$\left.\times(v^2\alpha^2 L^2-2v\alpha\omega L^3+\omega^2 L^4)\right]\,{}^{\mathrm{F}}w(\alpha,\eta)=\delta(\eta_1)\,\frac{PL^4}{2\pi D^*}\,\frac{\sin\frac{\alpha a}{L}}{\frac{\alpha a}{L}} \tag{5.59}$$

if at the same time the concentrated load is considered as distributed in direction ξ on the line segment $2a/L$.

The solution continues in a similar way to that in section 5.2, unlike the relationships for γ_1^2 **and** γ_2^2, which now have the form

$$\gamma_1^2=\alpha^2+\frac{K_2^* L^2}{2D^*}+\left[\frac{K_2^{*2} L^4}{4D^{*2}}-\frac{K_1 L^4}{D^*}+\frac{k_d \varrho h}{D^*}\left(v\alpha L-\omega L^2\right)^2\right]^{1/2} \tag{5.60}$$

$$\gamma_2^2=\alpha^2+\frac{K_2^* L^2}{2D^*}-\left[\frac{K_2^{*2} L^4}{4D^{*2}}-\frac{K_1^* L^4}{D^*}+\frac{k_d \varrho h}{D^*}(v\alpha L-\omega L^2)^2\right]^{1/2} \tag{5.61}$$

and similarly

$$\gamma_z^2=\frac{K_1^* L^2}{K_2^*}+\alpha^2-\frac{\varrho_z K_3(v\alpha-\omega L)^2}{K_2^*}. \tag{5.62}$$

The computation $F(i\omega)$ for the state vector components has to be performed for the constant value of moving speed v and various frequencies ω.

The spectral density of the corresponding state vector component $S_s(\omega)$ is given by the formula

$$S_s(\omega)=|F(i\omega)|^2 S_{\mathrm{p}}(\omega) \tag{5.63}$$

and the variance σ_{s}^2 is determined by the relationship

$$\sigma_{\mathrm{s}}^2=\int_0^\infty S_{\mathrm{s}}(\omega)\mathrm{d}\omega. \tag{5.64}$$

The standard deviation σ_s, referring to the value of the deterministic solution under the mean moving load corresponds to the coefficient of variation V_s.

The dynamic response of the system under a moving load is a non-stationary stochastic process, even though a stationary stochastic load was considered. The statistical characteristics of the system response are functions of the position and the time.

5.5.1 Numerical results

A numerical study was performed for the equivalent half-plate on subgrade, which corresponds to the rigid highway cement concrete pavement with input characteristics given in previous chapters.

Assuming the exponential covariance of the random load $\mathring{P}(t)$ in the form

$$C_{\mathrm{P}}(\tau) = \sigma_{\mathrm{P}}^2 \mathrm{e}^{-\omega_{\mathrm{g}}|\tau|} \tag{5.65}$$

the power spectral density according to (5.55) is given by the relationship

$$S_{\mathrm{P}}(\omega) = \sigma_{\mathrm{P}}^2 \frac{2\omega_{\mathrm{g}}}{\pi} / (\omega^2 + \omega_{\mathrm{g}}^2). \tag{5.66}$$

The variance of the load, σ_{P}^2, may be determined using the variance of the vehicle acceleration which is, according to [5.4], the product of the parameter of global dynamic vehicle transfer *I,* the parameter *C* as a measure of surface irregularities, and the vehicle speed *v*. It is expressed by the formula

$$\sigma_{\mathrm{P}}^2 = M^2 ICv. \tag{5.67}$$

The variance of the acceleration of the vehicle, *ICv*, is evaluated according to [5.4] by six degrees. For the first degree *ICv* does not exceed the value 0.5 m^2/s^4 and for the sixth degree *ICv* is higher than 10 m^2/s^4.

Numerical solutions, performed according to equations (5.63) and (5.64), assuming the covariance functions of the load according to (5.65) give for a rigid pavement structure the results plotted in Figs. 5.22–5.24 in terms of the ratio of the coefficients of variation V_s/V_P versus dimensionless load moving speed $C_P=v/c_2$ (c_2 is the velocity of shear waves in a cement concrete medium). In each case the motion of the load was considered on the track parallel to the pavement border at distance $\eta_1=0.01$.

The results in Fig. 5.22 correspond to the position and time given by coordinates $\xi=0.01$, $\eta=0.01$. The curves of the comparative coefficients of variation V_s/V_P for deflection *w*,

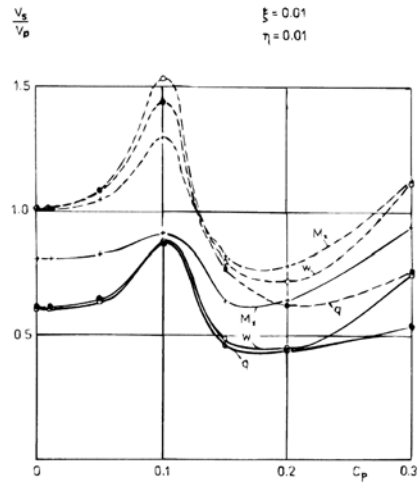

Fig. 5.22. Relationship of the coefficients of variation to speed factor C_P for state vector components of pavement.

subgrade reaction q and bending moment M_x are evaluated assuming (a) exponential covariance functions with dimensionless frequency $\beta_g=\omega_g h/c_2=0.1$ (full lines), and (b) constant covariance, i.e. $\beta_g=0$ (broken lines). The curves display maxima near the speed $C_p=0.1$ then, after decreasing, minima at speeds around $C_p=0.15$–0.22. In the region of real vehicle speeds the coefficient of variation of given state quantities V_s is practically the same as or lower than the coefficient of variation V_p. Assuming a constant covariance function ($\beta_g=0$), the ratio V_s/V_p is $V_s/V_p\approx1$, whereas for $\beta_g=0.1$ $V_s/V_p\approx0.6$ for w and q or $V_s/V_p\approx0.8$ for M_x.

The results Fig. 5.23 are similar but they correspond to the coordinates $\xi=-0.2$, $\eta=0.01$ and to the state vector components w, q and M_{xy}.

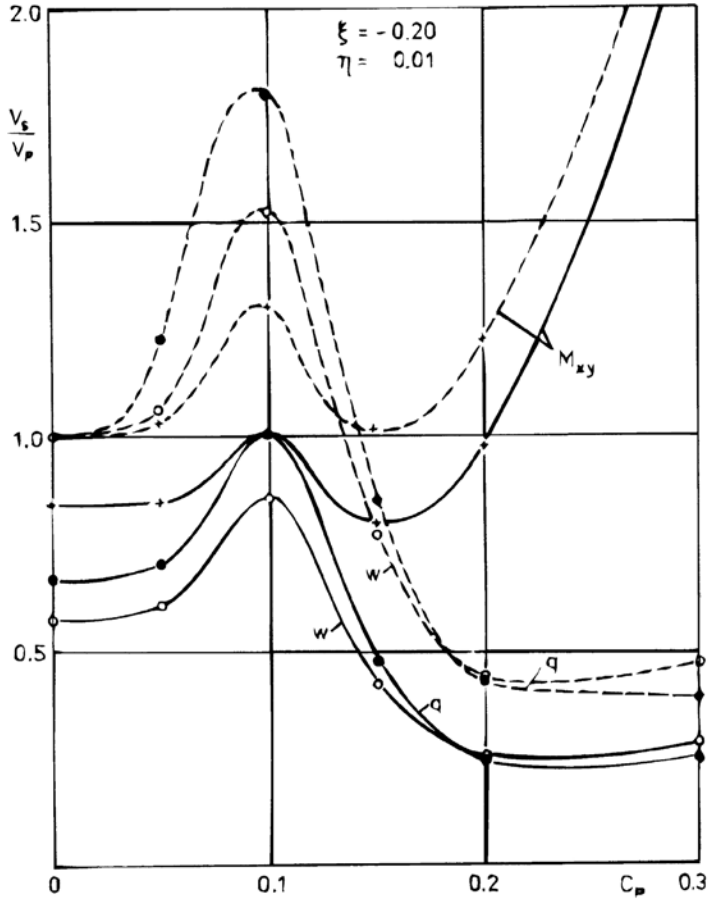

Fig. 5.23. Relationship of the coefficients of variation to speed factor C_p for state vector components of pavement.

The results in Fig. 5.24 correspond to the coordinates $\xi=0.1$, $\eta=0.01$ and show the variations of V_s/V_p for transverse force Q_x and twisting moment M_{xy}.

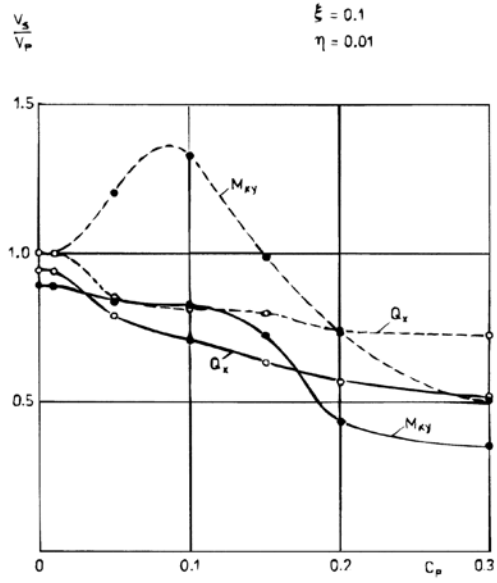

Fig. 5.24. Relationship of the coefficients of variation to speed factor C_p for state vector components of pavement.

The general conclusion following from the numerical solutions is that the dynamic response for the significant state vector components under a moving random load has statistical characteristics that for real vehicle speeds do not exceed the statistical characteristics of the load. From the practical point of view it is possible to consider for the decisive state vector components of the pavement the same values of the coefficients of variation as are supposed for random loads.

6
DYNAMIC RESPONSE OF PLATES WITH FREE BOUNDARIES ON UNBOUNDED SOIL BASE

At present the state of stresses and deformations for layered pavement structures is analysed on the basis of the static load of an unbounded system. The characteristic effects of dynamic loads on the equivalent plates on subgrade have been summarized in previous chapters. The object of this chapter is to draw attention to the differences between the dynamic response of bounded and unbounded pavement systems.

The method of boundary integral equations, which in the past was widely used for static solutions of plates [6.1–6.5] is also convenient for the solution of the dynamic forced vibration of a plate on subgrade. The solution using boundary elements can be applied if the dynamic fundamental solution is available.

6.1 Fundamental solutions for plate and subgrade

Using the theory of a thin plate and the dynamic simplified model of the subgrade the differential motion equation has the form

$$\nabla^2\nabla^2 w - \frac{K_2^*}{D^*}\,\nabla^2 w + \frac{K_1^*}{D^*} w + \frac{\varrho h}{D^*}\,\frac{\partial^2 w}{\partial t^2} + \frac{\varrho_0 K_3}{D^*}\,\frac{\partial^2 w}{\partial t^2} = \frac{p}{D^*}\,\mathrm{e}^{\mathrm{i}\omega t}. \tag{6.1}$$

This equation was analysed in section 3.4.8. The inertia forces of the equivalent plate and subgrade can be expressed by using the coefficient of mass increase of the plate k_d in the form

$$\frac{\varrho h}{D^*}\,\frac{\partial^2 w}{\partial t^2} + \frac{\varrho_0 K_3}{D^*}\,\frac{\partial^2 w}{\partial t^2} = \frac{k_d \varrho h}{D^*}\,\frac{\partial^2 w}{\partial t^2}. \tag{6.2}$$

If it is required to fulfil the exact form of the dispersion curve for flexural stress waves as determined by the more exact theory of a plate under the influence of shear and rotation inertia, it is possible to use the plate constant D^* in the form

$$D^* = Gh^3(1+\mathrm{i}\delta)\left[\frac{2\left(\frac{1}{1-\mu}+\frac{\kappa}{2}\right)\beta - \sqrt{4\left(\frac{1}{1-\mu}+\frac{\kappa}{2}\right)^2\beta^2 - \frac{8\kappa}{1-\mu}(\beta^2-12\kappa)}}{2(\beta^2-12\kappa)}\right]^2 \tag{6.3}$$

where $\beta=\omega h/c_2$ is the dimensionless frequency and $\kappa=(0.87+1.12\mu)^2/(1+\mu)^2$.

The function of dynamic deflection for the loading of an unbounded plate on subgrade by a harmonic unit concentrated force, i.e. the fundamental solution, Green's function, has the form

$$G(r,t) = \frac{-e^{i\omega t}3(1-\mu^2)i}{2Eh\Theta(1+i\delta)}\left[H_0^{(2)}(\gamma_1 r) - H_0^{(2)}(\gamma_2 r)\right] \tag{6.4}$$

where γ_1, γ_2, Ψ, Θ are given by

$$\gamma_{10}^2 = \gamma_1^2 h^2 = \Psi + \Theta, \quad \gamma_{20}^2 = \gamma_2^2 h^2 = \Psi - \Theta \tag{6.5}$$

$$\Psi = -\frac{K_2^* h^2}{2D^*} \tag{6.6}$$

$$\Theta = \sqrt{\left[\Psi^2 - \frac{K_1^* h^4}{D^*} + \frac{G\beta^2 h^3}{D^*} + \frac{G_0\beta_0^2 K_3 h^2}{D^*}\right]} \tag{6.7}$$

if the dimensionless frequencies are

$$\beta = \frac{\omega h}{c_2} = \frac{\omega h}{\sqrt{G/\varrho}}, \quad \beta_0 = \frac{\omega h}{\sqrt{G_0/\varrho}} \tag{6.8}$$

$H_0^{(2)}$ are Hankel's functions of the complex arguments $\gamma_1 r$, $\gamma_2 r$ with positive real part and negative imaginary part. In the case where the imaginary parts of arguments $\gamma_1 r$, $\gamma_2 r$ are positive, it is necessary to replace functions $H_0^{(2)}$ with functions $H_0^{(1)}$ in connection with the physical reality of the solution.

The soil base defined by the dynamic simplified model (section 3.4.1) described by the differential equation

$$K_2^* \nabla^2 w_0 - K_1^* w_0 - \varrho_0 K_3 \frac{\partial^2 w_0}{\partial t^2} = -\frac{\delta(r)}{2\pi r} e^{i\omega t} \tag{6.9}$$

where w_0 is a deflection of the subgrade and $\delta(r)$ is Dirac's generalized function, which is assumed to be a concentrated harmonic variable force acting on the surface of the subgrade.

Using Hankel's integral transformation we obtain the transform of Green's function ${}^{H}w_0$ in the form

$${}^{H}w_0(\alpha,t) = -\frac{e^{i\omega t}}{2\pi K_2^*} \frac{1}{\left(-\alpha^2 - \frac{K_1^*}{K_2^*} + \frac{\omega^2}{c_{R,0}^2}\right)} \tag{6.10}$$

where α is an integral parameter of Hankel's transformation and

$$c_{R,0}^{*2} = \frac{K_2^*}{\varrho_0 K_3}. \tag{6.11}$$

The original of the Green's function $w_0(r, t)$ is defined by relation

$$w_0(r,t) = \frac{e^{i\omega t}}{2\pi K_2^*} \int_0^\infty \frac{\alpha J_0(\alpha, r)}{\alpha^2 + \frac{K_1^*}{K_2^*} - \frac{\omega^2}{c_{R,0}^{*2}}} d\alpha. \tag{6.12}$$

Bessel's function $J_0(\alpha r)$ can be expressed by [1.18]

$$J_0(\alpha r) = -\frac{i}{\pi} \int_0^\infty \left(e^{i\alpha r \cosh v} - e^{-i\alpha r \cosh v}\right) dv. \tag{6.13}$$

Substituting into equation (6.12), the deflection after adjustment will have the form

$$w_0(r,t) = \frac{ie^{i\omega t}}{2\pi^2 K_2^*} \int_0^\infty dv \int_{-\infty}^\infty \frac{\alpha e^{-i\alpha r \cosh v}}{\alpha^2 + \frac{K_1^*}{K_2^*} - \frac{\omega^2}{c_{R,0}^{*2}}} d\alpha. \tag{6.14}$$

Using the method of residues in a lower complex half-plane the unproper internal integral gives the relation

$$\int_{-\infty}^\infty \frac{\alpha e^{-i\alpha r \cosh v}}{\alpha^2 + \frac{K_1^*}{K_2^*} - \frac{\omega^2}{c_{R,0}^{*2}}} d\alpha = -\pi i e^{-i\alpha_1 r \cosh v} \tag{6.15}$$

in which

$$\alpha_1 = \pm \sqrt{\frac{\omega^2}{c_{R,0}^{*2}} - \frac{K_1^*}{K_2^*}} \tag{6.16}$$

is a pole in the lower complex half-plane.

The validity of the relation [1.18]

$$\frac{2i}{\pi} \int_0^\infty e^{-i\alpha_1 r \cosh v} dv = H_0^{(2)}(\alpha_1 r) \tag{6.17}$$

where $H_0^{(2)}(\alpha_1 r)$ is Hankel's function of the second kind with complex argument, gives the Green's function $G_0(r, t)$ in the form

$$w_0(r,t) = G_0(r,t) = \frac{-e^{i\omega t_i}}{4K_2^*} H_0^{(2)}(\alpha_1 r). \tag{6.18}$$

6.2 Boundary integral formulation according to theorem of reciprocity

We assume that the plate occupies a region S with total boundary Γ on the unbounded subgrade S_0. The radius vector of the load point $\vec{\xi}$, of the unit force $\vec{r}$ and boundary point $\vec{\eta}$ are denoted in Fig. 6.1. We consider the bending moments M_{nn}, twisting moments M_{nt} and shear forces Q_n at the plate boundary. Because of thin plate theory it is necessary to consider the equivalent shear forces $H_n = Q_n + \partial M_{nt}/\partial t$.

Boundary integral formulations are obtained using the Rayleigh theorem of reciprocity. According to the theorem, in the case of a dynamic stationary task the virtual work of the system forces under unit concentrated force on deformations evoked by system load p is equal to the virtual work of system forces under load p on deformations evoked by unit concentrated force.

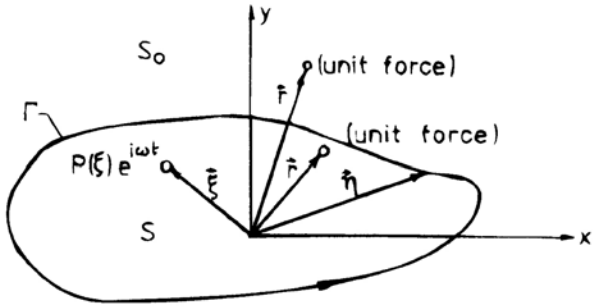

Fig. 6.1. Schematic diagram of the system and radius vectors.

Boundary integral formulations for the plate on subgrade have the form

$$\vartheta(\vec{r})\, w(\vec{r}) = \int_S p(\vec{\xi}) G(\varrho) \mathrm{d}S + \int_\Gamma \left[G(R)\, H_n(\vec{\eta}) - \frac{\partial G(R)}{\partial \vec{n}(\vec{\eta})} M_{nn}(\vec{\eta}) \right. \tag{6.19}$$

$$\left. - \hat{H}(R) w(\vec{\eta}) + \hat{M}_{nn}(R) \frac{\partial w(\vec{\eta})}{\partial \vec{n}(\vec{\eta})} \right] \mathrm{d}\Gamma + \sum_i (F_u G_u - \hat{F}_u w_u)_i$$

where

$$\vartheta(\vec{r}) = \begin{cases} 1 & \vec{r} \in S \\ 0 & \vec{r} \in (\Gamma \cup S) \end{cases}$$

and

$$R = |\vec{\eta} - \vec{r}| \quad ; \quad \varrho = |\vec{\xi} - \vec{r}|.$$

$\hat{H}_n$, $\hat{M}_{nn}$ are the equivalent shear forces and bending moments on the plate boundary under a unit concentrated load, and F_u $\hat{F}_u$, and w_u are corner forces and deflections under load p or a concentrated unit load.

The forces F_u, $\hat{F}_u$ arise at the corner points u of the plate boundary Γ (Fig. 6.2) because of the partial derivation of the twist moment in a tangential direction, and they are equal to the difference of twist moments $M_{nt(-)}-M_{nt(+)}$ at the corner point. The relationships have the form

$$F_u=(M_{nt(-)}-M_{nt(+)})_u$$

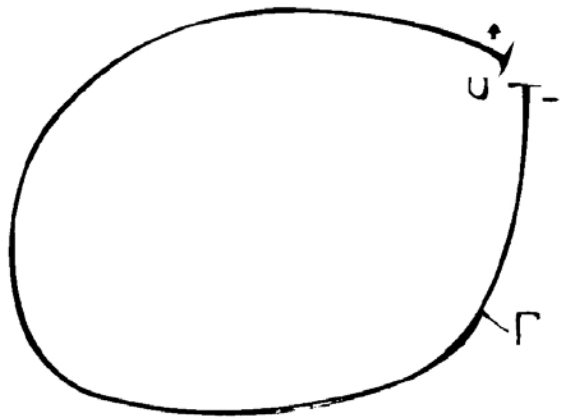

Fig. 6.2. Schematic diagram of the boundary corner point u.

$$\hat{F}_u = (\hat{M}_{nt(-)} - \hat{M}_{nt(+)})_u. \tag{6.21}$$

The integral formulation for soil base S_0 is given by the relationship

$$\vartheta(\vec{r})w_0(\vec{r}) = \int_{S_0} p_0(\vec{\xi})G_0(\varrho)\mathrm{d}S_0 + \int_{\Gamma} K_2\left[\frac{\partial w_0(\vec{\eta})}{\partial \vec{n}(\vec{\eta})}G_0(R)\right.$$

$$\left. - \frac{\partial G_0(R)}{\partial \vec{n}(\vec{\eta})}w_0(\vec{\eta})\right]\mathrm{d}\Gamma + \int_{\bar{\Gamma}} K_2^*\left[\frac{\partial w_0(\vec{\eta})}{\partial \vec{n}(\vec{\eta})}G_0(R) - \frac{\partial G_0(R)}{\partial \vec{n}(\vec{\eta})}w_0(\vec{\eta})\right]\mathrm{d}\bar{\Gamma} \tag{6.22}$$

if

$$\vartheta(\vec{r}) = \begin{cases} 1 & \vec{r} \in S_0 \\ 0 & \vec{r} \in (\Gamma \cup S_0) \end{cases} \tag{6.23}$$

and is $\bar{\Gamma}$ a fictitious circle boundary with its centre at the point of radius vector $\vec{\eta}$ and with radius *a,* which exceeds the boundary Γ.

6.2.1 Boundary conditions

The boundary conditions for the plate with free boundaries are given by

$$\begin{aligned} w(\vec{\eta}) &= w_0(\vec{\eta}) \\ M_{\mathrm{nn}}(\vec{n}) &= 0 \\ H_{\mathrm{n}}(\vec{\eta}) &= K_2^* \frac{\partial w_0(\vec{\eta})}{\partial \vec{n}(\vec{\eta})}. \end{aligned} \tag{6.24}$$

We assume equality of plate deflection and subgrade deflection on the plate boundary, no existence of bending moments, and the equality of the equivalent shear force of the system with the shear force of the subgrade $K_2^* \ \partial w_0(\vec{\eta})/\partial \vec{n}(\vec{\eta})$.

6.2.2 Integral formulations for an internal point of the plate and subgrade

Provided that the dynamic external load is acting on the plate surface, then using the boundary conditions the integral formulation for an internal point of the plate acquires the form

$$\begin{aligned} w(\vec{r}) = \int_S p(\vec{\xi}) G(\varrho) \mathrm{d}S + \int_\Gamma \Bigg[K_2^* G(R) \frac{\partial w_0(\vec{\eta})}{\partial \vec{n}(\vec{\eta})} - \hat{H}_{\mathrm{n}}(R)\, w(\vec{\eta}) \\ + \hat{M}_{\mathrm{nn}}(R) \frac{\partial w(\vec{\eta})}{\partial \vec{n}(\vec{\eta})} \Bigg] \mathrm{d}\Gamma + \sum_i (F_u G_u - \hat{F}_u w_u)_i \end{aligned} \tag{6.25}$$

and the integral formulation for the internal point of the subgrade is

$$\begin{aligned} w_0(\vec{r}) = \int_\Gamma K_2^* \left[\frac{\partial w_o(\vec{\eta})}{\partial \vec{n}(\vec{\eta})} G_0(R) - \frac{\partial G_0(R)}{\partial \vec{n}(\vec{\eta})} w(\vec{\eta}) \right] \mathrm{d}\Gamma \\ + \int_{\bar{\Gamma}} K_2^* \left[\frac{\partial w_0(\vec{\eta})}{\partial \vec{n}(\vec{\eta})} G_0(R) - \frac{\partial G_0(R)}{\partial \vec{n}(\vec{\eta})} w_0(\vec{\eta}) \right] \mathrm{d}\bar{\Gamma}. \end{aligned} \tag{6.26}$$

6.2.3 Boundary integral equations

By means of the limit transition on the boundary for $\vec{r} \to \vec{\zeta} \in \Gamma$ the boundary integral equation will be obtained from equation (6.25)

$$\frac{1}{2}\, w(\vec{\zeta}) - \int_{\Gamma} \left[K_2 G(R') \frac{\partial w_0(\vec{\eta})}{\partial \vec{n}(\vec{\eta})} - \hat{H}_{\mathrm{n}}(R') w(\vec{\eta}) + \to \hat{M}_{\mathrm{nn}}(R') \frac{\partial w(\vec{\eta})}{\partial \vec{n}(\vec{\eta})} \right] \mathrm{d}\Gamma$$

$$- \sum_{\mathrm{i}} (F_u G_u - \hat{F}_u w_u)_{\mathrm{i}} = \int_S p(\vec{\xi}) G(\varrho') \mathrm{d}S \tag{6.27}$$

in which the variable distances

$$R' = |\vec{\eta} - \vec{\zeta}|$$

$$\varrho' = |\vec{\xi} - \vec{\zeta}|. \tag{6.28}$$

Similarly, by means of the limit transition for $\vec{r} \to \vec{\zeta} \in \Gamma$ and limit transition for $a \to \infty$ of the circle boundary $\bar{\Gamma}$ the boundary integral equation is determined from equation (6.26)

$$\left(1 + \tfrac{1}{2}\right) w(\vec{\zeta}) - \int_{\Gamma} K_2^* \left[G_0(R') \frac{\partial w_0(\vec{\eta})}{\partial \vec{n}(\vec{\eta})} - \frac{\partial G_0(R')}{\partial \vec{n}(\vec{\eta})} w(\vec{\eta}) \right] \mathrm{d}\Gamma = 0. \tag{6.29}$$

Equation (6.29) reflects the reality that $G_0(R)$, $\partial G_0(R')/\partial \vec{n}(\vec{\eta})$ fulfil the condition of regularity by the limit transition for $a \to \infty$, and the boundary integral equation for the interior boundary of the unbounded regular region has identical form to the boundary integral equation of the bounded region. The regularity is interrupted in the case of a free member of integral formulation, because the deflection function is constant in the whole region. Since from a physical point of view the following equation is valid

$$\lim_{a \to \infty} \left[- \int_{\bar{\Gamma}} K_2 \frac{\partial G_0(R)}{\partial \eta(\vec{\eta})} \mathrm{d}\Gamma \right] = -1 \tag{6.31}$$

the coefficient of the free members has to acquire the value $1 + \frac{1}{2}$.

With regard to three unknown boundary quantities $\bar{w}(\vec{\eta}), \partial w_0(\vec{\eta})/\partial \vec{n}(\vec{\eta}), \partial w(\vec{\eta})/\partial \vec{n}(\vec{\eta})$ in the boundary integral equations (6.27), (6.29), it is necessary to formulate another integral equation.

Provided that for a concentrated moment we can write the fundamental solution

$$G_1(r,t) = \frac{\partial G(r,t)}{\partial r}\vec{r_n} \tag{6.31}$$

where $\vec{r_n}$ is the unit vector in direction *n,* then the boundary integral formulation has the form

$$\left[\frac{\partial w(\vec{r})}{\partial \vec{r}}\right]_{\vec{r_n}} = \int_S p(\vec{\xi})G_1(\varrho)\mathrm{d}S + \int_\Gamma \left[K_2^* G_1(R)\frac{\partial w_0(\vec{\eta})}{\partial \vec{n}(\vec{\eta})} - \hat{H}_{\mathrm{n}}^1(R)w(\vec{\eta})\right. \tag{6.32}$$

$$\left. + \hat{M}_{\mathrm{nn}}^1 \frac{\partial w(\vec{\eta})}{\partial \vec{n}(\vec{\eta})}\right]\mathrm{d}\Gamma + \sum_{\mathrm{i}}(F_u G_u^1 - \hat{F}_u^1 w_u)_{\mathrm{i}}.$$

By means of limit transition on the boundary integral equation we obtain

$$\frac{1}{2}\left[\frac{\partial w(\vec{\zeta})}{\partial \vec{\zeta}}\right]_{\vec{r_n}} - \int_\Gamma \left[K_2^* G_1(R')\frac{\partial w_0(\vec{\eta})}{\partial \vec{n}(\vec{\eta})} - \hat{H}_{\mathrm{n}}^1(R')w(\vec{\eta})\right. \tag{6.33}$$

$$\left. + \hat{M}_{\mathrm{nn}}^1(R')\frac{\partial w(\vec{\eta})}{\partial \vec{n}(\vec{\eta})}\right]\mathrm{d}\Gamma - \sum_{\mathrm{i}}(F_u G_u^1 - \hat{F}_u^1 w_u)_{\mathrm{i}} = \int_S p(\vec{\xi})G_1(\varrho')\mathrm{d}S.$$

6.3 Relations for calculation of internal forces and moments in plate on subgrade under virtual unit force and moment loads

The radial bending moment $\hat{M}_r$ evoked by virtual unit concentrated force is determined by a relationship which has the form

$$\hat{M}_r = -D\left(\frac{\mathrm{d}^2}{\mathrm{d}r^2} + \frac{\mu}{r}\frac{\mathrm{d}}{\mathrm{d}r}\right)G(r) \tag{6.34}$$

and the tangential bending moment $\hat{M}_{\mathrm{t}}$ is determined by the relationship

$$\hat{M}_{\mathrm{t}} = -D^*\left(\frac{1}{r}\frac{\mathrm{d}}{\mathrm{d}r} + \mu\frac{\mathrm{d}^2}{\mathrm{d}r^2}\right)G(r). \tag{6.35}$$

The bending moment $\hat{M}_{\mathrm{nn}}$ in the direction of normal line to the plate boundary is determined [6.6] by the equation

$$\hat{M}_{\mathrm{nn}} = \hat{M}_r \cos^2\alpha_n + \hat{M}_{\mathrm{t}} \sin^2\alpha_n \tag{6.36}$$

where the angle α_n according to the scheme in Fig. 6.3 is the angle between the direction *r* and normal direction to the plate boundary.

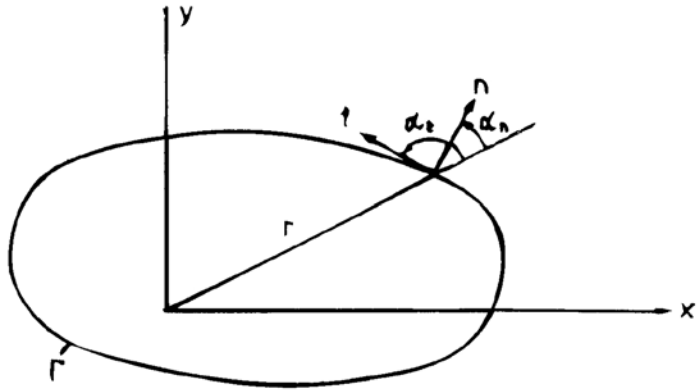

Fig. 6.3. Schematic diagram of the boundary angles.

The twisting moment $\widehat{M}_{nt}$ on the plate boundary is given by the relationship

$$\widehat{M}_{nt} = (\widehat{M}_r - \widehat{M}_t) \sin \alpha_n \cos \alpha_n. \tag{6.37}$$

The transverse force $\widehat{Q}_n$ of the system, i.e. of a plate resting on subgrade, is determined by the relationship

$$\widehat{Q}_n = D^* \left[\frac{d^3}{dr^3} + \frac{1}{r} \frac{d^2}{dr^2} - \frac{1}{r^2} \frac{d}{dr} + \frac{2\Psi}{h^2} \frac{d}{dr} \right] G(r) \tag{6.38}$$

where Ψ is given by equation (6.6) and h is the thickness of the plate.

The equivalent shear force $\widehat{H}_n$ on the plate boundary is given by

$$\widehat{H}_n = \widehat{Q}_n - \frac{\partial \widehat{M}_{nt}}{\partial \overrightarrow{t}}. \tag{6.39}$$

By the virtual load of unit moment the same relationships are valid for $\widehat{M}_r^1, \widehat{M}_t^1, \widehat{M}_{nn}^1, \widehat{M}_{nt}^1, \widehat{Q}_n^1$ and $\widehat{H}_n^1$, but related to Green's function G_1, determined in equation (6.31).

6.4 Solution of boundary integral equations using boundary elements

The boundary integral equations (6.27), (6.29), (6.33) form a system of three integral equations with unknown boundary quantities: deflection w, normal slopes of subgrade $\partial w_0/\partial n$ and plate $\partial w/\partial n$. Their solution is possible using the discretization of the plate boundary.

The total boundary curve can be divided into N boundary elements supposing constant, linear or quadratic approximations of sub-integral functions. The assumption of a constant

course along the element is simple. The unknown quantities are concentrated at the nodal points, which are at the centre of the element length. This assumption makes it possible to solve the pronounced singularities at the singular elements. Less precision can be compensated for by using a larger number of boundary elements.

Let us work out the virtual unit concentrated force at every nodal point of the boundary elements and similarly the unit moments in the normal direction to the boundary elements. Then it is possible to transform a system of integral equations into a system of $3N$ linear algebraical equations with the dimensionless unknown wE/ph, $E/p\ \partial w_0/\partial n$, $E/p\ \partial w/\partial n$ at the nodal points

$$
\begin{aligned}
&(1+\tfrac{1}{2})\left(\frac{wE}{ph}\right)_k + \sum_{\substack{j=1\\ j\neq k}}^{N} B_{kj}\left(\frac{wE}{ph}\right)_j + \sum_{j=1}^{N} A_{kj}\left(\frac{\partial w_0 E}{\partial np}\right)_j = 0\\
&\tfrac{1}{2}\left(\frac{wE}{ph}\right)_k + \sum_{\substack{j=1\\ j\neq k}}^{N} D_{kj}\left(\frac{wE}{ph}\right)_j + \sum_{j=1}^{N} C_{kj}\left(\frac{\partial w_0 E}{\partial np}\right)_j + \sum_{j=1}^{N} F_{kj}\left(\frac{\partial wE}{\partial np}\right)_j = P_k\\
&\sum_{j=1}^{N} E_{kj}\left(\frac{wE}{ph}\right)_j + \sum_{j=1}^{N} H_{kj}\left(\frac{\partial w_0 E}{\partial np}\right)_j + \frac{1}{2}\left(\frac{\partial wE}{\partial np}\right)_k + \sum_{\substack{j=1\\ j\neq k}}^{N} G_{kj}\left(\frac{\partial wE}{\partial np}\right)_j = PP_k\\
&k = 1, 2, \ldots N.
\end{aligned}
\tag{6.40}
$$

The coefficients of the system of equations are determined by the set of relationships

$$
\begin{aligned}
A_{kj} &= \frac{K_2^*}{h}\int_{\Gamma_j} G_0(R')\mathrm{d}\Gamma_j = -\frac{\mathrm{i}}{4}\frac{l_j}{h}\,H_0^{(2)}(\alpha R') = -\frac{\mathrm{i}}{4}\frac{l_j}{h}\,H_0^{(2)}\\
&\times\left(\sqrt{(\alpha\zeta_k)^2 + (\alpha\eta_j)^2 - 2\alpha\zeta_k\alpha\eta_j\,\cos\varphi_{kj}}\right)
\end{aligned}
\tag{6.41}
$$

$$
\begin{aligned}
B_{jk} &= K_2^*\int_{\Gamma_j}\frac{\partial G_0(R')}{\partial\vec{n}(\vec{\eta})}\mathrm{d}\Gamma_j = \frac{\mathrm{i}}{4}\frac{\alpha l_j}{h}\,\cos\alpha_{kj}H_1^{(2)}(\alpha R')\\
&= \frac{\mathrm{i}}{4}\frac{\alpha l_j}{h}\,\cos\alpha_k j\,H_1^{(2)}\left(\sqrt{\alpha\zeta_k)^2 + (\alpha\eta_j)^2 - 2\alpha\zeta_k\alpha\eta_j\,\cos\varphi_{kj}}\right)
\end{aligned}
\tag{6.42}
$$

in which l_j is the length of the j th boundary element and

$$\alpha = \alpha_1 h = \sqrt{\beta^2 \frac{c_2^2}{c_{\mathrm{R},0}^{*2}} - \frac{K_1^* h^2}{K_2^*}}$$

α_{kj} is an angle between the line connecting points ζ_k, η_j at the boundary curve and normal at boundary point η_j, and φ_{kj} is the angle between the radius vectors $\vec{\zeta}_k$ and $\vec{\eta}_j$. $H_0^{(2)}, H_0^{(2)}$ are Hankel's functions of zero and the first order, second kind with complex argument, in which the real part is positive and the imaginary part is negative.

$$C_{kj} = -\int_{\Gamma j} \frac{K_2^*}{h} G(R')\mathrm{d}\Gamma_j = \frac{\mathrm{i}3(1-\mu^2) l_j K_2^*}{2\Theta h^2 E^*} \left[H_0^{(2)}(\gamma_1 R') - H_0^{(2)}(\gamma_2 R')\right] \tag{6.43}$$

$$\begin{aligned} D_{kj} = \int_{\Gamma_j} \widehat{H}_\psi(R')\mathrm{d}\Gamma_j = -\frac{\mathrm{i}l_j \cos\alpha_{kj}}{8\Theta h} \Big[& \left(\gamma_{10}^3 - 2\Psi\gamma_{10}\right) H_1^{(2)}(\gamma_1 R') \\ & -(\gamma_{20}^3 - 2\Psi\gamma_{20}) \\ \times H_1^{(2)}(\gamma_2 R') + (1-\mu) \sin\alpha_{kj} \cos\alpha_{kj}^t & \left(\gamma_{10}^3 \left(1 - \frac{4}{(\gamma_1 R')^2}\right) H_1^{(2)}(\gamma_1 R')\right. \\ + \frac{2}{\gamma_1 R'} H_0^{(2)}(\gamma_1 R') - \gamma_{20}^3 & \left.\left(1 - \frac{4}{(\gamma_2 R')^2}\right) H_1^{(2)}(\gamma_2 R') - \frac{2}{\gamma_2 R'} H_0^{(2)}(\gamma_2 R')\right)\Big] \end{aligned} \tag{6.44}$$

$$\begin{aligned} F_{kj} = \int_{\Gamma j} \widehat{M}_{\mathrm{nn}}(R')\mathrm{d}\Gamma_j = \frac{-\mathrm{i}l_j}{8\Theta h} \Big\{ & \left(\cos^2\alpha_{kj} + \mu\sin^2\alpha_{kj}\right) \Big[\gamma_{10}^2 \Big(\frac{1}{\gamma_1 R'} H_1^{(2)}(\gamma_1 R') \\ & -H_0^{(2)}(\gamma_1 R')\Big) - \gamma_{20}^2 \Big(\frac{1}{\gamma_2 R'} H_1^{(2)}(\gamma_2 R') - H_0^{(2)}(\gamma_2 R')\Big)\Big] \\ & +(\mu\cos^2\alpha_{kj} + \sin^2\alpha_{kj}) \\ & \times \Big[-\frac{\gamma_{10}^2}{\gamma_1 R'} H_1^{(2)}(\gamma_1 R') + \frac{\gamma_{20}^2}{\gamma_2 R'} H_1^{(2)}(\gamma_2 R')\Big]\Big\} \end{aligned} \tag{6.45}$$

$$H_{kj} = \frac{-\mathrm{i}3(1-\mu^2) l_j K_2^*}{2\Theta h^2 E^*} \cos\alpha_{kj}^n \left[\gamma_{10} H_1^{(2)}(\gamma_1 R') - \gamma_{20} H_1^{(2)}(\gamma_2 R')\right] \tag{6.46}$$

$$E_{kj}=\frac{\mathrm{i}l_j}{8\Theta h}\cos\alpha_{kj}\cos\alpha_{kj}^{n}\left\{(\gamma_{10}^{4}-2\Psi\gamma_{10}^{2})\left[H_0^{(2)}(\gamma_1R')-\frac{1}{\gamma_1R'}H_1^{(2)}(\gamma_1R')\right]\right.$$

$$-(\gamma_{20}^{4}-2\Psi\gamma_{20}^{2})\left[H_0^{(2)}(\gamma_2R')-\frac{1}{\gamma_2R'}H_1^{(2)}(\gamma_2R')\right]-(1-\mu)\sin\alpha_{kj}\cos\alpha_{kj}^{t} \tag{6.47}$$

$$\times\left[\gamma_{10}^{4}\left(\left(\frac{12}{\gamma_1R'^{3}}-\frac{3}{\gamma_1R'}\right)H_1^{(2)}(\gamma_1R')+\left(1-\frac{6}{\gamma_1R'^{2}}\right)H_0^{(2)}(\gamma_1R')\right)\right.$$

$$\left.\left.-\gamma_{20}^{4}\left(\left(\frac{12}{\gamma_2R'^{3}}-\frac{3}{\gamma_1R'}\right)H_1^{(2)}(\gamma_2R')+\left(1-\frac{6}{\gamma_2R'^{2}}\right)H_0^{(2)}(\gamma_2R')\right)\right]\right\}$$

$$G_{kj}=\frac{-\mathrm{i}l_j}{8\Theta h}\cos\alpha_{kj}^{n}\left\{(\cos^2\alpha_{kj}+\mu\sin^2\alpha_{kj})\left[\gamma_{10}^{3}\left(\left(1-\frac{2}{\gamma_1R'^{2}}\right)H_1^{(2)}(\gamma_1R')\right.\right.\right.$$

$$\left.\left.+\frac{1}{\gamma_1R'}H_0^{(2)}(\gamma_1R')\right)-\gamma_{20}^{3}\left(\left(1-\frac{2}{\gamma_2R'^{2}}\right)H_1^{(2)}(\gamma_2R')+\frac{1}{\gamma_2R'}H_0^{(2)}(\gamma_2R')\right)\right] \tag{6.48}$$

$$+(\mu\cos^2\alpha_{kj}+\sin^2\alpha_{kj})\left[-\gamma_{10}^{3}\left(\frac{-2}{\gamma_1R'^{2}}H_1^{(2)}(\gamma_1R')+\frac{1}{\gamma_1R'}H_0^{(2)}(\gamma_1R')\right)\right.$$

$$\left.\left.+\gamma_{20}^{3}\left(-\frac{2}{\gamma_2R'^{2}}H_1^{(2)}(\gamma_2R')+\frac{1}{\gamma_2R'}H_0^{(2)}(\gamma_2R')\right)\right]\right\}.$$

In equations (6.44), (6.46), (6.47) and (6.48), α_{kj}^{t} is an angle between the line connecting points ζ_k, η_j at the boundary curve and tangent line at boundary point η_j, and α_{kj}^{n} is an angle between the line connecting points ζ_k, η_j at the boundary curve and normal line at boundary point ζ_k.

The calculation of the influence coefficients at singular elements A_{kk}, C_{kk}, F_{kk}, H_{kk} and E_{kk} requires special attention. Detailed analysis of the relations indicates that the coefficients H_{kk} and E_{kk} (assuming the constant approximation) are equal to zero. The other coefficients A_{kk}, C_{kk} and F_{kk} have to be calculated in the sense of a Cauchy principal value, by using the integrals with finite values and Gauss's quadrature formulas.

Absolute members of the equation system (6.40) depend on the external dynamic load. If, for instance, the plate on subgrade is under a dynamic load $pe^{\mathrm{i}\omega t}$ uniformly distributed on the circular area with radius e_0, equation (3.248) already derived is as follows

$$\int_S p e^{i\omega t} G(\varrho) dS = e^{i\omega t} p A^* e_0 \left[\frac{1}{\gamma_{10}} J_1(\gamma_1 e_0)\, H_0^{(2)}(\gamma_1 \varrho) \right.$$

$$\left. - \frac{1}{\gamma_{20}} J_1(\gamma_2 e_0) H_0^{(2)}(\gamma_2 \varrho) \right] \tag{6.49}$$

where

$$A^* = -\frac{\pi}{E} \frac{3(1-\mu^2)i}{\Theta(1+i\delta)}. \tag{6.50}$$

The right-hand sides of the equation system (6.40) at last have the form

$$P_k = \frac{-i3\pi(1-\mu^2)e_0}{\Theta(1+i\delta)} \left[\frac{1}{\gamma_{10}} J_1(\gamma_1 e_0) H_0^{(2)}(\gamma_1 \varrho') - \frac{1}{\gamma_{20}} J_1(\gamma_2 e_0) H_0^{(2)}(\gamma_2 \varrho') \right] \tag{6.51}$$

$$PP_k = \frac{3\pi(1-\mu^2)e_0}{\Theta(1+i\delta)h} \left[J_1(\gamma_1 e_0) H_1^{(2)}(\gamma_1 \varrho') - J_1(\gamma_2 e_0) H_1^{(2)}(\gamma_2 \varrho') \right]. \tag{6.52}$$

All coefficients and absolute members of the system (6.40) are complex. The unknown boundary quantities wE/ph, $E/p\ \partial w_0/\partial n$, $E/p\ \partial w_0/\partial n$, calculated from the system of equations, are determined by complex numbers, the characteristics of which are absolute value and phase angle.

Deflections in interior points of the plate or subgrade are established according to equations (6.25) and (6.26).

6.5 Numerical results

The submitted solution can be illustrated by the numerical results for the forced flexural vibration of a plate with free boundaries resting on the unbounded subgrade under a dynamic harmonic load, which is uniformly divided on the circle with radius e_0.

The following values for the parameters have been considered

$$\delta = 0.10, \delta_0 = 0.20, \mu = 0.20, \mu_0 = 0.35, c_2/c_{20} = 13.65,$$

$$\frac{K_1 h}{E} = 0.00188, \frac{K_2}{Eh} = 0.00197, \frac{K_2}{K_1 h^2} = 4.0, \frac{e_0}{h} = 0.25.$$

A plate on subgrade equivalent to a rigid pavement structure with equivalent thickness h=0.36 m has been assumed.

6.5.1 Square plate on subgrade

A square plate resting on subgrade with free boundaries and dimensions 4.80 m×4.80 m is loaded by a harmonic variable force $Pe^{i\omega t}$, which acts at the axis y (Fig. 6.4), where $P = \pi e_0^2 p$ and ω is an angular frequency.

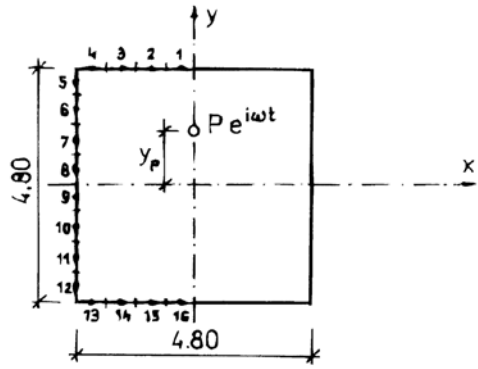

Fig. 6.4. Schematic diagram of boundary elements for square plate on subgrade.

Considering symmetry to axis y the boundary was divided into 16 boundary elements of length 0.6 m. The number of boundary unknowns was 3×16=48 and because of complex coefficients the problem was solved by a system of 96 equations. We assumed two load locations of the driving force $Pe^{i\omega t}$, with excentricities of working y_p=2.10 m and y_p=0.01 m.

The obtained amplitude—frequency characteristics of the deflections $|w|E/ph$ at boundary nodal points 1 and 16 are shown in Figs. 6.5 and 6.6. They are calculated for dimensionless frequencies $\beta=\omega h/c_2$ in the range 0.01–0.35.

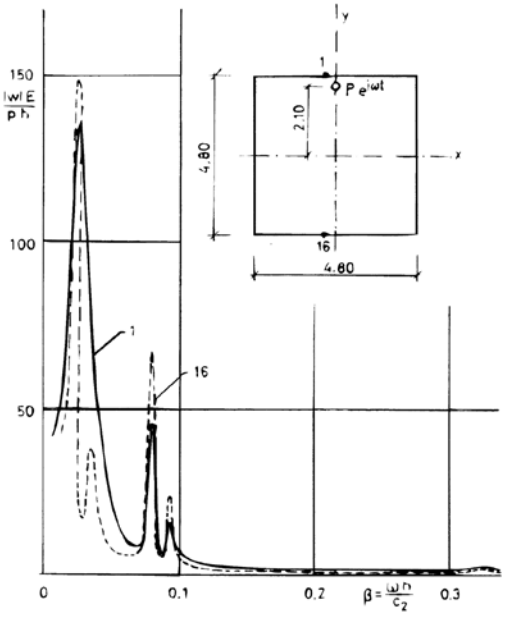

Fig. 6.5. Amplitude—frequency characteristics of deflection at boundary nodal points.

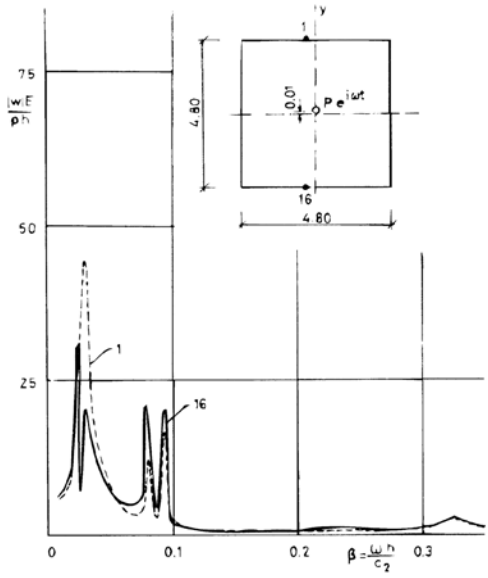

Fig. 6.6. Amplitude—frequency characteristics of deflection at boundary nodal points.

The deflection amplitudes of forced damped vibration of the plate at resonance frequencies β are shown in Figs. 6.7 and 6.8 for the load case with eccentricity y_p=2.10 m and in Figs. 6.9 and 6.10 for the load with eccentricity y_p=0.01 m.

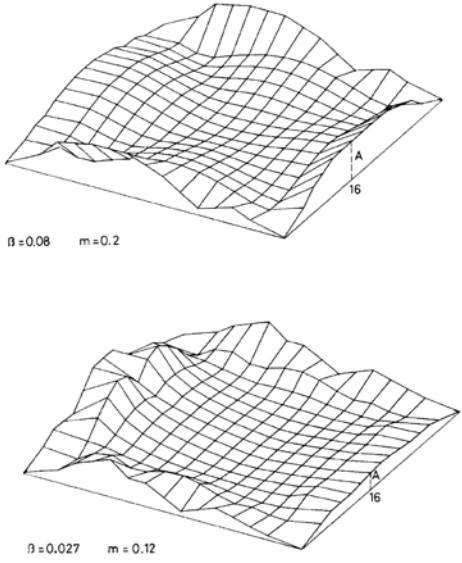

Fig. 6.7. Deflection amplitudes of forced vibration at frequencies β=0.08 and β=0.027.

The value of deflection amplitude $|w|E/ph$ can be determined by the division of vertical amplitude A with gauge m. The set of deflection amplitudes was calculated by using the

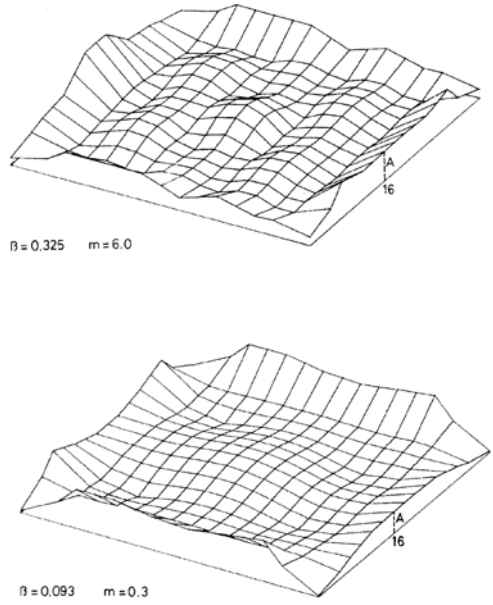

Fig. 6.8. Deflection amplitudes of forced vibration at frequencies β=0.093 and β=0.325.

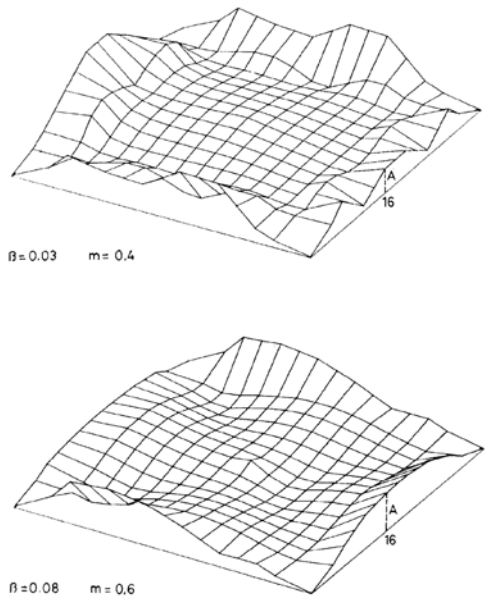

Fig. 6.9. Deflection amplitudes of forced vibration at frequencies β=0.03 and β=0.08.

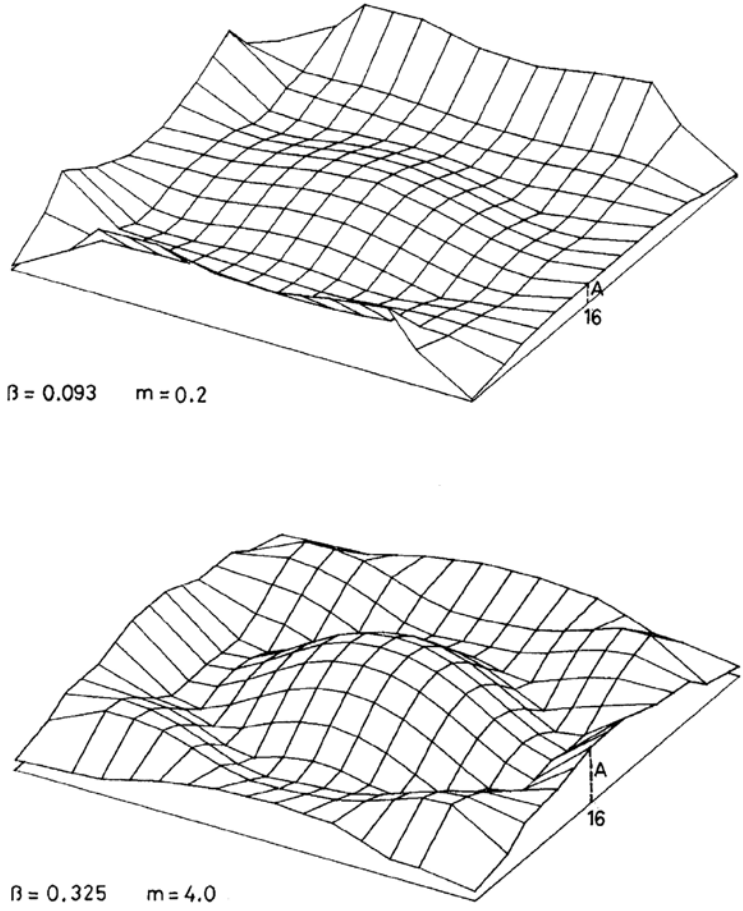

Fig. 6.10. Deflection amplitudes of forced vibration at frequencies β=0.093 and β=0.325.

boundary integral formulations and their transformation for a discrete solution applying boundary elements. The net of interior points had the basic dimension 0.3×0.3 m with the exception of the boundary zones, where the distance from the boundary was 0.6 m. The calculation of deflection amplitudes near the boundary has a small amount of precision with regard to the singular character of the fundamental solution.

The shape of the deflection amplitudes for the resonance frequencies β=0.08 and β=0.093 is similar to the vibration shapes of a free square plate with free boundaries, which corresponds to the second and third natural frequency [1.13]. According to [1.13] the relationship established for these frequencies of a square plate with side length l has the form

$$\omega_{2,3} = \omega^{*2}(1 \mp 0.6903\mu) \tag{6.53}$$

where

$$\omega^* = \frac{4.7300^2}{l^2}\sqrt{\frac{D}{\varrho h}}. \tag{6.54}$$

For Poisson's ratio μ=0.20 this can be expressed

$$\omega_2 = \frac{6.02}{l^2}\sqrt{\frac{Eh^2}{\varrho(1-\mu^2)}} = \frac{0.0535}{h}\sqrt{\frac{G}{\varrho}}$$

$$\omega_3 = \frac{6.93}{l^2}\sqrt{\frac{Eh^2}{\varrho(1-\mu^2)}} = \frac{0.0615}{h}\sqrt{\frac{G}{\varrho}}.$$

From the numerical solution of a square plate resting on subgrade the dimensionless frequencies $\beta=\omega h/c_2$ have correspondent values β_2=0.08, β_3=0.093. It can be seen that the interaction of the plate with the subgrade caused an increase in resonance frequencies by the ratios 0.080/0.0535 or 0.093/0.0654, i.e. approximately about 50%. The ratio of the frequencies which depends on the value of Poisson's ratio, is practically the same as for the free plate and corresponds very well to the value μ=0.20.

The first resonance zone in the frequency range β=0.025–0.035 probably corresponds to the vibration in which the vertical or rocking vibration of the plate mass on subgrade is determined. At the same time deformation of the plate shape is also present.

Provided that K_1h/G=0.00188, then a constant of vertical elasticity is approximately $C_z=K_1l^2$=0.00188$G\,l^2/h$ and the total mass of the plate $M = \varrho h l^2$. The angular frequency of vertical plate vibration on the subgrade considered as a rigid plate is given by

$$\omega = \sqrt{\frac{C_z}{M}} = \frac{0.043}{h}\sqrt{\frac{G}{\varrho}}.$$

At the same time deformity of the plate decreases the calculated value of angular frequency and forms a resonance zone in the frequency range β=0.025–0.035.

The third resonance zone at frequency β=0.325 has the amplitude shapes of forced vibration, which differ depending on the position of action of the driving harmonic force.

6.5.2 Rectangular plate on subgrade

The rectangular plate with free boundaries resting on subgrade has the dimensions: l_x=4.80 m, l_y=3.68 m.

Symmetry to the axis y is assumed again. The boundary is divided into 16 boundary elements. The length of the elements on the side l_y is 0.46 m. The numerical solution was

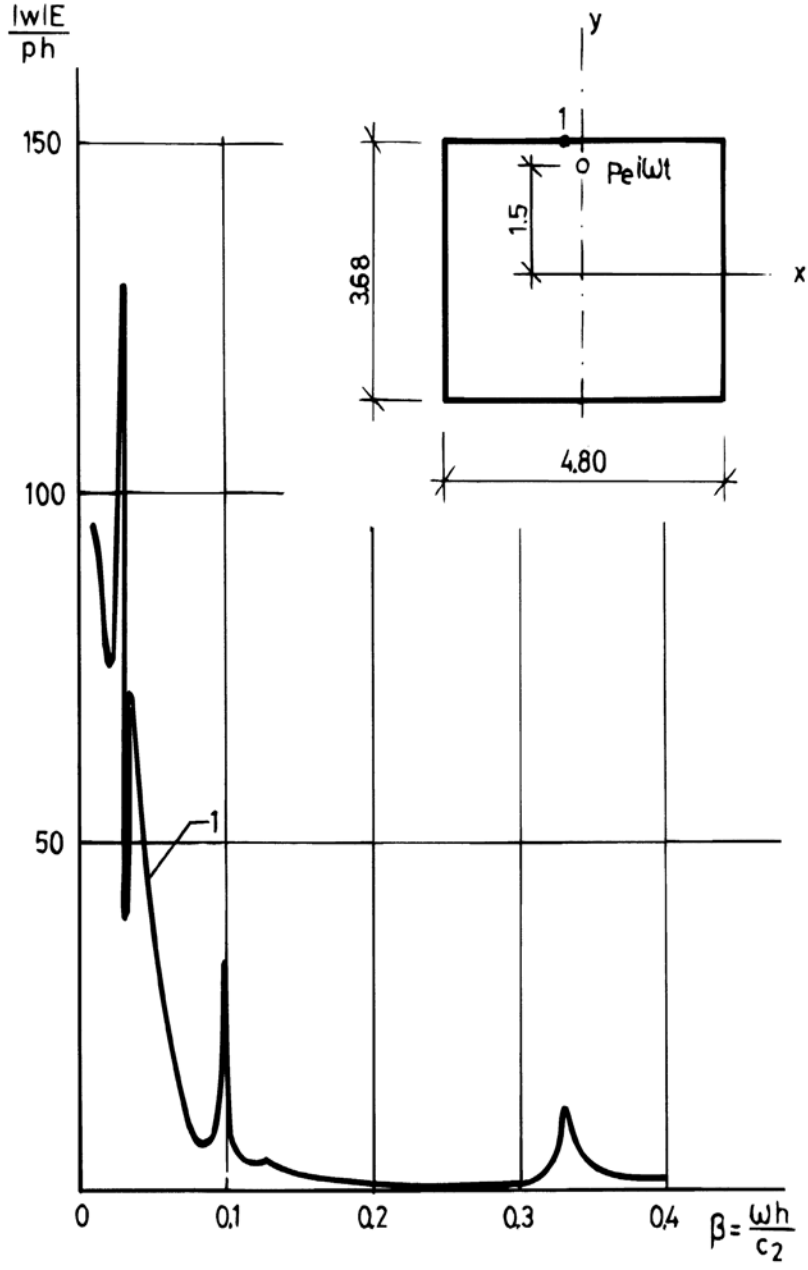

Fig. 6.11. Amplitude—frequency characteristic of deflection at boundary point of rectangular plate on subgrade.

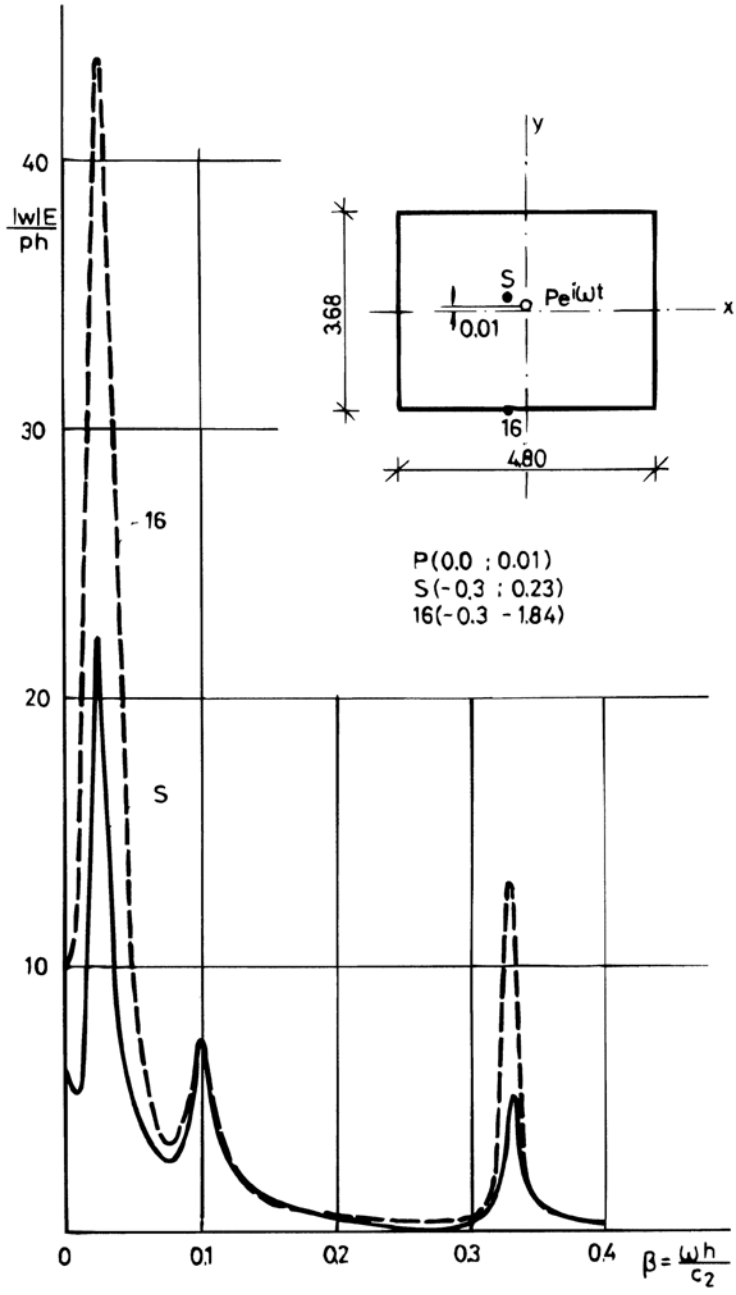

Fig. 6.12. Amplitude—frequency characteristics of deflection at boundary nodal points of rectangular plate on subgrade.

realized for two positions of a driving harmonic force, y_p=1.50 m and y_p=0.01 m. The amplitude-frequency characteristics of deflections $|w|E/ph$ in nodal points 1 and 16 or in interior point S are plotted in Figs. 6.11 and 6.12.

The deflection amplitudes of forced plate vibration on subgrade at resonance frequencies β are plotted in Figs. 6.13–6.15 for two load positions.

The shape of the deflection amplitudes corresponding to the second and third resonance frequencies are very similar, without regard to the position of the driving force.

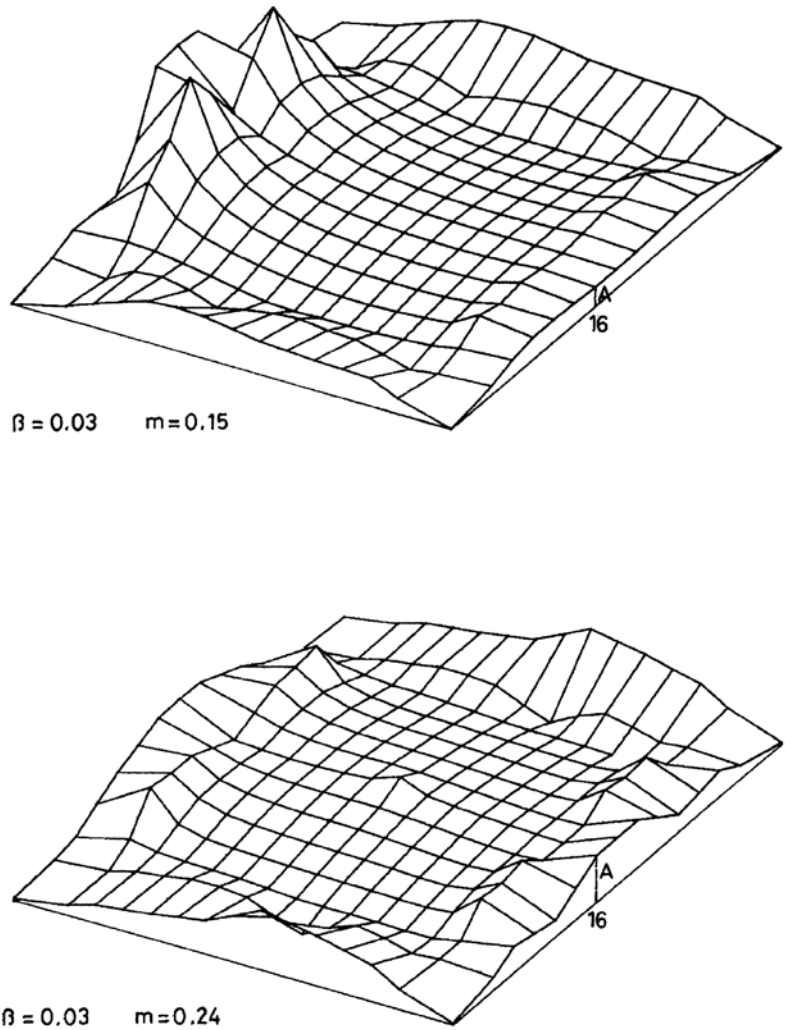

Fig. 6.13. Deflection amplitudes of forced vibration at frequency β=0.03 for two load positions.

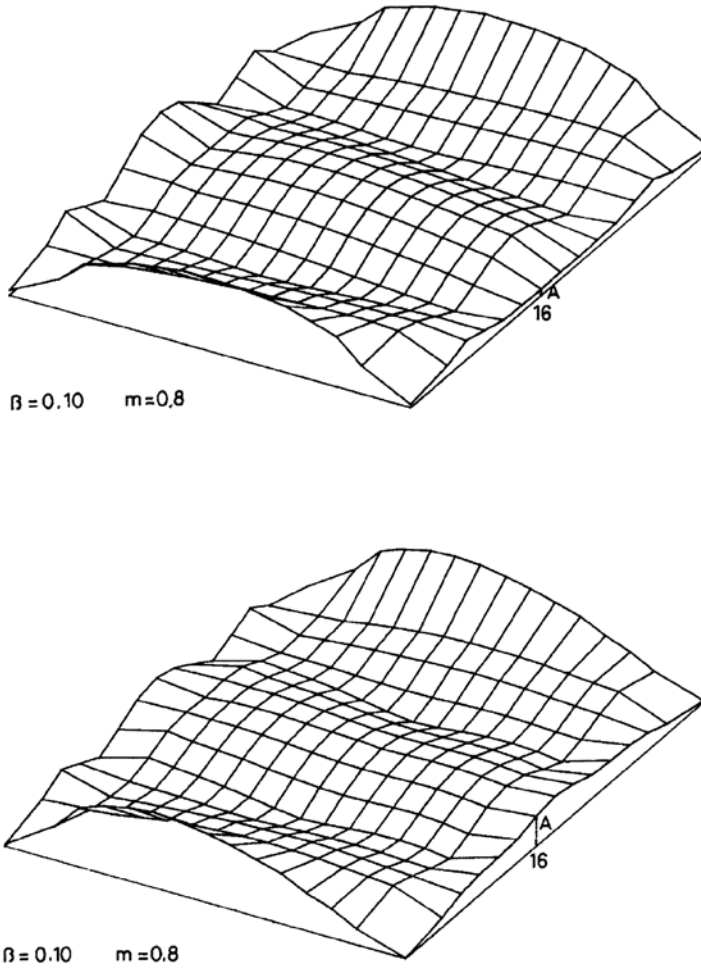

Fig. 6.14. Deflection amplitudes of forced vibration at frequency β=0.10 for two load positions.

6.5.3. Evaluation of application of the boundary element method

The theoretical procedures that have been presented, and compiled computer programs in FORTRAN 77 for IBM personal computers, demonstrate the considerable possibilities for and the advantage of the proposed methods in the application of the numerical solution of forced plate vibration resting on unbounded subgrade.

The advantage of the application of the method of integral equations is evident just in the cases of plate interaction with the subgrade. In such a case the method combines the exactness of the analytical solution with the efficacy of the numerical procedures for

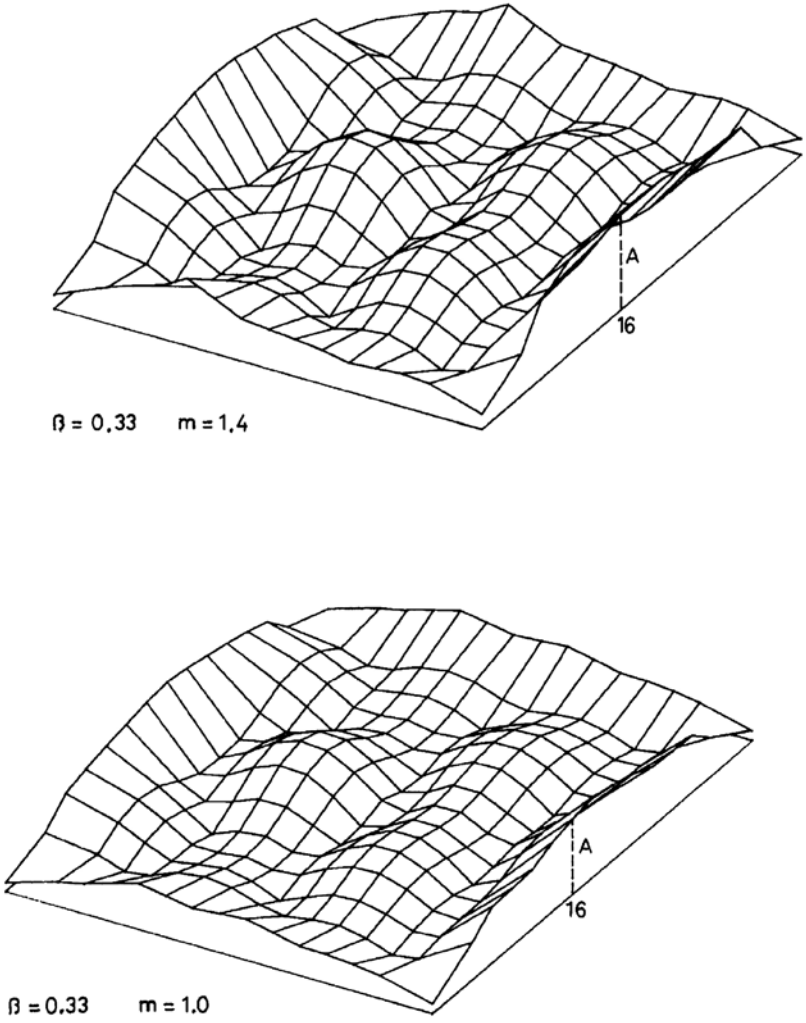

Fig. 6.15. Deflection amplitudes of forced vibration at frequency β=0.33 for two load positions.

fulfilling the boundary conditions. In comparison with the method of finite elements the method of boundary elements requires the solution of substantially smaller systems of equations. Another advantage is the possibility of its application for plates of arbitrary shape.

With regard to the singularity of fundamental solutions it is necessary to calculate some influence coefficients in the system of equations in the sense of a Cauchy principal value. For the same reason the calculation of the state vector components near the nodal points of boundary elements is insufficiently precise.

6.5.4. Effect of pulse loads

The differences between the dynamic response of a bounded and an unbounded plate resting on unbounded subgrade have their origin in the different forms of the amplitude—frequency characteristics. The amplitude—frequency characteristic of the unbounded plate is a monotonicall decreasing function, and in the case of a bounded plate resting on the subgrade there are resonance zones.

In order to study the effect of pulse loads the procedure of section 4.8 is adopted. The application of the indicated procedure to the dynamic response of a rectangular plate with free boundaries resting on subgrade allows us to obtain the corresponding dynamic coefficients ϑ_w of the deflection $|w|E/(ph)$. They are plotted in Fig. 6.16 for various values of the dimensionless parameter Ω_0, which corresponds to the time of pulse duration.

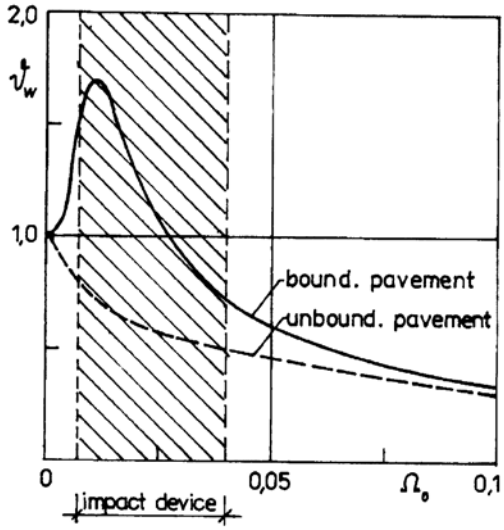

Fig. 6.16. Dynamic coefficients ϑ_w for effect of pulse loading on bounded and unbounded pavement structure.

The analysis of the dynamic response of a bounded plate resting on unbounded subgrade using the method of boundary elements confirms that the dynamic increment under a harmonic and pulse load is evident. These results are also important for layered pavement systems, because the equivalent plate with free boundaries presents a system which is in contrast to the model of an unbounded plate on subgrade.

7
CONCENTRATION OF THE VIBRATION ABOUT THE HOLES IN PLATE ON SUBGRADE

The method of boundary integral equations and the analysed procedures offer the possibility of studying some very interesting problems concerning the influence of holes of arbitrary shape in the plate on subgrade during the propagation of the vibration. In such a case the diffraction of the stress waves on the hole's boundaries is affected. The similarity of the problem with stress concentration about the holes in the static case is reinforced and transformed in dynamic problems because of dynamic increments in the resonance zones. These resonances can be formed by certain ratios of wavelength to the dimensions of the hole.

7.1 Integral formulations according to theorem of reciprocity

Let us assume thin plate theory and the simplified model of the soil base, and the fundamental solutions (6.4), (6.18).

In Fig. 7.1 a hole of arbitrary shape with boundary curve Γ is situated in an unbounded plate S resting on subgrade. The radius vector of the load position is $\vec{\xi}$, the radius vector of the unit concentrated force is $\vec{r}$, and the radius vector of the boundary point is $\vec{\eta}$.

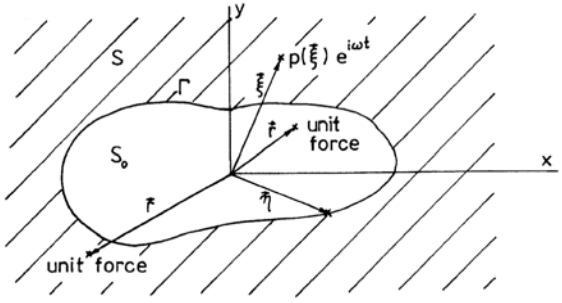

Fig. 7.1. Schematic diagram of system of a hole in plate on subgrade.

In general, the bending moments M_{nn}, the twisting moments M_{nt} and the shear forces Q_n of the system affect the hole boundary. Because of thin plate theory it is necessary to consider the equivalent shear forces $H_n = Q_n + \partial M_{nt}/\partial \vec{t}$.

According to Rayleigh's theorem of reciprocity the integral formulation for the plate has the form

$$\vartheta(\vec{r})\, w(\vec{r}) = \int_S p(\vec{\xi})\, G(\varrho)\, \mathrm{d}S + \int_\Gamma \Big[G(R)\, H_n(\vec{\eta}) - \frac{\partial G(R)}{\partial \vec{n}(\vec{\eta})}\, M_{nn}(\vec{\eta}) - \widehat{H}_n(R) w(\vec{\eta}) + \widehat{M}_{nn}(R) \frac{\partial w(\vec{\eta})}{\partial \vec{n}(\vec{\eta})} \Big] \mathrm{d}\Gamma + \int_{\bar{\Gamma}} \Big[G(R) H_n(\vec{\eta}) - \frac{\partial G(R)}{\partial \vec{n}(\vec{\eta})} M_{nn}(\vec{\eta}) - \widehat{H}_n(R) w(\vec{\eta}) + \widehat{M}_{nn}(R) \frac{\partial w(\vec{\eta})}{\partial \vec{n}(\vec{\eta})} \Big] \mathrm{d}\bar{\Gamma} + \sum_i (F_u G_u - \widehat{F}_u w_u)_i \tag{7.1}$$

where

$$\vartheta(\vec{r}) = \begin{cases} 1 & \vec{r} \in S \\ 0 & \vec{r} \bar{\in} (\Gamma \cup S) \end{cases}$$

and

$$R = |\vec{\eta} - \vec{r}| \quad , \quad \varrho = |\vec{\xi} - \vec{r}|.$$

The significance of the symbols and signs is the same as in Chapter 6.

The integral formulation for the medium of subgrade S_0 takes the form

$$\vartheta(\vec{r}) w_0(\vec{r}) = \int_{S_0} p_0(\vec{\xi})\, G_0(\varrho) \mathrm{d}S_0 + \int_\Gamma K_2^* \Big[\frac{\partial w_0(\vec{\eta})}{\partial \vec{n}(\vec{\eta})}\, G_0(R) - \frac{\partial G_0(R)}{\partial \vec{n}(\vec{\eta})} w_0(\vec{\eta}) \Big] \mathrm{d}\Gamma \tag{7.2}$$

if

$$\vartheta(\vec{r}) = \begin{cases} 1 & \vec{r} \in S_0 \\ 0 & \vec{r} \bar{\in} (\Gamma \cup S_0). \end{cases}$$

7.1.1 Boundary conditions

Provided that the boundaries of the hole in the plate are free, the boundary conditions are as follows:

$$w(\vec{\eta}) = w_0(\vec{\eta})$$

$$M_{nn}(\vec{\eta}) = 0 \tag{7.3}$$

$$H_n(\vec{\eta}) = K_2^* \frac{\partial w_0(\vec{\eta})}{\partial \vec{n}(\vec{\eta})}.$$

7.1.2 Boundary integral equations

Using the boundary conditions (7.3) and by means of the limit transition on the boundary for $\vec{r} \to \vec{\zeta} \in \Gamma$ and the limit transition of the circular boundary $\bar{\Gamma}$ for $a \to \infty$ the integral equation is established from equation (7.1) as follows:

$$\left(1 + \tfrac{1}{2}\right) w(\vec{\zeta}) = \int_{\Gamma} \left[K_2^* G(R') \frac{\partial w_0(\vec{\eta})}{\partial \vec{n}(\vec{\eta})} - \hat{H}_n(R') w(\vec{\eta}) \right.$$

$$\left. + \hat{M}_{nn}(R') \frac{\partial w(\vec{\eta})}{\partial \vec{n}(\vec{\eta})} \right] d\Gamma - \sum_i \left[F_u G_u - \hat{F}_u w_u \right]_i = \int_S p(\vec{\xi}) G(\varrho') dS \tag{7.4}$$

where

$$R' = |\vec{\eta} - \vec{\zeta}| \quad , \quad \varrho' = |\vec{\xi} - \vec{\zeta}|.$$

The boundary integral equation (7.4) expressed for the interior boundary of an unbounded regular region is identical in form to the boundary integral equation of the bounded region. Quantities $G(R)$, $\partial G(R)/\partial \vec{n}(\vec{\eta})$ and $\hat{M}_{nn}(R)$, $\hat{H}_n(R)$ fulfil the condition of regularity by limit transition for $a \to \infty$. The interruption of the regularity is actual in the case of a free member and because from a physical point of view the following relationship is valid:

$$\lim_{a \to \infty} \left[- \int_{\bar{\Gamma}} \hat{H}_n(R) \, d\bar{\Gamma} \right] = -1 \tag{7.5}$$

the coefficient of the free member is $1 + \frac{1}{2}$.

By means of the limit transition on the boundary for $\vec{r} \to \vec{\zeta} \in \Gamma$ the second integral boundary equation will be expressed from the integral formulation for the subgrade S_0 (7.2) in the form

$$\tfrac{1}{2} w(\vec{\zeta}) - \int_{\Gamma} K_2^* \left[G_0(R') \frac{\partial w_0(\vec{\eta})}{\partial \vec{n}(\vec{\eta})} - \frac{\partial G_0(R')}{\partial \vec{n}(\vec{\eta})} w(\vec{\eta}) \right] \mathrm{d}\Gamma = 0. \tag{7.6}$$

The third boundary integral equation can be expressed if the fundamental solution for the plate deflection $G_1(r; t)$ under a virtual unit polarized moment is established in the same way as in (6.31).

According to the Rayleigh theorem of reciprocity the integral formulation for the interior point of the plate is given by the relationship

$$\begin{aligned} \left[\frac{\partial w(\vec{r})}{\partial \vec{r}} \right]_{\vec{r}_n} = {} & \int_S p(\vec{\xi}) G_1(\varrho) \mathrm{d}S + \int_{\Gamma} \left[G_1(R)\, H_n^1(\vec{\eta}) - \frac{\partial G_1(R)}{\partial \vec{n}(\vec{\eta})} M_{nn}^1(\vec{\eta}) \right. \\ & \left. - \hat{H}_n^1(R) w(\vec{\eta}) + \hat{M}_{nn}^1(R) \frac{\partial w(\vec{\eta})}{\partial \vec{n}(\vec{\eta})} \right] \mathrm{d}\Gamma + \int_{\bar{\Gamma}} \left[G_1(R) H_{nn}^1(\vec{\eta}) \right. \\ & \left. - \frac{\partial G_1(R)}{\partial \vec{n}(\vec{\eta})} M_{nn}^1(\vec{\eta}) - \hat{H}_n^1(R) w(\vec{\eta}) + \hat{M}_{nn}^1(R) \frac{\partial w(\vec{\eta})}{\partial \vec{n}(\vec{\eta})} \right] \mathrm{d}\bar{\Gamma} \\ & + \sum_i \left(F_u G_u^1 - \hat{F}_u^1 w_u \right)_i . \end{aligned} \tag{7.7}$$

By using the boundary conditions (7.3), by means of transition on the boundary of the plate hole for $\vec{r} \to \vec{\zeta} \in \Gamma$ and by means of the limit transition to the boundary $\bar{\bar{\Gamma}}$ for $a \to \infty$, the integral boundary equation is expressed in the form

$$\begin{aligned} & \left(1 + \frac{1}{2}\right) \left[\frac{\partial w(\vec{\xi})}{\partial \vec{\xi}} \right]_{\vec{r}_n} - \int_{\Gamma} \left[K_2^* G_1(R') \frac{\partial w_0(\vec{\eta})}{\partial \vec{n}(\vec{\eta})} - \hat{H}_n^1(R')\, w(\vec{\eta}) \right. \\ & \left. + M_{nn}^1(R') \frac{\partial w(\vec{\eta})}{\partial \vec{n}(\vec{\eta})} \right] \mathrm{d}\Gamma - \sum_i \left(F_u G_u^1 - \hat{F}_u^1 w_u \right)_i = \int_S p(\vec{\xi}) G_1(\varrho') \mathrm{d}S. \end{aligned} \tag{7.8}$$

The validity of the relationship

$$\lim_{a \to \infty} \int_{\bar{\bar{\Gamma}}} \hat{M}_{nn}^1(R)\, \mathrm{d}\bar{\Gamma} = -1 \tag{7.9}$$

was considered by limit transition for $a \to \infty$.

The relationships for internal forces and moments in a plate on subgrade have already been derived and described in section 6.3. The significance of the angle α_n in this case is given according to the scheme of Fig. 7.2.

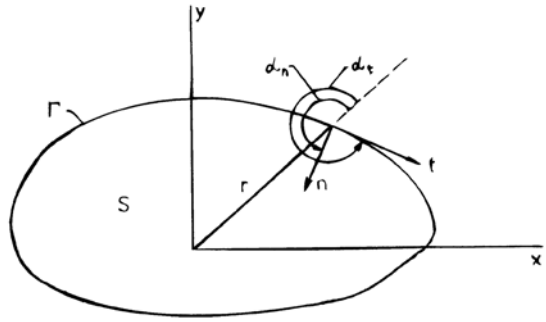

Fig. 7.2. Schematic diagram of boundary angles.

7.1.3. Solution of integral equations using boundary elements

Boundary integral equations (7.4), (7.6) and (7.8) have three unknown boundary quantities: deflection w, normal slope of the plate $\partial w/\partial n$ and normal slope of the subgrade $\partial w_0/\partial n$.

Their solution is possible using discretization of the plate boundary. Then, decomposing the entire boundary into boundary elements with N nodal points and assuming a constant course for the sub-integral function, the system of $3N$ linear algebraic equations with the dimensionless unknowns wE/ph, $E/p\ \partial w_0/\partial n$, $E/p\ \partial w/\partial n$ at the nodal points is obtained as follows

$$
\begin{aligned}
&\tfrac{1}{2}\left(\frac{wE}{ph}\right)_k + \sum_{\substack{j=1\\ j\neq k}}^{N} B_{kj}\left(\frac{wE}{ph}\right)_j + \sum_{j=1}^{N} A_{kj}\left(\frac{\partial w_0}{\partial n}\,\frac{E}{p}\right)_j = 0\\
&\left(1+\tfrac{1}{2}\right)\left(\frac{wE}{ph}\right)_k + \sum_{\substack{j=1\\ j\neq k}}^{N} D_{kj}\left(\frac{wE}{ph}\right)_j + \sum_{j=1}^{N} C_{kj}\left(\frac{\partial w_0}{\partial n}\,\frac{E}{p}\right)_j\\
&\qquad + \sum_{j=1}^{N} F_{kj}\left(\frac{\partial w}{\partial n}\,\frac{E}{p}\right)_j = P_k\\
&\sum_{j=1}^{N} E_{kj}\left(\frac{wE}{ph}\right)_j + \sum_{j=1}^{N} H_{kj}\left(\frac{\partial w_0 E}{\partial np}\right)_j + \left(1+\frac{1}{2}\right)\left(\frac{\partial wE}{\partial np}\right)_k\\
&\qquad + \sum_{\substack{j=1\\ j\neq k}}^{N} G_{kj}\left(\frac{\partial w}{\partial n}\,\frac{E}{p}\right)_j = PP_k\\
&k = 1, 2, \ldots N
\end{aligned}
\tag{7.10}
$$

The coefficients of the equation system are given by the relationships (6.41)–(6.48) of Chapter 6, but the angles α_{kj}, α^{t}_{kj}, α^{n}_{kj} have to relate in a tangential and normal direction in the boundary nodal points according to the scheme of Fig. 7.2.

The right-hand sides of the system of equations (7.10) have the form of relationships (6.51), (6.52) in the case of load $pe^{i\omega t}$, which is uniformly distributed in a circular area with radius e_0.

7.2 Numerical results

A submitted solution can be illustrated by the numerical results of the problem of stress-wave propagation in an unbounded plate, with a rectangular hole, resting on the subgrade. The boundaries of the hole are free.

A dynamic harmonic load acting on the surface of the plate is uniformly distributed on a circular area with radius e_0.

During the numerical study the following parameters and dimensionless values were used: δ=0.10, δ_0=0.20, μ=0.20, μ_0=0.35, c_2/c_{20}=13.65, K_1h/E=0.00188, K_2/Eh=0.00197, e_0/h=0.25.

The theoretical analysis and procedures were realized using a computer program in FORTRAN 77 on an IBM PC—AT personal computer. The numerical parametric study

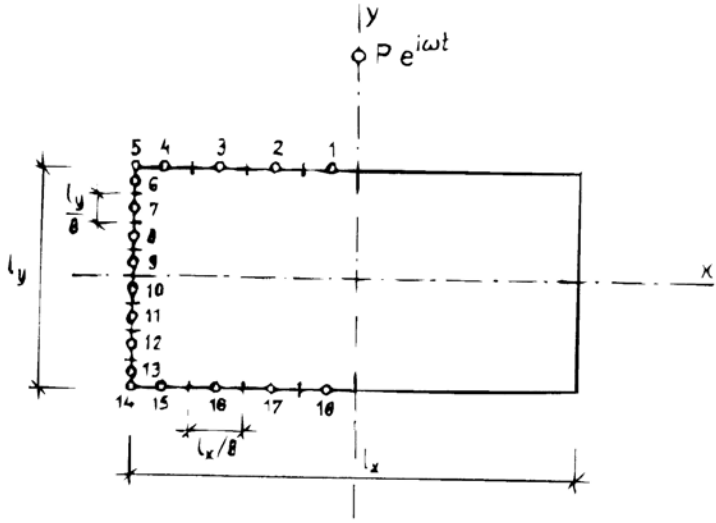

Fig. 7.3. Schematic diagram of boundary elements.

was carried out for rectangular holes in the plate on subgrade with various dimensions of hole sides. The number of boundary elements and nodal points was held to be the same. The elementary scheme of the hole and its division into boundary elements and nodal points are shown in Fig. 7.3.

Assuming symmetry of the system and division of every side into eight boundary elements, the total number of unknown boundary quantities will be 3×16+4(corner points)=52. Because of the complex values of the unknown quantities the task is transformed into the solution of 104 algebraic equations.

7.2.1 Diffraction of stress waves in plate on subgrade with rectangular hole

The dimensions of the sides of the rectangular hole in the plate are l_x=4.80 m, l_y=1.60 m. A dynamic harmonic load with angular frequency ω acts at the symmetry axis y at distance 2.80 m.

The calculation of the unknown quantities on the boundary of the plate hole was performed for various values of dimensionless frequency $\beta=\omega h/c_2$ in the range (0.0–0.30). Provided that the velocity of shear waves in concrete plate c_2=2400 m/s and the thickness of the plate h=0.30 m, the frequency range covers frequencies up to 380 Hz.

The amplitude—frequency characteristics of the deflection $|w|E/ph$ are drawn in Fig. 7.4 for nodal points 1, 6, 13 and 18. The dynamic response has two resonance zones in the analysed frequency range, the first near frequency β=0.025 and the second for β=0.165.

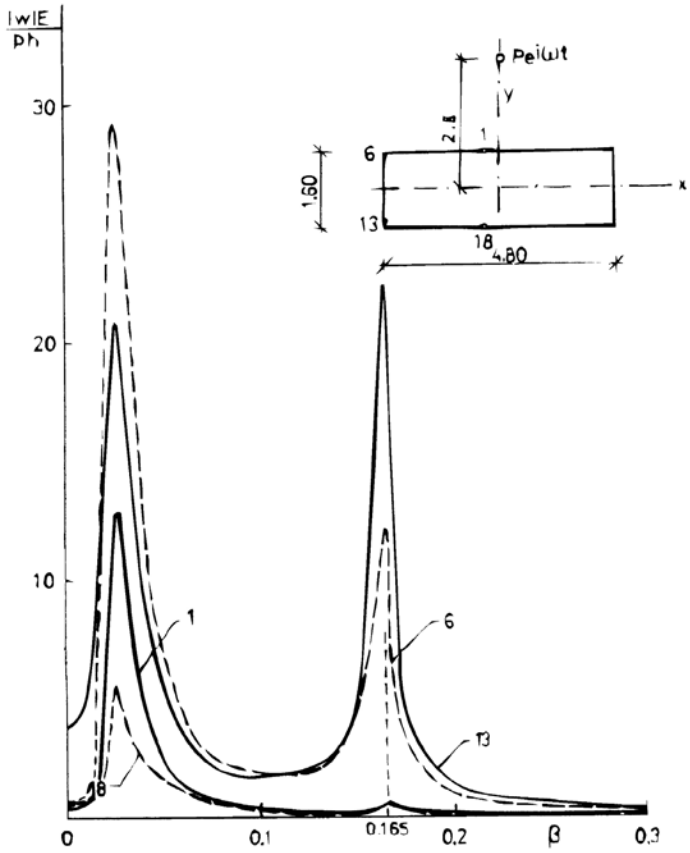

Fig. 7.4. Amplitude—frequency characteristics of deflection at nodal point of hole boundary.

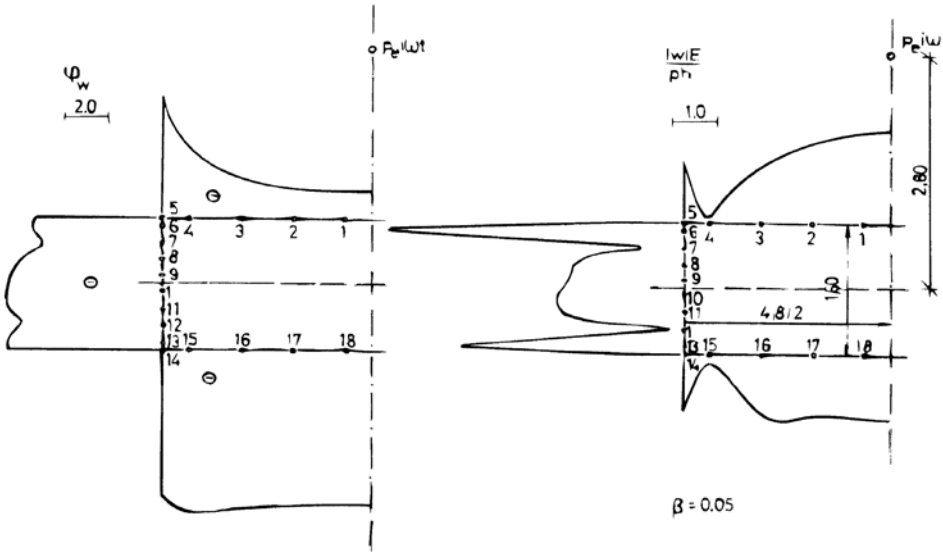

Fig. 7.5. Amplitudes of dynamic deflections $|w|E/(ph)$ and phase angles φ_w along hole boundaries at frequency β=0.05.

The distribution of the amplitudes of dynamic deflections $|w|E/ph$ and phase angles φ_w along the hole boundaries is plotted in Figs. 7.5– 7.7 for frequencies β=0.05, 0.10 and

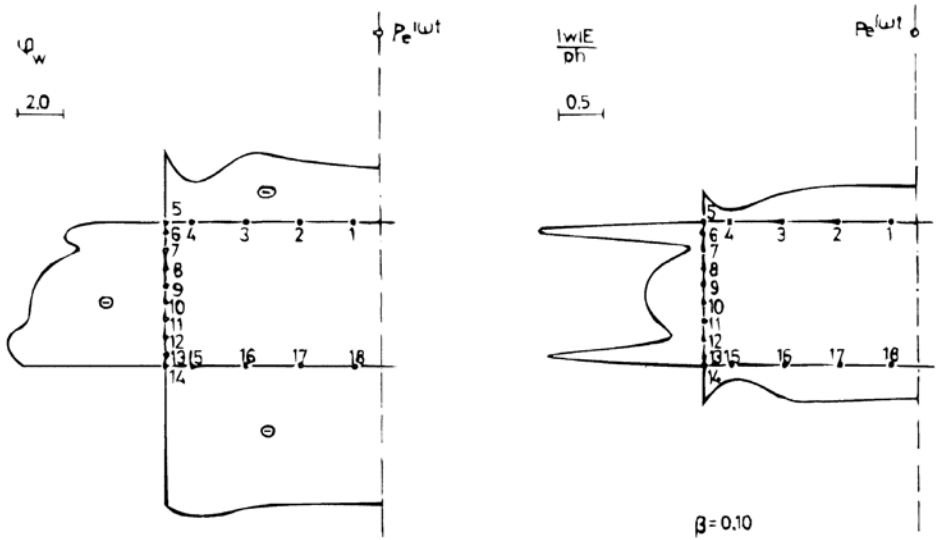

Fig. 7.6. Amplitudes of dynamic deflections $|w|E/(ph)$ and phase angles φ_w along hole boundaries at frequency β=0.10.

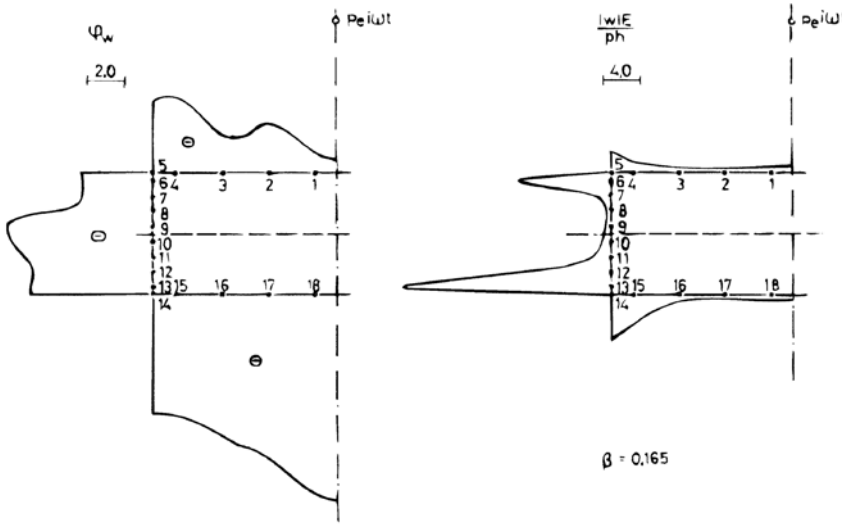

Fig. 7.7. Amplitudes of dynamic deflections $|w|E/(ph)$ and phase angles φ_w along hole boundaries at frequency β=0.165.

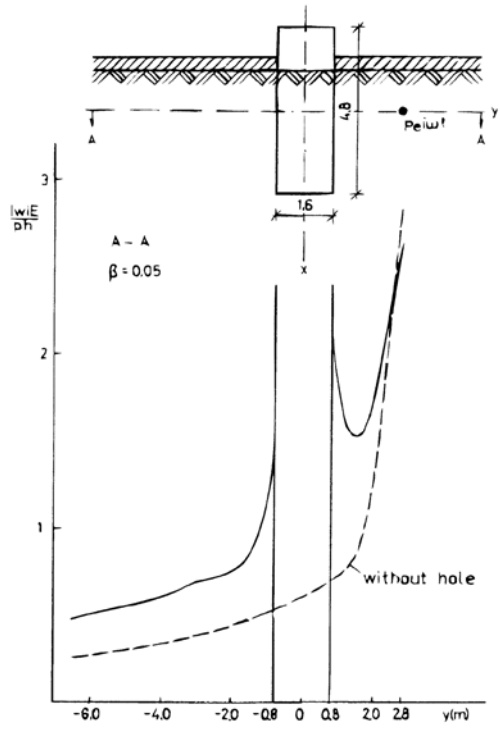

Fig. 7.8. Effect of plate hole on vibration amplitudes at frequency β=0.05.

0.165. It can be seen that the marked concentration of vibration along the sides of the rectangular hole is particularly noticeable near the corner of the lateral sides. The largest concentration of vibration at these places arises at the resonance frequency β=0.165.

The increase of the vibration amplitudes about the rectangular hole in comparison with the situation of vibration propagation in a plate on subgrade without a hole present, occurs along the cross-section A–A, i.e. along the axis y in Figs. 7.8–7.10.

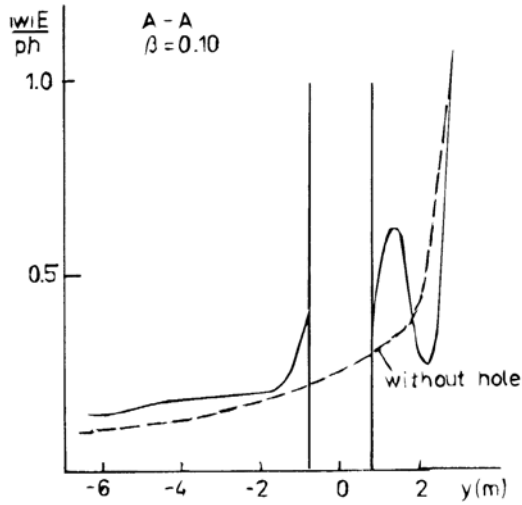

Fig. 7.9. Effect of plate hole on vibration amplitudes at frequency β=0.10.

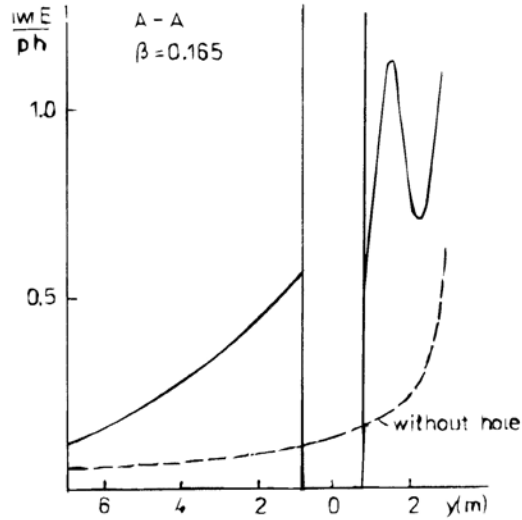

Fig. 7.10. Effect of plate hole on vibration amplitudes at frequency β=0.165.

The influence of the hole causes the concentration of vibration with the interference of direct and reflected waves in front of the frontal side of the rectangular hole but at the area behind the hole too. The concentration of the vibration is especially marked at the resonance frequencies. The hole becomes an amplifier of the vibration.

7.2.2 Influence of length of lateral sides of rectangular hole on resonance regions and vibration concentration

Let us assume a rectangular hole in a plate on subgrade with sides l_x=4.80 m, i.e. the same as in the previous analysis, but with the length of the lateral sides doubled, i.e. l_y=3.20 m. The location of dynamic load $Pe^{i\omega t}$ is on the axis y at distance 3.60 m. The amplitude—frequency

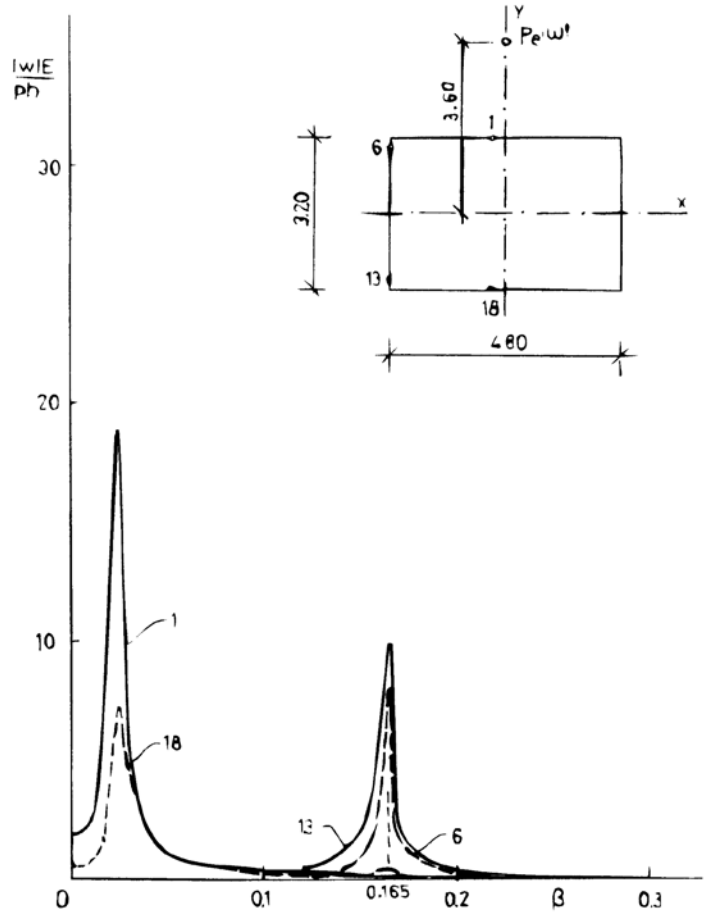

Fig. 7.11. Amplitude-frequency characteristics of deflection at nodal points of hole boundary.

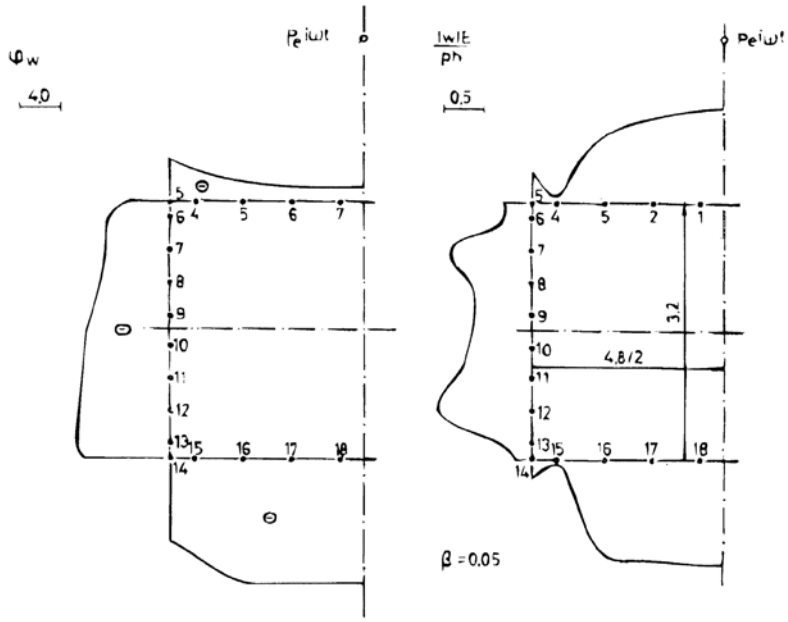

Fig. 7.12. Amplitudes of dynamic deflections $|w|E/(ph)$ and phase angles φ_w along hole boundaries at frequency β=0.05.

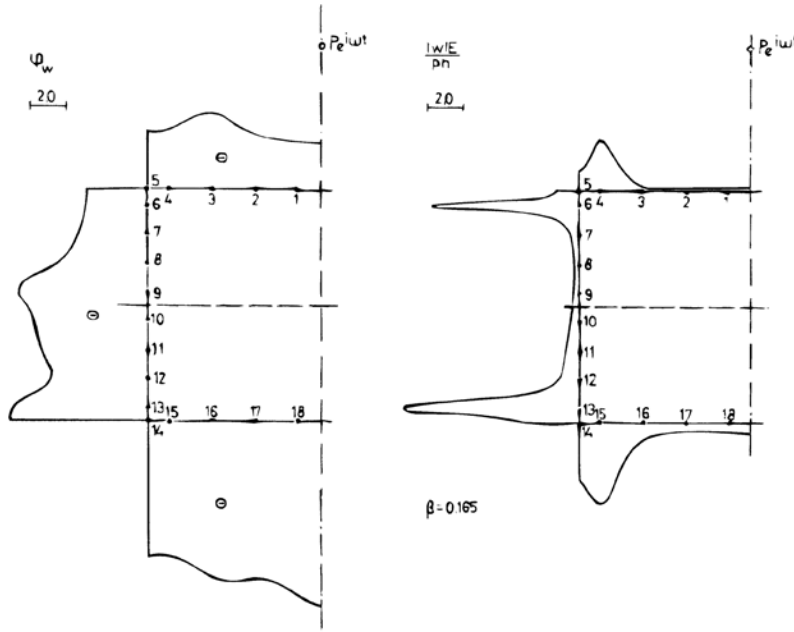

Fig. 7.13. Amplitudes of dynamic deflections $|w|E/(ph)$ and phase angles φ_w along hole boundaries at frequency β=0.165.

characteristics of deflection $|w|E/ph$ at the boundary nodal points 1, 18 or 6, 13 are shown in Fig. 7.11. Resonance zones rise again at frequencies β=0.025 and β=0.165. The results demonstrate that these resonances do not depend on the length of lateral side l_y of the rectangular hole.

The curves of the amplitudes of dynamic deflection $|w|E/ph$ and the phase angle φ_w at the boundary points are drawn in Figs. 7.12 and 7.13 for frequencies β=0.05 and β=0.165. They confirm the concentration of the vibration about the corner points of the rectangular hole, especially at the frequency β=0.165; at the same time, however, they indicate the subduing of the concentrated amplitudes of vibration at the lateral sides of the hole for the frequency β=0.05.

This trend is confirmed by the curves of the deflection amplitudes on the hole boundary in the case l_y=4.80 m, i.e. for a square hole as in Fig. 7.14; in contrast the increase of the concentration of vibration with reduction of the lateral hole sides, l_y=0.16 m, is presented in Fig. 7.15.

In conclusion it is possible to state that the length l_y of the lateral sides of a rectangular hole in a plate on subgrade for the analysed scheme of dynamic load activity has no

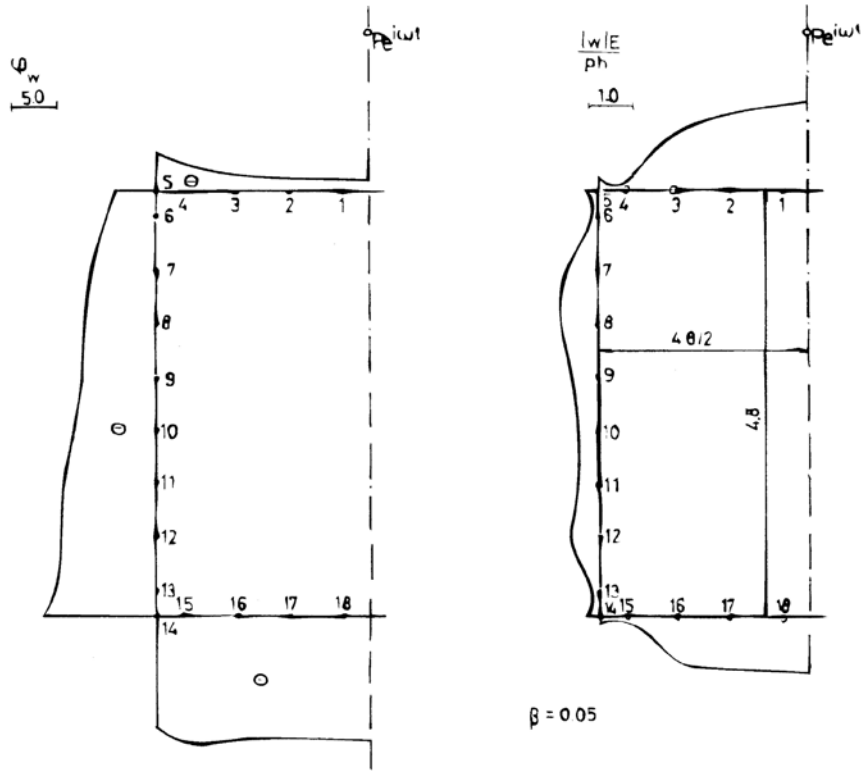

Fig. 7.14. Amplitudes of dynamic deflections $|w|E/(ph)$ and phase angles φ_w along hole boundaries at frequency β=0.05.

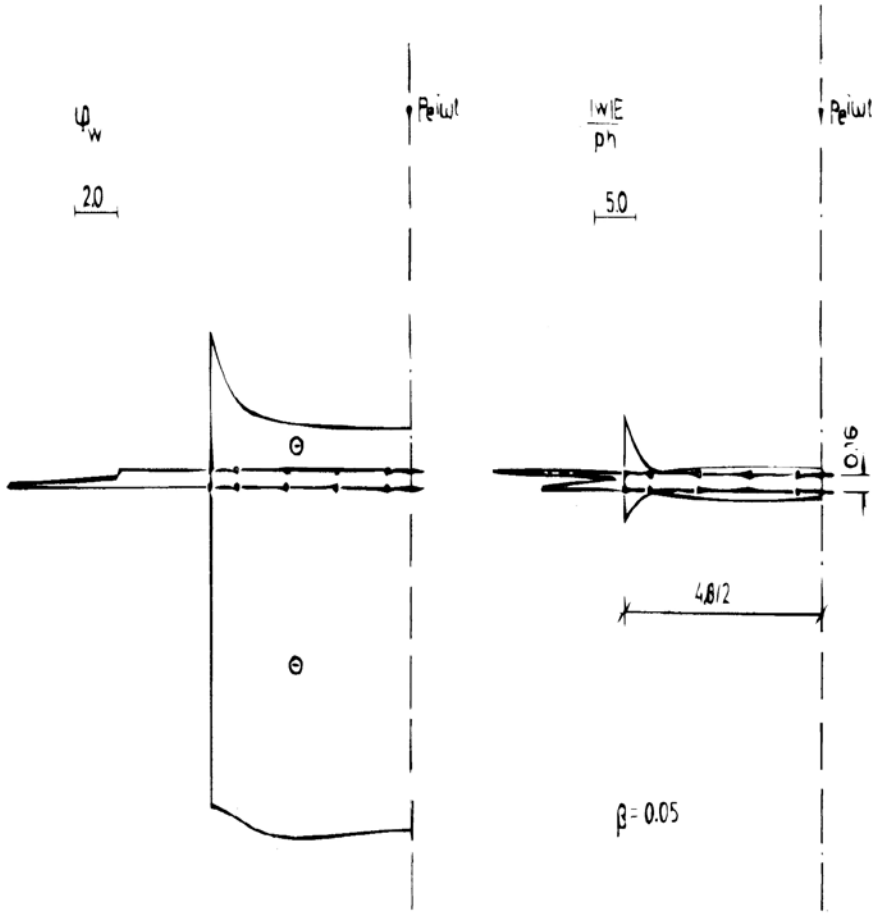

Fig. 7.15. Amplitudes of dynamic deflections $|w|E/(ph)$ and phase angles φ_w along hole boundaries at frequency β=0.05.

influence on resonance zones but alters the size of vibration concentration about the corner points of the hole, which increases with a reduction of the lateral side length.

7.2.3 Influence of length of frontal sides of a rectangular hole on resonance regions

Another series of numerical calculations was performed for the case of a rectangular hole with frontal side length l_x=6.40 m and lateral side length l_y=3.20 m.

The amplitude—frequency characteristics of a dynamic deflection at boundary points 1, 6, 13 and 18 are plotted in Fig. 7.16, and the curves of the deflection amplitude and phase angle φ_w along the hole boundary at frequency β=0.092 are plotted in Fig. 7.17.

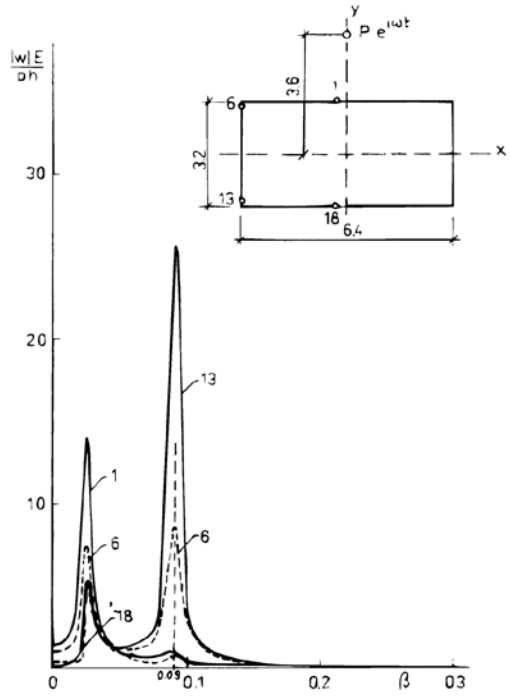

Fig. 7.16. Amplitude-frequency characteristics of deflection at nodal point of hole boundary.

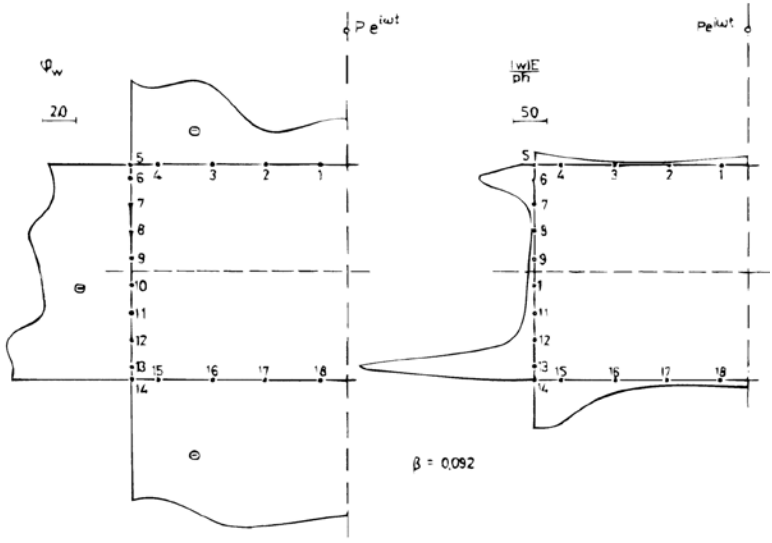

Fig. 7.17. Amplitudes of dynamic deflections $|w|E/(ph)$ and phase angles φ_w along hole boundaries at frequency β=0.092.

One can see that the amplitude—frequency characteristic contains the first resonance zone at the non-altered frequency β=0.025, but the second resonance zone has changed as a consequence of the alteration of frontal side length l_x. It has decreased from the value β=0.165 to β=0.092. The character of the vibration concentration about the corner points of the hole in the plate has remained similar to the previous cases.

It is evident that the second resonance frequency depends only on the length l_x of the frontal side of the rectangular hole. Proof is available. By the flexural vibration of the plates the resonance frequencies change in indirect proportion to the square of the side lengths. In this case this means that the ratio of resonance frequencies β=0.092 and β=0.165, i.e. 0.092/0.165=0.557, has to be equal to the ratio of the squares of frontal side lengths of the plate hole, i.e. $4.80^2/6.40^2$=0.561. In practical terms, this requirement is fulfilled.

The first resonance zone, which does not depend upon the lengths of the frontal or lateral hole sides, is probably connected to the stiffnesses of the subgrade and plate. In section 6.5 by the solution of the vibration of the bounded plate on subgrade similar resonance zones have arisen at frequencies β=0.025–0.035.

7.3 Influence of rectangular hole in plate on subgrade by pulse propagation

The method of boundary integral equations developed for the problem of flexural stress-wave propagation in a plate with a hole provides the dynamic response of the system, $S^*(\beta)$, under a dynamic harmonic load with arbitrary dimensionless frequency $\beta=\omega h/c_2$. The dynamic response $S^*(\beta)$ is a complex function with real part $S_R(\beta)$ and imaginary part $S_J(\beta)$.

In the cases of non-stationary vibration under a pulsed dynamic load it is possible to use Fourier's integral transformation according to the procedure in section 4.8. Although by its application the zero initial conditions are not fulfilled the dynamic response is sufficiently true and reliably reflects the reaction of the system under a pulse load.

The original of the state vector component is given by inverse transformation according to equation (4.79). The realization of such a procedure requires us to know the courses of functions $S_R(\beta)$ and $S_J(\beta)$ at the relevant frequency range and to replace the improper integral with a finite integral. We know the values of functions $S_R(\beta)$ and $S_J(\beta)$ only at discrete frequencies β this is why it has to be replaced in the numerical solution of equation (4.79) by continuous spline functions.

7.3.1 Numerical results

Let us assume that the plate on subgrade has a rectangular hole 6.40×3.20 m and the pulsed load is acting on the symmetry axis y at a distance 3.60 m. The results of the numerical solution using the method of boundary elements and harmonic load are known from section 7.2.3. The dynamic deflection response is presented as amplitude—frequency functions for boundary points 1 and 13 in Fig. 7.16. The characteristics for point 1 reflect essentially only the first resonance zone, while the characteristics for boundary point 13 comprise both resonances but reflect more the second resonance zone.

The curves of the real part $w_R E/ph$ and imaginary part $w_J E/ph$ of the dynamic deflection response at point 1 are shown in Fig. 7.18 and the calculated dynamic deflection to the pulse excitation in Fig. 7.19 for values of pulse duration represented by parameter Ω_0=0.012, 0.025, 0.050, 0.100 and 0.250. Parameter Ω_0 is indirectly proportional to the pulse duration.

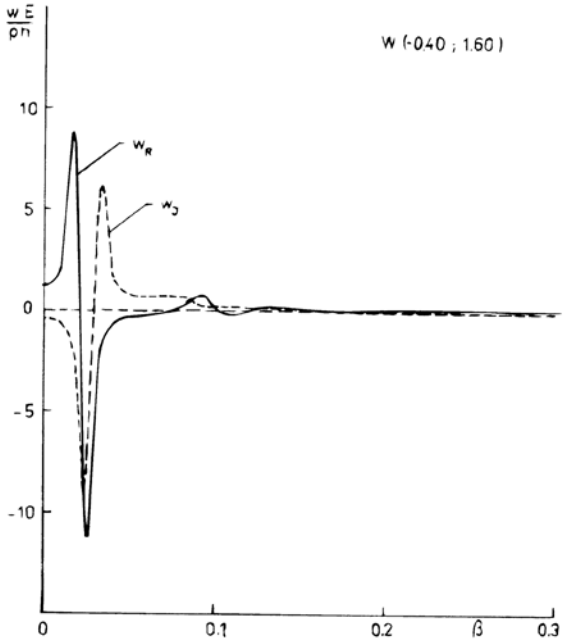

Fig. 7.18. Variation of real and imaginary parts of dynamic deflection response at hole boundary point 1.

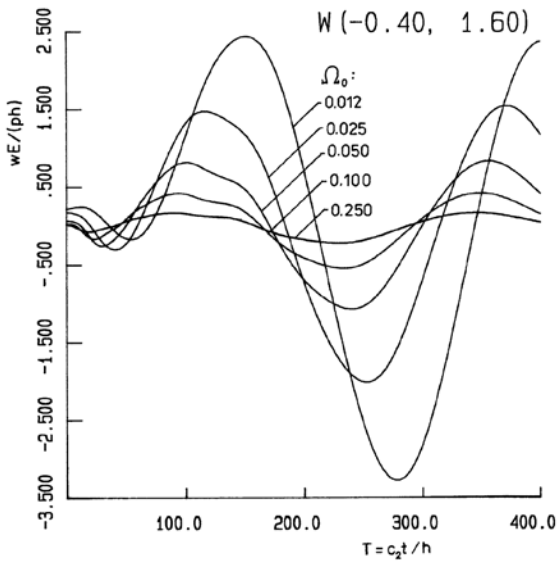

Fig. 7.19. Dynamic deflection responses at hole boundary point 1 under pulsed load for various values of pulse duration.

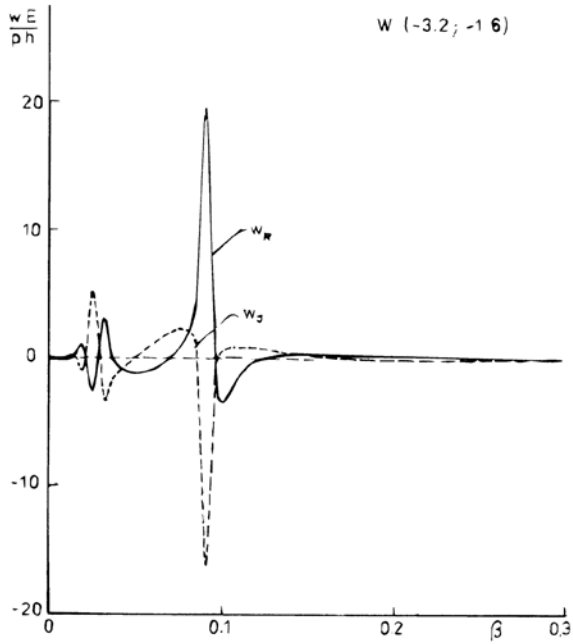

Fig. 7.20. Variation of real and imaginary parts of dynamic deflection response at hole boundary point 13.

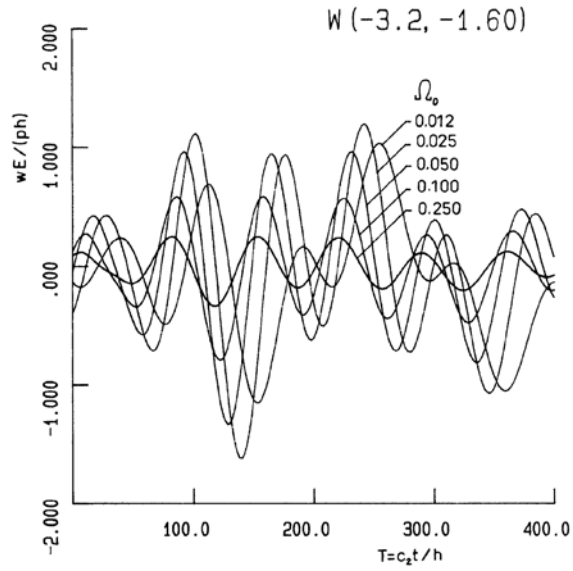

Fig. 7.21. Dynamic deflection responses at hole boundary point 13 under pulsed load for various values of pulse duration.

Similarly the real and imaginary part of the dynamic deflection response at boundary point 13 are given in Fig. 7.20 and the dynamic deflection under pulse load for various values of Ω_0 is shown in Fig. 7.21.

It can be seen that the dynamic response at point 1 is formed by the spectrum components of the first resonance frequency β=0.025 while the spectral components of the second resonance frequency β=0.092 predominate in the response at point 13.

The dynamic deflection response achieves its maximum amplitudes at point 1 for pulse parameter Ω_0=0.012 and at point 13 for β=0.025.

A relatively complicated and at present non-analysed problem of the vibration concentration near a hole in a plate on subgrade can be realized very well using the method of boundary integral equations.

Diffraction of the stress waves on the boundary of the hole causes concentration of the vibration in the surroundings by the process of propagation, which is magnified by means of resonance phenomena.

All these facts obtained by the problem solution are quite obvious and comprehensible from a physical point of view. Despite this the intensity of the concentration of vibration at some points of the plate hole is so expressive that it evokes the necessity of experimental identification of the phenomena.

The questions raised for solution in this section have no immediate use in the design of pavement structures but their contribution to theoretical fundamentals and further development in the mechanics of pavement structures is evident.

8
NON-LINEAR DYNAMIC RESPONSE OF UNBOUNDED PLATE ON SUBGRADE

Green's function w_0 for an unbounded plate on subgrade in the conception of a dynamic influence function of the deflection for stationary time courses is the solution of the equation

$$\nabla^2\nabla^2 w_0 - \frac{K_2^*}{D^*}\,\nabla^2 w_0 + \frac{K_1^*}{D^*} w_0 + \frac{k_d \varrho h}{D^*}\,\frac{\partial^2 w_0}{\partial t^2} = \frac{1}{D^*}\,\frac{\delta(r)}{2\pi r}\,\delta(t) \tag{8.1}$$

where $\delta(r)$, $\delta(t)$ are Dirac's generalized functions. By using Hankel's integral transformation and Fourier's integral transformation we obtain Green's function in the form

$$w_0(r,t) = \frac{-3(1-\mu^2)\mathrm{i}}{2Eh\Theta(1+\mathrm{i}\delta)} \int_{-\infty}^{\infty} \left[H_0^{(2)}(\gamma_1 r) - H_0^{(2)}(\gamma_2 r)\right] \mathrm{e}^{\mathrm{i}\omega t}\,\mathrm{d}\omega \tag{8.2}$$

if γ_1, γ_2, Θ are given by the equations (6.5)–(6.7).

8.1 Dynamic deflection of unbounded plate on non-linear soil base under a stationary load

A non-linear deflection may be established by the solution of a differential equation of motion in the form

$$\nabla^4 w - \frac{K_2^*}{D^*}\nabla^2 w + \frac{K_1}{D^*} w + \frac{k_\mathrm{d}\varrho h}{D^*}\,\frac{\partial^2 w}{\partial t^2} = \frac{p(r)\mathrm{e}^{\mathrm{i}\omega_1 t}}{D^*} - \frac{K_4^*}{D^*} w^3. \tag{8.3}$$

We suppose, then, a harmonically variable normal load with frequency

ω_1 and a non-linear cubic member with a coefficient of non-linear compression K_4^* in N/m^5.

The solution of equation (8.3) using Green's function w_0 is as follows

$$w(r,t)=\frac{-3(1-\mu^2)\mathrm{i}}{2Eh\Theta(1+\mathrm{i}\delta)}\frac{1}{2\pi}\int_{-\infty}^{\infty}\iint_{S}p(\vec{\varrho})\Big\{H_0^{(2)}[\gamma_1(\vec{r}-\vec{\varrho}]$$

$$-H_0^{(2)}[\gamma_2(\vec{r}-\vec{\varrho})]\Big\}\mathrm{d}S\int_{-\infty}^{\infty}\mathrm{e}^{\mathrm{i}\omega(t-\tau)}\mathrm{e}^{\mathrm{i}\omega_1\tau}\mathrm{d}\tau\mathrm{d}\omega \tag{8.4}$$

$$+\frac{3(1-\mu^2)\mathrm{i}\,K_4^*}{2Eh\Theta(1+\mathrm{i}\delta)}\frac{1}{2\pi}\int_{-\infty}^{\infty}\iint_{S}\int_{-\infty}^{\infty}\left\{H_0^{(2)}\left[\gamma_1(\vec{r}-\vec{\varrho})\right]-H_0^{(2)}\left[\gamma_2(\vec{r}-\vec{\varrho})\right]\right\}$$

$$\times\,\mathrm{e}^{\mathrm{i}\omega(t-\tau)}\mathrm{d}\omega\,w^3(\vec{\varrho},\tau)\,\mathrm{d}S(\vec{\varrho})\mathrm{d}\tau$$

where the sub-integral function is a vector function with the radius vector of deflection point $\vec{r}$ and the radius vector of the load point $\vec{\varrho}$.

Provided that the following equation is valid

$$\frac{1}{2\pi}\int_{-\infty}^{\infty}\mathrm{e}^{-\mathrm{i}(\omega-\omega_1)\tau}\mathrm{d}\tau=\delta(\omega-\omega_1) \tag{8.5}$$

if the integral is considered as generalized function, then equation (8.4) for deflection can be expressed

$$w=\bar{w}_{\mathrm{L}}+\frac{K_4^*6(1-\mu^2)}{Eh\Theta(1+\mathrm{i}\delta)}\frac{1}{2\pi}\int_{-\infty}^{\infty}\int_{-\infty}^{\infty}N(\vec{\varrho},\vec{r},\omega,\tau)\,\mathrm{e}^{\mathrm{i}\omega(t-\tau)}\mathrm{d}\omega\mathrm{d}\tau \tag{8.6}$$

if

$$\bar{w}_{\mathrm{L}}=\frac{-3(1-\mu^2)\mathrm{i}\,\mathrm{e}^{\mathrm{i}\omega_1 t}}{2Eh\Theta(1+\mathrm{i}\delta)}\iint_{S}\left\{H_0^{(2}\left[\gamma_1(\vec{r}-\vec{\varrho})\right]-H_0^{(2)}\left[\gamma_2(\vec{r}-\vec{\varrho})\right]p(\vec{\varrho})\mathrm{d}S\right. \tag{8.7}$$

and

$$N=\iint_{S}\frac{1}{4}\left\{H_0^{(2)}\left[\gamma_1(\vec{r}-\vec{\varrho})\right]-H_0^{(2)}\left[\gamma_2(\vec{r}-\vec{\varrho})\right]\right\}w^3(\vec{\varrho},\tau)\,\mathrm{d}S. \tag{8.8}$$

By using the procedure in [3.19] the value of integral N is determined by the relation

$$N = \frac{w^3(\gamma_1 r)}{\gamma_1^2} - \frac{w^3(\gamma_2 r)}{\gamma_2^2} \tag{8.9}$$

The nonlinear deflection of a plate on subgrade according to equation (8.6) is expressed by the equation

$$w = \bar{w}_{\mathrm{L}} + \frac{K_4^* \, 6(1-\mu^2)}{Eh\Theta(1+\mathrm{i}\delta)} \frac{1}{2\pi} \int_{-\infty}^{\infty}\int_{-\infty}^{\infty} \left[\frac{w^3(\gamma_1 r,\tau)}{\gamma_1^2(\omega)} - \frac{w^3(\gamma_2 r,\tau)}{\gamma_2^2(\omega)}\right] \mathrm{e}^{\mathrm{i}\omega(t-\tau)} \mathrm{d}\tau \, \mathrm{d}\omega \tag{8.10}$$

in which $\bar{w}_{\mathrm{L}}$ is the linear deflection of the plate.

The method of iteration can be used in the solution of integral equation (8.10). The first approximation expressed by linear deflection $\bar{w}_L$ gives the relationships

$$\begin{gathered} w = \bar{w}_{\mathrm{L}} = w_{\mathrm{L}} \mathrm{e}^{\mathrm{i}\omega_1 t} \\ w^3 = w_{\mathrm{L}}^3 \, \mathrm{e}^{\mathrm{i}\,3\omega_1 t} \end{gathered} \tag{8.11}$$

and substituting this into the right-hand side of equation (8.10), this relationship becomes

$$\begin{aligned} w = w_{\mathrm{L}} \, \mathrm{e}^{\mathrm{i}\omega_1 t} + \frac{K_4^* \, 6(1-\mu^2)}{Eh\theta(1+\mathrm{i}\delta)} \frac{1}{2\pi} \int_{-\infty}^{\infty}\int_{-\infty}^{\infty} \left[\frac{w_L^3(\gamma_1 r)}{\gamma_1^2(\omega)} - \frac{w_L^3(\gamma_2 r)}{\gamma_2^2(\omega)}\right] \\ \times \mathrm{e}^{-\mathrm{i}\tau(\omega-3\omega_1)} \mathrm{e}^{\mathrm{i}\omega t} \mathrm{d}\tau \, \mathrm{d}\omega \end{aligned} \tag{8.12}$$

Since the following equation is valid

$$\frac{1}{2\pi} \int_{-\infty}^{\infty} \mathrm{e}^{-\mathrm{i}\tau(\omega-3\omega_1)} \mathrm{d}\tau = \delta(\omega - 3\omega_1) \tag{8.13}$$

if the integral is considered as a generalized function then equation (8.12) becomes

$$\begin{aligned} w &= w_{\mathrm{L}} \, \mathrm{e}^{\mathrm{i}\omega_1 t} + \frac{K_4^* \, 6(1-\mu^2)}{Eh\Theta(1+\mathrm{i}\delta)} \int_{-\infty}^{\infty} \left[\frac{w_L^3(\gamma_1 r)}{\gamma_1^2(\omega)} - \frac{w_L^3(\gamma_2 r)}{\gamma_2^2(\omega)}\right] \delta(\omega - 3\omega_1) \, \mathrm{e}^{\mathrm{i}\omega t} \mathrm{d}\omega \\ &= w_{\mathrm{L}} \mathrm{e}^{\mathrm{i}\omega_1 t} + \frac{K_4^* \, 6(1-\mu^2)}{Eh\Theta(1+\mathrm{i}\delta)} \left[\frac{w_L^3(\gamma_1 r)}{\gamma_1^2(3\omega_1)} - \frac{w_L^3(\gamma_2 r)}{\gamma_2^2(3\omega_1)}\right] \mathrm{e}^{\mathrm{i}3\omega_1 t} \end{aligned} \tag{8.14}$$

In the following iteration step equation (8.14) will be used and by substituting it into (8.10) the second approximation will be obtained.

8.2 Non-stationary vibration problems of an unbounded plate on subgrade

For the stationary vibration of a plate on subgrade the damping of the material of the plate and subgrade is considered by the application of complex characteristics of elasticity E^*, K_1^*, K_2^* and K_4^*.

In the case of a non-stationary vibration problem it is better to consider viscous damping, because by using the complex characteristics of elasticity the problems with the fulfilling of the causation principle are established.

The differential equation of motion is considered in the form

$$\nabla^2\nabla^2 w - \frac{K_2}{D}\nabla^2 w + \frac{K_1}{D}w + \frac{k_d \varrho h}{D}\frac{\partial^2 w}{\partial t^2} + \frac{K_5}{D}\frac{\partial w}{\partial t} = \frac{P}{2\pi D}\frac{\delta(r)}{r}\,\delta(t) \tag{8.15}$$

in which K_1, K_2 and D are real characteristics of subgrade elasticity and plate rigidity, the damping characteristic K_5 (Ns/m^3) expresses the damping stress by unit moving velocity, and $\delta(r)$ and $\delta(t)$ are Dirac's generalized functions.

By using Hankel's integral transformation the original or Green's function $w_0(r, t)$ is established from equation (8.15) in the form

$$w_0(r,t) = -\frac{1}{2\pi D}\int_0^\infty \alpha J_0(\alpha r)\frac{1}{2\pi}\int_{-\infty}^{\infty}\frac{e^{-i\omega t}\,d\omega\,d\alpha}{\left(\frac{\varrho h k_d}{D}\omega^2 + \frac{i\omega K_5}{D} - \frac{K_1}{D} - \frac{K_2\alpha^2}{D} - \alpha^4\right)} \tag{8.16}$$

where α is an integral parameter of Hankel's transformation and ω is an integral parameter of Fourier's transformation.

Calculating the interior integral by the method of residua we obtain

$$w_0(r,t) = \frac{-e^{-\frac{\varepsilon_1}{2}t}}{2\pi\varrho h k_d}\int_0^\infty \frac{\alpha J_0(\alpha r)\sin\left(\sqrt{\frac{1}{\varrho h k_d}(K_1 + K_2\alpha^2 + D\alpha^4) - \frac{\varepsilon_1^2}{4}}\,t\right)}{\sqrt{\frac{1}{\varrho h k_d}\left(K_1 + K_2\alpha^2 + D\alpha^4 - \frac{\varepsilon_1^2}{4}\right)}}\,d\alpha \tag{8.17}$$

if

$$\varepsilon_1 = \frac{K_5}{\varrho h k_d}. \tag{8.18}$$

The improper integral (8.17) can be calculated numerically by substituting an integral with a sufficiently large value of upper limit α. The integral converges and has no singularity for

$$\frac{\varepsilon_1^2}{4} < \frac{1}{\varrho h k_d}\,(K_1 + K_2\alpha^2 + D\alpha^4).$$

In the case of a vertical normal load with intensity $p=P/\pi a^2$, which is uniformly divided on a circular area of the plate surface with radius a, equation (8.17) is given in the form

$$w_0(r,t) = \frac{P\,\mathrm{e}^{-\frac{\varepsilon_1}{2}t}}{2\pi^2 \varrho h k_d a}$$

$$\times \int_0^\infty \frac{J_1(\alpha a)\, J_0(\alpha r)\, \sin\left(\sqrt{\frac{1}{\varrho h k_d}(K_1 + K_2\alpha^2 + D\alpha^4) - \frac{\varepsilon_1^2}{4}}\, t\right)}{\sqrt{\frac{1}{\varrho h k_d}(K_1 + K_2\alpha^2 + D\alpha^4) - \frac{\varepsilon_1^2}{4}}}\,\mathrm{d}\alpha \tag{8.19}$$

Equations (8.17) and (8.19) are valid for an instantaneous pulse load (given by Dirac's generalized time function). In the cases of pulse loads formulated by the functions of non-stationary time course $f_1(\tau)$ the dynamic response of the system is determined by the relationship

$$w_0(r,t) = -\int_0^t \frac{f_1(\tau)\,\mathrm{e}^{-\frac{\varepsilon_1}{2}(t-\tau)} P}{2\pi^2 \varrho h k_d a}$$

$$\times \int_0^\infty J_1(\alpha a)\, J_0(\alpha r)\, \sin\frac{\left[\sqrt{\frac{1}{\varrho h k_d}(K_1 + K_2\alpha^2 + D\alpha^4) - \frac{\varepsilon_1^2}{4}}\,(t-\tau)\right]\mathrm{d}\alpha\mathrm{d}\tau}{\sqrt{\frac{1}{\varrho h k_d}(K_1 + K_2\alpha^2 + D\alpha^4) - \frac{\varepsilon_1^2}{4}}}. \tag{8.20}$$

8.3 Non-linear non-stationary vibration of a plate on subgrade

The assumption of the non-linear effect of subgrade leads to the differential equation of motion in the form

$$\nabla^2\nabla^2 w - \frac{K_2}{D}\nabla^2 w + \frac{K_1}{D} w + \frac{k_d \varrho h}{D}\frac{\partial^2 w}{\partial t^2} + \frac{K_5}{D}\frac{\partial w}{\partial t} = \frac{p(r,t)}{D} - \frac{K_4}{D} w^3. \tag{8.21}$$

Equation (8.17) was derived for Green's function $w_0(r, t)$ for non-stationary time courses. Then for the deflection w of the plate on subgrade according to (8.21) the relationship is given

$$w = \frac{1}{D}\int_0^t \int_{S_0} p(\vec{\varrho},\tau)\, w_0(\vec{r},\vec{\varrho},t,\tau)\,\mathrm{d}S_0\mathrm{d}\tau$$

$$-\frac{K_4}{D}\int_0^t \int_{S\infty} w^3(\vec{\varrho},\tau)\, w_0(\vec{r},\vec{\varrho},t,\tau)\mathrm{d}S\mathrm{d}\tau \tag{8.22}$$

where S_0 is the load area of the plate on subgrade and S_∞ is the unbounded region of the plate on subgrade.

The first part of equation (8.22) is the linear solution of the task, which can be marked by w_L.

Fourier's transform of the function $w_0(r, t)$ is given in the form

$$^{F}w_0 = \frac{-3(1-\mu^2)\mathrm{i}}{2EBh^3}\left\{H_0^{(2)}\left[\gamma_1(\vec{r}-\vec{\varrho})\right] - H_0^{(2)}\left[\gamma_2(\vec{r}-\vec{\varrho})\right]\right\} \tag{8.23}$$

if

$$\gamma_1^2 = A + B$$
$$\gamma_2^2 = A - B \tag{8.24}$$

and

$$A = -\frac{K_2}{2D} \tag{8.25}$$

$$B = \sqrt{A^2 - \frac{K_1}{D} + \mathrm{i}\omega\,\frac{K_5}{D} + \frac{\varrho h k_\mathrm{d}}{D}\omega^2}. \tag{8.26}$$

Equation (8.22) can be expressed as the relationship

$$w = w_\mathrm{L} + \frac{K_4}{D}\int_0^t \frac{1}{2\pi}\int_{-\infty}^{\infty}\int_{S\infty} w^3(\vec{\varrho},\tau)\left\{-\frac{3(1-\mu^2)\mathrm{i}}{2EBh^3}\left[H_0^{(2)}(\gamma_1(\vec{r}-\vec{\varrho}))\right.\right.$$
$$\left.\left. - H_0^{(2)}\left(\gamma_2(\vec{r}-\vec{\varrho})\right)\right]\right\}\mathrm{d}S\,\mathrm{e}^{\mathrm{i}\omega(t-\tau)}\,\mathrm{d}\omega\,\mathrm{d}\tau. \tag{8.27}$$

By using the procedure in [3.19] the relationships can be established in the form

$$\int_{S\infty} w^3(\vec{\varrho},\tau)\frac{\mathrm{i}}{4}\,H_0^{(2)}\left[\gamma_1(\vec{r}-\vec{\varrho})\right]\,\mathrm{d}S = \frac{w^3(r,\tau)}{\gamma_1^2}$$
$$\int_{S\infty} w^3(\vec{\varrho},\tau)\frac{\mathrm{i}}{4}\,H_0^{(2)}\left[\gamma_2(\vec{r}-\vec{\varrho})\right]\,\mathrm{d}S = \frac{w^3(r,\tau)}{\gamma_2^2}. \tag{8.28}$$

According to equation (8.28), equation (8.27) becomes

$$w = w_{\mathrm{L}} + A_1 \frac{6(1-\mu^2)}{Eh^3} \int_0^t w^3(r,\tau) \frac{1}{2\pi} \int_{-\infty}^{\infty} \frac{1}{B} \frac{\gamma_2^2 - \gamma_1^2}{\gamma_1^2 \gamma_2^2} \, \mathrm{e}^{-\mathrm{i}\omega(t-\tau)} \mathrm{d}\omega \mathrm{d}\tau \tag{8.29}$$

where

$$A_1 = \frac{K_4}{D}. \tag{8.30}$$

Because of the validity of the following relationships

$$\gamma_1^2 \gamma_2^2 = \frac{K_1}{D} - \mathrm{i}\omega \frac{K_5}{D} - \frac{\varrho h k_{\mathrm{d}}}{D} \omega^2 \tag{8.31}$$

$$\gamma_2^2 - \gamma_1^2 = -2B \tag{8.32}$$

the improper integral in equation (8.29) can be expressed using the method of residua in the form

$$\begin{aligned} &\frac{1}{2\pi} \int_{-\infty}^{\infty} \frac{-2 \, \mathrm{e}^{-\mathrm{i}\omega(t-\tau)} \mathrm{d}\omega}{\frac{K_1}{D} - \mathrm{i}\omega \frac{K_5}{D} - \frac{\varrho h k_{\mathrm{d}}}{D} \omega^2} \\ &= \frac{-2D}{\varrho h k_{\mathrm{d}}} \, \mathrm{e}^{-\frac{\varepsilon_1}{2}(t-\tau)} \sin \left[\frac{\sqrt{\frac{K_1}{\varrho h k_{\mathrm{d}}} - \frac{\varepsilon_1^2}{4}} \, (t-\tau)}{\sqrt{\frac{K_1}{\varrho h k_{\mathrm{d}}} - \frac{\varepsilon_1^2}{4}}} \right] \end{aligned} \tag{8.33}$$

Equation (8.33) is valid assuming that

$$\frac{K_1}{\varrho h k_{\mathrm{d}}} > \frac{\varepsilon_1^2}{4} \tag{8.34}$$

which is always fullfiled for the real values of the damping.

Then in the first approximation equation (8.29) becomes

$${}^1w = w_{\mathrm{L}} - \frac{K_4}{\varrho h k_{\mathrm{d}}} \int_0^t w_{\mathrm{L}}^3(r,\tau) \mathrm{e}^{-\frac{\varepsilon_1}{2}(t-\tau)} \sin \frac{\left[\sqrt{\frac{K_1}{\varrho h k_{\mathrm{d}}} - \frac{\varepsilon_1^2}{4}} \, (t-\tau) \right] d\tau}{\sqrt{\frac{K_1}{\varrho h k_{\mathrm{d}}} - \frac{\varepsilon_1^2}{4}}}. \tag{8.35}$$

8.4 Numerical applications

Equations (8.19), (8.20) and (8.35) can be calculated using numerical integration and computers. It is better to modify these relationships into dimensionless forms by introducing the dimensionless variables

$$\eta = \alpha a$$

$$t_1 = t\frac{c_0}{h} = t\frac{\sqrt{E/\varrho}}{h}$$

$$\tau_1 = \tau\frac{c_0}{h} \tag{8.36}$$

$$\varepsilon_0 = \varepsilon_1\frac{h}{c_0} = \frac{K_5\, c_0}{E\, k_d}.$$

Then equation (8.19) will acquire the form

$$\frac{w_0 E}{ph} = \frac{-e^{-\frac{\varepsilon_0}{2}t_1}}{2\pi k_d}\int_0^\infty \frac{J_1(\eta)\, J_0\left(\eta\frac{r}{a}\right)\, \sin\,(K(\eta)t_1)}{K(\eta)}\,d\eta \tag{8.37}$$

where

$$K(\eta) = \sqrt{\frac{K_1 h}{Ek_d} + \frac{K_2 h}{Ek_d a^2}\eta^2 + \frac{Dh}{Ek_d a^4}\eta^4 - \frac{\varepsilon_0^2}{4}}. \tag{8.38}$$

Equation (8.20) has, after modification, the form

$$\frac{w_0 E}{ph} = \frac{-1}{2\pi k_d}\int_0^{t_1}\int_0^\infty \frac{e^{-\frac{\varepsilon_0}{2}(t_1-\tau_1)} J_1(\eta)\, J_0\left(\eta\frac{r}{a}\right)\, \sin[K(\eta)(t_1-\tau_1)]\, f(\tau_1)}{K(\eta)}\,d\tau_1 d\eta \tag{8.39}$$

and equation (8.35) for non-linear dynamic response has the form

$$\frac{^1wE}{ph} = \frac{w_L E}{ph} - A_0\int_0^{t_1} \frac{\left(\frac{w_L E}{ph}\right)^3 e^{-\frac{\varepsilon_0}{2}(t_1-\tau_1)}\, \sin\left[\sqrt{\frac{K_1 h}{Ek_d} - \frac{\varepsilon_0^2}{4}}\,(t-\tau_1)\right]}{\sqrt{\frac{K_1 h}{Ek_d} - \frac{\varepsilon_0^2}{4}}}\,d\tau_1 \tag{8.40}$$

if

$$A_0 = \frac{K_4 p^2 h^3}{E^3 k_d}.$$

8.4.1 Effect of a trapezoid-shaped pulse

We may assume that a vertical normal load of intensity p=1, the time course of which is determined in Fig. 8.1, is acting on a circular area with radius a on the plate surface.

The numerical analysis is realized for the following values of parameters: μ=0, 25, k_d=2.50, K_1h/E=0.00078, K_2/Eh=0.00082, ε_0=0.02, h/a=1.73.

The variations of dimensionless deflection $W_o=wE/ph$ with the dimensionless time $t_1=tc_0/h$ are plotted in Figs. 8.2–8.4 for various distances from the exciting load which are given by the ratios r/a=5, 10 and 20.

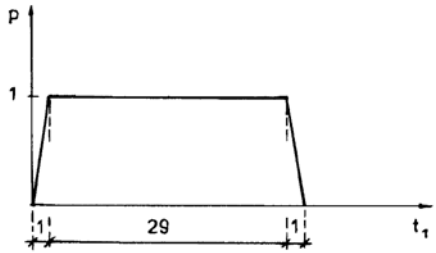

Fig. 8.1. Schematic diagram of trapezoid-shaped pulse.

The forms of the dynamic response confirm the characteristic laws of system action. From the dispersion curve of phase velocities it is evident that the phase velocities of the stress waves increase with increasing frequency or decreasing wavelength. It can be seen from Figs. 8.2–8.4 that the front of the pulse response with increasing distance from the exciting

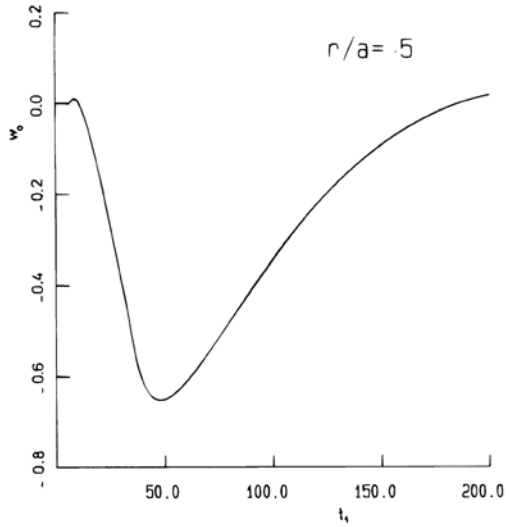

Fig. 8.2. Dynamic deflection response for r/a=5.

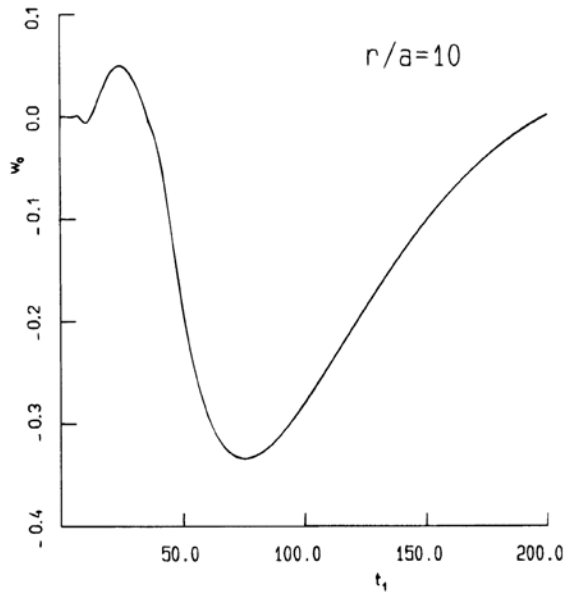

Fig. 8.3. Dynamic deflection response for *r/a*=10.

force is formed through wave components, the wavelength of which is shortest immediately at the front of the pulse. With time increase the wavelength gradually increases.

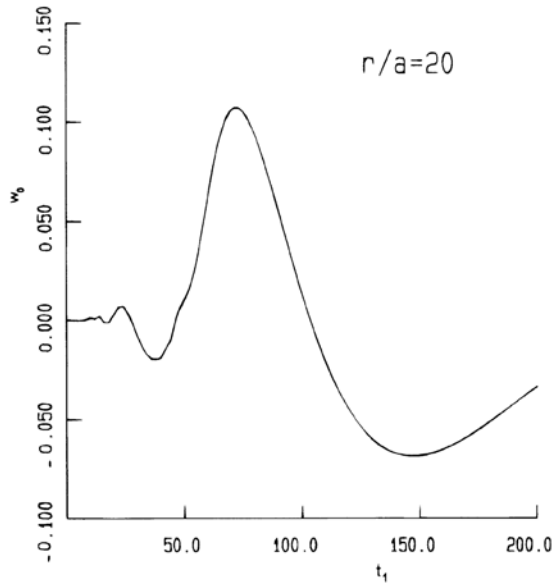

Fig. 8.4. Dynamic deflection response for *r/a*=20.

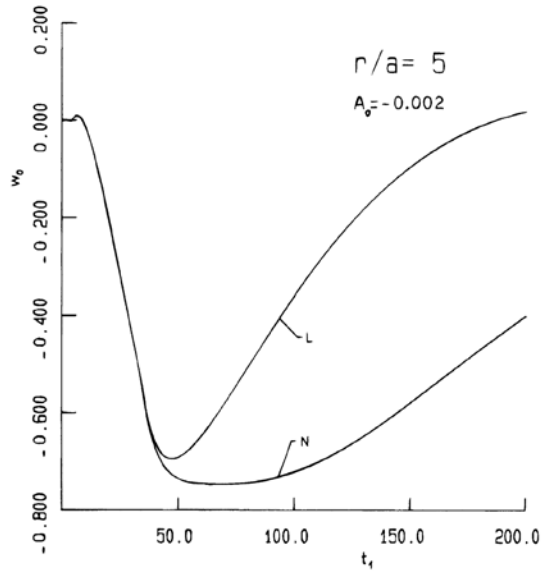

Fig. 8.5. Non-linear dynamic response for *r/a*=5 and decreasing rigidity of subgrade.

The non-linear dynamic responses for the same pulse load, calculated by the numerical integration of equation (8.40), are plotted in Figs. 8.5–8.10. The dynacmic response at the distance given by ratio *r/a*=5 is in Figs. 8.5 and 8.6, at distance *r/a*=10 in Figs. 8.7

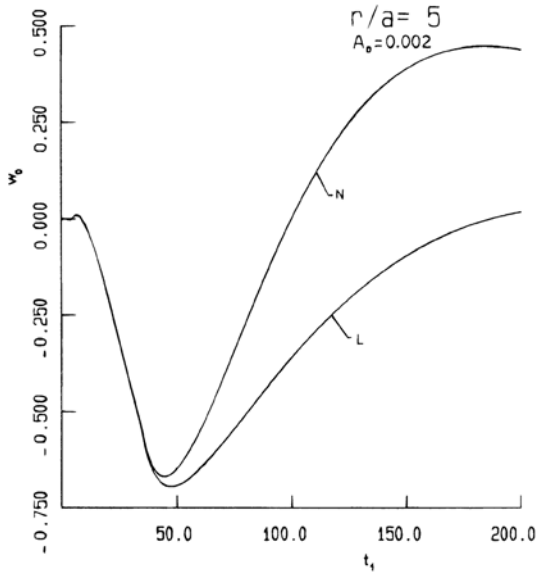

Fig. 8.6. Non-linear dynamic response for *r/a*=5 and increasing rigidity of subgrade.

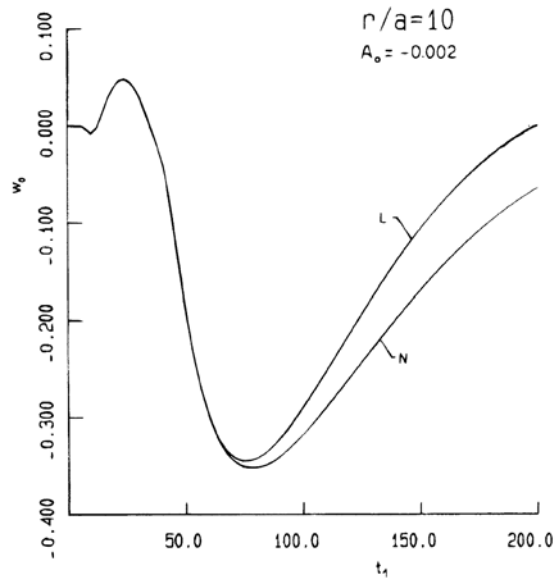

Fig. 8.7. Non-linear dynamic response for *r/a*=10 and decreasing rigidity of subgrade.

and 8.8, at distance *r/a*=10 in Figs. 8.7 and 8.8 and at distance *r/a*=20 in Figs. 8.9 and 8.10. The courses of the non-linear response correspond to the dimensionless characteristic of non-linearity A_0=−0.002, or A_0=0.002 and A_0=−0.05, i.e to decreasing or increasing

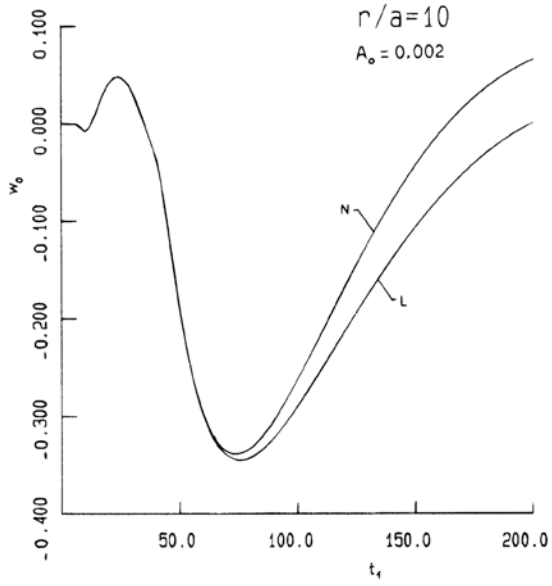

Fig. 8.8. Non-linear dynamic response for *r/a*=10 and increasing rigidity of subgrade.

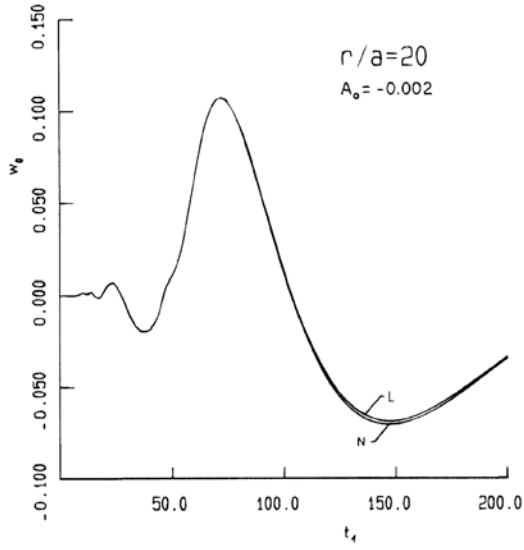

Fig. 8.9. Non-linear dynamic response for r/a=20 and characteristic of non-linearity A_0=−0.002.

rigidity of the subgrade. The physically real characteristic of nonlinearity certainly corresponds to decreasing rigidity of the subgrade by the increase of deflections. In the time variation of pulse response it manifests itself as an increase of maximum dynamic deflections and by the increase of the time t_1 in which these maxima set in.

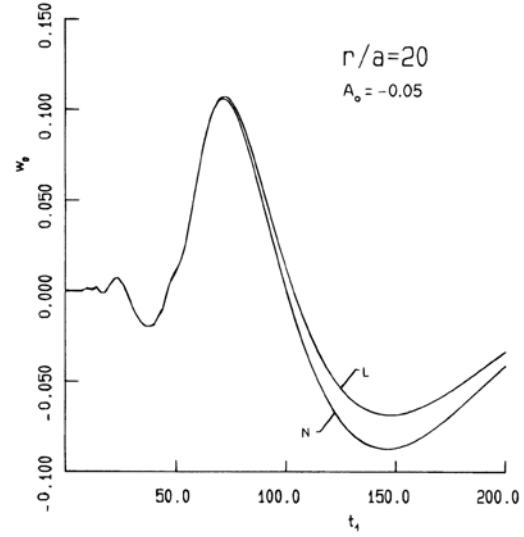

Fig. 8.10. Non-linear dynamic response for r/a=20 and characteristic of non-linearity A_0=−0.05.

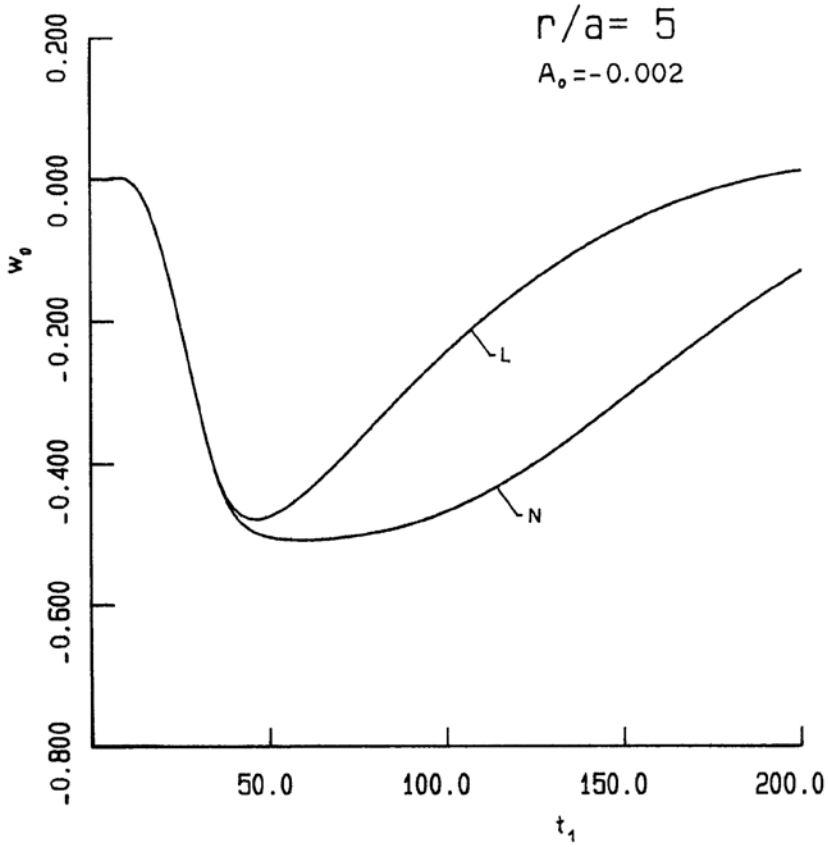

Fig. 8.11. Linear and non-linear response for *r/a*=5 under pulse of half-sinusoidal shape.

By increase the distance from the pulse source, the amplitudes of the response deflection decrease, as can be seen in Figs. 8.9 and 8.10 for the ratio *r/a*=20. The influence of non-linearity increases with increase of the value of A_0 (compare Figs. 8.9 and 8.30). The linear and non-linear dynamic response for a pulse load of half-sinusoidal shape with maximal amplitude *p*=1 and divided on an equal time section as shown in Fig. 8.1 is in Fig. 8.11. Comparing this with the response for a trapezoid-shaped pulse in Fig. 8.5, it can be seen that the dynamic deflections and the influence of non-linearity are both smaller. This corresponds to the reality of the situation because a pulse load of half-sinusiodal shape has a smaller value than a trapezoidshaped pulse.

8.4.2 Bending moment in plate on subgrade and subgrade reaction due to an instantaneous pulse load

The radial bending moment in a plate on subgrade is determined by the relationship

$$M_r = -D\left[\frac{\partial^2 w}{\partial r^2} + \frac{\mu}{r}\frac{\partial w}{\partial r}\right]. \tag{8.41}$$

According to equations (8.37), (8.38) and (8.41) the radial bending moment in the plate has, after rearranging, the form

$$\frac{M_r}{ph^2} = \frac{-e^{\frac{-\varepsilon_0}{2}t_1}\,h^2}{24\pi k_d(1-\mu^2)a^2} \times \int_0^\infty \frac{\sin(K(\eta)t_1)}{K(\eta)}\,\eta^2 J_1(\eta)\left[J_0\left(\eta\frac{r}{a}\right) - \frac{(1-\mu)}{\eta\frac{r}{a}}J_1\left(\eta\frac{r}{a}\right)\right]d\eta. \tag{8.42}$$

In the case of a non-linear subgrade the bending moment, in the first approximation, is given by the equation

$$\frac{{}^1M}{ph^2} = \frac{M_L}{ph^2} - A_0\int_0^{t_1}\left[3\left(\frac{w_L(\tau_1)E}{ph}\right)^2\frac{M_L(\tau_1)}{ph^2} - \frac{6w_L(\tau_1)E}{ph} \times \frac{e^{-\frac{\varepsilon_0}{2}\tau_1}h^2}{24\pi k_d(1-\mu^2)a^2}\int_0^\infty \frac{\sin(K(\eta)t_1)\,\eta^2 J_1(\eta)\,J_1\left(\eta\frac{r}{a}\right)^2 d\eta}{K(\eta)}\right] \times \frac{e^{-\frac{\varepsilon_0}{2}(t_1-\tau_1)}\sin\left[\sqrt{\frac{K_1h}{Ek_d}-\frac{\varepsilon_0^2}{4}}\,(t_1-\tau_1)\right]}{\sqrt{\frac{K_1h}{Ek_d}-\frac{\varepsilon_0^2}{4}}}\,d\tau_1. \tag{8.43}$$

The subgrade reaction q due to a pulse load is expressed by the relationship

$$q = K_1 w - K_2\,\nabla^2 w. \tag{8.44}$$

By using equations (8.37) and (8.38), the subgrade reaction in dimensionless form is given by the equation

$$\frac{q}{p} = \frac{-e^{\frac{-\varepsilon_0}{2}t_1}}{2\pi k_d}\int_0^\infty \frac{J_1(\eta)\left[\frac{K_1h}{E}+\frac{K_2h}{Ea^2}\eta^2\right]J_0\left(\eta\frac{r}{a}\right)\sin[K(\eta)t_1]}{K(\eta)}\,d\eta. \tag{8.45}$$

The non-linear reaction of the subgrade in the first approximation is determined in the form

$$\frac{^1q}{p} = \frac{q_L}{p} - A_0 \int_0^{t_1} \left[\frac{K_1 h}{E} w_L^3 + 3 w_L^2 q_L - 6 w_L \frac{e^{-\frac{\varepsilon_0}{2}\tau_1} K_2 h}{2\pi E k_d a^2} \right.$$

$$\left. \times \int_0^{\infty} \frac{\eta^2 J_1(\eta)\, J_1\left(\eta \frac{r}{a}\right)^2 \sin[K(\eta)\tau_1]\, d\eta}{K(\eta)} \right] \tag{8.46}$$

$$\times \frac{e^{-\frac{\varepsilon_0}{2}(t_1-\tau_1)} \sin\left[\sqrt{\frac{K_1 h}{E k_d} - \frac{\varepsilon_0^2}{4}}\,(t-\tau_1)\right]}{\sqrt{\frac{K_1 h}{E k_d} - \frac{\varepsilon_0^2}{4}}}\, d\tau_1.$$

Equations (8.42), (8.43) and (8.45), (8.46) refer to an instantaneous pulse load. It is simple to rearrange these equations for the case of a pulse load with time variation $f_1(\tau_1)$.

The courses of calculated dimensionless deflections $W_0 = w_0 E/ph$ dependent on dimensionless time t_1 are plotted in Fig. 8.12 for r/a=1, 5 and 10.

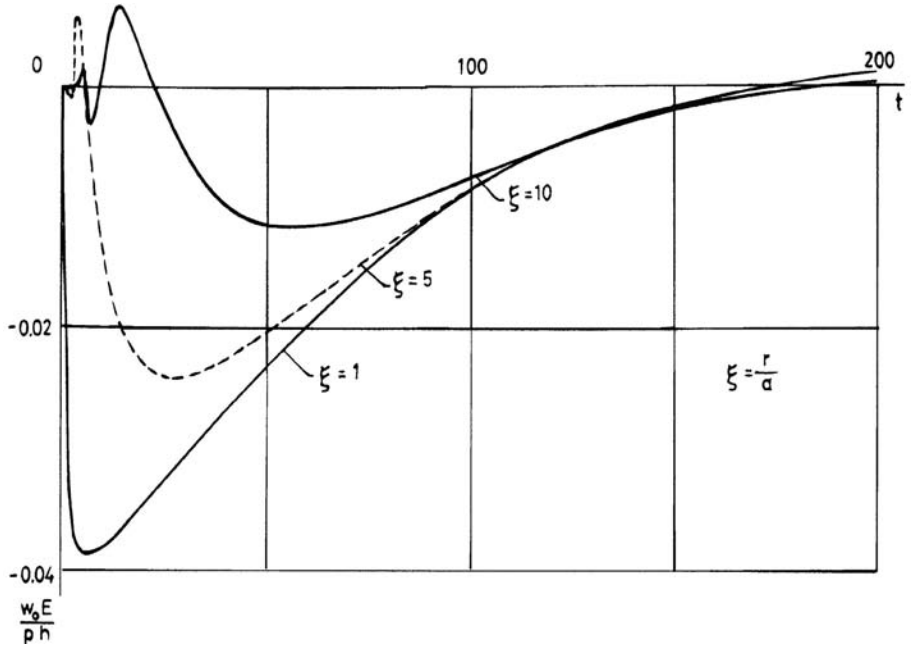

Fig. 8.12. Dynamic deflection response under unit instantaneous pulse at various ratios $\xi = r/a$.

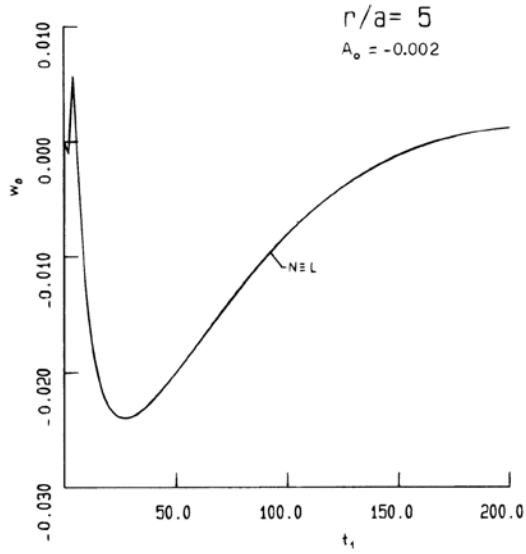

Fig. 8.13. Linear and non-linear deflection response under unit instantaneous pulse for r/a=5 and A_0=−0.002.

The values of the deflections are approximately 30 times smaller, because the value of a unit instantaneous pulse is 30 times smaller than the value of the trapezoid-shaped pulse in Fig. 8.1.

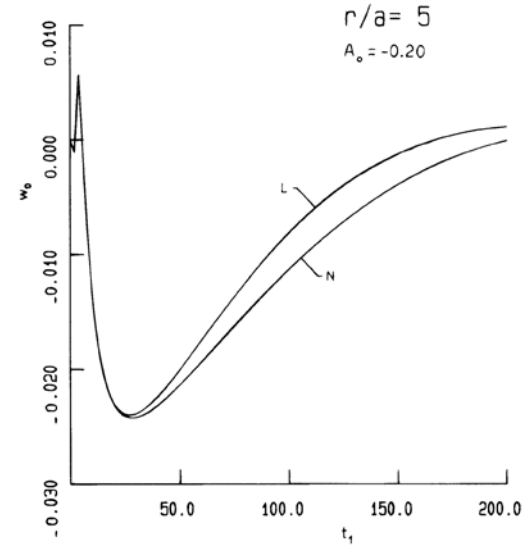

Fig. 8.14. Linear and non-linear deflection response under unit instantaneous pulse for r/a=5 and A_0=−0.20.

Very small values of deflections cause the influence of subgrade non-linearity to be visible only for the larger values of parameter A_0, as can be in Figs. 8.13 and 8.14.

The curves of bending moments of a plate on subgrade in dimensionless form $M_o=M_r/ph^2$ depending on t_1 at r/a=5 are plotted in Fig. 8.15 for a trapezoid-shaped pulse, in Fig. 8.16 for a triangle-shaped pulse and in Fig. 8.17 for a half-sinusoidal-shaped pulse. The time section of all the pulse shapes is the same as in Fig. 8.1. In Fig. 8.17 the course of bending moment for a triangle-shaped pulse is plotted as well.

The form of the moment response suggests that the instantaneous changes of pulse time variation $f_1(\tau_1)$ are reflected in intense changes of the variation of dynamic moment response. These changes are greatest for a trapezoid-shaped pulse and smallest for a half-sinusoidal-shaped pulse.

The subgrade reaction q/p in dimensionless form calculated for a half-sinusoidal-shaped pulse is plotted in Fig. 8.18 at the distances r/a=5 and r/a=10.

With regard to the theory of the equivalent plate on subgrade the results obtained and derived relationships and procedures in this section are an effective tool for the complex analysis of the influence of dynamic load of pavement structures. At the same time they form the theoretical basis for the development of dynamic diagnosis.

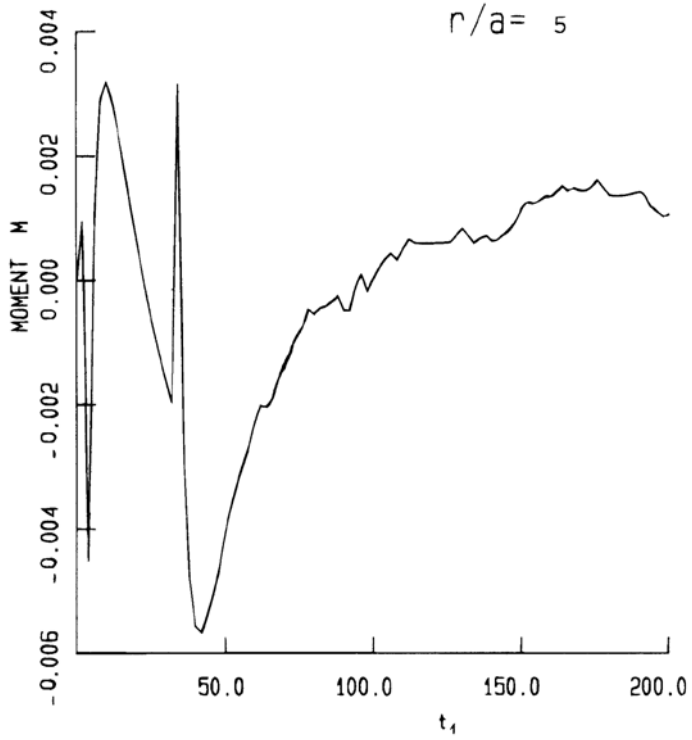

Fig. 8.15. Bending moment response of plate on subgrade under trapezoid-shaped pulse for r/a=5.

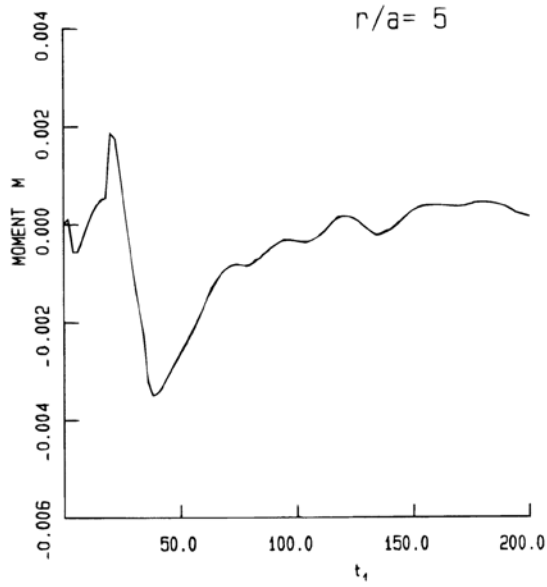

Fig. 8.16. Bending moment response of the plate on subgrade under triangle-shaped pulse for r/a=5.

An example of the computer program for the case of linear and nonlinear dynamic deflections of a plate on subgrade under a pulse load is given in Appendix 2.

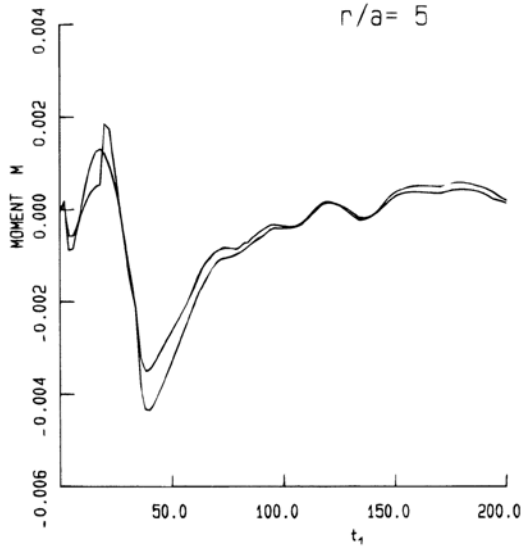

Fig. 8.17. Bending moment response under triangle- and half-sinusoidal-shaped pulse for r/a=5.

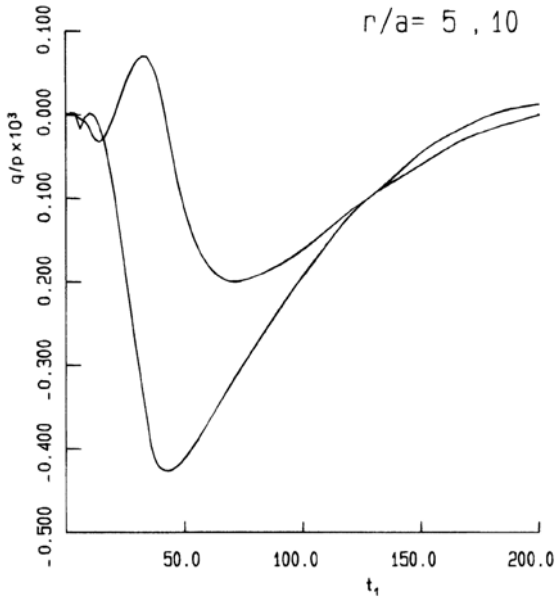

Fig. 8.18. Subgrade reaction response under half-sinusoidal-shaped pulse for r/a=5 and r/a=10.

9
EFFECTS OF VIBRATION-ISOLATING BARRIERS ON THE PROPAGATION OF VIBRATION IN SOIL BASES

Many experimental investigations performed on real or model soil bases [9.1]–[9.7] have shown that barriers in soil bases may be a very effective means for the vibration screening of objects or zones that are situated immediately behind the barrier. In particular, the barrier can be applied to the propagation of technical seismic effects or vibration evoked by traffic, when the majority of the frequency spectrum components have wavelengths smaller than or comparable to the dimensions of the barrier.

The problem has been treated in [9.2] using the method of finite elements as a two-dimensional problem, i.e. the plane strain problem.

9.1 Application of boundary element method

Our investigation has been performed theoretically by the use of the method of boundary integral equations and that of boundary elements respectively [6.1–6.4] assuming the soil base as described by the simplified dynamic model. We then assume the depth of a barrier larger than or comparable to the wavelength of the propagated force effect components. In this way, the influence of the shape and dimensions of the barrier on vibration-isolating effect can be investigated.

A harmonically variable dynamic force acting at the surface of the soil base generates dilatational and shear waves, which spread into the soil base, and surface Rayleigh waves which radiate at the surface with velocity c_R. The amplitudes of vertical displacements w and horizontal displacements u by Rayleigh waves are concentrated at the surface (Fig. 9.1). It is known [9.8] that the greater part of the energy (67 %) is radiated by the surface waves.

If the depth H of the obstacle (Fig. 9.1) is comparable to the wavelength Λ_R, we can expect the screening effect before the incoming waves.

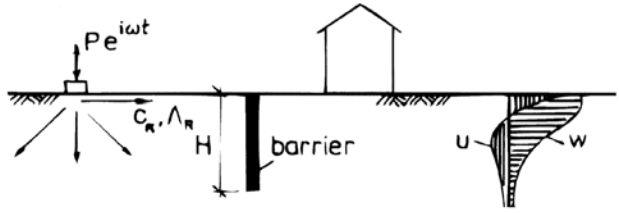

Fig. 9.1. Schematic diagram of barrier in soil base.

9.1.1 Simplified dynamic model of subgrade and fundamental solution

The simplified dynamic model of subgrade was analysed in section 3.4.1. The differential equation of motion for such a model of subgrade has the form

$$\nabla^2 w - \frac{K_1^*}{K_2^*} w - \frac{1}{c_R^{*2}} \frac{\partial^2 w}{\partial t^2} = -\frac{1}{K_2^*} \frac{\delta(r)}{2\pi r} \delta(t) \tag{9.1}$$

where $\delta(r)$, $\delta(t)$ are Dirac's generalized finctions, and c_R is a complex velocity of Rayleigh waves.

By using Hankel's and Fourier's integral transformations the transform of Green's function, ${}^{HF}w$ is given according to equation (9.1) in the form

$${}^{HF}w(\alpha, \omega) = -\frac{1}{4\pi^2 K_2^*} \frac{1}{\left(-\alpha^2 - K_1^*/K_2^* + \omega^2/c_R^{*2}\right)} \tag{9.2}$$

where α, ω are integral transformation parameters.

The original of Green's function $w(r, t)$ takes the form

$$w(r,t) = \frac{1}{4\pi^2 K_2^*} \int_{-\infty}^{\infty} \int_{0}^{\infty} \frac{\alpha J_0(\alpha r)\, e^{i\omega t}}{\alpha^2 + K_1^*/K_2^* - \omega^2/c_R^{*2}} \, d\alpha d\omega. \tag{9.3}$$

By using the procedure of section 6.1, Green's function for the subgrade is as follows

$$w(r,t) = -\frac{i}{8\pi K_2^*} \int_{-\infty}^{\infty} H_0^{(2)}(\alpha_1 r)\, e^{i\omega t} \, d\omega \tag{9.4}$$

if

$$\alpha_1 = \pm \sqrt{\frac{\omega^2}{c_R^{*2}} - \frac{K_1^*}{K_2^*}}. \tag{9.5}$$

Green's function as the dynamic influence function of the deflection under a harmonic unit concentrated force in the form

$$G(r,t) = \frac{-i}{4K_2^*} H_0^{(2)}(\alpha_1 r)\, e^{i\omega t} \tag{9.6}$$

represents the fundamental solution. The function $H_0^{(2)}(\alpha_1 r)$ is Hankel's function of complex argument $\alpha_1 r$ with positive real part and negative imaginary part.

9.1.2 Boundary integral formulation according to Rayleigh's theorem of reciprocity

Let us assume that the barrier occupies a region S_0 with boundary Γ in the unbounded subgrade *S*. The radius vector of the load point $\vec{\xi}$, of the unit force point $\vec{r}$ and boundary point $\vec{\eta}$ are indicated in Fig. 9.2.

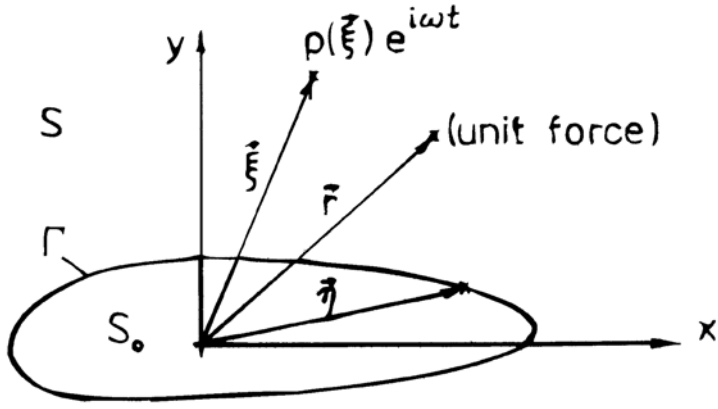

Fig. 9.2. Schematic diagram of system and coordinates.

The boundary integral formulation according to the theorem of reciprocity has the form

$$\vartheta(\vec{r})\, w(\vec{r}) = \int_S p(\vec{\xi}) G(\varrho) \mathrm{d}S + \int_\Gamma K_2^* \left[\frac{\partial w(\vec{\eta})}{\partial \vec{n}(\vec{\eta})}\, G(R) \right.$$

$$\left. - \frac{\partial G(R)}{\partial \vec{n}(\vec{\eta})\, w(\vec{\eta})} \right] \mathrm{d}\Gamma + \int_{\bar{\Gamma}} K_2^* \left[\frac{\partial w(\vec{\eta})}{\partial \vec{n}(\vec{\eta})}\, G(R) - \frac{\partial G(R)}{\partial \vec{n}(\vec{\eta})} w(\vec{\eta}) \right] \mathrm{d}\bar{\Gamma} \tag{9.7}$$

if

$$\vartheta(\vec{r}) = \begin{cases} 1 & \vec{r} \in S \\ 0 & \vec{r} \in \Gamma \cup S \end{cases}$$

and the variable distances $R = |\vec{\eta} - \vec{r}|$, $\varrho = |\vec{\xi} - \vec{r}|$. $\bar{\Gamma}$ is the fictitious boundary of the region *S*.

9.2 Barriers of different materials

If the barrier medium S_0 in the subgrade is made from a different material the integral formulation for the barrier medium has the form

$$\vartheta(\vec{r})\, w_0(\vec{r}) = \int_\Gamma K^*_{2,0}\left[\frac{\partial w_0(\vec{\eta})}{\partial \vec{n}(\vec{\eta})}\, G_{\mathrm{ba}}(R) - \frac{\partial G_{\mathrm{ba}}(R)}{\partial \vec{n}(\vec{\eta})}\, w_0(\vec{\eta})\right] \mathrm{d}\Gamma$$

$$\vartheta(\vec{r}) = \begin{cases} 1 & (\vec{r} \in S_0) \\ 0 & (\vec{r} \in \Gamma \cup S_0) \end{cases} \tag{9.8}$$

$G_{\mathrm{ba}}(R)$, $w_0(\vec{r})$, $K^*_{2,0}$ represent the fundamental solution, deflection and coefficient of shear transmission for the barrier medium.

The conditions at the boundary Γ are

$$w(\vec{\eta}) = w_0(\vec{\eta})$$

$$K^*_2 \frac{\partial w(\vec{\eta})}{\partial \vec{n}(\vec{\eta})} = K^*_{2,0}\, \frac{\partial w_0(\vec{\eta})}{\partial \vec{n}(\vec{\eta})}. \tag{9.9}$$

By means of limit transition on the boundary Γ for $\vec{r} \to \vec{\zeta} \in \Gamma$ and on the boundary $\bar{\Gamma}$ with the radius $\bar{R} \to \infty$, the boundary integral equations will be obtained from (9.7) and (9.8)

$$\left(1 + \tfrac{1}{2}\right) w(\vec{\zeta}) - \int_\Gamma K^*_2 \left[G(R')\frac{\partial w(\vec{\eta})}{\partial \vec{n}(\vec{\eta})} - \frac{\partial G(R')}{\partial \vec{n}(\vec{\eta})} w(\vec{\eta})\right] \mathrm{d}\Gamma$$

$$= \int_S p(\vec{\xi})\, G(\varrho')\mathrm{d}S$$

$$\tfrac{1}{2} w(\vec{\zeta}) - \int_\Gamma \left[K^*_2 G_{\mathrm{ba}}(R')\frac{\partial w(\vec{\eta})}{\partial \vec{n}(\vec{\eta})} - K^*_{2,0}\frac{\partial G_{\mathrm{ba}}(R')}{\partial \vec{n}(\vec{\eta})}\, w(\vec{\eta})\right] \mathrm{d}\Gamma = 0 \tag{9.10}$$

The distances R' and ϱ' are represented by equations (6.28). The coefficient of the free member in the first integral equation has the value $\mathbf{1} + \frac{1}{2}$, as it was given in section 6.2.3.

If the entire boundary is decomposed into boundary elements with nodal points, then it is possible to transform the system of integral equations into a system of $2N$ linear algebraic equations as follows

$$1.5\, \frac{w_k K_2}{pa^2} + \sum_{\substack{j=1 \\ j \neq k}}^{N} A_{kj} \frac{w_j K_2}{pa^2} + \sum_{j=1}^{N} B_{kj} \frac{\partial w_j}{\partial n}\, \frac{K_2}{pa} = P_k$$

$$0.5\, \frac{w_k K_2}{pa^2} + \sum_{\substack{j=1 \\ j \neq k}}^{N} C_{kj} \frac{w_j K_2}{pa^2} + \sum_{j=1}^{N} D_{kj} \frac{\partial w_j}{\partial n}\, \frac{K_2}{pa} = 0 \tag{9.11}$$

$$k = 1, 2, \ldots N$$

The dimensionless unknowns $w_j K_2/pa^2$, $K_2/pa\ \partial w_j/\partial n$ at the nodal points of the boundary can be determined by the solution of system (9.11).

The complex coefficients of the system (9.11), assuming a constant course of sub-integral function along the boundary element, have the form

$$A_{kj} = K_2^* \int_{\Gamma_j} \frac{\partial G(R')}{\partial \vec{n}(\vec{\eta})} \mathrm{d}\Gamma_j = \frac{i}{4}\,\alpha \frac{l_j}{a}\,\cos\alpha_{kj}\, H_1^{(2)}\left(\alpha \frac{R'}{a}\right)$$

$$B_{kj} = -K_2^* \int_{\Gamma_j} G(R')\mathrm{d}\Gamma_j = \frac{i}{4}\,\frac{l_j}{a}\, H_0^{(2)}\left(\alpha \frac{R'}{a}\right)$$

$$C_{kj} = K_{2,0}^* \int_{\Gamma_j} \frac{\partial G_{\mathrm{ba}}(R')}{\partial \vec{n}(\vec{\eta})} \mathrm{d}\Gamma_j = \frac{i}{4}\,\alpha_0 \frac{l_j}{a}\,\cos\alpha_{kj}^{\circ}\, H_1^{(2)}\left(\alpha_0 \frac{R'}{a}\right) \tag{9.12}$$

$$D_{kj} = K_{2,0}^* \int_{\Gamma_j} G_{\mathrm{ba}}(R')d\Gamma_j = -\frac{i}{4}\,\frac{l_j}{a}\gamma_{\mathrm{ba}}\, H_0^{(2)}\left(\alpha_0 \frac{R'}{a}\right)$$

where

$$\alpha^2 = (\alpha_1 a)^2 = \frac{\Omega^2}{1+\mathrm{i}\delta} - \frac{1}{\gamma}$$

$$\alpha_0^2 = \frac{\Omega^2}{\varepsilon} - \frac{1}{\gamma_0} \tag{9.13}$$

and α_{kj} is the angle between the direction of the normal at the boundary point η_j for subgrade medium and the direction of the line connected boundary points ξ_k and $\eta_j \cdot \alpha_{kj}^o$ is a similar angle for the barrier medium, l_j is the length of boundary element and dimensionless parameters are given in the form

$$\varepsilon = \frac{c_{\mathrm{R},0}^{*2}}{c_{\mathrm{R}}^2}, \quad \Omega = \frac{\omega a}{c_{\mathrm{R}}}, \quad \gamma = \frac{K_2^*}{K_1^* a^2}, \quad \gamma_0 = \frac{K_{2,0}^*}{K_{10}^* a^2}, \quad \gamma_{\mathrm{ba}} = \frac{K_0^*}{K_{2,0}^*}. \tag{9.14}$$

In the case of a uniform normal load $pe^{i\omega t}$ on a circular area of the subgrade with radius a, the right-hand side of the first equation (9.11) is expressed by the equation

$$P_k = -\frac{i\pi}{2\alpha}\, J_1(\alpha)\, H_0^{(2)}\left(\alpha\, \frac{|\vec{\xi} - \vec{\zeta}_k|}{a}\right) \tag{9.15}$$

where $J_1(\alpha)$ is the Bessel function of the first order.

9.2.1 Effect of a linear barrier

By numerical study of the effect of a linear barrier with length L=9.0 m and thickness B=0.6 m and with dimensionless parameters γ=10, γ_0=5 the boundary was divided into 32 boundary elements. A harmonic variable load $Pe^{i\omega t}$, uniformly distributed at the circular area with radius a=0.25 m, affects the subgrade according to the scheme of Fig. 9.3.

The calculated amplitudes of dynamic deflections $w_A=|w|K_2/pa^2$ are plotted along the boundary and along the section A–A for the cases with and without a barrier. The

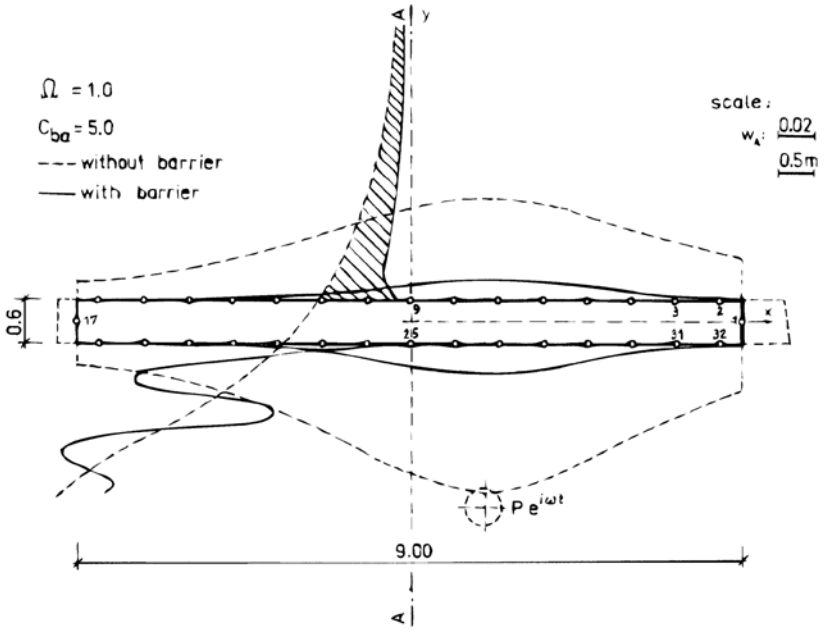

Fig. 9.3. Effect of linear barrier for C_{ba}=5.0 and vibration frequency Ω=1.0.

materials of the barrier and subgrade are given by the ratio $C_{ba}=c_{R,0}/c_R$=5.0 and dimensionless frequency of vibration Ω=1.0.

From Fig. 9.3 the dramatic vibration-isolating effect behind the barrier, and the superposition of direct and reflected waves before the barrier, can be seen.

9.2.2 Influence of various barrier rigidities on vibration isolation

The results in Fig. 9.4 represent the influence of parameter C_{ba} on the screening zone along the cross-section A–A at frequency Ω=1.0. The screening effect increases with increase of the ratio C_{ba} if the wave characteristic of the barrier medium is greater than the wave characteristic of the subgrade.

On the other side the results are more complicated if the material of the barrier has a lower value of velocity of surface waves that the subgrade.

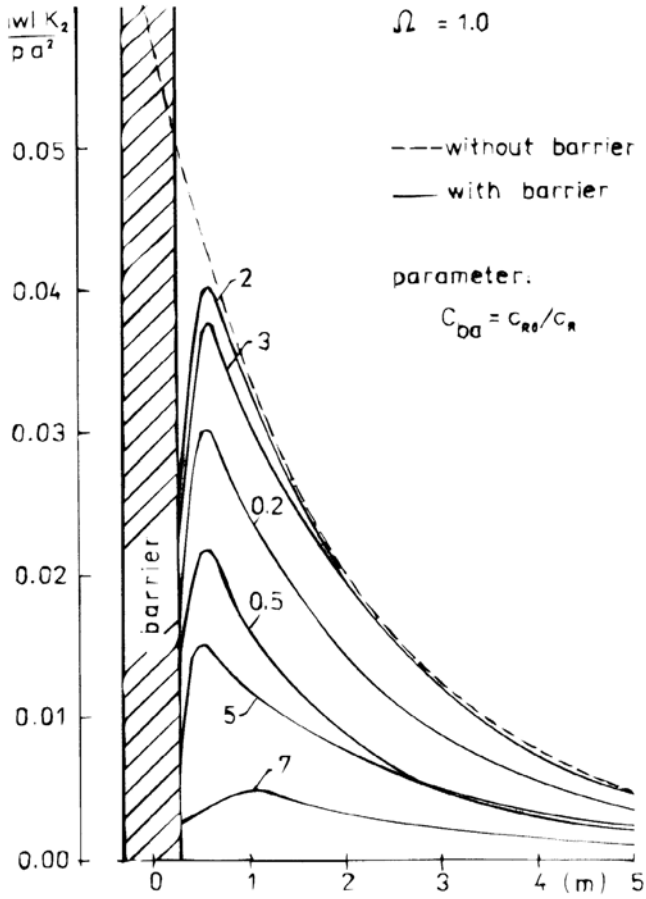

Fig. 9.4. Influence of parameter C_{ba} on screening zone at frequency Ω=1.0.

The results of a detailed study of barrier efficiency at various frequencies Ω at interval (0.3–1.0) and for various values of C_{ba} are given in Fig. 9.5. The efficiency expressed by amplitude reduction factor *ARF* is given in the screening zone by the ratio

$$ARF = \frac{\int_0^{L_0} \frac{|w_{BA}|(l)\,K_2}{pa^2}\,\mathrm{d}l}{\int_0^{L_0} \frac{|w|(l)\,K_2}{pa^2}\,\mathrm{d}l} \tag{9.16}$$

if $|w_{BA}|(l)$ is the course of the deflection amplitudes behind the barrier and $|w|(l)$ is the course of the deflections amplitudes in the same section of the subgrade without a barrier. The length of section is L_0=5.0 m.

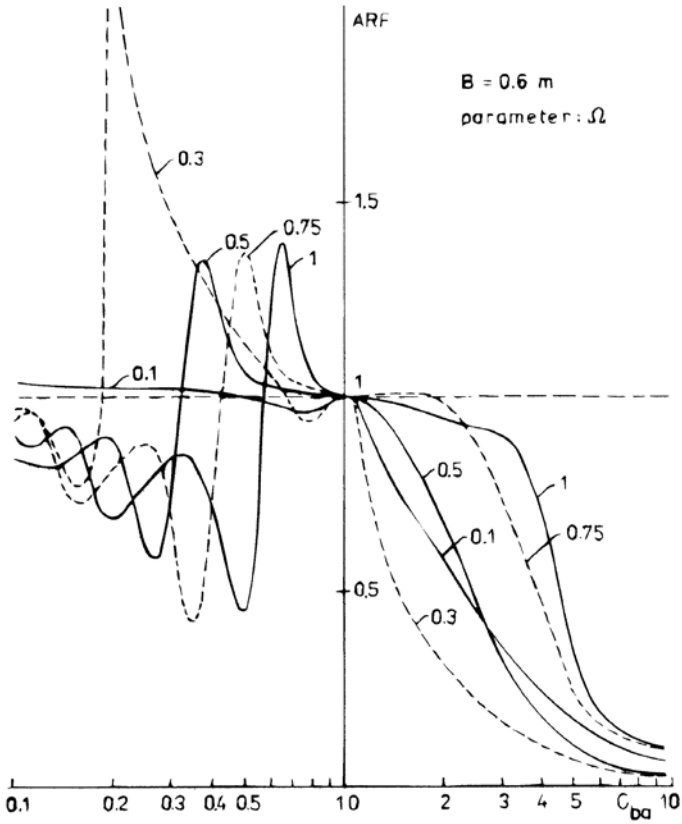

Fig. 9.5. Variations of amplitude reduction factor *ARF* with C_{ba} for various values of frequency Ω.

The trend of higher efficiency with increase of barrier medium rigidity is clear across the whole frequency range. In the region C_{ba}<1.0 the behaviour of *ARF* is very complicated. There are resonance zones, and in the first one *ARF*>1, i.e. the concentration of the vibration increases behind the barrier. However, the efficiency of the barrier is weaker at other resonances too. The results demonstrate that barriers made from material with wave characteristics lower than those of the subgrade characteristics, do not provide a sufficient vibration-isolating effect. For each frequency, intervals of values C_{ba} exist in which the barrier is a source of vibration concentration and thereby an amplifier of the vibration.

These phenomena are legitimate; they are connected with the diffraction of the stress waves on the boundaries of the barrier and with the resonances. It can be demonstrated that the resonances take place if the wavelength Λ_{ba} in the barrier medium has the values Λ_{ba}=25, *B*, 0.5*B*,…*B* is the thickness of barrier.

The efficiency of the barrier is also reduced in the region C_{ba}>1 at very high frequencies, if the wavelength in the subsoil is comparable with the thickness of the barrier.

9.2.3 Influence of various barrier thicknesses on vibration isolation

The effect of various barrier thicknesses was analysed through numerical study on the same linear barrier with thicknesses B=0.3, 0.6, 1.0 m. The rigidity of the barriers is always given by the ratio C_{ba}=5.0.

The variations of the subgrade deflection at the point (0.0, 2.0) in the screening area behind the barrier with the dimensionless frequency Ω is given in Fig. 9.6 for the barrier thicknesses B=0.3 m and B=1.0 m.

It can be seen that in the frequency range Ω=(0–2.0) the vibration-isolating effect of the barrier with B=1.0 m is considerably higher than for B=0.3 m.

A more general survey is given by the results in Fig. 9.7, where the variations of *ARF* factor with frequency are drawn for B=0.3, 0.6 and 1.0 m. These curves confirm that the vibration-isolating effect increases with increasing barrier thickness. It can be seen, however, that at higher values of frequencies above Ω=1.0 the isolating effect is influenced by resonance phenomena; the screening effect decreases and the vibration concentration increases.

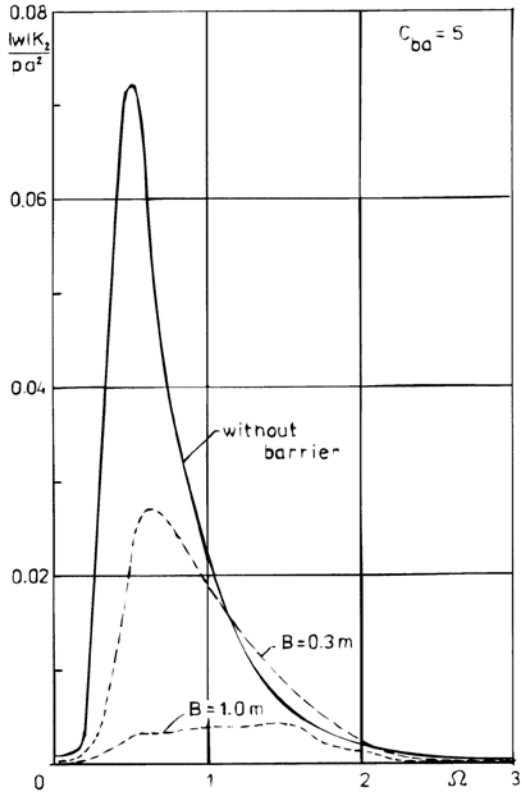

Fig. 9.6. Variations of subgrade deflection behind barrier with frequency Ω for barrier thickness B=0.3 m and B=1.0 m.

9.2.4 Dynamic deflection field around barrier

Contemporary computer techniques make it possible to calculate a whole field of dynamic deflections around the barrier and to show the deflection amplitudes graphically.

Such graphic images are presented in Fig. 9.8 for the frequency of exciting force Ω=0.3, in Fig. 9.9 for Ω=0.5, in Fig. 9.10 for Ω=1.0 and in Fig. 9.11 for Ω=1.5. All these results are valid for thickness B=0.6 m and parameter C_{ba}=5.0. The screening efect behind the barriers and the superposition of direct and reflected waves in the region between the source of vibration and the frontal side of barrier can be seen quite conclusively. The decrease of wavelength with increase of vibration frequency is evident too.

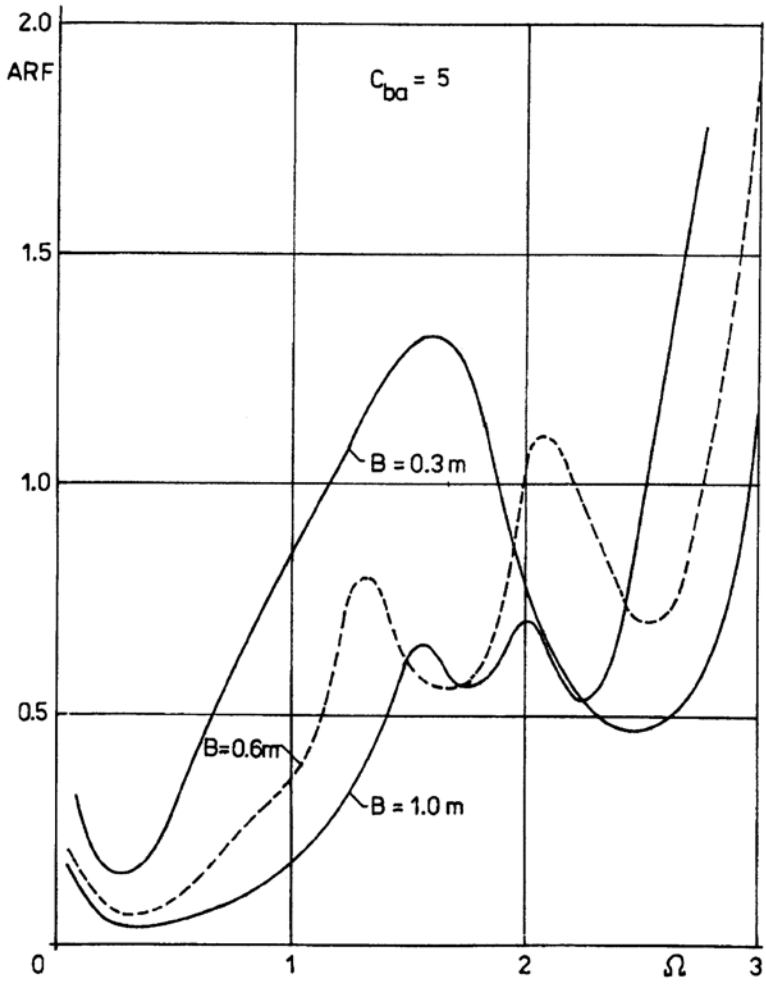

Fig. 9.7. Variations of amplitude reduction factor *ARF* with frequency Ω for barrier thickness B=0.3 m, B=0.6 m and B=1.0 m.

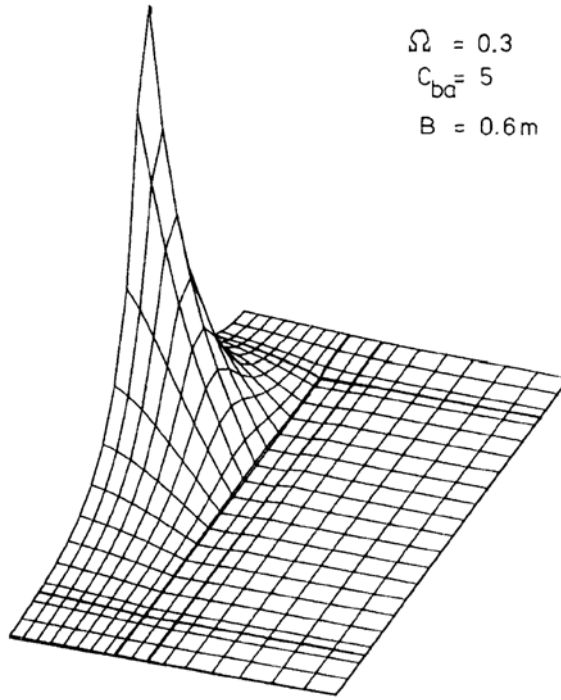

Fig. 9.8. Dynamic deflection field around barrier for vibration frequency Ω=0.3.

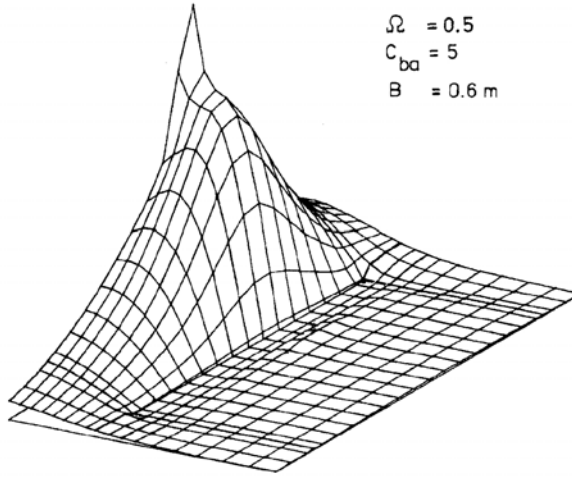

Fig. 9.9. Dynamic deflection field around barrier for vibration frequency Ω=0.5.

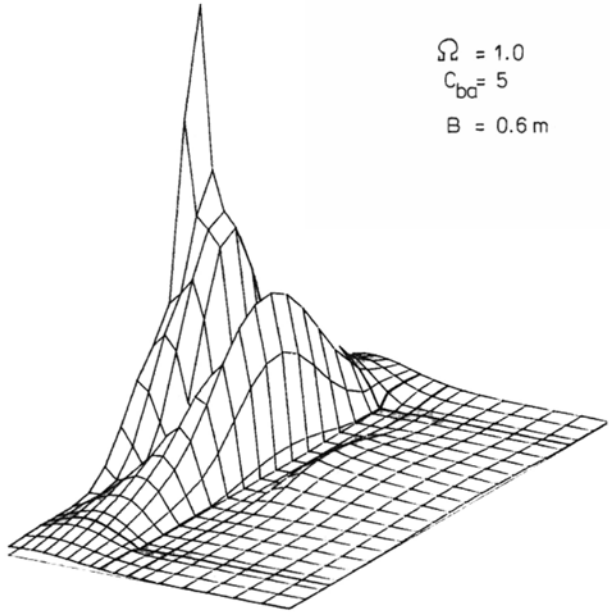

Fig. 9.10. Dynamic deflection field around barrier for vibration frequency Ω=1.0.

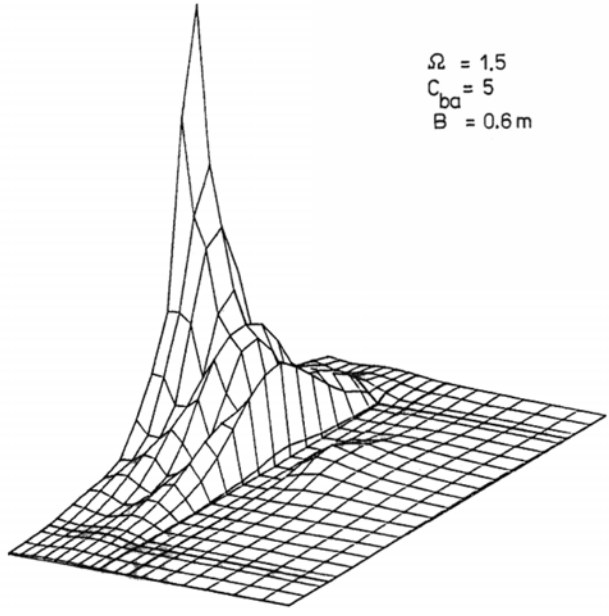

Fig. 9.11. Dynamic deflection field around barrier for vibration frequency Ω=1.5.

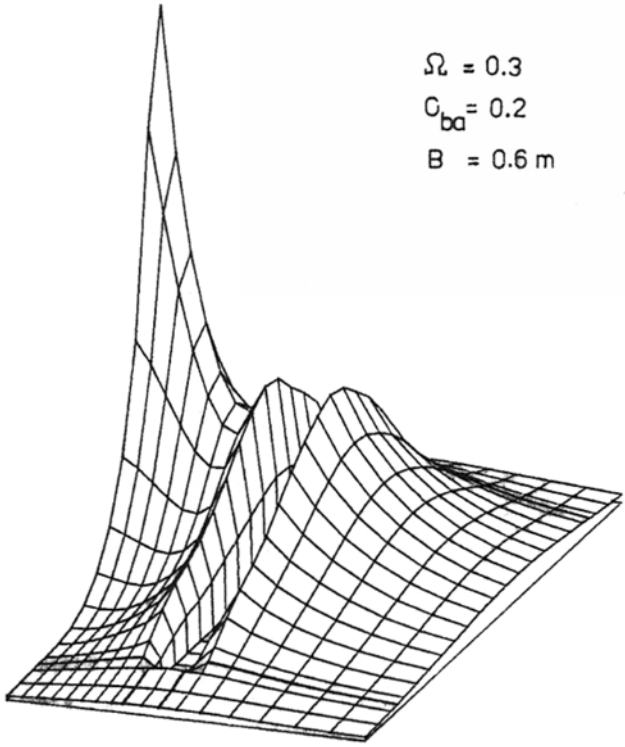

Fig. 9.12. Amplifying of vibration field around barrier for Ω=0.3, C_{ba}=0.2, B=0.6 m as a result of resonance phenomenon.

In contrast, the amplifying of the vibration field around the barrier is drawn in Fig. 9.12 for the parameters Ω=0.3, C_{ba}=0.1, B=0.6 m. The resonance phemonenon causes the barrier to become an amplifier of vibration.

9.3 Trench barriers

A barrier made by means of a trench with boundary Γ is a special case in which the following boundary condition applies:

$$Q_n(\vec{\eta}) = K_2^* \frac{\partial w(\vec{\eta})}{\partial \vec{n}(\vec{\eta})} = 0 \tag{9.17}$$

i.e we require zero shear forces $Q_n(\vec{\eta})$ on the boundary.

Then the boundary integral formulation for an interior point of the subgrade is established from equation (9.7) in the form

$$w(\vec{r}) = \int_S p(\vec{\xi}) G(\varrho) \mathrm{d}S - \int_\Gamma K_2^* \frac{\partial G(R)}{\partial \vec{n}(\vec{\eta})} w\vec{\eta}) \mathrm{d}\Gamma$$

$$- \int_{\bar{\Gamma}} K_2^* \frac{\partial G(R)}{\partial \vec{n}(\vec{\eta})} w(\vec{\eta}) \mathrm{d}\bar{\Gamma} \tag{9.18}$$

By limit transition on the boundary Γ for $\vec{r} \to \vec{\zeta} \in \Gamma$ and on the boundary $\bar{\Gamma}$ with radius $\bar{R} \to \infty$, the boundary integral equation is given as follows

$$\left(1 + \tfrac{1}{2}\right) w(\vec{\xi}) + \int_\Gamma K_2^* \frac{\partial G(R)}{\partial \vec{n}(\vec{\eta})} w(\vec{\eta}) \mathrm{d}\Gamma = \int_S p(\vec{\xi})\, G(\varrho') \mathrm{d}S \tag{9.19}$$

where the distances R', ϱ' are expressed by equations (6.28).

The solution of the integral equation (9.19) is possible by dividing the boundary Γ into N boundary elements. The constant, linear or quadratic course of the sub-integral functions along the elements can be assumed. The boundary integral equation (9.19), after discretization, is transformed into the following system of algebraical equations:

$$1.5 w_K + \sum_{\substack{j=1 \\ j \neq k}}^{N} A_{kj} \frac{w_j K_2}{pa^2} = P_k$$

$$k = 1, 2, \ldots N \tag{9.20}$$

where A_{kj} is given by the first equation (9.12) and P_k in the case of normal load p uniformly distributed on circular area with radius a is expressed by equation (9.15).

In the system (9.20), the coefficients A_{kj} and the right-hand sides P_k are complex quantities. The unknown boundary deflections at nodal points $w_j K_2/pa^2$ calculated by the solution of system (9.20) are complex too. The deflection at the arbitrary point of the subgrade is determined by using equation (9.18) and the known boundary deflections.

9.3.1 Linear trench barriers

A numerical study of a linear trench barrier with length L=10.0 m was carried out for various thicknesses: B_0=1.0 m, B_1=0.6 m and B_2=0.24 m.

The source of the dynamic harmonic load is situated excentrically to the symmetry axis of barrier at the point with coordinates (1.0, −2.50). All numerical calculations are performed for the dimensionless characteristic of the subgrade $\gamma = K_2^*/K_1^* a^2 = 10$, the damping parameter of subgrade medium δ=0.20 and the radius of load area a=0.25 m. The boundary of the trench barrier was divided into 32 boundary elements.

The results of the calculated dynamic amplitudes of deflection at the boundary nodal points and in the cross-section A–A can be seen in Fig. 9.13 for a trench barrier with B_2=0.24 m and frequency Ω=0.5.

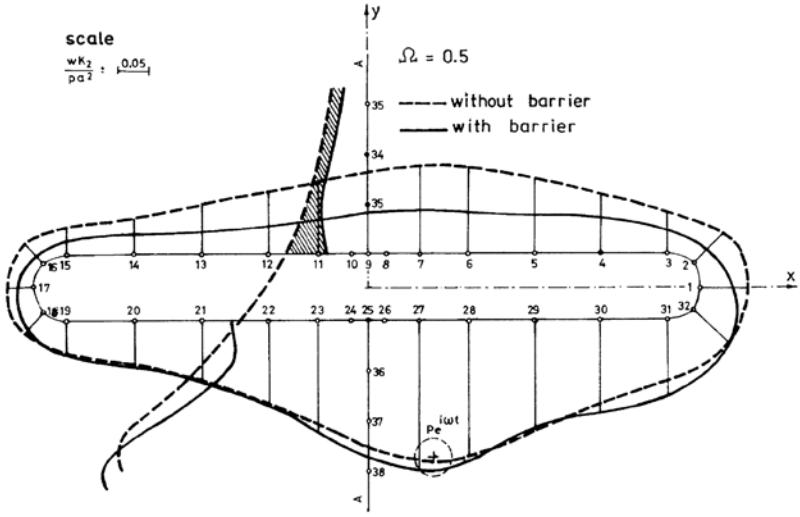

Fig. 9.13. Effect of linear trench barrier at vibration frequency Ω=0.5.

The deflection amplitudes in the screening zone behind the barrier and their variations along the cross-section A–A are marked in Fig. 9.14 for Ω=0.3 and thicknesses B_1, B_2 in Fig. 9.15 for Ω=0.5 and in Fig. 9.16 for Ω=1.0, in each case for B_0, B_1 and B_2. The results

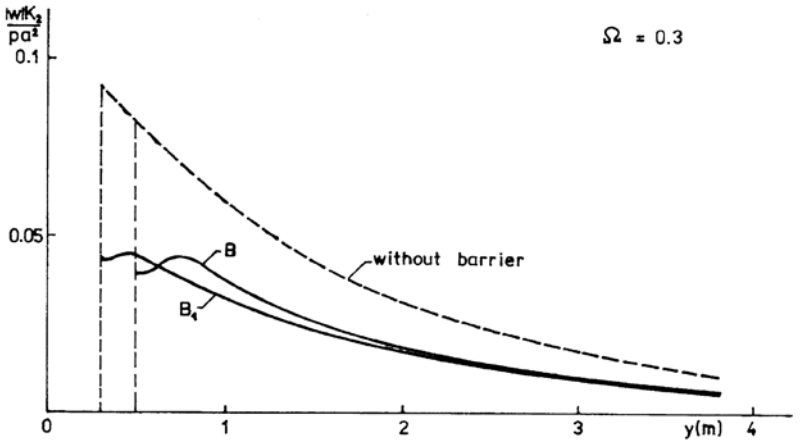

Fig. 9.14. Deflection amplitudes in screening zone behind trench barriers for Ω=0.3.

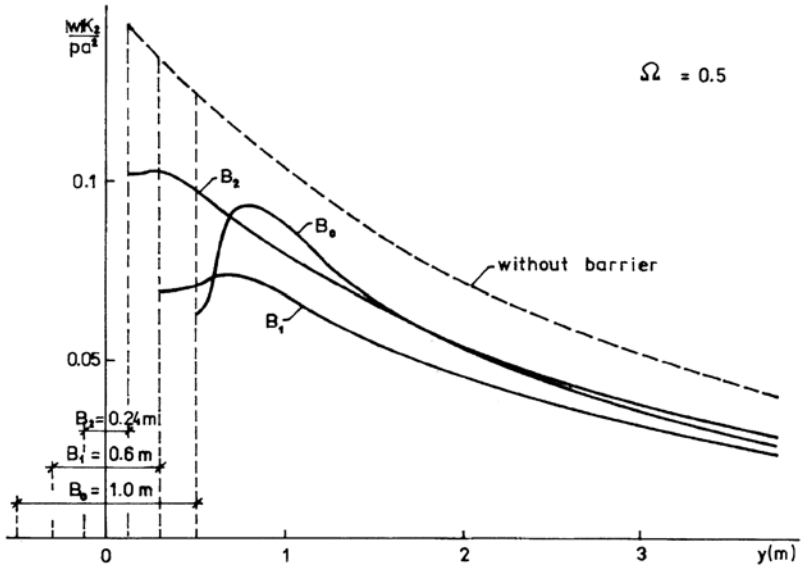

Fig. 9.15. Deflection amplitudes in screening zone behind trench barriers for Ω=0.5.

illustrate that the screening effect depends on the frequency and on the thickness of the barrier. Trench barriers, as a limited case of barriers with lower rigidity than the subgrade medium, demonstrate that the resonances influence the vibration-isolating effect and reduce its efficiency.

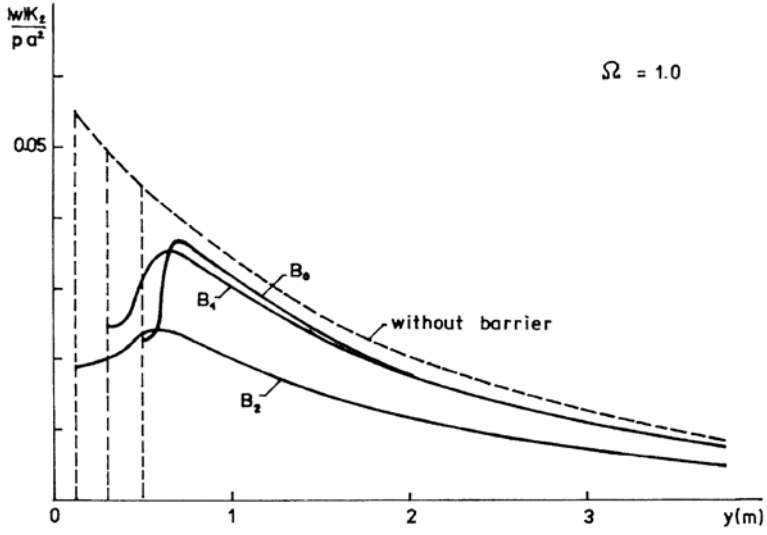

Fig. 9.16. Deflection amplitudes in screening zone behind trench barriers for Ω=1.0.

The variations of deflection amplitudes in Figs. 9.15–9.16 for Ω=0.5 and 12=1.0 confirm these conclusions.

9.4 Sheet piling barriers

Sheet piling barriers can take on an arbitrary shape: bounded curve or line, closed curve. If the depth of the barrier is greater than the wavelength of the stress waves propagated in the subgrade, the boundary condition on Γ may be expressed

$$w(\vec{\eta}) = 0. \tag{9.21}$$

We assume zero vertical deflection in the location of a sheet piling barrier.

The integral formulation according to Rayleigh's theorem of reciprocity has for the interior point of subgrade the form

$$w(\vec{r}) = \int_S p(\vec{\xi}) G(\varrho) \mathrm{d}S + \int_\Gamma K_2^* \frac{\partial w(\vec{\eta})}{\partial \vec{n}(\vec{\eta})} G(R) \mathrm{d}\Gamma + \int_{\bar{\Gamma}} K_2^* \frac{\partial w(\vec{\eta})}{\partial \vec{n}(\vec{\eta})} G(R) \mathrm{d}\bar{\Gamma} \tag{9.22}$$

By using the usual procedure of the transition to the boundaries and the condition (9.21) the boundary integral equation is as follows

$$-K_2^* \int_\Gamma G(R') \frac{\partial w(\vec{\eta})}{\partial \vec{n}(\vec{\eta})} \mathrm{d}\Gamma = \int_S p(\vec{\xi})\, G(\varrho') \mathrm{d}S \tag{9.23}$$

The solution of (9.23), applying boundary elements, generates a system of algebraical equations with unknown shear forces at the nodal points of the boundary.

After discretization into N boundary elements the system of equations has the form

$$\sum_{j=1}^{N} B_{kj} \frac{\partial w_j}{\partial n} \frac{K_2}{pa} = P_k \qquad k = 1, 2, \ldots N \tag{9.24}$$

Assuming a constant sub-integral function along the boundary element the complex coefficients B_{kj} are given by the equation (9.12) and P_k can be established according to equation (9.15).

The determination of the values of diagonal coefficients requires special aftention because Hankel's function $H_0^{(2)}$ gains an infinite value for the zero value of the argument.

Singular integrals $B_{kk} = \int_{\Gamma_k} G(R')\mathrm{d}\Gamma_k$ have to be calculated in the sense of the main value by using integral with finite values and Gauss's quadrature formulas.

9.4.1 Linear sheet piling barriers

A numerical study of a linear sheet piling barrier was performed for the characteristics γ=10, δ=0.20, a=0.25 m and L=9.6 m.

The barrier was divided into 32 boundary elements with the same length. The efficiency of the barrier was investigated by the calculation of deflection amplitudes $|w|K_2/pa^2$ along the cross-section in the screening zone behind the barrier, which is identical to the y axis. The source of the exciting harmonic force was at a point with distance 2.5 m before the barrier and with eccentricity 1.0 m from the symmetry axis of the barriers.

The variations of the deflection amplitudes are plotted in Fig. 9.17 for Ω=0.3, in Fig. 9.18 for Ω=0.5 and in Fig. 9.19 for Ω=1.0. The considerable vibration-isolating effect behind the barrier diminishes with increasing frequency.

An example of the computer program for the sheet piling barrier is in Appendix 3.

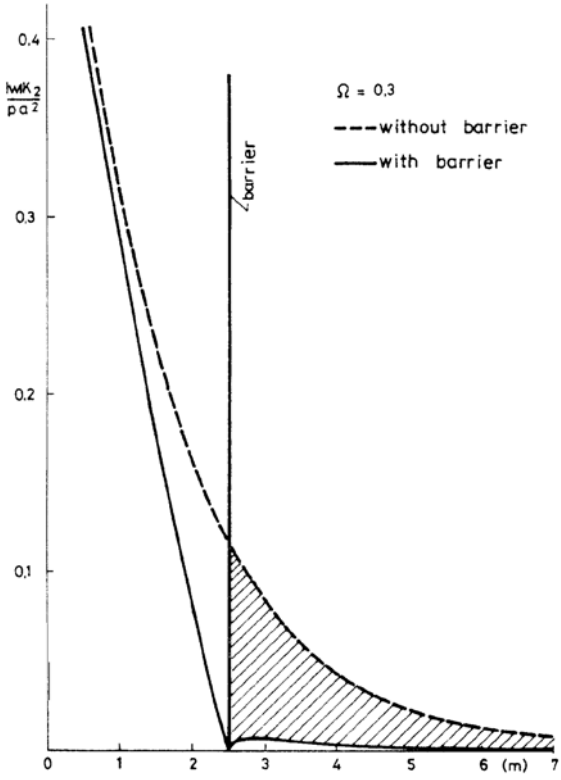

Fig. 9.17. Variation of deflections amplitudes with distance for sheet piling barrier and Ω=0.3.

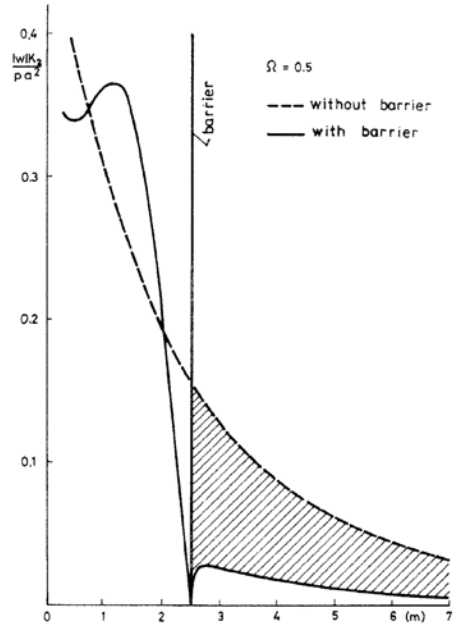

Fig. 9.18. Variation of deflection amplitudes with distance for sheet piling barrier and Ω=0.5.

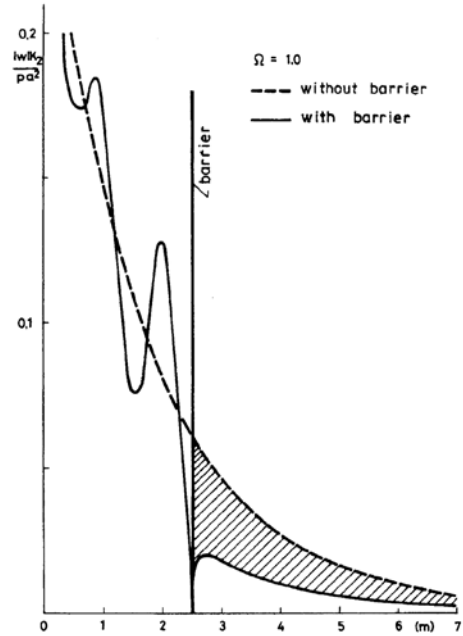

Fig. 9.19. Variation of deflection amplitudes with distance for sheet piling barrier and Ω=1.0.

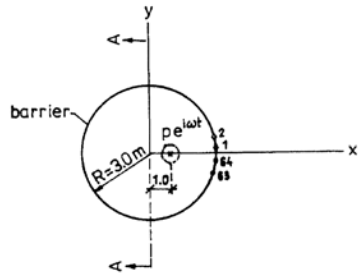

Fig. 9.20. Schematic diagram of closed circular sheet piling barrier.

9.4.2 Closed circular sheet piling barriers

The efficiency of a closed circular sheet piling barrier with radius R=3.0 m and with the source of the dynamic force according to the scheme of Fig. 9.20 was studied numerically by dividing the boundary curve into 64 boundary elements.

The variation of calculated dynamic deflection amplitudes $|w|K_2/(pa^2)$ along the cross-section A–A is drawn in Fig. 9.21 for Ω=0.5, in Fig. 9.22 for Ω=0.75, in Fig. 9.23 for Ω=1.00 and in Fig. 9.24 for Ω=2.0.

The variations of deflection amplitudes document the superposition of direct and reflected waves in the interior region of the barrier and the high degree of the vibration-isolating effect behind the closed barrier. The same effect can be expected if the exciting force is located on the exterior of the closed barrier. A passive vibration-isolating effect will be expected in the interior of the closed region. Such a case of passive vibration-isolation is the principle method for screening traffic vibration.

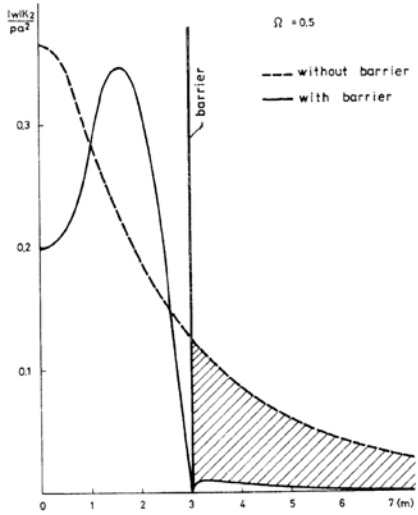

Fig. 9.21. Variation of deflection amplitudes with distance for closed barrier and Ω=0.5.

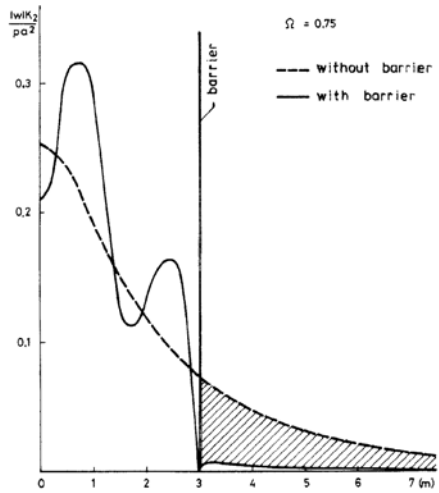

Fig. 9.22. Variation of deflection amplitudes with distance for closed barrier and Ω=0.75.

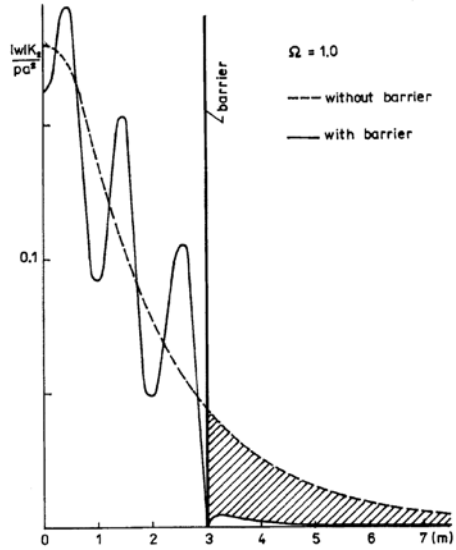

Fig. 9.23. Variation of deflection amplitudes with distance for closed barrier and Ω=1.0.

9.5 Screening effect for pulse loads

The method of boundary integral equations is a good means for the solution of problems in which the dynamic exciting force is a harmonically variable function of time with angular frequency ω.

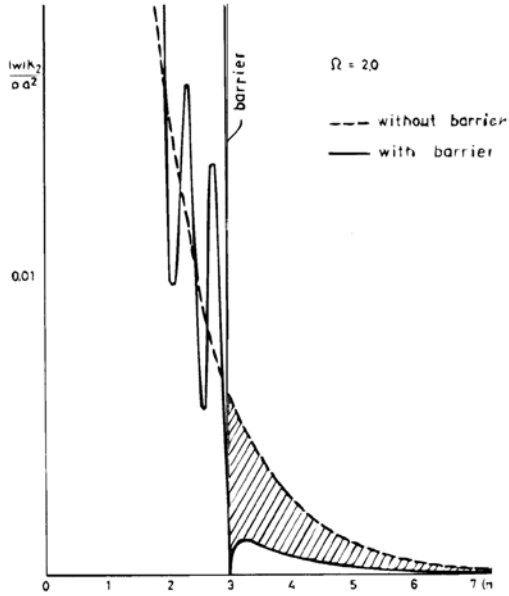

Fig. 9.24. Variation of deflection amplitudes with distance for closed barrier and Ω=2.0.

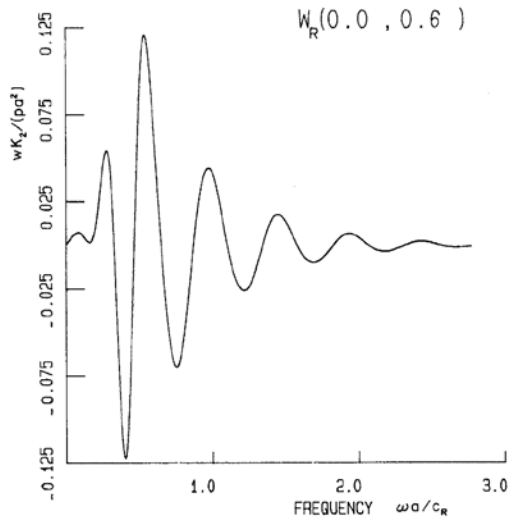

Fig. 9.25. Behaviour of real part of dynamic deflection response at point of subgrade medium without barrier.

In the cases of non-stationary vibration under a pulsed dynamic load the procedure of sections 4.8 and 7.3 can be applied. For illustration we present the results for a linear barrier with the parameters L=9.0 m, B=0.6 m, C_{ba}=5 and the scheme of Fig. 9.3.

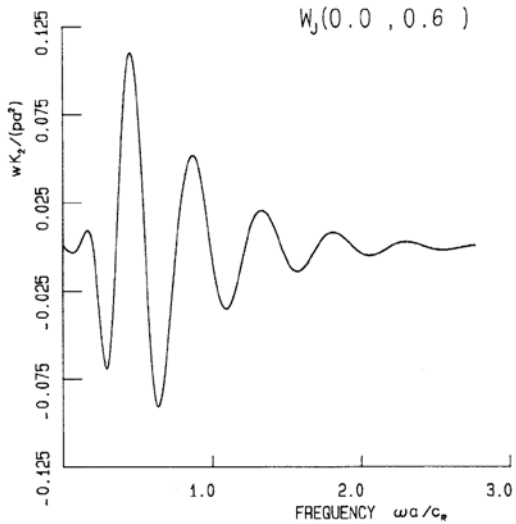

Fig. 9.26. Behaviour of imaginary part of dynamic deflection response at point of subgrade medium without barrier.

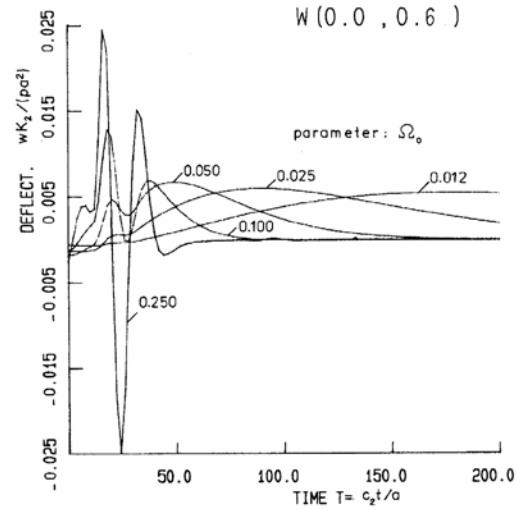

Fig. 9.27. Dynamic deflection response at point of subgrade medium under pulsed load for various values of pulse duration.

The courses of the real part $w_R K_2/pa^2$ and imaginary part $w_J K_2/pa^2$ of the dynamic deflection response at the point (0.0, 0.60) are shown in Figs. 9.25 and 9.26 for the subgrade

medium without the barrier. The corresponding variation of dynamic deflection as a time function for various values of pulse duration represented by parameter Ω_0=0.012, 0.025, 0.050, 0.100 and 0.250 is shown in Fig. 9.27.

Similarly, the real and imaginary parts of the dynamic deflection response for subgrade with a barrier are shown in Figs 9.28 and 9.29. The calculated dynamic deflection of the pulse excitation is shown in Fig. 9.30.

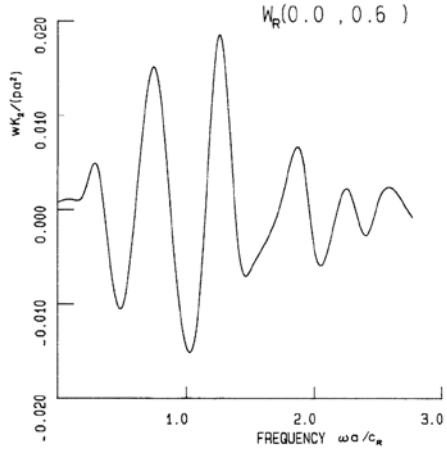

Fig. 9.28. Behaviour of real part of dynamic deflection response at point of subgrade medium with barrier.

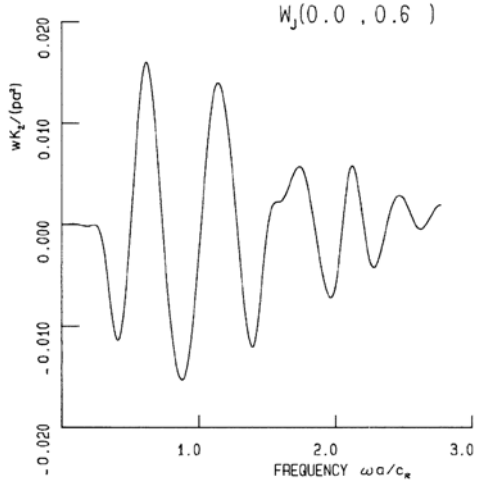

Fig. 9.29. Behaviour of imaginary part of dynamic deflection response at point of subgrade medium with barrier.

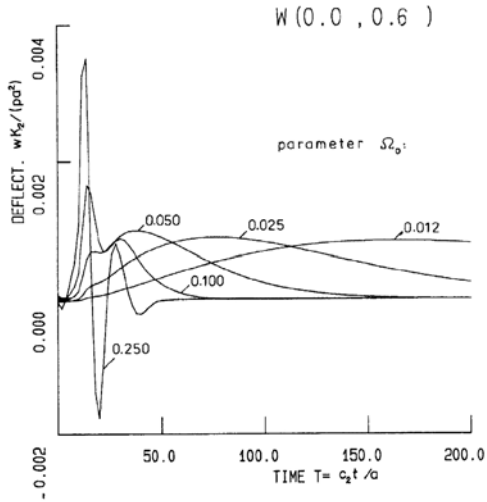

Fig. 9.30. Dynamic deflection response at point of subgrade medium with barrier under pulsed load for various values of pulse duration.

REFERENCES

1.1 VAKILI, J.: Dynamique d'un semiespace viscoélastique. *Bull. Liaison Labo. Runtiers P. et Ch., 40,* 1969, 155–176.

1.2 MATUŠINA, J.: The assessment of dynamic stiffness for runway pavements with cement concrete surfacing by using the method of phase velocities. In: *Nondestructive testing in building,* Brno, ČSVTS, Dům techniky 1977, 115–121. (In Czech)

1.3 ŠLACHTA, E.: The Application of the method of pulse wave propagation in layered medium. In: Utilisation of non-destructive methods in building. Košice, SVTS, Dom techniky 1974, VI. 1–28. (In Slovak)

1.4 JONES, R.: Surface wave technique for measuring the elastic properties and thickness of roads. Theoretical development. *Brit. J. Appl. Phys., 13,* 1962, 21–29.

1.5 JONES, R.: Following changes in the properties of road bases and subbases by the surface wave propagation method. *Civil Engng., 58,* 1963*,* 3–8.

1.6 JONES, R.-THROWER, E.N.: Effect of interfacial contact on the propagation of flexural waves along a composite plate. *J. Sound Vib.,* 2(2), 1965, 167–174.

1.7 Utilisation du vibreur Goodman en auscultation des chaussées. *Bulletin des laboratoires Routiers,* spécial J, juillet 1968.

1.8 GUILLEMIN, R.: Interpretation des vibrations de surface sur les structures routiéres. Laboratoire Central des Ponts et Chaussées, Paris, Sept. 1970, 70 p.

1.9 MARTINČEK, G.-POKORNÝ, M.: New assessment of elastic and inelastic properties of concrete using nondestructive testing methods. Research Report, Institut of Construction and Architecture of Slovak Academy of Sciences, Bratislava, 1965, 71 p. (In Slovak)

1.10 MARTINČEK, G.-POKORNÝ, M.: New apparatus for measuring the physical characteristics of material in elements and structures using dynamic non-destructive methods and its application. In: *The vibration and fatigue of building structures.* Bratislava, Publishing House of SAV, 1969, 113–147. (In Slovak)

1.11 MARTINČEK, G.: Simplified procedures of assessement of dynamic stiffness for pavement structures using the method of phase velocities. In: *Application of non-destructive method in building.* Košice, SVTS—Dom techniky 1974, 7, 1–10 (In Slovak)

1.12 MARTINČEK, G.: La diagnose de l'élasticité dynamique et de la rigidité des structures routiéres a l'aide de la méthode de vitesses de phase des ondes de contrainte. In: *New developments in non-destructive testing of non-metallic materials.* RILEM, Constanta 1974, 2, 35–42.

1.13 MARTINČEK, G.: *Theory and methods of dynamic non-destructive testing of flat elements.* Bratislava, Veda 1975, 316 p. (In Slovak)

1.14 MARTINČEK, G.: *Dynamic diagnosis of pavements.* Bratislava, Veda 1983, 190 p. (In Slovak)

1.15 POKORNÝ, M.: Apparatus for measuring the phase velocity of stress waves propagation. In: *Application of non-destructive methods in building.* Žilina, Dom techniky SVTS, 1972, 52–58. (In Slovak)

1.16 MARTINČEK, G.-POKORNÝ, M.: Technical theory of a dynamic equivalent layer on subgrade. Research Report, Bratislava, Institut of Construction and Architecture SAV, 1982, 118 p. (In Slovak)

1.17 KOLSKY, H.: *Stress waves in solids.* Oxford, 1953.

1.18 EWING, W.M.-JARDETZKY, W.S.-PRESS, F.: *Elastic waves in layered media.* New-York, London, McGraw-Hill 1957.
1.19 MARTINČEK, G.: Love's stress waves in viscoelastic layered media. *Stavebnícky časopis* 23, 1975, č. 6, 345–362. (In Slovak)
1.20 MARTINČEK, G.: Propagation of shear waves in layered media. In: *Proceedings of the Fifth European Conference on Earthquake Engineering.* Istanbul 1975, n. 19.
1.21 SOROKIN, E.S.: Internal and external resistence by the vibration of rigid bodies. *Nautchnoe sobshtchenje CNISK, 3,* Moskva 1957, 66 p. (In Russian)
1.22 SNOWDON, J.C.: *Vibration and shock in damped mechanical systems,* 1. ed. New York, London, Sydney, John Wiley, 1968, 486 p.
1.23 KOLSKY, H.: Viscoelastic waves. In: *Stress wave propagation in materials.* New York, Interscience Publishers 1960, 59–90.
1.24 HUET, C.: Une méthode d'étude en regime dynamique du comportement visco-élastique des matériaux enrobés. *Bulletin de liaison des labor. rout.,* Paris, *8,* 1964, 4.1.
1.25 ZAVERI, K.-OLESEN, H.P.: Messung des Elastizitätsmoduls und des Verlustfaktor von Asfalt. *Brüel-Kjaer Technical Review, 4,* 1972, 3–15.
1.26 PAGEN, C.A.: Rheological response of bituminous concrete. *Bituminous Materials and Mixes.* Highway Research Board, Washington 1965, 1–26.
1.27 LUXEMBURK, F.: Application of the theory of linear viscoelastic (Boltzmann) material, results in road building. SVTS, Dom techniky Košice, 1974, 2, 27–34. (In Czech)
1.28 VEVERKA, V.: Measuring of stiffness modulus for asphalt concrete by vibration method. *Siln. obzor, 3,* 1968, 73–76. (In Czech)
1.29 VEVERKA, V.: Research of testing and control methods for surfacing of bituminous pavements. Research Report, Praha, ČVUT, Fakulta stavební 1969.
1.30 MARTINČEK, G.-POKORNÝ, M.: The determination of viscoelastic characteristics of materials by the method of mechanical impendance and transmission. In: *Využitie nedeštruktívnych metód v stavebníctve,* SVTS—Dom techniky Košice, 1974, 10, 1–10. (In Slovak)
1.31 MARTINČEK, G.-POKORNÝ, M.: The assessement of viscoelastic characteristics of materials by using the method of mechanical impedance and transmissibility. In: *New developments in non-destructive testing of non-metallic materials.* RILEM, Constanta 1974, 2, 27–34.
1.32 MARTINČEK, G.-POKORNÝ, M.: The investigation of the dynamical viscoelastic properties of bituminous materials by the mechanical impedance method. In: *Proceedings of the Second International Symposium RILEM devoted to test in bituminous materials.* Budapest 1975, 463–473.
1.33 MARTINČEK, G.-POKORNÝ, M.: The assessement of dynamic viscoelastic properties of materials by mechanical impedance methods. In: *Dynamika stavebných konštrukcií*—ÚSTARCH—SAV, Smolenice 1977, 31–38. (In Slovak)
1.34 MARTINČEK, G.-POKORNÝ, M.: Method of mechanical impedance by using the longitudinal and torsional vibration of testing specimens. In: *Nedestruktivní zkoušení ve stavebnictví.* ČSVTS, Dům techniky Brno, 1977, 59–65. (In Slovak)
1.35 MARTINČEK, G.-SCHÁLEK, D.: Determination of dynamical viscoelastic characteristics of cohesive soils by the mechanical impedance method. In: *Proceedings of the Fifth Danube European Conference of Soils Mechanics and Foundation Engineering.* Bratislava 1977, 295–218.
1.36 TIMOSHENKO, S.: *Vibration in mechanical engineering.* Praha, SNTL 1960, 360 p. (In Czech)
1.37 MARTINČEK, G.: Dynamic vicoelastic properties of materials by the shear stress. Research Report, Bratislava, ÚSTARCH—SAV 1977, 94 p. (In Slovak)
1.38 MARTINČEK, G.: Use of the method of mechanical impedance for non-destructive testing of subgrade. In: *Nedeštruktívne skúšanie v stavebníctve 79.* Košice, Dom techniky 1979, 47–53. (In Slovak)

1.39 VAN DER POEL, C.: A general system describing the viscoelastic properties of bitumens and its relation to routine test data. *J. Appl. Chem., 4,* 1954, 5, p. 27.
1.40 MONISMITH, C.L.-ALEXANDER, R.L.-SECOR, K.E.: Rheologic behaviour of asphalt concrete. *Proceedings, Association of Asphalt Paving Technologists,* 35, 1966, 400–450.
1.41 KADLEČÍK, T.: Utilization of phase velocities for the quality testing of materials in pavement structure. In: *Využitie nedeštruktívnych metód v stavebníctve.* Košice, SVST—Dom techniky 1974, 7, 1–10. (In Slovak)
1.42 MARTINČEK, G.: Diagnostic of dynamic elasticity and rigidity of pavement structure. Research Report, Bratislava, ÚSTARCH—SAV 1978, 138 p. (In Slovak)
1.43 MARTINČEK, G.: Testing of pavement structures by using the method of phase velocities. In: *Zkoušení stavebních konstrukcí v teorii a praxi.* Svratka, ČVTS Brno 1971, 83–99. (In Slovak)
1.44 MARTINČEK, G.: Utilization of the method of phase velocities for non-destructive testing of pavements. Research Report, Bratislava, ÚS-TARCH—SAV-VÚIS 1970, 133 p. (In Slovak)
1.45 MARTINČEK, G.: The simplified procedures of the assessment of pavement dynamic rigidity using the method of phase velocities. In: *Využitie nedeštruktívnych metód v stavebníctve.* SVTS—Dom techniky Košice 1974, 7, 1–10. (In Slovak)
1.46 GSCHWENDT, J.: Tangential effect of trafic and influences of repeated loading established on circular testing track. Research Report, Bratislava, VÚIS 1972, 76 p. (In Slovak)
1.47 KADLEČÍK, T.: Dynamic moduli of elasticity for road materials determined by using the method of phase velocities. In: *Využitie nedeštruktívnych metód v stavebníctve.* Košice, SVTS—Dom techniky 1975, 14, 1–11. (In Slovak)
2.1 KOLAŘ, V.-NĚMEC, I.-DUBČÁK, J.: Stresses in layered pavements of slab and box bridges. *Stavebnícky časopis 24,* 1976, č. 1, 23–43. (In Czech)
3.1 REISSNER, E.: Stationare axialsymmetrische, durch eine shütternde Masse erregte Schwingungen eines homogenen elastischen Halbraumes. *Ingenieur Archiv,* dez. 1936, 838.
3.2 ŠECHTER, O. Ja.: Effect of inertia properties of soil-base by forced vertical vibration of rigid foundations. In: *NII, Symposium 12, Vibracii osnovanij i fundamentov,* Moskva, 1948, (In Russian)
3.3 BARKAN, D.D.: *Dynamics of bases and foundations.* McGraw-Hill, New York 1962, 434.
3.4 BYCROFT, G.N.: Forced vibrations of a rigid circular plate on a semiinfinite elastic space and on an elastic stratum. *Phil. Trans. of the R. Soc. of Lond.,* series 1, *248,* 1055–56, 327–368.
3.5 REISSNER, E.: Freie und erzwungene Torsionsschwingungen des elastischen Halbraumes. *Ingenieur—Archiv, 8,* 1937, 229–245.
3.6 REISSNER, E.-SAGOCI, H.F.: Forced torsional oscillations of an elastic half-space. *J. Appl. Phys*., 15, 1944, 652–662.
3.7 MARTINČEK, G.: Baugrunduntersuchungen nach der Methode der mechanischen Inpedanz. *Die Strasse,* 11/1981, 374–379.
3.8 MARTINČEK, G.: Determination of elasticity characteristics in plane structures without destruction. Research Report, ÚSTARCH-SAV, Bratislava 1970. (In Slovak)
3.9 UFLJAND, Ja. S.: Wave propagation by flexural vibration of bars and plates, *Prikladnaja matematika i mechanika, XII,* 1958, 287–300. (In Russian)
3.10 MINDLIN, R.D.: Influence of rotatory inertia and shear on flexural motion of isotropic elastic plates. *J. Appl. Mech. 18,* (1), 1951, 31–38.
3.11 MARTINČEK, G.: Influence of shear and rotatory inertia on plates vibration. *Strojnícky časopis XV*, X1964, č. 4, 337–357. (In Slovak)
3.12 NOVOTNÝ, B.-HANUŠKA, A.: *Theory of layered half-space.* Bratislava, VEDA 1983, 260 p. (In Slovak)
3.13 HAMPL, J.: Design of flexible pavement structures. Dissertation, Stavební fakulta ČVUT, Praha, 1990,122 p. (In Czech)

3.14 FILONENKO-BORODITCH, M.M.: Some approximate theories of elastic soil-base. *Utchenye zapiski MGU, 46,* Moskva, 1940.
3.15 PASTERNAK, P.L.: *Principle of the new design method of foundations on elastic subgrade by using two coefficients of compressibility.* Gosstrojizdat Moskva—Leningrad 1954. (In Russian)
3.16 VLASOV, V.Z.-LEONTJEV, N.N.: *Girders, plates and shells on elastic soil-base.* Gos. izd. fiziko-matem. literatury, Moskva 1960. (In Russian)
3.17 KOLÁŘ, V.-NĚMEC, L.: Energetic definitions and algorithms of the new subgrade model. *Stavebnícky časopis 26,* 1978, 565–581. (In Czech)
3.18 MARTINČEK, G.: Dynamic simplified model of subgrade. *Stavebnícky časopis, 32, 1984,* 21–43. (In Slovak)
3.19 MARTINČEK, G.-ALEXIEV, V.: Variants of inertia forces in nonlinear subgrade vibration. *Stavebnícky časopis,* 35, 1987, n. 10, 705–726. (In Slovak)
3.20 KORENEV, B.G.: *Some problems of the theory of elasticity and thermal conductivity solved in Bessel functions.* Gos. izd. fiziko-matem. literatury, Moskva 1960. (In Russian)
4.1 GIRKMANN, K.: *Flächentragwerke.* Springer-Verlag, Wien 1956.
5.1 FRÝBA, L.: *Vibration of solids and structures under moving loads.* Academia, Praha, 1972.
5.2 GHOSH, R.K.-RAMLAL-VIJAYARAGHAVAN, S.R.: Impact effect on rigid pavement corner having low spots. Central Road Research Institute, India, New Delhi.
5.3 BOLOTIN, V.V.: *Statistic methods in building mechanics.* GIS, Moskva 1961. (In Russian)
5.4 KROPÁČ, O.-PROCHÁZKA, M.-ŠPRINC, J.: Categorization and clasification of pavements according to the behaviour of system pavement vehicle. *Stavebnícky časopis, 32,* 1984, n. 5, 403–427. (In Czech)
6.1 BREBBIA, C.A.-TELLES, J.-WROBEL, L.: *Methods of boundary elements.* MIR, Moskva 1987. (In russian translation)
6.2 STERN, M.-LIN, T.L.: Thin elastic plates in bending. In: *Developments in boundary element method—4.* Elsevier, London—New York, 1986, 91–119.
6.3 BALAŠ, J.-SLÁDEK, J.-SLÁDEK, V.: *Stress analysis by the method of boundary integral equations.* VEDA, Bratislava, 359–410. (In Slovak)
6.4 BANERJEE, P.K.-BUTTERFIELD, R.: *Methods of boundary elements in applied sciences.* MIR, Moskva, 1984, 312–330. (In russian translation).
6.5 HARTMANN, F.: *Methode der Randelemente.* Springer—Verlag, Berlin, Tokyo 1987, 234–298.
6.6 TIMOSHENKO, S.P.-VOJNOVSKIJ-KRIGER, S.: *Plates and shells.* Gosud. izd. fiziko-matem. literatury. Moskva 1963 (In Russian translation)
9.1 BARKAN, D.D.: *Dynamics of bases and foundations.* McGraw-Hill, New York, London. 1962.
9.2 HAUPT, W.A.: Surface-waves in non-homogeneous halfspace. In: *Dynamic response and wave propagation in soils.* A.A.Balkema, Rotterdam, 1978, 335–367.
9.3 WOODS, R.D.: Holographic interferometry in soil dynamics. In: *Dynamic response and wave propagation in soils.* A.A.Balkema, Rotterdam, 1978, 39–55.
9.4 BENČAT, J.: Screening problems of surface stress waves in real mass medium. In: *Práce a štúdie Vysokej školy dopravy a spojov,* séria stav., zv. 7, Žilina 1982, 39–55. (In Slovak)
9.5 WOODS, R.D.: Screening of surface waves in soils. J. *Soil Mechanics and Foundations Division ASCE, 94* (SM4), 1968, 951–979.
9.6 WOODS, R.D.-BARNETT, N.E.-SAGESSER, R.: Holography—a new tool for soil dynamics. *J. Geotechnical Engineering Division, ASCE 100* (GT11), 1974, 1231–1247
9.7 BRAJA, M. DAS: *Fundamentals of soil dynamics.* Elsevier, New York, Amsterdam, Oxford 1983.
9.8 GRINTCHENKO, V.T.-MELESHKO, V.V.: *Harmonic vibrations and waves in elastic bodies.* Naukova dumka, Kijev 1981. (In Russian)

Appendix 1.
Computer program for the plate on half-space without the shear contact.

Program was developed for the case of plate on half-space and dimensionless frequency $\beta \to 0$, i.e static case. It makes possible to gain variations of the values of deflection, half-space reaction, bending moment and transversal force with the ratio r/h. The plate deflection is given by the relationship (3.122) and expressions (3.144) and (3.145) for $F(\xi, \beta \to 0)$ and $F_1(\xi, \beta \to 0)$. All others relationships are derived in section 3.3.

Input data:

DTA=δ

DTA1=δ_1

MI=μ

EPS1=$\varepsilon_1=c_2/c_{1z}$

EPS2=$\varepsilon_2=c_2/c_{2z}$

G1=G_z/G

$G2=a/h$

Output data:

W=wGa/P (r/h=0)

W1=wGa/P (r/h=1)

W2=wGa/P (r/h=2)

W3=wGa/P (r/h=3)

W5=wGa/P (r/h=5)

W10=wGa/P (r/h=10)

S=qah/P (r/h=0)

S1, S2, S3, S5, S10

Q1=Qa/P (r/h=1)

Q2, Q3, Q5, Q10

M=Ma/Ph (r/h=0)

M1, M2, M3, M5, M10

```
C     THE PLATE ON HALFSPACE WITHOUT THE SHEAR CONTACT-STATIC CASE
C     PROGRAM WPIS
      COMPLEX DTA,DTA1,W,W1,W2,W3,W5,W10,S,S1,S2,S3,S5,S10,Q,Q1,Q2,Q3,
     *Q5,Q10,M,M0,M1,M2,M3,M5,M10,FC,FM,FT1,FT,WA,W1A,W2A,W3A,W5A,W10A,
     *SA,S1A,S2A,S3A,S5A,S10A,Q1A,Q2A,Q3A,Q5A,Q10A,MOA,M1A,M2A,M3A,M5A,
     *M10A,V,WO,MA,MAA,QA,QAA
      REAL MI,KA
      OPEN(2, FILE='WPI.DAT')
      OPEN(3, FILE='WPO.DAT')
      READ(2,10)DTA,DTA1,MI,EPS1, EPS2,G1,G2
   10 FORMAT(2(F5.2,F5.2),F5.2,F6.2,F6.2, F8.5,F6.3)
      WRITE(3,11)DTA,DTA1,MI,EPS1,EPS2,G1,G2
   11 FORMAT(5X,6HDELTA=,F5.2,F5.2,3X,7HDELTA1=,F5.2,F5.2,3X,3HMI=,F5.2,
     *3X,5HEPS1=,F6.2,3X,5HEPS2=,F6.2,3X,3HG1=,F8.5,3X,3HG2=,F6.3,/)
      WA=CMPLX(0.,0.)
      W1A=CMPLX(0.,0.)
      W2A=CMPLX(0.,0.)
      W3A=CMPLX(0.,0.)
      W5A=CMPLX(0.,0.)
      W10A=CMPLX(0.,0.)
      SA=CMPLX(0.,0.)
      S1A=CMPLX(0.,0.)
      S2A=CMPLX(0.,0.)
      S3A=CMPLX(0.,0.)
      S5A=CMPLX(0.,0.)
      S10A=CMPLX(0.,0.)
      QAA=CMPLX(0.,0.)
      Q1A=CMPLX(0.,0.)
      Q2A=CMPLX(0.,0.)
      Q3A=CMPLX(0.,0.)
      Q5A=CMPLX(0.,0.)
      Q10A=CMPLX(0.,0.)
      M0A=CMPLX(0.,0.)
      MAA=CMPLX(0.,0.)
      M1A=CMPLX(0.,0.)
      M2A=CMPLX(0.,0.)
      M3A=CMPLX(0.,0.)
      M5A=CMPLX(0.,0.)
      M10A=CMPLX(0.,0.)
      ETA=0.0
      STEP=0.01
      DO 200 I=1,2000
      ETA=ETA+STEP
      B=ETA*G2
      FA0=BESS(0,B)
      FA1=BESS(1,B)
      B=ETA
      F10=BESS(0,B)
      F11=BESS(1,B)
```

```
B=ETA*2.
F20=BESS(0,B)
F21=BESS(1,B)
B=ETA*3.
F30=BESS(0,B)
F31=BESS(1,B)
B=ETA*5
F50=BESS(0,B)
F51=BESS(1,B)
B=ETA*10
F100=BESS(0,B)
F101=BESS(1,B)
B=ETA*G2
FG1=BESS(1,B)
FT1=2.*DTA1*(EPS1**2-EPS2**2)*ETA/(DTA*EPS2**2)
KA=((.87+1.12*MI)/(1+MI)) **2
FT=ETA**4-6.*(1-MI)*G1*FT1
W=6.*(1.-MI)/3.1415926*FG1/(FT*DTA)
W1=W*F10
W2=W*F20
W3=W*F30
W5=W*F50
W10=W*F100
S=-6.*(1.-MI)/3.1415926*G1*FT1*FG1/FT
S1=S*F10
S2=S*F20
S3=S*F30
S5=S*F50
S10=S*F100
Q=-(6.*(1.-MI)/3.1415926*(G1*FT1*DTA))/(FT*DTA)*FG1
QA=Q*FA1/ETA
Q1=Q*F11/ETA
Q2=Q*F21/ETA
Q3=Q*F31/ETA
Q5=Q*F51/ETA
Q10=Q*F101/ETA
M=(1./3.1415926*(ETA**2-G1*FT1/KA)/FT)*FG1
M0=M*(1.+MI)/2.
MA=M*(FAO-(1.-MI)*FA1/(G2*ETA))
M1=M*(F10-(1.-MI)*F11/ETA)
M2=M*(F20-(1.-MI)*F21/(2.*ETA))
M3=M*(F30-(1.-MI)*F31/(3.*ETA))
M5=M*(F50-(1.-MI)*F51/(5.*ETA))
M10=M*(F100-(1.-MI)*F101/(10.*ETA))
WA=WA+W
W1A=W1A+W1
W2A=W2A+W2
W3A=W3A+W3
W5A=W5A+W5
```

```
      W10A=W10A+W10
      SA=SA+S
      S1A=S1A+S1
      S2A=S2A+S2
      S3A=S3A+S3
      S5A=S5A+S5
      S10A=S10A+S10
      QAA=QAA+QA
      Q1A=Q1A+Q1
      Q2A=Q2A+Q2
      Q3A=Q3A+Q3
      Q5A=Q5A+Q5
      Q10A=Q10A+Q10
      M0A=M0A+M0
      MAA=MAA+MA
      M1A=M1A+M1
      M2A=M2A+M2
      M3A=M3A+M3
      M5A=M5A+M5
      M10A=M10A+M10
200   CONTINUE
      W0=-STEP*(G2*EPS2**2/(8.*3.1415926*G1*DTA1*(EPS1*2-EPS2**2)))
      W=STEP*WA+W0
      W1=STEP*W1A+W0
      W2=STEP*W2A+W0
      W3=STEP*W3A+W0
      W5=STEP*W5A+W0
      W10=STEP*W10A+W0
      S=STEP*SA
      S1=STEP*S1A
      S2=STEP*S2A
      S3=STEP*S3A
      S5=STEP*S5A
      S10=STEP*S10A
      QA=STEP*QAA-(1./(2.*3.1415926))
      Q1=STEP*Q1A-(1./(2.*3.1415926)*G2)
      Q2=STEP*Q2A-(1./(2.*3.1415926)*G2/2.)
      Q3=STEP*Q3A-(1./(2.*3.1415926)*G2/3.)
      Q5=STEP*Q5A-(1./(2.*3.1415926)*G2/5.)
      Q10=STEP*Q10A-(1./(2.*3.1415926)*G2/10.)
      M0=STEP*M0A+1./(12.*3.1415926*KA*G2)
      MA=STEP*MAA+1./(12.*3.1415926*KA*G2)
      M1=STEP*MIA+G2/(12.3.41926*KA)
      M2=STEP*M2A+G2/(12.*31415926*KA*4 )
      M3=STEP*M3A+G2/(12.*3.1415926*KA*9.)
      M5=STEP*M5A+G2/(12.*3.1415926*KA*25.)
      M10=STEP*M10A+G2/(12.*3.1415926*KA*100.)
      WRITE(3,12)
```

```
 12 FORMAT(5X,'DEFLECTIONS')
    CALL RIA(W)
    CALL RIA(W1)
    CALL (WA2)
    CALL RIA(W3)
    CALL RIA(W5)
    CALL RIA(W10)
    WRITE(3,13)
 13 FORMAT(5X,'HALFSPACE REACTIONS')
    CALL RIA(S)
    CALL RIA(S1)
    CALL RIA(S2)
    CALL RIA(S3)
    CALL RIA(S5)
    CALL RIA(S10)
    WRITE(3,14)
 14 FORMAT(5X,'TRANSVERSAL FORCES')
    CALL RIA(QA)
    CALL RIA(Q1)
    CALL RIA(Q2)
    CALL RIA(Q3)
    CALL RIA(Q5)
    CALL RIA(Q10)
    WRITE(3,15)
 15 FORMAT(5X,'BENDING MOMENTS')
    CALL RIA(M0)
    CALL RIA(MA)
    CALL RIA(M1)
    CALL RIA(M2)
    CALL RIA(M3)
    CALL RIA(M5)
    CALL RIA(M10)
    END

    SUBROUTINE RIA(V)
    COMPLEX V
    VR=REAL(V)
    VI=AIMAG(V)
    VA=CABS(V)
    VF=ATAN(VI/VR)
    WRITE(3,16)VR,VI,VA,VF
 16 FORMAT(5X,E14.6,3X,E14.6,3X,E14.6,3X,E14.6)
    RETURN
    END

    FUNCTION BESS(IA,B)
    DIMENSION CB(6,7)
    DATA CB/1.,.5,2*.79788456,2*.18539816,-2.2499997,-.56249985,
   1-7.7E-7,1.56E-6,.04166397,-.12499612,1.2656208,.21093573,
   2-5.5274E-3,0.01659667,3.954E-5,-5.65E-5,-.3163866,-.03954289,
```

```
 3-9.512E-5,1.7105E-4,-.00262573,.00637879,.0444479,.00443319,
 4.00137237,-.00249511,5.4125E-4,-7.4348E-4,-.0039444,-.
 500031761,-7.2805E-4,1.13653E-3,2.9333E-4,-7.9824E-4,2.1E
 6-4,i.io9E-5,i.4476E-4,-2.oo33E-4,-i.3558E-4,2.9i66E-4/
  IF(B-3.)1,1,3
1 X1=(B/3.)**2
  X=CB(IA+1,1)
  X2=1.
  DO 2 1=2,7
  X2=X2*X1
2 X=X+CB(IA+1,I)*X2
  IF(IA.EQ.1)X=X*B
  BESS=X
  RETURN
3 I1=IA+5
  I2=IA+3
  X2=CB(I2,1)
  X1=CB(I1,1)
  X3=3./B
  X4=1.
  X5=1.
  DO 4 1=2,7
  X4=X4*X3
  X5=X5*X3
  X2=X2+CB(I2,I)*X4
4 X1=X1+CB(I1,I)*X5
  IF(IA)5,5,6
5 X=X2*COS(B-X1)/SQRT(B)
  GOTO 7
6 X=X2*SIN(B-X1)/SQRT(B)
7 BESS=X
  RETURN
  END
```

Appendix 2.
Computer program for the linear and non-linear dynamic deflections of the plate on subgrade under pulse load.

Program was developed according to the relationship (8.39) and (8.38) for linear deflections and according to (8.40) for nonlinear deflections. The arbitrary shape of pulse load is given by means of thirty values F on the section T1 (0–30).

Input data:		**Output data:**
MI=μ	E0=$\varepsilon_0=\varepsilon_1 h/c_0=K_5 c_0/Ek_d$	T1=tc_0/h
KSI=r/a	E1=$K_1 h/E$	$W_0=w_0 E/ph$
HA=h/a	$E_2=K_2/Eh$	WN=$^{1}wE/ph$
$KD=k_d$	F=$f_1(\tau_1)$	

```
C     DYNAMIC NONLINEAR DEFLECTIONS OF THE PLATE ON SUBGRADE
C     PROGRAM NIMP
      DIMENSION T1(101),W0(101),W(101),WN(101)
      REAL KD
      OPEN(2,FILE='NIMP.DAT')
      OPEN(4,FILE='MIMPP.DAT')
      OPEN(3,FILE='NIMPP.DAT')
      READ(2,10)A0,E0,E1,KD
   10 FORMAT(4F7.5)
      PRINT 9,A0,E0,E1,KD
    9 FORMAT(5X,'A0=',F7.5,3X,'E0=',F7.5,3X,'E1=',F7.5,3X,'KD=',F7.5)
      READ(4,11)  (T1(K),W0(K),K=1,101)
   11 FORMAT(5X,F7. 3,3X,E14. 6)
      STE=2.
      WM=SQRT(E1/KD-E0**2/4.)
      DO 99 K=1,101
      IF(K.EQ.1)GOTO 20
      IF(K.EQ.2)GOTO 21
      WC=W0(2)**3*SIN(WM*STE/2.)*EXP(-E0*STE/4.)
      DO 100 J=1,K-1
      WC=WC+W0(J+1)**3*SIN(WM*(T1(K)-J*STE))*EXP(-E0*(T1(K)-J*STE)
     */2.)
  100 CONTINUE
      WC=WC*STE
      GOTO 30
   21 WC=W0(2)**3*SIN(WM*STE/2.)*EXP(-E0*STE/4.)
```

```
      WC=WC*STE/2.
      GOTO 30
   20 WC=0.
   30 W(K)=WC*A0/WM
      WN(K)=W0(K)-W(K)
      PRINT 12,T1(K),W0(K),WN(K)
   12 FORMAT(5X,F7.3,3X,E14.6,3X,E14.6)
      WRITE(3,13)T1(K),WN(K)
   13 FORMAT(5X,F7.3,3X,E14.6)
   99 CONTINUE
      END

C     DYNAMIC DEFLECTIONS OF THE PLATE ON SUBGRADE UNDER PULSE LOAD
C     PRORAM MIMP
      DIMENN F(30)
      REAL MI,KSI,KD
      OPEN(2,FILE='MIMP.DAT')
      OPEN(3,FILE='MIMP0.DAT')
      OPEN(4,FILE='MIMPP.DAT')
      M=30
      READ(2,10)MI,KSI,HA,KD,E0,E1,E2,F
   10 FORMAT(4F7.4,3F7.5,/,10F6.4,/10F6.4,/10F6.4)
      WRITE(3,11)MI,KSI,HA,KD,E0,E1,E2,F
      PRINT 11,MI,KSI,HA,KD,E0,E1,E2,F
   11 FORMAT(5X,'MI=',F7.4,3X,'KSI=',F7.4,3X,'HA=',F7.4,3X,'KD=',F7.4,
     */,5,'E0=',F7.5,3X,'E1=*,F7.5,3X,'E2=',F7.5,3X,/,5X,10F6
     *.4,5X,10F6.4,/5X,10F6.4)
      T1=-1.0
      STE=1.0
      DO 100 K=1,201
      T1=T1+STE
      IF(T1.EQ.0.)GOTO 14
      WA=0.
      ETA=0.
      STEP=0.01
      DO 200 I=1,1500
      ETA=ETA+STEP
      CALL BESSEL(1,ETA,B1)
      ETAR=ETA*KSI
      CALL BESSEL(0,ETAR,B0)
      WM=SQRT(E1/KD+E2*HA**2/KD*ETA**2+HA**4*ETA**4/KD/(12.*(1.-MI**2))
     *-E0**2/4.)
      IF(K.EQ.2) GOTO 20
      IF (K.LE.(M+1)) GOTO 21
      WC=BO*B1*1./2.*SIN(WM*STE/2.)*F(l)*EXP(-E0*STE/4.)
      DO 300 L=2,M
      WC=WC+B0*B1*SIN(WM*(T1-L*STE))*F(L)*EXP(-E0*(T1-L*STE)/2.)
  300 CONTINUE
      WC=WC*STE
```

```
      GO TO 30
   21 WC=B0*B1*1./2.*SIN(WM*STE/2.)*F(1)*EXP(-EO*STE/4.)
      DO 400 J=2,K-1
      WC=WC+B0*B1*SIN(WM*(T1-J*STE))*F(J)*EXP(-E0*(T1-J*STE)/2.)
  400 CONTINUE
      WC=WC*STE
      GOTO 30
   20 WC=B0*B1*SIN(WM*STE/2.)*F(1)*EXP(-E0*STE/4.)*STE/2.
   30 W=WC/WM
      WA=WA+W
  200 CONTINUE
      W=WA*STEP
      W0=-W/2./3.1415926/KD
      GOTO 15
   14 W0=0.
   15 PRINT 12,T1,W0
      WRITE(3,12)T1,W0
      WRITE(4,13)T1,W0
   12 FORMAT(5X,'T1=',F7.3,3X,'W0=',E14.6)
   13 FORMAT(5X,F7.3,3X,E14.6)
  100 CONTINUE
      END

      SUBROUTINE BESSEL(IA,B,BESS)
      DIMENSION CB(6,7)
      DATA CB/1.,.5,2*.79788456,2*.78539816,-2.2499997,-.56249985,
     1-7.7E-7,1.56E-6,.04166397,-.12499612,1.2656208,.21093573,
     2-5.5274E-3,0.01659667,3.954E-5,-5.65E-5.-.3163866,-.03954289,
     3-9.512E-5,1.7105E-4,-.00262573,.00637879,.0444479,.00443319,
     4.00137237,-.00249511,5.4125E-4,-7.4348E-4,-.0039444,-.
     500031761,-7.2805E-4,1.13653E-3,2.9333E-4,-7.9824E-4,2.1E
     6-4,1.109E-5,1.4476E-4,-2.0033E-4,-1.3558E-4,2.9166E-4/
      IF(B-3.)1,1,3
    1 X(B/3.)**2
      X=CB(IA+1,1)
      X2=1.
      DO 2 1=2,7
      X2=X2*X1
    2 X=X+CB(IA+1,I)*X2
      IF(IA.EQ.1)X=X*B
      BESS=X
      RETURN
    3 I1=IA+5
      I2=IA+3
      X2=CB(I2,1)
      X1=CB(I1,1)
      X3=3./B
      X4=1.
      X5=1.
```

```
      DO 4 1=2,7
      X4=X4*X3
      X5=X5*X3
      X2=X2+CB(I2,I)*X4
    4 X1=X1+CB(I1,I)*X5
      IF(IA)5,5,6
    5 X=X2*COS(B-X1)/SQRT(B)
      GOTO 7
    6 X=X2*SIN(B-X1)/SQRT(B)
    7 BESS=X
      RETURN
      END
```

Appendix 3.
Computer program for the dynamic deflection field around the sheet piling barrier in subgrade.

Program was developed according to the method of boundary elements as it is applied in chapter 9 and 9.4. It makes possible to solve the diffraction of the waves about the sheet piling barrier. The division of barrier is supposed into 32 boundary elements with the same length.

Input data:

NN number of boundary elements

X (J), J=1,NN coordinates of nodal element points

Y (J), J=1,NN coordinates of nodal element points

XX (M), M=1,20 coordinates of network points

YY (I), I=1,22 coordinates of network points

DLJ=l_j length of boundary element

XKSI, YKSI coordinates of load point

DTZ=δ damping parameter

GA = $\gamma = K_2^*/K_1^* a^2$

A radius of circular load area

OM=$\omega a/c_R$—dimensionless frequency

Output data:

ZZ—YY (K), XX (M) coordinates of network points

CABS (WP(M)) absolute values of dynamic deflections wK_2/pa^2

REAL (WP(M)) real parts of dynamic deflections wK_2/pa^2

AIMAG (WP(M)) imaginary parts of dynamic deflections wK_2/pa^2

```
C     VIBROISOLATING EFFECT OF SHEET PILING BARRIER
C     PROGRAM MA2
      COMMON/A1/ ETA(32),FI(32),DL(32),AL,ALEJ(32),W(32),
     *B(3,32),BZ(32)
      COMMON/A2/FIKSI,ETAKSI,ALKSI,A
      COMPLEX B,BZ,W,AL,ALEJ,DTZ,ALR(32,32),ALZP(20),
     *BP(0,32),BZP(20),WP(20),ALKSI
      DIMENSION X(32),Y(32),FIPJ(20,32),PSIP(20,32),ALFP(20,32),YY(22),
     *XX(0)
      OPEN(UNIT=2,FILE='MA2.DAT')
      OPEN(UNIT=3,FILE='MA20.DAT')
      OPEN(UNIT=4,FILE='MA2R.DAT')
      OPEN(UNIT=5,FILE='MA2I.DAT')
      READ(2,10)NN
   10 FORMAT(I4)
      PRINT 11,NN
   11 FORMAT(5X,3HNN=,I4,/)
      READ(2,12) (X(J),J=1,NN)
      READ(2,12) (Y(J),J=1,NN)
   12 FORMAT(12F6.2)
      PRINT 13,(X(J),J=1,NN),(Y(J),J=1,NN)
   13 FORMAT(12F6.2)
      CALL VSTUP(NN,X,Y)
      CALL MAT(NN,XKSI,YKSI,ALR)
      CALL SLVE(B,BZ,NN,.1E-12)
      READ(2,14) (YY(I),1=1,22)
   14 FORMAT(12F6.2)
      PRINT 15,(YY(I),1=1,22)
   15 RMAT(12F6.2)
      READ(2,16) (XX(M),M=1,20)
   16 RMAT(12F6.2)
      PRINT 17,(XX(M),M=1,20)
   17 FORMAT(12F6.2)
      DO 90 K=1,22
      ZZ=YY(K)
      CALL VYSTUP(NN,XX,ZZ,BP,BZP,WP)
   90 CONTINUE
      END

      SUBROUTINE VSTUP(NN,X,Y)
      COMMON/A1/ ETA(32),FI(32),DL(32),AL,ALEJ(32),W(32),
     *B(3,32),BZ(32)
      COMPLEX B,BZ,W,AL,ALEJ
      DIMENSION X(32),Y(32)
      DO 100 J=1,NN
      ETA(J)=SQRT(X(J)**2+Y(J)**2)
      IF(X(J).EQ.0.0.AND.Y(J).GT.0)GO TO 14
      IF(X(J).EQ.0.0.AND.Y(J).LT.0)GO TO 15
      IF(X(J).GT.0.AND.Y(J).EQ.0.0)GO TO 108
```

```
      IF(X(J).LT.0.AND.Y(J).EQ.0.0)GO TO 109
      GO TO 16
   14 (J)=3.1415926/2.
      GO TO 100
   15 (J)=3.1415926*3.72.
      GO TO 100
  108 FI(J)=0.
      GO TO 100
  109 FI(J)=3.1415926
      GO TO 100
   16 FI(J)=ATAN(ABS(Y(J))/ABS(X(J)))
      IF(X(J).GT.0.AND.Y(J).GT.0)GO TO 100
      IF(X(J).LT.0.AND.Y(J).GT.0)GO TO 17
      IF(X(J).LT.0.AND.Y(J).LT.0)GO TO 18
      IF(X(J).GT.0.AND.Y(J).LT.0)GO TO 19
   17 FI(J)=3.1415926-FI(J)
      GO TO 100
   18 FI(J)=3.1415926+FI(J)
      GO TO 100
   19 FI(J)=2.*3.1415926-FI(J)
  100 CONTINUE
      READ(2,20)DLJ
   20 FORMAT(F5.2)
      DO 101 J=1,32
  101 DL(J)=DLJ
      RETURN
      END

      SUBROUTINE MAT(NN,XKSI,YKSI,ALR)
      COMMON/A1/ ETA(32),FI(32),DL(32),AL,ALEJ(32),W(32),
     *B(3,32),BZ(32)
      COMMON /A2/ FIKSI,ETAKSI,ALKSI,A
      COMPLEX B,BZ,W,AL,ALEJ,DTZ,ALEK(32),ALR(32,32),ALKSI,ALZ(32),
     *B1RB2R,H1R,H2R,DLK(2),B1K,B2K,HIK,H2K,DLE,BIE,B2E,H1E,H2E,
     *B11B12,H11,H12,B01,B02,H01,H02
      DIMENSION FIKSIK(32),FIKJ(32,32),ALF(32,32),C(2)
      READ(2,8)XKSI,YKSI
    8 FMAT(2F6.2)
      PRINT 9,XKSI,YKSI
    9 FORMAT(5X,5HXKSI=,F6.2,3X,5HYKSI=,F6.2)
      READ(2,10)DTZ,GA,OM,A
   10 RMAT((F5.2,F5.2),3F6.2)
      PRINT 11,DTZ,GA,OM,A
   11 FORMAT(5X,4HDTZ=,(F5.2,F5.2),3X,3HGA=,F6.2,
     *3X,HOM=,F6.2,3X,2HA=,F6.2)
      AL=CSQRT(OM**2/DTZ-1./GA)
      IF(REAL(AL).LE.0)GO TO 12
      GO TO 13
   12 AL=-AL
```

```
 13 DO 100 K=1,NN
    ALEK(K)=AL*ETA(K)/A
    DO 100 J=1,NN
    FIKJ(K,J)=ABS(FI(K)-FI(J))
    ALEJ(J)=AL*ETA(J)/A
    IF(J.EQ.K)GO TO 100
    ALR(K, J)=CSQRT(ALEK(K)**2+ALEJ(J)**2-2.*ALEK(K)*ALEJ(J)*COS(FIKJ
   3(K,J)))
    IF(REAL(ALR(K,J)).LE.0)GO TO 14
    GO TO 15
 14 ALR(K,J)=-ALR(K,J)
 15 CALL HANK0(ALR(K,J),BIR,B2R,HIR,H2R,.00001)
    IF(AIMAG(ALR(K,J)).GE.0)GO TO 16
    IF(AIMAG(ALR(K,J)).LE.0)GO TO 17
 16 B(K,J)=-CMPLX(0.,1.)*DL(J)*H1R/4.
    GO TO 100
 17 B(K,J)=-CMPLX(0.,1.)*DL(J)*H2R/4.
100 CONTINUE
    DO 101 K=1,NN
    DLK(1)=DL(K)/2.*0.33998*AL/A*0.99
    DLK(2)=DL(K)/2.*0.86114*AL/A*0.99
    C(1)=0.65214
    C(2)=0.34785
    B(K,K)=(0.,0.)
    DO 102 I=1,2
    IF(REAL(DLK(I)).LE.0)GO TO 30
    GO TO 31
 30 DLK(I)=-DLK(I)
 31 CALL HANK0(DLK(I),B1K,B2K,H1K,H2K,.00001)
    IF(AIMAG(DLK(I)).GE.0)GO TO 32
    IF(AIMAG(DLK(I)).LE.0)GO TO 33
 32 B(K,K)=B(K,K)-CMPLX(0.,1.)*0.98*DL(K)*H1K*C(I)/4.
    GO TO 102
 33 B(K,K)=B(K,K)-CMPLX(0.,1.)*0.98*DL(K)*H2K*C(I)/4.
102 CONTINUE
    DLE=DL(K)/100.*AL/A
    IF(REAL(DLE).LE.0)GO TO 34
    GO TO 35
 34 DLE=-DLE
 35 CALL HANK0(DLE,B1E,B2E,H1E,H2E,.00001)
    IF(AIMAG(DLE).GE.0)GO TO 36
    IF(AIMAG(DLE).LE.0)GO TO 37
 36 B(K,K)=B(K,K)-CMPLX(0.,1.)*0.02*DL(K)*H1E/4.
    GO TO 101
 37 B(K,K)=B(K,K)-CMPLX(0.,1.)*0.02*DL(K)*H2E/4.
101 CONTINUE
    FIKSI=2.*3.1415926-ATAN(ABS(YKSI)/ABS(XKSI))
    ETAKSI=SQRT(XKSI**2+YKSI**2)
    CALL HANK1(AL,B11,B12,H11,H12,.00001)
```

```
      ALKSI=AL*ETAKSI/A
      DO 104 K=1,NN
      FIKSIK(K)=ABS(FI(K)-FIKSI)
      ALZ(K)=CSQRT(ALEK(K)**2+ALKSI**2-2.*ALEK(K)*ALKSI*COS(FIKSIK(K)))
      IF(REAL(ALZ(K)).LE.0)GO TO 22
      GO TO 19
   22 ALZ(K)=-ALZ(K)
   19 CALL HANK0(ALZ(K),B01,B02,H01,H02,.00001)
      IF(AIMAG(ALZ(K)).GE.0)GO TO 20
      IF(AIMAG(ALZ(K)).LE.0)GO TO 21
   20 BZ(K)=-CMPLX(0.,1.)*3.1415926/2./AL*B11*H01
      GO TO 104
   21 BZ(K)=-CMPLX(0.,1.)*3.1415926/2./AL*B11*H02
  104 CONTINUE
      DO 103 K=1,NN
      PRINT 23,REAL(B(K,K)),AIMAG(B(K,K)),CABS(B(K,K))
   23 FORMAT(5X,3E14.6)
      PRINT 24,REAL(BZ(K)),AIMAG(BZ(K)),CABS(BZ(K))
   24 FORMAT(2X,3E14.6)
  103 CONTINUE
      RETURN
      END

      SUBROUTINE SLVE(D,DZ,NN,EPS)
      DIMENSION FIW(32),D(32,32),DZ(32)
      COMPLEX B,BZ,DIV,DELT,W,ALEJ,AL,D,DZ
      COMMON/A1/ ETA(32),FI(32),DL(32),AL,ALEJ(32),W(32),
     *B(32,32),BZ(32)
      DO 9015 K=1,NN
      I=K
      IF(K-NN)9021,9007,9021
 9021 IF(CABS(D(K,K))-EPS)9006,9006,9007
9006 I=I+1
      DZ(K)=DZ(K)+DZ(I)
      DO 9023 J=1,NN
9023 D(K,J)=D(K,J)+D(I,J)
      GO TO 9021
9007 DIV=D(K,K)
      DZ(K)=DZ(K)/DIV
      DO 9009 J=1,NN
9009 D(K,J)=D(K,J)/DIV
      DO 9015 MM=1,NN
      DELT=D(MM,K)
      IF(CABS(DELT)-EPS)9015,9015,9016
9016 IF(MM-K)9010,9015,9010
9010 DZ(MM)=DZ(MM)-DZ(K)*DELT
      DO 9011 J=1,NN
      IF(CABS(D(MM,J)).LT.EPS)GO TO 11
      D(MM,J)=D(MM,J)-D(K,J)*DELT
```

```
  11 D(MfJ)=D(M,J)
9011 CONTINUE
9015 CONTINUE
     DO 99 MM=1,NN
     W(MM)=DZ(MM)
     FIW(MM)=ATAN(AIMAG(W(MM))/REAL(W(MM)))
     PRINT 10,REAL(W(MM)),AIMAG(W(MM)),CABS(W(MM))fFIW(MM)
  10 FORMAT(5X,4E14.6,)
  99 CONTINUE
     RETURN
     RETURN
     END

     SUBROUTINE VYSTUP(NN,XX,ZZ,BP,BZP,WP)
     COMMON/A1/ ETA(32),FI(32),DL(32),AL,ALEJ(32),W(32),B(32,32),
    *BZ(32)
     COMMON/A2/ FIKSI,ETAKSI,ALKSI,A
     DIMENSION FIPJ(20,32),ALRP(20,32),ALZP(20),BP(20,32),BZP(20),
    *WP(20),FIKSIP(20),FIWP(20),XX(20),EETA(20),FFI(20)
     COMPLEX B,BZ,W,AL,ALEJ,ALEM(20),ALKSI,ALZP,
    *ALRP,BBP(20),BP,BZP,WP,BIR,B2R,HIR,H2R,B01,B02,
    *H01,H02,B11,B12,H11,H12
     DO 91 M=1,20
     EETA(M)=SQRT(XX(M)**2+ZZ**2)
     IF(XX(M).EQ.0.0.AND.ZZ.GT.0)GOTO 74
     IF(XX(M).EQ.0.0.AND.ZZ.LT.0)GOTO 75
     IF(XX(M).GT.0.AND.ZZ.EQ.0.0)GOTO 78
     IF(XX(M).LT.0.AND.ZZ.EQ.0.0)GOTO 79
     GOTO 76
  74 FFI(M)=3.1415926/2.
     GOTO 91
  75 FFI(M)=3.1415926*3./2.
     GOTO 91
  78 FFI(M)=0
     GOTO 91
  79 FFI(M)=3.1415926
     GOTO 91
  76 FFI(M)=ATAN(ABS(ZZ)/ABS(XX(M)))
     IF(XX(M).GT.0.AND.ZZ.GT.0)GOTO 91
     IF(XX(M).LT.0.AND.ZZ.GT.0)GOTO 77
     IF(XX(M).LT.0.AND.ZZ.LT.0)GOTO 88
     IF(XX(M).GT.0.AND.ZZ.LT.0)GOTO 89
  77 FFI(M)=3.1415926-FFI(M)
     GOTO 91
  88 FFI(M)=3.1415926+FFI(M)
     GOTO 91
  89 FFI(M)=2.*3.1415926-FFI(M)
  91 CONTINUE
     DO 100 M=1,20
```

```
      DO 100 J=1,NN
  100 FIPJ(M,J)=ABS(FFI(M)-FI(J))
      DO 103 M=1,20
      ALEM(M)=AL*EETA(M)/A
      DO 103 J=1,NN
      ALRP(M,J)=CSQRT(ALEM(M)**2+ALEJ(J)**2
     *2.*ALEM(M)*ALEJ(J)*COS(FIPJ(M,J)))
      IF(REAL(ALRP(M,J)).LE.0)GO TO 14
      GO TO 15
   14 ALRP(M,J)=-ALRP(M,J)
   15 CALL HANK0(ALRP(M,J),BIR,B2R,HIR,H2R,.00001)
      IF(AIMAG(ALRP(M,J)).GE.0)GO TO 16
      IF(AIMAG(ALRP(M,J)).LE.0)GO TO 17
   16 BP(M,J)=-CMPLX(0.,1.)*DL(J)*H1R/4.
      GO TO 103
   17 BP(M, J)=-CMPLX(0.,1.)*DL(J)*H2R/4.
  103 CONTINUE
      CALL HANK1(AL,B11,B12,H11,H12,.00001)
      DO 104 M=1,20
      FIKSIP(M)=ABS(FFI(M)-FIKSI)
      ALZP(M)=CSQRT(ALEM(M)**2+ALKSI**2-2.*ALEM(M)*ALKSI*COS(FIKSIP(M)))
      IF(REAL(ALZP(M)).LE.0)GO TO 18
      GO TO 19
   18 ALZP(M)=-ALZP(M)
   19 CALL HANK0(ALZP(M),B01,B02,H01,H02,.00001)
      IF(AIMAG(ALZP(M)).GE.0)GO TO 20
      IF(AIMAG(ALZP(M)).LE.0)GO TO 21
   20 BZP(M)=-CMPLX(0.,1.)*3.1415926/2./AL*B11*H01
      GO TO 29
   21 BZP(M)=-CMPLX(0.,1,)*3.1415926/2./AL*B11*H02
   29 PRINT 30,REAL(BZP(M)),AIMAG(BZP(M)),CABS(BZP(M))
   30 FORMAT(3X,3E14.6)
  104 CONTINUE
      DO 105 M=1,20
      BBP(M)=(0.,0.)
      DO 106 J=1,NN
      BBP(M)=BBP(M)-BP(M,J)*W(J)
  106 CONTINUE
      WP(M)=BBP(M)+BZP(M)
      FIWP(M)=ATAN(AIMAG(WP(M))/REAL(WP(M)))
      PRINT 22,REAL(WP(M)),AIMAG(WP(M)),CABS(WP(M)),FIWP(M)
   22 FORMAT(5X,4E14.6,/)
      WRITE(3,23)ZZ,XX(M),CABS(WP(M))
   23 FORMAT (2F6.2,E14.6)
      WRITE(4,24)ZZ,XX(M),REAL(WP(M))
   24 FORMAT(2F6.2,E14.6)
      WRITE(5,25)ZZ,XX(M),AIMAG(WP(M))
   25 FORMAT(2F6.2,E14.6)
  105 CONTINUE
      RETURN
      END
```

```
      SUBROUTINE HANK0(C,BE01,BE02,H01,H02,DEL)
      COMPLEX C,BE01,BE02,H01,H02,H0,H00
      EXTERNAL NFAK
      REAL NFAK
      BE01=(0.,0.)
      C1=0.
      RO=CABS(C)
      IF(RO.GT.5.0)GO TO 19
      IF(REAL(C).LT.1.E-06)GO TO 5
      FI0=AIMAG(C)/REAL(C)
      FI=ATAN(FI0)
      GO TO 6
    5 FI=3.1415926/2.
    6 IF(REAL(C))9,9,10
    9 FI=FI+SIGN(1.,AIMAG(C))*3.1415926
   10 BE02=CMPLX(ALOG(RO/2.)+0.577216,FI)*2./3.1415926
      H01=(0.,0.)
      H02=(0.,0.)
      K=0
      DE01=1.
      GO TO 16
   15 IF(K.GT.30)GO TO 17
      DE011=1./NFAK(K)
      DE01=(-1)**K*DE011*(RO/2)**(2*K/3.)/NFAK(K)*(RO/2)**
      1(2*K/3.)*(RO/2)**(2*K/3.)
      GO TO 16
   17 DE01=(-2)**K*(RO/2)**(2*K/3.)/2.6525E32*(RO/2)**(2*K/3.)/2.6525
      2E32*(RO/2)**(2*K/3.)/NFAK(K)/NFAK(K)
   16 DE1=COS(2*K*FI)
      DE2=SIN(2*K*FI)
      BE01=BE01+CMPLX(DE01*DE1,DE01*DE2)
      IF(K)18,18,11
   11 B1=ALOG(RO/2.)+0.577216
      C1=C1+1./K
      F1=DE01*DE1*(B1-C1)-DE01*DE2*FI
      F2=DE01*DE2*(B1-C1)+DE01*DE1*FI
      BE02=BE02+CMPLX(F1,F2)*2./3.1415926
      F3=SQRT(F1**2+F2**2)
      F4=SQRT((DE01*DE1)**2H-(DE01*DE2)**2)
      IF(F3.LT.DEL.AND.F4.LT.DEL)GO TO 14
      IF(K.EQ.30)GO TO 14
   18 K=K+1
      GO TO 15
   14 H01=H01+CMPLX((REAL(BE01)-AIMAG(BE02)),
     2(AIMAG(BE01)+REAL(BE02)))
      H02=H02+CMPLX((REAL(BE01)+AIMAG(BE02)),
     3(AIMAG(BE01)-REAL(BE02)))
      GO TO 20
   19 H00=2.*CMPLX(0.,1.)*C
```

```
      H0=1.+1./4./H00+9./32./H00**2+1225./384./H00**3+
     211025./6144./H00**4
      H01=CSQRT(2./3.1415926/C)*CEXP(CMPLX(0.,1.)*(4.*C-3.1415926)/4.
     3)*H0
      H02=CSQRT(2./3.1415926/C)*CEXP(CMPLX(0.,-1.)*(4.*C-3.1415926)/4.
     4)*H0
      BE01=(H01+H02)/2.
      BE02=(H01-H02)/2./CMPLX(0.,1.)
   20 CONTINUE
      RETURN
      END

      SUBROUTINE HANK1(C,BE11,BE12,H11,H12,DEL)
      COMPLEX C,BE11,BE12,H11,H12,H1,H10
      EXTERNAL NFAK
      REAL NFAK
      BE11=(0.,0.)
      C1=0.
      RO=CABS(C)
      IF(RO.GT.5.)GO TO 20
      IF(REAL(C).LT.1.E-06)GO TO 5
      FI0=AIMAG(C)/REAL(C)
      FI=ATAN(FI0)
      GO TO 6
    5 FI=3.1415926/2.
    6 IF(REAL(C))9,9,10
    9 FI=FI+SIGN(1.,AIMAG(C))*3.1415926
   10 BE12=CMPLX(-COS(FI),SIN(FI))/RO*2./3.1415926
      H11=(0.,0.)
      H12=(0.,0.)
      K=0
      DE11=RO/2.
      GO TO 16
   15 IF(K.GT.30)GO TO 17
      DE111=1./NFAK(K+1)
      DE11=(-1)**K*DE111*(RO/2)**(2/3.*K-H1)/NFAK(K)*(RO/2)**(2/3.*K)*
     3(RO/2)**(2/3.*K)
      GO TO 16
   17 DE11=(-1)**KMRO/2)*M2/3.*K+1)/2.6525E32MRO/2)**(2/3.*K)
      3/2.6525E32*(RO/2)**(2/3.*K)/NFAK(K)/NFAK(K+1)
   16 DE1=COS((2*K+1)*FI)
      DE2=SIN((2*K+1)*FI)
      BE11=BE11+CMPLX(DE11*DE1,DE11*DE2)
      B1=ALOG(RO/2.)+0.577216-1./(2*K+2)
      IF(K)19,19,11
   19 BE12=BE12+CMPLX(DE11*(DE1*B1-DE2*FI),
     4DE11*(DE2*B1+DE1*FI))*2./3.1415926
      IF(K)18,18,11
   11 C1=C1+1./K
```

```
      F1=DE11*DE1*(B1-C1)-DE11*DE2*FI
      F2=DE11*DE2* (B1-C1)+DE11*DE1*FI
      BE12=BE12+CMPLX(F1,F2)*2./3.1415926
      F3=SQRT(F1**2+F2**2)
      F4=SQRT((DE11*DE1)**2+(DE11*DE2)**2)
      IF(F3.LT.DEL.AND.F4.LT.DEL)GO TO 14
      IF(K.EQ.30)GO TO 14
   18 K=K+1
      GO TO 15
   14 H11=H11+CMPLX((REAL(BE11)-AIMAG(BE12)),
     5(AIMAG(BE11)+REAL(BE12)))
      H12=H12+CMPLX((REAL(BE11)+AIMAG(BE12)),
     6(AIMAG(BE11)-REAL(BE12)))
      GO TO 21
   20 H10=2.*CMPLX(0.1.)*C
      H1=1.-3./4./H10-15./32./H10**2-4315./384./H10**3-14175./
     26144./H10**4
      H11=CSQRT(2./3.1415926/C)*CEXP(CMPLX(0.,1.)*(4.*C-3.*3.1415926)
     7/4.)*H1
      H12=CSQRT(2./3.1415926/C)*CEXP(CMPLX(0.,-1.)*(4.*C-3.*3.1415926)
     8/4.)*H1
      BE11=(H11+H12)/2.
      BE12=(H11-H12)/2./CMPLX(0.,1.)
   21 CONTINUE
      RETURN
      END
      REAL FUNCTION NFAK(N)
      NFAK=1.
      IF(N.LT.2)GO TO 4
      IF(N.GT.30)GO TO 6
      DO 5 I=1,N
    5 NFAK=NFAK*I
      CONTINUE
      GO TO 4
    6 NFAK=1.
      DO 7 I=31,N
    7 NFAK=NFAK*I
    4 RETURN
      END
```

SUBJECT INDEX